

**PHASE DIAGRAM STUDIES OF Bi-Mo-O AND
Pb-Mo-O SYSTEMS AND THE DEVELOPMENT OF A
HIGH TEMPERATURE PIEZOELECTRIC MATERIAL
FOR USE IN LIQUID METALS**

By

AISWARYA P M

CHEM02201204006

**Indira Gandhi Centre for Atomic Research,
Kalpakkam, Tamil Nadu, India**

*A thesis submitted to the
Board of Studies in Chemical Sciences
In partial fulfillment of requirements
for the Degree of*

DOCTOR OF PHILOSOPHY

of

HOMI BHABHA NATIONAL INSTITUTE



August, 2017

Homi Bhabha National Institute

Recommendations of the Viva Voce Committee

As members of the Viva Voce Committee, we certify that we have read the dissertation prepared by **Aiswarya P.M** entitled “**Phase diagram studies of Bi-Mo-O and Pb-Mo-O systems and the development of a high temperature piezoelectric material for use in liquid metals**” and recommend that it may be accepted as fulfilling the thesis requirement for the award of Degree of Doctor of Philosophy.

Chairman - Dr. S. Anthonysamy

Date:

Guide / Convener - Dr. T. Gnanasekaran

Date:

Examiner -

Date:

Member 1 - Dr. U. Kamachi Mudali

Date:

Member 2 - Dr. K. I. Gnanasekar

Date:

Member 3 - Dr. Rajesh Ganesan

Date:

Final approval and acceptance of this thesis is contingent upon the candidate's submission of the final copies of the thesis to HBNI.

I/We hereby certify that I/we have read this thesis prepared under my/our direction and recommend that it may be accepted as fulfilling the thesis requirement.

Date:

Place:

Dr. T. Gnanasekaran
(Guide)

STATEMENT BY AUTHOR

This dissertation has been submitted in partial fulfillment of requirements for an advanced degree at Homi Bhabha National Institute (HBNI) and is deposited in the Library to be made available to borrowers under rules of the HBNI.

Brief quotations from this dissertation are allowable without special permission, provided that accurate acknowledgement of source is made. Requests for permission for extended quotation from or reproduction of this manuscript in whole or in part may be granted by the Competent Authority of HBNI when in his or her judgment the proposed use of the material is in the interests of scholarship. In all other instances, however, permission must be obtained from the author.

Aiswarya P.M

DECLARATION

I, hereby declare that the investigation presented in the thesis has been carried out by me. The work is original and has not been submitted earlier as a whole or in part for a degree / diploma at this or any other Institution / University.

Aiswarya P.M

List of Publications arising from the thesis

I. Published:

1. Partial phase diagrams of Pb-Mo-O system and the standard molar Gibbs energy of formation of PbMoO_4 and Pb_2MoO_5 , P.M. Aiswarya, Rajesh Ganesan, T. Gnanasekaran, J. Nucl. Mater. **2017**, 493, 310-321.
2. The standard molar enthalpies of formation and heat capacities of PbMoO_4 (s) and Pb_2MoO_5 (s), P.M. Aiswarya, Rajesh Ganesan, T. Gnanasekaran, J. Chem. Thermodyn. **2018**, 116, 21-31.

II. Communicated:

1. Partial phase diagram of MoO_3 rich section of the ternary Bi-Mo-O system, P.M. Aiswarya, Rajesh Ganesan, R. Rajamadhavan, T. Gnanasekaran, Journal of Alloys and Compounds.

III. Manuscripts under preparation:

1. Partial phase diagrams of the ternary Bi-Mo-O system, P.M. Aiswarya, Rajesh Ganesan, T. Gnanasekaran.
2. The standard molar enthalpies of formation of bismuth molybdates, P.M. Aiswarya, Rajesh Ganesan, T. Gnanasekaran.
3. The standard molar Gibbs energy of formation and molar heat capacities of bismuth molybdates, P.M. Aiswarya, Rajesh Ganesan, T. Gnanasekaran.
4. Synthesis of highly resistive bismuth titanate for high temperature piezoelectric applications, P.M. Aiswarya, K.I. Gnanasekar, V. Jayaraman, T. Gnanasekaran.

IV. Conference presentations:

1. Studies on the Phase Diagram of Bi-Mo-O System, P.M. Aiswarya, R. Ganesan, T. Gnanasekaran, International Conference on Materials and Characterization Techniques- ICMCT 2014, VIT University, Vellore.

2. Studies on the phase diagram of Pb-Mo-O system, P.M. Aiswarya, R. Ganesan, T. Gnanasekaran, Inter disciplinary Symposium on Material Chemistry, ISMC-2014, 9-14 December 2014, BARC, Mumbai.
3. Phase equilibria in the Bi-Mo-O system, P.M. Aiswarya, R. Ganesan, T. Gnanasekaran, Nuclear Materials Conference, NUMAT-2014, 27-31 October-2014, Florida, USA
4. Studies on the phase diagram of Pb-Mo-O system, P.M. Aiswarya, R. Ganesan, T. Gnanasekaran, Nuclear Materials Conference NUMAT-2014, 27-31 October 2014, Florida, USA.
5. Thermochemical Studies on Pb-Mo-O system, P.M. Aiswarya, R. Ganesan, T. Gnanasekaran, CALPHAD XLIV, 30th May-5th June 2015, Loano, Italy.
6. Studies on Pb-Mo-O System, P.M. Aiswarya, R. Ganesan, T. Gnanasekaran, CHEMNUT-2015, 30-31 July 2015, IGCAR, Kalpakkam.
7. Phase diagram and thermodynamic studies on Pb-M-O and Bi-M-O (M: Fe, Cr, Mo) ternary systems, A.V Meera, P.M Aiswarya, S.K Sahu, R Ganesan, T. Gnanasekaran, Proceedings of the DAE-BRNS fifth Interdisciplinary Symposium on Materials Chemistry, 9-13 December 2014, Bhabha Atomic Research Centre, Mumbai.

Aiswarya P. M.

DEDICATED

To

My Mother

who taught me to be gentle and strong

My Father

who encouraged me to believe in myself

My Grandmother

for being my first teacher

ACKNOWLEDGEMENT

I wish to express my sincere gratitude to those who have contributed to this thesis and supported me throughout this amazing journey.

First and foremost I would like to express my sincere gratitude to my research supervisor, Dr. T Gnanasekaran for giving me the opportunity to work with him and for introducing me to the field of experimental thermodynamics. I am deeply indebted to him for the continuous support for my PhD study and related research, for his patience, motivation and immense knowledge. His enthusiasm for research was contagious and motivational for me and I appreciate all his contributions of time and ideas to make my PhD experience productive and stimulating.

I am deeply grateful to my technical advisor, Dr. Rajesh Ganesan who helped me throughout my PhD life. His expertise in experimental thermodynamics and his commitment towards research helped me in shaping most of the concepts in this thesis. I also remain indebted for his understanding and support during the toughest times. His deep insights helped me at various stages of my research.

I would like to thank my doctoral committee chairman, Dr. S. Anthonysamy, former chairman Dr. V. Ganesan and members, Dr. K. I. Gnanasekar and Dr. U. Kamachi Mudali for their valuable suggestions, support and useful discussions.

I would like to thank Dr. M. Joseph, Director, M & FCG and Dr. A. K. Badhuri, Director, IGCAR for permitting me to use the excellent research facilities at IGCAR. I thank Dr. N. Sivaraman, Dean of Chemical Sciences, for his constant support and help. I would be always thankful to Dr. V. Jayaraman, Dr. R. Sridharan and Dr. K. Chandran for their valuable suggestions and inspiration. I acknowledge DAE/IGCAR for financial support.

My sincere gratitude is reserved for Dr. E. Prabhu, Mr. Sajal Ghosh, Mr. Sree Rama Murthy and Mrs. Clinsha for their invaluable insights and fruitful discussions. I am grateful to them for all the helps and for the precious time they dedicated to me.

I sincerely acknowledge Dr. R. Sudha, Dr. Arup Dasgupta and Mr. Sai Kumaran for characterizing my samples using SEM and EDS. I express my sincere thanks to Mr. Rajamadhavan for characterizing my samples by XRD. I am grateful to

Dr. S. Vijayalakshmi, Mrs. S. Annapoorani, Mrs. V. Hemalatha Mrs. R. Uma Maheswari and Mr. S. Sriram for analyzing my samples using AAS and ICP-OES. I am thanking Mrs. E. Senthilvadivu for the analysis of my samples by XRF. I am thankful to Mr. K. Haridas of Central Glass Blowing Facility for vacuum sealing of my samples. I am also thankful to Mr. N. Eswaran, Mr. G. Lakshmanan, Mr. A. Praveen, Mr. Sathish Kumar and Mr. Khaja Mohideen for their help and support in constructing the experimental setup. I am grateful to Mr. K.A.S. Kutty for his neat drafting work. My sincere thanks to Mr. Henson Raj and Mr. G. Vijayaraghavan of Quality Control Division for their relentless support for helium leak testing. I also deeply acknowledge the help offered by Mr. Rama Murthy and Mr. Nagappan.

I thank Mrs. S. Premalatha, Mr. J.P. Rao and Mr. Ajay Kumar Kesari for their help in the setting up of solution calorimeter and emf units. I also thank Mr. G. Gunasekaran and Mr. G. Udaya Kumar for the timely help.

I deeply thank my lab members for their precious support in conducting my research. I would be immensely thankful to Mrs. Reshmi, Mr. Kishore Naick, Mrs. Nalini, Mrs. Muthu Ambika, Mr. VishnuVardhan, Mr. Lakshmi Gandhan, Mr. Jose, Mr. Shyam Kumar, Mr. Afijith, Dr. Soumen Das, Mr. Nagaraj, Mr. Sandeep Swamy, and Mr. Venkatesh, and for their endless support in carrying out the research. I would be always grateful to Mr. N. Sanil, Mr. Murugesan, Dr. Ashish Jain, Mr. Suranjan Bera, Mr. Trinadh and Mrs. Lali for the helps they offered.

I also thank my senior Dr. Sulata Kumari Sahu for her valuable advices and timely help.

It is a pleasure to thank my friends, Mrs. Meera, Mrs. Soja, Mrs. Rasmi and Mrs. Sabeena for the wonderful times we shared and unforgettable moments we cherished. Thanks to Meera for her continuous and unparalleled love, help and support and for holding my hand at the weakest times. I would be indebted to Soja and her mother for considering me as a family member and helping me to overcome the obstacles. Words cannot express my sincere gratitude to Rasmi and Sabeena for their constant encouragement, moral support and friendly advice. I cannot forget the good times which I had with Reshmi chechi, Deepu etan and their family. They stood for me at the miserable times and lot of heartfelt thanks to them for being my

guardians at Kalpakkam. Special thanks to Nalini, Dinu, Lavanya and Jayasree for the constant support.

I wish to thank my sister and brothers for their companionship and moral support. I am forever thankful to my dear friend Mr. Yatindra Kumar for being with me as a constant source of strength and encouragement and for making me comfortable always. I deeply thank him for being with me at times I needed the most and for taking care of my needs.

A special thanks to my family. Words cannot express how grateful I am to my mother, father, grandmother and relatives for all the sacrifices that they have made on my behalf. Their prayer for me was what sustained me thus far. They selflessly encouraged me to explore new directions in life and seek my own choices. This journey would not have been possible if not for them, and I dedicate this milestone to them.

Finally I thank my God, for letting me through all the difficulties. I have experienced his guidance every day and I will keep on trusting him for my future.

Thank You

Aiswarya P.M

CONTENTS

	Page No.
SYNOPSIS	xvi
LIST OF FIGURES	xx
LIST OF TABLES	xxiv
CHAPTER 1-INTRODUCTION	1
1.1 Use of liquid metals as coolant	1
1.2 Lead-Bismuth Eutectic (LBE) system	2
1.3 Accelerator Driven Systems (ADS) and use of liquid lead and LBE	3
1.4 Compatibility issues of liquid lead and LBE with structural steels	4
1.5 Mitigation of corrosion in liquid lead and LBE systems	7
1.5.1 Use of corrosion resistant structural materials	7
1.5.2 Corrosion resistant coatings	8
1.5.3 Active oxygen control	9
1.6 Thermodynamic basis for the protective oxide layer formation and active oxygen control	10
1.7 Characteristics of the oxide layer-from corrosion tests on steels	13
1.8 Kinetics of oxide layer formation	13
1.9 Use of piezoelectric materials	16
1.10 Aim	17
1.11 References	17
CHAPTER 2-EXPERIMENTAL METHODS	25
2.1 Preparation of the compounds	25
2.1.1 Solid state reaction method	25
2.1.2 Co-precipitation method	26
2.1.3 Molten salt method	27
2.2 Phase equilibration experiments	29
2.3 Techniques for materials characterization	30
2.3.1 X-ray Diffraction (XRD)	30
2.3.2 Scanning Electron Microscopy (SEM)	33
2.3.3 Impedance spectroscopy	34
2.4 Oxygen potential measurements employing solid oxide electrolytes	41

2.4.1	Defect equilibria and conduction mechanism in solid oxide electrolytes	43
2.4.2	Electrolytic domain	45
2.4.3	Application of solid electrolytes for emf measurements	47
2.5	Calorimetric techniques	48
2.5.1	Isoperibol calorimeters	49
2.5.2	Differential Scanning Calorimetry (DSC)	56
2.5.2.1	Heat flux DSC	56
2.5.2.2	Power compensation DSC	57
2.5.3	Calibration of DSC	58
2.5.3.1	Temperature calibration	58
2.5.3.2	Heat calibration	59
2.5.3.3	Heat flow rate calibration	59
2.5.4	Heat capacity measurement using a heat flux DSC	59
2.6	References	62
CHAPTER 3-THERMOCHEMICAL STUDIES ON Bi-Mo-O SYSTEM		65
3.1	Introduction	65
3.2	Literature survey	65
3.2.1	Bi-Mo system	65
3.2.2	Bi-O system	65
3.2.3	Mo-O system	67
3.2.4	Bi ₂ O ₃ -MoO ₃ system	70
3.3	Experimental details	84
3.3.1	Materials	84
3.3.2	Preparation of ternary compounds	85
3.3.3	Phase equilibration studies	85
3.3.3.1	Equilibrations of samples with compositions in the Bi ₂ O ₃ -MoO ₃ pseudo binary line	85
3.3.3.2	Equilibrations of samples with compositions in the line joining Bi ₂ O ₃ and MoO ₂	87
3.3.3.3	Partial reduction of ternary compounds followed by long term equilibrations	87
3.3.3.4	Long term equilibrations of phase mixtures using different starting components	91

3.3.3.5	Long term equilibrations of phase mixtures in liquid bismuth	94
3.3.3.6	Equilibrations to determine the stability ranges of $\text{Bi}_8\text{Mo}_3\text{O}_{21}$, $\text{Bi}_{14}\text{Mo}_5\text{O}_{36}$ and $\text{Bi}_6\text{Mo}_2\text{O}_{15}$	94
3.3.4	Electrical conductivity measurements	97
3.3.4.1	Conductivity measurements on $\text{Bi}_8\text{Mo}_3\text{O}_{21}$, $\text{Bi}_{14}\text{Mo}_5\text{O}_{36}$ and $\text{Bi}_6\text{Mo}_2\text{O}_{15}$	97
3.3.4.2	Conductivity measurements on $\text{Bi}_2\text{Mo}_2\text{O}_9$	99
3.3.4.3	Conductivity measurements on Bi_2MoO_6	99
3.3.5	Simultaneous equilibration experiments to follow the structural changes during conductivity measurements	100
3.3.6	Oxygen potential measurements using yttria stabilized zirconia solid electrolyte	102
3.3.7	Determination of standard molar enthalpies of formation of bismuth molybdates by solution calorimetry	107
3.3.8	Determination of molar heat capacities of bismuth molybdates by differential scanning calorimetry	109
3.4	Results and discussion	111
3.4.1	Preparation and characterization of starting components and ternary compounds	111
3.4.2	Studies involving equilibrations of samples with compositions in the Bi_2O_3 - MoO_3 pseudo binary line	112
3.4.3	Studies involving equilibrations of samples with compositions in the line joining Bi_2O_3 and MoO_2	114
3.4.4	Studies involving partial reduction of ternary compounds followed by long term equilibrations	114
3.4.5	Studies involving long term equilibrations of phase mixtures using different starting components and equilibrations in liquid bismuth	114
3.4.6	Investigation on the thermal stabilities of $\text{Bi}_8\text{Mo}_3\text{O}_{21}$, $\text{Bi}_{14}\text{Mo}_5\text{O}_{36}$ and $\text{Bi}_6\text{Mo}_2\text{O}_{15}$	117
3.4.7	Investigation on the thermal stability of $\text{Bi}_2\text{Mo}_2\text{O}_9$	122
3.4.8	Investigation on the polymorphic transformations of Bi_2MoO_6	123
3.4.9	Oxygen potential measurements	125
3.4.9.1	Standard molar Gibbs energy of formation of Bi_2MoO_6 (s)	125

3.4.10	Standard molar enthalpies of formation of bismuth molybdates	128
3.4.11	Heat capacity measurements	132
3.4.11.1	Molar heat capacity of MoO_3 (s)	132
3.4.11.2	Molar heat capacity of $\text{Bi}_2\text{Mo}_3\text{O}_{12}$ (s)	140
3.4.11.3	Molar heat capacity of monoclinic phase of Bi_2MoO_6 (s)	142
3.4.11.4	Molar heat capacity of $\text{Bi}_6\text{Mo}_2\text{O}_{15}$ (s)	144
3.4.12	Consistency of measured thermodynamic data	145
3.4.12.1	Monoclinic Bi_2MoO_6 (s)	145
3.5	References	147
CHAPTER 4-THERMOCHEMICAL STUDIES ON Pb-Mo-O SYSTEM		157
4.1	Introduction	157
4.2	Literature survey	157
4.2.1	Pb-Mo system	157
4.2.2	Pb-O system	157
4.2.3	PbO-MoO ₃ system	158
4.3	Experimental details	166
4.3.1	Materials	166
4.3.2	Preparation of ternary compounds	169
4.3.3	Phase equilibration studies	171
4.3.3.1	Equilibrations of samples with compositions on the PbO-MoO ₃ pseudo binary line and the line joining PbO and MoO ₂	171
4.3.3.2	Partial reduction of ternary compounds followed by long term equilibrations	171
4.3.3.3	Additional equilibrations using different starting components	173
4.3.3.4	Equilibrations in liquid lead	175
4.3.3.5	Equilibrations to determine the temperature range of stability of Pb_5MoO_8	179
4.3.4	Emf measurements	181
4.3.5	Determination of enthalpies of formation of lead molybdates by solution calorimetry	184
4.3.6	Determination of molar heat capacities of lead molybdates by	185

	differential scanning calorimetry	
4.4	Results and discussion	186
4.4.1	Preparation of ternary compounds	186
4.4.2	Studies involving equilibrations using PbO-MoO ₃ and PbO-MoO ₂ mixtures	187
4.4.3	Studies involving partial reduction of ternary compounds followed by long term equilibrations	187
4.4.4	Studies involving long term equilibrations using different starting components and equilibrations in liquid lead	188
4.4.5	Studies involving long term equilibrations to determine the temperature range of stability of Pb ₅ MoO ₈	189
4.4.6	Oxygen potential measurements	192
4.4.6.1	Standard molar Gibbs energy of formation of PbMoO ₄ (s)	192
4.4.6.2	Standard molar Gibbs energy of formation of Pb ₂ MoO ₅ (s)	195
4.4.6.3	Standard molar Gibbs energy of formation of Pb ₅ MoO ₈ (s)	197
4.4.7	Standard molar enthalpies of formation of PbMoO ₄ (s), Pb ₂ MoO ₅ (s) and Pb ₅ MoO ₈ (s)	198
4.4.8	Heat capacity measurements	203
4.4.8.1	Molar heat capacity of PbMoO ₄ (s)	203
4.4.8.2	Molar heat capacity of Pb ₂ MoO ₅ (s)	206
4.4.8.3	Deviations of C _p from Neumann-Kopp's rule (NKR)	210
4.4.9	Consistency of the measured thermodynamic data with the data reported in literature	213
4.4.9.1	PbMoO ₄ (s)	213
4.4.9.2	Pb ₂ MoO ₅ (s)	215
4.5	References	216
CHAPTER 5-DEVELOPMENT OF PIEZOELECTRIC MATERIAL FOR HIGH TEMPEARTURE APPLICATIONS IN LIQUID METALS		221
5.1	Introduction	221
5.1.1	Overview of piezoelectric elements suitable for high temperature applications	222

5.1.2	Bismuth titanate-structure and characteristic properties	224
5.2	Experimental details	228
5.2.1	Synthesis of bismuth titanate	228
5.2.1.1	Solid state reaction	228
5.2.1.2	Co-precipitation reaction	228
5.2.1.3	Reaction in molten salt medium	229
5.2.2	Synthesis of Nb-doped bismuth titanates	230
5.2.3	Structural and morphological characterizations	230
5.2.4	Conductivity measurements	230
5.2.5	Piezoelectric characterization	231
5.3	Results and discussion	232
5.3.1	Structural and morphological characterization of bismuth titanates	232
5.3.2	Electrical characterization of bismuth titanates	237
5.3.3	Piezoelectric characterization of bismuth titanates	242
5.4	References	242
	CHAPTER 6-SUMMARY AND CONCLUSIONS	247
6.1	Prediction of the nature of passive oxide layer	250
6.2	References	255
	CHAPTER 7-SCOPE FOR FUTURE STUDIES	257
7.1	References	257
	APPENDIX	259

SYNOPSIS

Liquid lead and Lead- Bismuth Eutectic (LBE) alloys are considered as spallation target as well as coolant in Accelerator Driven Systems (ADS). Because of their low reactivity towards air and water/steam, they are also considered as candidate coolants for fast breeder reactors [1]. However, these coolants are chemically incompatible with structural steels because of the high solubility of alloying elements of steels in them which leads to severe corrosion. Among the alloying components of steels, nickel has very high solubility in both liquid Pb and LBE. Hence, nickel free structural steels with optimum levels of Cr, Mo, Si, etc are being considered for Pb and LBE service. Solubility of Fe, Cr and Mo in these heavy metals is still significant and can lead to heavy corrosion effects. This corrosion and mass transport can be minimized by forming a protective oxide layer over the surface of the structural steels by careful control of oxygen concentration in the liquid metal coolant [2, 3]. To understand the stability and formation of this protective oxide film, the study of the thermochemical aspects of the interaction of alloying components of steel with Pb and Bi in the presence of dissolved oxygen is important. Towards this direction, data on the ternary phase diagrams of Pb-M-O and Bi-M-O (M=alloying elements in steels) systems and thermochemical properties of relevant ternary oxides in these systems are required. Systematic studies on the phased diagrams of Pb-Fe-O, Pb-Cr-O, Bi-Fe-O and Bi-Cr-O systems and the determination of thermochemical data of relevant ternary compounds present in these systems were carried out by Sahu et al. [4-9] and Meera et al. [10- 11]. In the present work, studies on Bi-Mo-O and Pb-Mo-O systems have been carried out.

The thesis also involves works related to the development of high temperature piezoelectric material to be used in liquid metals. High temperature ultrasonic transducers are employed for the inspection of components immersed in liquid metal systems. The piezoelectric materials, which are used in these ultrasonic transducers, must possess high Curie temperature and favorable piezoelectric properties. Presently, lead zirconate titanate (PZT) based ultra sonic transducers are used. Since the Curie temperature of PZT is only 623 K, it cannot be employed for high temperature applications. Piezoelectric materials such as lithium niobate, bismuth titanate, lead metaniobate and gallium orthophosphate etc possess high Curie temperature and are promising candidates. Among them, bismuth titanate has a Curie temperature of 948 K but it possesses highly anisotropic electrical conductivity with the maximum value along the plane of polarization. For piezoelectric applications, a low electrical conductivity is essential as it causes difficulty in poling [12] as well as during transducer application. Thus it is crucial to prepare bismuth titanate crystals with reduced electrical conductivity. In the present study, experiments were carried out to optimize the preparation conditions with niobium as the dopant to obtain highly resistive bismuth titanate crystals suitable for high temperature piezoelectric applications.

The objectives set for the present thesis work are

- (1) Determination of ternary phase diagrams of Bi-Mo-O and Pb-Mo-O systems.
- (2) Measurement of thermochemical properties such as Gibbs energy of formation, enthalpy of formation and the heat capacity of the ternary compounds in these systems.
- (3) Development of bismuth titanate based piezoelectric material to be used at high temperatures.

2. Organization of the thesis

The thesis consists of seven chapters. Chapter 1 contains the introduction to the present work. Experimental methods and techniques used in the present study are described in Chapter 2. Chapter 3 describes studies carried out on Bi-Mo-O ternary system and Chapter 4 describes the studies conducted on Pb-Mo-O ternary system. Chapter 5 discusses the preparation and characterization studies carried out towards the development of bismuth titanate based high temperature piezoelectric material. Chapter 6 provides the summary of the results and conclusions drawn from the present work. Chapter 7 presents the scope for future studies.

References

1. J. Zhang, N. Li, Review of the studies on fundamental issues in LBE corrosion, *J. Nucl. Mater.* 373 (2008) 351-377.
2. P.N. Martynov, Y.I. Orlov, Proceedings of Heavy Liquid Metal Coolants in Nuclear Technology (HLMC-98), Vol. 2, SSC RF-IPPE, Obninsk, 1998, pp. 565-576.
3. N. Li, active control of oxygen in molten lead-bismuth eutectic systems to prevent steel corrosion and coolant contamination, *J. Nucl. Mater.* 300 (2002) 73 -81.
4. S.K. Sahu, R. Ganesan, T. Gnanasekaran, Studies on phase diagram of Pb–Cr–O system, *J. Nucl. Mater.* 376 (2008) 366-370.
5. S.K. Sahu, R. Ganesan, T. Gnanasekaran, Standard molar Gibbs free energy of formation of $Pb_5CrO_8(s)$, $Pb_2CrO_5(s)$, and $PbCrO_4(s)$, *J. Chem. Thermodyn.* 42 (2010) 1–7.

6. S.K. Sahu, R. Ganesan, T.G. Srinivasan, T. Gnanasekaran, The standard molar enthalpies of formation of $\text{Pb}_2\text{CrO}_5(\text{s})$ and $\text{Pb}_5\text{CrO}_8(\text{s})$ by acid solution calorimetry, *J. Chem. Thermodyn.* 43 (2011) 750-753.
7. S.K. Sahu, M. Sahu, R.S. Srinivasa, T.Gnanasekaran, Determination of heat capacities of $\text{PbCrO}_4(\text{s})$, $\text{Pb}_2\text{CrO}_5(\text{s})$, and $\text{Pb}_5\text{CrO}_8(\text{s})$, *Monatsh. Chem.* 143 (2012) 1207–1214.
8. S.K. Sahu, R. Ganesan, T.Gnanasekaran, Studies on the phase diagram of Pb–Fe–O system and standard molar Gibbs energy of formation of ‘ $\text{PbFe}_5\text{O}_{8.5}$ ’ and $\text{Pb}_2\text{Fe}_2\text{O}_5$, *J. Nucl. Mater.* 426 (2012) 214-222.
9. S.K. Sahu, R. Ganesan, T. Gnanasekaran, The standard molar enthalpies of formation of $\text{Pb}_2\text{Fe}_2\text{O}_5(\text{s})$ and $\text{PbFe}_5\text{O}_{8.5}(\text{s})$ by acid solution calorimetry, *J. Chem. Thermodyn.* 56 (2013) 57–59.
10. A.V. Meera, R. Ganesan, T. Gnanasekaran, Partial phase diagram of Bi-Fe-O system and the standard molar Gibbs energy of formation of $\text{Bi}_2\text{Fe}_4\text{O}_9$, *J. Alloys. Comp.* 692 (2017) 841-847.
11. A.V. Meera, Joysurya Basu, R. Ganesan, T. Gnanasekaran, Studies on the phase diagram of Bi-Cr-O system, *J. Nucl. Mater.* 487 (2017) 174-185.
12. A. Fouskova, L.E. Cross, Dielectric properties of bismuth titanate, *J. Appl. Phys.* 41 (1970) 2834-2838.

LIST OF FIGURES

<i>Figure No</i>	<i>Figure Caption</i>	<i>Page No.</i>
1.1	Phase diagram of Pb-Bi system	3
1.2	Schematic diagram of accelerator driven system	4
1.3	Temperature dependence of solubility of alloying components of steel in liquid Pb	5
1.4	Temperature dependence of solubility of alloying components of steel in liquid Bi	6
1.5	Temperature dependence of solubility of alloying components of steel in LBE	6
1.6	Oxygen concentration effects on the corrosion behavior of steels in flowing liquid Pb after 3000 h at 823 K	11
1.7	Ellingham diagram showing the oxygen potentials of various metal/metal oxide equilibria	12
1.8	Oxidation kinetics of different steels tested at 823 K in flowing Pb	14
2.1	Typical representation of Nyquist plot	37
2.2	Typical representation of Bode plot	38
2.3	Equivalent electrical circuit of a solid ionic conductor, consisting of a series combination of parallelly connected resistors (R) and capacitors (C)	39
2.4	Impedance spectrum of a solid ionic conductor	40
2.5	Schematic of the conductivity cell	41
2.6	Fluorite structure	42
2.7	Variation of electrical conductivity with partial pressure	45
2.8	Schematic of the variation of electrical conductivity of ThO ₂ and ThO ₂ (Y ₂ O ₃) solid solutions with oxygen pressure at constant temperature	46
2.9	Electrolytic domain boundaries of calcia stabilized zirconia (CSZ) and yttria doped thoria	46
2.10	Schematic diagram of the isoperibol calorimeter	51
2.11-a	Temperature-time curve for exothermic process in isoperibol	53

	calorimeter: initial temperature higher than the temperature of the surroundings	
2.11-b	Temperature-time curve for exothermic process in isoperibol calorimeter: temperature of the surroundings is between initial and final temperature	53
2.11-c	Temperature-time curve for exothermic process in isoperibol calorimeter: final temperature is below the temperature of the surroundings	54
2.12	Illustration of determination of ΔT during the sample dissolution	55
2.13	Illustration of determination of ΔTC during the sample dissolution	55
2.14	Schematic of the heat flux DSC	57
2.15	Schematic of the power compensation DSC	58
2.16	Three step procedure for measuring heat capacity	60
2.17	Typical DSC run for blank, sample and reference	60
3.1	Phase diagram of Bi-Mo- system	66
3.2	Phase diagram of Bi-O system	66
3.3	Phase diagram of Mo-O system	67
3.4	Comparison of literature data on Gibbs energy of formation of MoO_2 (s)	68
3.5	Selected data on Gibbs energy of formation of MoO_2 (s) reported in literature	70
3.6	Compounds reported in the Bi_2O_3 - MoO_3 pseudo binary system	71
3.7	Bi_2O_3 - MoO_3 pseudo binary phase diagram	83
3.8	Schematic of the experimental assembly of the galvanic cell	105
3.9	Correlation between temperature rise and electrical energy	108
3.10	Partial phase diagram of Bi-Mo-O system at 773 K	116
3.11	Partial phase diagram of Bi-Mo-O system at 873 K	116
3.12	Partial phase diagram of Bi-Mo-O system at 1023 K	117
3.13	Variation of electrical conductivity of $\text{Bi}_8\text{Mo}_3\text{O}_{21}$ as a function of temperature	118
3.14	Variation of electrical conductivity of $\text{Bi}_{14}\text{Mo}_5\text{O}_{36}$ as a function of temperature	120

3.15	Variation of electrical conductivity of $\text{Bi}_6\text{Mo}_2\text{O}_{15}$ as a function of temperature	121
3.16	Variation of electrical conductivity of $\text{Bi}_2\text{Mo}_2\text{O}_9$ as a function of temperature	123
3.17	Variation of electrical conductivity of orthorhombic and monoclinic phases of Bi_2MoO_6 as a function of temperature	124
3.18	Variation of emf with temperature with $\text{Bi-MoO}_2\text{-Bi}_2\text{MoO}_6$ as sample	126
3.19	Variation of molar heat capacity of MoO_3 (s) with temperature	139
3.20	Variation of molar heat capacity of $\text{Bi}_2\text{Mo}_3\text{O}_{12}$ (s) with temperature	140
3.21	Variation of molar heat capacity of monoclinic- Bi_2MoO_6 with temperature	142
3.22	Variation of heat capacity of $\text{Bi}_6\text{Mo}_2\text{O}_{15}$ (s) with temperature	144
4.1	Phase diagram of Pb-Mo system	158
4.2	Phase diagram of Pb-O system	158
4.3	Compositions chosen for equilibrations	174
4.4	Compositions chosen for equilibrations	175
4.5	Schematic representation of the emf cell	181
4.6	Isothermal section of Pb-Mo-O system at 773 K	191
4.7	Isothermal section of Pb-Mo-O system at 998 K	191
4.8	Variation of emf with temperature in cell (I) for Pb- $\text{MoO}_2\text{-PbMoO}_4$ phase field	193
4.9	Comparison of $\Delta_f G_m^\circ < \text{PbMoO}_4 >$ from the present work and that reported in ref. [26]	194
4.10	Variation of emf with temperature in cell (II) for Pb- $\text{PbMoO}_4\text{-Pb}_2\text{MoO}_5$ phase field	196
4.11	Variation of emf with temperature in cell (III) for Pb- $\text{Pb}_2\text{MoO}_5\text{-Pb}_5\text{MoO}_8$ phase field	197
4.12	Variation of molar heat capacity of PbMoO_4 (s) with temperature	204
4.13	Comparison of measured heat capacity values of PbMoO_4 (s) with the values reported in literature	205
4.14	Variation of molar heat capacity of Pb_2MoO_5 (s) with temperature	207

4.15-a	Temperature dependence of enthalpies of formation of $\text{PbMoO}_4(\text{s})$	209
4.15-b	Temperature dependence of enthalpies of formation of Pb_2MoO_5	209
4.15-c	Difference in the temperature dependence of enthalpies of formation of $\text{PbMoO}_4(\text{s})$ and $\text{Pb}_2\text{MoO}_5(\text{s})$	210
5.1	Structure of bismuth titanate	226
5.2	Graphical comparison of XRD patterns of $\text{Bi}_4\text{Ti}_3\text{O}_{12}$	232
5.3	XRD patterns of $\text{Bi}_4\text{Ti}_3\text{O}_{12}$ prepared by oxalate co-precipitation method	233
5.4	Comparison of XRD patterns of Nb-doped bismuth titanate prepared by solid state reaction	234
5.5	Comparison of XRD patterns of Nb-doped bismuth titanate prepared by the reaction in molten salt medium	234
5.6	SEM images of pristine and Nb doped BIT prepared by solid state method	235
5.7	SEM images of pristine and Nb doped BIT prepared by molten salt method	236
5.8	Arrhenius plots of electrical conductivity of bismuth titanates prepared by different methods	237
5.9	Comparison of electrical conductivities of pristine and Nb-doped bismuth titanates prepared by solid state method	239
5.10	Comparison of electrical conductivities of pristine and Nb-doped bismuth titanates prepared by molten salt method	240
5.11	Variation of electrical conductivity as a function of Nb concentration	241
6.1	Oxygen potentials in liquid Bi containing different oxygen concentrations and with different chemical equilibria for 9Cr-1Mo steel	254
6.2	Oxygen potentials in liquid Pb containing different oxygen concentrations and with different chemical equilibria for 9Cr-1Mo steel	254
6.3	Oxygen potentials in LBE containing different oxygen concentrations and with different chemical equilibria for 9Cr-1Mo steel	255

LIST OF TABLES

<i>Table No</i>	<i>Table Caption</i>	<i>Page No.</i>
1.1	Comparison of thermophysical properties of liquid metal coolants and water	2
1.2	Solubility data of structural steel components in liquid Pb, Bi and LBE	5
1.3	Diffusion coefficient of oxygen	12
1.4	Standard Gibbs energy of dissolution of oxygen	12
1.5	Solubility of oxygen	12
3.1	Literature data on Gibbs energy of formation of MoO ₂ (s)	69
3.2	Literature data on Bi ₂ O ₃ -MoO ₃ pseudo binary system	75
3.3	Preparation of ternary compounds in the Bi ₂ O ₃ -MoO ₃ system	86
3.4	Details of equilibrations of samples with mixtures of Bi ₂ O ₃ and MoO ₃	88
3.5	Details of equilibrations of samples with Bi ₂ O ₃ and MoO ₂ mixtures	91
3.6	Details of equilibration of partially reduced ternary compounds	92
3.7	Details of equilibrations of phase mixtures using different starting components	93
3.8	Details of equilibrations in liquid bismuth	95
3.9	Details of equilibrations to study the stabilities of Bi ₈ Mo ₃ O ₂₁ , Bi ₁₄ Mo ₅ O ₃₆ and Bi ₆ Mo ₂ O ₁₅	98
3.10	Details of simultaneous equilibrations of Bi ₈ Mo ₃ O ₂₁ , Bi ₁₄ Mo ₅ O ₃₆ and Bi ₆ Mo ₂ O ₁₅ samples in air	103
3.11	Details of simultaneous equilibrations of Bi ₂ Mo ₂ O ₉ and Bi ₂ MoO ₆ samples in air	104
3.12	Variation of EMF with temperature in the Bi-MoO ₂ -Bi ₂ MoO ₆ phase field	126
3.13	Enthalpy of solution ($\Delta_{sol}H_m^o$) of TRIS* in 0.10 ± 0.01 mol / kgHCl	129
3.14	Experimentallydetermined values of enthalpies of dissolution	131

	(ΔH) and molar enthalpies of dissolution ($\Delta_{sol}H_m^o$) of Bi_2O_3 (s) and MoO_3 (s) in a mixture of 100 ml of 3 mol kg^{-1} NaOH and 25 ml of triethanolamine	
3.15	Experimentally determined values of enthalpies of dissolution (ΔH) and molar enthalpies of dissolution ($\Delta_{sol}H_m^o$) of $\text{Bi}_2\text{Mo}_3\text{O}_{12}$ (s), orthorhombic Bi_2MoO_6 (s), monoclinic Bi_2MoO_6 (s), $\text{Bi}_6\text{Mo}_2\text{O}_{15}$ (s) and $\text{Bi}_6\text{MoO}_{12}$ (s) in a mixture of 100 ml of 3 mol kg^{-1} NaOH and 25 ml of triethanolamine	133
3.16	Thermodynamic reaction schemes for obtaining the enthalpies of formation from oxides and elements for $\text{Bi}_2\text{Mo}_3\text{O}_{12}$ (s)	134
3.17	Thermodynamic reaction schemes for obtaining the enthalpies of formation from oxides and elements for orthorhombic Bi_2MoO_6 (s)	135
3.18	Thermodynamic reaction schemes for obtaining the enthalpies of formation from oxides and elements for monoclinic Bi_2MoO_6 (s)	136
3.19	Thermodynamic reaction schemes for obtaining the enthalpies of formation from oxides and elements for $\text{Bi}_6\text{Mo}_2\text{O}_{15}$ (s)	137
3.20	Thermodynamic reaction schemes for obtaining the enthalpies of formation from oxides and elements for $\text{Bi}_6\text{MoO}_{12}$ (s)	138
3.21	Heat capacity of MoO_3 (s)	139
3.22	Thermodynamic functions of $\text{Bi}_2\text{Mo}_3\text{O}_{12}$ (s)	141
3.23	Thermodynamic functions of monoclinic- Bi_2MoO_6 (s)	143
3.24	Thermodynamic functions of $\text{Bi}_6\text{Mo}_2\text{O}_{15}$ (s)	145
4.1	Literature data on PbO- MoO_3 pseudo binary system	161
4.2	Literature data on thermochemical properties of PbMoO_4 (s)	167
4.3	Preparation of compounds PbMo_5O_8 and $\text{Pb}_3\text{Mo}_{16}\text{O}_{24}$	170
4.4	Equilibration of samples with mixtures of (a) PbO and MoO_3 and (b) PbO and MoO_2	172
4.5	Equilibration of partially reduced ternary compounds	173
4.6	Details of additional equilibrations	176
4.7	Details of equilibration of samples of composition falling within the Pb-Mo- MoO_2 region	177
4.8	Details of samples equilibrated with excess liquid lead and the products obtained	178

4.9	Details of samples coated on alumina strips and equilibrated with excess liquid lead	179
4.10	Details of long term equilibration experiments to deduce the temperature range of stability of Pb_5MoO_8	180
4.11	Variation of emf of cell (I) with temperature	192
4.12	Comparison of $\Delta_f G_{298}^\circ < PbMoO_4 >$ reported in literature and that obtained in the present work	195
4.13	Variation of emf of cell (II) with temperature	195
4.14	Variation of emf of cell (III) with temperature	197
4.15	Experimentally determined values of enthalpies of dissolution (ΔH) and molar enthalpies of dissolution ($\Delta_{sol} H_m^\circ$) of $PbMoO_4$ (s), Pb_2MoO_5 (s), PbO (s) and MoO_3 (s) in 2.02 ± 0.01 mol / kg NaOH	199
4.16	Thermodynamic reaction schemes for obtaining the enthalpies of formation from oxides and elements for $PbMoO_4$ (s)	200
4.17	Thermodynamic reaction schemes for obtaining the enthalpies of formation from oxides and elements for Pb_2MoO_5 (s)	201
4.18	Thermodynamic reaction schemes for obtaining the enthalpies of formation from oxides and elements for Pb_5MoO_8 (s)	202
4.19	Thermodynamic functions of $PbMoO_4$ (s)	206
4.20	Thermodynamic functions of Pb_2MoO_5 (s)	208
4.21	Unit cell volumes of ternary oxides and component oxides	213
5.1	Properties of selected piezoelectric materials	222
5.2	Composition of Nb doped bismuth titanates ($Bi_4Ti_{3-x/4}Nb_{x/5}O_{12}$)	230

Chapter 1

Introduction

1.1 Use of liquid metals as coolant

Advanced nuclear systems use liquid metals as coolants for the effective heat removal from the reactor core. During the early stages of nuclear reactor development, liquid sodium as well as heavy liquid metals such as Lead and Lead-Bismuth Eutectic (LBE) were proposed and investigated as coolants for the Fast Breeder Reactors (FBRs) [1-5]. Superior heat transfer characteristics, low density, low neutron absorption cross section, inherent compatibility with structural materials and relatively low cost, made liquid sodium to be the preferred choice as coolant in FBRs in all countries. LBE was investigated as the primary coolant in Alpha submarine in Russia [6, 7]. Although liquid sodium is still the coolant of choice for fast reactors, its high chemical reactivity with air and water/steam and consequent hazards is a matter of concern. Any accidental failure of structural materials at the secondary heat exchanger of a fast breeder reactor can lead to violent and explosive reaction of liquid sodium with high pressure steam. This would form highly corrosive NaOH which would propagate the failure and costly shut down of the reactor. Because of very low chemical reactivity of liquid Pb and LBE with air and water/steam, they are being reconsidered as coolants for the secondary circuits of the fast reactors [1, 2]. In fact, Pb or LBE cooled fast reactors is one of the four types proposed for investigation by the Generation IV International Forum [8]. These heavy liquid metal coolants are the primary candidates for spallation neutron targets and coolants in Accelerator Driven Systems (ADS) because of their high spallation neutron yield, low neutron moderation, very high boiling point and low chemical

reactivity [6, 9-11]. Selected thermo physical properties of Na, Pb, LBE and water at 773 K (typical operating temperature of fast reactor) are compared in Table 1.1.

Table 1.1 Comparison of thermophysical properties of liquid metal coolants and water [12, 13]

Property	Sodium	Lead	LBE	H ₂ O
Melting point (K)	371	600.6	398	273
Boiling point (K)	1155	2021	1927	373
Density at 773 K (kg m ⁻³)	832	10452	10066	990 (at 323 K)
Thermal conductivity at 773 K (W m ⁻¹ K ⁻¹)	140	17.70	14.41	0.67 (at 323 K)
Specific heat at 773 K (J kg ⁻¹ K ⁻¹)	1264	144.82	141.05	1.339 (at 323 K)
Vapor pressure at 773 K (Pa)	5.51×10^2	2.12×10^{-3}	2.61×10^{-3}	101325 (at 373 K)
Viscosity at 773 K (Pa S)	2.36×10^{-4}	1.81×10^{-3}	1.31×10^{-3}	0.89 (at 298 K)
Surface tension at 773 K (Nm ⁻¹)	0.1563	0.4386	0.3867	71.99 (at 298 K)

1.2 Lead-Bismuth Eutectic (LBE) system

The phase diagram of Pb-Bi binary system is shown in Fig. 1.1 [14]. Lead and bismuth form a eutectic between them at 398.5 K and at 45 at% Pb. The terminal solid solubility of Bi in Pb is 22 at% at 460 K while maximum solid solubility of Pb in Bi is 0.5 at% at 398.5 K. It also shows the presence of an intermetallic phase designated as ϵ in the composition range of 27.5 to 40 at% Bi. The ϵ phase is a non-stoichiometric phase which melts peritectically at 460 K. Above the melting point of Pb, complete miscibility in liquid phase is observed in the entire composition range.

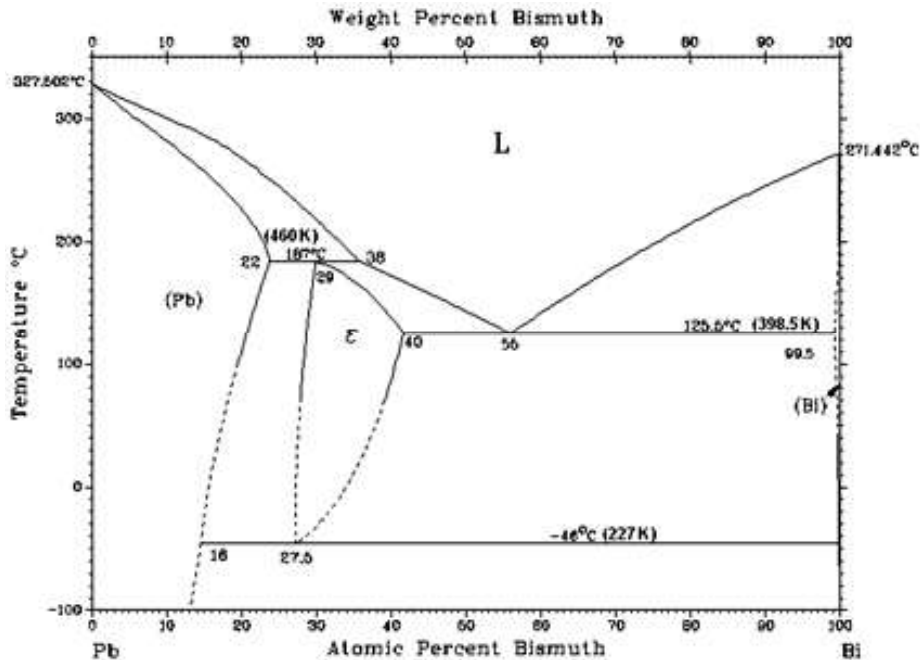


Fig. 1.1 Phase diagram of Pb-Bi system [14]

1.3 Accelerator Driven Systems (ADS) and use of liquid lead and LBE

Accelerator driven systems (ADS) are developed for the incineration of nuclear wastes which are generated in the conventional nuclear reactors. ADS can be considered as a better option for the transmutation of long lived radio isotopes into short lived radioactive or inert isotopes and thus serving in the safe disposal of nuclear wastes. The schematic diagram of ADS is shown in Fig. 1.2 [15]. In ADS, a superconducting linear accelerator is connected with a subcritical fast reactor. A high energy proton beam (~ 1.5 GeV) is generated by the accelerator and is injected on to the target. Spallation reactions take place when the high energy proton beam impinges on the target and as a result, neutrons are generated in the sub critical reactor core comprising of long lived minor actinides such as Am, Np, Cm, etc as the fuel along with U, Pu and Th. A heavy metal is preferred as the target to increase the yield of spallation neutrons. Use of heavy liquid metal as targets has additional advantages as the issues with respect to removal of heat from the reactor core and

radiation damages can be more easily solved. Liquid Pb and LBE are considered as the candidate material for both the subcritical reactor coolant as well as for the spallation target in ADS.

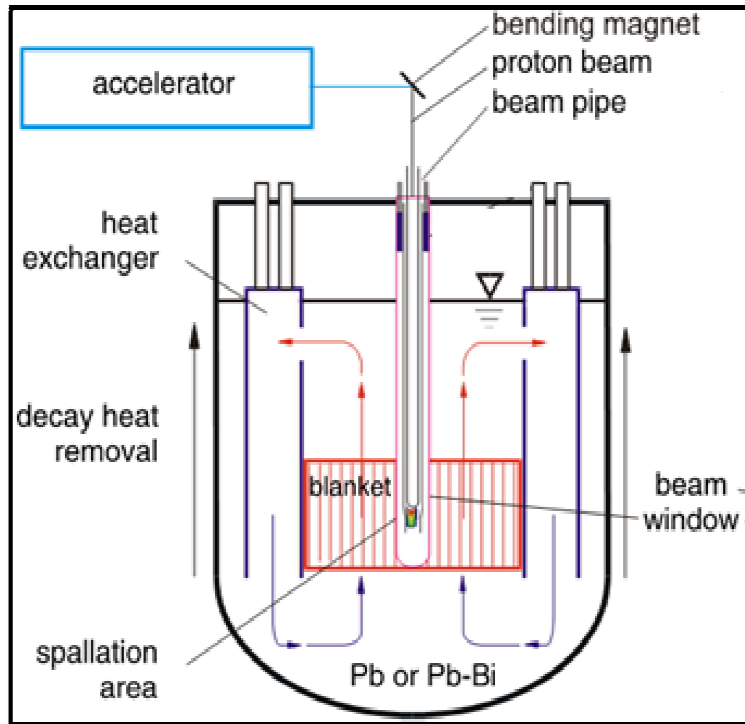


Fig. 1.2 Schematic diagram of accelerator driven system [15]

1.4 Compatibility issues of liquid lead and LBE with structural steels

The critical challenge in the use of liquid Pb and LBE in nuclear systems is to minimize the corrosion of the containment and structural materials in contact with them [16]. The corrosion occurs mainly because of the high solubility of the alloying components of steel in these heavy liquid metals. Since the solubility of components of the steel is different from each other, selective dissolution occurs. This causes compositional and micro structural changes which could lead to material failure. The data on solubility of Fe, Cr, Ni and Mo in liquid Pb, Bi and LBE are presented in Table 1.2. Figures 1.3 to 1.5 show the variation of these solubility values with temperature.

Table 1.2 Solubility data of structural steel components in liquid Pb, Bi and LBE

Metal	Liquid	Solubility (log (at%))	Temperature range (K)	Reference
Fe	Pb	1.68 – 3006 / T	800-1300	[17]
	Bi	2.75 - 3980 / T	973-1173	[17]
	LBE	0.5719 - 4398.6 / T	399-1173	[18]
Cr	Pb	4.30 - 6720 / T	1173-1473	[19]
	Bi	2.94 - 3610 / T	658-901	[20]
	LBE	-0.2757 - 3056.1 / T	500-1100	[18]
Ni	Pb	2.89 - 2189 / T	773-1073	[21]
	Bi	1.06 - 616 / T	755-1283	[22]
	LBE	2.8717- 2935.9 / T	528-742	[18]
Mo	Pb	1.6 – 6000 / T	1073-1473	[12]

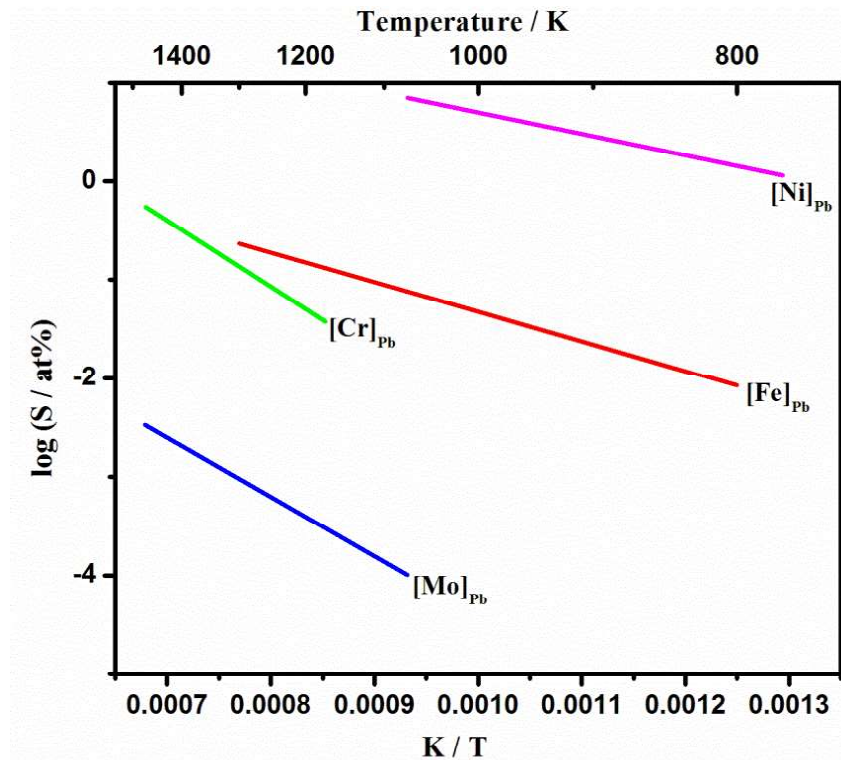


Fig. 1.3 Temperature dependence of solubility of alloying components of steel in liquid Pb

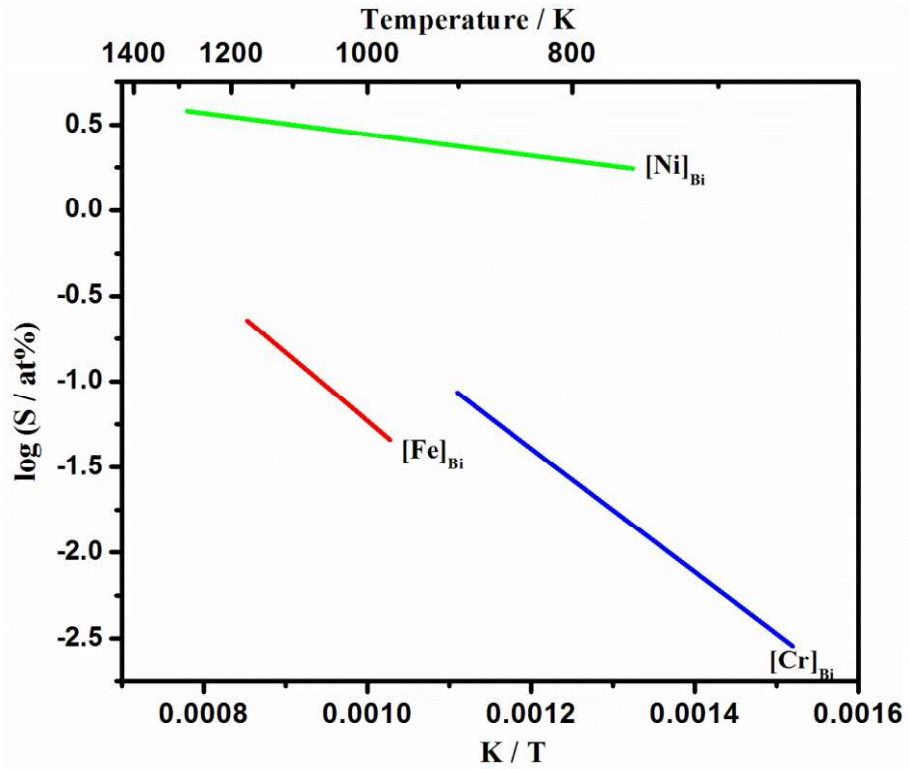


Fig. 1.4 Temperature dependence of solubility of alloying components of steel in liquid Bi

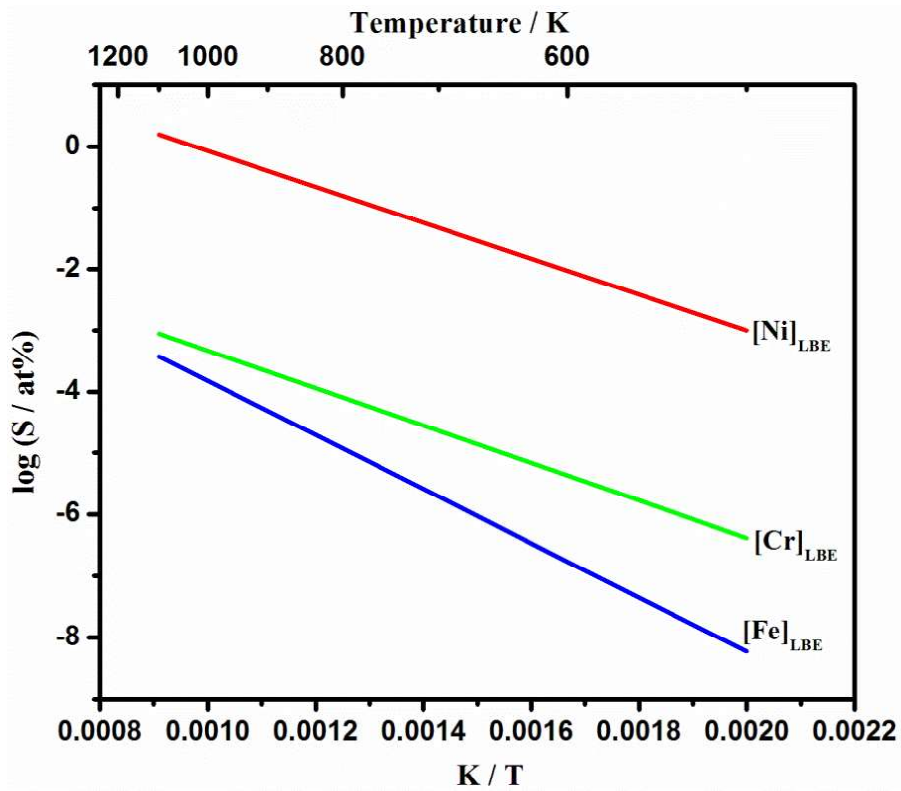


Fig. 1.5 Temperature dependence of solubility of alloying components of steel in LBE

It can be seen that solubility is a function of temperature and increases sharply with increase in temperature. As a result, mass transport occurs by the dissolution of the components of the steels at high temperature sections followed by the transfer and deposition of the corrosion products at the low temperature sections. The deposition of the corrosion products at low temperature sections can ultimately cause the clogging of the coolant pipes and reduce the heat transfer characteristics. Since the solubility of Ni in the heavy metals is much higher than those of Fe, Cr and Mo, nickel free steels are considered as structural materials for Pb and LBE systems.

1.5 Mitigation of corrosion in liquid lead and LBE systems

Different methods have been suggested for minimizing the corrosion of structural steels in liquid Pb and LBE. Corrosion can be minimized either by using the structural steels which have high corrosion resistance or by the addition of corrosion inhibitors. As mentioned earlier, because of solubility of Ni in liquid Pb and LBE is very high compared to those of other components of steels, Ni free ferritic steels with optimum concentrations of Cr, Mo, Si, etc are considered as candidate structural materials. However, the solubilities of other components are not low and are significantly high. Corrosion and mass transfer that would occur under high flow velocities over long periods of operation would still not be in acceptable range. Different methods adopted for the mitigation of corrosion of the structural steels in heavy liquid metal coolants are described in the following sections.

1.5.1 Use of corrosion resistant structural materials

One of the methods to minimize corrosion in liquid Pb and LBE systems would be to use metals with very low solubility. Examples of these metals are W and Mo whose solubility values at 1473 K are <0.0056 at% and <0.011 at%, respectively [23]. Mo has been reported to be highly corrosion resistant even after prolonged

exposures at 1273 K [4]. The investigation by Cathcart and Manly [24] on the relative resistances of 24 metals and alloys with respect to corrosion and mass transfer in liquid Pb showed that only Mo and Nb possess high degree of corrosion resistance. Certain alloys of these metals such as Nb-1Zr also exhibited considerable resistance to mass transfer and thus can be used as container materials for liquid Pb target. Experimental results on the compatibility studies of various steels indicated that alloys with high Ni content such as Ni-Cr-Fe alloy and 347-stainless steel showed lower resistance to corrosion by liquid Pb. Experiments have also shown that when structural steels are alloyed with appropriate concentrations of Al and Si, stable protective oxide scales would be formed on the surface by reaction with the dissolved oxygen in the heavy metal coolant. Very low corrosion rates were observed with Fe-Cr alloys containing 8 at% Al which had a protective alumina scale even at low oxygen potentials [24].

Cygan [25] has studied the compatibility of various steel alloys with LBE and observed that low carbon steels could be useful containers for LBE up to 727 K. The studies of Romano et al. [26] have shown that Croloy 1-1/4 (Fe-0.15C-1.25Cr-0.5Mo) steel exhibited corrosion resistance up to 5000 h in LBE at 623 to 923K. Other ferritic steels suggested for structural materials are 2-1/4Cr-1Mo, modified 9Cr-1Mo and 12Cr-1Mo [27].

1.5.2 Corrosion resistant coatings

It has been demonstrated that the corrosion resistance of the structural steels in heavy liquid metals can be enhanced by coating their surface with metals like Mo, W, Nb or their alloys [28]. These metals themselves have very low solubility in the coolants and are stable in LBE at low oxygen potentials and can protect the steels against the attack by LBE. Superalloys like MCrAlY (M = Fe, Ni, Co or NiCo)

exhibit corrosion resistance because of the alumina layers formed on their surface by selective oxidation and have gained interest because of the self healing properties of the oxide layer. Oxide, carbide and nitride coatings are also investigated as they can isolate the metals from the coolant [12]. Attempts have also been made to coat the structural materials with nitrides and borides of Ti and Zr, carbides of W, Al-Mg spinel [29] and $ZrO_2 + Y_2O_3$ [4]. However, these coatings were not dense enough to protect the steel from the diffusion of alloying components through them and do not possess any self healing ability [12]. They can crack during installation or operation due to their weak adherence. Failure during thermal cycling is also anticipated because of the difference in the coefficient of thermal expansions of the base metal and the coating. These failures can lead to the direct dissolution attack by Pb and LBE.

Films of carbides and nitrides such as ZrN, TiN, or TiN+TiC can be formed on the surfaces of steels by the addition of Ti and Zr (about 50 to 500 ppm) into the heavy liquid metal. These elements react with carbon and nitrogen present in the steel to form the film and protect the steels from direct contact with the coolant [30]. Again, it is difficult to ensure uniform formation of the film on the surface of steels. The integrity of the films also cannot be ascertained as they are brittle and tend to spall off.

1.5.3 Active oxygen control

It is found that by the careful control of dissolved oxygen concentration in the coolant, a protective oxide film can be formed on the steel surface, which can effectively separate the steel surface from the coolant. In order to promote the formation of a stable protective oxide layer, it is to be ensured that the oxygen potential in the liquid metal is above that needed for the formation of the film on the

structural material but below that required for the formation of the oxides of Pb or Bi. Once the passive oxide film is formed on the steel surface, direct dissolution of the structural material becomes negligible because of the very low diffusion coefficients of the alloying components of steel in the oxide layer [2].

The corrosion behavior of two different types of austenitic steels as a function of oxygen concentration in flowing Pb at 823 K after 3000 h of exposure is presented in Fig. 1.6 [31]. When oxygen concentration was below 10^{-7} at% in liquid Pb, corrosion rate increased significantly with decreasing oxygen concentration. Corrosion under these conditions was determined by the direct dissolution of the alloy components as there would be no protective oxide layer on the surface. When the oxygen concentration was higher than 10^{-7} at%, but below 10^{-6} at%, oxide films that prevent the direct dissolution of alloy components were formed on the surfaces of steels. When the oxygen concentration increases beyond 10^{-6} at%, corrosion depth was found to increase presumably because the surface oxide layer formed was no longer passive.

1.6 Thermodynamic basis for the protective oxide layer formation and active oxygen control

The formation and stability of the protective oxide layer over the structural steel surface are determined by the thermochemical properties of the oxide layer formed. The Ellingham diagram given in Fig. 1.7 shows the variation of oxygen potentials of metal-metal oxide equilibria corresponding to those of the components of steel along with those of Pb-PbO, Bi-Bi₂O₃, Al-Al₂O₃ and Si-SiO₂ with temperature. Using the data on activity, and solubility of oxygen in Pb and LBE, given in Tables 1.3 to 1.5 [32], and Gibbs energy of formation of PbO and Bi₂O₃, the oxygen potentials in the liquid metal at different dissolved oxygen levels were

calculated. These oxygen potentials are also shown in Fig. 1.7. It can be seen from the plot that the oxides of steel components, Al and Si are more stable than the oxides of Pb and Bi. Thus, when the oxygen potential in the liquid metal coolant is lower than that required for the formation of PbO and Bi₂O₃, either the oxides of the alloying elements of steel or the ternary oxides of Pb-M-O and Bi-M-O (where M = Fe, Cr, Mo, etc) systems could be formed at the steel–liquid metal interface which can act as the protective oxide layer.

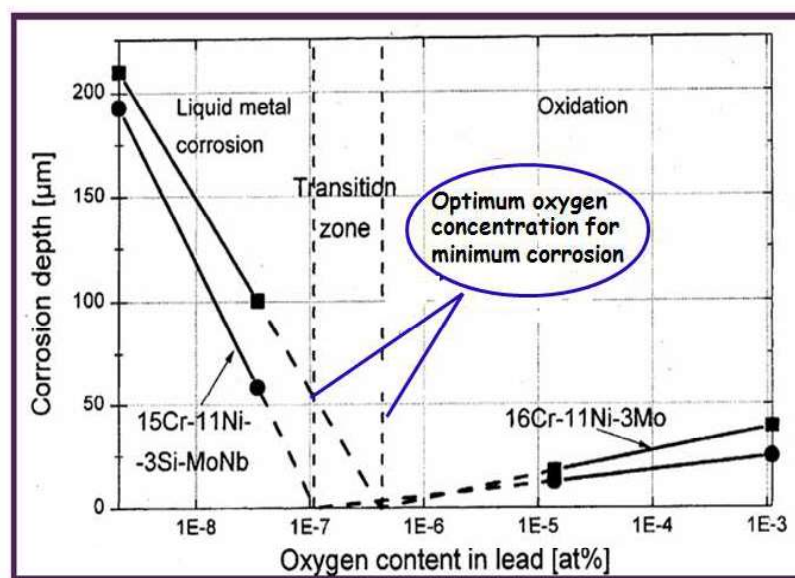


Fig. 1.6 Oxygen concentration effects on the corrosion behavior of steels in flowing liquid Pb after 3000 h at 823 K [31]

The protective oxide film formed can effectively separate the steel surface from undergoing direct dissolution. As the diffusion coefficients of the alloying components of steel through the oxide layer would be low, rate of dissolution of the steel components would also be suppressed. Knowledge on the thermochemical properties of the Pb-M-O and Bi-M-O systems is essential to understand the composition of the oxide films on the steel surface. Diffusion coefficients of oxygen and metal through the oxide layer would also be required to predict the film growth rate as well as the rate of corrosion.

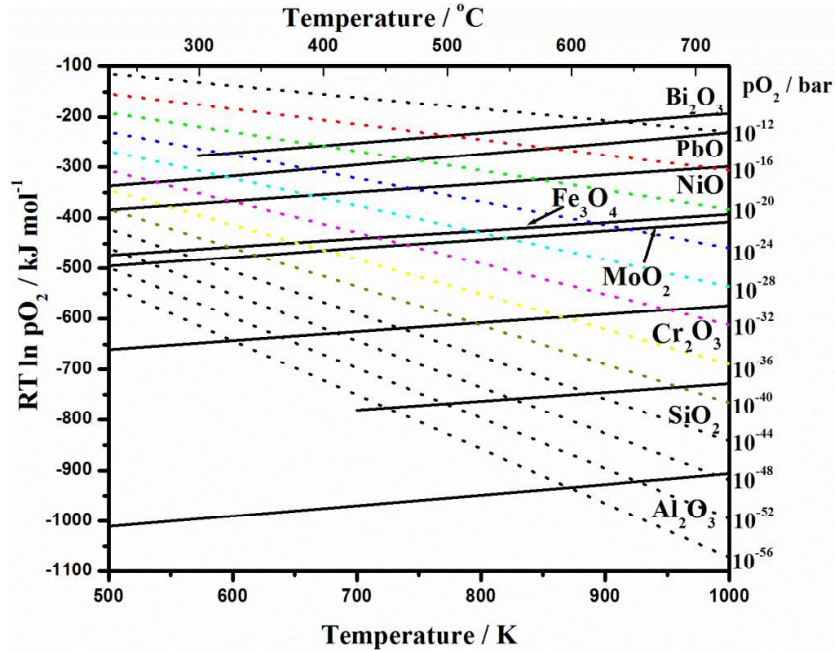


Fig. 1.7 Ellingham diagram showing the oxygen potentials of various metal/metaloxide equilibria

Table 1.3 Diffusion coefficient of oxygen [32]

Diffusivity of oxygen	Temperature range
Pb: $\log(D_O^{Pb} / cm^2 s^{-1}) = -2.554 - 2384/T$	818-1061 K
LBE: $\log(D_O^{LBE} / cm^2 s^{-1}) = -0.813 - 3612/T$	811-980 K

Table 1.4 Standard Gibbs energy of dissolution of oxygen [32]

Standard Gibbs energy of dissolution of oxygen	Temperature range
Pb: $G_{O(Pb)}^{XS} = -121349 + 16.906T J (g \text{ atom})^{-1}$	815-1090 K
LBE: $G_{O(LBE)}^{XS} = -127389 + 27.938T J (g \text{ atom})^{-1}$	812-1012 K

Table 1.5 Solubility of oxygen [32]

Solubility of oxygen	Temperature range
Pb: $\log(S / \text{at}\% \text{ O}) = -5100/T + 4.32$	815-1090 K
LBE: $\log(S / \text{at}\% \text{ O}) = -4287/T + 3.53$	812-1012 K

1.7 Characteristics of the oxide layer-from corrosion tests on steels

In order to understand the characteristics of the protective oxide film formed on the steel surface, corrosion tests have been performed on a number of steels exposed to flowing and static liquid Pb and LBE [33-40]. The experimental studies on different types of martensitic and austenitic steels indicated that they would be susceptible to dissolution in LBE even at a temperature as low as 673 K if the oxygen concentration in the coolant is $\leq 10^{-7}$ at%. However, the dissolution rate of austenitic steels was found to be lower than that of martensitic steels. For oxygen concentrations above 10^{-7} at%, formation of oxide layer was observed on the surfaces of both steels in the temperature range of 573-743 K. This thin protective oxide layer acted as a barrier against the direct dissolution of steel components into the coolant. Studies of Barbier et al. [33] showed that the thickness of the protective oxide film increased with increasing temperature and exposure time and the thickness of the layer formed depended upon the composition of the steel. It had been observed that martensitic steels form very thick oxide film and generally consisted of two layers with a porous outer layer of magnetite (Fe_3O_4) and a compact inner layer of Fe-Cr spinel ($(\text{Fe}, \text{Cr})_3\text{O}_4$). However, these thick oxide layers are found to be not protective and thus such steels cannot be used for long term applications. For austenitic steel, very thin oxide layer mainly composed of Fe-Cr spinel is formed at lower temperatures and this thin oxide layer was reported to be protective.

1.8 Kinetics of oxide layer formation [2]

The rate of formation of oxide layer over the steel surface can be represented by the following equation:

$$\delta = Kt^n = A \exp(-E_a / RT)t^n \quad (1.1)$$

δ = thickness of oxide film

t = time

K = oxidation rate constant (depends upon the composition of steel and operating conditions)

A = constant (depends on materials and environments)

E_a = activation energy for the process

n = constant (depends on the oxidation mechanism)

It is found that for temperatures below 773 K, value of n is $\frac{1}{2}$ for steels in LBE. Thus the oxidation rate equation becomes $\delta = Kt^{1/2}$ and hence, the growth of the oxide layer follows a parabolic law. However, with increasing temperature, value of n varies due to the complex kinetics of oxide layer formation. The oxidation kinetics of different steels in flowing Pb at 823 K was studied by Gorynin et al. [31] and shown in Fig. 1.8. The value of n obtained for different steels lies in the range of 0.317 to 0.813.

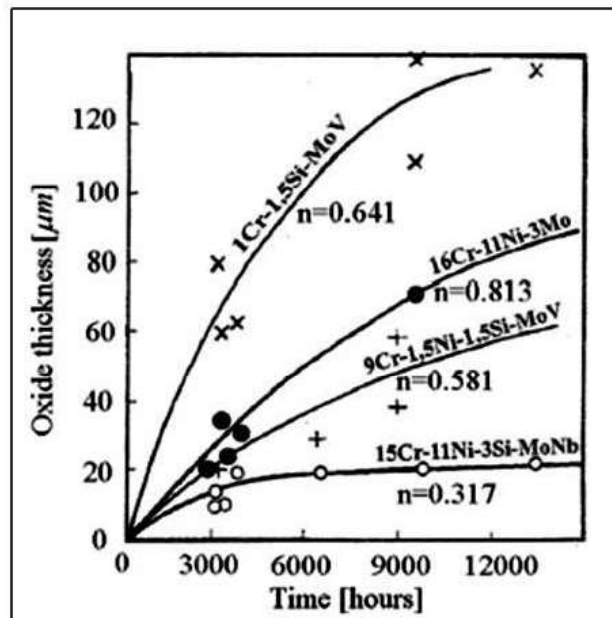


Fig. 1.8 Oxidation kinetics of different steels tested at 823 K in flowing Pb[31]

The parabolic rate constant of steels in flowing LBE can be calculated by the following equation:

$$K = \int_{P^1_{O_2}}^{P^2_{O_2}} \left(\alpha \frac{D(M)}{f_M} + \frac{D(O)}{f_O} \right) d[\ln P_{O_2}] \quad (1.2)$$

where $P^1_{O_2}$ and $P^2_{O_2}$ are the oxygen partial pressures at oxide/metal and oxide/liquid metal interface, respectively, M and O denotes the metal and oxygen, respectively, D is the diffusion coefficient, f is the correlation factor or correction factor for the self diffusion mechanism and is of the order unity and α is the molar ratio of oxygen to metal in the oxide. $P^1_{O_2}$ would be determined by the equilibrium established at the metal-oxide interface, i.e. binary M-O and ternary Pb-M-O and Bi-M-O systems. $P^2_{O_2}$ would be equal to oxygen partial pressure due to dissolved oxygen in the liquid metal.

Discussions on active oxygen control and kinetics of the formation of the protective oxide film show that for a better understanding of the nature of the protective oxide film, it is necessary to have a comprehensive knowledge on the chemical interaction of the components of structural steel with LBE containing dissolved oxygen. In this context, studies on phase diagrams of Bi-M-O and Pb-M-O (M=Fe, Cr, Mo, etc) systems are important and thermochemical data on the relevant ternary compounds in these systems are required. A systematic study on Pb-Fe-O and Pb-Cr-O systems was carried out by Sahu et al. [41-46]. Meera et al. [47, 48] established the phase diagrams of Bi-Fe-O and Bi-Cr-O systems and studied the thermochemical properties of the ternary compounds present in these systems. However, the interaction of Pb and Bi with Mo metal in the presence of dissolved oxygen has not been studied. Although, several studies on the pseudo binary phase

diagrams of $\text{Bi}_2\text{O}_3\text{-MoO}_3$ and PbO-MoO_3 systems have been carried out, data on the ternary phase diagrams are not available. Thermochemical data of the compounds present in these systems are scanty. In this thesis work, detailed studies on Bi-Mo-O and Pb-Mo-O systems have been carried out to establish the ternary phase diagrams and to determine the thermochemical properties of the ternary compounds in these systems.

1.9 Use of piezoelectric materials [49, 50]

High temperature ultrasonic transducers are employed for the inspection of components immersed in liquid metal systems. The piezoelectric materials, which are used in these ultrasonic transducers, must possess high Curie temperature and favorable piezoelectric properties. Ultrasonic transducers using pure and doped lead zirconate titanate (PZT) are widely used but the Curie temperature of these materials range between 623 and 653 K only. Hence, they cannot be employed for high temperature applications. Piezoelectric materials such as lithium niobate (Li_2NbO_3), bismuth titanate ($\text{Bi}_4\text{Ti}_3\text{O}_{12}$), lead metaniobate (PbNb_2O_6) and gallium orthophosphate (GaPO_4) etc possess high Curie temperatures and are promising candidates. Among them, bismuth titanate has a Curie temperature of 948 K but it possesses highly anisotropic electrical conductivity with the maximum value along the plane of polarization. For piezoelectric applications, a low electrical conductivity is essential which otherwise would cause difficulty in poling [51-54] as well as during transducer application. In the present study, experiments were carried out to optimize the preparation conditions with niobium as the dopant to obtain highly resistive bismuth titanate crystals suitable for high temperature piezoelectric applications.

1.10 Aim

In the present thesis, towards the application of Pb and LBE as a potential liquid metal coolant, the following aspects are explored.

1. Determination of ternary phase diagrams of Bi-Mo-O and Pb-Mo-O systems.
2. Experimental determination of thermochemical properties such as molar Gibbs energy of formation, enthalpy of formation and heat capacity of ternary compounds present in the Bi-Mo-O and Pb-Mo-O systems by employing solid oxide electrolyte based emf cells, solution calorimetry and differential scanning calorimetry.
3. Development of high temperature bismuth titanate based piezoelectric material for use in liquid metal coolants.

The experimental methods and techniques used in the present study are described in Chapter 2 of this thesis. The studies carried out on Bi-Mo-O and Pb-Mo-O systems are described in Chapters 3 and 4, respectively. Chapter 5 deals with the studies carried out towards the development of the high temperature piezoelectric material. The summary of the results and conclusions are given in Chapter 6, and Chapter 7 presents the scope for future studies.

1.11 References

1. S. Atmalingam, Choice of coolant for secondary circuit of LMFBRs in Proceedings of Heavy liquid metal coolants in nuclear technology (HLMC 98), Vol. 2, SSC RF-IPPE, Obninsk (1998) 361-365.
2. J. Zhang, N. Li, Review of studies on fundamental issues in LBE corrosion, J. Nucl. Mater. 373 (2008) 351-377.

3. R. Parkman, O.C. Shepard, Investigation of materials for use in a heat transfer system containing liquid lead alloys. Report No. XII, United States Atomic Energy Commission Report, 1951.
4. R.C. Asher, D. Davies, S.A. Beetham, Some observations on the compatibility of structural materials with molten lead, *Corrosion Sci.* 17 (1977) 545-557.
5. Liquid metal coolants for fast reactors cooled by sodium, lead and lead-bismuth eutectic, Nuclear Energy Series No. NP-T-1.6, International Atomic Energy Agency, Vienna, 2012.
6. B.F. Gromov (ed.), Heavy liquid metal coolants in nuclear technology (HLMC 98), Vols. 1 & 2, SSC RF-IPPE, Obninsk, 1999.
7. E.P. Lowen, A.T. Tookuhiro, Status of research and development of the lead-alloy-cooled fast reactor, *J. Nucl. Sci. Technol.* 40 (2003) 614-627.
8. T.K. Kim, C. Grandy, K. Natesan, J. Sienicki, R. Hill, Research and development roadmaps for liquid metal cooled reactors, ANL/ART-88, Nuclear Engineering Division, Argonne National Laboratory, April, 2017.
9. Accelerator Driven Systems (ADS) and fast reactors (FR) in advanced nuclear fuel cycles – A comparative study, Nuclear Energy Agency, Organization for Economic Cooperation and Development, NEA-3109, France, 2002.
10. F. Niu, R. Cendalino, N. Li, Effect of oxygen on fouling behavior in lead-bismuth coolant systems, *J. Nucl. Mater.* 366 (2007) 216-222.
11. Working material, Technical meeting to Review of national programmes on fast reactors and accelerator driven systems (ADS), IAEA-TM-25032, TWG-FR, IAEA, Vienna, 2002.
12. Handbook on lead-bismuth eutectic alloy and lead properties, materials compatibility, thermal hydraulics and technologies, OECD, NEA, 2015.

13. V. Sobolev, Database of thermophysical properties of liquid metal coolants for GEN-IV, Scientific report of the Belgian Nuclear Research Centre, SCK-CEN-BLG-1069, 2011.
14. N.A. Gocken, The Bi-Pb (bismuth-lead system), *J. Phase. Equilib.* 13 (1992) 21-32.
15. D.G. Pomonti, V. Russier, Liquid metals for nuclear applications, *J. Non-Cryst. Solids.* 353 (2007) 3600-3614.
16. N. Li, Active control of oxygen in molten lead-bismuth eutectic systems to prevent steel corrosion and coolant contamination, *J. Nucl. Mater.* 300 (2002) 73-81.
17. T.B. Massalski (ed. in chief) Binary alloys phase diagrams, The Materials Information Society, Materials Park, 1990.
18. S. Gosse, Thermodynamic assessment of solubility and activity of iron, chromium and nickel in lead bismuth eutectic, *J. Nucl. Mater.* 449 (2014) 122-131.
19. M. Venkataraman, J.P. Neumann, The Cr-Pb (chromium-lead) system, *Bull. Alloy Phase Diagr.* 9 (1988) 155-157.
20. M. Venkataraman, J.P. Neumann, The Bi-Cr (bismuth-chromium) system, *Bull. Alloy Phase Diagr.* 9 (1988) 271-273.
21. P. Nash, The Bi-Ni (bismuth-nickel) system, *Bull. Alloy Phase Diagr.* 6 (1985) 345-347.
22. P. Nash, The Ni-Pb (nickel-lead) system, *Bull. Alloy Phase Diagr.* 8 (1987) 264-268.

23. G. Muller, G. Schumacher, F. Zimmermann, Investigation on oxygen controlled liquid lead corrosion of surface treated steels, *J. Nucl. Mater.* 278 (2002) 85-89.
24. J.V. Cathcart, W.D. Manly, The mass transfer properties of various metals and alloys in liquid lead, *Corrosion.* 12 (1956) 43-47.
25. R. Cygan, Lead-Bismuth eutectic thermal convection loop, North American Aviation Report NAA-SR-1060, 1954.
26. A.J. Romano, C.J. Klumet, D.H. Gurinsky, The investigation of container materials for Bi and Pb alloys, Part 1, Thermal convection loops, Brookhaven National Laboratory Report BNL-811 (T-313), 1963.
27. J.J. Park, D.P. Butt, C.A. Beard, Review of liquid metal issues for potential containment materials for liquid lead and lead-bismuth eutectic spallation targets as a neutron source, *Nucl. Eng. Des.* 196 (2000) 315-325.
28. R.G. Ballinger, J. Lim, An overview of corrosion issues for the design and operation of high-temperature lead and lead-bismuth cooled reactor systems, *Nucl. Technol.* 147 (2004) 418-435.
29. R.I. Hodge, R.B. Turner, J.L. Platten, A 5000 h test of a lead-bismuth circuit constructed in steel and niobium, *Corrosion by Liquid metals*, AIME Proc. Plenum Press, NY, 1969.
30. G. Ilinev, Research results on the corrosion effects of liquid heavy metals Pb, Bi and Pb-Bi on structural materials with and without corrosion inhibitors, *Nucl. Eng. Des.* 217 (2002) 167-177.
31. I.V. Gorynin, G.P. Karzov, V.G. Markov, V.S. Lavrukhim, V.A. Yakovlev, Structural materials for power plants with heavy liquid metals as coolants in

- Proceedings of Heavy Liquid Metal Coolants in Nuclear Technology (HLMC-98), Obninsk, Russia, Vol. 1, 1988, p.120
32. R. Ganesan, T. Gnanasekaran, R.S. Srinivasa, Diffusivity, activity and solubility of oxygen in liquid lead and lead-bismuth eutectic alloy by electrochemical methods, *J. Nucl. Mater.* 349 (2006) 133-149.
 33. F. Barbier, G. Benamati, C. Fazio, A. Rusanov, Compatibility tests of steels in flowing liquid lead-bismuth, *J. Nucl. Mater.* 295 (2001) 149-156.
 34. F.B. Celerier, P. Deloffre, A. Terlain, A. Rusanov, Corrosion of metallic materials in flowing liquid lead-bismuth, *J. Phys. IV France.* 12 (2002) 177-190.
 35. H. Glasbrenner, J. Konys, G. Mueller, A. Rusanov, Corrosion investigation of steels in flowing lead at 400°C and 550°C, *J. Nucl. Mater.* 296 (2001) 237-242.
 36. C. Fazio, I. Ricapito, G. Scaddozzo, G. Benamati, Corrosion behavior of steels and refractory metals and tensile features of steels exposed to flowing Pb-Bi in the LECOR loop, *J. Nucl. Mater.* 318 (2003) 325-332.
 37. C. Fazio, G. Benamati, C. Martini, G. Palombarini, Compatibility tests on steels in molten lead-bismuth, *J. Nucl. Mater.* 296 (2001) 243-248.
 38. G. Benamati, C. Fazio, H. Piankova, A. Rusanov, Temperature effect on the corrosion mechanism of austenitic and martensitic steels in lead-bismuth, *J. Nucl. Mater.* 301 (2002) 23-27.
 39. G. Muller, A. Heinzl, J. Konys, G. Schumacher, A. Weisenburger, F. Zimmermann, V. Engelko, A. Rusanov, V. Markov, Results of steel corrosion tests in flowing liquid Pb/Bi at 420-600°C after 2000 h, *J. Nucl. Mater.* 301 (2002) 40-46.

40. L.S. Crespo, F.J.M. Munoz, D.G. Briceno, Short-term static corrosion tests in lead-bismuth, *J. Nucl. Mater.* 296 (2001) 273-281.
41. S.K. Sahu, R. Ganesan, T. Gnanasekaran, Studies on phase diagram of Pb–Cr–O system, *J. Nucl. Mater.* 376 (2008) 366-370.
42. S.K. Sahu, R. Ganesan, T. Gnanasekaran, Standard molar Gibbs free energy of formation of Pb_5CrO_8 (s), Pb_2CrO_5 (s), and PbCrO_4 (s), *J. Chem. Thermodyn.* 42 (2010) 1–7.
43. S.K. Sahu, R. Ganesan, T. G. Srinivasan, T. Gnanasekaran, The standard molar enthalpies of formation of Pb_2CrO_5 (s) and Pb_5CrO_8 (s) by acid solution calorimetry, *J. Chem. Thermodyn.* 43 (2011) 750-753.
44. S.K. Sahu, M. Sahu, R.S. Srinivasa, T. Gnanasekaran, Determination of heat capacities of PbCrO_4 (s), Pb_2CrO_5 (s), and Pb_5CrO_8 (s), *Monatsh. Chem.* 143 (2012) 1207–1214.
45. S.K. Sahu, R. Ganesan, T. Gnanasekaran, Studies on the phase diagram of Pb–Fe–O system and standard molar Gibbs energy of formation of ‘ $\text{PbFe}_5\text{O}_{8.5}$ ’ and $\text{Pb}_2\text{Fe}_2\text{O}_5$, *J. Nucl. Mater.* 426 (2012) 214-222.
46. S.K. Sahu, R. Ganesan, T. Gnanasekaran, The standard molar enthalpies of formation of $\text{Pb}_2\text{Fe}_2\text{O}_5$ (s) and $\text{PbFe}_5\text{O}_{8.5}$ (s) by acid solution calorimetry, *J. Chem. Thermodyn.* 56 (2013) 57–59.
47. A.V. Meera, R. Ganesan, T. Gnanasekaran, Partial phase diagram of Bi–Fe–O system and the standard molar Gibbs energy of formation of $\text{Bi}_2\text{Fe}_4\text{O}_9$, *J. Alloys. Comp.* 692 (2017) 841-847.
48. A.V. Meera, J. Basu, R. Ganesan, T. Gnanasekaran, Studies on the phase diagram of Bi–Cr–O system, *J. Nucl. Mater.* 487 (2017) 174-185.

49. T. Jardiel, A.C. Cabellero, M. Villegas, Aurivillius ceramics: $\text{Bi}_4\text{Ti}_3\text{O}_{12}$ -based piezoelectrics, *J. Ceram. Soc. Jpn.* 116 (2008) 511-518.
50. R.C. Turner, P.A. Fuiere, R.E. Newnham, T.R. Shrout, Materials for high temperature acoustic and vibration sensors: A review, *App. Acoustics.* 41 (1994) 299-324.
51. A. Fouskova, L.E. Cross, Dielectric properties of bismuth titanate, *J. Appl. Phys.* 41 (1970) 2834-2838.
52. S.E. Cummings, L.E. Cross, Electrical and Optical Properties of Ferroelectric $\text{Bi}_4\text{Ti}_3\text{O}_{12}$ Single Crystals. *J. Appl. Phys.* 39 (1968) 2268-2274.
53. M. Villegas, A.C. Caballero, C. Moure, P. Duran, J.F. Fernandez, Factors affecting the electrical conductivity of donor-doped $\text{Bi}_4\text{Ti}_3\text{O}_{12}$ piezoelectric ceramics, *J. Am. Ceram. Soc.* 82 (1999) 2411-2416.
54. H. Irie, M. Miyayama, T. Kudo, Electrical properties of a bismuth layer-structured $\text{Ba}_2\text{Bi}_4\text{Ti}_5\text{O}_{18}$ single crystal, *J. Am. Ceram. Soc.* 83 (2000) 2699-2704.

Chapter 2

Experimental Methods

The experimental methods involved in the thesis are discussed in this chapter. It includes discussion on the preparation of various compounds present in the Bi-Mo-O and Pb-Mo-O ternary systems, different preparatory methods adopted for the synthesis of bismuth titanate ceramics, long term phase equilibration studies carried out to establish the ternary phase diagrams, X-ray diffraction studies carried out for structural characterization of the samples, electron microscopy studies used for the morphological characterization of the samples and electrical conductivity measurements using impedance spectroscopy. Details of determination of thermochemical properties of the ternary oxygen compounds by emf and calorimetric measurements are also discussed in detail.

2.1 Preparation of the compounds

All the ternary compounds present in the Bi-Mo-O and Pb-Mo-O ternary systems were prepared by the solid state reaction between the constituent oxides. In addition to the solid state reaction method, coprecipitation and molten salt synthesis were also employed for the preparation of bismuth titanate ceramics. Details of different preparatory methods used in the study are discussed below.

2.1.1 Solid state reaction method [1, 2]

Solid state reaction method or the ceramic method is the most commonly used method for the preparation of metal oxides and other solid materials. This method involves the prolonged heating of the compacted pellets of a homogeneous mixture of constituent oxides at a particular temperature. The solid state reaction between the constituent components is initiated by the transport of reactants to the interface and

phase boundary reaction at the point of contact between the components. A product layer formed between the reacting particles acts as a barrier. This is followed by the diffusion of constituents through the product layer. As the reaction progresses, the diffusion paths become increasingly longer and the reaction rate becomes slower. Both thermodynamic and kinetic factors are important in solid state reactions. Thermodynamic factors determine the Gibbs energy changes associated with the process and predict the feasibility of the reaction whereas kinetic factors determine the rate at which the reaction occurs. Most of the solid state reaction methods require relatively high temperatures, as the reactivity of solids at low temperatures is low. For any solid state reaction, the reactants are thoroughly mixed together to increase the homogeneity. Also, it is essential to have intimate contact between the reactant components which can be facilitated by pressing the component mixture into pellets. The rate of the reaction can also be increased to some extent by intermittent grinding of the reactant mixture between the heating cycles for breaking the diffusion barrier i.e. product layer, and thus improve the contact between the reactants.

In the present study, all the ternary compounds in the Pb-Mo-O and Bi-Mo-O systems were prepared by this conventional method.

2.1.2 Co-precipitation method [1, 2]

In this method, the required metal cations, taken as soluble salts are co-precipitated as hydroxides, carbonates, oxalates, formates or citrates followed by heating to convert them to oxides. In general, the oxides or carbonates of the metals are taken in the stoichiometric amount and digested with an acid to form a solution to which the precipitating reagent is added. It is important that the solids formed upon precipitation are insoluble in the mother liquor. The precipitated solid is then filtered off, dried and calcined at a desired temperature. During calcination, the precipitates

get converted into fine and reactive metal oxide powders which in turn react among themselves to form the ternary or higher order oxides. This method can yield highly homogeneous and small particles. It also requires much lower reaction temperatures as compared to solid state reactions. However, this method cannot be used if significant differences exist in the solubilities of the products in the supernatant solution.

In the present study, co-precipitation method was employed for the preparation of bismuth titanate powders using bismuth nitrate and titanium isopropoxide as the precursor materials. Bismuth and titanium were co-precipitated as their oxalates using oxalic acid solution.

2.1.3 Molten salt method [3]

In this method, a low melting and non-reacting molten salt is used as the medium for preparing complex oxides from the constituent oxides. The reactant mixture is heated with the low melting salt (80-120 wt% of the reactant mixture) at temperatures above the melting point of the salt. Typical salts used in molten salt synthesis are generally binary or ternary eutectic chlorides and sulphates, for example, 50 mol% NaCl-50 mol% KCl (eutectic temperature = 923 K) or 63.5 mol% Li_2SO_4 -36.5 mol% Na_2SO_4 (eutectic temperature = 867 K). At the reaction temperature, the medium melts and acts as a solvent to facilitate the interaction of the reactants. The formation of the product particles occur in two stages: the reaction stage and the particle growth stage. In the reaction stage, the product particles are formed in the presence of solid reactant particles. The reactant particles dissolve in the molten salt and the product particles form. When all the reactant particles are consumed, the particle growth stage starts.

The formation of product particles in molten salt synthesis can occur either by solution-precipitation process or by solution-diffusion process and the mechanism of product formation is determined by the relative solubility of the reactants which is further dependent upon the particle size and surface area of the reactants. When the solubilities of both the reactants in the molten salt are comparable, both the reactants dissolve in the molten salt and the product particles precipitate under a high degree of supersaturation. This mechanism is termed as solution-precipitation mechanism. In this case, particles formed will have rectangular and irregularly rounded shapes. As the degree of supersaturation is high, it often results in the formation of aggregates also. Typical examples are the formation of Bi_2WO_6 from Bi_2O_3 and WO_3 using $\text{Li}_2\text{SO}_4\text{-Na}_2\text{SO}_4$ melt and TiZrO_4 preparation from TiO_2 and ZrO_2 using KCl . When the solubility of one of the reactants (A), is considerably higher than that of the other (B), the product layer formation take place on the surface of B and the product layer prevents the dissolution of B. As the solubility of A is high, large amount of A gets dissolved in the molten salt, diffuses through the medium, reaches on the surface of B and reacts with B. The reaction occurs by the diffusion of A from the molten salt-product layer interface to the product layer-B interface and results in an increase in the thickness of the product layer. Once both the reactants are completely consumed, product particles with almost the same shape as that of particle B are obtained. This mechanism is known as solution-diffusion process. An example is the preparation of LiFe_5O_8 from Li_2CO_3 and Fe_2O_3 using $\text{Li}_2\text{SO}_4\text{-Na}_2\text{SO}_4$ salt (solubility of Li_2CO_3 in $\text{Li}_2\text{SO}_4\text{-Na}_2\text{SO}_4$ melt is higher than that of Fe_2O_3).

The presence of molten salt increases the reaction rate. The increase in the reaction rate is a consequence of an increase in the contact area of the reactant particles and an increase in the mobility of the reactant species in the molten salt. In

the case of solid state reaction, the product formation occurs only at the contact points between the reactants and an increase in the product volume is caused by the material transport through the product layer. Whereas in molten salt synthesis, the reactant particles are covered with the melt and they become available to the reaction and the mobility of the species is fairly larger than that in solid state reaction.

After the heat treatment, the product in the form of slurry is cooled to room temperature and washed with appropriate solvent to remove the salt content. The complex oxide powder is obtained upon drying. The powders obtained by this method are found to be more homogeneous than those prepared by conventional methods. The grain size of powder obtained by molten salt synthesis is smaller than that obtained by solid state method. The shape of the particles formed by molten salt synthesis is determined by factors such as the salt used, reaction temperature, duration of heating and the powder characteristics of the reactants. Thus by proper control of these factors, particles with desired morphology can be obtained. Hence, this method is suitable for preparing highly textured ceramic powders and is widely used for the preparation of ferroelectric and ferromagnetic materials, semiconductors, photocatalysts, etc.

In the present study, molten salt method was used for the synthesis of bismuth titanate powder.

2.2 Phase equilibration experiments [4, 5]

To establish the phase fields in the ternary Bi-Mo-O and Pb-Mo-O systems, experiments involving equilibration of a mixture of phases, called henceforth as phase equilibration experiments were carried out. In these experiments, a sample of known composition and consisting of a mixture of different phases is made by homogeneously mixing the starting components in the stoichiometric amounts

followed by their pelletization. The pellets are then enclosed in inert crucibles and heated at a constant temperature until equilibrium is attained. When heating the sample, contamination from the container must be avoided. In order to avoid the volatilization and preserve the total composition as constant, sample pellet can be buried with the powder of same composition within a closed container. Generally, containers will have a temperature gradient. In such cases, hermetic sealing in low volume containers is used to prevent volatilization or reaction with atmosphere. This is useful when the volatility of the sample is not very high and time of equilibration is short. To determine the attainment of equilibrium, the sample is generally quenched to ambient conditions by rapidly cooling it into ice cold water or liquid nitrogen after a period of equilibration. This is followed by crushing the pellets and analyzing the phases by a combination of visual inspection, optical and electron microscopy and X-ray diffraction (XRD). After thorough grinding, the powdered sample is repelletized and subjected to heating under the same conditions. Presence of same phases at the end of both periods of equilibrations would indicate attainment of equilibrium. The attainment of equilibrium can also be ensured when same final phases are obtained with samples of identical composition but prepared from different phases. This method has the advantages of experimental simplicity and straightforward interpretation. The success of this method however, depends upon the preservation of the phases under equilibrium at the equilibration temperature by quenching to room temperature.

2.3 Techniques for materials characterization

2.3.1 X-ray Diffraction (XRD) [2, 6-9]

X-ray diffraction is the most important technique used for the characterization of crystalline materials and determination of their crystal structures. It is based on the

diffraction of characteristic X-ray beam on a crystalline solid. Crystalline solids consist of regular arrays of atoms or ions with inter-planar spacing in the order of angstrom. Because of the periodic nature of the internal structure, it is possible for the crystals to act as three dimensional grating to radiation. Since the wavelength of X-rays is of the same order as that of inter-planar spacing, diffraction of the radiation occurs. The characteristic X-rays are used for diffraction experiments as they are very narrow and have a FWHM less than 0.001 \AA with a very high intensity. The characteristic K-lines of a metal are generated when electrons having sufficient kinetic energy are made to strike the metal targets and knock out the electrons from the inner K shell of atoms. This is followed by filling up of vacancy in the K shell by the electrons from the outer shell with the emission of energy in the form of radiation of definite wavelength. When the vacancy in the K shell is filled up by electrons from the L and M shells, characteristic K_{α} and K_{β} lines are formed, respectively. The K_{α} lines are generally used for XRD. The target metal most commonly used is copper whose characteristic wavelength for K_{α} radiation is 1.5418 \AA . Other metal targets used in X-ray generating tubes include Cr ($K_{\alpha} = 2.29 \text{ \AA}$), Fe ($K_{\alpha} = 1.94 \text{ \AA}$), Co ($K_{\alpha} = 1.79 \text{ \AA}$), and Mo ($K_{\alpha} = 0.71 \text{ \AA}$).

When X-ray beams interact with electrons in the sample, scattering occurs. In order to satisfy the requirement for constructive interference, it is necessary that the scattered waves originating from the individual atoms be in phase with one another. The geometric condition to be satisfied for this to occur is given as Bragg's law:

$$n\lambda = 2d \sin \theta \quad (2.1)$$

where n is order of diffraction, λ is wavelength of the incident X-ray, d is inter-planar spacing and θ is angle of incidence.

A typical X-ray diffractometer consists of a source of radiation, a sample holder and a detector. Both single crystals and powders can be used as sample. X-rays are collimated and directed to the sample. When the incident beam strikes the sample, diffraction occurs in every possible orientation of 2θ . Diffracted beam can be detected by a movable detector which is set to scan over a range of 2θ values at a constant angular velocity. The detector records and processes this diffracted X-ray signal and converts the signal to a count rate which is then fed to a computer.

X-rays scattered by an atom are the resultant of the waves scattered by each electron in the atom. Thus the scattering factor or form factor of an atom is proportional to its atomic number and hence the intensity of the scattered X-rays is proportional to the atomic number. As a result, while determining the structure of crystals by XRD, location of light elements with less number of electrons is difficult as the intensity of scattered X-rays would be very low.

The X-ray diffraction pattern obtained is characteristic of the atomic arrangement within a given phase and acts as a fingerprint of that particular material. It can be used to identify and quantify the contents of the sample as well as to calculate the crystallite size, crystallinity and strain. Identification of different phases present in an unknown mixture is possible by comparing the diffraction pattern with the standard patterns known as Powder Diffraction Files (PDF) collected and maintained by Joint Committee of Powder Diffraction Standards (JCPDS).

The insitu investigation of the structural changes happening in a crystalline phase with changes in temperature can be carried out by using high temperature XRD. High temperature XRD can be used for studying solid state reactions, phase transitions, crystallite growth, thermal expansion, etc.

In the present work, XRD was used for the identification of equilibrium phases as well as to determine the phase purity of the prepared compounds. The analysis was carried out using an X-ray diffractometer (M/s Inel, France) with Cu K α radiation and graphite monochromator. Analyzed samples consisted of metals of Pb, Bi, Mo and Ti, their oxides as well as ternary oxides. As these are heavy elements, scattering factors are high and hence no difficulty was encountered for the identification of phases from the diffraction pattern of a mixture.

2.3.2 Scanning Electron Microscopy (SEM) [10, 11]

Scanning electron microscopy is widely used for studying the topology and morphology of solid samples. It enables to observe and characterize materials on nanometer to micrometer scale.

In SEM, the surface of the specimen is scanned under an accelerated electron beam. When the electron beam interacts with the specimen, phenomena such as absorption, reflection, backscattering, diffraction and emission of low energy secondary electrons and X-rays occur. The emission of secondary electrons and backscattered electrons is characteristic of the specimen under study and depends upon its composition and topography. Electrons due to these effects are collected, converted into electrical signals, amplified and displayed as modulations of brightness on the cathode ray tube. The magnification of the resultant image is determined by the ratio of the distance travelled by the recording beam in a given time interval to that travelled by the synchronously deflected scanning beam in the same time interval.

The elemental composition at the surface of the specimen can be determined by SEM using Energy Dispersive X-ray Spectroscopy or EDS. When the incident electron beam interacts with the surface atoms of the specimen, it causes the ejection

of electrons from the inner shells of the atoms. The resultant vacancies in the inner shells are filled up by electrons from the outer shells and this result in the emission of the characteristic X-rays. By measuring the energy of the characteristic X-rays, information about the elemental composition of the sample can be obtained. As the penetration depth of the electron beam is very low, it can interact only with the surface atoms and hence, the information obtained by this method corresponds to very narrow surface dimensions.

In the present study, SEM analysis was performed to study the surface morphology of bismuth titanate samples.

2.3.3 Impedance spectroscopy [12-14]

Impedance spectroscopy is a powerful technique for characterizing electrical properties of the materials and their interfaces with electronically conducting electrodes. It is a perturbation technique in which the system is perturbed by applying a small amplitude sinusoidal alternating voltage as a function of frequency and the response of the system is measured. The applied potential and the output current from the system are given by equations:

$$E = E_0 \sin(\omega t) \quad (2.2)$$

$$I = I_0 \sin(\omega t + \phi) \quad (2.3)$$

where ϕ is the phase difference. The output current has the same angular frequency ω but would differ in amplitude and phase from the voltage signal.

Impedance (Z) can be defined as the resistance to the flow of current and it can be obtained as the ratio of applied voltage to the resultant current.

$$Z = \frac{E}{I} = \frac{E_0 \sin(\omega t)}{I_0 \sin(\omega t + \phi)} = Z_0 \frac{\sin(\omega t)}{\sin(\omega t + \phi)} \quad (2.4)$$

Using Euler's relationship,

$$\exp(j\phi) = \cos \phi + j \sin \phi \quad (2.5)$$

it is possible to express impedance as a complex function. The potential is described as:

$$E = E_0 \exp(j\omega t) \quad (2.6)$$

and the current response as

$$I = I_0 \exp(j\omega t - \phi) \quad (2.7)$$

Impedance can be then represented as a complex number,

$$\begin{aligned} Z(\omega) &= \frac{E}{I} = Z_0 \exp(j\phi) = Z_0 (\cos \phi + j \sin \phi) \\ &= Z_0 \cos \phi - jZ_0 \sin \phi = Z' - jZ'' \end{aligned} \quad (2.8)$$

where $Z' = Z_0 \cos \phi$, $Z'' = Z_0 \sin \phi$ and $j = \sqrt{-1}$. Z' and Z'' are known as the real and imaginary parts of the impedance. The phase difference (ϕ) is given by

$$\phi = \tan^{-1} \left(\frac{Z''}{Z'} \right) \quad (2.9)$$

For a pure resistor, impedance is equal to its resistance R, i.e.

$$|Z| = R \quad (2.10)$$

There is no phase shift and the impedance value is independent of frequency.

Impedance of a capacitor (C) is 90° out of phase and it is given by:

$$|Z| = \frac{-j}{\omega C} \quad (2.11)$$

Impedance of a capacitor is dependent on frequency and it is larger for a lower frequency.

Typical electrochemical systems consist of process elements that can be described by various combinations of resistors, capacitors and inductors. Inductor is

seldom manifested in an electrochemical system and electrochemical processes have a behavior between a capacitor and a resistor. Further, the contributions of the capacitive and resistive components change with frequency. Hence, impedance measurements at a range of frequencies are performed and data thus obtained are used to determine the components of the system.

For a circuit consisting of a resistor and a capacitor connected in parallel (RC parallel), total impedance of the circuit can be obtained as follows:

$$\frac{1}{Z_{total}} = \frac{1}{Z_R} + \frac{1}{Z_C} = \frac{1}{R} + \frac{\omega C}{-j} \quad (2.12)$$

$$\text{Thus } Z_{total} = \frac{-jR}{\omega RC - j} \quad (2.13)$$

The above expression can be rearranged to get

$$Z_{total} = \frac{1 - j\omega R^2 C}{1 + \omega^2 R^2 C^2} \quad (2.14)$$

From this equation, the real and imaginary parts of impedance can be separated and hence,

$$Z_{real} = \frac{R}{1 + \omega^2 R^2 C^2} \quad (2.15)$$

$$Z_{imaginary} = \frac{R^2 C \omega}{1 + \omega^2 R^2 C^2} \quad (2.16)$$

By rearranging the impedance results for the RC parallel circuit, it can be shown that

$$\left(Z_{real} - \frac{R}{2}\right)^2 + Z_{imaginary}^2 = \frac{R^2}{4} \quad (2.17)$$

which is an equation of a circle, with the center at $(0, R/2)$ and the radius equal to $R/2$.

By plotting the real part of impedance along the x-axis and imaginary part along the y-axis, we get a Nyquist plot or Argand diagram as shown in Fig. 2.1. As

long as the axes are of equal scale, the appearance of the semicircle in the Nyquist plot signifies the existence of a parallel RC circuit. It is to be noted that for $\omega \rightarrow 0$, $Z_{\text{real}} \rightarrow R$ and for $\omega \rightarrow \text{infinity}$, $Z_{\text{real}} \rightarrow 0$. The angular frequency corresponding to the highest point in the imaginary axis is termed as the characteristic frequency or relaxation frequency, ω_0 and is given by:

$$\tau = RC = \frac{1}{\omega_0} \quad (2.18)$$

where τ is the time constant.

The physical meaning of a resistor and capacitor connected in series or parallel is that the phenomenon being represented has both resistive and capacitive qualities. At the relaxation frequency, the phase difference between current and voltage reaches a maximum. A semicircle is characteristic of a single time constant. The value of the resistance R can be easily determined directly from the diameter of the semicircle.

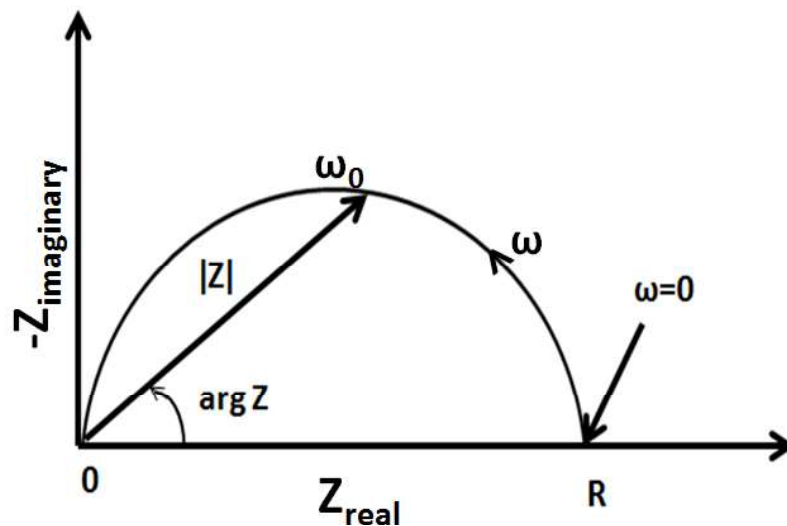


Fig. 2.1 Typical representation of Nyquist plot

Another popular representation method is the "Bode plot". Here the impedance is plotted with frequency on the X-axis and both the absolute value of the

impedance ($|Z| = Z_0$) and phase-shift on the Y-axis. Unlike the Nyquist plot, the Bode plot explicitly exhibits the behavior of R and C components of a material as a function of frequency. The frequency corresponding to the inflection point of the Bode plot is the relaxation frequency, ω_0 . A typical representation of Bode plot is shown in Fig. 2.2.

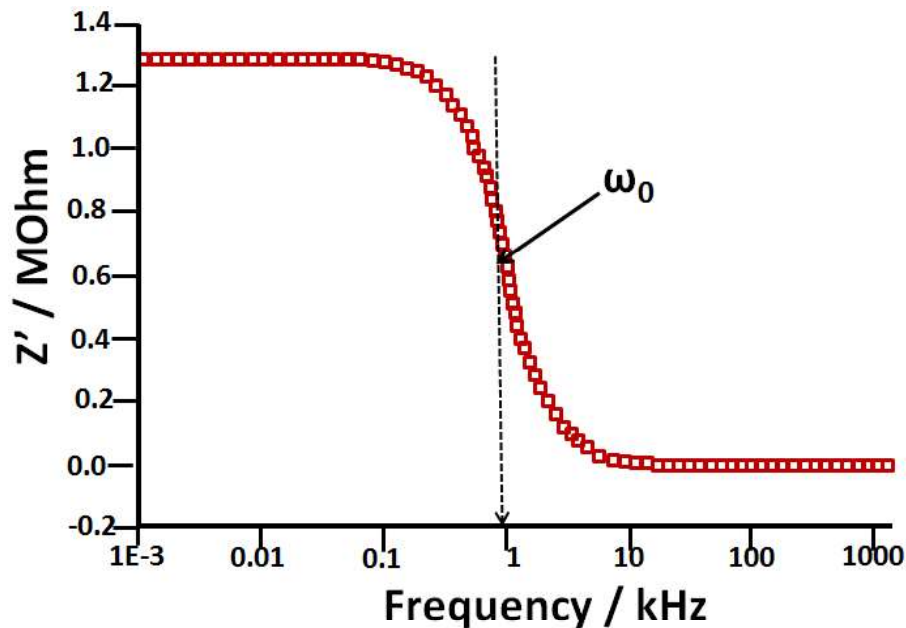


Fig. 2.2 Typical representation of Bode plot

When ac voltage is applied, charge transfer across a sample occurs. This consists of various processes at the electrode-sample interfaces and in the bulk of the sample. Processes at the electrode-sample interface could involve adsorption, diffusion and dissociation of adsorbed species and charge transfer to or from the electrode. Charge transport across the bulk of a polycrystalline sample can be a combination of transport through the grains and grain boundaries and could involve different ions also. The charge transport processes individually would have different time constants and hence, during the measurement of conductivity by ac methods, they would get separated in the frequency domain. The ordering of the semicircles

depends on their time constants. The circle with the shorter time constant will appear on the left side of the Nyquist plot. Each arc in the measured impedance can be correlated to various elementary processes occurring in the material and which can be understood by means of equivalent electrical circuits. The equivalent electrical circuit of a solid ionic conductor, consisting of a series combination of parallelly connected resistors (R) and capacitors (C), is shown in Fig. 2.3. The corresponding impedance spectrum is shown in Fig. 2.4. The first arc (bulk) is usually observed at low and medium temperatures and proportional to the sample length and density. It is attributed to the bulk or grain interior process. The low frequency arc (interface) is observed at high temperatures. This is inversely proportional to the electrode area and is attributed to the electrode-sample interfacial process. The impedance due to this is termed as Warburg impedance and is observed as a spike in the impedance spectrum. The intermediate arc (grain boundary) which is observed at low and medium temperatures is associated with the conductance and micro structural effects at the grain boundary.

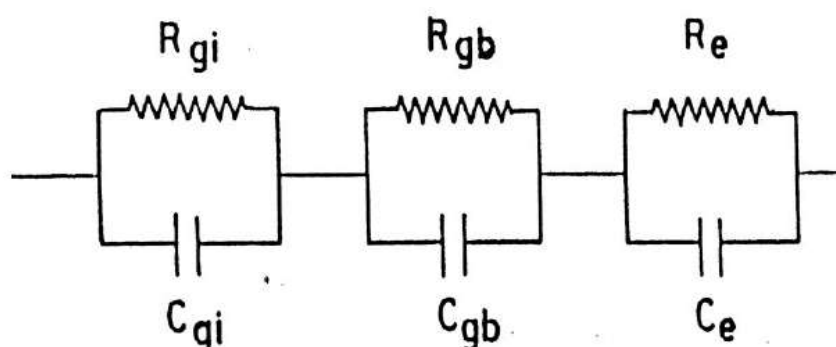


Fig. 2.3 Equivalent electrical circuit of a solid ionic conductor, consisting of a series combination of parallelly connected resistors (R) and capacitors (C)
(C_{gi} , C_{gb} and C_e are the capacitances and R_{gi} , R_{gb} and R_e are the resistances corresponding to the grain, grain boundary and electrode-electrolyte interface)

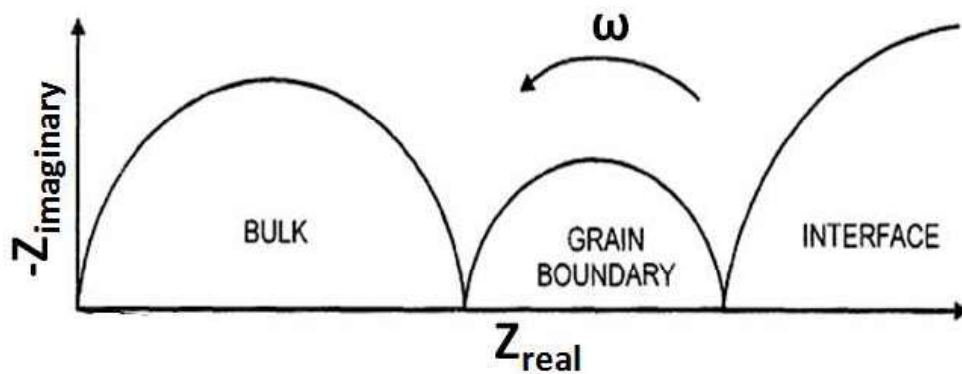


Fig. 2.4 Impedance spectrum of a solid ionic conductor

In the present study, the variation of conductivity with temperature for the ternary bismuth molybdates and bismuth titanates ($\text{Bi}_8\text{Mo}_3\text{O}_{21}$, $\text{Bi}_{14}\text{Mo}_5\text{O}_{36}$, $\text{Bi}_6\text{Mo}_2\text{O}_{15}$, $\text{Bi}_2\text{Mo}_2\text{O}_9$, Bi_2MoO_6 and pristine and Nb-doped $\text{Bi}_4\text{Ti}_3\text{O}_{12}$) was followed by impedance measurements using a conductivity cell, schematic of which is shown in Fig. 2.5. The conductivity cell consisted of two platinum electrical leads which were brazed to platinum pellets of identical dimension. The sintered sample pellet of known dimension was mounted between the platinum pellets by a spring loading arrangement. A K-type thermocouple was kept very close to the sample pellet, so that sample temperature could be accurately measured. Entire assembly was kept inside a quartz chamber which in turn was kept in a furnace for heating. Electrical conductivity was measured using a frequency response analyzer (Model SI 1225, Solartron, M/s Schlumberger, UK) coupled with an electrochemical interface (Model 1286, Solartron, M/s Schlumberger, UK) in the frequency range of 10 Hz to 1 MHz in air.

The impedance data obtained at each temperature can be fitted using the software Zview® [15]. The bulk resistance of the material can be obtained by fitting a semicircle to the experimentally obtained Nyquist plot. By incorporating the dimensions of the sample pellet, conductivity (σ) of the sample at the

experimental temperature (T) can be determined. Arrhenius plot for conductivity is then obtained by plotting $\log \sigma$ as a function of $1/T$. Activation energy can be calculated from the slope of the straight line. A change in the slope indicates the difference in the conduction mechanism and / or a phase change with the phases having different conductivities.

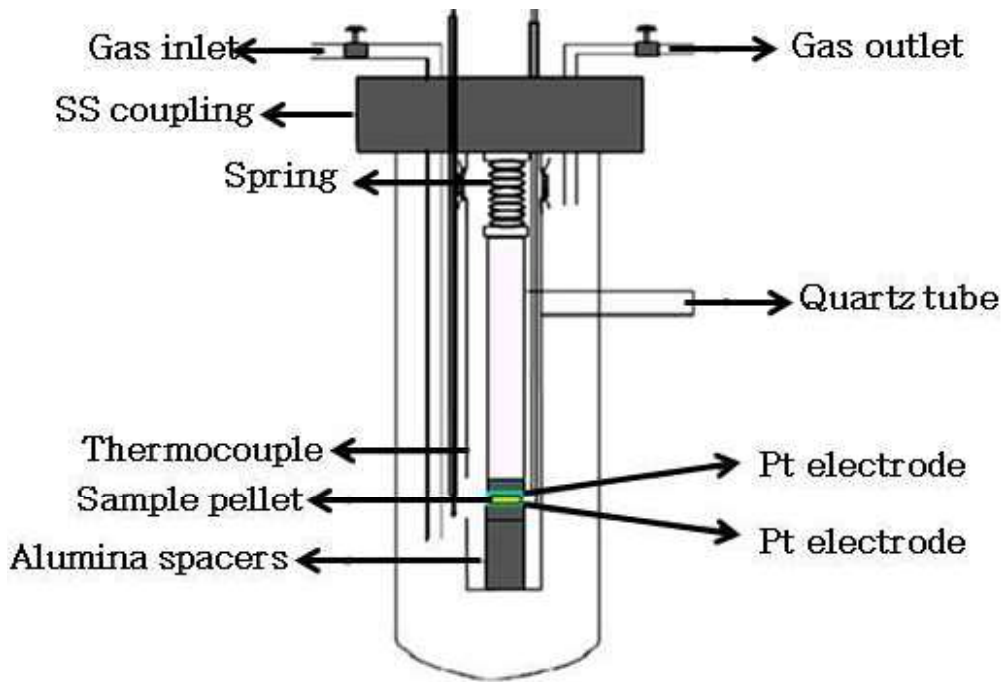


Fig. 2.5 Schematic of the conductivity cell

2.4 Oxygen potential measurements employing solid oxide electrolytes [16, 17]

In ionic solids, electrical conduction is mainly due to the presence of point defects such as vacancies, interstitials or impurities and the movement of these defects under a potential gradient gives rise to conductivity. The total electrical conductivity of the solid is the sum of contributions from ions, electrons and holes.

$$\text{i.e. } \sigma_T = \sigma_i + \sigma_e + \sigma_h \quad (2.19)$$

where σ_T is the total electrical conductivity, σ_i is the conductivity due to ions, σ_e is the conductivity due to electrons and σ_h is the conductivity due to holes. Ionic solids with very high ionic conductivity (10^{-3} - 10 Scm⁻¹) are termed as solid electrolytes. In technologically useful solid electrolytes, the ratio of ionic conductivity to electronic conductivity is 100 or greater.

Oxide solid electrolytes are the most commonly used solid electrolytes at elevated temperatures. Most of them are solid solutions with the fluorite structure as shown in Fig. 2.6.

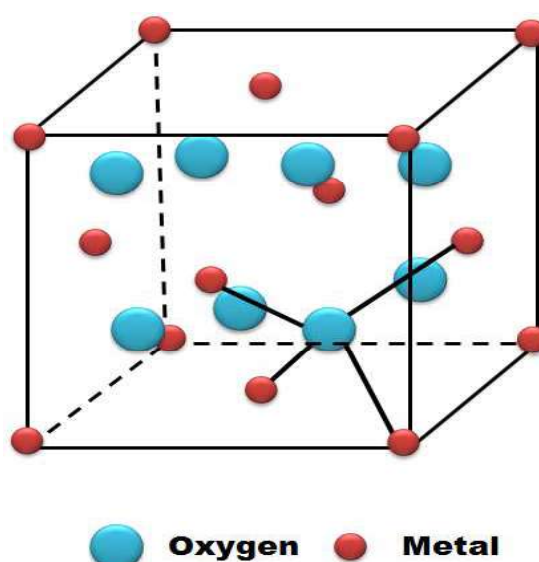


Fig. 2.6 Fluorite structure

Fluorite structure is a face centered cubic arrangement of cations with the anions occupying all the tetrahedral sites. In this structure, each metal cation is surrounded by eight oxygen anions and each oxygen anion is tetrahedrally coordinated by four metal cations. As the fluorite structure possesses large number of octahedral interstitial voids, it can be considered as an open structure where fast movement of oxide ions is possible from one lattice position to another. The most commonly used oxide solid electrolytes are based on ZrO₂ and ThO₂. ZrO₂ based

solid electrolytes are used in the high oxygen partial pressure range while ThO₂ based solid electrolytes is useful at low oxygen partial pressure range.

2.4.1 Defect equilibria and conduction mechanism in solid oxide electrolytes

Consider any ThO₂ based solid electrolyte with the fluorite structure. The predominant intrinsic defects present in this solid electrolyte are oxygen vacancies and oxygen interstitials. With these ionic defects, the electroneutrality in ThO₂ requires that

$$p + 2[V_O^{\bullet\bullet}] = n + 2[O_i^{\bullet}] \quad (\text{Using Kröger-Vink notation}) \quad (2.20)$$

where p is the concentration of holes, $V_O^{\bullet\bullet}$ is the oxide ion vacancy, O_i^{\bullet} is the interstitial oxide ion and n is the concentration of electrons. Considering only fully ionized defects, the formation of anionic Frenkel defect in ThO₂ can be represented as:



where O_o is the oxygen in an anionic lattice site. The equilibrium constant corresponding to the equilibrium 2.21 is

$$K_1 = [V_O^{\bullet\bullet}][O_i^{\bullet}] \quad (2.22)$$

As the formation of one anionic vacancy is accompanied by the formation of one interstitial,

$$[V_O^{\bullet\bullet}] = [O_i^{\bullet}] = K_1^{1/2} \quad (2.23)$$

Any variations in the oxygen partial pressure in equilibrium with ThO₂ can change the concentrations of ionic and electronic defects. Considering the case of high oxygen pressures, where the predominant defects are interstitial anions and holes, the defect equilibria can be represented as:



The corresponding equilibrium constant is given by

$$K_2 = [O_i^{\bullet}]p^2 / P_{O_2}^{1/2} \quad (2.25)$$

where P_{O_2} is the partial pressure of oxygen. With increase in the equilibrium oxygen pressure, the hole concentration increases to preserve the electroneutrality as required by equation (2.20). If $[O_i^{\bullet}]$ is large and essentially constant,

$K_2 = Kp^2 / P_{O_2}^{1/2}$ and hence $p \propto P_{O_2}^{1/4}$ which indicates a $P_{O_2}^{1/4}$ dependence of hole conductivity at high oxygen partial pressures.

At very low oxygen partial pressures, the predominant defects in ThO_2 will be oxygen vacancies and electrons, and the defect equilibria can be represented as:



Then the equilibrium constant is given by

$$K_3 = [V_o^{\bullet\bullet}]n^2 P_{O_2}^{1/2} \quad (2.27)$$

If $[V_o^{\bullet\bullet}]$ is large and constant, $n \propto P_{O_2}^{-1/4}$

Thus at low oxygen partial pressures, the n -type electronic conductivity is proportional to $P_{O_2}^{-1/4}$.

In the intermediate oxygen partial pressure range, the electrical conductivity is independent of the oxygen pressure. This can be schematically illustrated by Fig. 2.7 which shows the variation of electrical conductivity of ThO_2 with oxygen pressure at constant temperature. The diagram shows three regions: a low oxygen pressure region where the conductivity is due to electrons and having a dependence of $P_{O_2}^{-1/4}$, an intermediate oxygen pressure region where the conductivity is independent of P_{O_2} and a high pressure region where the conductivity is due to holes and proportional to $P_{O_2}^{1/4}$.

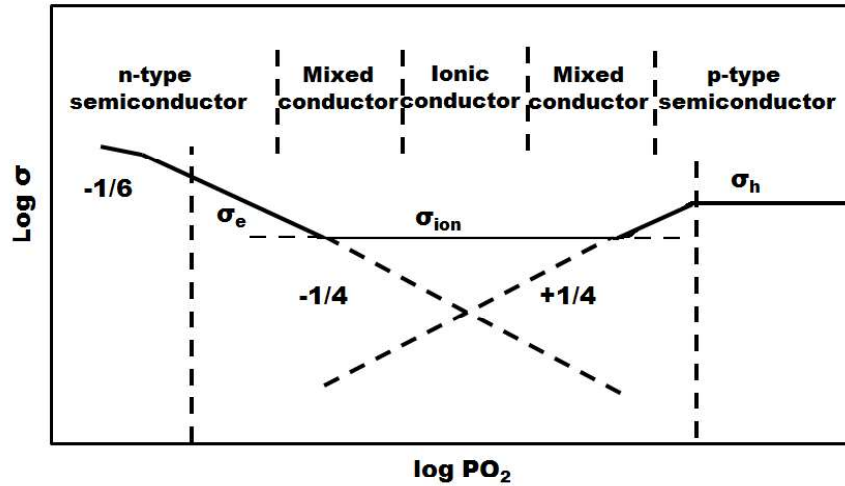


Fig. 2.7 Variation of electrical conductivity with oxygen partial pressure

It is known that addition of impurities can increase the defect concentration.

For example, consider the addition of Y_2O_3 in ThO_2 . Dissolution of yttria into the fluorite phase of ThO_2 can be written as:



Each addition of two yttrium ions creates one oxide ion vacancy. At a fixed oxygen pressure, any increase in the oxide ion vacancy concentration must decrease the concentration of oxygen interstitials as given by equation (2.22), increase the hole concentration (equation (2.25)) and decrease the electron concentration (equation (2.27)). Thus as a result of addition of Y_2O_3 in ThO_2 , the ionic conductivity and hole conductivity increases whereas the electron conductivity decreases. This is illustrated in Fig. 2.8.

2.4.2 Electrolytic domain

Most of the applications of solid electrolytes require that electronic conduction to be negligible. The temperature and pressure region of the solid electrolyte over which the electronic/hole conductivity is less than 1% is called the

electrolytic domain. The electrolytic domains of ThO_2 (15 mol% Y_2O_3) and ZrO_2 (15 mol% CaO) are shown in Fig. 2.9.

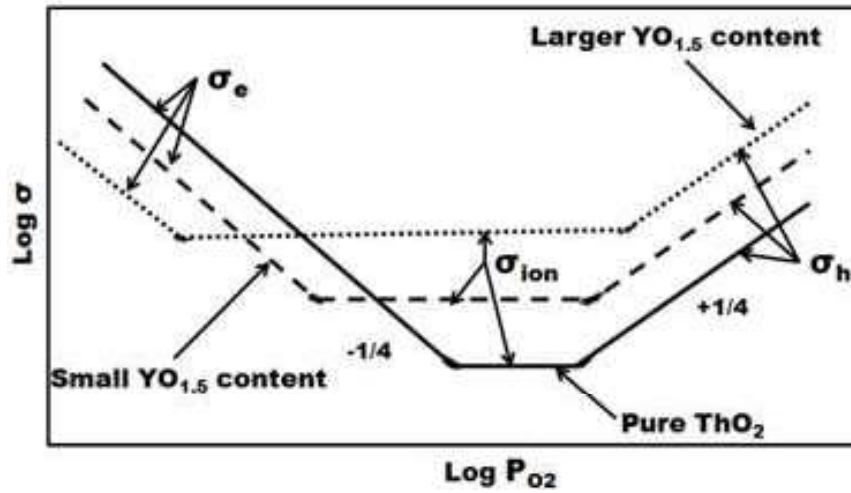


Fig. 2.8 Schematic of the variation of electrical conductivity of ThO_2 and ThO_2 (Y_2O_3) solid solutions with oxygen pressure at constant temperature

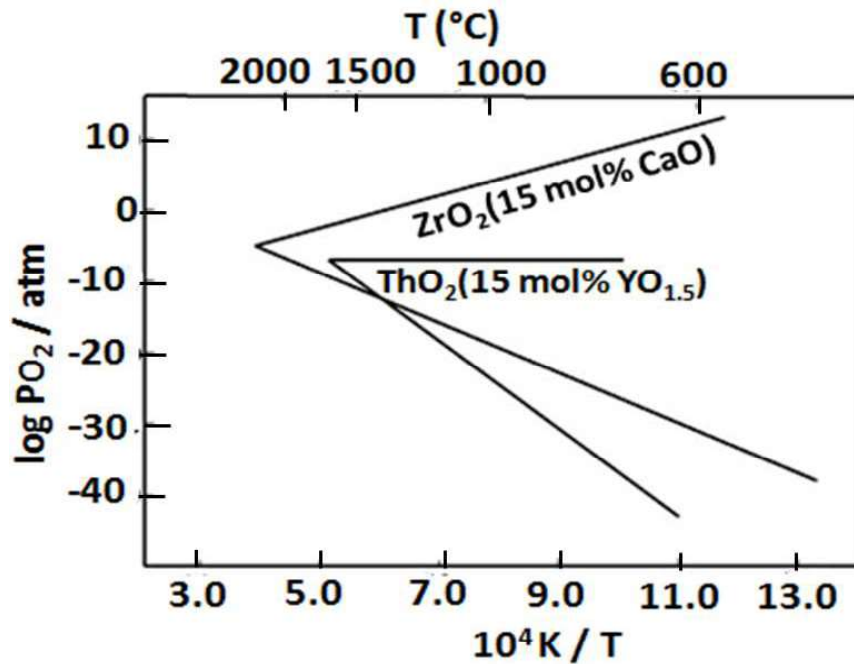


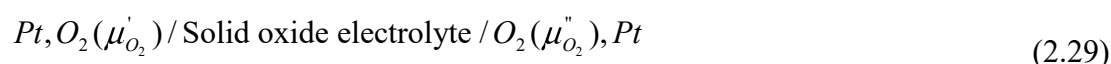
Fig. 2.9 Electrolytic domain boundaries of calcia stabilized zirconia (CSZ) and yttria doped thoria (YDT)

The upper boundary line is known as the upper electrolytic domain boundary and the lower boundary line is known as the lower electrolytic domain boundary. At all temperatures and pressures within the boundary line, the fraction of the ionic part in the total conductivity is greater than 0.99. Above the upper electrolytic domain boundary, p-type electronic conductivity will be greater than 1% and below the lower electrolytic domain boundary, n-type electronic conductivity will be greater than 1%. In the case of ZrO_2 (15 mol% CaO) the electrolytic domain boundary lies between $P_{O_2} \sim 10^5$ to $\sim 10^{-18}$ atm at 1273 K. For ThO_2 (15 mol% Y_2O_3), the domain lies between $P_{O_2} \sim 10^{-6}$ and $\sim 10^{-25}$ atm at 1273 K.

2.4.3 Application of solid electrolytes for emf measurements

Solid electrolytes are widely used for measuring thermochemical properties at elevated temperatures. Solid electrolytes used for these applications should predominantly conduct by ions and the ionic transference number should be greater than 0.99, i.e. the measurements should be carried out within the electrolytic domain boundaries of the solid electrolyte. It is also to be noted that different solid electrolytes possess different electrolytic domain boundaries. The chemical compatibility of the solid electrolyte with the electrode materials at the temperature ranges of study is another concern.

Galvanic cells can be constructed using solid oxide electrolytes for emf measurements. Any such cell can be represented as:



where μ'_{O_2} and μ''_{O_2} are the chemical potentials of oxygen at the two electrodes. The emf, E of the cell is given by

$$E = \frac{1}{4F} \int_{\mu_{O_2}}^{\mu_{O_2}''} t_{ion} d\mu_{O_2} \quad (2.30)$$

where 4 represents the number of charges involved in the transport of one oxygen molecule, F is the faraday constant and t_{ion} is the ionic transference number of the solid electrolyte. When the measurements are carried out within the electrolytic domain boundaries, $t_{ion} \approx 1$ and thus

$$E = \frac{1}{4F} \int_{\mu_{O_2}}^{\mu_{O_2}''} t_{ion} d\mu_{O_2} = \frac{RT}{4F} \ln \frac{p_{O_2}''}{p_{O_2}} \quad (2.31)$$

In the present study, yttria stabilized zirconia (YSZ) solid electrolyte was used for constructing the galvanic cells for measuring the equilibrium oxygen potentials in the different phase fields of Bi-Mo-O and Pb-Mo-O systems to deduce the standard molar Gibbs energy of formation of ternary compounds. YSZ is compatible with both bismuth and lead molybdates and the oxygen pressure ranges involved in these studies are within the electrolytic domain boundaries of YSZ.

2.5 Calorimetric techniques [18]

Calorimetry can be defined as the measurement of the heat absorbed or generated by a substance under study when it undergoes a change from an initial state to the final state. The change in state can result from chemical reaction, dissolution or dilution or physical changes such as fusion, vaporization or sublimation. Calorimetry can be classified into two categories based on the measurements on reacting and non-reacting systems. Reaction calorimetry involves measurements on the heat of mixing, dissolution and general chemical reactions. Non reaction calorimetry includes measurements of heat capacities and phase transitions. Both static and dynamic methods of measurements are possible in calorimetry. The static methods of

calorimetry are classified into three categories based on the variables: - temperature of the calorimeter T_c , temperature of the surroundings T_s and the heat Q produced per unit time. They are:

- i. Isothermal calorimetry, where $T_c = T_s = \text{constant}$ and only Q varies.
- ii. Adiabatic calorimetry, where $T_c = T_s$ but is not constant as Q varies.
- iii. Isoperibol calorimetry, where $T_s - T_c = \text{constant}$

The dynamic methods include differential scanning calorimetry (DSC), modulated DSC, AC calorimetry, heat capacity spectroscopy and relaxation calorimetry.

In the present work, thermochemical measurements were carried out by isoperibol calorimetry and DSC. Principles of these methods are detailed below.

2.5.1 Isoperibol calorimetry[19-21]

Isoperibol calorimetry is used for the determination of enthalpy of a reaction or dissolution. The basic principle involves the determination of enthalpy of dissolution of a substance AB by dissolving it in a suitable solvent. Corresponding amounts of A and B are also dissolved in the same solvent in separate experiments and the enthalpies of dissolution of the individual components are determined. From these data, standard molar enthalpy of formation of AB can be determined.

The choice of a suitable calorimetric solvent is very important in isoperibol calorimetry. The solvent must be able to dissolve the solutes in a reasonable time and it must have a low vapor pressure to avoid any evaporation losses. Also, the dissolution in the solvent must release moderate heat so as to minimize errors. Generally, aqueous mineral acids and bases such as hydrochloric acid, hydrofluoric acid, sodium hydroxide, etc are used as solvents. It is impossible to predict the suitability of any solvent to a particular compound and hence, preliminary trials

should be made to test the solvent. Non aqueous solvents such as ammonia are also used for measuring the heat of solution. The use of liquid metals such as mercury for the dissolution of alloys of lead with tin, zinc, bismuth, etc has also been reported [19].

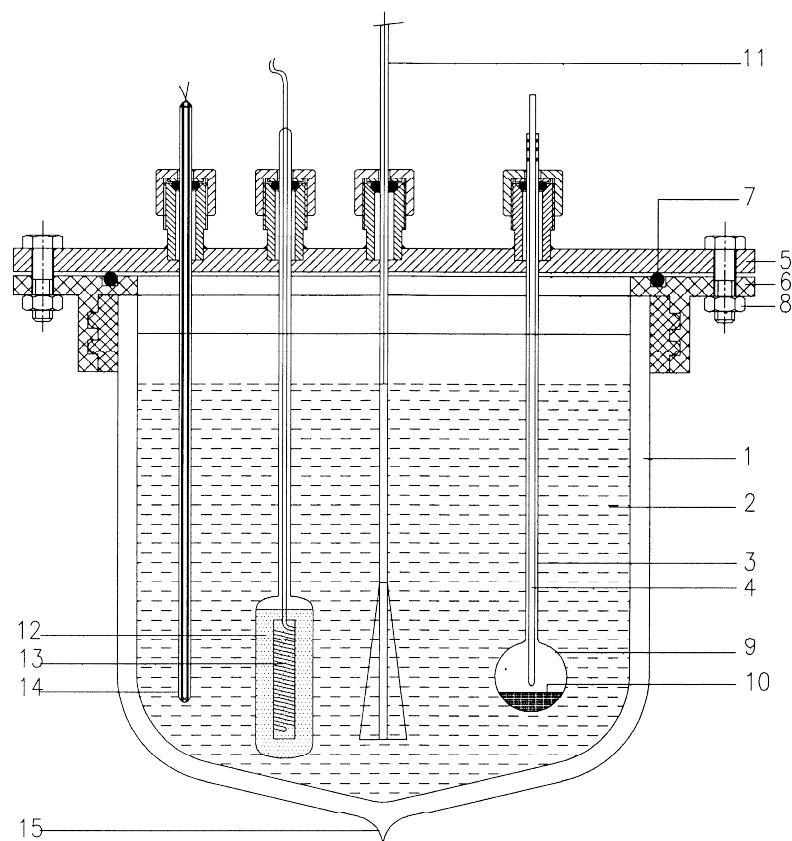
During the process of reaction, the temperature in the calorimeter rises or falls until the process of dissolution is complete. From the temperature change and the value of the energy equivalent of the calorimeter, the enthalpy of the process can be calculated. The energy equivalent of the calorimeter can be determined by carrying out insitu electrical calibration before and after the sample dissolution. In order to evaluate the evolution or absorption of the heat in the calorimeter, a correction must be made for the exchange of heat between the calorimeter and its surroundings [19, 20]. This is done by applying Newton's law of cooling:

$$\frac{dT_c}{dt} = k(T_c - T_s) \quad (2.32)$$

where T_c and T_s are the temperatures of the calorimeter and surroundings respectively, t is time and k is the cooling constant. Error due to this correction can be made small by having a small value of the cooling constant, which can be made possible by evacuating the annular gap of the calorimeter vessel (Dewar) placed in the constant temperature environment and by silvering both walls of the gap.

The isoperibol calorimeter used in this work essentially consists of a double walled glass Dewar of 200 ml capacity with a round bottom and with an evacuated inner space (Fig. 2.10). The top of the vessel is attached to a Teflon flange by means of a silicone gasket. This flange is attached to a stainless steel mating cover using a Viton O-ring. The mating cover has leak tight fittings for introducing a stirrer, sample bulb, heater and a thermistor. Provisions are given for submerging the entire

calorimeter assembly into a water bath. The temperature of water in the bath is kept constant within ± 0.01 K. The sample container is made up of a glass tube of 6 mm outer diameter with a thin walled bulb blown at the bottom of the tube. Sample is taken in the glass bulb and a sharp glass push rod is kept sealed to the inner wall of this sample tube using an O-ring. A stirrer, made up of PTFE and driven by a motor is provided for the uniform stirring of the calorimetric solvent in the Dewar. The speed of the stirrer is controlled by means of a controller and kept constant during the entire period of the experiment.



- | | | | |
|---|---|----|--------------------|
| 1 | DOUBLE WALLED EVACUATED GLASS DEWAR WITH SILVER COATING | 8 | BOLT & NUT |
| 2 | CALORIMETRIC FLUID | 9 | THIN WALLED BULB |
| 3 | SAMPLE HOLDER | 10 | SAMPLES |
| 4 | GLASS PUSH ROD | 11 | PTFE STIRRER |
| 5 | TOP S S FLANGE | 12 | SILICONE OIL |
| 6 | BOTTOM TEFLON FLANGE SET | 13 | CALIBRATION HEATER |
| 7 | 'O' RING | 14 | THERMISTOR |
| | | 15 | VACUUM SEAL |

Fig. 2.10 Schematic diagram of the isoperibol calorimeter

The calibration of the calorimeter is performed by electrical method. The electrical heater is made up of a PTFE coated manganin wire with very low temperature coefficient of resistance so that the change of resistance would be negligible during the calibration. The resistance of the heater is $17.425 \pm 0.005 \Omega$. The heater is kept immersed in silicone oil taken in a glass tube to enable conduction of heat from the heater to the calorimetric solvent. The electrical calibration is performed by applying a constant current using a stable power source, for a known period of time. Current passed is measured across a precision resistor connected in series. A thermistor (M/s Toshniwal Brothers Delhi Private Limited, Bangalore, India) is provided to measure the temperature as a function of time and which is connected to a data acquisition system, interfaced to a personal computer.

The chemical calibration of the calorimeter is performed by using tris(hydroxyl methyl) aminomethane (TRIS). The calorimetric solvent used for this calibration is 0.1 mol/kg HCl. In order to perform the chemical calibration, the required amount of the sample is accurately weighed and transferred into the sample bulb. The dissolution can be performed in 100 ml of the calorimetric solvent taken inside the Dewar flask. The sample bulb along with the other components is allowed to equilibrate at the bath temperature. A steady temperature signal is obtained once the calorimeter attains thermal equilibrium with the surrounding water bath. The sample bulb is then broken by pushing the glass rod and the sample is allowed to dissolve in the calorimetric solvent. The consequent variation in the temperature signal is monitored. Electrical calibration is performed in situ before and after of each of these experiments. Typical temperature-time curves obtained for an exothermic process are shown in Figs. 2.11a-c. The type of the curve depends upon the initial

temperature of the calorimeter with respect to the constant temperature surroundings (θ_0).

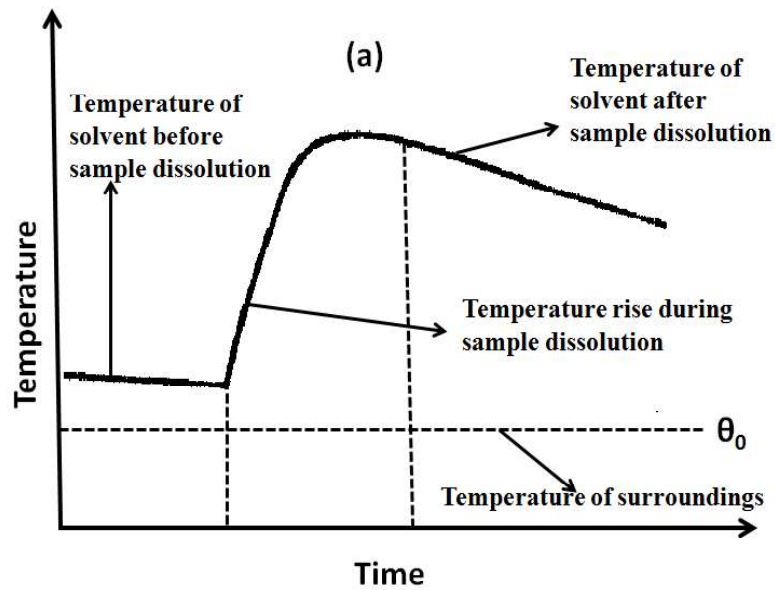


Fig. 2.11(a) Temperature-time curve for exothermic process in isoperibol calorimeter(initial temperature higher than the temperature of the surroundings) [19]

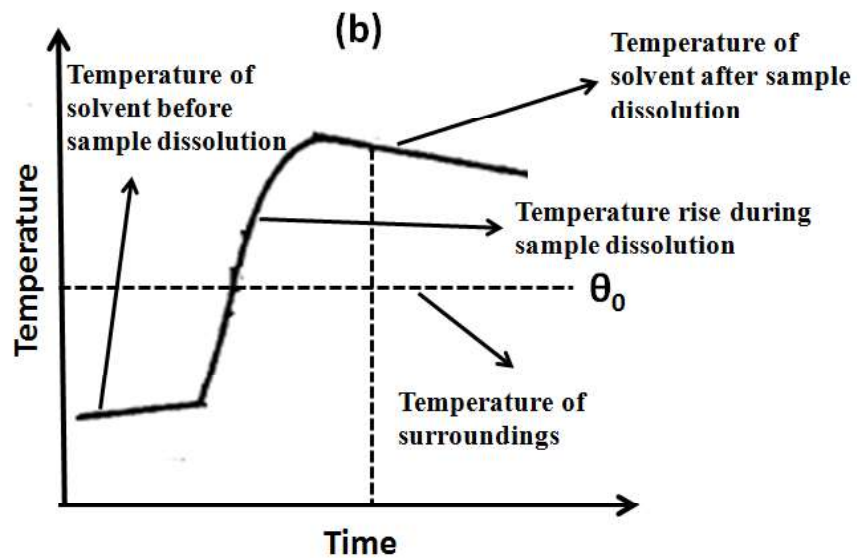


Fig. 2.11 (b) Temperature-time curve for exothermic process in isoperibol calorimeter (temperature of the surroundings is between initial and final temperature)[19]

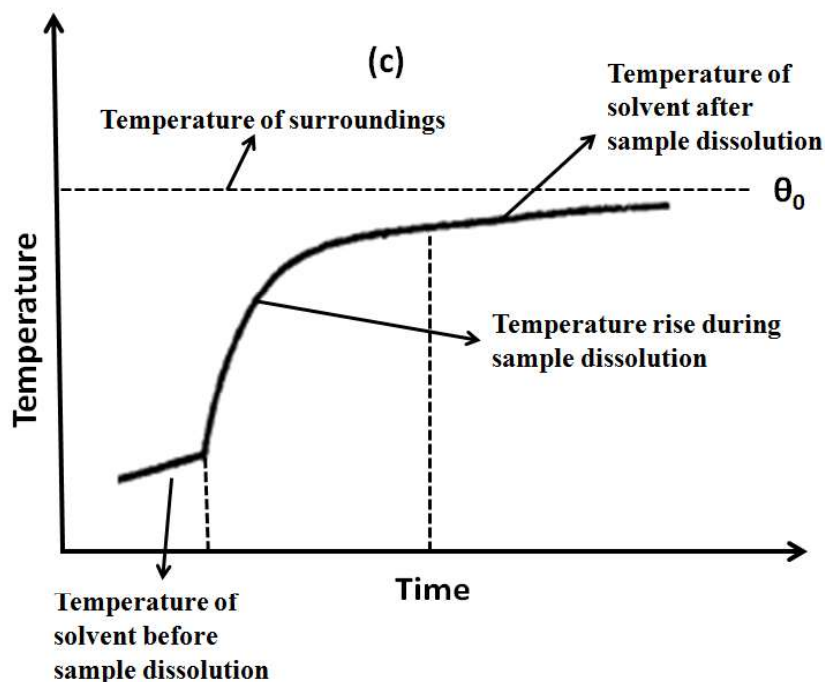


Fig. 2.11(c) Temperature-time curve for exothermic process in isoperibol calorimeter (final temperature is below the temperature of the surroundings) [19]

Figure 2.11a shows the temperature versus time plot when the initial temperature is higher than the surrounding temperature. Figure 2.11b shows the temperature variation when the temperature of the surroundings lies between the initial and final temperatures. Figure 2.11c shows the corresponding plot when the final temperatures lie below the temperature of the surroundings.

The determination of temperature change (ΔT) and the corrected temperature change (ΔT_c) from the temperature-time plot of sample dissolution are illustrated in Figs. 2.12 and 2.13 [19]. In Fig. 2.12, AB and CD represent the time dependence of temperature of the calorimeter before and after the sample dissolution. The line BC represents the increment in temperature due to the dissolution of the sample. The initial and final temperatures T_1 and T_2 corresponding to the commencement and ending of the reaction can be determined by extrapolating the lines AB and DC as BE and CF, respectively. The temperature change is then obtained as $\Delta T = T_2 - T_1$. The

mean temperature is then calculated as $T_m = T_1 + (0.63 \times \Delta T)$ as shown in Fig. 2.13. A vertical line passing through T_m is then drawn. The meeting point of the vertical line at AE and DF will give the corrected temperatures T_{C1} and T_{C2} . The corrected temperature change ΔT_C is given by $\Delta T_C = T_{C2} - T_{C1}$.

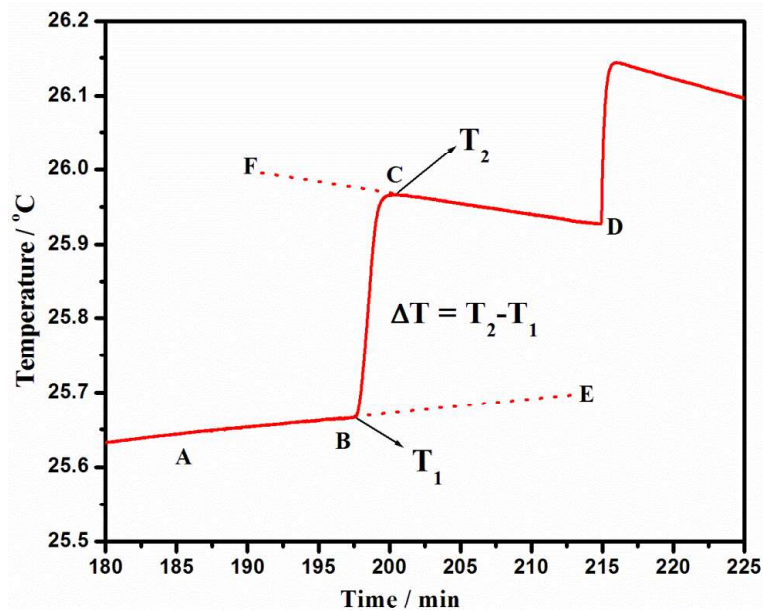


Fig. 2.12 Illustration of determination of ΔT during the sample dissolution

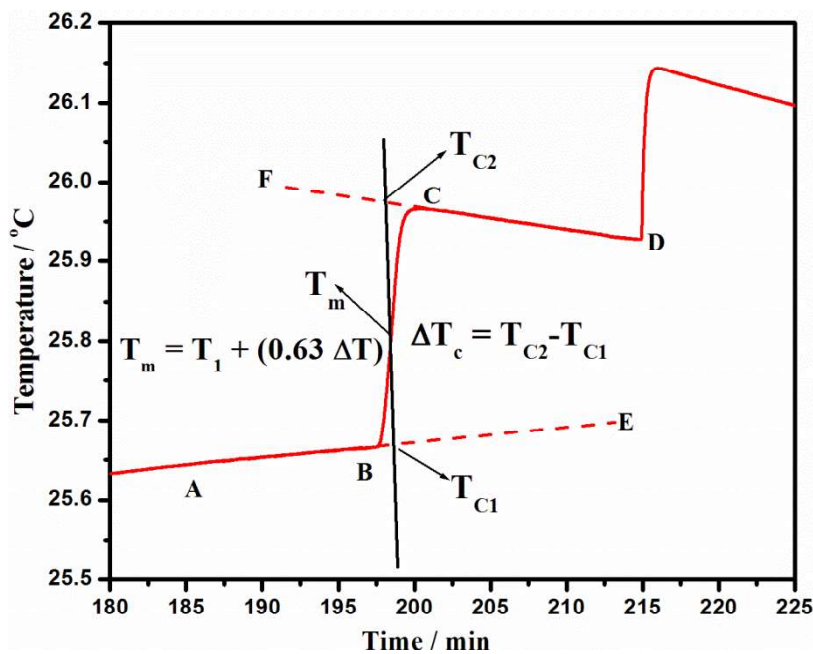


Fig. 2.13 Illustration of determination of ΔT_C during the sample dissolution

In the present work, standard molar enthalpies of formation of the ternary compounds, PbMoO_4 , Pb_2MoO_5 , Pb_5MoO_8 , $\text{Bi}_2\text{Mo}_3\text{O}_{12}$, Bi_2MoO_6 , $\text{Bi}_6\text{Mo}_2\text{O}_{15}$ and $\text{Bi}_6\text{MoO}_{12}$ were determined by solution calorimetry. 125 ml of 2.02 mol kg^{-1} NaOH solution was used as the calorimetric solvent for the dissolution of lead molybdates while a mixture of 100 ml of 3 mol kg^{-1} NaOH and 25 ml of triethanolamine was employed for the dissolution of bismuth molybdates.

2.5.2 Differential scanning calorimetry (DSC) [18, 22, 23]

In Differential Scanning Calorimetry (DSC), the heat flow rate to the sample is measured as a function of time or temperature. Here both the sample and the reference materials are heated in a programmed way. The temperature of the sample and reference are maintained the same throughout the experiment and the difference in the amount of heat required to raise the temperature of the sample and reference are measured. DSC can be used for determining the heat capacity and for studying phenomena such as phase transitions, chemical reactions, adsorption, etc occurring on materials. Two designs of DSC are available: heat flux DSC and power compensating DSC.

2.5.2.1 Heat flux DSC

In heat flux DSC (Fig. 2.14), the difference in heat flow into the sample and reference is measured while the sample temperature is changed at the constant rate. The characteristic feature of this measuring system is that the main heat flow from the furnace to the samples passes symmetrically through a disk made of a material of good thermal conductivity [23]. The sample and reference pans are positioned on this disk symmetrical to the centre of the furnace. The temperature sensors are integrated into the disk. When the furnace is heated, heat flows through the disk to the samples. When the arrangement of sample and reference pans is ideally symmetrical (identical

with respect to the mass, material and position or arrangement), equal amount of heat flows into the pans. Then the differential temperature signal would be zero. However, if this steady state equilibrium is disturbed by any transition occurring in the sample, a differential signal is generated which is proportional to the difference between the heat flow rates to the sample and to the reference material.

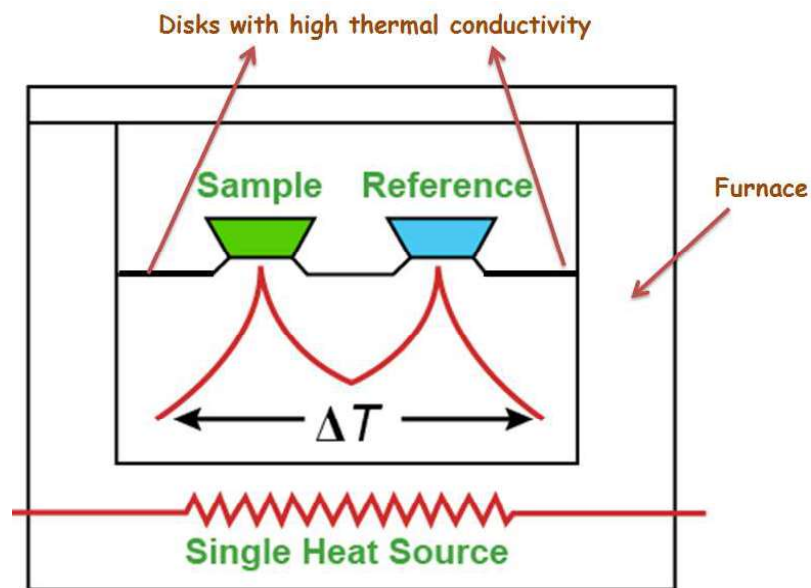


Fig. 2.14 Schematic of the heat flux DSC

2.5.2.2 Power compensation DSC

Power compensating DSC (Fig. 2.15) consists of two microfurnaces of the same type, each of which contains a temperature sensor and a heating resistor. Both the microfurnaces are thermally decoupled from each other and are positioned in a silver block of constant temperature. During heating, same heating power is supplied to both the furnaces by means of a control circuit. When the thermal symmetry is ideal, the temperature of both microfurnaces would be the same. When an asymmetry occurs as a result of any thermal event in the sample, a temperature difference arises between the microfurnaces. This temperature difference is both the measurement signal and the input signal of a second control circuit. This second control circuit tries

to compensate the reaction heat flow rate through proportional control by increasing or decreasing an additional heating power. The compensating heating power is proportional to the temperature difference. The time integral over the compensating heating power is proportional to the heat which was released or consumed by the sample.

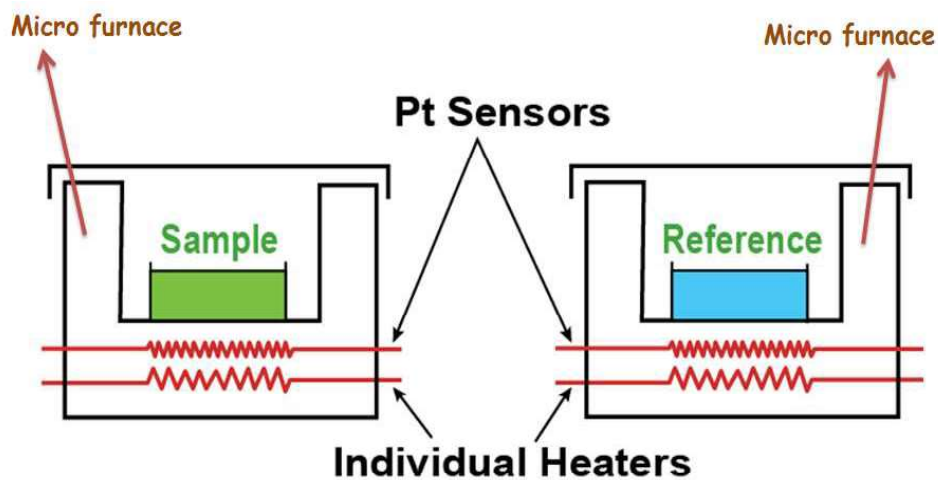


Fig. 2.15 Schematic of the power compensation DSC

2.5.3 Calibration of DSC

DSC is not an absolute heat and temperature measuring device. Hence, the relative data obtained by DSC must be correlated to absolute values by calibration. The calibration procedure involves temperature calibration, heat calibration and heat flow rate calibration (in case of heat flux DSC).

2.5.3.1 Temperature calibration

Temperature calibration involves the explicit assignment of the temperature indicated by the instrument to the true temperature. It is accomplished by using melting points of high purity metals. The thermodynamically defined transition temperature is always the equilibrium temperature whereas DSC measurements are dynamic. Therefore, DSC calibration results must be extrapolated to equilibrium conditions to ensure a temperature calibration, which is independent of the heating

rate used. This is carried out by measuring the melting points of reference materials such as In, Sn, Pb and Zn as a function of heating rate and extrapolating the obtained values to zero heating rates.

2.5.3.2 Heat calibration

Heat calibration involves the determination of the proportionality factor between the exchanged heat measured by the instrument and the actual heat exchanged by the sample due to any thermal event in the sample. The heat calibration can be carried out by using the enthalpy of melting of NBS standards such as In, Sn, Pb and Zn.

2.5.3.3 Heatflow rate calibration

The heat flow rate calibration involves the determination of the proportionality factor between the measured heat flow rate and the true heat flow rate (released or consumed) by the sample. It can be performed with a sample of known heat capacity. The materials used for heat flow rate calibration should not undergo any phase transition in the temperature range of study. Sapphire ($\alpha\text{-Al}_2\text{O}_3$) is generally used for heat flow rate calibration.

2.5.4 Heat capacity measurement using a heat flux DSC

A three step procedure is generally adopted for the measurement of heat capacity. The three steps are: i) blank run, ii) calibration run and iii) sample run and these are illustrated in Figs. 2.16 and 2.17.

At each step, the temperature program used for the measurement consisted of three segments: an isothermal segment at the initial temperature with a fixed dwelling period, followed by a dynamic segment at a defined heating rate and finally another prefixed isothermal segment at the final temperature. At the isothermal segment, the heat flow rate from the furnace to the sample is close to zero whereas during the

dynamic heating segment, an exponential endothermic effect is observed due to the flow of heat from the furnace to the sample and it is proportional to the heat capacity of the sample. The slope of the line during the dynamic segment indicates the variation of heat capacity of the sample with temperature. Generally aluminium pans are used for the sample and reference and are hermetically sealed with a pin hole on the lid to ensure that the entire sample is at a uniform temperature when the measurements are carried out.

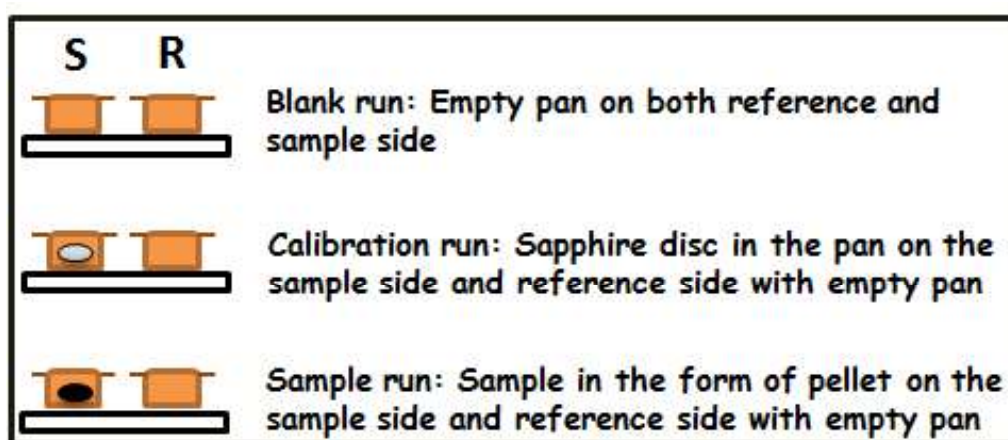


Fig. 2.16 Three step procedure for measuring heat capacity

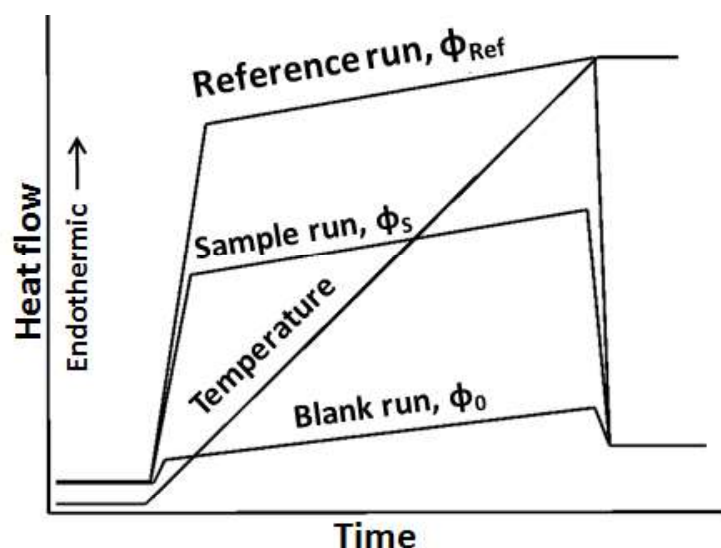


Fig. 2.17 Typical DSC run for blank, sample and reference

- 1) Blank run: In the blank run, the heat flow rate is determined (Φ_0) using empty aluminium pans of equal mass in the sample and reference sides.
- 2) Calibration run: In the calibration run, a calibration substance of known heat capacity such as sapphire is placed in to the sample pan whereas the reference side is unchanged and the heat flow rate is measured as in the case of blank run.

The following expression is valid:

$$C_{Ref}m_{Ref}\beta = K\Phi(T)(\Phi_{Ref} - \Phi_0) \quad (2.33)$$

where C_{Ref} is heat capacity of the reference material, β is heating rate, m_{Ref} is the mass of the reference material, Φ_{Ref} and Φ_0 are the heat flow rates for the reference run and the blank run respectively, $K\Phi(T)$ is the temperature dependant calibration factor.

- 3) Sample run: During the sample run, sapphire in the sample pan is replaced with the sample and the heat flow rate is measured. Thus

$$C_Sm_S\beta = K\Phi(T)(\Phi_S - \Phi_0) \quad (2.34)$$

where C_S is the heat capacity of the sample, m_S is the mass of the sample and Φ_S is the heat flow rate for the sample run.

Based on the above two equations, heat capacity of the sample can be determined as below:

$$C_S = \frac{C_{Ref}(\Phi_S - \Phi_0)m_{Ref}}{(\Phi_{Ref} - \Phi_0)m_S} \quad (2.35)$$

In order to have good thermal contact between the pan and the sample and to eliminate any possible errors due to the temperature gradient within the sample, heat capacity measurements are generally carried out with sample taken in the form of a disc similar to that of the reference material.

In the present work, molar heat capacities of the ternary compounds in the Bi-Mo-O and Pb-Mo-O systems were measured using a heat flux DSC (M/s Mettler Toledo-Model No.DSC827e, Switzerland).

2.6 References

1. C.N.R. Rao, K. Biswas, Ceramic methods in essentials of inorganic materials synthesis, John Wiley & Sons Inc. Hoboken, NJ, 2015.
2. A.R. West, Solid state chemistry and its applications, John Wiley & Sons Inc. Singapore, 2003.
3. T. Kimura, Molten salt synthesis of ceramic powders (in Advances in ceramics-synthesis and characterization, processing and specific applications, Edited by C. Sikalidis), InTech, 2011, p. 75.
4. A.M. Alper, Phase diagrams: Materials science and technology, (in Theory, principles and techniques of phase diagrams), Academic Press Inc. New York, 1970, p. 115.
5. J.G. Zhao, Methods of phase diagram determination of ceramic systems, Elsevier, 2007.
6. R.A. Meyers, Encyclopedia of analytical chemistry, (X-ray technique: Overview), John Wiley & Sons Ltd, Chichester, 2000.
7. S.E. Dann, Reactions and characterization of solids, The Royal Society of Chemistry, 2002.
8. L.E. Smart, E.A. Moore, Solid state chemistry- an introduction, CRC press, Taylor and Francis group, Suite, 2005.
9. B.D. Cullity, S.R. Stock, Elements of X-ray diffraction, Prentice Hall, NJ, 2001.

10. D.E. Newbury, D.C. Joy, P. Echlen, C.E. Fiori, J.I. Goldstein, *Advanced scanning electron microscopy and X-ray microanalysis*, Plenum Press, New York, 1986.
11. K. Mills, J.R. Davis, D.A. Dieterich, *Metallography and microstructure*, ASM handbook, International Soc. ASM, Material Park, USA, 1998.
12. E. Barsoukov, R. Macdonald, *Impedance spectroscopy, Theory, Experiment and applications*, John Wiley and Sons, Inc. NJ, 2005.
13. M.E. Orazem, B. Tribollet, *Electrochemical impedance spectroscopy*, John Wiley & Sons, NJ, 2008.
14. P. Vanysek, *Introduction to electrochemical impedance*, Calgary, 1994.
15. Z view®-Impedance software, Scribner Associates, Inc. North Carolina, USA, 2005.
16. S. Geller, *Solid electrolytes*, Springer, New York, 1977.
17. E.C. Subbarao, *Solid electrolytes and their applications*, Plenum Press, New York, 1980.
18. M. Sorai, *Comprehensive handbook of calorimetry and thermal analysis*, John Wiley & Sons, Ltd, Chichester, 2004.
19. O. Kubachewski, C.B. Alcock, *Metallurgical thermochemistry*, 5th Ed., Pergamon, Oxford, 1993.
20. J.K. Grime, *Analytical solution calorimetry*, Vol. 79, John Wiley & Sons, Ltd, Canada, 1976.
21. K.N. Marsh, P.A.G. O'Hare, *Solution calorimetry-Experimental thermodynamics*, Blackwell Scientific Publications, Australia, 1994.
22. M.E. Brown, *Handbook of thermal analysis and calorimetry*, Vol. 1, Principles and practice, 1998.

23. G. Hohne, W. Hemminger, H.J. Flammersheim, Differential scanning calorimetry-An introduction for practitioners, Springer, Germany, 1996.

Chapter 3

Thermochemical studies on Bi-Mo-O system

3.1 Introduction

As discussed in chapter 1, the heavy corrosion and mass transport effects due to high dissolution of structural steel components in liquid Pb and LBE can be minimized by the insitu formation of a passive oxide layer over the steel surface by the careful control of oxygen concentration in the coolant. To understand the formation and stability of the passive oxide film, the interaction of alloying components of steel with Pb and Bi in the presence of dissolved oxygen has to be studied. In this context, a detailed knowledge on the phase diagrams of Bi-M-O and Pb-M-O (M = Fe, Cr, Mo, etc) systems as well as thermochemical data of relevant ternary compounds in these systems are required. Studies carried out on Bi-Mo-O system are described in this chapter.

3.2 Literature survey

3.2.1 Bi-Mo system

Data on Bi-Mo system has been reviewed by Brewer [1] and by Elliott [2]. The binary phase diagram of Bi-Mo system is shown in Fig. 3.1 [3]. No intermetallic phases exist in the system. Horsely and Maskreg [4] attempted to determine the solubility of Mo in Bi over a range of temperatures and concluded that the solubility is below the limits of analytical detection (1 ppm) up to 1303 K.

3.2.2 Bi-O system

The Bi-O phase diagram at 1 bar total pressure is shown in Fig. 3.2. The data on Bi-O system has been reviewed by Risold et al. [5]. Bismuth, which exists in the rhombohedral form, has a melting point of 544 K. The solubility of oxygen in

bismuth is 5 at% at 1400 K and it increases to 30 at% at 1650 K. Ganesan et al. [6] have reported the solubility of oxygen in liquid bismuth and is given by the following expressions:

$$\log(S/at\%O) = -4476/T K^{-1} + 4.05 \quad (T : 753-988 K) \quad (3.1)$$

$$\log(S/at\%O) = -3786/T K^{-1} + 3.36 \quad (T : 988-1020 K) \quad (3.2)$$

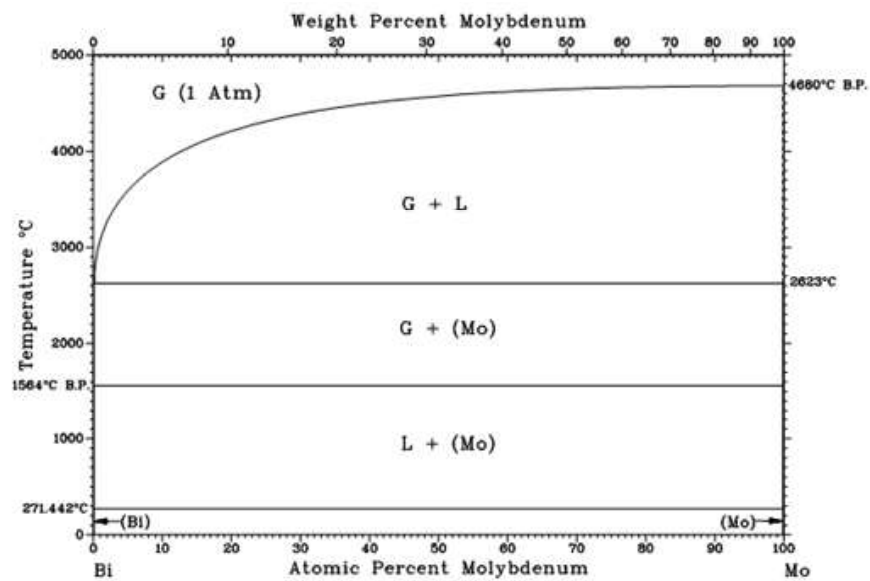


Fig. 3.1 Phase diagram of Bi-Mo- system [3]

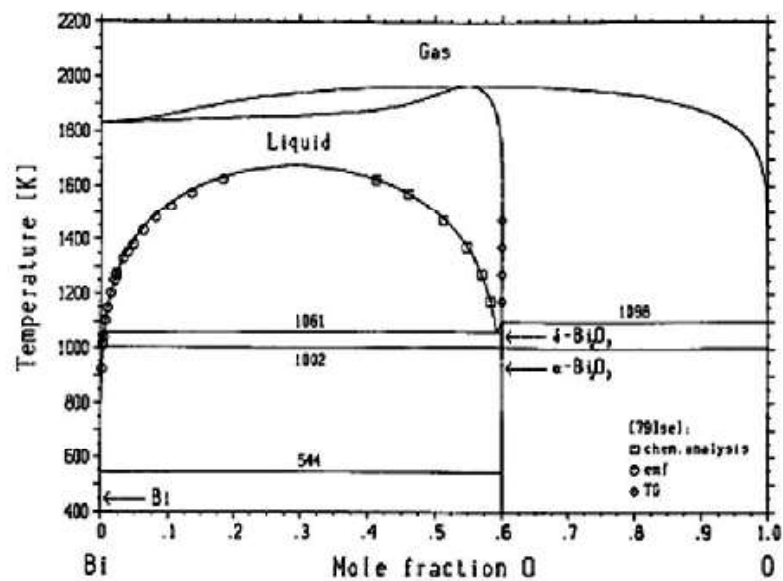


Fig. 3.2 Phase diagram of Bi-O system [4]

The only stable compound in the Bi-O system is Bi_2O_3 , which exhibits polymorphism with four modifications: α , β , γ and δ - Bi_2O_3 . Among which, α and δ phases are the stable phases while β and γ phases are metastable phases. The low temperature α - Bi_2O_3 has a monoclinic structure and the high temperature δ - Bi_2O_3 has fcc structure. α phase is stable up to 1002 K and where it transforms to the δ phase, which melts at 1098 K. The β and γ phases are having tetragonal and bcc structure, respectively. These metastable phases are formed upon cooling the δ phase. The formation temperatures of β and γ phases are reported to be ~ 920 and ~ 910 K, respectively. The β to α transition take place at temperatures between 920 and 700 K while the γ phase can be preserved at room temperature. The liquid exhibits miscibility gap between Bi and Bi_2O_3 from 1061 K and complete miscibility in liquid phase occurs at temperatures above 1650 K.

3.2.3 Mo-O system

The binary phase diagram of Mo-O system is presented in Fig. 3.3. A detailed review on this system has been given in ref 7.

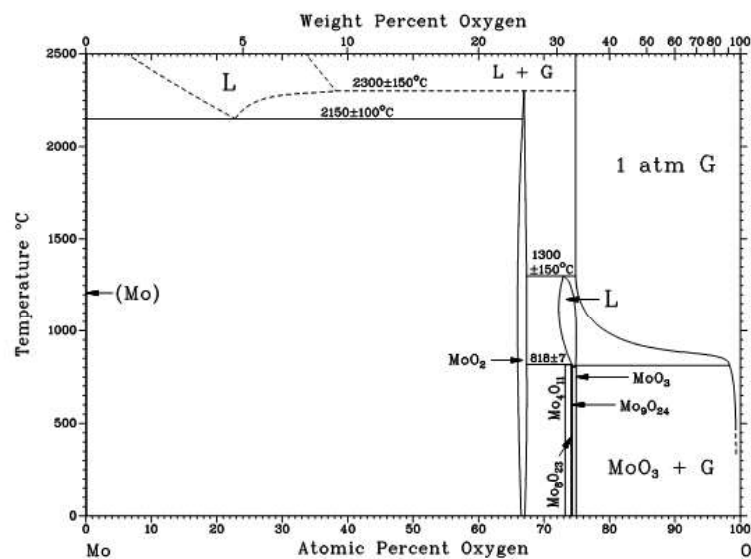


Fig. 3.3 Phase diagram of Mo-O system [6]

The various oxides of Mo reported to be present are MoO_2 , Mo_4O_{11} , Mo_8O_{23} , Mo_9O_{26} and MoO_3 . The melting points of MoO_3 and MoO_2 are determined to be 1073 ± 5 K and 2873 ± 5 K, respectively. Mo_4O_{11} undergoes disproportionation into MoO_2 and liquid at 1091 K.

The standard molar Gibbs energy of formation of MoO_2 (s) has been reported by several investigators [8-23]. Both emf and gas equilibrations techniques were used by these investigators. However, there is considerable differences exist among the reported data. The summary of the literature data on the Gibbs energy of formation of MoO_2 (s) and the experimental techniques employed are given in Table 3.1. The graphical comparison of the literature data is shown in Fig. 3.4.

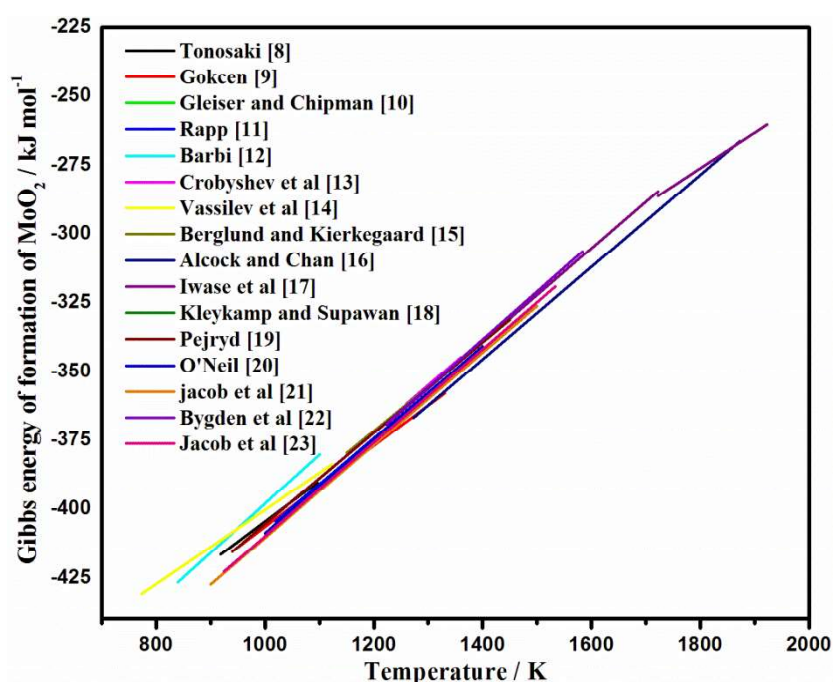


Fig. 3.4 Comparison of literature data on Gibbs energy of formation of MoO_2 (s)

The data reported by Gleiser and Chipman [10], O'Neill [20], Rapp [11] and Jacob et al. [21, 23] are in good agreement in the temperature range of 925 to 1500 K and are shown separately in Fig. 3.5. It is to be noted that these closely agreeing results are obtained by a variety of techniques.

Table 3.1 Literature data on Gibbs energy of formation of MoO₂ (s)

Investigators	Techniques	Molar Gibbs energy of formation of MoO ₂ / kJ mol ⁻¹	Temperature range/ K
Tonosaki, 1940 [8]	Gas equilibration (H ₂ /H ₂ O)	-550.199 + 0.1457T	918-1096
Gokcen, 1953 [9]	Gas equilibration (H ₂ /H ₂ O)	-553.334 + 0.1469T	950-1330
Gleiser and Chipman, 1962 [10]	Gas equilibration (CO/CO ₂)	-576.932 + 0.1681T	1200-1350
Rapp, 1963 [11]	Emf (Fe/FeO and Ni/NiO as reference electrode)	-575.300+0.1674T	1020-1320
Barbi, 1964 [12]	Emf (FeO/Fe ₃ O ₄ and Fe/Fe ₃ O ₄ as reference electrode)	-575.856+0.1778T	840-1100
Drobyshev et al., 1965 [13]	Emf (Fe/FeO as reference electrode)	-575.635+0.1697T	1260-1360
Vassilev et al., 1968 [14]	Gas equilibration (H ₂ /H ₂ O)	-533.887+0.1336T	773-1123
Berglund and Kierkegaard, 1969 [15]	Emf (air as reference electrode)	-564.798+0.161T	1150-1450
Alcock and Chan, 1972 [16]	Emf (CO/CO ₂ as reference electrode)	-579.902+0.1674T	1273-1873
Iwase et al., 1979 [17]	Emf (Co/CoO and air as reference electrode)	-576.100+0.1692T	1223-1723
Kleykamp and Supawan, 1979 [18]	Emf (Fe/FeO as reference electrode)	-509.600+0.1297T	1723-1923
Pejryd, 1984 [19]	Emf (air as reference electrode)	-571.800+0.1662T	1070-1320
O'Neill, 1986 [20]	Emf (Fe/FeO as reference electrode)	-529.21-0.1268T+0.0362TlnT	940-1450
Jacob et al., 1987 [21]	Emf (O ₂ as reference electrode)	-603.268-0.3375T-0.0207TlnT	1000-1400
Bygden et al., 1994 [22]	Emf (Fe/FeO as reference electrode)	-578.880+0.1685T	900-1500
Jacob et al., 2007 [23]	Emf (O ₂ as reference electrode)	-580.560+0.173T	1224-1584
		-579.821+0.170T	925-1533

Gleiser and Chipman [10] used the gas equilibration method, Rapp [11] used the emf method with Ni/NiO and Fe/FeO as the reference electrodes, O'Neill [20] used the emf method with Fe/FeO reference electrodes while Jacob et al. [21, 23] used pure oxygen gas as reference. The data reported by Tonosaki [8], Vassilev et al. [14] and Barbi [12] are significantly more positive.

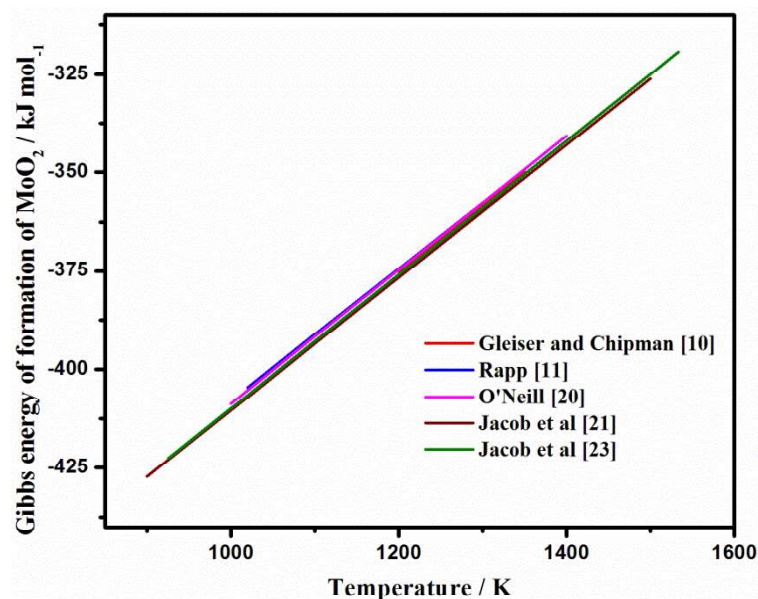


Fig. 3.5 Selected data on Gibbs energy of formation of MoO₂ (s) reported in literature

3.2.4 Bi₂O₃-MoO₃ system

The Bi₂O₃-MoO₃ pseudo binary system has been studied by several groups and it is characterized by the presence of several compounds and solid solutions. Extensive studies on thermal stabilities, oxide ion conductivities and catalytic properties of bismuth molybdates have been reported in literature. Spectroscopic investigations of several bismuth molybdates have been carried out in the past to unravel the mechanisms of their catalytic activities [24-26]. MoO₃rich section of this system in the composition range of 0 to 50 mol% Bi₂O₃ consists of three ternary compounds, namely, Bi₂Mo₃O₁₂, Bi₂Mo₂O₉ and Bi₂MoO₆. These compounds exhibit significant oxide ion conductivity and are known to catalyze selective oxidation of

several organic compounds and ammoxidation of olefins [27-29]. However, the Bi_2O_3 rich section of the system ($\text{Bi}_2\text{O}_3/\text{MoO}_3 \geq 1$) is rather complicated due to the presence of several ternary compounds and solid solutions. The temperature ranges of stabilities of most of the compounds in this composition range are not well established. All the reported ternary compounds in this system are labeled and presented in Fig. 3.6. The literature data concerning the existence and stabilities of bismuth molybdates and solid solutions are described below and the salient features are given in Table 3.2.

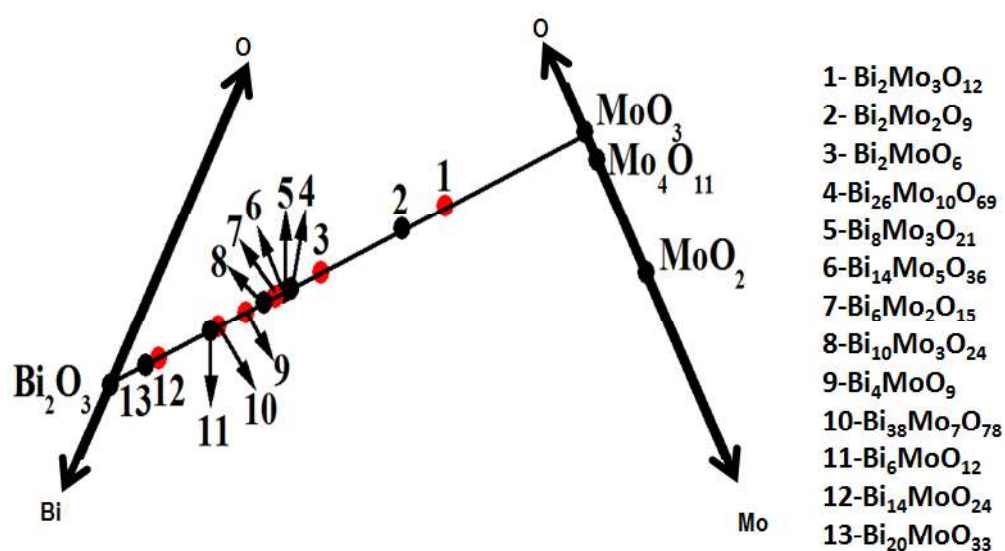


Fig. 3.6 Compounds reported in the Bi_2O_3 - MoO_3 pseudo binary system

a. $\text{Bi}_{20}\text{MoO}_{33}$

The existence of this Bi_2O_3 rich compound was first reported by Sillen and Lundborg [30] based on the studies involving XRD. The presence of this compound was indicated in the later studies by Kohlmuller and Badaud also [31]. However, Egashira et al. [32] carried out a detailed analysis of the data reported by Sillen and Lundborg [30] and showed that the XRD pattern attributed to $\text{Bi}_{20}\text{MoO}_{33}$ was that of

a mixture of the XRD patterns of Bi_2O_3 and $\text{Bi}_{14}\text{MoO}_{24}$ and thus ruled out the existence of $\text{Bi}_{20}\text{MoO}_{33}$.

b. $\text{Bi}_{14}\text{MoO}_{24}$

Egashira et al. [32] showed the existence of this Bi_2O_3 rich compound, during their investigation of the phase diagram of Bi_2O_3 - MoO_3 system. Structural characterization of this compound was later carried out by Ling et al. [33]. The formation of an eutectoid between Bi_2O_3 and $\text{Bi}_{14}\text{MoO}_{24}$ at ~ 998 K to form the solid solution δ (73-100 mol% Bi_2O_3) was suggested by Tomasi et al. [34].

c. $\text{Bi}_6\text{MoO}_{12}$

Belyaev and Smolyaninov [35] reported this compound and according to them, it forms continuous series of solid solutions with Bi_2O_3 as well as with Bi_2MoO_6 . The phase diagrams of Bi_2O_3 - MoO_3 system which were later reported by Bleijenberg et al. [36] and Vitting [37] showed the presence of $\text{Bi}_6\text{MoO}_{12}$ while that reported by Kohlmuller and Badaud [31] did not include it. Kohlmuller and Badaud [31] reported the composition corresponding to $\text{Bi}_6\text{MoO}_{12}$ to be falling within a solid solution with a composition of ~ 75 to 85 mol% Bi_2O_3 and melting congruently at 1253 K.

d. Bi_4MoO_9

The presence of Bi_4MoO_9 was first indicated by Gattow [38] based on their studies involving XRD and DTA. During their studies on Bi_2O_3 - MoO_3 system, Belyaev and Smolyaninov [35] observed the existence of a solid solution between $\text{Bi}_6\text{MoO}_{12}$ and Bi_2MoO_6 with a minimum at 33.3 mol% MoO_3 at 1203 K. They showed this corresponded to the composition of Bi_4MoO_9 and hence ruled out the existence of this compound.

e. $\text{Bi}_{38}\text{Mo}_7\text{O}_{78}$

Investigations of the Bi_2O_3 -rich section of the system by Buttrey et al. [39] using XRD and high resolution electron microscopy showed the presence of a new phase of composition $\text{Bi}_{38}\text{Mo}_7\text{O}_{78}$ with a defective fluorite structure. They determined its lattice parameters and ascribed it to be the same phase as described previously as $\text{Bi}_6\text{MoO}_{12}$. It is to be pointed out that Buttrey et al. [39] prepared $\text{Bi}_{38}\text{Mo}_7\text{O}_{78}$ by solid state reaction between Bi_2O_3 and MoO_3 at 1123 K in air while the earlier investigators [32, 36] prepared $\text{Bi}_6\text{MoO}_{12}$ by the reaction between the oxides at 873 K in air. $\text{Bi}_{38}\text{Mo}_7\text{O}_{78}$ was structurally characterized by Spinolo and Tomasi [40] and Sharma et al. [41]. Based on the studies involving DTA and impedance spectroscopy, Tomasi et al. [34] suggested an eutectoid reaction between $\text{Bi}_{14}\text{MoO}_{24}$ and $\text{Bi}_{38}\text{Mo}_7\text{O}_{78}$ at ~ 1063 K to form the solid solution δ (73-100 mol% Bi_2O_3). Tomasi et al. [34] also indicated the existence of a wide non stoichiometry in $\text{Bi}_{38}\text{Mo}_7\text{O}_{78}$.

f. $\text{Bi}_{10}\text{Mo}_3\text{O}_{24}$

The existence of $\text{Bi}_{10}\text{Mo}_3\text{O}_{24}$ was reported by Vila et al. [42] and their work showed it to be appearing as stable phase at 823 K and decomposing to $\text{Bi}_{38}\text{Mo}_7\text{O}_{78}$ and a high temperature solid solution at 1093 K. The structural characterization of this compound was later carried out by Galy et al. [43].

g. $\text{Bi}_6\text{Mo}_2\text{O}_{15}$

Based on the studies involving growth of single crystals and their characterization, Miyazawa et al. [44] reported a new compound of composition $\text{Bi}_6\text{Mo}_2\text{O}_{15}$ belonging to the monoclinic system and melting congruently at 1243 ± 5 K. Egashira et al. [32] also reported this compound and indicated the formation of an

eutectic between it and $\text{Bi}_6\text{MoO}_{12}$ at 1223 K. They also suggested this compound to be undergoing a phase transition at around 1023 K. Boon and Metselaar [45] reported the phase transition temperature to be between 973 and 1073 K. Vila et al. [46] studied the polymorphism and electrical properties of $\text{Bi}_6\text{Mo}_2\text{O}_{15}$. They observed the transition of $\text{Bi}_6\text{Mo}_2\text{O}_{15}$ to a $[\text{Bi}_{12}\text{O}_{14}]$ based columnar structured phase which belong to the high temperature solid solution at around 973 K. This solid solution was also reported to undergo an irreversible transition into another columnar type solid solution phase at ~ 1133 K.

h. $\text{Bi}_8\text{Mo}_3\text{O}_{21}$ and $\text{Bi}_{14}\text{Mo}_5\text{O}_{36}$

The presence of these two compounds was observed by Vila et al. [47]. Their investigations showed these compounds to be appearing as stable phases at temperatures close to 853 K. They found these compounds transformed to the high temperature solid solution at temperatures higher than 923 K.

i. Bi_2MoO_6

Zemann [48] reported this compound belonging to orthorhombic system. Although, subsequent investigators reported it to be congruently melting [31, 35, and 36], studies by Erman et al. [49] and Chen and Smith [50] showed it to be peritectically decomposing to liquid rich in MoO_3 and the solid solution with composition 1.26:1 $\text{Bi}_2\text{O}_3:\text{MoO}_3$ at ~ 1220 K. A high temperature modification of this compound was first reported by Blasse [51]. Later work by Erman et al. [52] showed three polymorphic forms of this compound to be present: i) γ - the low temperature phase (orthorhombic structure), ii) γ'' - the intermediate phase (tetragonal structure) and iii) γ' - the high temperature phase (monoclinic structure).

Table 3.2 Literature data on Bi₂O₃-MoO₃ pseudo binary system

Compound	Author	Preparation route	Experimental techniques employed	Observations
Bi ₂₀ MoO ₃₃	Sillen and Lundborg [30] Kohlmuller and Badaud[31] Egashira et al. [32]	Solid state reaction between Bi ₂ O ₃ and MoO ₃	XRD [30-32] DTA [31, 32]	<ul style="list-style-type: none"> ➤ Reported the presence of this compound [30, 31] ➤ Observed that Bi₂₀MoO₃₃ consisted of a mixture of Bi₂O₃ and Bi₁₄MoO₂₄ [32]
Bi ₁₄ MoO ₂₄	Ling et al. [33]Tomasi et al. [34] Spinolo and Tomasi [40]	Solid state reaction between Bi ₂ O ₃ and MoO ₃ at 1073 K	DTA [34] XRD [33, 34, 40] Impedance spectroscopy [34]	<ul style="list-style-type: none"> ➤ Structural characterizations of Bi₁₄MoO₂₄ [33, 40] ➤ Eutectoid reaction with Bi₂O₃ to form the solid solution δ (73-100 mol% Bi₂O₃): ~998 K [34] ➤ Eutectoid reaction with Bi₃₈Mo₇₈ to form the solid solution δ (73-100 mol% Bi₂O₃): ~1063 K [34]
Bi ₆ MoO ₁₂	Kohlmuller and Badaud[31] Egashira et al. [32] Belyaev & Smolyaninov [35] Bleijenberg et al. [36] Erman et al. [49]	Solid state reaction between Bi ₂ O ₃ and MoO ₃ at 873 K [36, 32] Fusion of oxide mixtures followed by recrystallization [35] Fusion of oxide mixtures followed by quenching and subsequent heating at 1023 K [49]	XRD and DTA[31, 32, 36, 49] Visual polythermal method [35]	<ul style="list-style-type: none"> ➤ Congruent melting point :1253 K [31], 1263 K [35], 1268 K [36] ➤ Bi₆MoO₁₂ is within the solid solution field of δ-Bi₂O₃ [49] ➤ The solid solutions based on δ-Bi₂O₃ possess a maximum at 76-77 mol% Bi₂O₃ corresponding to 3:1 Bi₂O₃:MoO₃ (i.e. Bi₆MoO₁₂) [31] ➤ Eutectic with Bi₆Mo₂O₁₅ : 1223 K [32]

Bi ₄ MoO ₉	Belyaev and Smolyaninov [35] Gattow [38]	Fusion of oxide mixtures followed by crystallization [35] Coprecipitation method [38]	Visual polythermal method [35] XRD and DTA[38]	<ul style="list-style-type: none"> ➤ Melting point: 1193 K [38] ➤ The minimum of Bi₆MoO₁₂-Bi₂MoO₆ solid solution corresponding to the composition of Bi₄MoO₉ [35]
Bi ₃₈ Mo ₇ O ₇₈	Tomasi et al. [34] Buttrey et al. [39] Spinolo and Tomasi [40]	Solid state reaction between Bi ₂ O ₃ and MoO ₃ at 1113 K [39], 1073 K [34, 40]	XRD [34, 39, 40] SAED [39] DTA [34] Impedance spectroscopy [34]	<ul style="list-style-type: none"> ➤ Characterized Bi₃₈Mo₇O₇₈ and ascribed it as the same phase as Bi₆MoO₁₂ [39] ➤ Suggested non - stoichiometry [34] ➤ Structural characterizations of Bi₃₈Mo₇O₇₈ [40]
Bi ₁₀ Mo ₃ O ₂₄	Vila et al. [42]	Wet chemical method	XRD Impedance spectroscopy	<ul style="list-style-type: none"> ➤ Appears as stable phase at 823 K ➤ Decomposes at temperatures above 1023 K to Bi₃₈Mo₇O₇₈ and a high temperature solid solution polymorph
Bi ₆ Mo ₂ O ₁₅	Egashira [32] Miyazawa et al. [44] Boon and Metselaar [45] Vila et al. [46]	Single crystal growth by Czochralski method [44] Solid state reaction at 873 K [32], 1073 K [45] Wet chemical method [46]	DTA [32, 46] XRD [32, 44-46] Impedance spectroscopy [45, 46]	<ul style="list-style-type: none"> ➤ Congruent melting point : 1243 K [44] ➤ Appears as stable phase at 773 K [32] ➤ Phase transition at 1023 K [32], 973-1073 K [45] ➤ Eutectic with Bi₆MoO₁₂ : 1223 K [32] ➤ Transforms to a high temperature solid solution polymorph at 973 K [46]
Bi _{11,4} Mo ₅ O ₃₆	Vila et al. [47]	Wet chemical method	XRD Impedance spectroscopy	<ul style="list-style-type: none"> ➤ Formation temperature between 823 to 853 K ➤ Transforms to a high temperature solid solution polymorph at 923 K
Bi ₈ Mo ₃ O ₂₁	Vila et al. [47]	Wet chemical method	XRD	<ul style="list-style-type: none"> ➤ Formation temperature between 853 to 903 K

			Impedance spectroscopy	
Bi ₂ MoO ₆	Egashira et al. [32] Belyaev and Smolyaninov [35] Bleijenberg et al. [36] Erman et al. [49, 52] Chen and Smith [50] Blasse [51] Watanabe and Kodama [53] Lim et al. [55]	Fusion of oxide mixtures followed by crystallization [35] Fusion of oxide mixtures followed by quenching and subsequent heating at 873 K [49, 52] Fusion of oxide mixtures followed by annealing at 873-943 K [50] Solid state reaction at 873 K [36, 32], 1023 K [51], 800 K [53] Single crystal growth [55]	Visual polythermal method [35] DTA [32, 36, 49, 50, 53, 55] XRD [32, 36, 49, 50, 51, 53] High temperature XRD [52] Dilatometry [53] DSC [53]	<ul style="list-style-type: none"> ➤ Transforms to a high temperature solid solution polymorph at 943 K ➤ Congruent melting point : 1243 K [35], 1211 K [36] ➤ Eutectic with Bi₂Mo₃O₁₂ : 909 K [35] ➤ Eutectic with Bi₂Mo₂O₉: 909 K [49, 50] ➤ Peritectic decomposition: 1193 K [35], 1173 K [36], 1220 K [50] ➤ Observed only the low temperature orthorhombic (γ) phase [36] ➤ Observed three polymorphic forms [49, 52] ➤ Observed the high temperature modification (γ' phase) [51] ➤ Observed only γ and γ' modifications; γ to γ' transition at 873 K and irreversible [32] ➤ Transition of the low temperature phase (γ) to the intermediate phase (γ'') at : 593-793 K [53], 877 K [54], 533 K [55] and is reversible ➤ Transition of the intermediate phase (γ'') to the high temperature phase (γ') at 823-913 K [52], 913 to 943 K [53], 918 K [55] and is irreversible ➤ $\Delta H_{transition}$ for γ to γ'' transition : 0.1 kcal/mol [52] ➤ $\Delta H_{transition}$ for γ'' to γ' transition: 3.2 kcal/mol [53]
Bi ₂ Mo ₂ O ₉	Erman et al. [49, 57, 58] Chen and Smith [50] Egashira et al. [32]	Fusion of oxide mixtures followed by crystallization and by coprecipitation [49, 57,	XRD [32, 49, 50, 57, 58] DTA [32, 49, 50]	<ul style="list-style-type: none"> ➤ Structural characterization and determination of lattice parameters [58] ➤ Peritectic decomposition: 938 K [49], 955 K [50], 923 K [49, 57]

			58] Fusion of oxide mixtures followed by annealing at 873-943 K [50] Solid state reaction at 873 K [32]		<ul style="list-style-type: none"> ➤ Eutectic with Bi_2MoO_6: 909 K [57] ➤ Eutectic with $\text{Bi}_2\text{Mo}_3\text{O}_{12}$: 913 K [32], 909 K [57] ➤ Stable range: 813 to 938 K [32]
$\text{Bi}_2\text{Mo}_3\text{O}_{12}$	Zambonini [61] Belyaev and Smolyaninov [35] Bleijenberg et al. [36] Erman et al. [49, 57] Chen and Smith [50] Egashira et al. [32] Miyazawa et al. [44]	Visual polythermal method [35] XRD [32, 36, 49, 50, 57] DTA [36, 49, 50]	Fusion of oxide mixtures followed by recrystallization [35, 49, 57] Solid state reaction at 873 K [36, 32] Fusion of oxide mixtures followed by annealing at 873-943 K [50] Coprecipitation [57] Single crystal growth by Czochralski method [44]	<ul style="list-style-type: none"> ➤ Reported the existence [61] ➤ Congruent melting point : 921 K [35], 949 K [36], 935 K [50], 943 K [44] ➤ Eutectic with MoO_3 : 909 K [49, 57], 891 K [35, 50] ➤ Eutectic with $\text{Bi}_2\text{Mo}_2\text{O}_9$: 913 K [32] ➤ Eutectic with Bi_2MoO_6: 909 K [35, 57] ➤ Peritectic decomposition: 913 K [49] 	
Solid solutions	Tomasi et al. [34] Erman et al. [49] Chen and Smith [50] Vannier et al. [63, 64] Buttrey et al. [65]	DTA [34, 49] XRD [49, 50, 63, 64, 66, 67] Impedance spectroscopy	Fusion of oxide mixtures followed by quenching and subsequent heating at 1023 K [49]	<ul style="list-style-type: none"> ➤ Observed the following solid solutions with variable lattice parameters [49] <ul style="list-style-type: none"> a) ϵ- phase (40 to 60 mol% Bi_2O_3) b) θ- phase (60 to ~70 mol% Bi_2O_3) c) Ω-phase (~70 to 75 mol% Bi_2O_3) 	

	<p>Enjalbert et al. [66] Huveet al. [67]</p>	<p>Fusion of oxide mixtures followed by annealing at 873-943 K [50] Solid state reaction between Bi₂O₃ and MoO₃ [34, 63-66]</p>	<p>[63, 64, 34] SAED [65, 67] NPD [64]</p>	<p>d) η-phase (~80 to ~90 mol% Bi₂O₃) e) δ-phase (60 to ~97 mol% Bi₂O₃) ➤ Observed the ε phase (13 Bi₂O₃:10MoO₃) [49, 50] ➤ Structural investigation of Bi_xMo₁₀O₆₉ (x = 25.75 to 27.75) and confirmed the solid solubility range as between 2.6 ≤ Bi/Mo ≤ 2.8 [63-65] ➤ Determined the the solid solution range of Bi_xMo₁₀O₆₉ with x = 28.6 to 35 [66] ➤ Confirmed the solid solution range of Bi_xMo₁₀O₆₉ with x = 26 to 28 [67] ➤ All compositions within this solid solution field are monoclinic [63]. ➤ Observed a lens shaped biphasic region separating the liquid and solid solution field (~84 to 100% Bi₂O₃) [34]</p>
--	--	---	--	--

Several studies have been carried out on the polymorphic transformations of Bi_2MoO_6 [32, 49, 52-56], but the reported transition temperatures are in disagreement. Erman et al. [52] reported a reversible transition of γ to γ'' at temperatures between 593 K and 793 K and an irreversible transition of γ'' to γ' at temperatures between 823 K and 913 K based on high temperature X-ray diffraction studies whereas Lim et al. [55] reported 533 and 918 K as the corresponding transition temperatures. Polymorphism of the compound was not observed in the studies of Bleijenberg et al. [36] and Chen and Smith [50]. They observed only the γ phase of Bi_2MoO_6 . Egashira et al. [32] observed only the γ and γ' phases of Bi_2MoO_6 with a transition temperature ~ 873 K. Studies by Watanabe and Kodama [53, 54] showed the γ to γ'' transition (877 K) to be reversible while γ'' to γ' transition (913 K) to be irreversible and reported the corresponding enthalpies of transitions as 0.42 kJ mol^{-1} and 13.4 kJ mol^{-1} , respectively. Buttrey et al. [56] also reported the γ to γ'' transition to be reversible and occurring at ~ 840 K and the γ'' to γ' transition to be irreversible and occurring at ~ 880 K.

j. $\text{Bi}_2\text{Mo}_2\text{O}_9$

Erman et al. [57] reported the existence of $\text{Bi}_2\text{Mo}_2\text{O}_9$ which was formed by the peritectic reaction between MoO_3 rich liquid and Bi_2MoO_6 at 923 K. Structure of this compound was established by them in their later study [58]. They showed that $\text{Bi}_2\text{Mo}_2\text{O}_9$ formed an eutectic with $\text{Bi}_2\text{Mo}_3\text{O}_{12}$ at 909 K with a eutectic composition of 72.5 mol% MoO_3 . Erman et al. [49] reported that the peritectic decomposition of $\text{Bi}_2\text{Mo}_2\text{O}_9$ was erroneously considered as the eutectic between $\text{Bi}_2\text{Mo}_3\text{O}_{12}$ and Bi_2MoO_6 in the studies reported in references 31, 35, and 36 and did not include the presence of $\text{Bi}_2\text{Mo}_2\text{O}_9$ in the phase diagrams reported in these works. Later studies by

Chen and Smith [50] confirmed the results of Erman et al. [49]. Results of the studies made by Egashira et al. [32] were also similar except for small differences in the eutectic and peritectic temperatures. Investigations by Batist et al. [59] and Grzybowska et al. [60] on thermal stability of $\text{Bi}_2\text{Mo}_2\text{O}_9$ showed it to be decomposing to $\text{Bi}_2\text{Mo}_3\text{O}_{12}$ and Bi_2MoO_6 below 823 K. Investigations by Egashira et al. [32] showed $\text{Bi}_2\text{Mo}_2\text{O}_9$ to be stable in a very narrow range of temperature viz., 813 to 938 K and it disproportionated to form $\text{Bi}_2\text{Mo}_3\text{O}_{12}$ and Bi_2MoO_6 at 813 K.

k. $\text{Bi}_2\text{Mo}_3\text{O}_{12}$

Zambonini et al. [61] reported the presence of this compound and structurally characterized it. Later, several authors [32, 35-37, 44, 49, 50, 57, 62] have studied this compound and showed it to be congruently melting at ~930 K. Erman et al. [57] reported an eutectic to be formed between $\text{Bi}_2\text{Mo}_3\text{O}_{12}$ and MoO_3 and this has been supported by the later works of Bleijenberg et al. [36], Egashira et al. [32] and Chen [62].

l. Solid solutions in the Bi_2O_3 - MoO_3 system

Many investigators have observed the presence of solid solutions in the Bi_2O_3 rich part of the system [32, 34-36, 49, 50]. Erman et al. [49] reported the presence of five solid solutions above 773 K in the composition ranges of a) 40 to 60 mol% Bi_2O_3 , b) 60 to ~70 mol% Bi_2O_3 , c) ~70 to 75 mol% Bi_2O_3 , d) ~80 to ~90 mol% Bi_2O_3 and e) a high temperature phase with 60 to ~97 mol% Bi_2O_3 . Studies by Chen and Smith [50] also showed the presence of the solid solution at around 56.5 mol% Bi_2O_3 . Erman et al. [49] also reported that the high temperature phase with ~75 mol% Bi_2O_3 had a melting point maximum and that with ~67 mol% Bi_2O_3 had the minimum. They suggested that these compositions corresponded to the compositions of

$\text{Bi}_6\text{MoO}_{12}$ and Bi_4MoO_9 reported by Belyaev and Smolyaninov [35] and Gattow [38], respectively. Studies by Tomasi et al. [34] also showed the existence of a high temperature solid solution with the composition ranging from ~73 to 100 mol% Bi_2O_3 and with a defective fluorite structure. They observed that a lens shaped biphasic region separated this solid solution field from the liquid phase. They also reported that both $\text{Bi}_{14}\text{MoO}_{24}$ and $\text{Bi}_{38}\text{Mo}_7\text{O}_{78}$ were stable below this solid solution field.

Vannier et al. [63, 64] observed the domain of a solid solution around $\text{Bi}_x\text{Mo}_{10}\text{O}_{69}$ ($x = 25.75$ to 27.75) with a structure based on $[\text{Bi}_{12}\text{O}_{14}]$ columns, which was reported earlier by Erman et al. [49] and Chen & Smith [50]. The composition of the parent compound of this solid solution field was formulated as $\text{Bi}_{26}\text{Mo}_{10}\text{O}_{69}$. They also observed that the structure of compositions within this solid solution field to be monoclinic. These results were later confirmed by Buttrey et al. [65]. However, Enjalbert et al. [66] disputed the stoichiometry range of the solid solution and based on crystallographic investigations, they proposed its composition as with $x = 28.6$ to 35.0 . Huve et al. [67] carried out structural analysis of the family of the compounds belonging to the $[\text{Bi}_{12}\text{O}_{14}]$ columns and confirmed the solid solution field to be limited within the range of $x = 26$ to 28 .

Phase diagrams of the Bi_2O_3 - MoO_3 system and the liquidus boundaries are reported in references [31, 32, 34-36, 49, 50]. It is to be pointed out that in the course of the investigations of the system by employing various techniques, new compounds and solid solutions have been identified. Hence, phase diagrams reported by earlier investigators were not complete. Buttrey [68] in 2008 proposed a phase diagram of this system by taking into account of the data available in literature. Although it shows the presence of $\text{Bi}_2\text{Mo}_3\text{O}_{12}$, $\text{Bi}_2\text{Mo}_2\text{O}_9$, Bi_2MoO_6 , $\text{Bi}_8\text{Mo}_3\text{O}_{21}$, $\text{Bi}_{14}\text{Mo}_5\text{O}_{36}$, $\text{Bi}_6\text{Mo}_2\text{O}_{15}$, $\text{Bi}_{10}\text{Mo}_3\text{O}_{24}$, $\text{Bi}_{38}\text{Mo}_7\text{O}_{78}$ and $\text{Bi}_{14}\text{MoO}_{24}$, presence of $\text{Bi}_6\text{MoO}_{12}$ had not

It is clear from the literature data that MoO₃ rich section of the system consists of only three ternary compounds, namely, Bi₂Mo₃O₁₂, Bi₂Mo₂O₉ and Bi₂MoO₆. The Bi₂O₃ rich section of the system is not well established. Although several compounds were reported in the past, subsequent studies have shown the presence of the following compounds in this part of the system: Bi₈Mo₃O₂₁, Bi₁₄Mo₅O₃₆, Bi₆Mo₂O₁₅, Bi₁₀Mo₃O₂₄, Bi₃₈Mo₇O₇₈, Bi₆MoO₁₂ and Bi₁₄MoO₂₄. It is known that a solid solution Bi_xMo₁₀O₆₉ (x = 26 to 28) exists at high temperatures. This solid solution will be designated as ‘Bi₂₆Mo₁₀O₆₉’ further in the discussions. Bi₈Mo₃O₂₁, Bi₁₄Mo₅O₃₆ and Bi₆Mo₂O₁₅ appear as stable phases at temperatures between 773 and 873 K and they transform to ‘Bi₂₆Mo₁₀O₆₉’ at higher temperatures although the exact transformation temperatures are not known. The exact temperatures at which these ternary compounds appear as stable phases and the corresponding invariant reactions at these temperatures are also not known. Since, the phase diagram reported by Buttrey [68] does not include the presence of Bi₆MoO₁₂, existence of this compound also need to be studied.

Although the pseudo binary phase diagram of Bi₂O₃-MoO₃ system has been investigated by several authors, no data exist on the ternary Bi-Mo-O system and the thermochemical properties of the ternary compounds of the system are not available.

3.3 Experimental details

3.3.1 Materials

Bi₂O₃ powder (99.99% purity on metal basis, M/s Alfa Aesar, USA), Bi powder (99.9% purity on metal basis, M/s Alfa Aesar, USA) and Mo powder (99.9% purity on metal basis, M/s Alfa Aesar, USA) were used. Bi₂O₃ powder was calcined at 1023 K in air for about 6 h to remove any carbonate impurity and adsorbed moisture present in it. The calcined powder was stored in a desiccator. MoO₃ powder

was prepared by heating ammonium heptamolybdate tetrahydrate (99.96% purity on metal basis, M/s Sigma-Aldrich, USA) at 723 K in air for 24 h. MoO₂ was prepared by the reduction of MoO₃ at 823 K for 16 h under flowing hydrogen gas saturated with water vapour. All the compounds were characterized by an X-ray diffractometer (M/s Inel, France) with Cu K_α radiation and graphite monochromator. The XRD patterns were matched with the corresponding PCPDF patterns.

3.3.2 Preparation of ternary compounds

The ternary compounds reported to be present in the Bi₂O₃-MoO₃ pseudo binary system were prepared by the solid state reaction between Bi₂O₃ and MoO₃ in air. For this, stoichiometric amounts of Bi₂O₃ and MoO₃ were homogeneously mixed and made into pellets. The pellets were placed in alumina crucibles and heated at different chosen temperatures. The pellets were ground at the end of half the total duration of heating. The powders were homogenized, repelletized and heated again. The samples were quenched to room temperature and the phases in them were characterized by XRD. Although the mass loss of the samples while heating in open crucibles were very low (~0.01 to 0.03%), the ternary compounds were also prepared under vacuum by placing the alumina crucibles containing the sample pellets in small volume (~20 ml) evacuated and sealed quartz ampoules. The ampoules were kept inside a constant temperature zone of the furnace and heated at the chosen temperature. The experimental details are given in Table 3.3.

3.3.3 Phase equilibration studies

3.3.3.1 Equilibrations of samples with compositions in the Bi₂O₃-MoO₃ pseudo binary line

To examine the possible existence of any new compound other than those reported in the Bi₂O₃-MoO₃ pseudo binary system, samples with different molar

ratios of Bi_2O_3 and MoO_3 were prepared and equilibrated. The overall composition of each sample was chosen such that it would correspond to a composition between those of two reported adjacent ternary compounds. Initial mixture of Bi_2O_3 and MoO_3 were thoroughly ground and made into pellets. The pellets were then kept inside alumina crucibles and enclosed in quartz ampoules under vacuum. Samples were equilibrated for prolonged periods at 773, 873 and 1023 K. After the equilibration, samples were quenched to room temperature and the products formed were identified by XRD. The details of these experiments are given in Table 3.4.

Table 3.3 Preparation of ternary compounds in the Bi_2O_3 - MoO_3 system

Compound	Molar ratios of Bi_2O_3 and MoO_3	Temperature	Duration of heating	Product formed*
$\text{Bi}_2\text{Mo}_3\text{O}_{12}$	$1\text{Bi}_2\text{O}_3 : 3\text{MoO}_3$	873 K	48 h	$\text{Bi}_2\text{Mo}_3\text{O}_{12}$
$\text{Bi}_2\text{Mo}_2\text{O}_9$	$1\text{Bi}_2\text{O}_3 : 2\text{MoO}_3$	773 K	48 h	$\text{Bi}_2\text{Mo}_3\text{O}_{12}$, γ - Bi_2MoO_6 (orthorhombic phase)
		873 K	48 h	$\text{Bi}_2\text{Mo}_2\text{O}_9$
Bi_2MoO_6	$1\text{Bi}_2\text{O}_3 : 1\text{MoO}_3$	773 K	48 h	γ - Bi_2MoO_6 (orthorhombic phase)
		873 K	48 h	γ' - Bi_2MoO_6 (monoclinic phase)
$\text{Bi}_6\text{Mo}_2\text{O}_{15}$	$3\text{Bi}_2\text{O}_3 : 2\text{MoO}_3$	873 K	48 h	$\text{Bi}_6\text{Mo}_2\text{O}_{15}$
$\text{Bi}_{10}\text{Mo}_3\text{O}_{24}$	$5\text{Bi}_2\text{O}_3 : 3\text{MoO}_3$	1023 K	48 h	$\text{Bi}_{10}\text{Mo}_3\text{O}_{24}$
$\text{Bi}_6\text{MoO}_{12}$	$3\text{Bi}_2\text{O}_3 : 1\text{MoO}_3$	873 K	48 h	$\text{Bi}_6\text{MoO}_{12}$
$\text{Bi}_{38}\text{Mo}_7\text{O}_{78}$	$19\text{Bi}_2\text{O}_3 : 7\text{MoO}_3$	1023 K	48 h	$\text{Bi}_{38}\text{Mo}_7\text{O}_{78}$
$\text{Bi}_{14}\text{MoO}_{24}$	$7\text{Bi}_2\text{O}_3 : 1\text{MoO}_3$	873 K	48 h	$\text{Bi}_{14}\text{MoO}_{24}$
$\text{Bi}_{26}\text{Mo}_{10}\text{O}_{69}$	$13\text{Bi}_2\text{O}_3 : 5\text{MoO}_3$	1023 K	48 h	' $\text{Bi}_{26}\text{Mo}_{10}\text{O}_{69}$ '

**Same phases were obtained at the end of 24 h of heating*

As mentioned earlier, Buttrey et al. [39] considered $\text{Bi}_{38}\text{Mo}_7\text{O}_{78}$ to be the same as the compound $\text{Bi}_6\text{MoO}_{12}$, although their compositions are significantly different ($3\text{Bi}_2\text{O}_3 : 1\text{MoO}_3$ in $\text{Bi}_6\text{MoO}_{12}$ and $2.71\text{Bi}_2\text{O}_3 : \text{MoO}_3$ in $\text{Bi}_{38}\text{Mo}_7\text{O}_{78}$) and XRD patterns of the two compounds have marked difference. It is also to be pointed

out that subsequent to the report by Buttrey et al. [39], no further data has been reported in literature about these compounds. To verify the existence of $\text{Bi}_6\text{MoO}_{12}$, samples with different molar ratios of Bi_2O_3 and MoO_3 , whose compositions lie between those of $\text{Bi}_{10}\text{Mo}_3\text{O}_{24}$ and $\text{Bi}_{14}\text{MoO}_{24}$, were equilibrated. The sample mixtures were thoroughly ground, made into pellets, kept in alumina crucibles and sealed in evacuated quartz ampoules. The ampoules were equilibrated at 773, 873 and 1023 K for prolonged duration. After the equilibration, samples were quenched to room temperature. The details of the overall compositions chosen and the products identified by XRD are given in Table 3.4.

3.3.3.2 Equilibrations of samples with compositions in the line joining Bi_2O_3 and MoO_2

Samples containing different molar ratios of Bi_2O_3 and MoO_2 were equilibrated for prolonged periods to examine the existence of any ternary compound involving Bi_2O_3 and MoO_2 . For this, mixtures of Bi_2O_3 and MoO_2 were compacted into pellets and taken in alumina crucibles. The crucibles were then kept enclosed in evacuated quartz ampoules and subjected to long term equilibration at 773 and 1023 K. After the equilibrations, samples were quenched to room temperature and the products were identified by XRD. The results obtained from these equilibration experiments are given in Table 3.5.

3.3.3.3 Partial reduction of ternary compounds followed by long term equilibrations

To obtain preliminary information on the coexisting phases in the Bi-Mo-O system, the ternary compounds were subjected to partial reduction under flowing hydrogen gas at 773 K for about 15 min.

Table 3.4 Details of equilibrations of samples with mixtures of Bi₂O₃ and MoO₃

No	Composition chosen	Products obtained after equilibration*		
		At 773 K (960 h)	At 873 K (720 h)	At 1023 K (480 h)
1	1Bi ₂ O ₃ : 7MoO ₃ (between MoO ₃ and Bi ₂ Mo ₃ O ₁₂)	MoO ₃ , Bi ₂ Mo ₃ O ₁₂	MoO ₃ , Bi ₂ Mo ₃ O ₁₂	-
2	1Bi ₂ O ₃ : 2.5MoO ₃ (between Bi ₂ Mo ₃ O ₁₂ and Bi ₂ Mo ₂ O ₉)	Bi ₂ Mo ₃ O ₁₂ , Bi ₂ MoO ₆	Bi ₂ Mo ₃ O ₁₂ , Bi ₂ Mo ₂ O ₉	-
3	1Bi ₂ O ₃ : 1.4MoO ₃ (between Bi ₂ Mo ₂ O ₉ and Bi ₂ MoO ₆)	Bi ₂ Mo ₃ O ₁₂ , Bi ₂ MoO ₆	Bi ₂ Mo ₂ O ₉ , Bi ₂ MoO ₆	-
4	1.08Bi ₂ O ₃ : 1MoO ₃ (between Bi ₂ MoO ₆ and 'Bi ₂₆ Mo ₁₀ O ₆₉ ')	Bi ₂ MoO ₆ , Bi ₆ Mo ₂ O ₁₅	Bi ₂ MoO ₆ , Bi ₆ Mo ₂ O ₁₅	Bi ₂ MoO ₆ , 'Bi ₂₆ Mo ₁₀ O ₆₉ '
5	1.17Bi ₂ O ₃ : 1MoO ₃ (between Bi ₂ MoO ₆ and 'Bi ₂₆ Mo ₁₀ O ₆₉ ')	Bi ₂ MoO ₆ , Bi ₆ Mo ₂ O ₁₅	Bi ₂ MoO ₆ , Bi ₆ Mo ₂ O ₁₅	Bi ₂ MoO ₆ , 'Bi ₂₆ Mo ₁₀ O ₆₉ '
6	1.25Bi ₂ O ₃ : 1MoO ₃ (between Bi ₂ MoO ₆ and 'Bi ₂₆ Mo ₁₀ O ₆₉ ')	Bi ₂ MoO ₆ , Bi ₆ Mo ₂ O ₁₅	Bi ₂ MoO ₆ , Bi ₈ Mo ₃ O ₂₁	Bi ₂ MoO ₆ , 'Bi ₂₆ Mo ₁₀ O ₆₉ '
7	1.31Bi ₂ O ₃ : 1MoO ₃ (between 'Bi ₂₆ Mo ₁₀ O ₆₉ ' and Bi ₈ Mo ₃ O ₂₁)	Bi ₂ MoO ₆ , Bi ₆ Mo ₂ O ₁₅	Bi ₂ MoO ₆ , Bi ₈ Mo ₃ O ₂₁	Bi ₂ MoO ₆ , 'Bi ₂₆ Mo ₁₀ O ₆₉ '
8	1.32Bi ₂ O ₃ : 1MoO ₃ (between 'Bi ₂₆ Mo ₁₀ O ₆₉ ' and Bi ₈ Mo ₃ O ₂₁)	Bi ₂ MoO ₆ , Bi ₆ Mo ₂ O ₁₅	Bi ₂ MoO ₆ , Bi ₈ Mo ₃ O ₂₁	Bi ₂ MoO ₆ , 'Bi ₂₆ Mo ₁₀ O ₆₉ '
9	1.375Bi ₂ O ₃ : 1MoO ₃ (between Bi ₈ Mo ₃ O ₂₁ and	Bi ₂ MoO ₆ , Bi ₆ Mo ₂ O ₁₅	Bi ₈ Mo ₃ O ₂₁ , Bi ₁₄ Mo ₅ O ₃₆	'Bi ₂₆ Mo ₁₀ O ₆₉ '

	$\text{Bi}_{14}\text{Mo}_5\text{O}_{36}$				
10	1.43 Bi_2O_3 : 1 MoO_3 (between $\text{Bi}_{14}\text{Mo}_5\text{O}_{36}$ and $\text{Bi}_6\text{Mo}_2\text{O}_{15}$)	Bi_2MoO_6 , $\text{Bi}_6\text{Mo}_2\text{O}_{15}$	$\text{Bi}_8\text{Mo}_3\text{O}_{21}$, $\text{Bi}_{14}\text{Mo}_5\text{O}_{36}$		' $\text{Bi}_{26}\text{Mo}_{10}\text{O}_{69}$ '
11	1.47 Bi_2O_3 : 1 MoO_3 (between $\text{Bi}_{14}\text{Mo}_5\text{O}_{36}$ and $\text{Bi}_6\text{Mo}_2\text{O}_{15}$)	Bi_2MoO_6 , $\text{Bi}_6\text{Mo}_2\text{O}_{15}$	$\text{Bi}_{14}\text{Mo}_5\text{O}_{36}$, $\text{Bi}_6\text{Mo}_2\text{O}_{15}$		' $\text{Bi}_{26}\text{Mo}_{10}\text{O}_{69}$ '
12	1.54 Bi_2O_3 : 1 MoO_3 (between $\text{Bi}_6\text{Mo}_2\text{O}_{15}$ and $\text{Bi}_{10}\text{Mo}_3\text{O}_{24}$)	Bi_2MoO_6 , $\text{Bi}_6\text{Mo}_2\text{O}_{15}$	$\text{Bi}_{14}\text{Mo}_5\text{O}_{36}$, $\text{Bi}_6\text{Mo}_2\text{O}_{15}$		' $\text{Bi}_{26}\text{Mo}_{10}\text{O}_{69}$ '
13	1.61 Bi_2O_3 : 1 MoO_3 (between $\text{Bi}_6\text{Mo}_2\text{O}_{15}$ and $\text{Bi}_{10}\text{Mo}_3\text{O}_{24}$)	$\text{Bi}_6\text{Mo}_2\text{O}_{15}$, $\text{Bi}_{10}\text{Mo}_3\text{O}_{24}$	$\text{Bi}_6\text{Mo}_2\text{O}_{15}$, $\text{Bi}_{10}\text{Mo}_3\text{O}_{24}$		' $\text{Bi}_{26}\text{Mo}_{10}\text{O}_{69}$ ', $\text{Bi}_{10}\text{Mo}_3\text{O}_{24}$
14	1.78 Bi_2O_3 : 1 MoO_3 (between $\text{Bi}_{10}\text{Mo}_3\text{O}_{24}$ and ' $\text{Bi}_{38}\text{Mo}_7\text{O}_{78}$ ')	$\text{Bi}_6\text{Mo}_2\text{O}_{15}$, $\text{Bi}_{10}\text{Mo}_3\text{O}_{24}$	$\text{Bi}_6\text{Mo}_2\text{O}_{15}$, $\text{Bi}_{10}\text{Mo}_3\text{O}_{24}$		' $\text{Bi}_{26}\text{Mo}_{10}\text{O}_{69}$ ', $\text{Bi}_{10}\text{Mo}_3\text{O}_{24}$
15	2.01 Bi_2O_3 : 1 MoO_3 (between $\text{Bi}_{10}\text{Mo}_3\text{O}_{24}$ and ' $\text{Bi}_{38}\text{Mo}_7\text{O}_{78}$ ')	$\text{Bi}_{10}\text{Mo}_3\text{O}_{24}$, $\text{Bi}_6\text{MoO}_{12}$	$\text{Bi}_{10}\text{Mo}_3\text{O}_{24}$, $\text{Bi}_6\text{MoO}_{12}$		$\text{Bi}_{10}\text{Mo}_3\text{O}_{24}$, ' $\text{Bi}_{38}\text{Mo}_7\text{O}_{78}$ '
16	2.84 Bi_2O_3 : 1 MoO_3 (between ' $\text{Bi}_{38}\text{Mo}_7\text{O}_{78}$ ' and $\text{Bi}_6\text{MoO}_{12}$)	$\text{Bi}_{10}\text{Mo}_3\text{O}_{24}$, $\text{Bi}_6\text{MoO}_{12}$	$\text{Bi}_{10}\text{Mo}_3\text{O}_{24}$, $\text{Bi}_6\text{MoO}_{12}$		$\text{Bi}_{10}\text{Mo}_3\text{O}_{24}$, ' $\text{Bi}_{38}\text{Mo}_7\text{O}_{78}$ '
17	6.125 Bi_2O_3 : 1 MoO_3 (between $\text{Bi}_6\text{MoO}_{12}$ and $\text{Bi}_{14}\text{MoO}_{24}$)	$\text{Bi}_{10}\text{Mo}_3\text{O}_{24}$, $\text{Bi}_6\text{MoO}_{12}$	$\text{Bi}_{10}\text{Mo}_3\text{O}_{24}$, $\text{Bi}_6\text{MoO}_{12}$		$\text{Bi}_{10}\text{Mo}_3\text{O}_{24}$, ' $\text{Bi}_{38}\text{Mo}_7\text{O}_{78}$ '
18	6.82 Bi_2O_3 : 1 MoO_3 (between $\text{Bi}_6\text{MoO}_{12}$ and $\text{Bi}_{14}\text{MoO}_{24}$)	$\text{Bi}_6\text{MoO}_{12}$, $\text{Bi}_{14}\text{MoO}_{24}$	$\text{Bi}_6\text{MoO}_{12}$, $\text{Bi}_{14}\text{MoO}_{24}$		' $\text{Bi}_{38}\text{Mo}_7\text{O}_{78}$ ', $\text{Bi}_{14}\text{MoO}_{24}$
19	10.44 Bi_2O_3 : 1 MoO_3 (between $\text{Bi}_{14}\text{MoO}_{24}$ and	$\text{Bi}_6\text{MoO}_{12}$, $\text{Bi}_{14}\text{MoO}_{24}$	$\text{Bi}_6\text{MoO}_{12}$, $\text{Bi}_{14}\text{MoO}_{24}$		' $\text{Bi}_{38}\text{Mo}_7\text{O}_{78}$ ', $\text{Bi}_{14}\text{MoO}_{24}$

	Bi ₂ O ₃)				
20	10.53Bi ₂ O ₃ : 1MoO ₃ (between Bi ₁₄ MoO ₂₄ and Bi ₂ O ₃)	Bi ₁₄ MoO ₂₄ , Bi ₂ O ₃	Bi ₁₄ MoO ₂₄ , Bi ₂ O ₃	Bi ₁₄ MoO ₂₄ , Bi ₂ O ₃	Bi ₁₄ MoO ₂₄ , Bi ₂ O ₃
21	10Bi ₂ O ₃ : 1MoO ₃ (between Bi ₁₄ MoO ₂₄ and Bi ₂ O ₃)	Bi ₁₄ MoO ₂₄ , Bi ₂ O ₃	Bi ₁₄ MoO ₂₄ , Bi ₂ O ₃	Bi ₁₄ MoO ₂₄ , Bi ₂ O ₃	Bi ₁₄ MoO ₂₄ , Bi ₂ O ₃
Equilibrations to verify the existence of Bi₆MoO₁₂					
22	4.25Bi ₂ O ₃ : 1MoO ₃ (between Bi ₁₄ MoO ₂₄ and Bi ₆ MoO ₁₂)	Bi ₆ MoO ₁₂ , Bi ₁₄ MoO ₂₄	Bi ₆ MoO ₁₂ , Bi ₁₄ MoO ₂₄	Bi ₆ MoO ₁₂ , Bi ₁₄ MoO ₂₄	'Bi ₃₈ Mo ₇ O ₇₈ ', Bi ₁₄ MoO ₂₄
23	3Bi ₂ O ₃ : 1MoO ₃ (Bi ₆ MoO ₁₂)	Bi ₆ MoO ₁₂	Bi ₆ MoO ₁₂	Bi ₆ MoO ₁₂	'Bi ₃₈ Mo ₇ O ₇₈ '
24	2.82Bi ₂ O ₃ : 1MoO ₃ (between Bi ₆ MoO ₁₂ and 'Bi ₃₈ Mo ₇ O ₇₈ ')	Bi ₆ MoO ₁₂ , Bi ₁₀ Mo ₃ O ₂₄	Bi ₆ MoO ₁₂ , Bi ₁₀ Mo ₃ O ₂₄	Bi ₆ MoO ₁₂ , Bi ₁₀ Mo ₃ O ₂₄	'Bi ₃₈ Mo ₇ O ₇₈ '
25	2.94Bi ₂ O ₃ : 1MoO ₃ (between Bi ₆ MoO ₁₂ and 'Bi ₃₈ Mo ₇ O ₇₈ ')	Bi ₆ MoO ₁₂ , Bi ₁₀ Mo ₃ O ₂₄	Bi ₆ MoO ₁₂ , Bi ₁₀ Mo ₃ O ₂₄	Bi ₆ MoO ₁₂ , Bi ₁₀ Mo ₃ O ₂₄	'Bi ₃₈ Mo ₇ O ₇₈ '
26	2.71Bi ₂ O ₃ : 1MoO ₃ ('Bi ₃₈ Mo ₇ O ₇₈ ')	Bi ₆ MoO ₁₂ , Bi ₁₀ Mo ₃ O ₂₄	Bi ₆ MoO ₁₂ , Bi ₁₀ Mo ₃ O ₂₄	Bi ₆ MoO ₁₂ , Bi ₁₀ Mo ₃ O ₂₄	'Bi ₃₈ Mo ₇ O ₇₈ '
27	2.12Bi ₂ O ₃ : 1MoO ₃ (between 'Bi ₃₈ Mo ₇ O ₇₈ ' and Bi ₁₀ Mo ₃ O ₂₄)	Bi ₆ MoO ₁₂ , Bi ₁₀ Mo ₃ O ₂₄	Bi ₆ MoO ₁₂ , Bi ₁₀ Mo ₃ O ₂₄	Bi ₆ MoO ₁₂ , Bi ₁₀ Mo ₃ O ₂₄	'Bi ₃₈ Mo ₇ O ₇₈ ', Bi ₁₀ Mo ₃ O ₂₄

**Same phases were obtained at the end of 50% of the total duration of heating. At 773 K, orthorhombic phase of Bi₂MoO₆ was obtained. At 873 and 1023 K, monoclinic phase of Bi₂MoO₆ was obtained.*

Table 3.5 Details of equilibrations of samples with Bi₂O₃ and MoO₂ mixtures

No	Molar ratios of oxides taken	T / K	Phases obtained after equilibration*
28	1:3Bi ₂ O ₃ : MoO ₂	773K, 960h	Bi, MoO ₂ , Bi ₂ MoO ₆ (orthorhombic phase)
		1023K, 480h	Bi, MoO ₂ , Bi ₂ MoO ₆ (monoclinic phase)
29	1:1 Bi ₂ O ₃ : MoO ₂	773K, 960h	Bi, MoO ₂ , Bi ₂ MoO ₆ (orthorhombic phase)
		1023K, 480h	Bi, MoO ₂ , Bi ₂ MoO ₆ (monoclinic phase)
30	3:1 Bi ₂ O ₃ : MoO ₂	773K, 960h	Bi, Bi ₁₀ Mo ₃ O ₂₄ , Bi ₆ MoO ₁₂
		1023K, 480h	Bi, Bi ₁₀ Mo ₃ O ₂₄ , 'Bi ₃₈ Mo ₇ O ₇₈ '

**Same phases were obtained at the end of 50% of the total duration of heating*

The overall composition of the products obtained after this reduction was then determined based on the final mass of the product by assuming the mass loss was solely due to removal of oxygen (i.e. Bi to Mo ratio remained constant during reduction). The products obtained were ground well and made into pellets, which were then kept in alumina crucibles and sealed in low volume quartz ampoules under vacuum. Different pellets of the samples were equilibrated at 773, 873 and 1023 K for prolonged periods. After equilibration, they were quenched to room temperature and the phases in the products were analyzed by XRD. The details of the samples are given in Table 3.6.

3.3.3.4 Long term equilibrations of phase mixtures using different starting components

To obtain information about the coexisting phases in the ternary Bi-Mo-O system, experiments involving long term equilibrations were performed. For these experiments, samples with different overall compositions were prepared using different starting components. Samples prepared by taking appropriate molar ratios of different starting components were thoroughly mixed and made into pellets. The

pellets were then kept inside alumina crucibles and enclosed in small volume evacuated quartz ampoules. The samples were equilibrated at 773, 873 and 1023 K. At the end of about half the total duration of heating, the ampoules were quenched to room temperature. Samples were retrieved, ground well and analyzed by XRD. Samples were then repelletized and equilibration was continued in an identical manner. Details of the samples and equilibration parameters are given in Table 3.7.

Table 3.6 Details of equilibrations of partially reduced ternary compounds

No	Starting compound	Overall composition after partial reduction	Temperature and duration of equilibration	Phases obtained after equilibration*
31	Bi ₂ Mo ₃ O ₁₂	Bi _{0.17} Mo _{0.26} O _{0.56}	873K, 720h	Bi, MoO ₂ , Bi ₂ MoO ₆
			1023K, 480h	Bi, MoO ₂ , Bi ₂ MoO ₆
32	Bi ₂ Mo ₂ O ₉	Bi _{0.24} Mo _{0.24} O _{0.52}	873K, 720h	Bi, MoO ₂ , Bi ₂ MoO ₆
			1023K, 480h	Bi, MoO ₂ , Bi ₂ MoO ₆
33	Bi ₂ MoO ₆	Bi _{0.35} Mo _{0.17} O _{0.48}	873K, 720h	Bi, MoO ₂ , Bi ₂ MoO ₆
			1023K, 480h	Bi, MoO ₂ , Bi ₂ MoO ₆
34	Bi ₆ Mo ₂ O ₁₅	Bi _{0.33} Mo _{0.11} O _{0.56}	773K, 960h	Bi, MoO ₂ , Bi ₂ MoO ₆
			873K, 720h	Bi, MoO ₂ , Bi ₂ MoO ₆
			1023K, 480h	Bi, MoO ₂ , Bi ₂ MoO ₆
35	Bi ₆ MoO ₁₂	Bi _{0.48} Mo _{0.08} O _{0.43}	773K, 960h	Bi, MoO ₂ , Bi ₂ MoO ₆
36	Bi ₁₄ MoO ₂₄	Bi _{0.70} Mo _{0.05} O _{0.29}	773K, 960h	Bi, MoO ₂ , Bi ₂ MoO ₆
			873K, 720h	Bi, MoO ₂ , Bi ₂ MoO ₆

*Same phases were obtained at the end of 50% of the total duration of heating. At 773 K, orthorhombic phase of Bi₂MoO₆ was obtained. At 873 and 1023 K, monoclinic phase of Bi₂MoO₆ was obtained.

Table 3.7 Details of equilibrations of phase mixtures using different starting components

No	Molar ratios of phases taken for equilibration	Products obtained after equilibration*		
		At 773 K (960 h)	At 873 K (720 h)	At 1023 K (480 h)
37	1Bi ₂ O ₃ : 2Mo: 5.4MoO ₃	Bi ₂ MoO ₆ , MoO ₂ , Bi ₂ Mo ₃ O ₁₂	Bi ₂ MoO ₆ , MoO ₂ , Bi ₂ Mo ₂ O ₉	-
38	1Bi ₂ O ₃ : 2.3MoO ₂ : 1.5MoO ₃	Bi ₂ MoO ₆ , MoO ₂ , Bi ₂ Mo ₃ O ₁₂	Bi ₂ Mo ₂ O ₉ , MoO ₂ , Bi ₂ Mo ₃ O ₁₂	-
39	1Bi ₂ O ₃ : 6Mo: 1.8MoO ₂	Bi, Mo, MoO ₂	Bi, Mo, MoO ₂	Bi, Mo, MoO ₂
40	10Bi: 28.6Mo: 1MoO ₃	Bi, Mo, MoO ₂	Bi, Mo, MoO ₂	Bi, Mo, MoO ₂
41	1Bi ₂ O ₃ : 0.71Mo: 1.7MoO ₂	Bi, MoO ₂ , Bi ₂ MoO ₆	-	Bi, MoO ₂ , Bi ₂ MoO ₆
42	3.4Bi ₂ O ₃ : 1Mo: 1.8MoO ₂	Bi, MoO ₂ , Bi ₂ MoO ₆	-	Bi, MoO ₂ , Bi ₂ MoO ₆
43	1.6Bi ₂ O ₃ : 1Mo: 3MoO ₂	Bi, MoO ₂ , Bi ₂ MoO ₆	-	Bi, MoO ₂ , Bi ₂ MoO ₆
44	4.7Bi ₂ O ₃ : 1Mo: 4.6MoO ₃	Bi, MoO ₂ , Bi ₂ MoO ₆	-	Bi, MoO ₂ , Bi ₂ MoO ₆
45	14.3Bi ₂ O ₃ : 1MoO ₃ : 35.5MoO ₂	-	Bi, MoO ₂ , Bi ₂ MoO ₆	Bi, MoO ₂ , Bi ₂ MoO ₆
46	4.3Bi ₂ O ₃ : 1MoO ₃ : 11.1MoO ₂	-	Bi, MoO ₂ , Bi ₂ MoO ₆	Bi, MoO ₂ , Bi ₂ MoO ₆
47	1.2Bi ₂ O ₃ : 1MoO ₃ : 3.7MoO ₂	-	Bi, MoO ₂ , Bi ₂ MoO ₆	Bi, MoO ₂ , Bi ₂ MoO ₆
48	1Bi ₂ O ₃ : 3MoO ₂ : 2.75MoO ₃	-	Bi ₂ Mo ₂ O ₉ , MoO ₂ , Bi ₂ Mo ₃ O ₁₂	-
49	1Bi ₂ O ₃ : 6.3MoO ₂ : 2.3MoO ₃	-	Bi ₂ MoO ₆ , MoO ₂ , Bi ₂ Mo ₂ O ₉	-
50	1.1Bi: 1.5Bi ₂ O ₃ : 1MoO ₂	Bi, Bi ₂ MoO ₆ , Bi ₆ Mo ₂ O ₁₅	-	Bi, Bi ₂ MoO ₆ , 'Bi ₂₆ Mo ₁₀ O ₆₉ '
51	2Bi: 2.4Bi ₂ O ₃ : 1MoO ₂	Bi, Bi ₁₀ Mo ₃ O ₂₄ , Bi ₆ MoO ₁₂	-	Bi, Bi ₁₀ Mo ₃ O ₂₄ , 'Bi ₃₈ Mo ₇ O ₇₈ '
52	4.6Bi: 4.6Bi ₂ O ₃ : 1MoO ₂	Bi, Bi ₆ MoO ₁₂ , Bi ₁₄ MoO ₂₄	-	Bi, 'Bi ₃₈ Mo ₇ O ₇₈ ', Bi ₁₄ MoO ₂₄
53	16.1Bi: 14.7.4Bi ₂ O ₃ : 1MoO ₂	Bi, Bi ₁₄ MoO ₂₄ , Bi ₂ O ₃	Bi, Bi ₁₄ MoO ₂₄ , Bi ₂ O ₃	Bi, Bi ₁₄ MoO ₂₄ , Bi ₂ O ₃
54	1Bi: 4.9Bi ₂ O ₃ : 3MoO ₂	Bi, Bi ₂ MoO ₆ , Bi ₆ Mo ₂ O ₁₅	-	Bi, Bi ₂ MoO ₆ , 'Bi ₂₆ Mo ₁₀ O ₆₉ '
55	1Bi: 2.1Bi ₂ O ₃ : 1.3MoO ₂	Bi, Bi ₁₀ Mo ₃ O ₂₄ , Bi ₆ MoO ₁₂	-	Bi, Bi ₁₀ Mo ₃ O ₂₄ , 'Bi ₃₈ Mo ₇ O ₇₈ '
56	1Bi: 9.6Bi ₂ O ₃ : 1.8MoO ₂	Bi, Bi ₆ MoO ₁₂ , Bi ₁₄ MoO ₂₄	-	Bi, 'Bi ₃₈ Mo ₇ O ₇₈ ', Bi ₁₄ MoO ₂₄
57	1Bi: 22.4Bi ₂ O ₃ : 1.9MoO ₂	Bi, Bi ₁₄ MoO ₂₄ , Bi ₂ O ₃	Bi, Bi ₁₄ MoO ₂₄ , Bi ₂ O ₃	Bi, Bi ₁₄ MoO ₂₄ , Bi ₂ O ₃

*Same phases were obtained at the end of 50% of the total duration of heating. At 773 K, orthorhombic phase of Bi₂MoO₆ was obtained. At 873 and 1023 K, monoclinic phase of Bi₂MoO₆ was obtained.

3.3.3.5 Long term equilibrations of phase mixtures in liquid bismuth

To confirm the phases that coexist with liquid bismuth, additional long term equilibrations were carried out. For these experiments, pellets of the samples were prepared by mixing different sets of starting components. Homogeneous mixture of these phases was made as porous pellets. Excess bismuth metal taken in alumina crucibles was melted in an argon atmosphere glove box. Each sample pellet was forcefully immersed into the liquid metal using an alumina strip. The strip was tied to the crucible by means of a binding wire. The crucible containing the sample was later sealed under vacuum in quartz ampoule. Samples enclosed in quartz ampoules were then subjected to long term equilibration at 773, 873 and 1023 K. After the equilibration, samples were quenched to room temperature. Sample pellets were retrieved after melting bismuth metal. The powdered samples were then characterized by XRD. Details of these experiments are given in Table 3.8.

3.3.3.6 Equilibrations to determine the stability ranges of $\text{Bi}_8\text{Mo}_3\text{O}_{21}$, $\text{Bi}_{14}\text{Mo}_5\text{O}_{36}$ and $\text{Bi}_6\text{Mo}_2\text{O}_{15}$

To unravel the temperature ranges of stability of $\text{Bi}_8\text{Mo}_3\text{O}_{21}$, $\text{Bi}_{14}\text{Mo}_5\text{O}_{36}$ and $\text{Bi}_6\text{Mo}_2\text{O}_{15}$, pellets of these compounds were equilibrated at different temperatures for prolonged periods. In the case of $\text{Bi}_8\text{Mo}_3\text{O}_{21}$, pellets of 6 mm diameter and 3 mm thickness were made and taken in small quartz crucibles. They were in turn stacked at precisely known heights in a 1 m long and one end closed 16 mm diameter quartz tube using quartz spacers. Similarly, sample pellets of $\text{Bi}_{14}\text{Mo}_5\text{O}_{36}$ and $\text{Bi}_6\text{Mo}_2\text{O}_{15}$ were stacked in separate quartz tubes. About 15 samples were placed in each of the quartz tubes. The quartz tubes were then placed in a vertical furnace which provided an axial temperature gradient. The temperature within the furnace was maintained between 748 and 1023 K.

Table 3.8 Details of equilibrations in liquid bismuth

a) Using Bi, Bi ₂ O ₃ and MoO ₂ as starting components		Phases obtained after equilibration		
		At 773 K / 960 h	At 873 K / 720 h	At 1023 K / 480 h
No	Composition chosen			
58	5.52Bi:18.09Bi ₂ O ₃ :1MoO ₂	Bi, Bi ₁₄ MoO ₂₄ , Bi ₂ O ₃	-	Bi, Bi ₁₄ MoO ₂₄ , Bi ₂ O ₃
59	22.29Bi:12.11Bi ₂ O ₃ :1MoO ₂	Bi, Bi ₁₄ MoO ₂₄ , Bi ₂ O ₃	-	Bi, Bi ₁₄ MoO ₂₄ , Bi ₂ O ₃
60	Bi:6.22Bi ₂ O ₃ :1.28MoO ₂	Bi, Bi ₆ MoO ₁₂ , Bi ₁₄ MoO ₂₄	Bi, Bi ₆ MoO ₁₂ , Bi ₁₄ MoO ₂₄	Bi, 'Bi ₃₈ Mo ₇ O ₇₈ ', Bi ₁₄ MoO ₂₄
61	2.1Bi:5.06Bi ₂ O ₃ :1MoO ₂	Bi, Bi ₆ MoO ₁₂ , Bi ₁₄ MoO ₂₄	Bi, Bi ₆ MoO ₁₂ , Bi ₁₄ MoO ₂₄	Bi, 'Bi ₃₈ Mo ₇ O ₇₈ ', Bi ₁₄ MoO ₂₄
62	1Bi:11.09Bi ₂ O ₃ :5.34MoO ₂	Bi, Bi ₁₀ Mo ₃ O ₂₄ , Bi ₆ MoO ₁₂	Bi, Bi ₁₀ Mo ₃ O ₂₄ , Bi ₆ MoO ₁₂	Bi, Bi ₁₀ Mo ₃ O ₂₄ , 'Bi ₃₈ Mo ₇ O ₇₈ '
63	1Bi:5.98Bi ₂ O ₃ :3.03MoO ₂	Bi, Bi ₁₀ Mo ₃ O ₂₄ , Bi ₆ MoO ₁₂	Bi, Bi ₁₀ Mo ₃ O ₂₄ , Bi ₆ MoO ₁₂	Bi, Bi ₁₀ Mo ₃ O ₂₄ , 'Bi ₃₈ Mo ₇ O ₇₈ '
b) Using Bi, Bi ₂ O ₃ and MoO ₃ as starting components				
64	1Bi ₂ O ₃ :2Bi:2.5MoO ₃	Bi, MoO ₂ , Bi ₂ MoO ₆	-	Bi, MoO ₂ , Bi ₂ MoO ₆
65	8.9Bi:1Mo:0.43MoO ₃	Bi, MoO ₂ , Bi ₂ MoO ₆	-	Bi, MoO ₂ , Bi ₂ MoO ₆
66	6.19Bi:17.76Bi ₂ O ₃ :1MoO ₃	Bi, Bi ₁₄ MoO ₂₄ , Bi ₂ O ₃	-	Bi, Bi ₂ O ₃ , Bi ₁₄ MoO ₂₄
67	12.77Bi:21.96Bi ₂ O ₃ :1MoO ₃	Bi, Bi ₁₄ MoO ₂₄ , Bi ₂ O ₃	-	Bi, Bi ₂ O ₃ , Bi ₁₄ MoO ₂₄
68	1.45Bi:4.52Bi ₂ O ₃ :1MoO ₃	Bi, Bi ₆ MoO ₁₂ , Bi ₁₄ MoO ₂₄	Bi, Bi ₆ MoO ₁₂ , Bi ₁₄ MoO ₂₄	Bi, 'Bi ₃₈ Mo ₇ O ₇₈ ', Bi ₁₄ MoO ₂₄
69	2.77Bi:4.72Bi ₂ O ₃ :1MoO ₃	Bi, Bi ₆ MoO ₁₂ , Bi ₁₄ MoO ₂₄	Bi, Bi ₆ MoO ₁₂ , Bi ₁₄ MoO ₂₄	Bi, 'Bi ₃₈ Mo ₇ O ₇₈ ', Bi ₁₄ MoO ₂₄
70	1Bi:5.6Bi ₂ O ₃ :2.87MoO ₃	Bi, Bi ₁₀ Mo ₃ O ₂₄ , Bi ₆ MoO ₁₂	Bi, Bi ₁₀ Mo ₃ O ₂₄ , Bi ₆ MoO ₁₂	Bi, Bi ₁₀ Mo ₃ O ₂₄ , 'Bi ₃₈ Mo ₇ O ₇₈ '

71	1Bi:2.83Bi ₂ O ₃ :1.45MoO ₃	Bi, Bi ₁₀ Mo ₃ O ₂₄ , Bi ₆ MoO ₁₂	Bi, Bi ₁₀ Mo ₃ O ₂₄ , Bi ₆ MoO ₁₂	Bi, Bi ₁₀ Mo ₃ O ₂₄ , 'Bi ₃₈ Mo ₇ O ₇₈ '
72	1Bi:18.9Bi ₂ O ₃ :10.6MoO ₃	Bi, Bi ₆ Mo ₂ O ₁₅ , Bi ₁₀ Mo ₃ O ₂₄ ,	Bi, Bi ₆ Mo ₂ O ₁₅ , Bi ₁₀ Mo ₃ O ₂₄	Bi, 'Bi ₂₆ Mo ₁₀ O ₆₉ ', Bi ₁₀ Mo ₃ O ₂₄
73	1Bi:11.57Bi ₂ O ₃ :7.22MoO ₃	Bi, Bi ₆ Mo ₂ O ₁₅ , Bi ₁₀ Mo ₃ O ₂₄	Bi, Bi ₆ Mo ₂ O ₁₅ , Bi ₁₀ Mo ₃ O ₂₄	Bi, 'Bi ₂₆ Mo ₁₀ O ₆₉ ', Bi ₁₀ Mo ₃ O ₂₄
74	1Bi:38.85Bi ₂ O ₃ :24.7MoO ₃	Bi, Bi ₆ Mo ₂ O ₁₅ , Bi ₁₀ Mo ₃ O ₂₄	Bi, Bi ₆ Mo ₂ O ₁₅ , Bi ₁₀ Mo ₃ O ₂₄	Bi, 'Bi ₂₆ Mo ₁₀ O ₆₉ ', Bi ₁₀ Mo ₃ O ₂₄
75	1Bi:41.42Bi ₂ O ₃ :28.61MoO ₃	Bi, Bi ₂ MoO ₆ , Bi ₆ Mo ₂ O ₁₅	Bi, Bi ₁₄ Mo ₅ O ₃₆ , Bi ₆ Mo ₂ O ₁₅	-
76	1Bi:20.72Bi ₂ O ₃ :14.16MoO ₃	Bi, Bi ₂ MoO ₆ , Bi ₆ Mo ₂ O ₁₅	Bi, Bi ₁₄ Mo ₅ O ₃₆ , Bi ₆ Mo ₂ O ₁₅	-
77	1Bi:5.41Bi ₂ O ₃ :3.75MoO ₃	Bi, Bi ₂ MoO ₆ , Bi ₆ Mo ₂ O ₁₅	Bi, Bi ₁₄ Mo ₅ O ₃₆ , Bi ₆ Mo ₂ O ₁₅	-
78	1Bi:2.8Bi ₂ O ₃ :1.96MoO ₃	Bi, Bi ₂ MoO ₆ , Bi ₆ Mo ₂ O ₁₅	Bi, Bi ₈ Mo ₃ O ₂₁ , Bi ₁₄ Mo ₅ O ₃₆	-
79	1.01Bi:1.41Bi ₂ O ₃ :1MoO ₃	Bi, Bi ₂ MoO ₆ , Bi ₆ Mo ₂ O ₁₅	Bi, Bi ₈ Mo ₃ O ₂₁ , Bi ₁₄ Mo ₅ O ₃₆	-
80	1.13Bi:1.39Bi ₂ O ₃ :1MoO ₃	Bi, Bi ₂ MoO ₆ , Bi ₆ Mo ₂ O ₁₅	Bi, Bi ₈ Mo ₃ O ₂₁ , Bi ₁₄ Mo ₅ O ₃₆	-
81	1Bi:3.19Bi ₂ O ₃ :2.85MoO ₃	Bi, Bi ₂ MoO ₆ , Bi ₆ Mo ₂ O ₁₅	Bi, Bi ₂ MoO ₆ , Bi ₈ Mo ₃ O ₂₁	-
82	1Bi:2.25Bi ₂ O ₃ :2.02MoO ₃	Bi, Bi ₂ MoO ₆ , Bi ₆ Mo ₂ O ₁₅	Bi, Bi ₂ MoO ₆ , Bi ₈ Mo ₃ O ₂₁	-

At 773 K, orthorhombic phase of Bi₂MoO₆ was obtained. At 873 and 1023 K, monoclinic phase of Bi₂MoO₆ was obtained.

A stainless steel pipe of 45 mm OD and 1.5 m long was also kept additionally in the furnace, surrounding the quartz tubes for providing radially uniform temperature (Fig.1 in the Appendix). Size of the sample pellets was small such that the temperature within each pellet would be constant throughout the period of equilibration. Using a K-type thermocouple which could be moved very slowly (10 mm/min) from bottom to top of the furnace and close to the quartz tube with the help of a motor, the temperature at which each sample pellet was equilibrated could be measured. The samples were equilibrated for 600 h and quenched to room temperature. The powdered samples were then analyzed by XRD. The details of equilibrations are given in Table 3.9.

3.3.4 Electrical conductivity measurements

3.3.4.1 Conductivity measurements on $\text{Bi}_8\text{Mo}_3\text{O}_{21}$, $\text{Bi}_{14}\text{Mo}_5\text{O}_{36}$ and $\text{Bi}_6\text{Mo}_2\text{O}_{15}$

In order to determine the temperatures at which $\text{Bi}_8\text{Mo}_3\text{O}_{21}$, $\text{Bi}_{14}\text{Mo}_5\text{O}_{36}$ and $\text{Bi}_6\text{Mo}_2\text{O}_{15}$ transform into the high temperature solid solution phase ' $\text{Bi}_{26}\text{Mo}_{10}\text{O}_{69}$ ', conductivity measurements were carried out in air. For these measurements, sintered pellets of the compounds were used.

In the case of $\text{Bi}_8\text{Mo}_3\text{O}_{21}$, conductivity measurements were carried out in the temperature range of 773 to 943 K. The first measurement of conductivity was carried out at 773 K followed by increasing the sample temperature by 10 K. After maintaining the sample at that temperature for about 2 h, its conductivity was measured at that temperature. This was continued till 943 K. For $\text{Bi}_{14}\text{Mo}_5\text{O}_{36}$, measurements were carried out in the temperature range of 748 to 990 K in a similar way. The conductivity of $\text{Bi}_6\text{Mo}_2\text{O}_{15}$ was measured in the temperature range of 718 to 917 K.

Table 3.9 Details of equilibrations to study the stabilities of $\text{Bi}_8\text{Mo}_3\text{O}_{21}$, $\text{Bi}_{14}\text{Mo}_5\text{O}_{36}$ and $\text{Bi}_6\text{Mo}_2\text{O}_{15}$

$\text{Bi}_8\text{Mo}_3\text{O}_{21}$		$\text{Bi}_{14}\text{Mo}_5\text{O}_{36}$		$\text{Bi}_6\text{Mo}_2\text{O}_{15}$	
T / K	Phases obtained	T / K	Phases obtained	T / K	Phases obtained
771	Bi_2MoO_6 , $\text{Bi}_6\text{Mo}_2\text{O}_{15}$	766	Bi_2MoO_6 , $\text{Bi}_6\text{Mo}_2\text{O}_{15}$	745	$\text{Bi}_6\text{Mo}_2\text{O}_{15}$
788	Bi_2MoO_6 , $\text{Bi}_6\text{Mo}_2\text{O}_{15}$	782	Bi_2MoO_6 , $\text{Bi}_6\text{Mo}_2\text{O}_{15}$	753	$\text{Bi}_6\text{Mo}_2\text{O}_{15}$
805	Bi_2MoO_6 , $\text{Bi}_6\text{Mo}_2\text{O}_{15}$	798	Bi_2MoO_6 , $\text{Bi}_6\text{Mo}_2\text{O}_{15}$	768	$\text{Bi}_6\text{Mo}_2\text{O}_{15}$
841	$\text{Bi}_8\text{Mo}_3\text{O}_{21}$	817	Bi_2MoO_6 , $\text{Bi}_{14}\text{Mo}_5\text{O}_{36}$, $\text{Bi}_6\text{Mo}_2\text{O}_{15}$	784	$\text{Bi}_6\text{Mo}_2\text{O}_{15}$
862	$\text{Bi}_8\text{Mo}_3\text{O}_{21}$	838	Bi_2MoO_6 , $\text{Bi}_{14}\text{Mo}_5\text{O}_{36}$, $\text{Bi}_6\text{Mo}_2\text{O}_{15}$	801	$\text{Bi}_6\text{Mo}_2\text{O}_{15}$
888	$\text{Bi}_8\text{Mo}_3\text{O}_{21}$	859	Bi_2MoO_6 , $\text{Bi}_{14}\text{Mo}_5\text{O}_{36}$, $\text{Bi}_6\text{Mo}_2\text{O}_{15}$	817	$\text{Bi}_6\text{Mo}_2\text{O}_{15}$
912	$\text{Bi}_8\text{Mo}_3\text{O}_{21}$	883	$\text{Bi}_{14}\text{Mo}_5\text{O}_{36}$	836	$\text{Bi}_6\text{Mo}_2\text{O}_{15}$
931	' $\text{Bi}_{26}\text{Mo}_{10}\text{O}_{69}$ '	907	$\text{Bi}_{14}\text{Mo}_5\text{O}_{36}$	857	$\text{Bi}_6\text{Mo}_2\text{O}_{15}$
952	' $\text{Bi}_{26}\text{Mo}_{10}\text{O}_{69}$ '	927	$\text{Bi}_{14}\text{Mo}_5\text{O}_{36}$	883	$\text{Bi}_6\text{Mo}_2\text{O}_{15}$
970	' $\text{Bi}_{26}\text{Mo}_{10}\text{O}_{69}$ '	947	$\text{Bi}_{14}\text{Mo}_5\text{O}_{36}$	901	$\text{Bi}_6\text{Mo}_2\text{O}_{15}$
986	' $\text{Bi}_{26}\text{Mo}_{10}\text{O}_{69}$ '	968	' $\text{Bi}_{26}\text{Mo}_{10}\text{O}_{69}$ '	928	' $\text{Bi}_{26}\text{Mo}_{10}\text{O}_{69}$ '
999	' $\text{Bi}_{26}\text{Mo}_{10}\text{O}_{69}$ '	984	' $\text{Bi}_{26}\text{Mo}_{10}\text{O}_{69}$ '	949	' $\text{Bi}_{26}\text{Mo}_{10}\text{O}_{69}$ '
1011	' $\text{Bi}_{26}\text{Mo}_{10}\text{O}_{69}$ '	998	' $\text{Bi}_{26}\text{Mo}_{10}\text{O}_{69}$ '	968	' $\text{Bi}_{26}\text{Mo}_{10}\text{O}_{69}$ '
1023	' $\text{Bi}_{26}\text{Mo}_{10}\text{O}_{69}$ '	1009	' $\text{Bi}_{26}\text{Mo}_{10}\text{O}_{69}$ '	983	' $\text{Bi}_{26}\text{Mo}_{10}\text{O}_{69}$ '
-	-	1022	' $\text{Bi}_{26}\text{Mo}_{10}\text{O}_{69}$ '	998	' $\text{Bi}_{26}\text{Mo}_{10}\text{O}_{69}$ '
-	-	1023	' $\text{Bi}_{26}\text{Mo}_{10}\text{O}_{69}$ '	-	-

3.3.4.2 Conductivity measurements on $\text{Bi}_2\text{Mo}_2\text{O}_9$

It is reported in literature that $\text{Bi}_2\text{Mo}_2\text{O}_9$ is unstable at low temperatures and decomposes to $\text{Bi}_2\text{Mo}_3\text{O}_{12}$ and Bi_2MoO_6 . The decomposition temperature has been reported to be 813 K [32] as well as 823 K [59, 60]. In the present work, electrical conductivity of $\text{Bi}_2\text{Mo}_2\text{O}_9$ was measured by complex impedance spectroscopy to determine its decomposition temperature. The $\text{Bi}_2\text{Mo}_2\text{O}_9$ sample was prepared by the solid state reaction between stoichiometric amounts of Bi_2O_3 and MoO_3 at 873 K in air for 48 h. A sintered pellet of $\text{Bi}_2\text{Mo}_2\text{O}_9$ having 8 mm diameter and 3 mm thickness was made and used for conductivity measurements. The pellet was sintered in air at 903 K for about 6 h. The conductivity measurements were carried out in air in the temperature range of 905 to 754 K in the frequency range of 10 Hz to 1 MHz with an applied perturbation potential of 500 mV.

First measurement of conductivity was made at 905 K after heating the sample for 24 h at that temperature. This was followed by decreasing the sample temperature by 10 K and maintaining at that temperature for about 2 h. Conductivity was then measured at each temperature. This was continued till the final temperature of 754 K was reached.

3.3.4.3 Conductivity measurements on Bi_2MoO_6

Electrical conductivity of Bi_2MoO_6 was measured to determine the temperature at which it undergoes phase transitions. For these measurements, sintered pellets of both the orthorhombic and monoclinic phases of Bi_2MoO_6 were used. The monoclinic phase of Bi_2MoO_6 was prepared by the solid state reaction between stoichiometric amounts of Bi_2O_3 and MoO_3 at 873 K in air for 48 h whereas the reaction at 773 K for 48 h yielded the orthorhombic phase of Bi_2MoO_6 . With the orthorhombic phase as the sample pellet, measurements were carried out on heating it

first from 700 to 963 K in steps of 10 K. The sample was maintained at the initial temperature of 700 K for about 24 h and the conductivity was measured at that temperature. This is followed by raising the sample temperature by 10 K and maintaining at that temperature for about 2 h. The conductivity was then measured. When the starting phase was the high temperature monoclinic phase, conductivity was measured while cooling the sample in steps from 973 to 723 K.

All the conductivity experiments were carried out using the conductivity cell described in chapter 2. The electrical conductivity was measured using a frequency response analyzer (Model SI 1225, Solartron, M/s Schlumberger, UK) coupled with an electrochemical interface (Model 1286, Solartron, M/s Schlumberger, UK). The measurements were carried out in the frequency range of 10 Hz to 1 MHz with an applied perturbation potential of 500 mV. The impedance data obtained at each temperature was fitted using the software Zview®. The bulk resistance of the material was obtained by fitting a semicircle to the experimentally obtained Nyquist plot. By incorporating the dimensions of the pellet, the conductivity (σ) of the sample at each temperature (T) was determined. The Arrhenius plot for conductivity was obtained by plotting $\log \sigma$ as a function of $1/T$. A change in the slope indicates the difference in the conduction mechanism and / or a phase change. At the end of the conductivity measurements, the sample pellets were retrieved, powdered and characterized by XRD to establish any structural changes that had occurred during the measurement.

3.3.5 Simultaneous equilibration experiments to follow the structural changes during conductivity measurements

The structural changes that could occur during conductivity measurements were followed by performing separate equilibration experiments at different selected temperatures falling within the temperature ranges of conductivity measurements. For

these experiments, sample pellets of $\text{Bi}_8\text{Mo}_3\text{O}_{21}$, $\text{Bi}_{14}\text{Mo}_5\text{O}_{36}$, $\text{Bi}_6\text{Mo}_2\text{O}_{15}$, $\text{Bi}_2\text{Mo}_2\text{O}_9$, and Bi_2MoO_6 , were individually kept inside alumina crucibles and equilibrated in air at different temperatures by following the temperature program used for conductivity measurements.

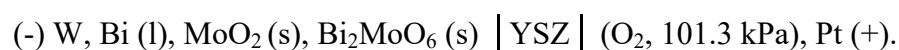
For $\text{Bi}_8\text{Mo}_3\text{O}_{21}$, the equilibrations were carried out at 873, 898, 923, 948 and 973 K. The equilibration temperatures for $\text{Bi}_{14}\text{Mo}_5\text{O}_{36}$ were 873, 923, 948 and 973 K whereas for $\text{Bi}_6\text{Mo}_2\text{O}_{15}$, equilibrations were carried out at 873, 898 and 923 K, respectively. In the case of $\text{Bi}_2\text{Mo}_2\text{O}_9$, equilibrations were carried out at 873, 823, 798 and 773 K and for the monoclinic phase of Bi_2MoO_6 , equilibrations were performed at 973, 873, 823 and 773 K.

The equilibration of all the compounds ($\text{Bi}_2\text{Mo}_2\text{O}_9$, monoclinic phase of Bi_2MoO_6 , $\text{Bi}_8\text{Mo}_3\text{O}_{21}$, $\text{Bi}_{14}\text{Mo}_5\text{O}_{36}$ and $\text{Bi}_6\text{Mo}_2\text{O}_{15}$) were performed in such a way that the first pellet of each sample was first equilibrated at the highest temperature for 24 h and then quenched to room temperature. The second pellet of each compound was first equilibrated at the highest temperature for 24 h which was followed by increasing the temperature by 10 K and maintained at that temperature for 2 h. This was followed by quenching the sample to room temperature. Similarly, third pellet was first equilibrated at the highest temperature for 24 h, followed by successively raising its temperature by 10 K at a time and holding at each temperature for 2 h. This is continued till equilibration at the desired final temperature is completed. After equilibrating at the final temperature, the pellet was quenched to room temperature. In order to check the low temperature stability of $\text{Bi}_8\text{Mo}_3\text{O}_{21}$ and $\text{Bi}_{14}\text{Mo}_5\text{O}_{36}$, pellets of these compounds were also heated at 788 and 773 K, respectively for 24 h followed by quenching them to room temperature and XRD analysis.

In the case of orthorhombic phase of Bi_2MoO_6 , equilibrations were carried out at 773, 823, 843, 853, 873, 923 and 973 K in air by following the identical procedure used for conductivity measurements. First pellet was equilibrated at the lowest temperature for 24 h followed by quenching it to room temperature. Equilibration of the next pellet started at the lowest temperature for 24 h followed by raising its temperature by 10 K and maintaining at that temperature for 2 h. This raise of temperature and dwelling at that temperature was continued till the desired temperature of equilibration was reached and after which the sample was quenched to room temperature. All the samples quenched to room temperature were powdered and analyzed by XRD. Details of these experiments are given in Tables 3.10 and 3.11.

3.3.6 Oxygen potential measurements using yttria stabilized zirconia solid electrolyte

To determine the Gibbs energy of formation of Bi_2MoO_6 (s), a galvanic cell based on yttria stabilized zirconia solid electrolyte was constructed (Fig. 3.8). The galvanic cell can be represented as given below:



The reference electrode for the cell was prepared by applying platinum paste (M/s Eltecks Corporation, India) over the inner bottom surface of the solid electrolyte tube and heating it in air at 1373 K for 2 h. This resulted in a uniform and porous platinum coating over the electrolyte surface. A platinum wire, which had been spot welded to platinum mesh was cofired with the platinum paste. This served as the electrical lead for the reference electrode. A similar porous platinum electrode was formed at the external bottom surface of the electrolyte tube. The solid electrolyte tube was then fastened to a Veeco coupling by means of a high temperature epoxy seal.

Table 3.10 Details of simultaneous equilibrations of $\text{Bi}_8\text{Mo}_3\text{O}_{21}$, $\text{Bi}_{14}\text{Mo}_5\text{O}_{36}$ and $\text{Bi}_6\text{Mo}_2\text{O}_{15}$ samples in air

Sample details	Phases obtained after quenching the samples from						
	873 K	898 K	923 K	948 K	973 K	788 K*	773 K**
1. $\text{Bi}_8\text{Mo}_3\text{O}_{21}$	$\text{Bi}_8\text{Mo}_3\text{O}_{21}$	$\text{Bi}_8\text{Mo}_3\text{O}_{21}$	' $\text{Bi}_{26}\text{Mo}_{10}\text{O}_{69}$ '	' $\text{Bi}_{26}\text{Mo}_{10}\text{O}_{69}$ '	' $\text{Bi}_{26}\text{Mo}_{10}\text{O}_{69}$ '	Bi_2MoO_6 , $\text{Bi}_6\text{Mo}_2\text{O}_{15}$	-
2. $\text{Bi}_{14}\text{Mo}_5\text{O}_{36}$	$\text{Bi}_{14}\text{Mo}_5\text{O}_{36}$	-	$\text{Bi}_{14}\text{Mo}_5\text{O}_{36}$	$\text{Bi}_{14}\text{Mo}_5\text{O}_{36}$	' $\text{Bi}_{26}\text{Mo}_{10}\text{O}_{69}$ '	-	Bi_2MoO_6 , $\text{Bi}_6\text{Mo}_2\text{O}_{15}$
3. $\text{Bi}_6\text{Mo}_2\text{O}_{15}$	$\text{Bi}_6\text{Mo}_2\text{O}_{15}$	' $\text{Bi}_{26}\text{Mo}_{10}\text{O}_{69}$ '	' $\text{Bi}_{26}\text{Mo}_{10}\text{O}_{69}$ '	-	-	-	

1. Heated from 773 to 973 K in steps of 10 K with a dwelling period of 2 h at each temperature and quenched to room temperature from the respective temperatures.

2. Heated from 773 to 973 K in steps of 10 K with a dwelling period of 2 h at each temperature and quenched to room temperature from the respective temperatures.

3. Heated from 700 to 923 K in steps of 10 K with a dwelling period of 2 h at each temperature and quenched to room temperature from the respective temperatures.

* Heated at 788 K for 24 h and quenched to room temperature.

** Heated at 773 K for 24 h and quenched to room temperature.

Table 3.11 Details of simultaneous equilibrations of $\text{Bi}_2\text{Mo}_2\text{O}_9$ and Bi_2MoO_6 samples in air

Sample details	Phases obtained after quenching the samples from									
	773 K	798 K	823 K	843 K	853 K	873 K	923 K	973 K		
$\text{Bi}_2\text{Mo}_2\text{O}_9^*$	$\text{Bi}_2\text{Mo}_3\text{O}_{12}$, Bi_2MoO_6	$\text{Bi}_2\text{Mo}_3\text{O}_{12}$, Bi_2MoO_6	$\text{Bi}_2\text{Mo}_2\text{O}_9$	-	-	$\text{Bi}_2\text{Mo}_2\text{O}_9$	-	-		
$\text{Bi}_2\text{MoO}_6^{**}$ (monoclinic phase)	Bi_2MoO_6 (monoclinic phase)	-	Bi_2MoO_6 (monoclinic phase)	-	-	Bi_2MoO_6 (monoclinic phase)	-	-	Bi_2MoO_6 (monoclinic phase)	Bi_2MoO_6 (monoclinic phase)
$\text{Bi}_2\text{MoO}_6^{***}$ (orthorhombic phase)	Bi_2MoO_6 (orthorhombic phase)	-	Bi_2MoO_6 (orthorhombic phase)							

* Cooled from 873 to 773 K in steps of 10 K with a dwelling period of 2 h at each temperature and quenched to room temperature from the respective temperatures. For equilibration at 873 K, the duration of heating was 24 h.

** Cooled from 973 to 773 K in steps of 10 K with a dwelling period of 2 h at each temperature and quenched to room temperature from the respective temperatures. For equilibration at 973 K, the duration of heating was 24 h.

*** Heated from 773 to 973 K in steps of 10 K with a dwelling period of 2 h at each temperature and quenched to room temperature from the respective temperatures. For equilibration at 773 K, the duration of heating was 24 h

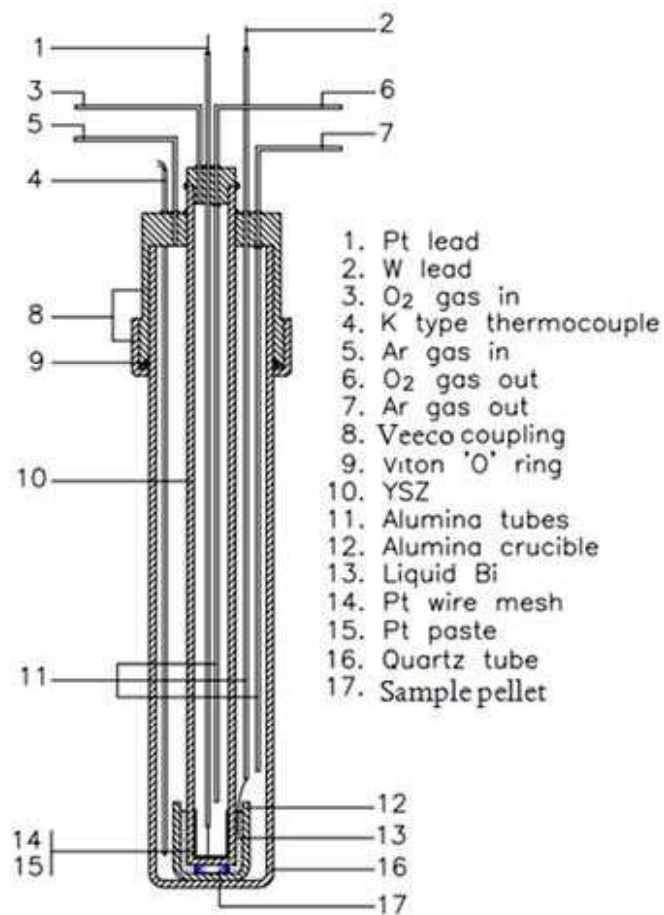


Fig. 3.8 Schematic of the experimental assembly of the galvanic cell

A K-type thermocouple was inserted through the stainless steel coupling and kept very close to the electrode-electrolyte assembly for measuring the cell temperature. The thermocouple used in the experiment was calibrated prior to the actual measurements against a standard calibrated thermocouple supplied by National Physical Laboratory, India.

The entire cell assembly was then kept enclosed in a one end closed quartz tube and sealed using a Viton O-ring. Cell assembly had provisions for flowing gases through the sample and reference compartments. The performance of the emf cell was tested by measuring the null emf by maintaining identical oxygen pressures on both sides of the electrolyte (air-air and oxygen-oxygen). Performance of the cell was also checked by passing oxygen at one electrode and air at the other electrode. Later, the

coated platinum electrode and the platinum lead present at the external surface of the electrolyte tube were removed. A tungsten electrode fastened to the stainless steel coupling through a thin alumina tube using high temperature epoxy seal served as the electrical lead for the sample electrode. Tungsten was chosen as it is compatible with liquid bismuth.

Two sample pellets whose composition falling within the Bi-MoO₂-Bi₂MoO₆ phase field was used for emf measurement. Pellets of the sample electrodes were made by compacting the homogeneous mixture of the constituent phases. The emf cell was assembled inside the argon atmosphere glove box. Appropriate amount of bismuth metal was taken in a recrystallized alumina crucible and melted. Sample pellet was then kept immersed in liquid bismuth by placing the solid electrolyte tube over it in such a way that the lower end of the tungsten wire dipped into liquid bismuth. After cooling, the cell assembly was taken outside the glove box and placed in the constant temperature zone of the furnace. A long hollow cylindrical stainless steel block was also kept in the constant temperature zone of the furnace to further enhance the uniformity of the temperature in the zone. During emf measurements, high purity argon and oxygen gases were passed through the sample and reference compartments, respectively. The cell emf was measured using a high impedance electrometer (input impedance $> 10^{14} \Omega$, M/s Keithley, Model 617) and the thermocouple output was measured using a multimeter (M/s Agilent Technologies, Malaysia, Model-34970A, data acquisition /switch unit). Data were recorded using a computer interface.

Emf measurements were carried out in the temperature range of 773 to 1023 K. First measurement with each cell was carried out at high temperatures (1023 K for cell-I and 936 K for cell-II) to enable faster equilibrium at the sample electrode-

electrolyte interface. At each temperature, the readings were recorded when the cell emf was stable within ± 0.05 mV at least for four hours. The reproducibility of the cell emf was confirmed by the emf data obtained during the random heating and cooling cycles.

The thermo-emf between the two dissimilar electrical leads, i.e. tungsten and platinum was measured in a separate experiment by forming a junction between the two electrical leads followed by the measurement of the thermo-emf between them as a function of temperature. Measured data were fitted to a polynomial expression of order two and is given by:

$$E \pm 0.16 / mV = -1.56 - 7.97 \times 10^{-4} T + 1.84 \times 10^{-5} T^2 \quad [T: 337-1076 \text{ K}] \quad (3.3)$$

The uncertainty expressed is the expanded uncertainty with 0.95 level of confidence. The cell emf was then corrected using this thermo-emf data. At the end of the emf measurements sample pellets were retrieved and analyzed by XRD to confirm the coexisting phases.

3.3.7 Determination of standard molar enthalpies of formation of bismuth molybdates by solution calorimetry

Enthalpies of dissolution of the ternary compounds, namely, $\text{Bi}_2\text{Mo}_3\text{O}_{12}$ (s), monoclinic and orthorhombic phases of Bi_2MoO_6 (s), $\text{Bi}_6\text{Mo}_2\text{O}_{15}$ (s) and $\text{Bi}_6\text{MoO}_{12}$ (s) were determined by using an isoperibol calorimeter as described in Chapter 2. The calibration of the calorimeter was performed by both electrical and chemical methods. The electrical calibration was performed by applying a constant current using a stable power source, for a known period of time. 125 ml of 2 mol kg^{-1} NaOH solution was used as the calorimetric solvent during electrical calibration. The current was measured across a precision resistor connected in series. The temperature was measured using a thermistor (M/s Toshniwal Brothers Delhi Private Limited,

Bangalore, India) connected to a data acquisition system, interfaced to a personal computer and was recorded as a function of time. Fig. 3.9 shows the plot of temperature rise against energy supplied. The correlation between temperature rise and energy in joules was found to be linear up to 500 J.

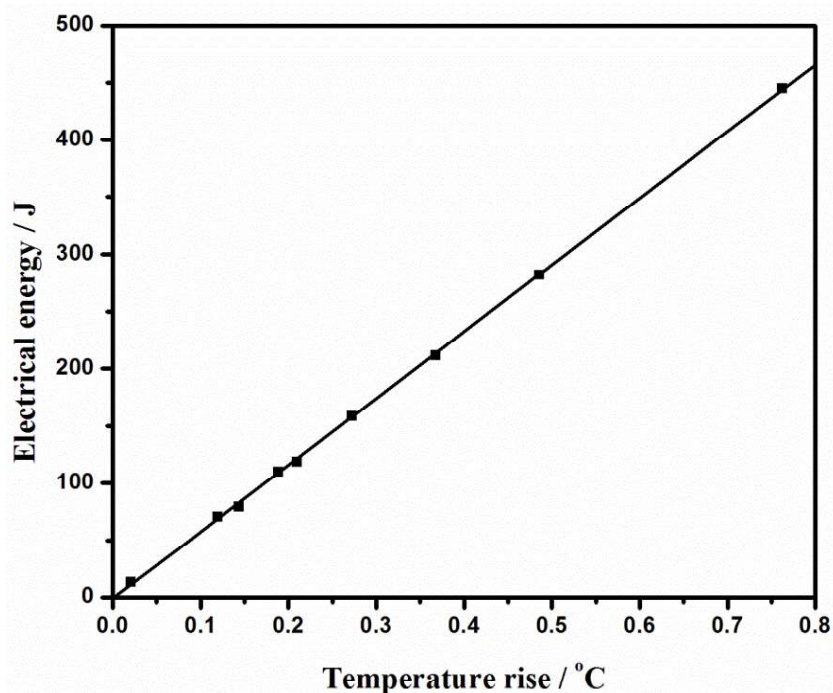


Fig. 3.9 Correlation between temperature rise and electrical energy

The chemical calibration of the calorimeter was carried out by using tris(hydroxyl methyl) aminomethane (s) (TRIS) (99.8% purity, M/s Merck, UK). The calorimetric solvent used was 0.1mol kg^{-1} HCl. The sample required for the calibration was accurately weighed and transferred into the sample bulb. 100 ml of the calorimetric solvent was taken inside the Dewar flask. The sample bulb along with the other components was allowed to equilibrate at the bath temperature. A steady temperature signal was obtained once the calorimeter attained thermal equilibrium with the surrounding water bath. The sample bulb was then broken by pushing the glass rod and the sample was allowed to dissolve in the calorimetric solvent. The

consequent variation in the temperature signal was monitored. Electrical calibration was performed insitu before and after of each of these experiments.

Similar experiments were performed for the calorimetric measurements of samples of ternary bismuth molybdates as well as for the binary oxides viz., Bi_2O_3 (s) and MoO_3 (s). In each case the calorimetric solvent used was a mixture of 100 ml of 3 mol kg^{-1} NaOH and 25 ml of triethanolamine. The volume of triethanolamine was chosen in such a way that the molar ratio of metals to triethanolamine was maintained at $\sim 1:80$ for the dissolution experiments. The current and duration of its passage for the insitu electrical calibration was decided by the time taken for the sample to dissolve completely under the experimental conditions and the weight of the sample taken for each experiment. The maximum time taken for the dissolution of the samples was around 4 min. The temperature change, ΔT , during the experiment with the ternary compounds and starting components was also corrected for the heat exchange between calorimeter and surroundings as explained in Chapter 2 and was used for the evaluation of the enthalpy change for the reaction. Calorimetric measurements were repeated several times to obtain the reproducible data.

3.3.8 Determination of molar heat capacities of bismuth molybdates by differential scanning calorimetry

The heat capacity of bismuth molybdates were measured using a heat flux DSC (Mettler Toledo-Model No.DSC827e, Switzerland). Temperature calibration was carried out by measuring the melting points of high purity indium and zinc metals and the standard uncertainty in the temperature measurement was found to be ± 0.4 K. A three step procedure was adopted for the measurement of heat capacity. The three steps are i) blank run, ii) calibration run and iii) sample run. In the blank run, the heat flow rate is determined using empty aluminium pans of equal weight in the sample

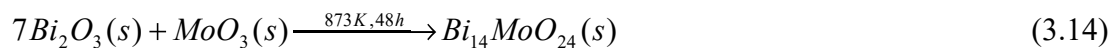
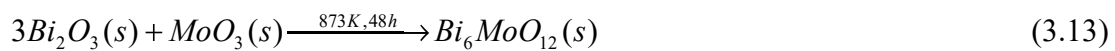
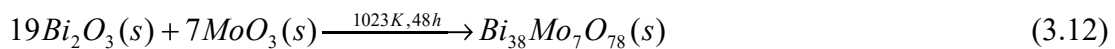
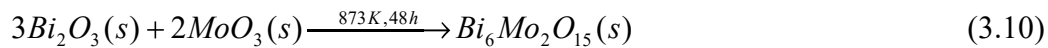
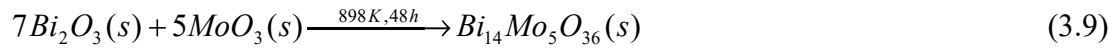
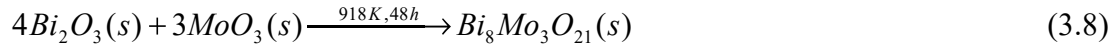
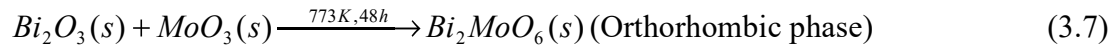
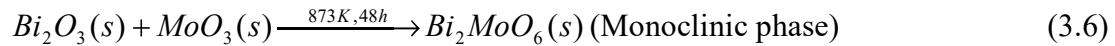
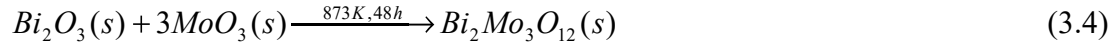
and reference sides. A disc of sapphire (NIST, USA) is used as the calibration reference. In the calibration run, sapphire is placed into the sample pan while the reference side is unchanged and the heat flow rate is measured as in the case of blank run. During sample run, sapphire in the sample pan is replaced by the sample and the heat flow rate is measured. In addition to the heat flow calibration by sapphire, performance of DSC was also verified by measuring the heat capacity of MoO₃ (s). Sample pellets were prepared by compaction of the powders followed by sintering them under vacuum. The sintered pellets (~110 mg) were then sealed in 40 mm³ aluminium pans and used for the measurement. For each sample, reproducibility was checked by repeating the measurement atleast for five to six times. Measurements were also repeated with two different pellets of the same sample. DSC measurements were carried out under high purity argon atmosphere maintained at a flow rate of 50 ml min⁻¹ upto a temperature of ~800 K at a heating rate of 10 K min⁻¹. The temperature program used for the measurement consisted of three segments: an isothermal segment at the initial temperature with a dwelling period of 10 min, followed by a dynamic segment at a heating rate of 10 K min⁻¹ and finally an isothermal segment at the final temperature for 10 min. Samples used for measurements were characterized by XRD before and after the calorimetric runs. The weight loss of the samples after DSC measurements was very low (~0.02-0.03%) indicating that vaporization losses are negligible. The heat capacity data at each temperature was obtained by taking the average of the calorimetric runs carried out with two sample pellets.

3.4 Results and discussion

3.4.1 Preparation and characterization of starting components and ternary compounds

The starting components MoO_3 and MoO_2 prepared in this study were characterized by XRD and the XRD patterns matched with PCPDF file nos. 00-005-0508 and 00-032-0671, respectively.

The solid state reactions leading to the formation of ternary bismuth molybdates can be represented by the following equations:



XRD patterns of the ternary compounds matched with PCPDF file nos. 00-021-0103, 00-033-0209, respectively for $\text{Bi}_2\text{Mo}_3\text{O}_{12}$ and $\text{Bi}_2\text{Mo}_2\text{O}_9$. Preparation of Bi_2MoO_6 at 773 K yielded the orthorhombic phase while the preparation at 873 K

yielded the monoclinic phase. The XRD patterns of the above two phases matched with PCPDF files 00-084-0787 and 04-009-3413, respectively. Similarly, XRD patterns of the other ternary compounds prepared by the solid state reaction between Bi_2O_3 and MoO_3 matched with the PCPDF file nos. 01-082-3470, 00-059-0526, 00-056-1473, 00-058-0668, 00-038-0249, 00-089-6667 and 00-050-1730, respectively for $\text{Bi}_8\text{Mo}_3\text{O}_{21}$, $\text{Bi}_{14}\text{Mo}_5\text{O}_{36}$, $\text{Bi}_6\text{Mo}_2\text{O}_{15}$, $\text{Bi}_{10}\text{Mo}_3\text{O}_{24}$, $\text{Bi}_{38}\text{Mo}_7\text{O}_{78}$, $\text{Bi}_{14}\text{MoO}_{24}$ and ' $\text{Bi}_{26}\text{Mo}_{10}\text{O}_{69}$ '. The XRD pattern of the compound $\text{Bi}_6\text{MoO}_{12}$ matched with those reported by Bleijenberg et al. [36].

3.4.2 Studies involving equilibrations of samples with compositions in the Bi_2O_3 - MoO_3 pseudo binary line

Table 3.4 shows the details of equilibration experiments performed to find out the presence of any ternary compound other than those reported by earlier investigators in the Bi_2O_3 - MoO_3 pseudo binary system. The XRD patterns of the products obtained after the long term equilibrations of different molar ratios of Bi_2O_3 and MoO_3 have shown the presence of either a mixture of two ternary compounds reported in literature or that of a ternary compound and the metal oxide. It is to be noted that the orthorhombic phase of Bi_2MoO_6 was obtained when equilibration was carried out at 773 K while the monoclinic phase was obtained when the equilibration was at 873 and 1023 K. Presence of the intermediate phase (γ'') reported in literature was not observed. Similarly presence of $\text{Bi}_2\text{Mo}_2\text{O}_9$ was not observed when equilibration was carried out at 773 K whereas it was observed when equilibrations were carried out at 873 K. This is in agreement with the data reported in literature. The equilibration of sample no 21 given in Table 3.4, which had an overall composition corresponding to the compound $\text{Bi}_{20}\text{MoO}_{33}$ reported by Sillen and Lundborg [30] and Kohlmuller and Badaud [31] at 773 as well as at 873 K yielded a

mixture of $\text{Bi}_{14}\text{MoO}_{24}$ and Bi_2O_3 as products indicating the non existence of $\text{Bi}_{20}\text{MoO}_{33}$. This is in agreement with that reported by Bleijenberg et al. [36]. Also the presence of $\text{Bi}_6\text{Mo}_2\text{O}_{15}$ was not observed at 1023 K, but it had transformed into the high temperature polymorph belonging to the ' $\text{Bi}_{26}\text{Mo}_{10}\text{O}_{69}$ ' solid solution. This observation is in agreement with those reported by previous investigators [42, 46].

XRD patterns obtained for the equilibration of compositions 15 to 17 indicate the presence of mixtures of $\text{Bi}_6\text{MoO}_{12}$ and $\text{Bi}_{10}\text{Mo}_3\text{O}_{24}$ at 773 and 873 K while equilibrations at 1023 K yielded mixtures of $\text{Bi}_{38}\text{Mo}_7\text{O}_{78}$ and $\text{Bi}_{10}\text{Mo}_3\text{O}_{24}$. This observation was further confirmed by results obtained for samples 22 to 27 given in Table 3.4. The overall composition of the sample 23 exactly corresponded to 3:1 Bi_2O_3 : MoO_3 and the XRD results have shown the presence of the compound $\text{Bi}_6\text{MoO}_{12}$ at 773 and 873 K. $\text{Bi}_{38}\text{Mo}_7\text{O}_{78}$ was present only after equilibration at 1023 K. Similarly the overall composition of the sample 26 corresponds to 2.71:1 Bi_2O_3 : MoO_3 and results of the equilibrations were same as in the case of sample 23. These results indicate that $\text{Bi}_{38}\text{Mo}_7\text{O}_{78}$ is not stable at 773 and 873 K while it is stable at 1023 K. At low temperatures, $\text{Bi}_6\text{MoO}_{12}$ is stable. It is to be pointed out that no other phase was found to be present along with $\text{Bi}_{38}\text{Mo}_7\text{O}_{78}$, and this indicates the presence of a wide non-stoichiometry in $\text{Bi}_{38}\text{Mo}_7\text{O}_{78}$ phase as suggested by Tomasi et al. [34]. Hereafter in the text, the solid solution based on $\text{Bi}_{38}\text{Mo}_7\text{O}_{78}$ phase will be designated as ' $\text{Bi}_{38}\text{Mo}_7\text{O}_{78}$ '.

Thus based on the equilibration along the Bi_2O_3 - MoO_3 pseudo binary line, presence of ten ternary compounds, namely, $\text{Bi}_2\text{Mo}_3\text{O}_{12}$, $\text{Bi}_2\text{Mo}_2\text{O}_9$, Bi_2MoO_6 , $\text{Bi}_8\text{Mo}_3\text{O}_{21}$, $\text{Bi}_{14}\text{Mo}_5\text{O}_{36}$, $\text{Bi}_6\text{Mo}_2\text{O}_{15}$, $\text{Bi}_{10}\text{Mo}_3\text{O}_{24}$, $\text{Bi}_{38}\text{Mo}_7\text{O}_{78}$, $\text{Bi}_6\text{MoO}_{12}$ and $\text{Bi}_{14}\text{MoO}_{24}$ along with the high temperature solid solution ' $\text{Bi}_{26}\text{Mo}_{10}\text{O}_{69}$ ' are confirmed.

3.4.3 Studies involving equilibrations of samples with compositions in the line joining Bi_2O_3 and MoO_2

The long term equilibrations of samples with different molar ratios of Bi_2O_3 and MoO_2 as starting materials have shown that there are no ternary compounds involving Bi_2O_3 and MoO_2 (Table 3.5). However, the results revealed the existence of the phase fields $\text{Bi-MoO}_2\text{-Bi}_2\text{MoO}_6$ at 773 and 1023 K, $\text{Bi-Bi}_{10}\text{Mo}_3\text{O}_{24}\text{-Bi}_6\text{MoO}_{12}$ at 773 K and $\text{Bi-Bi}_{10}\text{Mo}_3\text{O}_{24}\text{-Bi}_{38}\text{Mo}_7\text{O}_{78}$ at 1023 K.

3.4.4 Studies involving partial reduction of ternary compounds followed by long term equilibrations

The equilibrium phases obtained after the long term equilibrations of partially reduced ternary compounds are given in Table 3.6. Upon partial reduction, the overall composition of reduced samples has moved towards lower oxygen content. The XRD analysis of these samples after long term equilibrations confirmed the existence of $\text{Bi-MoO}_2\text{-Bi}_2\text{MoO}_6$ phase field at 773 as well as at 1023 K.

3.4.5 Studies involving long term equilibrations of phase mixtures using different starting components and equilibrations in liquid bismuth

In order to determine the coexisting phases in the ternary Bi-Mo-O system, several long term equilibrations were performed by taking different starting components. These equilibrations revealed the existence of different phase fields (Table 3.7). The phase fields identified are: (1) Bi-Mo-MoO_2 , (2) $\text{Bi-MoO}_2\text{-Bi}_2\text{MoO}_6$, (3) $\text{Bi}_2\text{MoO}_6\text{-MoO}_2\text{-Bi}_2\text{Mo}_3\text{O}_{12}$, (4) $\text{Bi-Bi}_2\text{MoO}_6\text{-Bi}_6\text{Mo}_2\text{O}_{15}$, (5) $\text{Bi-Bi}_{10}\text{Mo}_3\text{O}_{24}\text{-Bi}_6\text{MoO}_{12}$ (6) $\text{Bi-Bi}_6\text{MoO}_{12}\text{-Bi}_{14}\text{MoO}_{24}$ and (7) $\text{Bi-Bi}_{14}\text{MoO}_{24}\text{-Bi}_2\text{O}_3$ at 773 K, (1) Bi-Mo-MoO_2 , (2) $\text{Bi-MoO}_2\text{-Bi}_2\text{MoO}_6$, (3) $\text{Bi}_2\text{MoO}_6\text{-MoO}_2\text{-Bi}_2\text{Mo}_2\text{O}_9$, (4) $\text{Bi}_2\text{Mo}_2\text{O}_9\text{-MoO}_2\text{-Bi}_2\text{Mo}_3\text{O}_{12}$ and (5) $\text{Bi-Bi}_{14}\text{MoO}_{24}\text{-Bi}_2\text{O}_3$ at 873 K and (1) Bi-Mo-MoO_2 , (2) $\text{Bi-MoO}_2\text{-Bi}_2\text{MoO}_6$, (3) $\text{Bi-Bi}_2\text{MoO}_6\text{-'Bi}_{26}\text{Mo}_{10}\text{O}_{69}'$, (4) $\text{Bi-Bi}_{10}\text{Mo}_3\text{O}_{24}\text{-'Bi}_{38}\text{Mo}_7\text{O}_{78}'$, (5) $\text{Bi-'Bi}_{38}\text{Mo}_7\text{O}_{78}'\text{-Bi}_{14}\text{MoO}_{24}$ and (6) $\text{Bi-Bi}_{14}\text{MoO}_{24}\text{-Bi}_2\text{O}_3$ at 1023 K.

Further evidences for the presence of additional phase fields were obtained from the results of several long term equilibrations in liquid bismuth. These experiments also helped to confirm the existence of the phase fields which were identified in the previous equilibration studies. The results are summarized in Table 3.8. The data in the table shows the existence of the following phase fields: (1) Bi-MoO₂-Bi₂MoO₆, (2) Bi-Bi₂MoO₆-Bi₆Mo₂O₁₅, (3) Bi-Bi₆Mo₂O₁₅-Bi₁₀Mo₃O₂₄, (4) Bi-Bi₁₀Mo₃O₂₄-Bi₆MoO₁₂, (5) Bi-Bi₆MoO₁₂-Bi₁₄MoO₂₄ and (6) Bi-Bi₁₄MoO₂₄-Bi₂O₃ at 773 K, (1) Bi-Bi₂MoO₆-Bi₈Mo₃O₂₁, (2) Bi-Bi₈Mo₃O₂₁-Bi₁₄Mo₅O₃₆, (3) Bi-Bi₁₄Mo₅O₃₆-Bi₆Mo₂O₁₅, (4) Bi-Bi₆Mo₂O₁₅-Bi₁₀Mo₃O₂₄, (5) Bi-Bi₁₀Mo₃O₂₄-Bi₆MoO₁₂ and (6) Bi-Bi₆MoO₁₂-Bi₁₄MoO₂₄ at 873 K and (1) Bi-MoO₂-Bi₂MoO₆, (2) Bi-‘Bi₂₆Mo₁₀O₆₉’-Bi₁₀Mo₃O₂₄, (3) Bi-Bi₁₀Mo₃O₂₄-‘Bi₃₈Mo₇O₇₈’, (4) Bi-‘Bi₃₈Mo₇O₇₈’-Bi₁₄MoO₂₄ and (5) Bi-Bi₁₄MoO₂₄-Bi₂O₃ at 1023 K.

Using these results, the partial phase diagrams of the ternary Bi-Mo-O system valid at 773, 873 and 1023 K have been constructed and are shown in Figs. 3.10 to 3.12.

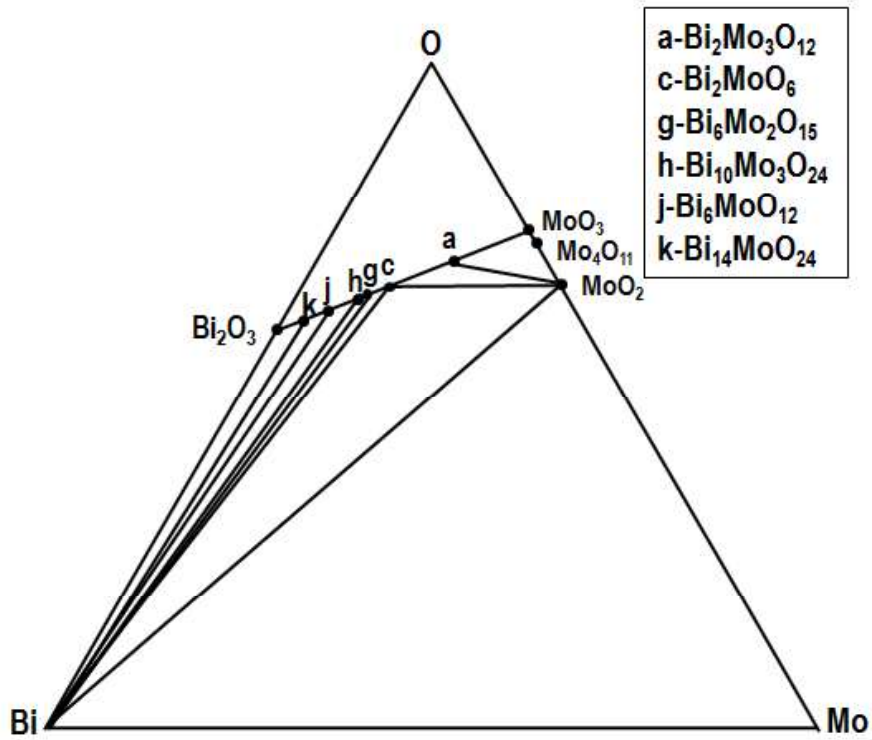


Fig. 3.10 Partial phase diagram of Bi-Mo-O system at 773 K

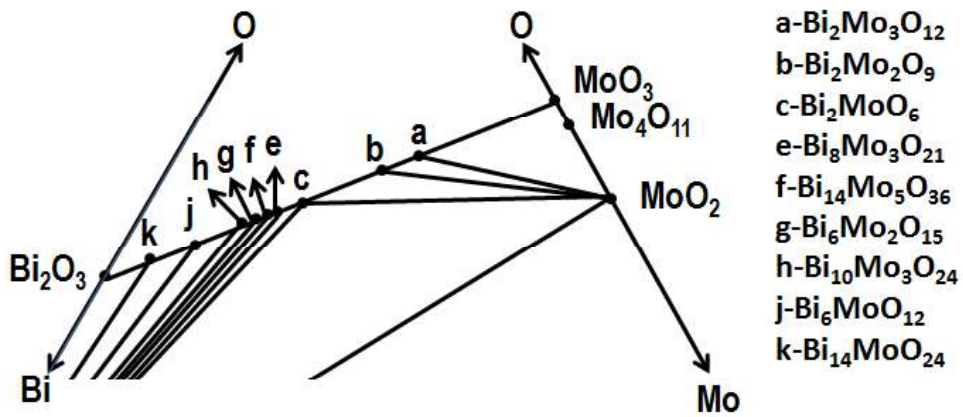


Fig. 3.11 Partial phase diagram of Bi-Mo-O system at 873 K

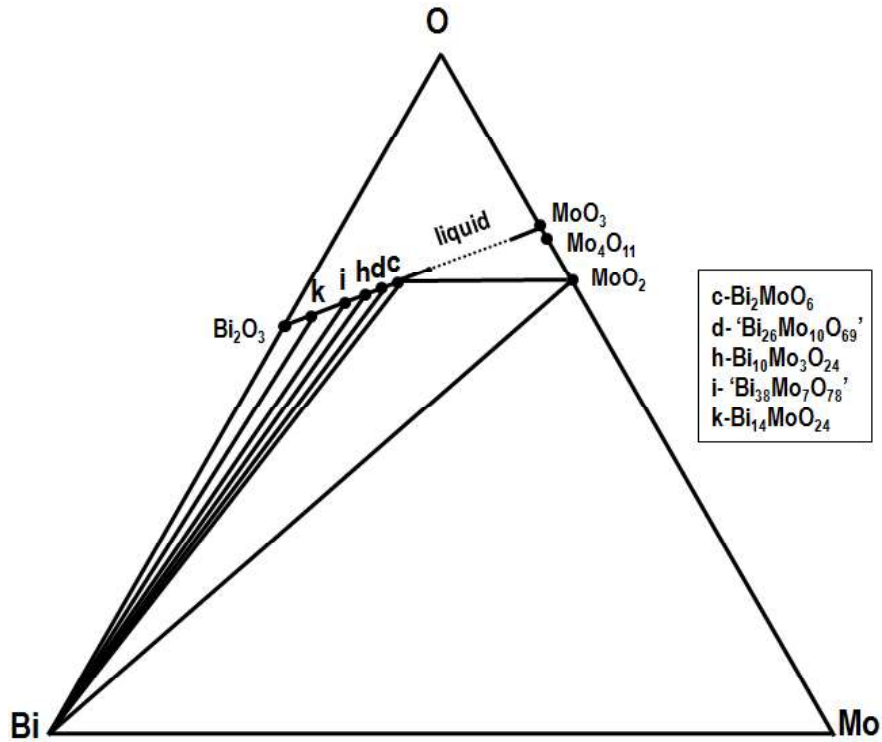


Fig. 3.12 Partial phase diagram of Bi-Mo-O system at 1023 K

3.4.6 Investigation on the thermal stabilities of $\text{Bi}_8\text{Mo}_3\text{O}_{21}$, $\text{Bi}_{14}\text{Mo}_5\text{O}_{36}$ and $\text{Bi}_6\text{Mo}_2\text{O}_{15}$

Experimental results obtained for the long term equilibrations of $\text{Bi}_8\text{Mo}_3\text{O}_{21}$ at different temperatures are given in Table 3.9. It can be seen that upon equilibration at 771, 788 and 805 K, $\text{Bi}_8\text{Mo}_3\text{O}_{21}$ has decomposed to give a mixture of Bi_2MoO_6 and $\text{Bi}_6\text{Mo}_2\text{O}_{15}$ phases. This indicates that $\text{Bi}_8\text{Mo}_3\text{O}_{21}$ is not stable at temperatures below 805 K. However, for equilibrations in the temperature range of 841 to 912 K, the $\text{Bi}_8\text{Mo}_3\text{O}_{21}$ phase was retained which shows that $\text{Bi}_8\text{Mo}_3\text{O}_{21}$ is stable at these temperatures. Hence, $\text{Bi}_8\text{Mo}_3\text{O}_{21}$ appears as a stable phase at temperature lying between 805 and 841 K. The equilibration of $\text{Bi}_8\text{Mo}_3\text{O}_{21}$ at temperatures between 931 and 1023 K has resulted in the formation of ' $\text{Bi}_{26}\text{Mo}_{10}\text{O}_{69}$ ' phase only which suggests that $\text{Bi}_8\text{Mo}_3\text{O}_{21}$ undergoes transition into the high temperature polymorph belonging to the solid solution phase at temperature falling between 912 and 931 K.

The plot of electrical conductivity of $\text{Bi}_8\text{Mo}_3\text{O}_{21}$ as a function of reciprocal temperature is shown in Fig. 3.13. The conductivity measurements were carried out from 773 to 973 K. As seen from the plot, a slope change is observed at 917 ± 5 K. XRD analysis of the sample retrieved after the conductivity measurements at 973 K has shown the presence of ' $\text{Bi}_{26}\text{Mo}_{10}\text{O}_{69}$ ' phase. This indicates that at 917 ± 5 K, $\text{Bi}_8\text{Mo}_3\text{O}_{21}$ would transform to the high temperature solid solution ' $\text{Bi}_{26}\text{Mo}_{10}\text{O}_{69}$ '.

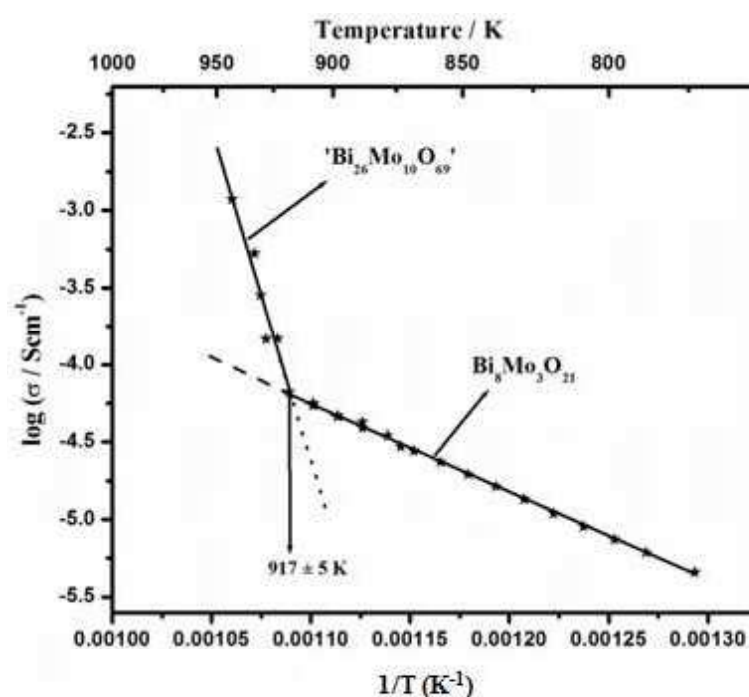


Fig. 3.13 Variation of electrical conductivity of $\text{Bi}_8\text{Mo}_3\text{O}_{21}$ as a function of temperature

The results based on the XRD patterns of the products obtained after the simultaneous equilibrations of $\text{Bi}_8\text{Mo}_3\text{O}_{21}$ at different temperatures in air are given in Table 3.10. The data indicates that upon equilibrations at 873 and 898 K, the $\text{Bi}_8\text{Mo}_3\text{O}_{21}$ phase was retained while equilibrations at 923, 948 and 973 K had led to the formation of the ' $\text{Bi}_{26}\text{Mo}_{10}\text{O}_{69}$ ' phase. This supports the conclusion based on electrical conductivity measurement. The activation energy determined from the Arrhenius plot is found to be 1.13 eV for the temperature range of 773 to 917 K

indicating the conductivity due to oxide ions as reported in reference [47]. Results obtained from the long term equilibrations of $\text{Bi}_8\text{Mo}_3\text{O}_{21}$ samples at different temperatures clearly show that $\text{Bi}_8\text{Mo}_3\text{O}_{21}$ is unstable at temperatures below 805 K and it decomposes to give a mixture of Bi_2MoO_6 and $\text{Bi}_6\text{Mo}_2\text{O}_{15}$ phases. Equilibration at 788 K for 24 h (Table 3.10) also supports this. However, in the electrical conductivity measurements, no slope change corresponding to the decomposition was observed. This can be attributed to the structural similarities of $\text{Bi}_8\text{Mo}_3\text{O}_{21}$, Bi_2MoO_6 and $\text{Bi}_6\text{Mo}_2\text{O}_{15}$ as all of them crystallize in the monoclinic system and hence they could possess similar conductivity values.

Results obtained for the long term equilibrations of $\text{Bi}_{14}\text{Mo}_5\text{O}_{36}$ at different temperatures are given in Table 3.9. It is seen that the equilibration of $\text{Bi}_{14}\text{Mo}_5\text{O}_{36}$ at temperatures 766, 782 and 798 K has given a mixture of Bi_2MoO_6 and $\text{Bi}_6\text{Mo}_2\text{O}_{15}$ phases. This indicates that $\text{Bi}_{14}\text{Mo}_5\text{O}_{36}$ is unstable at these temperatures and undergoes decomposition at temperatures below 798 K. Equilibrations at 817, 838 and 883 K has resulted in a mixture of Bi_2MoO_6 and $\text{Bi}_6\text{Mo}_2\text{O}_{15}$ along with $\text{Bi}_{14}\text{Mo}_5\text{O}_{36}$. It shows that $\text{Bi}_{14}\text{Mo}_5\text{O}_{36}$ is stable at these temperatures and it is appearing to be as a stable phase at temperatures between 798 and 817 K. Single phase of $\text{Bi}_{14}\text{Mo}_5\text{O}_{36}$ was present after equilibrations at temperatures between 883 and 947 K whereas equilibrations between 968 and 1023 K had yielded the ' $\text{Bi}_{26}\text{Mo}_{10}\text{O}_{69}$ ' phase. This shows the temperature at which $\text{Bi}_{14}\text{Mo}_5\text{O}_{36}$ would undergo transformation in to the high temperature solid solution phase lies between 947 and 968 K.

Variation of logarithm of electrical conductivity of $\text{Bi}_{14}\text{Mo}_5\text{O}_{36}$ with reciprocal temperature obtained is shown in Fig. 3.14. Conductivity had been measured in the temperature range of 748 to 990 K and a change in slope is seen at

963 ± 5 K corresponding to the transition of $\text{Bi}_{14}\text{Mo}_5\text{O}_{36}$ to ' $\text{Bi}_{26}\text{Mo}_{10}\text{O}_{69}$ ' phase. This observation is in accordance with the results obtained from the simultaneous equilibration experiments (Table 3.10). $\text{Bi}_{14}\text{Mo}_5\text{O}_{36}$ was retained on equilibrations at 873, 923 and 948 K whereas on equilibration at 973 K it transformed to ' $\text{Bi}_{26}\text{Mo}_{10}\text{O}_{69}$ '. Further, XRD analysis of the pellet retrieved after the conductivity measurements at 990 K has shown the presence of ' $\text{Bi}_{26}\text{Mo}_{10}\text{O}_{69}$ ' phase only. Activation energy determined from the Arrhenius plot is found to be 1.39 eV for the temperature range of 748 to 963 K. As in the case of $\text{Bi}_8\text{Mo}_3\text{O}_{21}$, long term equilibration experiments at different temperatures (Table 3.9) along with equilibration at 773 K for 24 h (Table 3.10) had shown that $\text{Bi}_{14}\text{Mo}_5\text{O}_{36}$ is unstable at temperatures below 817 K and it had partially decomposed to Bi_2MoO_6 and $\text{Bi}_6\text{Mo}_2\text{O}_{15}$ phases. However, we could not observe any slope change corresponding to this decomposition in the Arrhenius plot of conductivity. Since all the three ternary compounds involved in this disproportionation reaction have monoclinic structure, they are expected to have similar conductivities and hence this behavior.

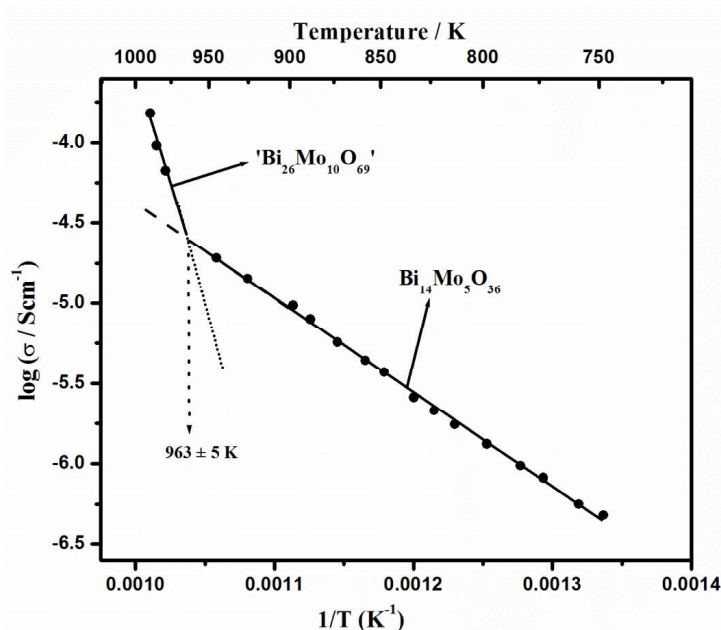


Fig. 3.14 Variation of electrical conductivity of $\text{Bi}_{14}\text{Mo}_5\text{O}_{36}$ as a function of temperature

Equilibration of $\text{Bi}_6\text{Mo}_2\text{O}_{15}$ at different temperatures between 745 and 901 K for prolonged duration has shown that $\text{Bi}_6\text{Mo}_2\text{O}_{15}$ is stable at these temperatures. The XRD patterns have shown the presence of single phase of $\text{Bi}_6\text{Mo}_2\text{O}_{15}$ only (Table 3.9). However, upon equilibrations at temperatures between 928 and 998 K, ' $\text{Bi}_{26}\text{Mo}_{10}\text{O}_{69}$ ' phase was obtained. This indicates the transition of $\text{Bi}_6\text{Mo}_2\text{O}_{15}$ to the high temperature solid solution phase occurs at a temperature falling between 901 and 928 K.

The plot of variation of electrical conductivity of $\text{Bi}_6\text{Mo}_2\text{O}_{15}$ with temperature, as presented in Fig. 3.15, showed a slope change at 891 ± 5 K. These observations were further verified by carrying out simultaneous equilibration experiments (Table 3.10).

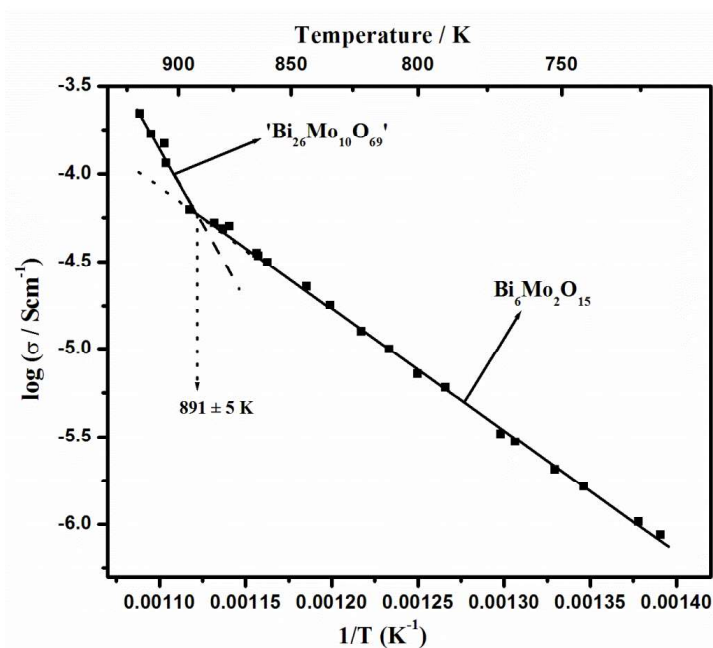


Fig. 3.15 Variation of electrical conductivity of $\text{Bi}_6\text{Mo}_2\text{O}_{15}$ as a function of temperature

It can be seen that upon equilibration at 873 K, $\text{Bi}_6\text{Mo}_2\text{O}_{15}$ phase remains unaltered whereas after equilibrations at 898 and 923 K, ' $\text{Bi}_{26}\text{Mo}_{10}\text{O}_{69}$ ' was formed. Further, XRD analysis of the pellet retrieved from the conductivity cell after

measurement at 917 K showed the presence of 'Bi₂₆Mo₁₀O₆₉' phase. Activation energy determined from the Arrhenius plot is found to be 1.16 eV for the temperature range of 718 to 891 K.

3.4.7 Investigation of thermal stability of Bi₂Mo₂O₉

To identify the temperature above which Bi₂Mo₂O₉ is stable, its electrical conductivity as a function of temperature was measured.

The variation of conductivity with temperature as $\log \sigma$ Vs $1/T$ is shown in Fig. 3.16. As seen from the figure, a slope change is observed at 817 ± 5 K. The XRD analysis of the sample retrieved after the conductivity measurements (sample quenched to room temperature from 754 K) has shown the presence of Bi₂MoO₆ (orthorhombic phase) and Bi₂Mo₃O₁₂ phases. The results of simultaneous equilibration of Bi₂Mo₂O₉ at different temperatures in air (Table 3.11) also show that Bi₂Mo₂O₉ is stable at 823 and 873 K but undergoes decomposition at 773 and 798 K. Consideration of conductivity data in conjunction with these XRD data indicates that Bi₂Mo₂O₉ would decompose to form Bi₂MoO₆ and Bi₂Mo₃O₁₂ at 817 ± 5 K. The activation energies determined from the Arrhenius plot are found to be 1.19 eV and 1.44 eV, respectively for the temperature ranges of 753 to 817 K and 817 to 913 K. Hartmanova et al. [69] have also measured electrical conductivity of Bi₂Mo₂O₉ in the temperature range of 454 to 713 K and reported the activation energy as 1.15 eV which is in good agreement with the present value of 1.19 eV obtained for conduction in the low temperature regime.

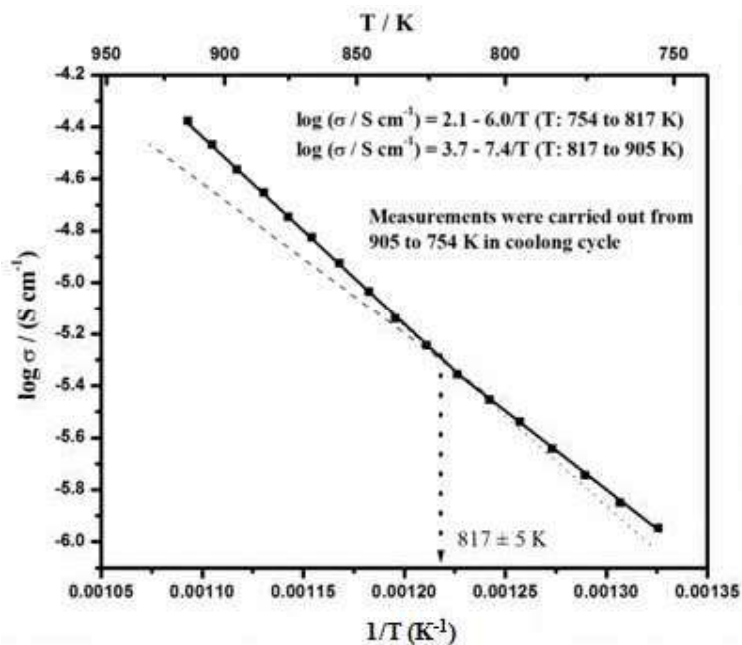


Fig. 3.16 Variation of electrical conductivity of $\text{Bi}_2\text{Mo}_2\text{O}_9$ as a function of temperature (Below 817 K, the phases present are $\text{Bi}_2\text{Mo}_3\text{O}_{12}$ and Bi_2MoO_6)

3.4.8 Investigation on the polymorphic transformations of Bi_2MoO_6

The variation of conductivity of the orthorhombic phase of Bi_2MoO_6 with temperature is shown in Fig. 3.17. Conductivities were measured during a heating cycle from 700 to 963 K. It can be seen that at temperatures between 868 and 871 K a sharp drop in conductivity occurred. Further increase in the temperature resulted in the steady increase in conductivity. The XRD analysis of the samples equilibrated at 773, 823, 843 and 853 K (Table 3.11) had shown the presence of orthorhombic phase of Bi_2MoO_6 while the equilibrations at 873, 923 and 973 K had shown the presence of the monoclinic phase. Hence, the drop in conductivity is due to the transformation of orthorhombic phase to monoclinic phase at ~ 870 K. The presence of an intermediate phase (γ'') has been reported in literature in the temperature range of ~ 840 to 877 K. However, in samples after equilibration at 843 and 853 K, we could observe only the orthorhombic phase of Bi_2MoO_6 . Intermediate γ'' phase could not be observed in

samples from both conductivity and equilibration experiments. The activation energies for conductivity deduced from the plot are 1.85 eV and 1.97 eV, respectively for the temperature ranges of 763 to 868 K and 872 to 963 K corresponding to the orthorhombic and monoclinic phases of Bi_2MoO_6 . Arrhenius plot obtained for the electrical conductivity measurements carried out while cooling the monoclinic phase of Bi_2MoO_6 is also shown in Fig. 3.17. No change in slope is observed in the conductivity plot suggesting that the compound had not undergone any phase transition at low temperatures and this is in agreement with the irreversible nature of the orthorhombic to monoclinic phase transition reported in literature. This is also supported by the results of the equilibration experiments with the monoclinic phase of Bi_2MoO_6 given in Table 3.11. XRD analysis of the samples obtained after equilibration at all temperatures (773, 823, 873 and 973 K) showed the presence of monoclinic phase of Bi_2MoO_6 only.

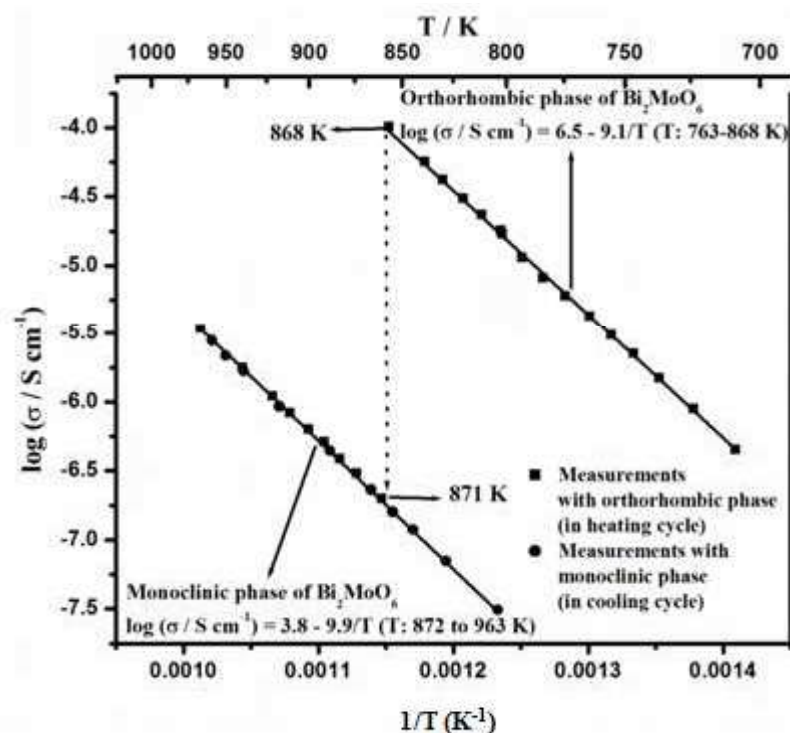


Fig. 3.17 Variation of electrical conductivity of orthorhombic and monoclinic phases of Bi_2MoO_6 as a function of temperature

3.4.9 Oxygen potential measurements

3.4.9.1 Standard molar Gibbs energy of formation of Bi_2MoO_6 (s)

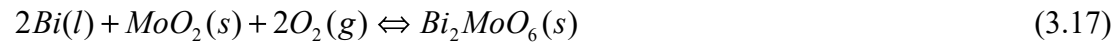
The XRD analysis of the sample pellets retrieved at the end of emf measurements showed the presence of Bi, MoO_2 and Bi_2MoO_6 phases. Monoclinic phase of Bi_2MoO_6 was observed to be present. As mentioned earlier, first temperature of operation in each cell was in the temperature range of 1023 K for cell-I and 936 K for cell-II, where the monoclinic phase of Bi_2MoO_6 is stable. It is known that the transition of Bi_2MoO_6 from the orthorhombic phase to monoclinic phase is irreversible and the electrical conductivity measurements have shown that the transformation occurring at ~ 868 K. The monoclinic form of Bi_2MoO_6 is known to be metastable at room temperature. Hence, the phase that was present during emf measurements was the monoclinic form of Bi_2MoO_6 .

The emf values measured as a function of temperature in the case of sample with composition within the Bi- MoO_2 - Bi_2MoO_6 phase field are given in Table 3.12. The variation of cell emf with temperature is shown in Fig. 3.18 and can be expressed by the following least squares fitted expression:

$$E \pm 0.7 / \text{mV} = 1039.7 - 0.4358 (T/\text{K}) \quad (T: 772\text{-}1023 \text{ K}) \quad (3.16)$$

The error indicated is the expanded uncertainty with 0.95 level of confidence.

The chemical equilibrium at the sample electrode is represented as below:



$$\Delta_f G_m^\circ < \text{Bi}_2\text{MoO}_6 > = \Delta_f G_m^\circ < \text{MoO}_2 > + 2RT \ln p_{\text{O}_2}^s \quad (3.18)$$

where $p_{\text{O}_2}^s$ is the partial pressure of oxygen at the sample electrode.

Table 3.12 Variation of EMF with temperature in the Bi-MoO₂-Bi₂MoO₆ phase field

Sample 1		Sample 2	
Temperature / K	Emf / mV	Temperature / K	Emf / mV
1022.7	595.4	936.3	631.8
921.5	638.2	911.6	642.5
823.9	680.9	886.5	653.6
998.5	605.3	873.7	659.5
899.1	648.3	861.1	664.6
947.0	627.2	1014.3	597.6
849.0	670.0	911.2	641.2
1010.5	599.7	936.9	630.2
985.4	610.2	864.3	662.3
961.0	620.9	962.1	619.3
-	-	987.9	608.3
-	-	772.6	703.3
-	-	799.2	691.7

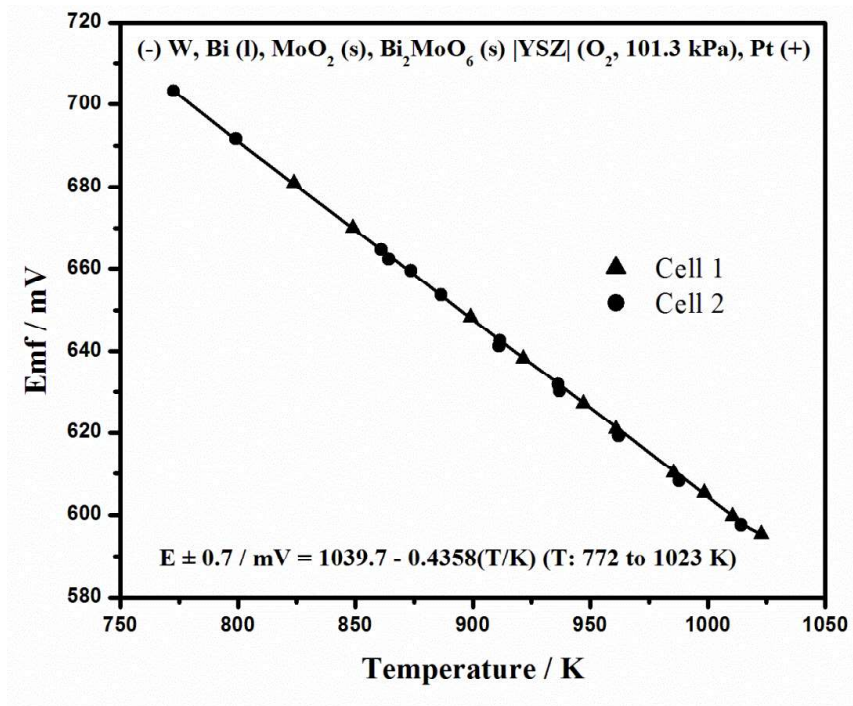


Fig. 3.18 Variation of emf with temperature with Bi- MoO₂-Bi₂MoO₆ as sample

The cell emf is given by

$$E = \frac{RT}{4F} \ln \frac{P_{O_2}^R}{P_{O_2}^S} \quad (3.19)$$

where E is the electromotive force in volts, R is the universal gas constant (8.314 J K⁻¹ mol⁻¹), F is the Faraday constant (96485 C mol⁻¹) and $P_{O_2}^R$ is the partial pressure of oxygen in the reference electrode. Equation (3.19) can be written as

$$4FE = RT \ln P_{O_2}^R - RT \ln P_{O_2}^S \quad (3.20)$$

Since $P_{O_2}^R = 1 \text{ atm}$, $RT \ln p_{O_2}^S = -4FE$

Thus the standard molar Gibbs energy of formation of the monoclinic phase of Bi₂MoO₆(s) can be obtained from the measured emf values as given below:

$$\Delta_f G_m^\circ < Bi_2MoO_6 > = \Delta_f G_m^\circ < MoO_2 > - 8FE \quad (3.21)$$

By substituting the emf data given by expression (3.16) and using the following data on molar Gibbs energy of formation of MoO₂ (s) from ref. 23

$$\Delta_f G^\circ < MoO_2 > \pm 0.6 / kJ mol^{-1} = -579.8 + 0.1700(T / K) \quad (T : 925 - 1533 K) \quad (3.22)$$

The standard molar Gibbs energy of formation of monoclinic phase of Bi₂MoO₆(s) was derived and is given below:

$$\Delta_f G^\circ < Bi_2MoO_6 > \pm 0.8 / kJ mol^{-1} = -1382.3 + 0.5064(T / K) \quad (T : 772 - 1023 K) \quad (3.23)$$

To determine the uncertainties introduced in the Gibbs energy of formation of Bi₂MoO₆ (s) due to variation in the total local atmospheric pressure of the site, atmospheric pressure during the experimental period was continuously monitored.

The variation was found to be $\pm 0.008 \text{ atm}$.

The uncertainties introduced due to this variation are calculated as below:

The standard molar Gibbs energy of formation of Bi₂MoO₆ (s) is deduced from the following equation:

$$\Delta_f G_m^\circ < Bi_2MoO_6 > = \Delta_f G_m^\circ < MoO_2 > + 2RT \ln P_{O_2}^R - 8FE \quad (3.24)$$

When $P_{O_2}^R = 1$ atm, the expression (3.24) could be written as:

$$\Delta_f G_m^\circ < Bi_2MoO_6 > = \Delta_f G_m^\circ < MoO_2 > - 8FE$$

At the maximum temperature of emf measurement ($T = 1023$ K),

$$\Delta_f G_m^\circ < Bi_2MoO_6 > = -864.3 \pm 0.8 \text{ kJ mol}^{-1}.$$

When there is deviation in $P_{O_2}^R$ from 1 atm, i.e. $P_{O_2}^R = 1 \pm 0.008$ atm, the errors introduced at the maximum temperature of 1023 K is calculated as below:

At $T = 1023$ K and $P = 1.008$ atm,

$$2RT \ln 1.008 = 0.136 \text{ kJ mol}^{-1}$$

And when $P = 0.992$ atm,

$$2RT \ln 0.992 = -0.136 \text{ kJ mol}^{-1}$$

Hence, the error due to the variation of reference pressure = $\pm 0.136 \text{ kJ mol}^{-1}$.

Therefore,

$$\Delta_f G_m^\circ < Bi_2MoO_6 > = \Delta_f G_m^\circ < MoO_2 > + 2RT \ln P_{O_2}^R - 8FE = -864.3 \pm 0.136 \text{ kJ mol}^{-1}$$

at 1023 K.

This error is negligible compared to the uncertainty reported for the Gibbs energy of formation of Bi_2MoO_6 (s) ($\pm 0.8 \text{ kJ mol}^{-1}$).

3.4.10 Standard molar enthalpies of formation of bismuth molybdates

The experimental results obtained for the enthalpy of dissolution of TRIS are given in Table 3.13. The molar enthalpy of solution of TRIS obtained in the present work is $(-29.62 \pm 0.44) \text{ kJ mol}^{-1}$ which is in good agreement with the reported value of $(-29.770 \pm 0.032) \text{ kJ mol}^{-1}$ [70]. Thus it ensures the suitability of the experimental set up for calorimetric measurements.

Table 3.13 Enthalpy of solution ($\Delta_{sol}H_m^{\circ}$) of TRIS* in 0.10 ± 0.01 mol / kg HCl (mass of solvent = 99.52 ± 0.01 g) at 298.15 K[@] and 0.1 MPa^a (Molar mass of TRIS = 121.1 g mol⁻¹)

Run	Weight of TRIS (w / g) ^a	Experimental enthalpy change (ΔH / J)	Molar enthalpy of solution ($\Delta_{sol}H_m^{\circ}$ / kJ mol ⁻¹)
1	0.2354	-57.73	-29.70
2	0.2313	-57.07	-29.87
3	0.2295	-55.71	-29.40
4	0.2295	-56.15	-29.63
5	0.2161	-52.62	-29.48
			Average: (-29.62 ± 0.44)^b

*Tris(hydroxymethyl)aminomethane (s), [@]Temperature stability inside the calorimeter prior to start of experiment was within ± 0.001 K. ^a Standard uncertainty, *u*, are $u(P) = 0.8$ kPa and $u(w) = 0.001$, ^b Expanded uncertainty $U(\Delta_{sol}H_m^{\circ})$ is calculated as 2σ of the mean with 0.95 level of confidence. Uncertainty from calibration was also included into the final uncertainty of the dissolution enthalpies.

In the present study, the standard molar enthalpies of formation of bismuth molybdates were determined by measuring their enthalpies of dissolution. A suitable solvent which can dissolve the ternary bismuth molybdates as well as the component oxides, Bi₂O₃ (s) and MoO₃ (s) has to be used for the dissolution experiments. Also the samples should dissolve in the solvent in a reasonable period of time. Several mineral acids and alkalis were tried for the solubility experiments and the bismuth molybdates were found to be insoluble in all of them.

It is known from literature that triethanolamine (TEA) is a versatile ligand and can readily form coordination complexes with almost all metal ions and behave as N and O-donor ligands [71]. TEA can form complexes with Bi³⁺ and Mo⁶⁺ ions as well. The complexes of TEA with Bi find its application in medical fields. For the preparation of medically relevant Bi-TEA complexes, the ratio of Bi to TEA used was reported to be ranging from 1:2.6 to 1:5.2 [72]. Miller described the conditions for the

formation of complexes of TEA with bismuth and reported that TEA forms 1:1 complex with bismuth ions [72]. Based on differential pulse polarography experiments, Hancock et al. [73] determined the formation constant ($\log K$) of this 1:1 complex and it is found to be 9.2. The complexation of molybdenum ions with TEA was studied by Szalontai et al. [74]. Under alkaline pH, the mononuclear molybdate anion exists in the tetrahedral form while upon chelation with triethanolamine, it forms soluble oxomolybdate (VI) complexes which exist in the octahedral or distorted octahedral configuration. It is also reported that water soluble complexes of Mo-TEA could form when the ratio of Mo to TEA is 1:3 [74]. In the present experiments, the ratio of metals to TEA was maintained as 1:80, so as to maintain a large excess of TEA. The final solution obtained after the dissolution of bismuth molybdates as well as the component oxides were clear and there were no perceptible precipitates. Based on the reports in literature, it is clear that both bismuth and molybdenum salts can form water soluble complexes with triethanolamine under alkaline conditions. This fact has been employed in the present study. The solubility of ternary bismuth molybdates along with that of Bi_2O_3 (s) and MoO_3 (s) was checked in a mixture of triethanolamine and NaOH solution. It was observed that all the ternary bismuth molybdates as well as the component oxides were soluble in the solvent and the maximum time taken for the dissolution was found to be ~4 min under the chosen experimental conditions.

The experimental results obtained for the measurement of enthalpy of solution of the starting components, Bi_2O_3 (s) and MoO_3 (s) and that for ternary components are given in Tables 3.14 and 3.15, respectively.

Table 3.14 Experimentally determined values of enthalpies of dissolution (ΔH) and molar enthalpies of dissolution ($\Delta_{sol}H_m^o$) of Bi_2O_3 (s) and MoO_3 (s) in a mixture of 100 ml of 3 mol kg^{-1} NaOH and 25 ml of triethanolamine at 298.15 K* and 0.1 MPa^a

Sample	Weight of sample (w / g) ^a	Experimental enthalpy change (ΔH / J)	Molar enthalpy of solution ($\Delta_{sol}H_m^o$ / kJ mol^{-1})
Bi_2O_3 (s) (molar mass = 465.96 g mol^{-1})	0.6923	-62.34	-41.96
	0.4020	-36.97	-42.86
	0.4400	-39.84	-42.18
	0.4388	-41.00	-43.54
	0.2650	-24.52	-43.11
	0.3645	-33.37	-42.66
	0.2002	-18.87	-43.93
	0.3152	-28.30	-41.83
	0.2568	-23.45	-42.56
Average: (-42.74 \pm 0.77)^b			
MoO_3 (s) (molar mass = 143.9382 g mol^{-1})	0.3239	-178.67	-79.39
	0.2459	-136.19	-79.72
	0.2699	-150.62	-80.32
	0.2392	-131.89	-79.36
	0.2450	-136.71	-80.32
Average: (-79.82 \pm 1.19)^b			

*Temperature stability inside the calorimeter prior to start of experiment was within ± 0.001 K. ^a Standard uncertainties, u , are $u(P) = 0.8$ kPa and $u(w) = 0.0001$ g. ^bExpanded uncertainty, $U(\Delta_{sol}H_m^o)$, is calculated as 2σ of the mean with 0.95 level of confidence. Uncertainty from calibration was also included into the final uncertainty of the dissolution enthalpies.

The molar enthalpies of solution, $\Delta_{sol}H_m^o$ of Bi_2O_3 (s), MoO_3 (s), $\text{Bi}_2\text{Mo}_3\text{O}_{12}$ (s), orthorhombic- Bi_2MoO_6 (s), monoclinic- Bi_2MoO_6 (s), $\text{Bi}_6\text{Mo}_2\text{O}_{15}$ (s), and $\text{Bi}_6\text{MoO}_{12}$ (s), obtained are (-42.74 \pm 0.77), (-79.82 \pm 1.19), (-172.72 \pm 2.69), (-31.28 \pm 0.98), (-52.79 \pm 1.24), (-145.40 \pm 2.55) and (-60.15 \pm 1.08) kJ mol^{-1} , respectively. The molar enthalpy of formation of the ternary compounds from the component elements were obtained by considering suitable thermochemical reaction schemes

presented in Tables 3.16 to 3.20. For the calculation of enthalpies of formation from elements, values of enthalpies of formation of binary oxides were taken from references 74 and 75. The calculated enthalpies of formation from elements, $\Delta_f H_{298}^\circ$, are (-2915.8 ± 5.7) , (-1407.2 ± 3.8) , (-1385.7 ± 3.9) , (-3345.0 ± 10.9) and (-2605.2 ± 10.4) kJ mol⁻¹, respectively for Bi₂Mo₃O₁₂ (s), orthorhombic Bi₂MoO₆ (s), monoclinic Bi₂MoO₆ (s), Bi₆Mo₂O₁₅ (s) and Bi₆MoO₁₂ (s).

3.4.11 Heat capacity measurements

3.4.11.1 Molar heat capacity of MoO₃ (s)

The performance of the differential scanning calorimeter was verified by measuring the heat capacity of MoO₃ (s) in the temperature range of 318 to 763 K and shown in Fig. 3.19 and the selected values are given in Table 3.21. The measured data given in Table 3.21 is the mean of ten measurements. The experimental heat capacity is compared with the literature data [77]. It is seen that the measured C_p values are in good agreement with the reported C_p values at temperatures between 428 and 703 K. Deviations from the literature data are observed at temperatures below and above this range. The maximum deviation is found to be 3%.

The combined expanded uncertainty associated with the heat capacity measurements of the samples were calculated by incorporating the relative uncertainties of experimental data and the relative uncertainty attributed to the instrument. The relative uncertainty of the instrument was determined from the measured C_p values of MoO₃(s) (Table 3.21). The relative uncertainty in the measured heat capacity of the samples were calculated as $\Delta x/x$ where Δx is the maximum standard uncertainty observed and x is the smallest measured C_p value.

Table 3.15 Experimentally determined values of enthalpies of dissolution (ΔH) and molar enthalpies of dissolution ($\Delta_{sol}H_m^o$) of $\text{Bi}_2\text{Mo}_3\text{O}_{12}(\text{s})$, orthorhombic $\text{Bi}_2\text{MoO}_6(\text{s})$, monoclinic $\text{Bi}_2\text{MoO}_6(\text{s})$, $\text{Bi}_6\text{Mo}_2\text{O}_{15}(\text{s})$ and $\text{Bi}_6\text{MoO}_{12}(\text{s})$ in a mixture of 100 ml of 3 mol kg^{-1} NaOH and 25 ml of triethanolamine at 298.15 K^{*} and 0.1 MPa^a.

Sample	Weight of sample (w / g) ^a	Experimental enthalpy change ΔH (J)	Molar enthalpy of solution $\Delta_{sol}H_m^o$ (kJ mol ⁻¹)
$\text{Bi}_2\text{Mo}_3\text{O}_{12}(\text{s})$ (molar mass = 897.7728 g mol ⁻¹)	0.4921	-94.11	-171.69
	0.5156	-99.64	-173.49
	0.5338	-103.83	-174.63
	0.5340	-102.63	-172.54
	0.5442	-103.81	-171.26
Average: (-172.72 ± 2.69)^b			
$\text{Bi}_2\text{MoO}_6(\text{s})$ - orthorhombic phase (molar mass = 609.8964 g mol ⁻¹)	0.3043	-15.76	-31.59
	0.2758	-14.71	-32.53
	0.2392	-11.94	-30.44
	0.2204	-10.89	-30.14
	0.2952	-15.35	-31.71
Average: (-31.28 ± 0.98)^b			
$\text{Bi}_2\text{MoO}_6(\text{s})$ - monoclinic phase (molar mass = 609.8964 g mol ⁻¹)	0.4308	-38.62	-54.68
	0.3217	-27.46	-52.06
	0.3745	-31.57	-51.42
	0.3240	-27.57	-51.89
	0.4677	-41.13	-53.63
0.5418	-47.12	-53.04	
Average: (-52.79 ± 1.24)^b			
$\text{Bi}_6\text{Mo}_2\text{O}_{15}(\text{s})$ - (molar mass = 1685.7534 g mol ⁻¹)	0.3892	-32.11	-142.76
	0.3556	-29.68	-144.80
	0.1739	-15.06	-145.98
	0.4455	-38.96	-147.42
	0.2834	-24.55	-146.06
Average: (-145.40 ± 2.55)^b			
$\text{Bi}_6\text{MoO}_{12}(\text{s})$ - (molar mass = 1541.8152 g mol ⁻¹)	0.2653	-10.25	-59.61
	0.3770	-14.79	-60.48
	0.2108	-8.29	-60.66
	0.4186	-16.53	-60.91
	0.4363	-16.72	-59.10
Average: (-60.15 ± 1.08)^b			

^{*}Temperature stability inside the calorimeter prior to start of experiment was within ± 0.001 K. ^aStandard uncertainties, u , are $u(P) = 0.8$ kPa and $u(w) = 0.0001$ g. ^bExpanded uncertainty, $U(\Delta_{sol}H_m^o)$, is calculated as 2σ of the mean with 0.95 level of confidence. Uncertainty from calibration was also included into the final uncertainty of the dissolution enthalpies.

Table 3.16 Thermodynamic reaction schemes for obtaining the enthalpies of formation from oxides and elements for $\text{Bi}_2\text{Mo}_3\text{O}_{12}$ (s) at $T = 298.15 \text{ K}^a$. (s = solid, soln = aqueous solution, g = gas)

No	Reaction	Enthalpies (kJ mol^{-1})	Source of data
1	Bi_2O_3 (s) + 6 NaOH (soln) = $(2 \text{ Bi}^{3+} + 6 \text{ OH}^- + 6 \text{ Na}^+ + 3 \text{ O}^{2-})$ (soln)	$\Delta H_1 = (-42.74 \pm 0.77)^b$	This work
2	MoO_3 (s) + 2 NaOH (soln) = $(2 \text{ Na}^+ + \text{MoO}_4^{2-} + \text{H}_2\text{O})$ (soln)	$\Delta H_2 = (-79.82 \pm 1.19)^b$	This work
3	$\text{Bi}_2\text{Mo}_3\text{O}_{12}$ (s) + 12 NaOH (soln) = $(2 \text{ Bi}^{3+} + 6 \text{ OH}^- + 12 \text{ Na}^+ + 3 \text{ O}^{2-} + 3 \text{ MoO}_4^{2-} + 3 \text{ H}_2\text{O})$ (soln)	$\Delta H_3 = (-172.72 \pm 2.69)^b$	This work
4	2 Bi (s) + $3/2 \text{ O}_2$ (g) = Bi_2O_3 (s)	$\Delta H_4 = \Delta_f H_{298}^\circ$ of Bi_2O_3 (s) = (-570.70 ± 3.35)	[75]
5	Mo (s) + $3/2 \text{ O}_2$ (g) = MoO_3 (s)	$\Delta H_5 = \Delta_f H_{298}^\circ$ of MoO_3 (s) = (-745.2 ± 0.4)	[76]
6	2 Bi (s) + 3 Mo (s) + 6 O_2 (g) = $\text{Bi}_2\text{Mo}_3\text{O}_{12}$ (s)	$\Delta H_6 = \Delta H_1 + 3\Delta H_2 + \Delta H_4 + 3 \Delta H_5 - \Delta H_3 = \Delta_f H_{298}^\circ$ of $\text{Bi}_2\text{Mo}_3\text{O}_{12}$ (s) = $(-2915.8 \pm 5.7)^c$	-

^aTemperature of the calorimeter prior to the actual experiment was stable within $\pm 0.001 \text{ K}$. ^bExpanded uncertainties, $U_c(\Delta H_i)$ are calculated as 2σ of the mean and are at the 95 % confidence level. ^cCombined expanded uncertainties, $U_c(\Delta H)$, are calculated as 2σ of the mean and are at the 95 % confidence level.

Table 3.17 Thermodynamic reaction schemes for obtaining the enthalpies of formation from oxides and elements for orthorhombic Bi_2MoO_6 (s) at $T = 298.15 \text{ K}^a$ (s = solid, soln = aqueous solution, g = gas)

No	Reaction	Enthalpies (kJ mol^{-1})	Source of data
1	Bi_2O_3 (s) + 6 NaOH (soln) = $(2 \text{ Bi}^{3+} + 6 \text{ OH}^- + 6 \text{ Na}^+ + 3 \text{ O}^{2-})$ (soln)	$\Delta H_1 = (-42.74 \pm 0.77)^b$	This work
2	MoO_3 (s) + 2 NaOH (soln) = $(2 \text{ Na}^+ + \text{MoO}_4^{2-} + \text{H}_2\text{O})$ (soln)	$\Delta H_2 = (-79.82 \pm 1.19)^b$	This work
3	Bi_2MoO_6 (s) + 8 NaOH (soln) = $(2 \text{ Bi}^{3+} + 6 \text{ OH}^- + 8 \text{ Na}^+ + 3 \text{ O}^{2-} + \text{MoO}_4^{2-} + \text{H}_2\text{O})$ (soln)	$\Delta H_3 = (-31.28 \pm 0.98)^b$	This work
4	2 Bi (s) + $3/2 \text{ O}_2$ (g) = Bi_2O_3 (s)	$\Delta H_4 = \Delta_f H_{298}^\circ$ of Bi_2O_3 (s) = (-570.70 ± 3.35)	[75]
5	Mo (s) + $3/2 \text{ O}_2$ (g) = MoO_3 (s)	$\Delta H_5 = \Delta_f H_{298}^\circ$ of MoO_3 (s) = (-745.2 ± 0.4)	[76]
6	2 Bi (s) + Mo (s) + 3 O_2 (g) = Bi_2MoO_6 (s)	$\Delta H_6 = \Delta H_1 + \Delta H_2 + \Delta H_4 + \Delta H_5 - \Delta H_3 =$ $\Delta_f H_{298}^\circ$ of Bi_2MoO_6 (s) = $(-1407.2 \pm 3.8)^c$	-

^aTemperature of the calorimeter prior to the actual experiment was stable within $\pm 0.001 \text{ K}$. ^bExpanded uncertainties, $U_c(\Delta H)$, are calculated as 2σ of the mean and are at the 95 % confidence level. ^cCombined expanded uncertainties, $U_c(\Delta H)$, are calculated as 2σ of the mean and are at the 95 % confidence level.

Table 3.18 Thermodynamic reaction schemes for obtaining the enthalpies of formation from oxides and elements form monoclinic $\text{Bi}_2\text{MoO}_6(\text{s})$ at $T = 298.15 \text{ K}^{\text{a}}$ (s = solid, soln = aqueous solution, g = gas)

No	Reaction	Enthalpies (kJ mol^{-1})	Source of data
1	$\text{Bi}_2\text{O}_3(\text{s}) + 6 \text{ NaOH}(\text{soln}) = (2 \text{ Bi}^{3+} + 6 \text{ OH}^- + 6 \text{ Na}^+ + 3 \text{ O}^{2-})(\text{soln})$	$\Delta H_1 = (-42.74 \pm 0.77)^{\text{b}}$	This work
2	$\text{MoO}_3(\text{s}) + 2 \text{ NaOH}(\text{soln}) = (2 \text{ Na}^+ + \text{MoO}_4^{2-} + \text{H}_2\text{O})(\text{soln})$	$\Delta H_2 = (-79.82 \pm 1.19)^{\text{b}}$	This work
3	$\text{Bi}_2\text{MoO}_6(\text{s}) + 8 \text{ NaOH}(\text{soln}) = (2 \text{ Bi}^{3+} + 6 \text{ OH}^- + 8 \text{ Na}^+ + 3 \text{ O}^{2-} + \text{MoO}_4^{2-} + \text{H}_2\text{O})(\text{soln})$	$\Delta H_3 = (-52.79 \pm 1.24)^{\text{b}}$	This work
4	$2 \text{ Bi}(\text{s}) + 3/2 \text{ O}_2(\text{g}) = \text{Bi}_2\text{O}_3(\text{s})$	$\Delta H_4 = \Delta_f H_{298}^\circ \text{ of Bi}_2\text{O}_3(\text{s}) = (-570.70 \pm 3.35)$	[75]
5	$\text{Mo}(\text{s}) + 3/2 \text{ O}_2(\text{g}) = \text{MoO}_3(\text{s})$	$\Delta H_5 = \Delta_f H_{298}^\circ \text{ of MoO}_3(\text{s}) = (-745.2 \pm 0.4)$	[76]
6	$2 \text{ Bi}(\text{s}) + \text{Mo}(\text{s}) + 3 \text{ O}_2(\text{g}) = \text{Bi}_2\text{MoO}_6(\text{s})$	$\Delta H_6 = \Delta H_1 + \Delta H_2 + \Delta H_4 + \Delta H_5 - \Delta H_3 =$ $\Delta_f H_{298}^\circ \text{ of Bi}_2\text{MoO}_6(\text{s}) = (-1385.7 \pm 3.9)^{\text{c}}$	-

^aTemperature of the calorimeter prior to the actual experiment was stable within $\pm 0.001 \text{ K}$. ^bExpanded uncertainties, $U_c(\Delta H_i)$ are calculated as 2σ of the mean and are at the 95 % confidence level. ^cCombined expanded uncertainties, $U_c(\Delta H)$, are calculated as 2σ of the mean and are at the 95 % confidence level.

Table 3.19 Thermodynamic reaction schemes for obtaining the enthalpies of formation from oxides and elements for $\text{Bi}_6\text{Mo}_2\text{O}_{15}$ (s) at $T = 298.15 \text{ K}^a$ (s = solid, soln = aqueous solution, g = gas)

No	Reaction	Enthalpies (kJ mol^{-1})	Source of data
1	Bi_2O_3 (s) + 6 NaOH (soln) = $(2 \text{ Bi}^{3+} + 6 \text{ OH}^- + 6 \text{ Na}^+ + 3 \text{ O}^{2-})$ (soln)	$\Delta H_1 = (-42.74 \pm 0.77)^b$	This work
2	MoO_3 (s) + 2 NaOH (soln) = $(2 \text{ Na}^+ + \text{MoO}_4^{2-} + \text{H}_2\text{O})$ (soln)	$\Delta H_2 = (-79.82 \pm 1.19)^b$	This work
3	$\text{Bi}_6\text{Mo}_2\text{O}_{15}$ (s) + 22 NaOH (soln) = $(6 \text{ Bi}^{3+} + 18 \text{ OH}^- + 22 \text{ Na}^+ + 9 \text{ O}^{2-} + 2 \text{ MoO}_4^{2-} + 2 \text{ H}_2\text{O})$ (soln)	$\Delta H_3 = (-145.40 \pm 2.55)^b$	This work
4	2 Bi (s) + $3/2 \text{ O}_2$ (g) = Bi_2O_3 (s)	$\Delta H_4 = \Delta_f H_{298}^\circ$ of Bi_2O_3 (s) = (-570.70 ± 3.35)	[75]
5	5 Mo (s) + $3/2 \text{ O}_2$ (g) = MoO_3 (s)	$\Delta H_5 = \Delta_f H_{298}^\circ$ of MoO_3 (s) = (-745.2 ± 0.4)	[76]
6	6 Bi (s) + 2 Mo (s) + $15/2 \text{ O}_2$ (g) = $\text{Bi}_6\text{Mo}_2\text{O}_{15}$ (s)	$\Delta H_6 = 3\Delta H_1 + 2\Delta H_2 + 3\Delta H_4 + 2\Delta H_5 - \Delta H_3 =$ $\Delta_f H_{298}^\circ$ of $\text{Bi}_6\text{Mo}_2\text{O}_{15}$ (s) = $(-3345.0 \pm 10.9)^c$	-

^aTemperature of the calorimeter prior to the actual experiment was stable within $\pm 0.001 \text{ K}$. ^bExpanded uncertainties, U_c (ΔH_i) are calculated as 2σ of the mean and are at the 95 % confidence level. ^cCombined expanded uncertainties, $U_c(\Delta H)$, are calculated as 2σ of the mean and are at the 95 % confidence level.

Table 3.20 Thermodynamic reaction schemes for obtaining the enthalpies of formation from oxides and elements for $\text{Bi}_6\text{MoO}_{12}(\text{s})$ at $T = 298.15 \text{ K}^{\text{a}}$ (s = solid, soln = aqueous solution, g = gas)

No	Reaction	Enthalpies (kJ mol^{-1})	Source of data
1	$\text{Bi}_2\text{O}_3(\text{s}) + 6 \text{NaOH}(\text{soln}) = (2 \text{Bi}^{3+} + 6 \text{OH}^- + 6 \text{Na}^+ + 3 \text{O}^{2-})(\text{soln})$	$\Delta H_1 = (-42.74 \pm 0.77)^{\text{b}}$	This work
2	$\text{MoO}_3(\text{s}) + 2 \text{NaOH}(\text{soln}) = (2 \text{Na}^+ + \text{MoO}_4^{2-} + \text{H}_2\text{O})(\text{soln})$	$\Delta H_2 = (-79.82 \pm 1.19)^{\text{b}}$	This work
3	$\text{Bi}_6\text{MoO}_{12}(\text{s}) + 20 \text{NaOH}(\text{soln}) = (6 \text{Bi}^{3+} + 18 \text{OH}^- + 20 \text{Na}^+ + 9 \text{O}^{2-} + \text{MoO}_4^{2-} + \text{H}_2\text{O})(\text{soln})$	$\Delta H_3 = (-60.15 \pm 1.08)^{\text{b}}$	This work
4	$2 \text{Bi}(\text{s}) + 3/2 \text{O}_2(\text{g}) = \text{Bi}_2\text{O}_3(\text{s})$	$\Delta H_4 = \Delta_f H_{298}^\circ \text{ of Bi}_2\text{O}_3(\text{s}) = (-570.70 \pm 3.35)$	[75]
5	$\text{Mo}(\text{s}) + 3/2 \text{O}_2(\text{g}) = \text{MoO}_3(\text{s})$	$\Delta H_5 = \Delta_f H_{298}^\circ \text{ of MoO}_3(\text{s}) = (-745.2 \pm 0.4)$	[76]
6	$6 \text{Bi}(\text{s}) + \text{Mo}(\text{s}) + 6 \text{O}_2(\text{g}) = \text{Bi}_6\text{MoO}_{12}(\text{s})$	$\Delta H_6 = 3\Delta H_1 + \Delta H_2 + 3\Delta H_4 + \Delta H_5 - \Delta H_3 =$ $\Delta_f H_{298}^\circ \text{ of Bi}_6\text{MoO}_{12}(\text{s}) = (-2605.2 \pm 10.4)^{\text{c}}$	-

^aTemperature of the calorimeter prior to the actual experiment was stable within $\pm 0.001 \text{ K}$. ^bExpanded uncertainties, $U_c(\Delta H)$, are calculated as 2σ of the mean and are at the 95 % confidence level. ^cCombined expanded uncertainties, $U_c(\Delta H)$ are calculated as 2σ of the mean and are at the 95 % confidence level.

Using these relative uncertainties, the combined expanded uncertainty was calculated by multiplying with the highest value of the measured heat capacity and is given in the fitted expressions of heat capacities of bismuth molybdates.

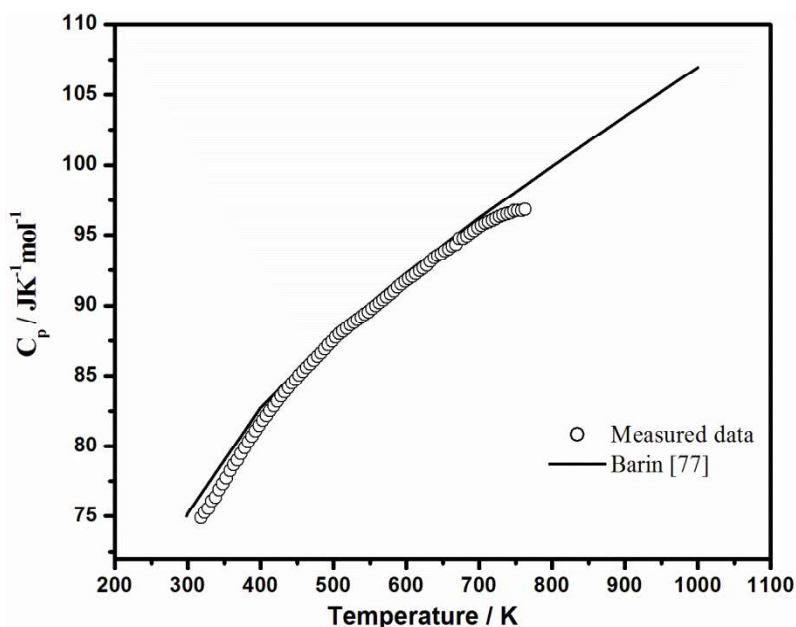


Fig. 3.19 Variation of molar heat capacity of MoO_3 (s) with temperature

Table 3.21 Heat capacity of MoO_3 (s) at $P = 0.1\text{MPa}^a$

T / K^a	$C_p / \text{J K}^{-1} \text{mol}^{-1}$		Observed deviation from the reported values / $\text{J K}^{-1} \text{mol}^{-1}$
	Measured data ^b	Reported values [77] ^c	
318	74.9	76.9	2.0
353	77.7	79.7	2.0
403	81.8	82.9	1.1
453	85.1	85.7	0.6
503	87.7	88.1	0.4
553	89.8	90.4	0.6
603	91.9	92.4	0.5
653	93.9	94.4	0.5
703	95.7	96.4	0.7
753	96.7	98.2	1.5
763	96.8	98.6	1.8

^a Standard uncertainties, u , are $u(T) = 0.4 \text{ K}$ and $u(P) = 0.8 \text{ kPa}$. ^b Maximum relative uncertainty is 0.03 with 0.95 level of confidence. ^c Barin [77]

3.4.11.2 Molar heat capacity of $\text{Bi}_2\text{Mo}_3\text{O}_{12}$ (s)

The XRD patterns of the $\text{Bi}_2\text{Mo}_3\text{O}_{12}$ (s) samples retrieved after heat capacity measurements were identical to their XRD patterns before the measurements indicating that the compound had not undergone any changes during the measurements. Fig. 3.20 represents the experimental heat capacity of $\text{Bi}_2\text{Mo}_3\text{O}_{12}$ (s) as a function of temperature over the range of 328 to 818 K. The data can be fitted to the following least squares expression:

$$C_p \pm 16.4 / \text{J K}^{-1} \text{mol}^{-1} = 416.7 - 7.1 \times 10^{-3} T - 8.8 \times 10^6 T^{-2}; T = 328\text{-}818 \text{ K} \quad (3.25)$$

The error given in the expression is the combined expanded uncertainty with 0.95 level of confidence.

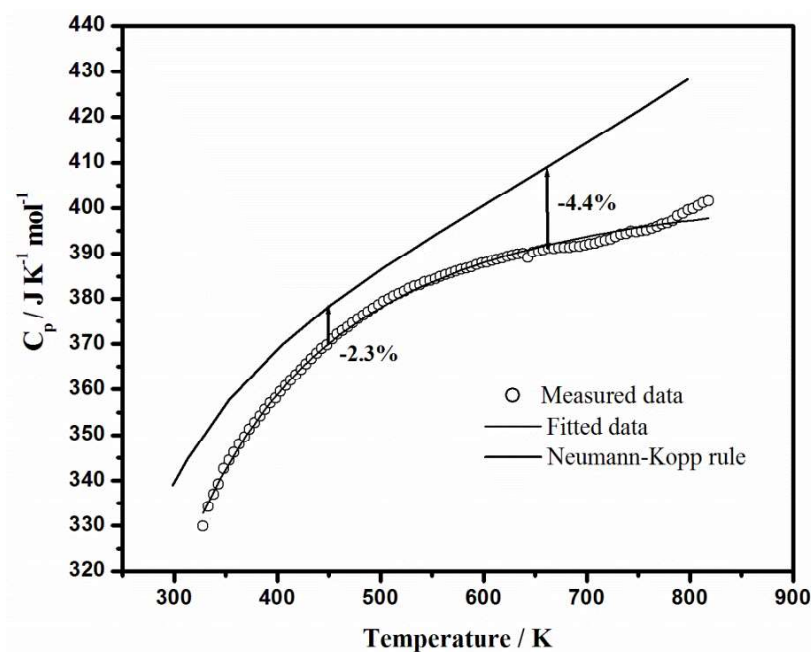


Fig. 3.20 Variation of molar heat capacity of $\text{Bi}_2\text{Mo}_3\text{O}_{12}$ (s) with temperature

The measured heat capacity values of $\text{Bi}_2\text{Mo}_3\text{O}_{12}$ (s) along with the fitted values for the selected temperatures are given in Table 3.22. The heat capacity of $\text{Bi}_2\text{Mo}_3\text{O}_{12}$ (s) was also computed by Neumann-Kopp's rule (NKR) using the heat capacity data for Bi_2O_3 (s) and MoO_3 (s) [78], and is compared with the measured

data in Fig. 3.20. The comparison plot reveals that the experimental heat capacity is lower than the estimated data and the percentage deviation is $\sim 3\%$ at 573 K, which is the mean temperature of the measurement.

Table 3.22 Thermodynamic functions of $\text{Bi}_2\text{Mo}_3\text{O}_{12}$ (s) at $P = 0.1 \text{ MPa}^a$

T / K ^a	$C_p / \text{J K}^{-1} \text{ mol}^{-1}$		$H_T^\circ - H_{298}^\circ$ / J mol^{-1b}	S_T° / $\text{J K}^{-1} \text{ mol}^{-1b}$	$-(G_T^\circ - H_{298}^\circ) / T$ / $\text{J K}^{-1} \text{ mol}^{-1b}$
	Measured data	Fitted values			
298.15	-	315.6	0	358.2 ± 1.4	358.5 ± 1.4
328	329.9	332.6	9687.0 ± 489.5	389.1 ± 1.6	359.9 ± 2.2
353	344.4	343.6	18144.8 ± 899.5	414.0 ± 2.8	362.9 ± 3.8
403	359.5	359.7	35754.6 ± 1719.5	460.6 ± 4.9	372.2 ± 6.5
453	371.0	370.6	54029.6 ± 2539.5	503.3 ± 6.9	384.4 ± 8.9
503	379.4	378.3	72766.3 ± 3359.5	542.6 ± 8.6	398.2 ± 10.9
553	384.5	384.0	91834.6 ± 4179.5	578.7 ± 10.1	413.0 ± 12.6
603	388.1	388.2	111147.8 ± 4999.5	612.1 ± 11.6	428.2 ± 14.2
653	390.6	391.4	130645.6 ± 5819.5	643.2 ± 12.9	443.5 ± 15.6
703	392.1	393.9	150284.8 ± 6639.5	672.2 ± 14.1	458.7 ± 16.9
753	395.0	395.8	170033.8 ± 7459.5	699.3 ± 15.2	473.9 ± 18.1
798	399.5	397.2	187882.0 ± 8197.5	722.3 ± 16.1	487.2 ± 19.1
818	401.6	397.7	195833.3 ± 8525.5	732.1 ± 16.6	493.1 ± 19.6

^aStandard uncertainties, u , are $u(T) = 0.4 \text{ K}$ and $u(P) = 0.8 \text{ kPa}$. The reported uncertainties are the combined expanded uncertainties. The combined expanded uncertainty, U_c , is $U_c(C_p) = 16.4 \text{ J K}^{-1} \text{ mol}^{-1}$.

As no thermochemical data are available for $\text{Bi}_2\text{Mo}_3\text{O}_{12}$ (s), the S_{298}° value of $\text{Bi}_2\text{Mo}_3\text{O}_{12}$ (s) was computed by NKR using the S_{298}° values of Bi_2O_3 (s) and MoO_3 (s) [78]. Since the experimental value of C_p of $\text{Bi}_2\text{Mo}_3\text{O}_{12}$ (s) at 298.15 K is 6.9% lower than that obtained by the NKR estimation, it is assumed that the S_{298}° value of $\text{Bi}_2\text{Mo}_3\text{O}_{12}$ (s) will also be 6.9% lower than the estimated S_{298}° value. Similar assumption has been made in the earlier works [79-81]. Based on this assumption, the

S_{298}° value computed for $\text{Bi}_2\text{Mo}_3\text{O}_{12}$ (s) is $358.2 \text{ J K}^{-1} \text{ mol}^{-1}$. Using this value, other thermodynamic functions of $\text{Bi}_2\text{Mo}_3\text{O}_{12}$ (s) were computed and are given in Table 3.22.

3.4.11.3 Molar heat capacity of monoclinic phase of Bi_2MoO_6 (s)

XRD pattern of the monoclinic phase of Bi_2MoO_6 (s) pellets after the heat capacity measurements were identical to the initial pattern, indicating that no changes had happened to the compound during the calorimetric runs. The temperature dependence of heat capacity of Bi_2MoO_6 (s) obtained by measurement over the temperature range of 318 to 818 K is shown in Fig. 3.21 and can be represented by the least squares fitted expression:

$$C_p \pm 8.8 / \text{J K}^{-1} \text{ mol}^{-1} = 221.4 - 1.5 \times 10^{-3} T - 3.9 \times 10^6 T^{-2} \quad (T : 318 - 818 \text{ K}) \quad (3.26)$$

The error given in the expression is the combined expanded uncertainty with 0.95 level of confidence.

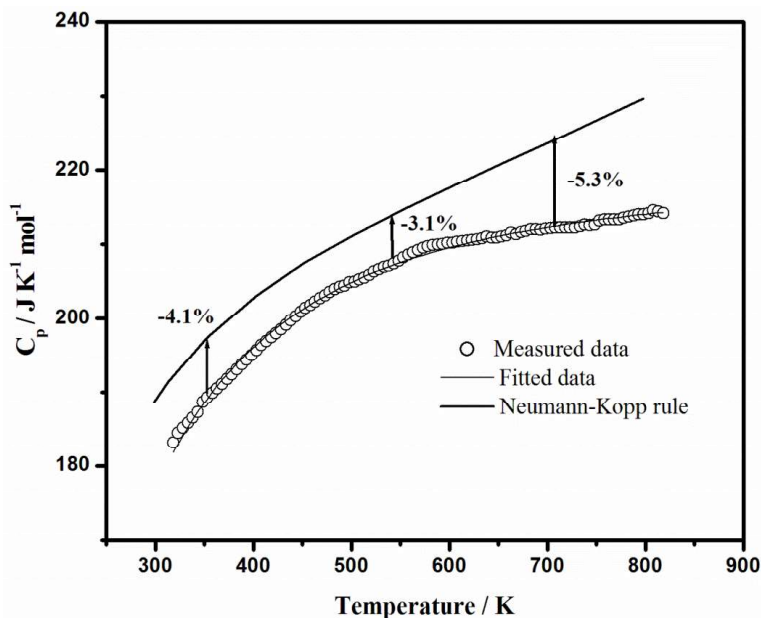


Fig. 3.21 Variation of molar heat capacity of monoclinic- Bi_2MoO_6 with temperature

The measured heat capacity values of Bi_2MoO_6 (s) along with the fitted values for the selected temperatures are given in Table 3.23. Each measured data is the mean of sixteen measurements obtained by measuring the C_p using two sample pellets. The heat capacity of Bi_2MoO_6 (s) was also computed by Neumann-Kopp's rule (NKR) using the heat capacity data for Bi_2O_3 (s) and MoO_3 (s) [78], and is compared with the measured data in Fig. 3.21.

Table 3.23 Thermodynamic functions of monoclinic- Bi_2MoO_6 (s) at $P = 0.1\text{MPa}$ ^a

T / K ^a	$C_p / \text{J K}^{-1} \text{mol}^{-1}$		$H_T^\circ - H_{298}^\circ$ / J mol^{-1b}	S_T° / $\text{J K}^{-1} \text{mol}^{-1b}$	$-(G_T^\circ - H_{298}^\circ)/T$ / $\text{J K}^{-1} \text{mol}^{-1b}$
	Measured data	Fitted values			
298.15	-	177.1	0	214.3 ± 0.5	214.3 ± 0.5
318	183.2	182.4	3569.1 ± 174.7	225.8 ± 0.6	214.7 ± 0.8
328	185.1	184.7	5404.4 ± 262.7	231.5 ± 0.8	215.1 ± 1.2
353	189.3	189.6	10084.5 ± 482.7	245.2 ± 1.5	216.7 ± 2.0
403	195.7	196.8	19755.4 ± 922.7	270.8 ± 2.7	221.9 ± 3.5
453	201.4	201.7	29725.2 ± 1362.7	294.1 ± 3.7	228.6 ± 4.8
503	204.9	205.2	39903.5 ± 1802.7	315.4 ± 4.6	236.2 ± 5.8
553	208.2	207.8	50232.9 ± 2242.7	334.9 ± 5.4	244.2 ± 6.8
603	210.2	209.8	60674.8 ± 2682.7	353.0 ± 6.2	252.5 ± 7.6
653	211.0	211.3	71202.4 ± 3122.7	369.7 ± 6.9	260.9 ± 8.4
703	212.2	212.5	81796.8 ± 3562.7	385.4 ± 7.5	269.2 ± 9.1
753	213.2	213.4	92443.8 ± 4002.7	400.0 ± 8.2	277.4 ± 9.7
818	214.2	214.3	106346.7 ± 4574.7	417.7 ± 8.9	287.8 ± 10.5

^a Standard uncertainties, u , are $u(T) = 0.4 \text{ K}$ and $u(P) = 0.8 \text{ kPa}$. ^bThe reported uncertainties are the combined expanded uncertainties. The combined expanded uncertainty, U_c , is $U_c(C_p) = 8.8 \text{ J K}^{-1} \text{mol}^{-1}$

As seen in the figure, the experimental heat capacity is lower than the estimated data and the percentage deviation is $\sim 3.1\%$ at 568 K, which is the mean temperature of the measurement. As no thermochemical data of Bi_2MoO_6 (s) are available, its S_{298}° value was computed by Neumann-Kopp Rule (NKR) using the S_{298}° values of Bi_2O_3 (s) and MoO_3 (s) [78]. Based on this assumption, the S_{298}° value

computed for Bi_2MoO_6 (s) is $208.8 \text{ J K}^{-1} \text{ mol}^{-1}$. Using this value, the thermodynamic functions of Bi_2MoO_6 (s) were computed and given in Table 3.23.

3.4.11.4 Molar heat capacity of $\text{Bi}_6\text{Mo}_2\text{O}_{15}$ (s)

The XRD pattern of $\text{Bi}_6\text{Mo}_2\text{O}_{15}$ (s) retrieved after DSC measurements was identical to the initial pattern indicating that no changes had happened to the compound during the calorimetric runs. The variation of molar heat capacity of $\text{Bi}_6\text{Mo}_2\text{O}_{15}$ (s) obtained is shown in Fig. 3.22 and the fitted expression is given below:

$$C_p \pm 23.4 / \text{J K}^{-1} \text{ mol}^{-1} = 529.8 - 67.9 \times 10^{-3} T - 6.3 \times 10^6 T^{-2} \quad (T : 318 - 808 \text{ K}) \quad (3.27)$$

The error given in the expression is the combined expanded uncertainty with 0.95 level of confidence.

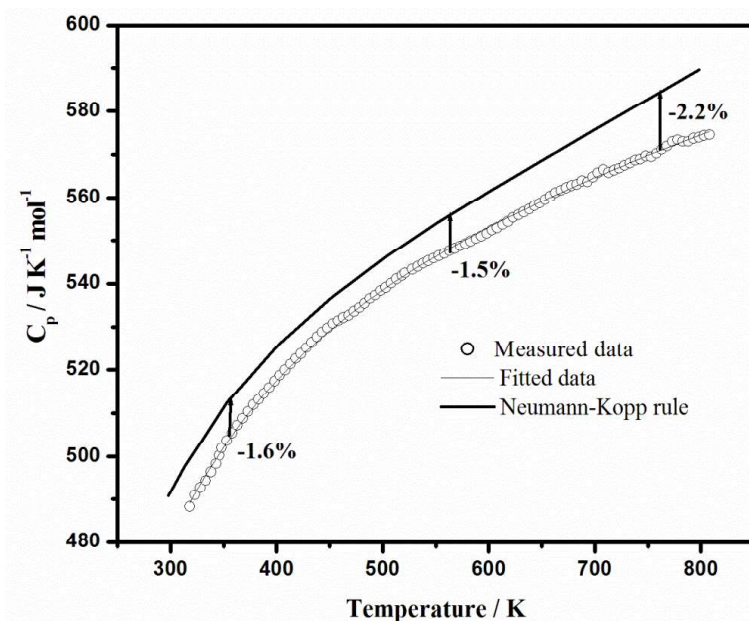


Fig. 3.22 Variation of heat capacity of $\text{Bi}_6\text{Mo}_2\text{O}_{15}$ (s) with temperature

The thermodynamic functions of $\text{Bi}_6\text{Mo}_2\text{O}_{15}$ (s) were calculated based on the measured heat capacity data and presented in Table 3.24. Fig.3.22 also shows the comparison of experimentally obtained heat capacities and those estimated by NKR. It is found that the measured heat capacities are lower than the estimated heat

capacities and the percentage deviation is ~1.5 % at the mean temperature of measurement (563 K).

Table 3.24 Thermodynamic functions of Bi₆Mo₂O₁₅ (s) at P = 0.1MPa^a

T / K ^a	C _p / J K ⁻¹ mol ⁻¹		H _T ^o - H ₂₉₈ ^o / J mol ^{-1b}	S _T ^o / J K ⁻¹ mol ^{-1b}	-(G _T ^o - H ₂₉₈ ^o)/T / J K ⁻¹ mol ^{-1b}
	Measured data	Fitted values			
298.15	-	479.1	0	545.0 ± 1.1	545.0 ± 1.1
318	489.1	489.0	9610.8 ± 464.5	576.2 ± 1.5	545.9 ± 2.1
343	499.5	499.5	21970.9 ± 1049.5	613.6 ± 3.3	549.5 ± 4.5
401	517.9	517.8	51504.5 ± 2406.7	693.1 ± 6.9	564.6 ± 9.2
451	529.4	529.4	77697.6 ± 3576.7	754.6 ± 9.7	582.3 ± 12.5
500	538.7	538.5	103870.4 ± 4723.3	809.7 ± 12.1	602.0 ± 15.3
550	546.4	546.3	130997.5 ± 5893.3	861.4 ± 14.3	623.2 ± 17.9
600	553.1	553.1	158485.8 ± 7063.3	909.2 ± 16.4	645.1 ± 20.2
650	559.1	559.1	186291.3 ± 8233.3	953.8 ± 18.2	667.2 ± 22.2
700	564.5	564.5	214382.3 ± 9403.3	995.4 ± 20.0	689.1 ± 24.1
750	569.6	569.6	242735.8 ± 10573.3	1034.5 ± 21.6	710.9 ± 25.8
800	574.3	574.3	271334.4 ± 11743.3	1071.4 ± 23.1	732.3 ± 27.4
808	575.0	575.1	275932.0 ± 11930.5	1077.1 ± 23.3	735.6 ± 27.6

^aStandard uncertainties, u , are $u(T) = 0.4$ K and $u(P) = 0.8$ kPa. ^bThe reported uncertainties are the combined expanded uncertainties. The combined expanded uncertainty, U_c , is $U_c(C_p) = 23.4$ J K⁻¹ mol⁻¹

3.4.12 Consistency of the measured thermodynamic data

The consistency between the standard enthalpy of formation of Bi₂MoO₆(s) determined by solution calorimetry experiments, with the standard enthalpy of formation at the mid temperature of emf measurements is determined as follows:

3.4.12.1 Monoclinic Bi₂MoO₆ (s)

The standard molar Gibbs energy of formation of monoclinic Bi₂MoO₆ (s) obtained by emf method is given by the expression (3.23);

$$\Delta_f G^\circ < Bi_2MoO_6 > \pm 0.8 / kJ mol^{-1} = -1382.3 + 0.5064(T / K) \quad (T : 772 - 1023K) \quad (3.23)$$

The mid temperature of this measurement is 898 K. By expressing the standard Gibbs energy of formation as $\Delta G = \Delta H - T\Delta S$, the enthalpy of formation of $Bi_2MoO_6(s)$ at 898 K can be deduced as

$$\Delta_f H_{898}^\circ < Bi_2MoO_6 > = -1382.3 kJ mol^{-1}$$

This can be related to the standard molar enthalpy of formation of $Bi_2MoO_6(s)$ at 298.15 K as below:

$$\Delta_f H_{298K}^\circ < Bi_2MoO_6 > = \Delta_f H_{898K}^\circ < Bi_2MoO_6 > - \left[\int_{298}^{544} \Delta C_p dT - 2\Delta H_{fusion}^{Bi} + \int_{544}^{898} \Delta C_p dT \right] \quad (3.28)$$

where ΔC_p is the difference in the heat capacities of $Bi_2MoO_6(s)$ and its constituent elements Bi (solid / liquid), Mo and O_2 and ΔH_{fusion}^{Bi} is the enthalpy of fusion of Bi at 544 K. The second term of the equation (3.28) can be obtained as:

$$\begin{aligned} \int_{298}^{544} \Delta C_p dT - 2\Delta H_{fusion}^{Bi} + \int_{544}^{898} \Delta C_p dT &= \int_{298}^{544} [C_p^{Bi_2MoO_6} - (2C_p^{Bi(s)} + C_p^{Mo(s)} + 3C_p^{O_2(g)})] dT - \\ 2\Delta H_{fusion}^{Bi} + \int_{544}^{898} [C_p^{Bi_2MoO_6} - (2C_p^{Bi(l)} + C_p^{Mo(s)} + 3C_p^{O_2(g)})] dT & \quad (3.29) \end{aligned}$$

The data of heat capacity for Bi, Mo and O_2 were taken from ref [78] and that of $Bi_2MoO_6(s)$ from our experimental studies as given by equation (3.26) and are given below:

$$C_p < Bi_2MoO_6 > / JK^{-1} mol^{-1} = 221.4 - 1.5 \times 10^{-3} T - 3.9 \times 10^{-6} T^{-2} \quad (T : 318 - 818K) \quad (3.26)$$

$$C_p < Bi > / JK^{-1} mol^{-1} = 28.033 - 24.267 \times 10^{-3} T + 50.208 \times 10^{-6} T^2 \quad (T : 298 - 544K) \quad (3.30)$$

$$C_p \{Bi\} / JK^{-1} mol^{-1} = 23.359 - 9.736 \times 10^{-3} T - 0.280 \times 10^{-6} T^{-2} + 3.238 \times 10^{-6} T \quad (T : 544 - 1835K) \quad (3.31)$$

$$C_p < Mo > / JK^{-1} mol^{-1} = 29.732 + 3.138 \times 10^{-3} T + 1.661 \times 10^{-6} T^{-2} - 0.720 \times 10^{-6} T \quad (T : 298 - 2896K) \quad (3.32)$$

$$C_p(O_2) / JK^{-1}mol^{-1} = 29.154 + 6.477 \times 10^{-3} T - 0.184 \times 10^{-6} T^2 - 1.017 \times 10^{-6} T \quad (T: 298-3200 K) \quad (3.33)$$

By substituting the above values in equation (3.29), we get

$$\int_{298}^{544} \Delta C_p dT - 2\Delta H_{fusion}^{Bi} + \int_{544}^{898} \Delta C_p dT = -5.24 kJ mol^{-1} \text{ and hence,}$$

$$\Delta_f H_{298K}^o < Bi_2MoO_6 > = -1382.3 + 5.24 = -1377.1 kJ mol^{-1}.$$

$\Delta_f H_{298K}^o < Bi_2MoO_6 >$ obtained by solution calorimetry experiment is -1385.7 kJ mol⁻¹ and is found to be in agreement with the deduced value of -1377.1 kJ mol⁻¹.

3.5 References

1. L. Brewer, Molybdenum: Physico-chemical properties of its compounds and alloys, Atomic Energy Review Special issue No.7, International Atomic Energy Agency, Vienna, 1980.
2. R.P. Elliott, Constitution of binary alloys, First supplement, McGraw Hill book company, USA, 1965.
3. T.B. Massalski (Ed.), Binary Alloy Phase Diagrams, 2nd Ed., ASM International, 1990.
4. G.W. Horsley, J.T. Maskreg, J. Inst. Metals, 86 (1957) 401-402.
5. D. Risold, B. Hallstedt, L.J. Gauckler, The bismuth-oxygen system, J. Phase. Equilibria. 16 (1995) 223-234.
6. R. Ganesan, T. Gnanasekaran, R.S. Srinivasa, Electrochemical study on determination of diffusivity, activity and solubility of oxygen in liquid bismuth, J. Chem. Thermodyn. 38 (2006) 739-747.

7. L. Brewer, R.H. Lamoreaux, The Mo-O system, Bull. Alloy Phase Diagr. 1 (1980) 85-89.
8. K. Tonosaki, Bull. Inst. Phys. Chem. Res. Jpn. 19 (1940) 126-132.
9. N.A. Gokcen, Thermodynamic properties of molybdenum dioxide, J. Met. 197 (1953) 1019-1020.
10. M. Gleiser, J. Chapman, Free energy of formation of molybdenum oxide and carbide, J. Phys. Chem. 66 (1962) 1539-1540.
11. R.A. Rapp, The standard free energy of formation of MoO₂, Trans. Metall. Soc. AIME 227 (1963) 371-374.
12. G.B. Barbi, Thermodynamic functions and phase stability limits by electromotive force measurements on solid electrolyte cells, J. Phys. Chem. 68 (1964) 1025-1029.
13. V.N. Drobyshev, T.N. Rezhukhina, L.A. Tarasova, Thermodynamic properties of cobalt-molybdenum alloys, Russ. J. Phys. Chem. 39 (1965) 70-73.
14. C. Vassilev, T. Nikolov, M. Chimbulev, Trans. Inst. Min. Metall. 77 (1968) C36-C38.
15. S. Berglund, P. Kierkegaard, The free energies of formation of WO₂ and MoO₂, Acta Chem. Scand. 23 (1969) 329-330.
16. C.B. Alcock, J.C. Chan, The oxygen permeability of stabilized zirconia electrolytes at high temperatures, Can. Metall. Quart. 11 (1972) 559-567.

17. M. Iwase, M. Yasuda, T. Mori, Free energy of formation of MoO₂ at steelmaking temperature from EMF measurement, *Electrochim. Acta* 24 (1979) 261-266.
18. H. Kleykamp, A. Supawan, Gibbs energies of formation of MoO₂ and Mo₄O₁₁, *J. Less Comm. Met.* 63 (1979) 261L.
19. L. Pejryd, Phase relations and stabilities in the system Ni-MoO₂-O in the temperature range 850-1500 K, *High Temp-High Press.* 16 (1984) 403-408.
20. H.St.C. O'Neill, Mo-MoO₂ (MOM) oxygen buffer and the free energy of formation of MoO₂, *Am. Mineral.* 71 (1986) 1007-1010.
21. K.T. Jacob, G.M. Kale, G.N.K. Iyengar, Phase equilibria and thermodynamic properties in the system Ni-Mo-O, *J. Mater. Sci.* 22 (1987) 4274-4280.
22. J. Bygden, D. Sichen, S. Seetharaman, A thermodynamic study of the molybdenum-oxygen system, *Metall. Mater. Trans. B* 25 (1994) 885-891.
23. K.T. Jacob, V.S. Saji, J. Gopalakrishnan, Y. Waseda, Thermodynamic evidence for phase transition in MoO₂-δ, *J. Chem. Thermodyn.* 39 (2007) 1539-1545.
24. M.R. Antonio, R.G. Teller, D.R. Sandstrom, M. Mehicic, J.F. Brazdil, Structural characterization of bismuth molybdates by X-ray absorption spectroscopy and powder neutron diffraction profile analysis, *J. Phys. Chem.* 92 (1988) 2939-2944.

25. F.D. Hardcastle, I.E. Wachs, Molecular structure of molybdenum oxide in bismuth molybdates by Raman spectroscopy, *J. Phys. Chem.* 95 (1991) 10763-10772.
26. M.T. Le, W.J.M.V. Well, I.V. Driessche, S. Hoste, Spray drying, a versatile synthetic method to control purity in single phases and mixed phases of bismuth molybdates, *Can. J. Chem. Eng.* 83 (2005) 336-343.
27. R.B. Licht, D. Vogt, A.T. Bell, The mechanism and kinetics of propene ammoxidation over α -bismuth molybdates, *J. Catal.* 339 (2016) 228-241.
28. A.P.V. Soares, L.D. Dimitrov, M.C.R.A. Oliveira, L. Hilaire, M.F. Portela, R.K. Grasselli, Synergy effects between β and γ phases of bismuth molybdates in the selective catalytic oxidation of 1-butene, *Appl. Catal. A.* 253 (2003) 191-200.
29. B. Farin, A.H.A.M. Videla, S. Specchia, E.M. Gaigneaux, Bismuth molybdates prepared by solution combustion synthesis for the partial oxidation of propene, *Catal. Today.* 257 (2015) 11-17.
30. L. Sillen, K. Lundberg, *Arkiv Kemi*, 17A (1943) 21.
31. R. Kohlmuller, J. P. Baduad, Etude du systeme $\text{Bi}_2\text{O}_3\text{-MoO}_3$, *Bull. Soc. Chim. Fr.* 10 (1969) 3434-3439.
32. M. Egashira, K. Matsuo, S. Kagawa, T. Seiyama, Phase diagram of the system $\text{Bi}_2\text{O}_3\text{-MoO}_3$, *J. Catal.* 58 (1979) 409-418.

33. C.D. Ling, R.L. Withers, J.G. Thompson, S. Schmid, Structures of $\text{Bi}_{14}\text{WO}_{24}$ and $\text{Bi}_{14}\text{MoO}_{24}$ from neutron powder diffraction data, *Acta. Cryst. B* 55 (1999) 306-312.
34. C. Tomasi, G. Spinolo, G. Chiodelli, A. Magistris, Phase equilibria in the Bi-rich part of the Bi, Mo/O system, *Solid State Ionics*. 99 (1997) 263–268.
35. I.N. Belyaev, N.P. Smolyaninov, The Bi_2O_3 - MoO_3 - PbO ternary system, *Russ. J. Inorg. Chem.* 5 (1962) 579–581.
36. A.C.A.M. Bleijenberg, B. C. Lippens, G. C. A. Schuit, Catalytic oxidation of 1-Butene over bismuth molybdate catalysts: the system Bi_2O_3 - MoO_3 , *J. Catal.* 4 (1965) 581–585.
37. L.M. Vitting, *Vestnik Moskow. Univ., Ser. Khim.* 2 (1966) 60.
38. G. Gattow, Beitrag zur kristallchemie des systems Bi_2O_3 - MoO_3 , *Z. Anorg. Chem.* 298 (1958) 64-71.
39. D.J. Buttrey, D.A. Jefferson, J.M. Thomas, Characterization of a new bismuth molybdate phase – $\text{Bi}_{38}\text{Mo}_7\text{O}_{78}$, *Mat. Res. Bull.* 21 (1986) 739–744.
40. G. Spinolo, C. Tomasi, Fluorite-related phases in the Bi-rich part of the Bi, Mo/O system, *Powder Diffraction*. 12 (1997) 16-19.
41. N. Sharma, R.B. Macquart, M. Christensen, M. Avdeev, Y.S. Chen, C.D. Ling, Structure and crystal chemistry of fluorite-related $\text{Bi}_{38}\text{Mo}_7\text{O}_{78}$ from single crystal X-ray diffraction and ab initio calculations, *J. Solid. State. Chem.* 182 (2009) 1312-1318.

42. E. Vila, J.E. Iglesias, J. Galy, A. Castro, Synthesis and characterization of a novel bismuth-molybdenum oxide and study of its ionic conducting behavior, *Solid State Sci.* 7 (2005) 1369-1376.
43. J. Galy, J.H. Velasco, A.R.L. Canovas, E. Vila, A. Castro, Ab initio structure determination and Rietveld refinement of $\text{Bi}_{10}\text{Mo}_3\text{O}_{24}$ the member $n = 3$ of the $\text{Bi}_{2n+4}\text{Mo}_n\text{O}_{6(n+1)}$ series, *J. Solid. State. Chem.* 182 (2009) 1177-1187.
44. S. Miyazawa, A. Kawana, H. Koizumi, H. Iwasaki, Single crystals in the Bi_2O_3 - MoO_3 binary system: growth and optical properties, *Mat. Res. Bull.* 9 (1974) 41–52.
45. L. Boon, R. Metselaar, Transport properties of $\text{Bi}_6\text{Mo}_2\text{O}_{15}$, *Solid State Ionics.* 16 (1985) 201–210.
46. E. Vila, J.M. Rojo, J.E. Iglesias, A. Castro, Polymorphism and electrical properties in the new oxide $\text{Bi}_6\text{Mo}_2\text{O}_{15}$, *Chem. Mater.* 16 (2004) 1732-1739.
47. E. Vila, A.R.L. Canovas, J. Galy, J.E. Iglesias, A. Castro, $\text{Bi}_{2n+4}\text{Mo}_n\text{O}_{6(n+1)}$ with $n = 3, 4, 5, 6$: A new series of low-temperature stable phases in the $m\text{Bi}_2\text{O}_3$ - MoO_3 system ($1.0 < m < 1.7$): Structural relationships and conductor properties, *J. Solid State Chem.* 180 (2007) 661-669.
48. J. Zemann, Die Kristallstruktur von koechlinit, Bi_2MoO_6 , *Heidelberger Beitr. Mineral. Petrogr.* 5 (1956) 139-145.
49. L.Ya. Erman, E.L. Galperin, B.P. Sobolev, Equilibrium diagram of the Bi_2O_3 - MoO_3 system, *Russ. J. Inorg. Chem.* 16 (1971) 258-261.

50. T. Chen, G.S. Smith, The compounds and the phase diagram of MoO₃-rich Bi₂O₃-MoO₃ system, *J. Solid State Chem.* 13 (1975) 288–297.
51. G. Blasse, Polymorphism of Bi₂MoO₆, *J. Inorg. Nucl. Chem.* 28 (1966) 1124–1125.
52. L.Ya. Erman, E.L. Galperin, Modifications of Bi₂MoO₆, *Russ. J. Inorg. Chem.* 13 (1968) 487.
53. A. Watanabe, H. Kodama, Polymorphic transformations of Bi₂MoO₆, *J. Solid State Chem.* 35 (1980) 240–245.
54. H. Kodama, A. Watanabe, The relative stabilities of Bi₂MoO₆ polymorphs, *J. Solid State Chem.* 56 (1985) 225-229.
55. A.R. Lim, J.H. Chang, S.H. Choh, M.S. Jang, A study of the phase transition in Bi₂MoO₆ single crystals, *J. Korean Phys. Soc.* 25 (1992) 109-112.
56. D.J. Buttrey, T. Vogt, B.D. White, High-temperature incommensurate-to-commensurate phase transition in the Bi₂MoO₆ catalyst, *J. Solid State Chem.* 155 (2000) 206-215.
57. L.Ya. Erman, E.L. Galperin, I.K. Kolchin, G.F. Dobrzhanskii, K.S. Chernyshev, The Bi₂O₃-MoO₃ system, *Russ. J. Inorg. Chem.* 9 (1964) 1174-1176.
58. L.Ya. Erman, E.L. Galperin, New data on the crystal structure of Bi₂O₃.2MoO₃, *Russ. J. Inorg. Chem.* 11 (1966) 122.

59. Ph.A. Batist, A.H.W.M. der Kinderen, Y. Leeuwenburgh, F.A.M.G. Metz, G.C.A. Schuit, Catalytic oxidation of 1-Butene over bismuth molybdate catalysts: dependence of activity on structures of catalysts, *J. Catal.* 12 (1968) 45-60.
60. B. Grzybowska, J. Haber, J. Komorek, Chemistry of Bi-Mo oxide catalysts: phase composition of catalysts and its relation to structure of precursors, *J. Catal.* 25 (1972) 25-32.
61. F. Zambonini, *Gazz. Chim. Ital.* 50 (1920) 128.
62. T. Chen, Crystal growth of BaMoO_4 , $\text{Bi}_2\text{O}_3 \cdot 3\text{MoO}_3$ and $\text{Bi}_2\text{O}_3 \cdot 2\text{MoO}_3$ from molten salt solution by pulling seed method, *J. Cryst. Growth.* 20 (1973) 29-37.
63. R.N. Vannier, G. Mairesse, F. Abraham, G. Nowogrocki, $\text{Bi}_{26}\text{Mo}_{10}\text{O}_8$ solid solution type in the Bi_2O_3 - MoO_3 - V_2O_5 ternary diagram, *J. Solid State Chem.* 122 (1996) 394-406.
64. R.N. Vannier, F. Abraham, G. Nowogrocki, G. Mairesse, New structural and electrical data on Bi-Mo mixed oxides with a structure based on $[\text{Bi}_{12}\text{O}_{14}]_\infty$ columns, *J. Solid State. Chem.* 142 (1999) 294-304.
65. D.J. Buttrey, T. Vogt, G.P.A. Yap, A.L. Rheingold, The structure of $\text{Bi}_{26}\text{Mo}_{10}\text{O}_{69}$, *Mat. Res. Bull.* 32 (1997) 947-963.
66. R. Enjalbert, G. Hasselmann, J. Galy, $[\text{Bi}_{12}\text{O}_{14}\text{E}_{12}]_n$ columns and lone pairs E in $\text{Bi}_{13}\text{Mo}_4\text{VO}_3\text{E}_{13}$: synthesis, crystal structure and chemistry of the Bi_2O_3 - MoO_3 - V_2O_5 system, *J. Solid. State. Chem.* 131 (1997) 236-245.

67. M. Huve, R.N. Vannier, G. Mairesse, EDS and TEM study of the family of compounds with a structure based on $[\text{Bi}_{12}\text{O}_{14}]_{\infty}$ columns in the Bi_2O_3 - MoO_3 binary system, *J. Solid. State. Chem.* 149 (2000) 276-283.
68. D.J. Buttrey, A survey of the Bi_2O_3 - MoO_3 binary system in Turning points in solid state materials and surface science- A book in celebration of the life and work of Sir John Meurig Thomas edited by K.D.M. Harris, P.P. Edwards, Royal Society of Chemistry, Cambridge, UK, 2008, p. 754-777.
69. M. Hartmanova, M.T. Le, I.V. Driessche, S. Hoste, F. Kundracik, Phase composition and charge transport in bismuth molybdates, *Russ.J. Electrochem.* 41 (2005) 455-460.
70. R. Sabbah, A.X. Wu, J.S. Chickos, M.L.P. Leitao, M.V. Roux, L.A. Torres, Reference materials for calorimetry and differential thermal analysis, *Thermochim. Acta.* 331 (1999) 93-204.
71. K. Majid, R. Mushtaq, S. Ahmad, Synthesis, characterization and coordinating behavior of aminoalcohol complexes with transition metals, *E-J.Chem.* 5 (2008) 969-979.
72. W.T. Miller, Some complex sodium bismuth salts of triethanolamine and triisopropanolamine, *J. Am. Chem. Soc.* 62 (1940) 2707-2709.
73. R.D. Hancock, I. Cukrowski, J. Baloyi, J. Mashishi, The affinity of bismuth (III) for nitrogen donor ligands, *J. Chem. Soc. Dalton Trans.* (1993) 2895-2899.

74. G. Szalontai, G. Kiss, L. Bartha, Equilibria of mononuclear oxomolybdenum (VI) complexes of triethanolamine- A multinuclear dynamic magnetic resonance study of structure and exchange mechanisms, *Spectrochim. Acta Part A* 59 (2003) 1995-2007.
75. O. Kubachewski, C.B. Alcock, *Metallurgical thermochemistry*, fifth ed., Pergamon, Oxford, 1979.
76. G.B. Naumov, B.N. Ryzhenko, I.L. Khodakovsky, *Reference book of thermodynamic values (for geologists) (in Russian)*: Atomizdat: Moskva, 1971
77. I. Barin, *Thermochemical data of pure substances*, third ed., VCH, Weinheim (Federal Republic of Germany), 1995.
78. O. Knacke, O. Kubachewski, K. Hesselmann, *Thermochemical properties of inorganic substances*, Vol 2, second ed., Springer, Berlin, 1991.
79. R. Venkatakrisnan, K. Nagarajan, P.R. Vasudeva Rao, Heat capacity measurements on BaThO₃ and BaCeO₃, *J. Nucl. Mater.* 299 (2001) 28–31.
80. R. Ganesan, R. Venkatakrisnan, R. Asuvathraman, K. Nagarajan, T. Gnanasekaran, R.S. Srinivasa, Heat capacities of PbBi₁₂O₁₉(s) and Φ -Pb₅Bi₈O₁₇(s), *Thermochim Acta* 439 (2005) 27-31.
81. S.K. Sahu, M. Sahu, R.S. Srinivasa, T. Gnanasekaran, Determination of heat capacities of PbCrO₄(s), Pb₂CrO₅(s) and Pb₅CrO₈(s), *Monatsh Chem.* 143 (2012) 1207-1214.

Chapter 3

Thermochemical studies on Bi-Mo-O system

3.1 Introduction

As discussed in chapter 1, the heavy corrosion and mass transport effects due to high dissolution of structural steel components in liquid Pb and LBE can be minimized by the insitu formation of a passive oxide layer over the steel surface by the careful control of oxygen concentration in the coolant. To understand the formation and stability of the passive oxide film, the interaction of alloying components of steel with Pb and Bi in the presence of dissolved oxygen has to be studied. In this context, a detailed knowledge on the phase diagrams of Bi-M-O and Pb-M-O (M = Fe, Cr, Mo, etc) systems as well as thermochemical data of relevant ternary compounds in these systems are required. Studies carried out on Bi-Mo-O system are described in this chapter.

3.2 Literature survey

3.2.1 Bi-Mo system

Data on Bi-Mo system has been reviewed by Brewer [1] and by Elliott [2]. The binary phase diagram of Bi-Mo system is shown in Fig. 3.1 [3]. No intermetallic phases exist in the system. Horsely and Maskreg [4] attempted to determine the solubility of Mo in Bi over a range of temperatures and concluded that the solubility is below the limits of analytical detection (1 ppm) up to 1303 K.

3.2.2 Bi-O system

The Bi-O phase diagram at 1 bar total pressure is shown in Fig. 3.2. The data on Bi-O system has been reviewed by Risold et al. [5]. Bismuth, which exists in the rhombohedral form, has a melting point of 544 K. The solubility of oxygen in

bismuth is 5 at% at 1400 K and it increases to 30 at% at 1650 K. Ganesan et al. [6] have reported the solubility of oxygen in liquid bismuth and is given by the following expressions:

$$\log(S/at\%O) = -4476/T K^{-1} + 4.05 \quad (T : 753-988 K) \quad (3.1)$$

$$\log(S/at\%O) = -3786/T K^{-1} + 3.36 \quad (T : 988-1020 K) \quad (3.2)$$

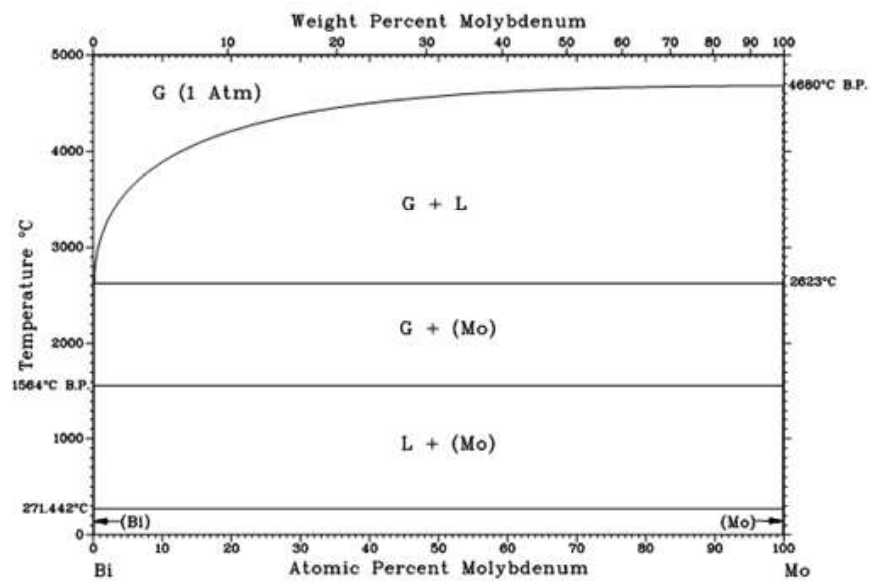


Fig. 3.1 Phase diagram of Bi-Mo- system [3]

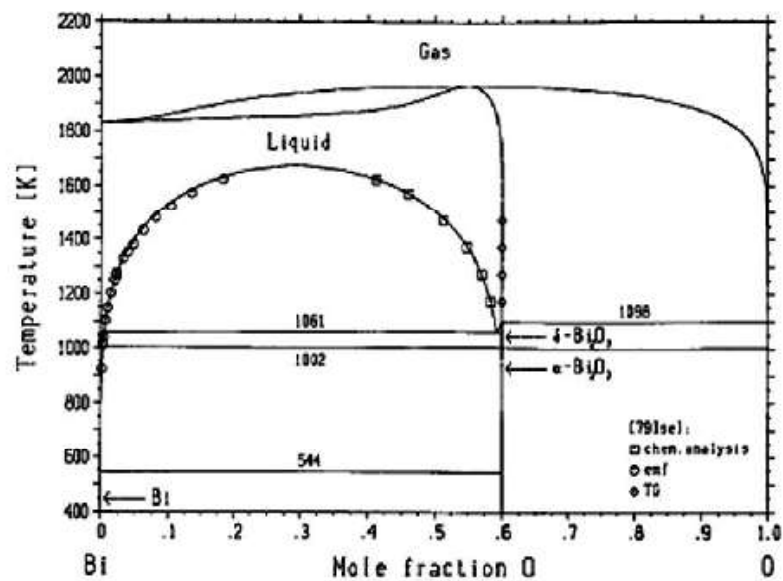


Fig. 3.2 Phase diagram of Bi-O system [4]

The only stable compound in the Bi-O system is Bi_2O_3 , which exhibits polymorphism with four modifications: α , β , γ and δ - Bi_2O_3 . Among which, α and δ phases are the stable phases while β and γ phases are metastable phases. The low temperature α - Bi_2O_3 has a monoclinic structure and the high temperature δ - Bi_2O_3 has fcc structure. α phase is stable up to 1002 K and where it transforms to the δ phase, which melts at 1098 K. The β and γ phases are having tetragonal and bcc structure, respectively. These metastable phases are formed upon cooling the δ phase. The formation temperatures of β and γ phases are reported to be ~ 920 and ~ 910 K, respectively. The β to α transition take place at temperatures between 920 and 700 K while the γ phase can be preserved at room temperature. The liquid exhibits miscibility gap between Bi and Bi_2O_3 from 1061 K and complete miscibility in liquid phase occurs at temperatures above 1650 K.

3.2.3 Mo-O system

The binary phase diagram of Mo-O system is presented in Fig. 3.3. A detailed review on this system has been given in ref 7.

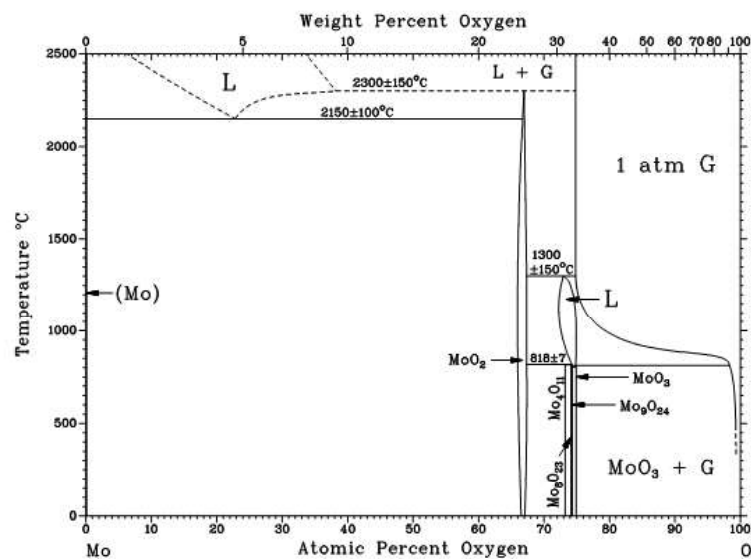


Fig. 3.3 Phase diagram of Mo-O system [6]

The various oxides of Mo reported to be present are MoO_2 , Mo_4O_{11} , Mo_8O_{23} , Mo_9O_{26} and MoO_3 . The melting points of MoO_3 and MoO_2 are determined to be 1073 ± 5 K and 2873 ± 5 K, respectively. Mo_4O_{11} undergoes disproportionation into MoO_2 and liquid at 1091 K.

The standard molar Gibbs energy of formation of MoO_2 (s) has been reported by several investigators [8-23]. Both emf and gas equilibrations techniques were used by these investigators. However, there is considerable differences exist among the reported data. The summary of the literature data on the Gibbs energy of formation of MoO_2 (s) and the experimental techniques employed are given in Table 3.1. The graphical comparison of the literature data is shown in Fig. 3.4.

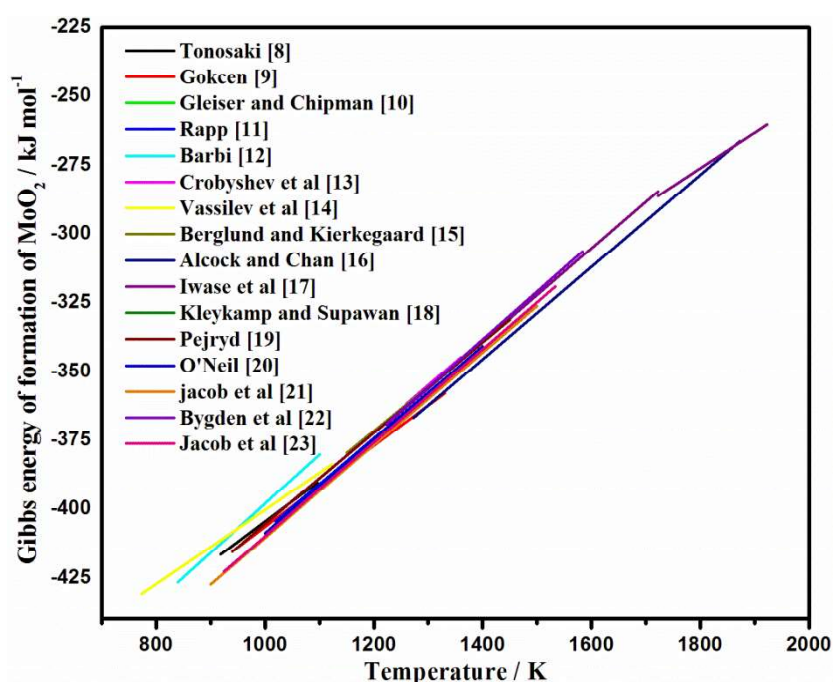


Fig. 3.4 Comparison of literature data on Gibbs energy of formation of MoO_2 (s)

The data reported by Gleiser and Chipman [10], O'Neill [20], Rapp [11] and Jacob et al. [21, 23] are in good agreement in the temperature range of 925 to 1500 K and are shown separately in Fig. 3.5. It is to be noted that these closely agreeing results are obtained by a variety of techniques.

Table 3.1 Literature data on Gibbs energy of formation of MoO₂ (s)

Investigators	Techniques	Molar Gibbs energy of formation of MoO ₂ / kJ mol ⁻¹	Temperature range/ K
Tonosaki, 1940 [8]	Gas equilibration (H ₂ /H ₂ O)	-550.199 + 0.1457T	918-1096
Gokcen, 1953 [9]	Gas equilibration (H ₂ /H ₂ O)	-553.334 + 0.1469T	950-1330
Gleiser and Chipman, 1962 [10]	Gas equilibration (CO/CO ₂)	-576.932 + 0.1681T	1200-1350
Rapp, 1963 [11]	Emf (Fe/FeO and Ni/NiO as reference electrode)	-575.300+0.1674T	1020-1320
Barbi, 1964 [12]	Emf (FeO/Fe ₃ O ₄ and Fe/Fe ₃ O ₄ as reference electrode)	-575.856+0.1778T	840-1100
Drobyshev et al., 1965 [13]	Emf (Fe/FeO as reference electrode)	-575.635+0.1697T	1260-1360
Vassilev et al., 1968 [14]	Gas equilibration (H ₂ /H ₂ O)	-533.887+0.1336T	773-1123
Berglund and Kierkegaard, 1969 [15]	Emf (air as reference electrode)	-564.798+0.161T	1150-1450
Alcock and Chan, 1972 [16]	Emf (CO/CO ₂ as reference electrode)	-579.902+0.1674T	1273-1873
Iwase et al., 1979 [17]	Emf (Co/CoO and air as reference electrode)	-576.100+0.1692T	1223-1723
Kleykamp and Supawan, 1979 [18]	Emf (Fe/FeO as reference electrode)	-509.600+0.1297T	1723-1923
Pejryd, 1984 [19]	Emf (air as reference electrode)	-571.800+0.1662T	1070-1320
O'Neill, 1986 [20]	Emf (Fe/FeO as reference electrode)	-529.21-0.1268T+0.0362TlnT	940-1450
Jacob et al., 1987 [21]	Emf (O ₂ as reference electrode)	-603.268-0.3375T-0.0207TlnT	1000-1400
Bygden et al., 1994 [22]	Emf (Fe/FeO as reference electrode)	-578.880+0.1685T	900-1500
Jacob et al., 2007 [23]	Emf (O ₂ as reference electrode)	-580.560+0.173T	1224-1584
		-579.821+0.170T	925-1533

Gleiser and Chipman [10] used the gas equilibration method, Rapp [11] used the emf method with Ni/NiO and Fe/FeO as the reference electrodes, O'Neill [20] used the emf method with Fe/FeO reference electrodes while Jacob et al. [21, 23] used pure oxygen gas as reference. The data reported by Tonosaki [8], Vassilev et al. [14] and Barbi [12] are significantly more positive.

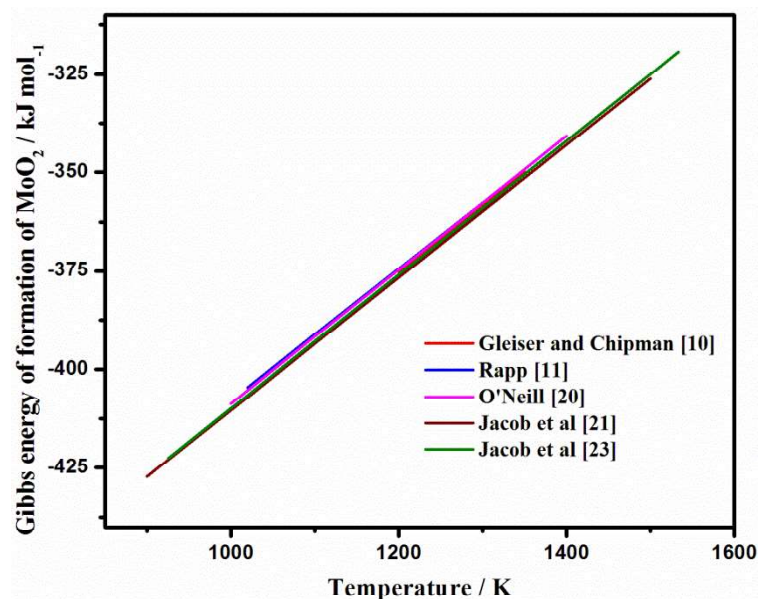


Fig. 3.5 Selected data on Gibbs energy of formation of MoO₂ (s) reported in literature

3.2.4 Bi₂O₃-MoO₃ system

The Bi₂O₃-MoO₃ pseudo binary system has been studied by several groups and it is characterized by the presence of several compounds and solid solutions. Extensive studies on thermal stabilities, oxide ion conductivities and catalytic properties of bismuth molybdates have been reported in literature. Spectroscopic investigations of several bismuth molybdates have been carried out in the past to unravel the mechanisms of their catalytic activities [24-26]. MoO₃rich section of this system in the composition range of 0 to 50 mol% Bi₂O₃ consists of three ternary compounds, namely, Bi₂Mo₃O₁₂, Bi₂Mo₂O₉ and Bi₂MoO₆. These compounds exhibit significant oxide ion conductivity and are known to catalyze selective oxidation of

several organic compounds and ammoxidation of olefins [27-29]. However, the Bi_2O_3 rich section of the system ($\text{Bi}_2\text{O}_3/\text{MoO}_3 \geq 1$) is rather complicated due to the presence of several ternary compounds and solid solutions. The temperature ranges of stabilities of most of the compounds in this composition range are not well established. All the reported ternary compounds in this system are labeled and presented in Fig. 3.6. The literature data concerning the existence and stabilities of bismuth molybdates and solid solutions are described below and the salient features are given in Table 3.2.

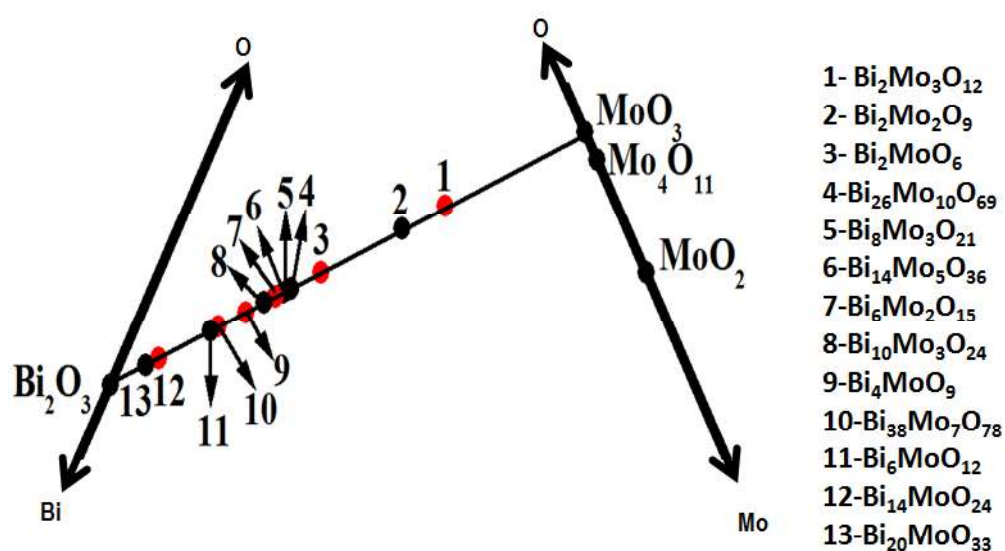


Fig. 3.6 Compounds reported in the Bi_2O_3 - MoO_3 pseudo binary system

a. $\text{Bi}_{20}\text{MoO}_{33}$

The existence of this Bi_2O_3 rich compound was first reported by Sillen and Lundborg [30] based on the studies involving XRD. The presence of this compound was indicated in the later studies by Kohlmuller and Badaud also [31]. However, Egashira et al. [32] carried out a detailed analysis of the data reported by Sillen and Lundborg [30] and showed that the XRD pattern attributed to $\text{Bi}_{20}\text{MoO}_{33}$ was that of

a mixture of the XRD patterns of Bi_2O_3 and $\text{Bi}_{14}\text{MoO}_{24}$ and thus ruled out the existence of $\text{Bi}_{20}\text{MoO}_{33}$.

b. $\text{Bi}_{14}\text{MoO}_{24}$

Egashira et al. [32] showed the existence of this Bi_2O_3 rich compound, during their investigation of the phase diagram of Bi_2O_3 - MoO_3 system. Structural characterization of this compound was later carried out by Ling et al. [33]. The formation of an eutectoid between Bi_2O_3 and $\text{Bi}_{14}\text{MoO}_{24}$ at ~ 998 K to form the solid solution δ (73-100 mol% Bi_2O_3) was suggested by Tomasi et al. [34].

c. $\text{Bi}_6\text{MoO}_{12}$

Belyaev and Smolyaninov [35] reported this compound and according to them, it forms continuous series of solid solutions with Bi_2O_3 as well as with Bi_2MoO_6 . The phase diagrams of Bi_2O_3 - MoO_3 system which were later reported by Bleijenberg et al. [36] and Vitting [37] showed the presence of $\text{Bi}_6\text{MoO}_{12}$ while that reported by Kohlmuller and Badaud [31] did not include it. Kohlmuller and Badaud [31] reported the composition corresponding to $\text{Bi}_6\text{MoO}_{12}$ to be falling within a solid solution with a composition of ~ 75 to 85 mol% Bi_2O_3 and melting congruently at 1253 K.

d. Bi_4MoO_9

The presence of Bi_4MoO_9 was first indicated by Gattow [38] based on their studies involving XRD and DTA. During their studies on Bi_2O_3 - MoO_3 system, Belyaev and Smolyaninov [35] observed the existence of a solid solution between $\text{Bi}_6\text{MoO}_{12}$ and Bi_2MoO_6 with a minimum at 33.3 mol% MoO_3 at 1203 K. They showed this corresponded to the composition of Bi_4MoO_9 and hence ruled out the existence of this compound.

e. $\text{Bi}_{38}\text{Mo}_7\text{O}_{78}$

Investigations of the Bi_2O_3 -rich section of the system by Buttrey et al. [39] using XRD and high resolution electron microscopy showed the presence of a new phase of composition $\text{Bi}_{38}\text{Mo}_7\text{O}_{78}$ with a defective fluorite structure. They determined its lattice parameters and ascribed it to be the same phase as described previously as $\text{Bi}_6\text{MoO}_{12}$. It is to be pointed out that Buttrey et al. [39] prepared $\text{Bi}_{38}\text{Mo}_7\text{O}_{78}$ by solid state reaction between Bi_2O_3 and MoO_3 at 1123 K in air while the earlier investigators [32, 36] prepared $\text{Bi}_6\text{MoO}_{12}$ by the reaction between the oxides at 873 K in air. $\text{Bi}_{38}\text{Mo}_7\text{O}_{78}$ was structurally characterized by Spinolo and Tomasi [40] and Sharma et al. [41]. Based on the studies involving DTA and impedance spectroscopy, Tomasi et al. [34] suggested an eutectoid reaction between $\text{Bi}_{14}\text{MoO}_{24}$ and $\text{Bi}_{38}\text{Mo}_7\text{O}_{78}$ at ~ 1063 K to form the solid solution δ (73-100 mol% Bi_2O_3). Tomasi et al. [34] also indicated the existence of a wide non stoichiometry in $\text{Bi}_{38}\text{Mo}_7\text{O}_{78}$.

f. $\text{Bi}_{10}\text{Mo}_3\text{O}_{24}$

The existence of $\text{Bi}_{10}\text{Mo}_3\text{O}_{24}$ was reported by Vila et al. [42] and their work showed it to be appearing as stable phase at 823 K and decomposing to $\text{Bi}_{38}\text{Mo}_7\text{O}_{78}$ and a high temperature solid solution at 1093 K. The structural characterization of this compound was later carried out by Galy et al. [43].

g. $\text{Bi}_6\text{Mo}_2\text{O}_{15}$

Based on the studies involving growth of single crystals and their characterization, Miyazawa et al. [44] reported a new compound of composition $\text{Bi}_6\text{Mo}_2\text{O}_{15}$ belonging to the monoclinic system and melting congruently at 1243 ± 5 K. Egashira et al. [32] also reported this compound and indicated the formation of an

eutectic between it and $\text{Bi}_6\text{MoO}_{12}$ at 1223 K. They also suggested this compound to be undergoing a phase transition at around 1023 K. Boon and Metselaar [45] reported the phase transition temperature to be between 973 and 1073 K. Vila et al. [46] studied the polymorphism and electrical properties of $\text{Bi}_6\text{Mo}_2\text{O}_{15}$. They observed the transition of $\text{Bi}_6\text{Mo}_2\text{O}_{15}$ to a $[\text{Bi}_{12}\text{O}_{14}]$ based columnar structured phase which belong to the high temperature solid solution at around 973 K. This solid solution was also reported to undergo an irreversible transition into another columnar type solid solution phase at ~ 1133 K.

h. $\text{Bi}_8\text{Mo}_3\text{O}_{21}$ and $\text{Bi}_{14}\text{Mo}_5\text{O}_{36}$

The presence of these two compounds was observed by Vila et al. [47]. Their investigations showed these compounds to be appearing as stable phases at temperatures close to 853 K. They found these compounds transformed to the high temperature solid solution at temperatures higher than 923 K.

i. Bi_2MoO_6

Zemann [48] reported this compound belonging to orthorhombic system. Although, subsequent investigators reported it to be congruently melting [31, 35, and 36], studies by Erman et al. [49] and Chen and Smith [50] showed it to be peritectically decomposing to liquid rich in MoO_3 and the solid solution with composition 1.26:1 $\text{Bi}_2\text{O}_3:\text{MoO}_3$ at ~ 1220 K. A high temperature modification of this compound was first reported by Blasse [51]. Later work by Erman et al. [52] showed three polymorphic forms of this compound to be present: i) γ - the low temperature phase (orthorhombic structure), ii) γ'' - the intermediate phase (tetragonal structure) and iii) γ' - the high temperature phase (monoclinic structure).

Table 3.2 Literature data on Bi₂O₃-MoO₃ pseudo binary system

Compound	Author	Preparation route	Experimental techniques employed	Observations
Bi ₂₀ MoO ₃₃	Sillen and Lundborg [30] Kohlmuller and Badaud[31] Egashira et al. [32]	Solid state reaction between Bi ₂ O ₃ and MoO ₃	XRD [30-32] DTA [31, 32]	<ul style="list-style-type: none"> ➤ Reported the presence of this compound [30, 31] ➤ Observed that Bi₂₀MoO₃₃ consisted of a mixture of Bi₂O₃ and Bi₁₄MoO₂₄ [32]
Bi ₁₄ MoO ₂₄	Ling et al. [33]Tomasi et al. [34] Spinolo and Tomasi [40]	Solid state reaction between Bi ₂ O ₃ and MoO ₃ at 1073 K	DTA [34] XRD [33, 34, 40] Impedance spectroscopy [34]	<ul style="list-style-type: none"> ➤ Structural characterizations of Bi₁₄MoO₂₄ [33, 40] ➤ Eutectoid reaction with Bi₂O₃ to form the solid solution δ (73-100 mol% Bi₂O₃): ~998 K [34] ➤ Eutectoid reaction with Bi₃₈Mo₇₈O₇₈ to form the solid solution δ (73-100 mol% Bi₂O₃): ~1063 K [34]
Bi ₆ MoO ₁₂	Kohlmuller and Badaud[31] Egashira et al. [32] Belyaev & Smolyaninov [35] Bleijenberg et al. [36] Erman et al. [49]	Solid state reaction between Bi ₂ O ₃ and MoO ₃ at 873 K [36, 32] Fusion of oxide mixtures followed by recrystallization [35] Fusion of oxide mixtures followed by quenching and subsequent heating at 1023 K [49]	XRD and DTA[31, 32, 36, 49] Visual polythermal method [35]	<ul style="list-style-type: none"> ➤ Congruent melting point :1253 K [31], 1263 K [35], 1268 K [36] ➤ Bi₆MoO₁₂ is within the solid solution field of δ-Bi₂O₃ [49] ➤ The solid solutions based on δ-Bi₂O₃ possess a maximum at 76-77 mol% Bi₂O₃ corresponding to 3:1 Bi₂O₃:MoO₃ (i.e. Bi₆MoO₁₂) [31] ➤ Eutectic with Bi₆Mo₂O₁₅ : 1223 K [32]

Bi ₄ MoO ₉	Belyaev and Smolyaninov [35] Gattow [38]	Fusion of oxide mixtures followed by crystallization [35] Coprecipitation method [38]	Visual polythermal method [35] XRD and DTA[38]	<ul style="list-style-type: none"> ➤ Melting point: 1193 K [38] ➤ The minimum of Bi₆MoO₁₂-Bi₂MoO₆ solid solution corresponding to the composition of Bi₄MoO₉ [35]
Bi ₃₈ Mo ₇ O ₇₈	Tomasi et al. [34] Buttrey et al. [39] Spinolo and Tomasi [40]	Solid state reaction between Bi ₂ O ₃ and MoO ₃ at 1113 K [39], 1073 K [34, 40]	XRD [34, 39, 40] SAED [39] DTA [34] Impedance spectroscopy [34]	<ul style="list-style-type: none"> ➤ Characterized Bi₃₈Mo₇O₇₈ and ascribed it as the same phase as Bi₆MoO₁₂ [39] ➤ Suggested non - stoichiometry [34] ➤ Structural characterizations of Bi₃₈Mo₇O₇₈ [40]
Bi ₁₀ Mo ₃ O ₂₄	Vila et al. [42]	Wet chemical method	XRD Impedance spectroscopy	<ul style="list-style-type: none"> ➤ Appears as stable phase at 823 K ➤ Decomposes at temperatures above 1023 K to Bi₃₈Mo₇O₇₈ and a high temperature solid solution polymorph
Bi ₆ Mo ₂ O ₁₅	Egashira [32] Miyazawa et al. [44] Boon and Metselaar [45] Vila et al. [46]	Single crystal growth by Czochralski method [44] Solid state reaction at 873 K [32], 1073 K [45] Wet chemical method [46]	DTA [32, 46] XRD [32, 44-46] Impedance spectroscopy [45, 46]	<ul style="list-style-type: none"> ➤ Congruent melting point : 1243 K [44] ➤ Appears as stable phase at 773 K [32] ➤ Phase transition at 1023 K [32], 973-1073 K [45] ➤ Eutectic with Bi₆MoO₁₂ : 1223 K [32] ➤ Transforms to a high temperature solid solution polymorph at 973 K [46]
Bi _{11,4} Mo ₅ O ₃₆	Vila et al. [47]	Wet chemical method	XRD Impedance spectroscopy	<ul style="list-style-type: none"> ➤ Formation temperature between 823 to 853 K ➤ Transforms to a high temperature solid solution polymorph at 923 K
Bi ₈ Mo ₃ O ₂₁	Vila et al. [47]	Wet chemical method	XRD	<ul style="list-style-type: none"> ➤ Formation temperature between 853 to 903 K

			Impedance spectroscopy	
Bi ₂ MoO ₆	Egashira et al. [32] Belyaev and Smolyaninov [35] Bleijenberg et al. [36] Erman et al. [49, 52] Chen and Smith [50] Blasse [51] Watanabe and Kodama [53] Lim et al. [55]	Fusion of oxide mixtures followed by crystallization [35] Fusion of oxide mixtures followed by quenching and subsequent heating at 873 K [49, 52] Fusion of oxide mixtures followed by annealing at 873-943 K [50] Solid state reaction at 873 K [36, 32], 1023 K [51], 800 K [53] Single crystal growth [55]	Visual polythermal method [35] DTA [32, 36, 49, 50, 53, 55] XRD [32, 36, 49, 50, 51, 53] High temperature XRD [52] Dilatometry [53] DSC [53]	<ul style="list-style-type: none"> ➤ Transforms to a high temperature solid solution polymorph at 943 K ➤ Congruent melting point : 1243 K [35], 1211 K [36] ➤ Eutectic with Bi₂Mo₃O₁₂ : 909 K [35] ➤ Eutectic with Bi₂Mo₂O₉: 909 K [49, 50] ➤ Peritectic decomposition: 1193 K [35], 1173 K [36], 1220 K [50] ➤ Observed only the low temperature orthorhombic (γ) phase [36] ➤ Observed three polymorphic forms [49, 52] ➤ Observed the high temperature modification (γ' phase) [51] ➤ Observed only γ and γ' modifications; γ to γ' transition at 873 K and irreversible [32] ➤ Transition of the low temperature phase (γ) to the intermediate phase (γ'') at : 593-793 K [53], 877 K [54], 533 K [55] and is reversible ➤ Transition of the intermediate phase (γ'') to the high temperature phase (γ') at 823-913 K [52], 913 to 943 K [53], 918 K [55] and is irreversible ➤ $\Delta H_{transition}$ for γ to γ'' transition : 0.1 kcal/mol [52] ➤ $\Delta H_{transition}$ for γ'' to γ' transition: 3.2 kcal/mol [53]
Bi ₂ Mo ₂ O ₉	Erman et al. [49, 57, 58] Chen and Smith [50] Egashira et al. [32]	Fusion of oxide mixtures followed by crystallization and by coprecipitation [49, 57, 58]	XRD [32, 49, 50, 57, 58] DTA [32, 49, 50]	<ul style="list-style-type: none"> ➤ Structural characterization and determination of lattice parameters [58] ➤ Peritectic decomposition: 938 K [49], 955 K [50], 923 K [49, 57]

			58] Fusion of oxide mixtures followed by annealing at 873-943 K [50] Solid state reaction at 873 K [32]		<ul style="list-style-type: none"> ➤ Eutectic with Bi_2MoO_6: 909 K [57] ➤ Eutectic with $\text{Bi}_2\text{Mo}_3\text{O}_{12}$: 913 K [32], 909 K [57] ➤ Stable range: 813 to 938 K [32]
$\text{Bi}_2\text{Mo}_3\text{O}_{12}$	Zambonini [61] Belyaev and Smolyaninov [35] Bleijenberg et al. [36] Erman et al. [49, 57] Chen and Smith [50] Egashira et al. [32] Miyazawa et al. [44]	Visual polythermal method [35] XRD [32, 36, 49, 50, 57] DTA [36, 49, 50]	Fusion of oxide mixtures followed by recrystallization [35, 49, 57] Solid state reaction at 873 K [36, 32] Fusion of oxide mixtures followed by annealing at 873-943 K [50] Coprecipitation [57] Single crystal growth by Czochralski method [44]	<ul style="list-style-type: none"> ➤ Reported the existence [61] ➤ Congruent melting point : 921 K [35], 949 K [36], 935 K [50], 943 K [44] ➤ Eutectic with MoO_3 : 909 K [49, 57], 891 K [35, 50] ➤ Eutectic with $\text{Bi}_2\text{Mo}_2\text{O}_9$: 913 K [32] ➤ Eutectic with Bi_2MoO_6: 909 K [35, 57] ➤ Peritectic decomposition: 913 K [49] 	
Solid solutions	Tomasi et al. [34] Erman et al. [49] Chen and Smith [50] Vannier et al. [63, 64] Buttrey et al. [65]	DTA [34, 49] XRD [49, 50, 63, 64, 66, 67] Impedance spectroscopy	Fusion of oxide mixtures followed by quenching and subsequent heating at 1023 K [49]	<ul style="list-style-type: none"> ➤ Observed the following solid solutions with variable lattice parameters [49] <ul style="list-style-type: none"> a) ϵ- phase (40 to 60 mol% Bi_2O_3) b) θ- phase (60 to ~70 mol% Bi_2O_3) c) Ω-phase (~70 to 75 mol% Bi_2O_3) 	

	<p>Enjalbert et al. [66] Huveet al. [67]</p>	<p>Fusion of oxide mixtures followed by annealing at 873-943 K [50] Solid state reaction between Bi₂O₃ and MoO₃ [34, 63-66]</p>	<p>[63, 64, 34] SAED [65, 67] NPD [64]</p>	<p>d) η-phase (~80 to ~90 mol% Bi₂O₃) e) δ-phase (60 to ~97 mol% Bi₂O₃) ➤ Observed the ε phase (13 Bi₂O₃:10MoO₃) [49, 50] ➤ Structural investigation of Bi_xMo₁₀O₆₉ (x = 25.75 to 27.75) and confirmed the solid solubility range as between 2.6 ≤ Bi/Mo ≤ 2.8 [63-65] ➤ Determined the the solid solution range of Bi_xMo₁₀O₆₉ with x = 28.6 to 35 [66] ➤ Confirmed the solid solution range of Bi_xMo₁₀O₆₉ with x = 26 to 28 [67] ➤ All compositions within this solid solution field are monoclinic [63]. ➤ Observed a lens shaped biphasic region separating the liquid and solid solution field (~84 to 100% Bi₂O₃) [34]</p>
--	--	---	--	--

Several studies have been carried out on the polymorphic transformations of Bi_2MoO_6 [32, 49, 52-56], but the reported transition temperatures are in disagreement. Erman et al. [52] reported a reversible transition of γ to γ'' at temperatures between 593 K and 793 K and an irreversible transition of γ'' to γ' at temperatures between 823 K and 913 K based on high temperature X-ray diffraction studies whereas Lim et al. [55] reported 533 and 918 K as the corresponding transition temperatures. Polymorphism of the compound was not observed in the studies of Bleijenberg et al. [36] and Chen and Smith [50]. They observed only the γ phase of Bi_2MoO_6 . Egashira et al. [32] observed only the γ and γ' phases of Bi_2MoO_6 with a transition temperature ~ 873 K. Studies by Watanabe and Kodama [53, 54] showed the γ to γ'' transition (877 K) to be reversible while γ'' to γ' transition (913 K) to be irreversible and reported the corresponding enthalpies of transitions as 0.42 kJ mol^{-1} and 13.4 kJ mol^{-1} , respectively. Buttrey et al. [56] also reported the γ to γ'' transition to be reversible and occurring at ~ 840 K and the γ'' to γ' transition to be irreversible and occurring at ~ 880 K.

j. $\text{Bi}_2\text{Mo}_2\text{O}_9$

Erman et al. [57] reported the existence of $\text{Bi}_2\text{Mo}_2\text{O}_9$ which was formed by the peritectic reaction between MoO_3 rich liquid and Bi_2MoO_6 at 923 K. Structure of this compound was established by them in their later study [58]. They showed that $\text{Bi}_2\text{Mo}_2\text{O}_9$ formed an eutectic with $\text{Bi}_2\text{Mo}_3\text{O}_{12}$ at 909 K with a eutectic composition of 72.5 mol% MoO_3 . Erman et al. [49] reported that the peritectic decomposition of $\text{Bi}_2\text{Mo}_2\text{O}_9$ was erroneously considered as the eutectic between $\text{Bi}_2\text{Mo}_3\text{O}_{12}$ and Bi_2MoO_6 in the studies reported in references 31, 35, and 36 and did not include the presence of $\text{Bi}_2\text{Mo}_2\text{O}_9$ in the phase diagrams reported in these works. Later studies by

Chen and Smith [50] confirmed the results of Erman et al. [49]. Results of the studies made by Egashira et al. [32] were also similar except for small differences in the eutectic and peritectic temperatures. Investigations by Batist et al. [59] and Grzybowska et al. [60] on thermal stability of $\text{Bi}_2\text{Mo}_2\text{O}_9$ showed it to be decomposing to $\text{Bi}_2\text{Mo}_3\text{O}_{12}$ and Bi_2MoO_6 below 823 K. Investigations by Egashira et al. [32] showed $\text{Bi}_2\text{Mo}_2\text{O}_9$ to be stable in a very narrow range of temperature viz., 813 to 938 K and it disproportionated to form $\text{Bi}_2\text{Mo}_3\text{O}_{12}$ and Bi_2MoO_6 at 813 K.

k. $\text{Bi}_2\text{Mo}_3\text{O}_{12}$

Zambonini et al. [61] reported the presence of this compound and structurally characterized it. Later, several authors [32, 35-37, 44, 49, 50, 57, 62] have studied this compound and showed it to be congruently melting at ~930 K. Erman et al. [57] reported an eutectic to be formed between $\text{Bi}_2\text{Mo}_3\text{O}_{12}$ and MoO_3 and this has been supported by the later works of Bleijenberg et al. [36], Egashira et al. [32] and Chen [62].

l. Solid solutions in the Bi_2O_3 - MoO_3 system

Many investigators have observed the presence of solid solutions in the Bi_2O_3 rich part of the system [32, 34-36, 49, 50]. Erman et al. [49] reported the presence of five solid solutions above 773 K in the composition ranges of a) 40 to 60 mol% Bi_2O_3 , b) 60 to ~70 mol% Bi_2O_3 , c) ~70 to 75 mol% Bi_2O_3 , d) ~80 to ~90 mol% Bi_2O_3 and e) a high temperature phase with 60 to ~97 mol% Bi_2O_3 . Studies by Chen and Smith [50] also showed the presence of the solid solution at around 56.5 mol% Bi_2O_3 . Erman et al. [49] also reported that the high temperature phase with ~75 mol% Bi_2O_3 had a melting point maximum and that with ~67 mol% Bi_2O_3 had the minimum. They suggested that these compositions corresponded to the compositions of

$\text{Bi}_6\text{MoO}_{12}$ and Bi_4MoO_9 reported by Belyaev and Smolyaninov [35] and Gattow [38], respectively. Studies by Tomasi et al. [34] also showed the existence of a high temperature solid solution with the composition ranging from ~73 to 100 mol% Bi_2O_3 and with a defective fluorite structure. They observed that a lens shaped biphasic region separated this solid solution field from the liquid phase. They also reported that both $\text{Bi}_{14}\text{MoO}_{24}$ and $\text{Bi}_{38}\text{Mo}_7\text{O}_{78}$ were stable below this solid solution field.

Vannier et al. [63, 64] observed the domain of a solid solution around $\text{Bi}_x\text{Mo}_{10}\text{O}_{69}$ ($x = 25.75$ to 27.75) with a structure based on $[\text{Bi}_{12}\text{O}_{14}]$ columns, which was reported earlier by Erman et al. [49] and Chen & Smith [50]. The composition of the parent compound of this solid solution field was formulated as $\text{Bi}_{26}\text{Mo}_{10}\text{O}_{69}$. They also observed that the structure of compositions within this solid solution field to be monoclinic. These results were later confirmed by Buttrey et al. [65]. However, Enjalbert et al. [66] disputed the stoichiometry range of the solid solution and based on crystallographic investigations, they proposed its composition as with $x = 28.6$ to 35.0 . Huve et al. [67] carried out structural analysis of the family of the compounds belonging to the $[\text{Bi}_{12}\text{O}_{14}]$ columns and confirmed the solid solution field to be limited within the range of $x = 26$ to 28 .

Phase diagrams of the Bi_2O_3 - MoO_3 system and the liquidus boundaries are reported in references [31, 32, 34-36, 49, 50]. It is to be pointed out that in the course of the investigations of the system by employing various techniques, new compounds and solid solutions have been identified. Hence, phase diagrams reported by earlier investigators were not complete. Buttrey [68] in 2008 proposed a phase diagram of this system by taking into account of the data available in literature. Although it shows the presence of $\text{Bi}_2\text{Mo}_3\text{O}_{12}$, $\text{Bi}_2\text{Mo}_2\text{O}_9$, Bi_2MoO_6 , $\text{Bi}_8\text{Mo}_3\text{O}_{21}$, $\text{Bi}_{14}\text{Mo}_5\text{O}_{36}$, $\text{Bi}_6\text{Mo}_2\text{O}_{15}$, $\text{Bi}_{10}\text{Mo}_3\text{O}_{24}$, $\text{Bi}_{38}\text{Mo}_7\text{O}_{78}$ and $\text{Bi}_{14}\text{MoO}_{24}$, presence of $\text{Bi}_6\text{MoO}_{12}$ had not

been considered. Presence of high temperature solid solutions such as δ phase (with composition $\text{Bi}_x\text{Mo}_{10}\text{O}_{69}$ with $x = 26$ to 28) and ϵ phase (with composition of ~ 82 - 87 mol% Bi_2O_3) are also indicated. It is to be pointed out that the Bi_2O_3 rich portion of the phase diagram by Buttrey [68] is considerably different from those reported by earlier investigators. Tomasi et al. [34] had reported the presence of an eutectoid between Bi_2O_3 and $\text{Bi}_{14}\text{MoO}_{24}$ at ~ 998 K and another eutectoid between $\text{Bi}_{14}\text{MoO}_{24}$ and $\text{Bi}_{38}\text{Mo}_7\text{O}_{78}$ at ~ 1063 K and these are not indicated in the phase diagram proposed by Buttrey [68]. Also, the presence of the high temperature solid solution at ~ 73 to 100 mol% Bi_2O_3 and the lens shaped biphasic region above this solid solution field suggested by Tomasi et al. [34] had not been considered. The temperatures above which the compounds $\text{Bi}_8\text{Mo}_3\text{O}_{21}$ and $\text{Bi}_{14}\text{Mo}_5\text{O}_{36}$ appear as stable phases and the invariant reactions that would involve the appearance of these compounds in this system have not yet been established. Phase diagram of Bi_2O_3 - MoO_3 system which was adapted from that reported by Buttrey et al. [68] is shown in Fig. 3.7.

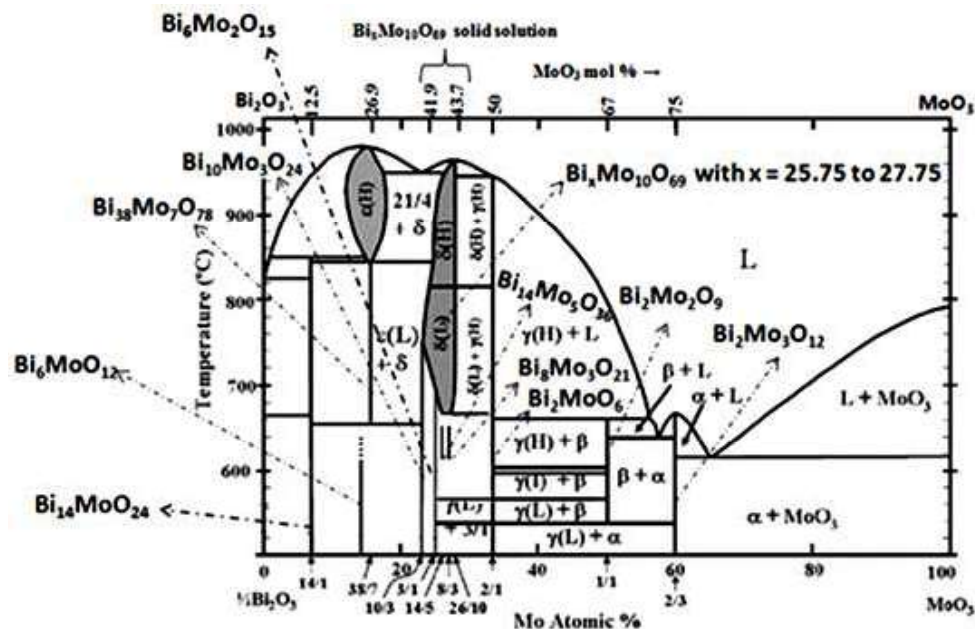


Fig. 3.7 Bi_2O_3 - MoO_3 pseudo binary phase diagram adapted from ref. 68 showing the composition of the compounds and solid solutions [In ref. 68, existence of $\text{Bi}_6\text{MoO}_{12}$ is not considered]

It is clear from the literature data that MoO₃ rich section of the system consists of only three ternary compounds, namely, Bi₂Mo₃O₁₂, Bi₂Mo₂O₉ and Bi₂MoO₆. The Bi₂O₃ rich section of the system is not well established. Although several compounds were reported in the past, subsequent studies have shown the presence of the following compounds in this part of the system: Bi₈Mo₃O₂₁, Bi₁₄Mo₅O₃₆, Bi₆Mo₂O₁₅, Bi₁₀Mo₃O₂₄, Bi₃₈Mo₇O₇₈, Bi₆MoO₁₂ and Bi₁₄MoO₂₄. It is known that a solid solution Bi_xMo₁₀O₆₉ (x = 26 to 28) exists at high temperatures. This solid solution will be designated as ‘Bi₂₆Mo₁₀O₆₉’ further in the discussions. Bi₈Mo₃O₂₁, Bi₁₄Mo₅O₃₆ and Bi₆Mo₂O₁₅ appear as stable phases at temperatures between 773 and 873 K and they transform to ‘Bi₂₆Mo₁₀O₆₉’ at higher temperatures although the exact transformation temperatures are not known. The exact temperatures at which these ternary compounds appear as stable phases and the corresponding invariant reactions at these temperatures are also not known. Since, the phase diagram reported by Buttrey [68] does not include the presence of Bi₆MoO₁₂, existence of this compound also need to be studied.

Although the pseudo binary phase diagram of Bi₂O₃-MoO₃ system has been investigated by several authors, no data exist on the ternary Bi-Mo-O system and the thermochemical properties of the ternary compounds of the system are not available.

3.3 Experimental details

3.3.1 Materials

Bi₂O₃ powder (99.99% purity on metal basis, M/s Alfa Aesar, USA), Bi powder (99.9% purity on metal basis, M/s Alfa Aesar, USA) and Mo powder (99.9% purity on metal basis, M/s Alfa Aesar, USA) were used. Bi₂O₃ powder was calcined at 1023 K in air for about 6 h to remove any carbonate impurity and adsorbed moisture present in it. The calcined powder was stored in a desiccator. MoO₃ powder

was prepared by heating ammonium heptamolybdate tetrahydrate (99.96% purity on metal basis, M/s Sigma-Aldrich, USA) at 723 K in air for 24 h. MoO₂ was prepared by the reduction of MoO₃ at 823 K for 16 h under flowing hydrogen gas saturated with water vapour. All the compounds were characterized by an X-ray diffractometer (M/s Inel, France) with Cu K_α radiation and graphite monochromator. The XRD patterns were matched with the corresponding PCPDF patterns.

3.3.2 Preparation of ternary compounds

The ternary compounds reported to be present in the Bi₂O₃-MoO₃ pseudo binary system were prepared by the solid state reaction between Bi₂O₃ and MoO₃ in air. For this, stoichiometric amounts of Bi₂O₃ and MoO₃ were homogeneously mixed and made into pellets. The pellets were placed in alumina crucibles and heated at different chosen temperatures. The pellets were ground at the end of half the total duration of heating. The powders were homogenized, repelletized and heated again. The samples were quenched to room temperature and the phases in them were characterized by XRD. Although the mass loss of the samples while heating in open crucibles were very low (~0.01 to 0.03%), the ternary compounds were also prepared under vacuum by placing the alumina crucibles containing the sample pellets in small volume (~20 ml) evacuated and sealed quartz ampoules. The ampoules were kept inside a constant temperature zone of the furnace and heated at the chosen temperature. The experimental details are given in Table 3.3.

3.3.3 Phase equilibration studies

3.3.3.1 Equilibrations of samples with compositions in the Bi₂O₃-MoO₃ pseudo binary line

To examine the possible existence of any new compound other than those reported in the Bi₂O₃-MoO₃ pseudo binary system, samples with different molar

ratios of Bi_2O_3 and MoO_3 were prepared and equilibrated. The overall composition of each sample was chosen such that it would correspond to a composition between those of two reported adjacent ternary compounds. Initial mixture of Bi_2O_3 and MoO_3 were thoroughly ground and made into pellets. The pellets were then kept inside alumina crucibles and enclosed in quartz ampoules under vacuum. Samples were equilibrated for prolonged periods at 773, 873 and 1023 K. After the equilibration, samples were quenched to room temperature and the products formed were identified by XRD. The details of these experiments are given in Table 3.4.

Table 3.3 Preparation of ternary compounds in the Bi_2O_3 - MoO_3 system

Compound	Molar ratios of Bi_2O_3 and MoO_3	Temperature	Duration of heating	Product formed*
$\text{Bi}_2\text{Mo}_3\text{O}_{12}$	$1\text{Bi}_2\text{O}_3 : 3\text{MoO}_3$	873 K	48 h	$\text{Bi}_2\text{Mo}_3\text{O}_{12}$
$\text{Bi}_2\text{Mo}_2\text{O}_9$	$1\text{Bi}_2\text{O}_3 : 2\text{MoO}_3$	773 K	48 h	$\text{Bi}_2\text{Mo}_3\text{O}_{12}$, γ - Bi_2MoO_6 (orthorhombic phase)
		873 K	48 h	$\text{Bi}_2\text{Mo}_2\text{O}_9$
Bi_2MoO_6	$1\text{Bi}_2\text{O}_3 : 1\text{MoO}_3$	773 K	48 h	γ - Bi_2MoO_6 (orthorhombic phase)
		873 K	48 h	γ' - Bi_2MoO_6 (monoclinic phase)
$\text{Bi}_6\text{Mo}_2\text{O}_{15}$	$3\text{Bi}_2\text{O}_3 : 2\text{MoO}_3$	873 K	48 h	$\text{Bi}_6\text{Mo}_2\text{O}_{15}$
$\text{Bi}_{10}\text{Mo}_3\text{O}_{24}$	$5\text{Bi}_2\text{O}_3 : 3\text{MoO}_3$	1023 K	48 h	$\text{Bi}_{10}\text{Mo}_3\text{O}_{24}$
$\text{Bi}_6\text{MoO}_{12}$	$3\text{Bi}_2\text{O}_3 : 1\text{MoO}_3$	873 K	48 h	$\text{Bi}_6\text{MoO}_{12}$
$\text{Bi}_{38}\text{Mo}_7\text{O}_{78}$	$19\text{Bi}_2\text{O}_3 : 7\text{MoO}_3$	1023 K	48 h	$\text{Bi}_{38}\text{Mo}_7\text{O}_{78}$
$\text{Bi}_{14}\text{MoO}_{24}$	$7\text{Bi}_2\text{O}_3 : 1\text{MoO}_3$	873 K	48 h	$\text{Bi}_{14}\text{MoO}_{24}$
$\text{Bi}_{26}\text{Mo}_{10}\text{O}_{69}$	$13\text{Bi}_2\text{O}_3 : 5\text{MoO}_3$	1023 K	48 h	' $\text{Bi}_{26}\text{Mo}_{10}\text{O}_{69}$ '

**Same phases were obtained at the end of 24 h of heating*

As mentioned earlier, Buttrey et al. [39] considered $\text{Bi}_{38}\text{Mo}_7\text{O}_{78}$ to be the same as the compound $\text{Bi}_6\text{MoO}_{12}$, although their compositions are significantly different ($3\text{Bi}_2\text{O}_3 : 1\text{MoO}_3$ in $\text{Bi}_6\text{MoO}_{12}$ and $2.71\text{Bi}_2\text{O}_3 : \text{MoO}_3$ in $\text{Bi}_{38}\text{Mo}_7\text{O}_{78}$) and XRD patterns of the two compounds have marked difference. It is also to be pointed

out that subsequent to the report by Buttrey et al. [39], no further data has been reported in literature about these compounds. To verify the existence of $\text{Bi}_6\text{MoO}_{12}$, samples with different molar ratios of Bi_2O_3 and MoO_3 , whose compositions lie between those of $\text{Bi}_{10}\text{Mo}_3\text{O}_{24}$ and $\text{Bi}_{14}\text{MoO}_{24}$, were equilibrated. The sample mixtures were thoroughly ground, made into pellets, kept in alumina crucibles and sealed in evacuated quartz ampoules. The ampoules were equilibrated at 773, 873 and 1023 K for prolonged duration. After the equilibration, samples were quenched to room temperature. The details of the overall compositions chosen and the products identified by XRD are given in Table 3.4.

3.3.3.2 Equilibrations of samples with compositions in the line joining Bi_2O_3 and MoO_2

Samples containing different molar ratios of Bi_2O_3 and MoO_2 were equilibrated for prolonged periods to examine the existence of any ternary compound involving Bi_2O_3 and MoO_2 . For this, mixtures of Bi_2O_3 and MoO_2 were compacted into pellets and taken in alumina crucibles. The crucibles were then kept enclosed in evacuated quartz ampoules and subjected to long term equilibration at 773 and 1023 K. After the equilibrations, samples were quenched to room temperature and the products were identified by XRD. The results obtained from these equilibration experiments are given in Table 3.5.

3.3.3.3 Partial reduction of ternary compounds followed by long term equilibrations

To obtain preliminary information on the coexisting phases in the Bi-Mo-O system, the ternary compounds were subjected to partial reduction under flowing hydrogen gas at 773 K for about 15 min.

Table 3.4 Details of equilibrations of samples with mixtures of Bi₂O₃ and MoO₃

No	Composition chosen	Products obtained after equilibration*		
		At 773 K (960 h)	At 873 K (720 h)	At 1023 K (480 h)
1	1Bi ₂ O ₃ : 7MoO ₃ (between MoO ₃ and Bi ₂ Mo ₃ O ₁₂)	MoO ₃ , Bi ₂ Mo ₃ O ₁₂	MoO ₃ , Bi ₂ Mo ₃ O ₁₂	-
2	1Bi ₂ O ₃ : 2.5MoO ₃ (between Bi ₂ Mo ₃ O ₁₂ and Bi ₂ Mo ₂ O ₉)	Bi ₂ Mo ₃ O ₁₂ , Bi ₂ MoO ₆	Bi ₂ Mo ₃ O ₁₂ , Bi ₂ Mo ₂ O ₉	-
3	1Bi ₂ O ₃ : 1.4MoO ₃ (between Bi ₂ Mo ₂ O ₉ and Bi ₂ MoO ₆)	Bi ₂ Mo ₃ O ₁₂ , Bi ₂ MoO ₆	Bi ₂ Mo ₂ O ₉ , Bi ₂ MoO ₆	-
4	1.08Bi ₂ O ₃ : 1MoO ₃ (between Bi ₂ MoO ₆ and 'Bi ₂₆ Mo ₁₀ O ₆₉ ')	Bi ₂ MoO ₆ , Bi ₆ Mo ₂ O ₁₅	Bi ₂ MoO ₆ , Bi ₆ Mo ₂ O ₁₅	Bi ₂ MoO ₆ , 'Bi ₂₆ Mo ₁₀ O ₆₉ '
5	1.17Bi ₂ O ₃ : 1MoO ₃ (between Bi ₂ MoO ₆ and 'Bi ₂₆ Mo ₁₀ O ₆₉ ')	Bi ₂ MoO ₆ , Bi ₆ Mo ₂ O ₁₅	Bi ₂ MoO ₆ , Bi ₆ Mo ₂ O ₁₅	Bi ₂ MoO ₆ , 'Bi ₂₆ Mo ₁₀ O ₆₉ '
6	1.25Bi ₂ O ₃ : 1MoO ₃ (between Bi ₂ MoO ₆ and 'Bi ₂₆ Mo ₁₀ O ₆₉ ')	Bi ₂ MoO ₆ , Bi ₆ Mo ₂ O ₁₅	Bi ₂ MoO ₆ , Bi ₈ Mo ₃ O ₂₁	Bi ₂ MoO ₆ , 'Bi ₂₆ Mo ₁₀ O ₆₉ '
7	1.31Bi ₂ O ₃ : 1MoO ₃ (between 'Bi ₂₆ Mo ₁₀ O ₆₉ ' and Bi ₈ Mo ₃ O ₂₁)	Bi ₂ MoO ₆ , Bi ₆ Mo ₂ O ₁₅	Bi ₂ MoO ₆ , Bi ₈ Mo ₃ O ₂₁	Bi ₂ MoO ₆ , 'Bi ₂₆ Mo ₁₀ O ₆₉ '
8	1.32Bi ₂ O ₃ : 1MoO ₃ (between 'Bi ₂₆ Mo ₁₀ O ₆₉ ' and Bi ₈ Mo ₃ O ₂₁)	Bi ₂ MoO ₆ , Bi ₆ Mo ₂ O ₁₅	Bi ₂ MoO ₆ , Bi ₈ Mo ₃ O ₂₁	Bi ₂ MoO ₆ , 'Bi ₂₆ Mo ₁₀ O ₆₉ '
9	1.375Bi ₂ O ₃ : 1MoO ₃ (between Bi ₈ Mo ₃ O ₂₁ and	Bi ₂ MoO ₆ , Bi ₆ Mo ₂ O ₁₅	Bi ₈ Mo ₃ O ₂₁ , Bi ₁₄ Mo ₅ O ₃₆	'Bi ₂₆ Mo ₁₀ O ₆₉ '

	$\text{Bi}_{14}\text{Mo}_5\text{O}_{36}$				
10	1.43 Bi_2O_3 : 1 MoO_3 (between $\text{Bi}_{14}\text{Mo}_5\text{O}_{36}$ and $\text{Bi}_6\text{Mo}_2\text{O}_{15}$)	Bi_2MoO_6 , $\text{Bi}_6\text{Mo}_2\text{O}_{15}$	$\text{Bi}_8\text{Mo}_3\text{O}_{21}$, $\text{Bi}_{14}\text{Mo}_5\text{O}_{36}$		' $\text{Bi}_{26}\text{Mo}_{10}\text{O}_{69}$ '
11	1.47 Bi_2O_3 : 1 MoO_3 (between $\text{Bi}_{14}\text{Mo}_5\text{O}_{36}$ and $\text{Bi}_6\text{Mo}_2\text{O}_{15}$)	Bi_2MoO_6 , $\text{Bi}_6\text{Mo}_2\text{O}_{15}$	$\text{Bi}_{14}\text{Mo}_5\text{O}_{36}$, $\text{Bi}_6\text{Mo}_2\text{O}_{15}$		' $\text{Bi}_{26}\text{Mo}_{10}\text{O}_{69}$ '
12	1.54 Bi_2O_3 : 1 MoO_3 (between $\text{Bi}_6\text{Mo}_2\text{O}_{15}$ and $\text{Bi}_{10}\text{Mo}_3\text{O}_{24}$)	Bi_2MoO_6 , $\text{Bi}_6\text{Mo}_2\text{O}_{15}$	$\text{Bi}_{14}\text{Mo}_5\text{O}_{36}$, $\text{Bi}_6\text{Mo}_2\text{O}_{15}$		' $\text{Bi}_{26}\text{Mo}_{10}\text{O}_{69}$ '
13	1.61 Bi_2O_3 : 1 MoO_3 (between $\text{Bi}_6\text{Mo}_2\text{O}_{15}$ and $\text{Bi}_{10}\text{Mo}_3\text{O}_{24}$)	$\text{Bi}_6\text{Mo}_2\text{O}_{15}$, $\text{Bi}_{10}\text{Mo}_3\text{O}_{24}$	$\text{Bi}_6\text{Mo}_2\text{O}_{15}$, $\text{Bi}_{10}\text{Mo}_3\text{O}_{24}$		' $\text{Bi}_{26}\text{Mo}_{10}\text{O}_{69}$ ', $\text{Bi}_{10}\text{Mo}_3\text{O}_{24}$
14	1.78 Bi_2O_3 : 1 MoO_3 (between $\text{Bi}_{10}\text{Mo}_3\text{O}_{24}$ and ' $\text{Bi}_{38}\text{Mo}_7\text{O}_{78}$ ')	$\text{Bi}_6\text{Mo}_2\text{O}_{15}$, $\text{Bi}_{10}\text{Mo}_3\text{O}_{24}$	$\text{Bi}_6\text{Mo}_2\text{O}_{15}$, $\text{Bi}_{10}\text{Mo}_3\text{O}_{24}$		' $\text{Bi}_{26}\text{Mo}_{10}\text{O}_{69}$ ', $\text{Bi}_{10}\text{Mo}_3\text{O}_{24}$
15	2.01 Bi_2O_3 : 1 MoO_3 (between $\text{Bi}_{10}\text{Mo}_3\text{O}_{24}$ and ' $\text{Bi}_{38}\text{Mo}_7\text{O}_{78}$ ')	$\text{Bi}_{10}\text{Mo}_3\text{O}_{24}$, $\text{Bi}_6\text{MoO}_{12}$	$\text{Bi}_{10}\text{Mo}_3\text{O}_{24}$, $\text{Bi}_6\text{MoO}_{12}$		$\text{Bi}_{10}\text{Mo}_3\text{O}_{24}$, ' $\text{Bi}_{38}\text{Mo}_7\text{O}_{78}$ '
16	2.84 Bi_2O_3 : 1 MoO_3 (between ' $\text{Bi}_{38}\text{Mo}_7\text{O}_{78}$ ' and $\text{Bi}_6\text{MoO}_{12}$)	$\text{Bi}_{10}\text{Mo}_3\text{O}_{24}$, $\text{Bi}_6\text{MoO}_{12}$	$\text{Bi}_{10}\text{Mo}_3\text{O}_{24}$, $\text{Bi}_6\text{MoO}_{12}$		$\text{Bi}_{10}\text{Mo}_3\text{O}_{24}$, ' $\text{Bi}_{38}\text{Mo}_7\text{O}_{78}$ '
17	6.125 Bi_2O_3 : 1 MoO_3 (between $\text{Bi}_6\text{MoO}_{12}$ and $\text{Bi}_{14}\text{MoO}_{24}$)	$\text{Bi}_{10}\text{Mo}_3\text{O}_{24}$, $\text{Bi}_6\text{MoO}_{12}$	$\text{Bi}_{10}\text{Mo}_3\text{O}_{24}$, $\text{Bi}_6\text{MoO}_{12}$		$\text{Bi}_{10}\text{Mo}_3\text{O}_{24}$, ' $\text{Bi}_{38}\text{Mo}_7\text{O}_{78}$ '
18	6.82 Bi_2O_3 : 1 MoO_3 (between $\text{Bi}_6\text{MoO}_{12}$ and $\text{Bi}_{14}\text{MoO}_{24}$)	$\text{Bi}_6\text{MoO}_{12}$, $\text{Bi}_{14}\text{MoO}_{24}$	$\text{Bi}_6\text{MoO}_{12}$, $\text{Bi}_{14}\text{MoO}_{24}$		' $\text{Bi}_{38}\text{Mo}_7\text{O}_{78}$ ', $\text{Bi}_{14}\text{MoO}_{24}$
19	10.44 Bi_2O_3 : 1 MoO_3 (between $\text{Bi}_{14}\text{MoO}_{24}$ and	$\text{Bi}_6\text{MoO}_{12}$, $\text{Bi}_{14}\text{MoO}_{24}$	$\text{Bi}_6\text{MoO}_{12}$, $\text{Bi}_{14}\text{MoO}_{24}$		' $\text{Bi}_{38}\text{Mo}_7\text{O}_{78}$ ', $\text{Bi}_{14}\text{MoO}_{24}$

	Bi_2O_3)				
20	10.53 Bi_2O_3 : 1 MoO_3 (between $\text{Bi}_{14}\text{MoO}_{24}$ and Bi_2O_3)	$\text{Bi}_{14}\text{MoO}_{24}$, Bi_2O_3	$\text{Bi}_{14}\text{MoO}_{24}$, Bi_2O_3	$\text{Bi}_{14}\text{MoO}_{24}$, Bi_2O_3	$\text{Bi}_{14}\text{MoO}_{24}$, Bi_2O_3
21	10 Bi_2O_3 : 1 MoO_3 (between $\text{Bi}_{14}\text{MoO}_{24}$ and Bi_2O_3)	$\text{Bi}_{14}\text{MoO}_{24}$, Bi_2O_3	$\text{Bi}_{14}\text{MoO}_{24}$, Bi_2O_3	$\text{Bi}_{14}\text{MoO}_{24}$, Bi_2O_3	$\text{Bi}_{14}\text{MoO}_{24}$, Bi_2O_3
Equilibrations to verify the existence of $\text{Bi}_6\text{MoO}_{12}$					
22	4.25 Bi_2O_3 : 1 MoO_3 (between $\text{Bi}_{14}\text{MoO}_{24}$ and $\text{Bi}_6\text{MoO}_{12}$)	$\text{Bi}_6\text{MoO}_{12}$, $\text{Bi}_{14}\text{MoO}_{24}$	$\text{Bi}_6\text{MoO}_{12}$, $\text{Bi}_{14}\text{MoO}_{24}$	$\text{Bi}_6\text{MoO}_{12}$, $\text{Bi}_{14}\text{MoO}_{24}$	' $\text{Bi}_{38}\text{Mo}_7\text{O}_{78}$ ', $\text{Bi}_{14}\text{MoO}_{24}$
23	3 Bi_2O_3 : 1 MoO_3 ($\text{Bi}_6\text{MoO}_{12}$)	$\text{Bi}_6\text{MoO}_{12}$	$\text{Bi}_6\text{MoO}_{12}$	$\text{Bi}_6\text{MoO}_{12}$	' $\text{Bi}_{38}\text{Mo}_7\text{O}_{78}$ '
24	2.82 Bi_2O_3 : 1 MoO_3 (between $\text{Bi}_6\text{MoO}_{12}$ and ' $\text{Bi}_{38}\text{Mo}_7\text{O}_{78}$ ')	$\text{Bi}_6\text{MoO}_{12}$, $\text{Bi}_{10}\text{Mo}_3\text{O}_{24}$	$\text{Bi}_6\text{MoO}_{12}$, $\text{Bi}_{10}\text{Mo}_3\text{O}_{24}$	$\text{Bi}_6\text{MoO}_{12}$, $\text{Bi}_{10}\text{Mo}_3\text{O}_{24}$	' $\text{Bi}_{38}\text{Mo}_7\text{O}_{78}$ '
25	2.94 Bi_2O_3 : 1 MoO_3 (between $\text{Bi}_6\text{MoO}_{12}$ and ' $\text{Bi}_{38}\text{Mo}_7\text{O}_{78}$ ')	$\text{Bi}_6\text{MoO}_{12}$, $\text{Bi}_{10}\text{Mo}_3\text{O}_{24}$	$\text{Bi}_6\text{MoO}_{12}$, $\text{Bi}_{10}\text{Mo}_3\text{O}_{24}$	$\text{Bi}_6\text{MoO}_{12}$, $\text{Bi}_{10}\text{Mo}_3\text{O}_{24}$	' $\text{Bi}_{38}\text{Mo}_7\text{O}_{78}$ '
26	2.71 Bi_2O_3 : 1 MoO_3 (' $\text{Bi}_{38}\text{Mo}_7\text{O}_{78}$ ')	$\text{Bi}_6\text{MoO}_{12}$, $\text{Bi}_{10}\text{Mo}_3\text{O}_{24}$	$\text{Bi}_6\text{MoO}_{12}$, $\text{Bi}_{10}\text{Mo}_3\text{O}_{24}$	$\text{Bi}_6\text{MoO}_{12}$, $\text{Bi}_{10}\text{Mo}_3\text{O}_{24}$	' $\text{Bi}_{38}\text{Mo}_7\text{O}_{78}$ '
27	2.12 Bi_2O_3 : 1 MoO_3 (between ' $\text{Bi}_{38}\text{Mo}_7\text{O}_{78}$ ' and $\text{Bi}_{10}\text{Mo}_3\text{O}_{24}$)	$\text{Bi}_6\text{MoO}_{12}$, $\text{Bi}_{10}\text{Mo}_3\text{O}_{24}$	$\text{Bi}_6\text{MoO}_{12}$, $\text{Bi}_{10}\text{Mo}_3\text{O}_{24}$	$\text{Bi}_6\text{MoO}_{12}$, $\text{Bi}_{10}\text{Mo}_3\text{O}_{24}$	' $\text{Bi}_{38}\text{Mo}_7\text{O}_{78}$ ', $\text{Bi}_{10}\text{Mo}_3\text{O}_{24}$

*Same phases were obtained at the end of 50% of the total duration of heating. At 773 K, orthorhombic phase of Bi_2MoO_6 was obtained. At 873 and 1023 K, monoclinic phase of Bi_2MoO_6 was obtained.

Table 3.5 Details of equilibrations of samples with Bi₂O₃ and MoO₂ mixtures

No	Molar ratios of oxides taken	T / K	Phases obtained after equilibration*
28	1:3Bi ₂ O ₃ : MoO ₂	773K, 960h	Bi, MoO ₂ , Bi ₂ MoO ₆ (orthorhombic phase)
		1023K, 480h	Bi, MoO ₂ , Bi ₂ MoO ₆ (monoclinic phase)
29	1:1 Bi ₂ O ₃ : MoO ₂	773K, 960h	Bi, MoO ₂ , Bi ₂ MoO ₆ (orthorhombic phase)
		1023K, 480h	Bi, MoO ₂ , Bi ₂ MoO ₆ (monoclinic phase)
30	3:1 Bi ₂ O ₃ : MoO ₂	773K, 960h	Bi, Bi ₁₀ Mo ₃ O ₂₄ , Bi ₆ MoO ₁₂
		1023K, 480h	Bi, Bi ₁₀ Mo ₃ O ₂₄ , 'Bi ₃₈ Mo ₇ O ₇₈ '

**Same phases were obtained at the end of 50% of the total duration of heating*

The overall composition of the products obtained after this reduction was then determined based on the final mass of the product by assuming the mass loss was solely due to removal of oxygen (i.e. Bi to Mo ratio remained constant during reduction). The products obtained were ground well and made into pellets, which were then kept in alumina crucibles and sealed in low volume quartz ampoules under vacuum. Different pellets of the samples were equilibrated at 773, 873 and 1023 K for prolonged periods. After equilibration, they were quenched to room temperature and the phases in the products were analyzed by XRD. The details of the samples are given in Table 3.6.

3.3.3.4 Long term equilibrations of phase mixtures using different starting components

To obtain information about the coexisting phases in the ternary Bi-Mo-O system, experiments involving long term equilibrations were performed. For these experiments, samples with different overall compositions were prepared using different starting components. Samples prepared by taking appropriate molar ratios of different starting components were thoroughly mixed and made into pellets. The

pellets were then kept inside alumina crucibles and enclosed in small volume evacuated quartz ampoules. The samples were equilibrated at 773, 873 and 1023 K. At the end of about half the total duration of heating, the ampoules were quenched to room temperature. Samples were retrieved, ground well and analyzed by XRD. Samples were then repelletized and equilibration was continued in an identical manner. Details of the samples and equilibration parameters are given in Table 3.7.

Table 3.6 Details of equilibrations of partially reduced ternary compounds

No	Starting compound	Overall composition after partial reduction	Temperature and duration of equilibration	Phases obtained after equilibration*
31	Bi ₂ Mo ₃ O ₁₂	Bi _{0.17} Mo _{0.26} O _{0.56}	873K, 720h	Bi, MoO ₂ , Bi ₂ MoO ₆
			1023K, 480h	Bi, MoO ₂ , Bi ₂ MoO ₆
32	Bi ₂ Mo ₂ O ₉	Bi _{0.24} Mo _{0.24} O _{0.52}	873K, 720h	Bi, MoO ₂ , Bi ₂ MoO ₆
			1023K, 480h	Bi, MoO ₂ , Bi ₂ MoO ₆
33	Bi ₂ MoO ₆	Bi _{0.35} Mo _{0.17} O _{0.48}	873K, 720h	Bi, MoO ₂ , Bi ₂ MoO ₆
			1023K, 480h	Bi, MoO ₂ , Bi ₂ MoO ₆
34	Bi ₆ Mo ₂ O ₁₅	Bi _{0.33} Mo _{0.11} O _{0.56}	773K, 960h	Bi, MoO ₂ , Bi ₂ MoO ₆
			873K, 720h	Bi, MoO ₂ , Bi ₂ MoO ₆
			1023K, 480h	Bi, MoO ₂ , Bi ₂ MoO ₆
35	Bi ₆ MoO ₁₂	Bi _{0.48} Mo _{0.08} O _{0.43}	773K, 960h	Bi, MoO ₂ , Bi ₂ MoO ₆
36	Bi ₁₄ MoO ₂₄	Bi _{0.70} Mo _{0.05} O _{0.29}	773K, 960h	Bi, MoO ₂ , Bi ₂ MoO ₆
			873K, 720h	Bi, MoO ₂ , Bi ₂ MoO ₆

*Same phases were obtained at the end of 50% of the total duration of heating. At 773 K, orthorhombic phase of Bi₂MoO₆ was obtained. At 873 and 1023 K, monoclinic phase of Bi₂MoO₆ was obtained.

Table 3.7 Details of equilibrations of phase mixtures using different starting components

No	Molar ratios of phases taken for equilibration	Products obtained after equilibration*		
		At 773 K (960 h)	At 873 K (720 h)	At 1023 K (480 h)
37	1Bi ₂ O ₃ : 2Mo: 5.4MoO ₃	Bi ₂ MoO ₆ , MoO ₂ , Bi ₂ Mo ₃ O ₁₂	Bi ₂ MoO ₆ , MoO ₂ , Bi ₂ Mo ₂ O ₉	-
38	1Bi ₂ O ₃ : 2.3MoO ₂ : 1.5MoO ₃	Bi ₂ MoO ₆ , MoO ₂ , Bi ₂ Mo ₃ O ₁₂	Bi ₂ Mo ₂ O ₉ , MoO ₂ , Bi ₂ Mo ₃ O ₁₂	-
39	1Bi ₂ O ₃ : 6Mo: 1.8MoO ₂	Bi, Mo, MoO ₂	Bi, Mo, MoO ₂	Bi, Mo, MoO ₂
40	10Bi: 28.6Mo: 1MoO ₃	Bi, Mo, MoO ₂	Bi, Mo, MoO ₂	Bi, Mo, MoO ₂
41	1Bi ₂ O ₃ : 0.71Mo: 1.7MoO ₂	Bi, MoO ₂ , Bi ₂ MoO ₆	-	Bi, MoO ₂ , Bi ₂ MoO ₆
42	3.4Bi ₂ O ₃ : 1Mo: 1.8MoO ₂	Bi, MoO ₂ , Bi ₂ MoO ₆	-	Bi, MoO ₂ , Bi ₂ MoO ₆
43	1.6Bi ₂ O ₃ : 1Mo: 3MoO ₂	Bi, MoO ₂ , Bi ₂ MoO ₆	-	Bi, MoO ₂ , Bi ₂ MoO ₆
44	4.7Bi ₂ O ₃ : 1Mo: 4.6MoO ₃	Bi, MoO ₂ , Bi ₂ MoO ₆	-	Bi, MoO ₂ , Bi ₂ MoO ₆
45	14.3Bi ₂ O ₃ : 1MoO ₃ : 35.5MoO ₂	-	Bi, MoO ₂ , Bi ₂ MoO ₆	Bi, MoO ₂ , Bi ₂ MoO ₆
46	4.3Bi ₂ O ₃ : 1MoO ₃ : 11.1MoO ₂	-	Bi, MoO ₂ , Bi ₂ MoO ₆	Bi, MoO ₂ , Bi ₂ MoO ₆
47	1.2Bi ₂ O ₃ : 1MoO ₃ : 3.7MoO ₂	-	Bi, MoO ₂ , Bi ₂ MoO ₆	Bi, MoO ₂ , Bi ₂ MoO ₆
48	1Bi ₂ O ₃ : 3MoO ₂ : 2.75MoO ₃	-	Bi ₂ Mo ₂ O ₉ , MoO ₂ , Bi ₂ Mo ₃ O ₁₂	-
49	1Bi ₂ O ₃ : 6.3MoO ₂ : 2.3MoO ₃	-	Bi ₂ MoO ₆ , MoO ₂ , Bi ₂ Mo ₂ O ₉	-
50	1.1Bi: 1.5Bi ₂ O ₃ : 1MoO ₂	Bi, Bi ₂ MoO ₆ , Bi ₆ Mo ₂ O ₁₅	-	Bi, Bi ₂ MoO ₆ , 'Bi ₂₆ Mo ₁₀ O ₆₉ '
51	2Bi: 2.4Bi ₂ O ₃ : 1MoO ₂	Bi, Bi ₁₀ Mo ₃ O ₂₄ , Bi ₆ MoO ₁₂	-	Bi, Bi ₁₀ Mo ₃ O ₂₄ , 'Bi ₃₈ Mo ₇ O ₇₈ '
52	4.6Bi: 4.6Bi ₂ O ₃ : 1MoO ₂	Bi, Bi ₆ MoO ₁₂ , Bi ₁₄ MoO ₂₄	-	Bi, 'Bi ₃₈ Mo ₇ O ₇₈ ', Bi ₁₄ MoO ₂₄
53	16.1Bi: 14.7.4Bi ₂ O ₃ : 1MoO ₂	Bi, Bi ₁₄ MoO ₂₄ , Bi ₂ O ₃	Bi, Bi ₁₄ MoO ₂₄ , Bi ₂ O ₃	Bi, Bi ₁₄ MoO ₂₄ , Bi ₂ O ₃
54	1Bi: 4.9Bi ₂ O ₃ : 3MoO ₂	Bi, Bi ₂ MoO ₆ , Bi ₆ Mo ₂ O ₁₅	-	Bi, Bi ₂ MoO ₆ , 'Bi ₂₆ Mo ₁₀ O ₆₉ '
55	1Bi: 2.1Bi ₂ O ₃ : 1.3MoO ₂	Bi, Bi ₁₀ Mo ₃ O ₂₄ , Bi ₆ MoO ₁₂	-	Bi, Bi ₁₀ Mo ₃ O ₂₄ , 'Bi ₃₈ Mo ₇ O ₇₈ '
56	1Bi: 9.6Bi ₂ O ₃ : 1.8MoO ₂	Bi, Bi ₆ MoO ₁₂ , Bi ₁₄ MoO ₂₄	-	Bi, 'Bi ₃₈ Mo ₇ O ₇₈ ', Bi ₁₄ MoO ₂₄
57	1Bi: 22.4Bi ₂ O ₃ : 1.9MoO ₂	Bi, Bi ₁₄ MoO ₂₄ , Bi ₂ O ₃	Bi, Bi ₁₄ MoO ₂₄ , Bi ₂ O ₃	Bi, Bi ₁₄ MoO ₂₄ , Bi ₂ O ₃

*Same phases were obtained at the end of 50% of the total duration of heating. At 773 K, orthorhombic phase of Bi₂MoO₆ was obtained. At 873 and 1023 K, monoclinic phase of Bi₂MoO₆ was obtained.

3.3.3.5 Long term equilibrations of phase mixtures in liquid bismuth

To confirm the phases that coexist with liquid bismuth, additional long term equilibrations were carried out. For these experiments, pellets of the samples were prepared by mixing different sets of starting components. Homogeneous mixture of these phases was made as porous pellets. Excess bismuth metal taken in alumina crucibles was melted in an argon atmosphere glove box. Each sample pellet was forcefully immersed into the liquid metal using an alumina strip. The strip was tied to the crucible by means of a binding wire. The crucible containing the sample was later sealed under vacuum in quartz ampoule. Samples enclosed in quartz ampoules were then subjected to long term equilibration at 773, 873 and 1023 K. After the equilibration, samples were quenched to room temperature. Sample pellets were retrieved after melting bismuth metal. The powdered samples were then characterized by XRD. Details of these experiments are given in Table 3.8.

3.3.3.6 Equilibrations to determine the stability ranges of $\text{Bi}_8\text{Mo}_3\text{O}_{21}$, $\text{Bi}_{14}\text{Mo}_5\text{O}_{36}$ and $\text{Bi}_6\text{Mo}_2\text{O}_{15}$

To unravel the temperature ranges of stability of $\text{Bi}_8\text{Mo}_3\text{O}_{21}$, $\text{Bi}_{14}\text{Mo}_5\text{O}_{36}$ and $\text{Bi}_6\text{Mo}_2\text{O}_{15}$, pellets of these compounds were equilibrated at different temperatures for prolonged periods. In the case of $\text{Bi}_8\text{Mo}_3\text{O}_{21}$, pellets of 6 mm diameter and 3 mm thickness were made and taken in small quartz crucibles. They were in turn stacked at precisely known heights in a 1 m long and one end closed 16 mm diameter quartz tube using quartz spacers. Similarly, sample pellets of $\text{Bi}_{14}\text{Mo}_5\text{O}_{36}$ and $\text{Bi}_6\text{Mo}_2\text{O}_{15}$ were stacked in separate quartz tubes. About 15 samples were placed in each of the quartz tubes. The quartz tubes were then placed in a vertical furnace which provided an axial temperature gradient. The temperature within the furnace was maintained between 748 and 1023 K.

Table 3.8 Details of equilibrations in liquid bismuth

a) Using Bi, Bi ₂ O ₃ and MoO ₂ as starting components		Phases obtained after equilibration		
		At 773 K / 960 h	At 873 K / 720 h	At 1023 K / 480 h
No	Composition chosen			
58	5.52Bi:18.09Bi ₂ O ₃ :1MoO ₂	Bi, Bi ₁₄ MoO ₂₄ , Bi ₂ O ₃	-	Bi, Bi ₁₄ MoO ₂₄ , Bi ₂ O ₃
59	22.29Bi:12.11Bi ₂ O ₃ :1MoO ₂	Bi, Bi ₁₄ MoO ₂₄ , Bi ₂ O ₃	-	Bi, Bi ₁₄ MoO ₂₄ , Bi ₂ O ₃
60	Bi:6.22Bi ₂ O ₃ :1.28MoO ₂	Bi, Bi ₆ MoO ₁₂ , Bi ₁₄ MoO ₂₄	Bi, Bi ₆ MoO ₁₂ , Bi ₁₄ MoO ₂₄	Bi, 'Bi ₃₈ Mo ₇ O ₇₈ ', Bi ₁₄ MoO ₂₄
61	2.1Bi:5.06Bi ₂ O ₃ :1MoO ₂	Bi, Bi ₆ MoO ₁₂ , Bi ₁₄ MoO ₂₄	Bi, Bi ₆ MoO ₁₂ , Bi ₁₄ MoO ₂₄	Bi, 'Bi ₃₈ Mo ₇ O ₇₈ ', Bi ₁₄ MoO ₂₄
62	1Bi:11.09Bi ₂ O ₃ :5.34MoO ₂	Bi, Bi ₁₀ Mo ₃ O ₂₄ , Bi ₆ MoO ₁₂	Bi, Bi ₁₀ Mo ₃ O ₂₄ , Bi ₆ MoO ₁₂	Bi, Bi ₁₀ Mo ₃ O ₂₄ , 'Bi ₃₈ Mo ₇ O ₇₈ '
63	1Bi:5.98Bi ₂ O ₃ :3.03MoO ₂	Bi, Bi ₁₀ Mo ₃ O ₂₄ , Bi ₆ MoO ₁₂	Bi, Bi ₁₀ Mo ₃ O ₂₄ , Bi ₆ MoO ₁₂	Bi, Bi ₁₀ Mo ₃ O ₂₄ , 'Bi ₃₈ Mo ₇ O ₇₈ '
b) Using Bi, Bi ₂ O ₃ and MoO ₃ as starting components				
64	1Bi ₂ O ₃ :2Bi:2.5MoO ₃	Bi, MoO ₂ , Bi ₂ MoO ₆	-	Bi, MoO ₂ , Bi ₂ MoO ₆
65	8.9Bi:1Mo:0.43MoO ₃	Bi, MoO ₂ , Bi ₂ MoO ₆	-	Bi, MoO ₂ , Bi ₂ MoO ₆
66	6.19Bi:17.76Bi ₂ O ₃ :1MoO ₃	Bi, Bi ₁₄ MoO ₂₄ , Bi ₂ O ₃	-	Bi, Bi ₂ O ₃ , Bi ₁₄ MoO ₂₄
67	12.77Bi:21.96Bi ₂ O ₃ :1MoO ₃	Bi, Bi ₁₄ MoO ₂₄ , Bi ₂ O ₃	-	Bi, Bi ₂ O ₃ , Bi ₁₄ MoO ₂₄
68	1.45Bi:4.52Bi ₂ O ₃ :1MoO ₃	Bi, Bi ₆ MoO ₁₂ , Bi ₁₄ MoO ₂₄	Bi, Bi ₆ MoO ₁₂ , Bi ₁₄ MoO ₂₄	Bi, 'Bi ₃₈ Mo ₇ O ₇₈ ', Bi ₁₄ MoO ₂₄
69	2.77Bi:4.72Bi ₂ O ₃ :1MoO ₃	Bi, Bi ₆ MoO ₁₂ , Bi ₁₄ MoO ₂₄	Bi, Bi ₆ MoO ₁₂ , Bi ₁₄ MoO ₂₄	Bi, 'Bi ₃₈ Mo ₇ O ₇₈ ', Bi ₁₄ MoO ₂₄
70	1Bi:5.6Bi ₂ O ₃ :2.87MoO ₃	Bi, Bi ₁₀ Mo ₃ O ₂₄ , Bi ₆ MoO ₁₂	Bi, Bi ₁₀ Mo ₃ O ₂₄ , Bi ₆ MoO ₁₂	Bi, Bi ₁₀ Mo ₃ O ₂₄ , 'Bi ₃₈ Mo ₇ O ₇₈ '

71	1Bi:2.83Bi ₂ O ₃ :1.45MoO ₃	Bi, Bi ₁₀ Mo ₃ O ₂₄ , Bi ₆ MoO ₁₂	Bi, Bi ₁₀ Mo ₃ O ₂₄ , Bi ₆ MoO ₁₂	Bi, Bi ₁₀ Mo ₃ O ₂₄ , 'Bi ₃₈ Mo ₇ O ₇₈ '
72	1Bi:18.9Bi ₂ O ₃ :10.6MoO ₃	Bi, Bi ₆ Mo ₂ O ₁₅ , Bi ₁₀ Mo ₃ O ₂₄ ,	Bi, Bi ₆ Mo ₂ O ₁₅ , Bi ₁₀ Mo ₃ O ₂₄	Bi, 'Bi ₂₆ Mo ₁₀ O ₆₉ ', Bi ₁₀ Mo ₃ O ₂₄
73	1Bi:11.57Bi ₂ O ₃ :7.22MoO ₃	Bi, Bi ₆ Mo ₂ O ₁₅ , Bi ₁₀ Mo ₃ O ₂₄	Bi, Bi ₆ Mo ₂ O ₁₅ , Bi ₁₀ Mo ₃ O ₂₄	Bi, 'Bi ₂₆ Mo ₁₀ O ₆₉ ', Bi ₁₀ Mo ₃ O ₂₄
74	1Bi:38.85Bi ₂ O ₃ :24.7MoO ₃	Bi, Bi ₆ Mo ₂ O ₁₅ , Bi ₁₀ Mo ₃ O ₂₄	Bi, Bi ₆ Mo ₂ O ₁₅ , Bi ₁₀ Mo ₃ O ₂₄	Bi, 'Bi ₂₆ Mo ₁₀ O ₆₉ ', Bi ₁₀ Mo ₃ O ₂₄
75	1Bi:41.42Bi ₂ O ₃ :28.61MoO ₃	Bi, Bi ₂ MoO ₆ , Bi ₆ Mo ₂ O ₁₅	Bi, Bi ₁₄ Mo ₅ O ₃₆ , Bi ₆ Mo ₂ O ₁₅	-
76	1Bi:20.72Bi ₂ O ₃ :14.16MoO ₃	Bi, Bi ₂ MoO ₆ , Bi ₆ Mo ₂ O ₁₅	Bi, Bi ₁₄ Mo ₅ O ₃₆ , Bi ₆ Mo ₂ O ₁₅	-
77	1Bi:5.41Bi ₂ O ₃ :3.75MoO ₃	Bi, Bi ₂ MoO ₆ , Bi ₆ Mo ₂ O ₁₅	Bi, Bi ₁₄ Mo ₅ O ₃₆ , Bi ₆ Mo ₂ O ₁₅	-
78	1Bi:2.8Bi ₂ O ₃ :1.96MoO ₃	Bi, Bi ₂ MoO ₆ , Bi ₆ Mo ₂ O ₁₅	Bi, Bi ₈ Mo ₃ O ₂₁ , Bi ₁₄ Mo ₅ O ₃₆	-
79	1.01Bi:1.41Bi ₂ O ₃ :1MoO ₃	Bi, Bi ₂ MoO ₆ , Bi ₆ Mo ₂ O ₁₅	Bi, Bi ₈ Mo ₃ O ₂₁ , Bi ₁₄ Mo ₅ O ₃₆	-
80	1.13Bi:1.39Bi ₂ O ₃ :1MoO ₃	Bi, Bi ₂ MoO ₆ , Bi ₆ Mo ₂ O ₁₅	Bi, Bi ₈ Mo ₃ O ₂₁ , Bi ₁₄ Mo ₅ O ₃₆	-
81	1Bi:3.19Bi ₂ O ₃ :2.85MoO ₃	Bi, Bi ₂ MoO ₆ , Bi ₆ Mo ₂ O ₁₅	Bi, Bi ₂ MoO ₆ , Bi ₈ Mo ₃ O ₂₁	-
82	1Bi:2.25Bi ₂ O ₃ :2.02MoO ₃	Bi, Bi ₂ MoO ₆ , Bi ₆ Mo ₂ O ₁₅	Bi, Bi ₂ MoO ₆ , Bi ₈ Mo ₃ O ₂₁	-

At 773 K, orthorhombic phase of Bi₂MoO₆ was obtained. At 873 and 1023 K, monoclinic phase of Bi₂MoO₆ was obtained.

A stainless steel pipe of 45 mm OD and 1.5 m long was also kept additionally in the furnace, surrounding the quartz tubes for providing radially uniform temperature (Fig.1 in the Appendix). Size of the sample pellets was small such that the temperature within each pellet would be constant throughout the period of equilibration. Using a K-type thermocouple which could be moved very slowly (10 mm/min) from bottom to top of the furnace and close to the quartz tube with the help of a motor, the temperature at which each sample pellet was equilibrated could be measured. The samples were equilibrated for 600 h and quenched to room temperature. The powdered samples were then analyzed by XRD. The details of equilibrations are given in Table 3.9.

3.3.4 Electrical conductivity measurements

3.3.4.1 Conductivity measurements on $\text{Bi}_8\text{Mo}_3\text{O}_{21}$, $\text{Bi}_{14}\text{Mo}_5\text{O}_{36}$ and $\text{Bi}_6\text{Mo}_2\text{O}_{15}$

In order to determine the temperatures at which $\text{Bi}_8\text{Mo}_3\text{O}_{21}$, $\text{Bi}_{14}\text{Mo}_5\text{O}_{36}$ and $\text{Bi}_6\text{Mo}_2\text{O}_{15}$ transform into the high temperature solid solution phase ' $\text{Bi}_{26}\text{Mo}_{10}\text{O}_{69}$ ', conductivity measurements were carried out in air. For these measurements, sintered pellets of the compounds were used.

In the case of $\text{Bi}_8\text{Mo}_3\text{O}_{21}$, conductivity measurements were carried out in the temperature range of 773 to 943 K. The first measurement of conductivity was carried out at 773 K followed by increasing the sample temperature by 10 K. After maintaining the sample at that temperature for about 2 h, its conductivity was measured at that temperature. This was continued till 943 K. For $\text{Bi}_{14}\text{Mo}_5\text{O}_{36}$, measurements were carried out in the temperature range of 748 to 990 K in a similar way. The conductivity of $\text{Bi}_6\text{Mo}_2\text{O}_{15}$ was measured in the temperature range of 718 to 917 K.

Table 3.9 Details of equilibrations to study the stabilities of $\text{Bi}_8\text{Mo}_3\text{O}_{21}$, $\text{Bi}_{14}\text{Mo}_5\text{O}_{36}$ and $\text{Bi}_6\text{Mo}_2\text{O}_{15}$

$\text{Bi}_8\text{Mo}_3\text{O}_{21}$		$\text{Bi}_{14}\text{Mo}_5\text{O}_{36}$		$\text{Bi}_6\text{Mo}_2\text{O}_{15}$	
T / K	Phases obtained	T / K	Phases obtained	T / K	Phases obtained
771	$\text{Bi}_2\text{MoO}_6, \text{Bi}_6\text{Mo}_2\text{O}_{15}$	766	$\text{Bi}_2\text{MoO}_6, \text{Bi}_6\text{Mo}_2\text{O}_{15}$	745	$\text{Bi}_6\text{Mo}_2\text{O}_{15}$
788	$\text{Bi}_2\text{MoO}_6, \text{Bi}_6\text{Mo}_2\text{O}_{15}$	782	$\text{Bi}_2\text{MoO}_6, \text{Bi}_6\text{Mo}_2\text{O}_{15}$	753	$\text{Bi}_6\text{Mo}_2\text{O}_{15}$
805	$\text{Bi}_2\text{MoO}_6, \text{Bi}_6\text{Mo}_2\text{O}_{15}$	798	$\text{Bi}_2\text{MoO}_6, \text{Bi}_6\text{Mo}_2\text{O}_{15}$	768	$\text{Bi}_6\text{Mo}_2\text{O}_{15}$
841	$\text{Bi}_8\text{Mo}_3\text{O}_{21}$	817	$\text{Bi}_2\text{MoO}_6, \text{Bi}_{14}\text{Mo}_5\text{O}_{36}, \text{Bi}_6\text{Mo}_2\text{O}_{15}$	784	$\text{Bi}_6\text{Mo}_2\text{O}_{15}$
862	$\text{Bi}_8\text{Mo}_3\text{O}_{21}$	838	$\text{Bi}_2\text{MoO}_6, \text{Bi}_{14}\text{Mo}_5\text{O}_{36}, \text{Bi}_6\text{Mo}_2\text{O}_{15}$	801	$\text{Bi}_6\text{Mo}_2\text{O}_{15}$
888	$\text{Bi}_8\text{Mo}_3\text{O}_{21}$	859	$\text{Bi}_2\text{MoO}_6, \text{Bi}_{14}\text{Mo}_5\text{O}_{36}, \text{Bi}_6\text{Mo}_2\text{O}_{15}$	817	$\text{Bi}_6\text{Mo}_2\text{O}_{15}$
912	$\text{Bi}_8\text{Mo}_3\text{O}_{21}$	883	$\text{Bi}_{14}\text{Mo}_5\text{O}_{36}$	836	$\text{Bi}_6\text{Mo}_2\text{O}_{15}$
931	' $\text{Bi}_{26}\text{Mo}_{10}\text{O}_{69}$ '	907	$\text{Bi}_{14}\text{Mo}_5\text{O}_{36}$	857	$\text{Bi}_6\text{Mo}_2\text{O}_{15}$
952	' $\text{Bi}_{26}\text{Mo}_{10}\text{O}_{69}$ '	927	$\text{Bi}_{14}\text{Mo}_5\text{O}_{36}$	883	$\text{Bi}_6\text{Mo}_2\text{O}_{15}$
970	' $\text{Bi}_{26}\text{Mo}_{10}\text{O}_{69}$ '	947	$\text{Bi}_{14}\text{Mo}_5\text{O}_{36}$	901	$\text{Bi}_6\text{Mo}_2\text{O}_{15}$
986	' $\text{Bi}_{26}\text{Mo}_{10}\text{O}_{69}$ '	968	' $\text{Bi}_{26}\text{Mo}_{10}\text{O}_{69}$ '	928	' $\text{Bi}_{26}\text{Mo}_{10}\text{O}_{69}$ '
999	' $\text{Bi}_{26}\text{Mo}_{10}\text{O}_{69}$ '	984	' $\text{Bi}_{26}\text{Mo}_{10}\text{O}_{69}$ '	949	' $\text{Bi}_{26}\text{Mo}_{10}\text{O}_{69}$ '
1011	' $\text{Bi}_{26}\text{Mo}_{10}\text{O}_{69}$ '	998	' $\text{Bi}_{26}\text{Mo}_{10}\text{O}_{69}$ '	968	' $\text{Bi}_{26}\text{Mo}_{10}\text{O}_{69}$ '
1023	' $\text{Bi}_{26}\text{Mo}_{10}\text{O}_{69}$ '	1009	' $\text{Bi}_{26}\text{Mo}_{10}\text{O}_{69}$ '	983	' $\text{Bi}_{26}\text{Mo}_{10}\text{O}_{69}$ '
-	-	1022	' $\text{Bi}_{26}\text{Mo}_{10}\text{O}_{69}$ '	998	' $\text{Bi}_{26}\text{Mo}_{10}\text{O}_{69}$ '
-	-	1023	' $\text{Bi}_{26}\text{Mo}_{10}\text{O}_{69}$ '	-	-

3.3.4.2 Conductivity measurements on $\text{Bi}_2\text{Mo}_2\text{O}_9$

It is reported in literature that $\text{Bi}_2\text{Mo}_2\text{O}_9$ is unstable at low temperatures and decomposes to $\text{Bi}_2\text{Mo}_3\text{O}_{12}$ and Bi_2MoO_6 . The decomposition temperature has been reported to be 813 K [32] as well as 823 K [59, 60]. In the present work, electrical conductivity of $\text{Bi}_2\text{Mo}_2\text{O}_9$ was measured by complex impedance spectroscopy to determine its decomposition temperature. The $\text{Bi}_2\text{Mo}_2\text{O}_9$ sample was prepared by the solid state reaction between stoichiometric amounts of Bi_2O_3 and MoO_3 at 873 K in air for 48 h. A sintered pellet of $\text{Bi}_2\text{Mo}_2\text{O}_9$ having 8 mm diameter and 3 mm thickness was made and used for conductivity measurements. The pellet was sintered in air at 903 K for about 6 h. The conductivity measurements were carried out in air in the temperature range of 905 to 754 K in the frequency range of 10 Hz to 1 MHz with an applied perturbation potential of 500 mV.

First measurement of conductivity was made at 905 K after heating the sample for 24 h at that temperature. This was followed by decreasing the sample temperature by 10 K and maintaining at that temperature for about 2 h. Conductivity was then measured at each temperature. This was continued till the final temperature of 754 K was reached.

3.3.4.3 Conductivity measurements on Bi_2MoO_6

Electrical conductivity of Bi_2MoO_6 was measured to determine the temperature at which it undergoes phase transitions. For these measurements, sintered pellets of both the orthorhombic and monoclinic phases of Bi_2MoO_6 were used. The monoclinic phase of Bi_2MoO_6 was prepared by the solid state reaction between stoichiometric amounts of Bi_2O_3 and MoO_3 at 873 K in air for 48 h whereas the reaction at 773 K for 48 h yielded the orthorhombic phase of Bi_2MoO_6 . With the orthorhombic phase as the sample pellet, measurements were carried out on heating it

first from 700 to 963 K in steps of 10 K. The sample was maintained at the initial temperature of 700 K for about 24 h and the conductivity was measured at that temperature. This is followed by raising the sample temperature by 10 K and maintaining at that temperature for about 2 h. The conductivity was then measured. When the starting phase was the high temperature monoclinic phase, conductivity was measured while cooling the sample in steps from 973 to 723 K.

All the conductivity experiments were carried out using the conductivity cell described in chapter 2. The electrical conductivity was measured using a frequency response analyzer (Model SI 1225, Solartron, M/s Schlumberger, UK) coupled with an electrochemical interface (Model 1286, Solartron, M/s Schlumberger, UK). The measurements were carried out in the frequency range of 10 Hz to 1 MHz with an applied perturbation potential of 500 mV. The impedance data obtained at each temperature was fitted using the software Zview®. The bulk resistance of the material was obtained by fitting a semicircle to the experimentally obtained Nyquist plot. By incorporating the dimensions of the pellet, the conductivity (σ) of the sample at each temperature (T) was determined. The Arrhenius plot for conductivity was obtained by plotting $\log \sigma$ as a function of $1/T$. A change in the slope indicates the difference in the conduction mechanism and / or a phase change. At the end of the conductivity measurements, the sample pellets were retrieved, powdered and characterized by XRD to establish any structural changes that had occurred during the measurement.

3.3.5 Simultaneous equilibration experiments to follow the structural changes during conductivity measurements

The structural changes that could occur during conductivity measurements were followed by performing separate equilibration experiments at different selected temperatures falling within the temperature ranges of conductivity measurements. For

these experiments, sample pellets of $\text{Bi}_8\text{Mo}_3\text{O}_{21}$, $\text{Bi}_{14}\text{Mo}_5\text{O}_{36}$, $\text{Bi}_6\text{Mo}_2\text{O}_{15}$, $\text{Bi}_2\text{Mo}_2\text{O}_9$, and Bi_2MoO_6 , were individually kept inside alumina crucibles and equilibrated in air at different temperatures by following the temperature program used for conductivity measurements.

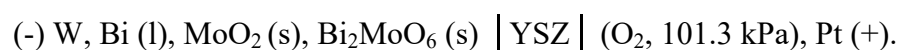
For $\text{Bi}_8\text{Mo}_3\text{O}_{21}$, the equilibrations were carried out at 873, 898, 923, 948 and 973 K. The equilibration temperatures for $\text{Bi}_{14}\text{Mo}_5\text{O}_{36}$ were 873, 923, 948 and 973 K whereas for $\text{Bi}_6\text{Mo}_2\text{O}_{15}$, equilibrations were carried out at 873, 898 and 923 K, respectively. In the case of $\text{Bi}_2\text{Mo}_2\text{O}_9$, equilibrations were carried out at 873, 823, 798 and 773 K and for the monoclinic phase of Bi_2MoO_6 , equilibrations were performed at 973, 873, 823 and 773 K.

The equilibration of all the compounds ($\text{Bi}_2\text{Mo}_2\text{O}_9$, monoclinic phase of Bi_2MoO_6 , $\text{Bi}_8\text{Mo}_3\text{O}_{21}$, $\text{Bi}_{14}\text{Mo}_5\text{O}_{36}$ and $\text{Bi}_6\text{Mo}_2\text{O}_{15}$) were performed in such a way that the first pellet of each sample was first equilibrated at the highest temperature for 24 h and then quenched to room temperature. The second pellet of each compound was first equilibrated at the highest temperature for 24 h which was followed by increasing the temperature by 10 K and maintained at that temperature for 2 h. This was followed by quenching the sample to room temperature. Similarly, third pellet was first equilibrated at the highest temperature for 24 h, followed by successively raising its temperature by 10 K at a time and holding at each temperature for 2 h. This is continued till equilibration at the desired final temperature is completed. After equilibrating at the final temperature, the pellet was quenched to room temperature. In order to check the low temperature stability of $\text{Bi}_8\text{Mo}_3\text{O}_{21}$ and $\text{Bi}_{14}\text{Mo}_5\text{O}_{36}$, pellets of these compounds were also heated at 788 and 773 K, respectively for 24 h followed by quenching them to room temperature and XRD analysis.

In the case of orthorhombic phase of Bi_2MoO_6 , equilibrations were carried out at 773, 823, 843, 853, 873, 923 and 973 K in air by following the identical procedure used for conductivity measurements. First pellet was equilibrated at the lowest temperature for 24 h followed by quenching it to room temperature. Equilibration of the next pellet started at the lowest temperature for 24 h followed by raising its temperature by 10 K and maintaining at that temperature for 2 h. This raise of temperature and dwelling at that temperature was continued till the desired temperature of equilibration was reached and after which the sample was quenched to room temperature. All the samples quenched to room temperature were powdered and analyzed by XRD. Details of these experiments are given in Tables 3.10 and 3.11.

3.3.6 Oxygen potential measurements using yttria stabilized zirconia solid electrolyte

To determine the Gibbs energy of formation of Bi_2MoO_6 (s), a galvanic cell based on yttria stabilized zirconia solid electrolyte was constructed (Fig. 3.8). The galvanic cell can be represented as given below:



The reference electrode for the cell was prepared by applying platinum paste (M/s Eltecks Corporation, India) over the inner bottom surface of the solid electrolyte tube and heating it in air at 1373 K for 2 h. This resulted in a uniform and porous platinum coating over the electrolyte surface. A platinum wire, which had been spot welded to platinum mesh was cofired with the platinum paste. This served as the electrical lead for the reference electrode. A similar porous platinum electrode was formed at the external bottom surface of the electrolyte tube. The solid electrolyte tube was then fastened to a Veeco coupling by means of a high temperature epoxy seal.

Table 3.10 Details of simultaneous equilibrations of $\text{Bi}_8\text{Mo}_3\text{O}_{21}$, $\text{Bi}_{14}\text{Mo}_5\text{O}_{36}$ and $\text{Bi}_6\text{Mo}_2\text{O}_{15}$ samples in air

Sample details	Phases obtained after quenching the samples from						
	873 K	898 K	923 K	948 K	973 K	788 K*	773 K**
1. $\text{Bi}_8\text{Mo}_3\text{O}_{21}$	$\text{Bi}_8\text{Mo}_3\text{O}_{21}$	$\text{Bi}_8\text{Mo}_3\text{O}_{21}$	' $\text{Bi}_{26}\text{Mo}_{10}\text{O}_{69}$ '	' $\text{Bi}_{26}\text{Mo}_{10}\text{O}_{69}$ '	' $\text{Bi}_{26}\text{Mo}_{10}\text{O}_{69}$ '	Bi_2MoO_6 , $\text{Bi}_6\text{Mo}_2\text{O}_{15}$	-
2. $\text{Bi}_{14}\text{Mo}_5\text{O}_{36}$	$\text{Bi}_{14}\text{Mo}_5\text{O}_{36}$	-	$\text{Bi}_{14}\text{Mo}_5\text{O}_{36}$	$\text{Bi}_{14}\text{Mo}_5\text{O}_{36}$	' $\text{Bi}_{26}\text{Mo}_{10}\text{O}_{69}$ '	-	Bi_2MoO_6 , $\text{Bi}_6\text{Mo}_2\text{O}_{15}$
3. $\text{Bi}_6\text{Mo}_2\text{O}_{15}$	$\text{Bi}_6\text{Mo}_2\text{O}_{15}$	' $\text{Bi}_{26}\text{Mo}_{10}\text{O}_{69}$ '	' $\text{Bi}_{26}\text{Mo}_{10}\text{O}_{69}$ '	-	-	-	

1. Heated from 773 to 973 K in steps of 10 K with a dwelling period of 2 h at each temperature and quenched to room temperature from the respective temperatures.

2. Heated from 773 to 973 K in steps of 10 K with a dwelling period of 2 h at each temperature and quenched to room temperature from the respective temperatures.

3. Heated from 700 to 923 K in steps of 10 K with a dwelling period of 2 h at each temperature and quenched to room temperature from the respective temperatures.

* Heated at 788 K for 24 h and quenched to room temperature.

** Heated at 773 K for 24 h and quenched to room temperature.

Table 3.11 Details of simultaneous equilibrations of $\text{Bi}_2\text{Mo}_2\text{O}_9$ and Bi_2MoO_6 samples in air

Sample details	Phases obtained after quenching the samples from									
	773 K	798 K	823 K	843 K	853 K	873 K	923 K	973 K		
$\text{Bi}_2\text{Mo}_2\text{O}_9^*$	$\text{Bi}_2\text{Mo}_3\text{O}_{12}$, Bi_2MoO_6	$\text{Bi}_2\text{Mo}_3\text{O}_{12}$, Bi_2MoO_6	$\text{Bi}_2\text{Mo}_2\text{O}_9$	-	-	$\text{Bi}_2\text{Mo}_2\text{O}_9$	-	-		
$\text{Bi}_2\text{MoO}_6^{**}$ (monoclinic phase)	Bi_2MoO_6 (monoclinic phase)	-	Bi_2MoO_6 (monoclinic phase)	-	-	Bi_2MoO_6 (monoclinic phase)	-	-	Bi_2MoO_6 (monoclinic phase)	Bi_2MoO_6 (monoclinic phase)
$\text{Bi}_2\text{MoO}_6^{***}$ (orthorhombic c phase)	Bi_2MoO_6 (orthorhombic phase)	-	Bi_2MoO_6 (orthorhombic phase)	Bi_2MoO_6 (orthorhombic phase)	Bi_2MoO_6 (orthorhombic c phase)	Bi_2MoO_6 (monoclinic phase)				

* Cooled from 873 to 773 K in steps of 10 K with a dwelling period of 2 h at each temperature and quenched to room temperature from the respective temperatures. For equilibration at 873 K, the duration of heating was 24 h.

** Cooled from 973 to 773 K in steps of 10 K with a dwelling period of 2 h at each temperature and quenched to room temperature from the respective temperatures. For equilibration at 973 K, the duration of heating was 24 h.

*** Heated from 773 to 973 K in steps of 10 K with a dwelling period of 2 h at each temperature and quenched to room temperature from the respective temperatures. For equilibration at 773 K, the duration of heating was 24 h

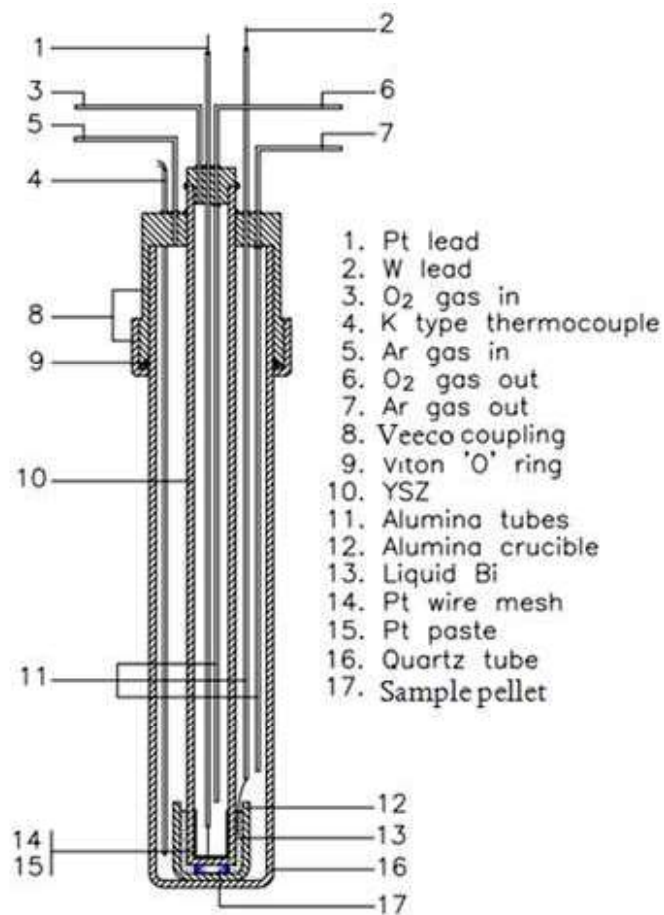


Fig. 3.8 Schematic of the experimental assembly of the galvanic cell

A K-type thermocouple was inserted through the stainless steel coupling and kept very close to the electrode-electrolyte assembly for measuring the cell temperature. The thermocouple used in the experiment was calibrated prior to the actual measurements against a standard calibrated thermocouple supplied by National Physical Laboratory, India.

The entire cell assembly was then kept enclosed in a one end closed quartz tube and sealed using a Viton O-ring. Cell assembly had provisions for flowing gases through the sample and reference compartments. The performance of the emf cell was tested by measuring the null emf by maintaining identical oxygen pressures on both sides of the electrolyte (air-air and oxygen-oxygen). Performance of the cell was also checked by passing oxygen at one electrode and air at the other electrode. Later, the

coated platinum electrode and the platinum lead present at the external surface of the electrolyte tube were removed. A tungsten electrode fastened to the stainless steel coupling through a thin alumina tube using high temperature epoxy seal served as the electrical lead for the sample electrode. Tungsten was chosen as it is compatible with liquid bismuth.

Two sample pellets whose composition falling within the Bi-MoO₂-Bi₂MoO₆ phase field was used for emf measurement. Pellets of the sample electrodes were made by compacting the homogeneous mixture of the constituent phases. The emf cell was assembled inside the argon atmosphere glove box. Appropriate amount of bismuth metal was taken in a recrystallized alumina crucible and melted. Sample pellet was then kept immersed in liquid bismuth by placing the solid electrolyte tube over it in such a way that the lower end of the tungsten wire dipped into liquid bismuth. After cooling, the cell assembly was taken outside the glove box and placed in the constant temperature zone of the furnace. A long hollow cylindrical stainless steel block was also kept in the constant temperature zone of the furnace to further enhance the uniformity of the temperature in the zone. During emf measurements, high purity argon and oxygen gases were passed through the sample and reference compartments, respectively. The cell emf was measured using a high impedance electrometer (input impedance > 10¹⁴ Ω, M/s Keithley, Model 617) and the thermocouple output was measured using a multimeter (M/s Agilent Technologies, Malaysia, Model-34970A, data acquisition /switch unit). Data were recorded using a computer interface.

Emf measurements were carried out in the temperature range of 773 to 1023 K. First measurement with each cell was carried out at high temperatures (1023 K for cell-I and 936 K for cell-II) to enable faster equilibrium at the sample electrode-

electrolyte interface. At each temperature, the readings were recorded when the cell emf was stable within ± 0.05 mV at least for four hours. The reproducibility of the cell emf was confirmed by the emf data obtained during the random heating and cooling cycles.

The thermo-emf between the two dissimilar electrical leads, i.e. tungsten and platinum was measured in a separate experiment by forming a junction between the two electrical leads followed by the measurement of the thermo-emf between them as a function of temperature. Measured data were fitted to a polynomial expression of order two and is given by:

$$E \pm 0.16 / mV = -1.56 - 7.97 \times 10^{-4} T + 1.84 \times 10^{-5} T^2 \quad [T: 337-1076 \text{ K}] \quad (3.3)$$

The uncertainty expressed is the expanded uncertainty with 0.95 level of confidence. The cell emf was then corrected using this thermo-emf data. At the end of the emf measurements sample pellets were retrieved and analyzed by XRD to confirm the coexisting phases.

3.3.7 Determination of standard molar enthalpies of formation of bismuth molybdates by solution calorimetry

Enthalpies of dissolution of the ternary compounds, namely, $\text{Bi}_2\text{Mo}_3\text{O}_{12}$ (s), monoclinic and orthorhombic phases of Bi_2MoO_6 (s), $\text{Bi}_6\text{Mo}_2\text{O}_{15}$ (s) and $\text{Bi}_6\text{MoO}_{12}$ (s) were determined by using an isoperibol calorimeter as described in Chapter 2. The calibration of the calorimeter was performed by both electrical and chemical methods. The electrical calibration was performed by applying a constant current using a stable power source, for a known period of time. 125 ml of 2 mol kg^{-1} NaOH solution was used as the calorimetric solvent during electrical calibration. The current was measured across a precision resistor connected in series. The temperature was measured using a thermistor (M/s Toshniwal Brothers Delhi Private Limited,

Bangalore, India) connected to a data acquisition system, interfaced to a personal computer and was recorded as a function of time. Fig. 3.9 shows the plot of temperature rise against energy supplied. The correlation between temperature rise and energy in joules was found to be linear up to 500 J.

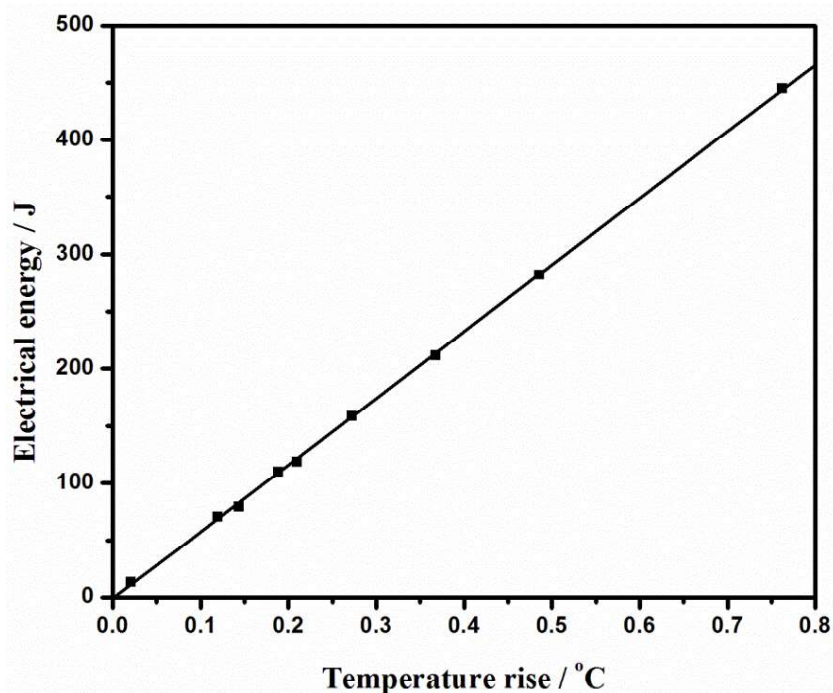


Fig. 3.9 Correlation between temperature rise and electrical energy

The chemical calibration of the calorimeter was carried out by using tris(hydroxyl methyl) aminomethane (s) (TRIS) (99.8% purity, M/s Merck, UK). The calorimetric solvent used was 0.1mol kg^{-1} HCl. The sample required for the calibration was accurately weighed and transferred into the sample bulb. 100 ml of the calorimetric solvent was taken inside the Dewar flask. The sample bulb along with the other components was allowed to equilibrate at the bath temperature. A steady temperature signal was obtained once the calorimeter attained thermal equilibrium with the surrounding water bath. The sample bulb was then broken by pushing the glass rod and the sample was allowed to dissolve in the calorimetric solvent. The

consequent variation in the temperature signal was monitored. Electrical calibration was performed insitu before and after of each of these experiments.

Similar experiments were performed for the calorimetric measurements of samples of ternary bismuth molybdates as well as for the binary oxides viz., Bi_2O_3 (s) and MoO_3 (s). In each case the calorimetric solvent used was a mixture of 100 ml of 3 mol kg^{-1} NaOH and 25 ml of triethanolamine. The volume of triethanolamine was chosen in such a way that the molar ratio of metals to triethanolamine was maintained at $\sim 1:80$ for the dissolution experiments. The current and duration of its passage for the insitu electrical calibration was decided by the time taken for the sample to dissolve completely under the experimental conditions and the weight of the sample taken for each experiment. The maximum time taken for the dissolution of the samples was around 4 min. The temperature change, ΔT , during the experiment with the ternary compounds and starting components was also corrected for the heat exchange between calorimeter and surroundings as explained in Chapter 2 and was used for the evaluation of the enthalpy change for the reaction. Calorimetric measurements were repeated several times to obtain the reproducible data.

3.3.8 Determination of molar heat capacities of bismuth molybdates by differential scanning calorimetry

The heat capacity of bismuth molybdates were measured using a heat flux DSC (Mettler Toledo-Model No.DSC827e, Switzerland). Temperature calibration was carried out by measuring the melting points of high purity indium and zinc metals and the standard uncertainty in the temperature measurement was found to be ± 0.4 K. A three step procedure was adopted for the measurement of heat capacity. The three steps are i) blank run, ii) calibration run and iii) sample run. In the blank run, the heat flow rate is determined using empty aluminium pans of equal weight in the sample

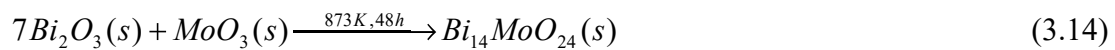
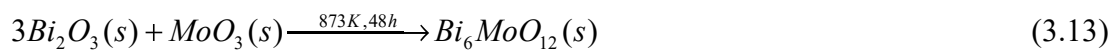
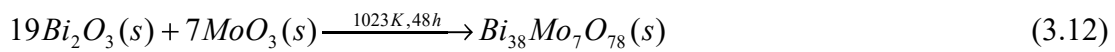
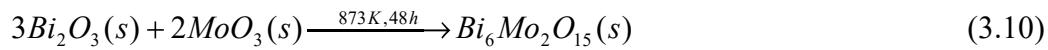
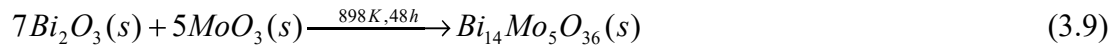
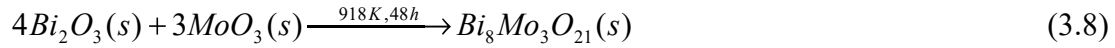
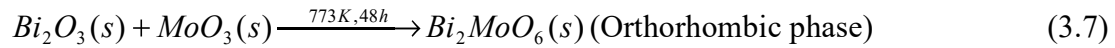
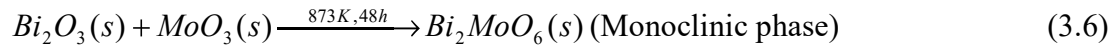
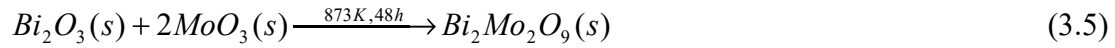
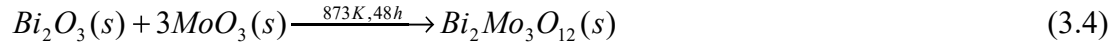
and reference sides. A disc of sapphire (NIST, USA) is used as the calibration reference. In the calibration run, sapphire is placed into the sample pan while the reference side is unchanged and the heat flow rate is measured as in the case of blank run. During sample run, sapphire in the sample pan is replaced by the sample and the heat flow rate is measured. In addition to the heat flow calibration by sapphire, performance of DSC was also verified by measuring the heat capacity of MoO₃ (s). Sample pellets were prepared by compaction of the powders followed by sintering them under vacuum. The sintered pellets (~110 mg) were then sealed in 40 mm³ aluminium pans and used for the measurement. For each sample, reproducibility was checked by repeating the measurement atleast for five to six times. Measurements were also repeated with two different pellets of the same sample. DSC measurements were carried out under high purity argon atmosphere maintained at a flow rate of 50 ml min⁻¹ upto a temperature of ~800 K at a heating rate of 10 K min⁻¹. The temperature program used for the measurement consisted of three segments: an isothermal segment at the initial temperature with a dwelling period of 10 min, followed by a dynamic segment at a heating rate of 10 K min⁻¹ and finally an isothermal segment at the final temperature for 10 min. Samples used for measurements were characterized by XRD before and after the calorimetric runs. The weight loss of the samples after DSC measurements was very low (~0.02-0.03%) indicating that vaporization losses are negligible. The heat capacity data at each temperature was obtained by taking the average of the calorimetric runs carried out with two sample pellets.

3.4 Results and discussion

3.4.1 Preparation and characterization of starting components and ternary compounds

The starting components MoO_3 and MoO_2 prepared in this study were characterized by XRD and the XRD patterns matched with PCPDF file nos. 00-005-0508 and 00-032-0671, respectively.

The solid state reactions leading to the formation of ternary bismuth molybdates can be represented by the following equations:



XRD patterns of the ternary compounds matched with PCPDF file nos. 00-021-0103, 00-033-0209, respectively for $\text{Bi}_2\text{Mo}_3\text{O}_{12}$ and $\text{Bi}_2\text{Mo}_2\text{O}_9$. Preparation of Bi_2MoO_6 at 773 K yielded the orthorhombic phase while the preparation at 873 K

yielded the monoclinic phase. The XRD patterns of the above two phases matched with PCPDF files 00-084-0787 and 04-009-3413, respectively. Similarly, XRD patterns of the other ternary compounds prepared by the solid state reaction between Bi_2O_3 and MoO_3 matched with the PCPDF file nos. 01-082-3470, 00-059-0526, 00-056-1473, 00-058-0668, 00-038-0249, 00-089-6667 and 00-050-1730, respectively for $\text{Bi}_8\text{Mo}_3\text{O}_{21}$, $\text{Bi}_{14}\text{Mo}_5\text{O}_{36}$, $\text{Bi}_6\text{Mo}_2\text{O}_{15}$, $\text{Bi}_{10}\text{Mo}_3\text{O}_{24}$, $\text{Bi}_{38}\text{Mo}_7\text{O}_{78}$, $\text{Bi}_{14}\text{MoO}_{24}$ and ' $\text{Bi}_{26}\text{Mo}_{10}\text{O}_{69}$ '. The XRD pattern of the compound $\text{Bi}_6\text{MoO}_{12}$ matched with those reported by Bleijenberg et al. [36].

3.4.2 Studies involving equilibrations of samples with compositions in the Bi_2O_3 - MoO_3 pseudo binary line

Table 3.4 shows the details of equilibration experiments performed to find out the presence of any ternary compound other than those reported by earlier investigators in the Bi_2O_3 - MoO_3 pseudo binary system. The XRD patterns of the products obtained after the long term equilibrations of different molar ratios of Bi_2O_3 and MoO_3 have shown the presence of either a mixture of two ternary compounds reported in literature or that of a ternary compound and the metal oxide. It is to be noted that the orthorhombic phase of Bi_2MoO_6 was obtained when equilibration was carried out at 773 K while the monoclinic phase was obtained when the equilibration was at 873 and 1023 K. Presence of the intermediate phase (γ'') reported in literature was not observed. Similarly presence of $\text{Bi}_2\text{Mo}_2\text{O}_9$ was not observed when equilibration was carried out at 773 K whereas it was observed when equilibrations were carried out at 873 K. This is in agreement with the data reported in literature. The equilibration of sample no 21 given in Table 3.4, which had an overall composition corresponding to the compound $\text{Bi}_{20}\text{MoO}_{33}$ reported by Sillen and Lundborg [30] and Kohlmuller and Badaud [31] at 773 as well as at 873 K yielded a

mixture of $\text{Bi}_{14}\text{MoO}_{24}$ and Bi_2O_3 as products indicating the non existence of $\text{Bi}_{20}\text{MoO}_{33}$. This is in agreement with that reported by Bleijenberg et al. [36]. Also the presence of $\text{Bi}_6\text{Mo}_2\text{O}_{15}$ was not observed at 1023 K, but it had transformed into the high temperature polymorph belonging to the ' $\text{Bi}_{26}\text{Mo}_{10}\text{O}_{69}$ ' solid solution. This observation is in agreement with those reported by previous investigators [42, 46].

XRD patterns obtained for the equilibration of compositions 15 to 17 indicate the presence of mixtures of $\text{Bi}_6\text{MoO}_{12}$ and $\text{Bi}_{10}\text{Mo}_3\text{O}_{24}$ at 773 and 873 K while equilibrations at 1023 K yielded mixtures of $\text{Bi}_{38}\text{Mo}_7\text{O}_{78}$ and $\text{Bi}_{10}\text{Mo}_3\text{O}_{24}$. This observation was further confirmed by results obtained for samples 22 to 27 given in Table 3.4. The overall composition of the sample 23 exactly corresponded to 3:1 Bi_2O_3 : MoO_3 and the XRD results have shown the presence of the compound $\text{Bi}_6\text{MoO}_{12}$ at 773 and 873 K. $\text{Bi}_{38}\text{Mo}_7\text{O}_{78}$ was present only after equilibration at 1023 K. Similarly the overall composition of the sample 26 corresponds to 2.71:1 Bi_2O_3 : MoO_3 and results of the equilibrations were same as in the case of sample 23. These results indicate that $\text{Bi}_{38}\text{Mo}_7\text{O}_{78}$ is not stable at 773 and 873 K while it is stable at 1023 K. At low temperatures, $\text{Bi}_6\text{MoO}_{12}$ is stable. It is to be pointed out that no other phase was found to be present along with $\text{Bi}_{38}\text{Mo}_7\text{O}_{78}$, and this indicates the presence of a wide non-stoichiometry in $\text{Bi}_{38}\text{Mo}_7\text{O}_{78}$ phase as suggested by Tomasi et al. [34]. Hereafter in the text, the solid solution based on $\text{Bi}_{38}\text{Mo}_7\text{O}_{78}$ phase will be designated as ' $\text{Bi}_{38}\text{Mo}_7\text{O}_{78}$ '.

Thus based on the equilibration along the Bi_2O_3 - MoO_3 pseudo binary line, presence of ten ternary compounds, namely, $\text{Bi}_2\text{Mo}_3\text{O}_{12}$, $\text{Bi}_2\text{Mo}_2\text{O}_9$, Bi_2MoO_6 , $\text{Bi}_8\text{Mo}_3\text{O}_{21}$, $\text{Bi}_{14}\text{Mo}_5\text{O}_{36}$, $\text{Bi}_6\text{Mo}_2\text{O}_{15}$, $\text{Bi}_{10}\text{Mo}_3\text{O}_{24}$, $\text{Bi}_{38}\text{Mo}_7\text{O}_{78}$, $\text{Bi}_6\text{MoO}_{12}$ and $\text{Bi}_{14}\text{MoO}_{24}$ along with the high temperature solid solution ' $\text{Bi}_{26}\text{Mo}_{10}\text{O}_{69}$ ' are confirmed.

3.4.3 Studies involving equilibrations of samples with compositions in the line joining Bi_2O_3 and MoO_2

The long term equilibrations of samples with different molar ratios of Bi_2O_3 and MoO_2 as starting materials have shown that there are no ternary compounds involving Bi_2O_3 and MoO_2 (Table 3.5). However, the results revealed the existence of the phase fields $\text{Bi-MoO}_2\text{-Bi}_2\text{MoO}_6$ at 773 and 1023 K, $\text{Bi-Bi}_{10}\text{Mo}_3\text{O}_{24}\text{-Bi}_6\text{MoO}_{12}$ at 773 K and $\text{Bi-Bi}_{10}\text{Mo}_3\text{O}_{24}\text{-Bi}_{38}\text{Mo}_7\text{O}_{78}$ at 1023 K.

3.4.4 Studies involving partial reduction of ternary compounds followed by long term equilibrations

The equilibrium phases obtained after the long term equilibrations of partially reduced ternary compounds are given in Table 3.6. Upon partial reduction, the overall composition of reduced samples has moved towards lower oxygen content. The XRD analysis of these samples after long term equilibrations confirmed the existence of $\text{Bi-MoO}_2\text{-Bi}_2\text{MoO}_6$ phase field at 773 as well as at 1023 K.

3.4.5 Studies involving long term equilibrations of phase mixtures using different starting components and equilibrations in liquid bismuth

In order to determine the coexisting phases in the ternary Bi-Mo-O system, several long term equilibrations were performed by taking different starting components. These equilibrations revealed the existence of different phase fields (Table 3.7). The phase fields identified are: (1) Bi-Mo-MoO_2 , (2) $\text{Bi-MoO}_2\text{-Bi}_2\text{MoO}_6$, (3) $\text{Bi}_2\text{MoO}_6\text{-MoO}_2\text{-Bi}_2\text{Mo}_3\text{O}_{12}$, (4) $\text{Bi-Bi}_2\text{MoO}_6\text{-Bi}_6\text{Mo}_2\text{O}_{15}$, (5) $\text{Bi-Bi}_{10}\text{Mo}_3\text{O}_{24}\text{-Bi}_6\text{MoO}_{12}$ (6) $\text{Bi-Bi}_6\text{MoO}_{12}\text{-Bi}_{14}\text{MoO}_{24}$ and (7) $\text{Bi-Bi}_{14}\text{MoO}_{24}\text{-Bi}_2\text{O}_3$ at 773 K, (1) Bi-Mo-MoO_2 , (2) $\text{Bi-MoO}_2\text{-Bi}_2\text{MoO}_6$, (3) $\text{Bi}_2\text{MoO}_6\text{-MoO}_2\text{-Bi}_2\text{Mo}_2\text{O}_9$, (4) $\text{Bi}_2\text{Mo}_2\text{O}_9\text{-MoO}_2\text{-Bi}_2\text{Mo}_3\text{O}_{12}$ and (5) $\text{Bi-Bi}_{14}\text{MoO}_{24}\text{-Bi}_2\text{O}_3$ at 873 K and (1) Bi-Mo-MoO_2 , (2) $\text{Bi-MoO}_2\text{-Bi}_2\text{MoO}_6$, (3) $\text{Bi-Bi}_2\text{MoO}_6\text{-'Bi}_{26}\text{Mo}_{10}\text{O}_{69}'$, (4) $\text{Bi-Bi}_{10}\text{Mo}_3\text{O}_{24}\text{-'Bi}_{38}\text{Mo}_7\text{O}_{78}'$, (5) $\text{Bi-'Bi}_{38}\text{Mo}_7\text{O}_{78}'\text{-Bi}_{14}\text{MoO}_{24}$ and (6) $\text{Bi-Bi}_{14}\text{MoO}_{24}\text{-Bi}_2\text{O}_3$ at 1023 K.

Further evidences for the presence of additional phase fields were obtained from the results of several long term equilibrations in liquid bismuth. These experiments also helped to confirm the existence of the phase fields which were identified in the previous equilibration studies. The results are summarized in Table 3.8. The data in the table shows the existence of the following phase fields: (1) Bi-MoO₂-Bi₂MoO₆, (2) Bi-Bi₂MoO₆-Bi₆Mo₂O₁₅, (3) Bi-Bi₆Mo₂O₁₅-Bi₁₀Mo₃O₂₄, (4) Bi-Bi₁₀Mo₃O₂₄-Bi₆MoO₁₂, (5) Bi-Bi₆MoO₁₂-Bi₁₄MoO₂₄ and (6) Bi-Bi₁₄MoO₂₄-Bi₂O₃ at 773 K, (1) Bi-Bi₂MoO₆-Bi₈Mo₃O₂₁, (2) Bi-Bi₈Mo₃O₂₁-Bi₁₄Mo₅O₃₆, (3) Bi-Bi₁₄Mo₅O₃₆-Bi₆Mo₂O₁₅, (4) Bi-Bi₆Mo₂O₁₅-Bi₁₀Mo₃O₂₄, (5) Bi-Bi₁₀Mo₃O₂₄-Bi₆MoO₁₂ and (6) Bi-Bi₆MoO₁₂-Bi₁₄MoO₂₄ at 873 K and (1) Bi-MoO₂-Bi₂MoO₆, (2) Bi-‘Bi₂₆Mo₁₀O₆₉’-Bi₁₀Mo₃O₂₄, (3) Bi-Bi₁₀Mo₃O₂₄-‘Bi₃₈Mo₇O₇₈’, (4) Bi-‘Bi₃₈Mo₇O₇₈’-Bi₁₄MoO₂₄ and (5) Bi-Bi₁₄MoO₂₄-Bi₂O₃ at 1023 K.

Using these results, the partial phase diagrams of the ternary Bi-Mo-O system valid at 773, 873 and 1023 K have been constructed and are shown in Figs. 3.10 to 3.12.

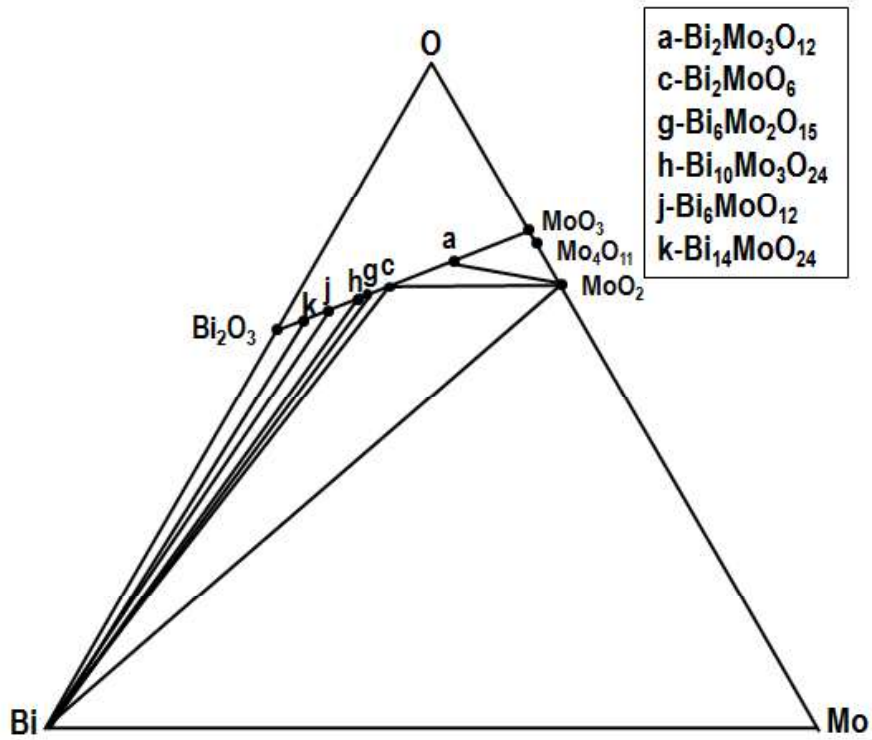


Fig. 3.10 Partial phase diagram of Bi-Mo-O system at 773 K

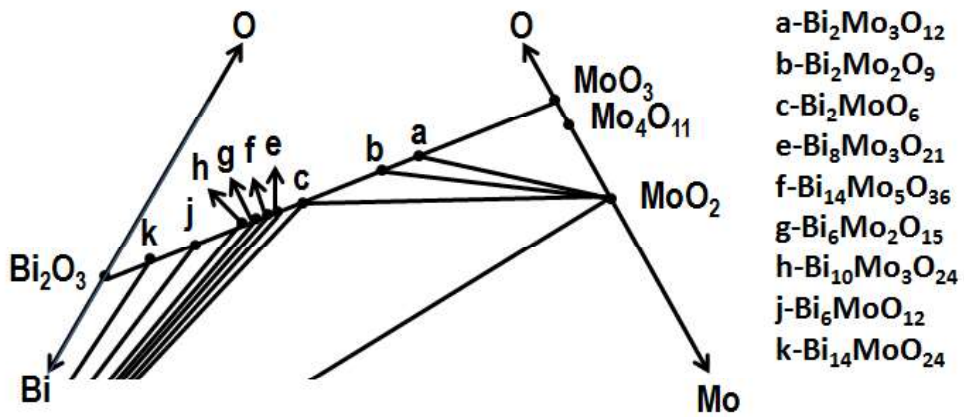


Fig. 3.11 Partial phase diagram of Bi-Mo-O system at 873 K

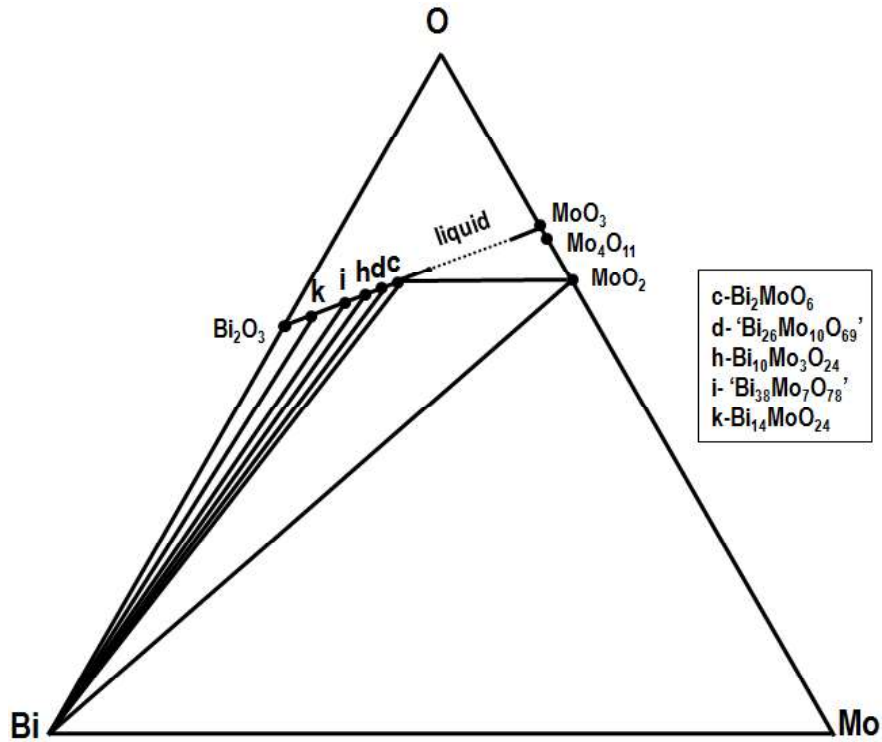


Fig. 3.12 Partial phase diagram of Bi-Mo-O system at 1023 K

3.4.6 Investigation on the thermal stabilities of $\text{Bi}_8\text{Mo}_3\text{O}_{21}$, $\text{Bi}_{14}\text{Mo}_5\text{O}_{36}$ and $\text{Bi}_6\text{Mo}_2\text{O}_{15}$

Experimental results obtained for the long term equilibrations of $\text{Bi}_8\text{Mo}_3\text{O}_{21}$ at different temperatures are given in Table 3.9. It can be seen that upon equilibration at 771, 788 and 805 K, $\text{Bi}_8\text{Mo}_3\text{O}_{21}$ has decomposed to give a mixture of Bi_2MoO_6 and $\text{Bi}_6\text{Mo}_2\text{O}_{15}$ phases. This indicates that $\text{Bi}_8\text{Mo}_3\text{O}_{21}$ is not stable at temperatures below 805 K. However, for equilibrations in the temperature range of 841 to 912 K, the $\text{Bi}_8\text{Mo}_3\text{O}_{21}$ phase was retained which shows that $\text{Bi}_8\text{Mo}_3\text{O}_{21}$ is stable at these temperatures. Hence, $\text{Bi}_8\text{Mo}_3\text{O}_{21}$ appears as a stable phase at temperature lying between 805 and 841 K. The equilibration of $\text{Bi}_8\text{Mo}_3\text{O}_{21}$ at temperatures between 931 and 1023 K has resulted in the formation of ' $\text{Bi}_{26}\text{Mo}_{10}\text{O}_{69}$ ' phase only which suggests that $\text{Bi}_8\text{Mo}_3\text{O}_{21}$ undergoes transition into the high temperature polymorph belonging to the solid solution phase at temperature falling between 912 and 931 K.

The plot of electrical conductivity of $\text{Bi}_8\text{Mo}_3\text{O}_{21}$ as a function of reciprocal temperature is shown in Fig. 3.13. The conductivity measurements were carried out from 773 to 973 K. As seen from the plot, a slope change is observed at 917 ± 5 K. XRD analysis of the sample retrieved after the conductivity measurements at 973 K has shown the presence of ' $\text{Bi}_{26}\text{Mo}_{10}\text{O}_{69}$ ' phase. This indicates that at 917 ± 5 K, $\text{Bi}_8\text{Mo}_3\text{O}_{21}$ would transform to the high temperature solid solution ' $\text{Bi}_{26}\text{Mo}_{10}\text{O}_{69}$ '.

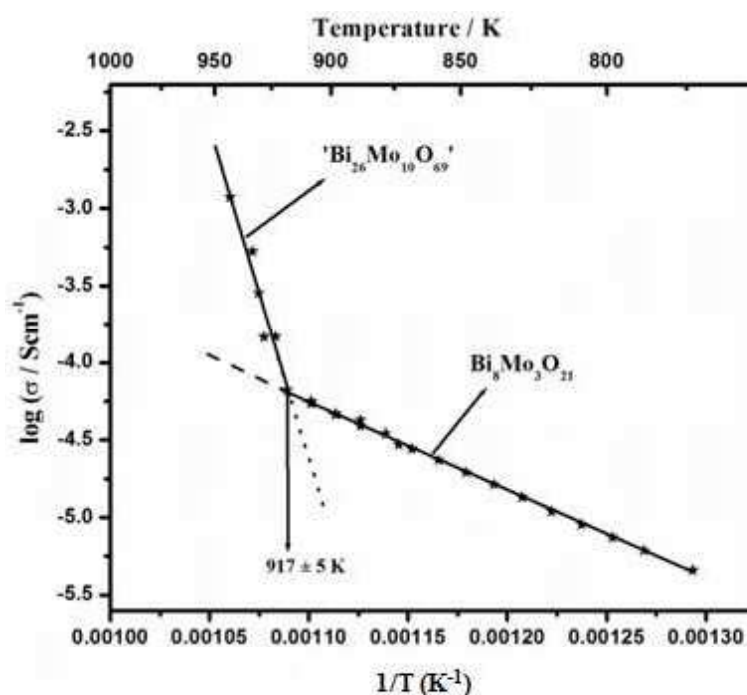


Fig. 3.13 Variation of electrical conductivity of $\text{Bi}_8\text{Mo}_3\text{O}_{21}$ as a function of temperature

The results based on the XRD patterns of the products obtained after the simultaneous equilibrations of $\text{Bi}_8\text{Mo}_3\text{O}_{21}$ at different temperatures in air are given in Table 3.10. The data indicates that upon equilibrations at 873 and 898 K, the $\text{Bi}_8\text{Mo}_3\text{O}_{21}$ phase was retained while equilibrations at 923, 948 and 973 K had led to the formation of the ' $\text{Bi}_{26}\text{Mo}_{10}\text{O}_{69}$ ' phase. This supports the conclusion based on electrical conductivity measurement. The activation energy determined from the Arrhenius plot is found to be 1.13 eV for the temperature range of 773 to 917 K

indicating the conductivity due to oxide ions as reported in reference [47]. Results obtained from the long term equilibrations of $\text{Bi}_8\text{Mo}_3\text{O}_{21}$ samples at different temperatures clearly show that $\text{Bi}_8\text{Mo}_3\text{O}_{21}$ is unstable at temperatures below 805 K and it decomposes to give a mixture of Bi_2MoO_6 and $\text{Bi}_6\text{Mo}_2\text{O}_{15}$ phases. Equilibration at 788 K for 24 h (Table 3.10) also supports this. However, in the electrical conductivity measurements, no slope change corresponding to the decomposition was observed. This can be attributed to the structural similarities of $\text{Bi}_8\text{Mo}_3\text{O}_{21}$, Bi_2MoO_6 and $\text{Bi}_6\text{Mo}_2\text{O}_{15}$ as all of them crystallize in the monoclinic system and hence they could possess similar conductivity values.

Results obtained for the long term equilibrations of $\text{Bi}_{14}\text{Mo}_5\text{O}_{36}$ at different temperatures are given in Table 3.9. It is seen that the equilibration of $\text{Bi}_{14}\text{Mo}_5\text{O}_{36}$ at temperatures 766, 782 and 798 K has given a mixture of Bi_2MoO_6 and $\text{Bi}_6\text{Mo}_2\text{O}_{15}$ phases. This indicates that $\text{Bi}_{14}\text{Mo}_5\text{O}_{36}$ is unstable at these temperatures and undergoes decomposition at temperatures below 798 K. Equilibrations at 817, 838 and 883 K has resulted in a mixture of Bi_2MoO_6 and $\text{Bi}_6\text{Mo}_2\text{O}_{15}$ along with $\text{Bi}_{14}\text{Mo}_5\text{O}_{36}$. It shows that $\text{Bi}_{14}\text{Mo}_5\text{O}_{36}$ is stable at these temperatures and it is appearing to be as a stable phase at temperatures between 798 and 817 K. Single phase of $\text{Bi}_{14}\text{Mo}_5\text{O}_{36}$ was present after equilibrations at temperatures between 883 and 947 K whereas equilibrations between 968 and 1023 K had yielded the ' $\text{Bi}_{26}\text{Mo}_{10}\text{O}_{69}$ ' phase. This shows the temperature at which $\text{Bi}_{14}\text{Mo}_5\text{O}_{36}$ would undergo transformation into the high temperature solid solution phase lies between 947 and 968 K.

Variation of logarithm of electrical conductivity of $\text{Bi}_{14}\text{Mo}_5\text{O}_{36}$ with reciprocal temperature obtained is shown in Fig. 3.14. Conductivity had been measured in the temperature range of 748 to 990 K and a change in slope is seen at

963 ± 5 K corresponding to the transition of $\text{Bi}_{14}\text{Mo}_5\text{O}_{36}$ to ' $\text{Bi}_{26}\text{Mo}_{10}\text{O}_{69}$ ' phase. This observation is in accordance with the results obtained from the simultaneous equilibration experiments (Table 3.10). $\text{Bi}_{14}\text{Mo}_5\text{O}_{36}$ was retained on equilibrations at 873, 923 and 948 K whereas on equilibration at 973 K it transformed to ' $\text{Bi}_{26}\text{Mo}_{10}\text{O}_{69}$ '. Further, XRD analysis of the pellet retrieved after the conductivity measurements at 990 K has shown the presence of ' $\text{Bi}_{26}\text{Mo}_{10}\text{O}_{69}$ ' phase only. Activation energy determined from the Arrhenius plot is found to be 1.39 eV for the temperature range of 748 to 963 K. As in the case of $\text{Bi}_8\text{Mo}_3\text{O}_{21}$, long term equilibration experiments at different temperatures (Table 3.9) along with equilibration at 773 K for 24 h (Table 3.10) had shown that $\text{Bi}_{14}\text{Mo}_5\text{O}_{36}$ is unstable at temperatures below 817 K and it had partially decomposed to Bi_2MoO_6 and $\text{Bi}_6\text{Mo}_2\text{O}_{15}$ phases. However, we could not observe any slope change corresponding to this decomposition in the Arrhenius plot of conductivity. Since all the three ternary compounds involved in this disproportionation reaction have monoclinic structure, they are expected to have similar conductivities and hence this behavior.

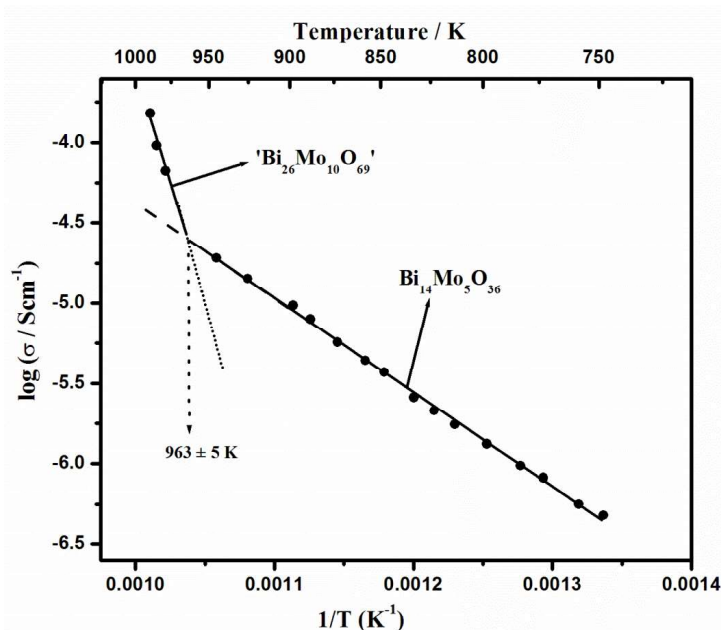


Fig. 3.14 Variation of electrical conductivity of $\text{Bi}_{14}\text{Mo}_5\text{O}_{36}$ as a function of temperature

Equilibration of $\text{Bi}_6\text{Mo}_2\text{O}_{15}$ at different temperatures between 745 and 901 K for prolonged duration has shown that $\text{Bi}_6\text{Mo}_2\text{O}_{15}$ is stable at these temperatures. The XRD patterns have shown the presence of single phase of $\text{Bi}_6\text{Mo}_2\text{O}_{15}$ only (Table 3.9). However, upon equilibrations at temperatures between 928 and 998 K, ' $\text{Bi}_{26}\text{Mo}_{10}\text{O}_{69}$ ' phase was obtained. This indicates the transition of $\text{Bi}_6\text{Mo}_2\text{O}_{15}$ to the high temperature solid solution phase occurs at a temperature falling between 901 and 928 K.

The plot of variation of electrical conductivity of $\text{Bi}_6\text{Mo}_2\text{O}_{15}$ with temperature, as presented in Fig. 3.15, showed a slope change at 891 ± 5 K. These observations were further verified by carrying out simultaneous equilibration experiments (Table 3.10).

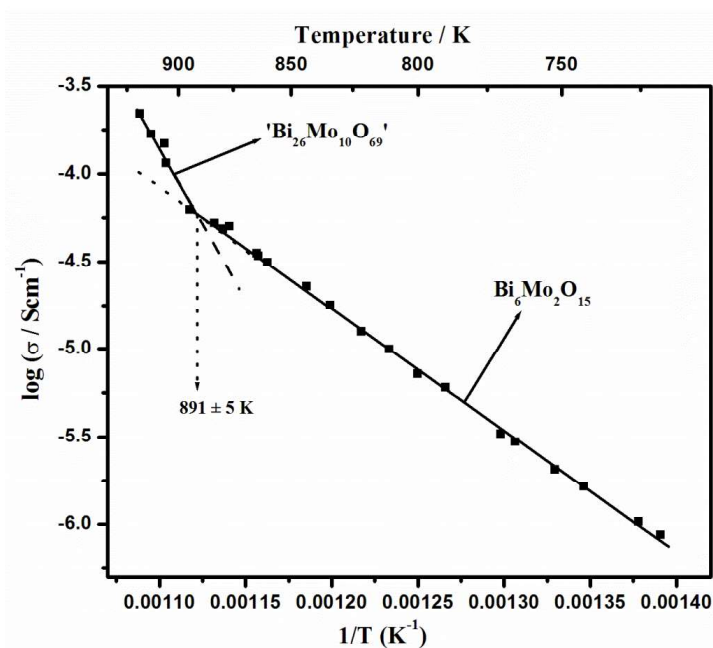


Fig. 3.15 Variation of electrical conductivity of $\text{Bi}_6\text{Mo}_2\text{O}_{15}$ as a function of temperature

It can be seen that upon equilibration at 873 K, $\text{Bi}_6\text{Mo}_2\text{O}_{15}$ phase remains unaltered whereas after equilibrations at 898 and 923 K, ' $\text{Bi}_{26}\text{Mo}_{10}\text{O}_{69}$ ' was formed. Further, XRD analysis of the pellet retrieved from the conductivity cell after

measurement at 917 K showed the presence of 'Bi₂₆Mo₁₀O₆₉' phase. Activation energy determined from the Arrhenius plot is found to be 1.16 eV for the temperature range of 718 to 891 K.

3.4.7 Investigation of thermal stability of Bi₂Mo₂O₉

To identify the temperature above which Bi₂Mo₂O₉ is stable, its electrical conductivity as a function of temperature was measured.

The variation of conductivity with temperature as $\log \sigma$ Vs $1/T$ is shown in Fig. 3.16. As seen from the figure, a slope change is observed at 817 ± 5 K. The XRD analysis of the sample retrieved after the conductivity measurements (sample quenched to room temperature from 754 K) has shown the presence of Bi₂MoO₆ (orthorhombic phase) and Bi₂Mo₃O₁₂ phases. The results of simultaneous equilibration of Bi₂Mo₂O₉ at different temperatures in air (Table 3.11) also show that Bi₂Mo₂O₉ is stable at 823 and 873 K but undergoes decomposition at 773 and 798 K. Consideration of conductivity data in conjunction with these XRD data indicates that Bi₂Mo₂O₉ would decompose to form Bi₂MoO₆ and Bi₂Mo₃O₁₂ at 817 ± 5 K. The activation energies determined from the Arrhenius plot are found to be 1.19 eV and 1.44 eV, respectively for the temperature ranges of 753 to 817 K and 817 to 913 K. Hartmanova et al. [69] have also measured electrical conductivity of Bi₂Mo₂O₉ in the temperature range of 454 to 713 K and reported the activation energy as 1.15 eV which is in good agreement with the present value of 1.19 eV obtained for conduction in the low temperature regime.

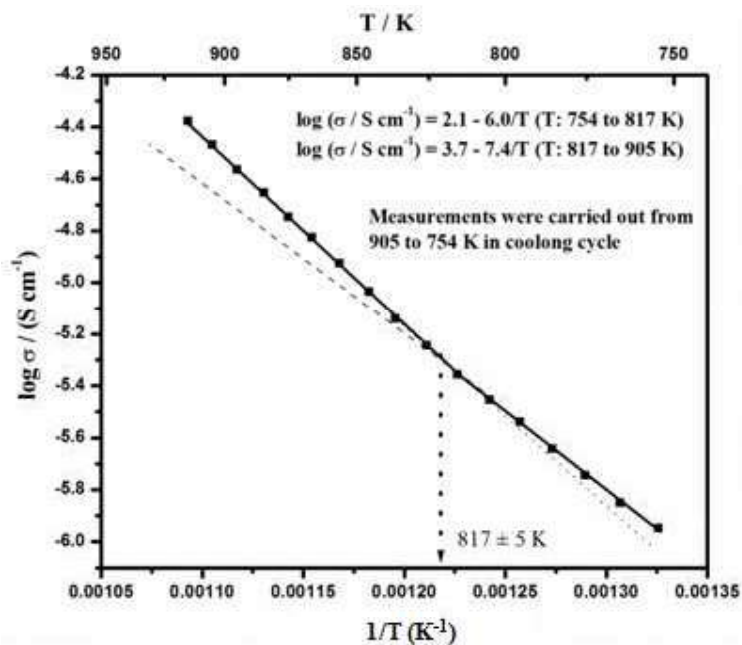


Fig. 3.16 Variation of electrical conductivity of $\text{Bi}_2\text{Mo}_2\text{O}_9$ as a function of temperature (Below 817 K, the phases present are $\text{Bi}_2\text{Mo}_3\text{O}_{12}$ and Bi_2MoO_6)

3.4.8 Investigation on the polymorphic transformations of Bi_2MoO_6

The variation of conductivity of the orthorhombic phase of Bi_2MoO_6 with temperature is shown in Fig. 3.17. Conductivities were measured during a heating cycle from 700 to 963 K. It can be seen that at temperatures between 868 and 871 K a sharp drop in conductivity occurred. Further increase in the temperature resulted in the steady increase in conductivity. The XRD analysis of the samples equilibrated at 773, 823, 843 and 853 K (Table 3.11) had shown the presence of orthorhombic phase of Bi_2MoO_6 while the equilibrations at 873, 923 and 973 K had shown the presence of the monoclinic phase. Hence, the drop in conductivity is due to the transformation of orthorhombic phase to monoclinic phase at ~ 870 K. The presence of an intermediate phase (γ'') has been reported in literature in the temperature range of ~ 840 to 877 K. However, in samples after equilibration at 843 and 853 K, we could observe only the orthorhombic phase of Bi_2MoO_6 . Intermediate γ'' phase could not be observed in

samples from both conductivity and equilibration experiments. The activation energies for conductivity deduced from the plot are 1.85 eV and 1.97 eV, respectively for the temperature ranges of 763 to 868 K and 872 to 963 K corresponding to the orthorhombic and monoclinic phases of Bi_2MoO_6 . Arrhenius plot obtained for the electrical conductivity measurements carried out while cooling the monoclinic phase of Bi_2MoO_6 is also shown in Fig. 3.17. No change in slope is observed in the conductivity plot suggesting that the compound had not undergone any phase transition at low temperatures and this is in agreement with the irreversible nature of the orthorhombic to monoclinic phase transition reported in literature. This is also supported by the results of the equilibration experiments with the monoclinic phase of Bi_2MoO_6 given in Table 3.11. XRD analysis of the samples obtained after equilibration at all temperatures (773, 823, 873 and 973 K) showed the presence of monoclinic phase of Bi_2MoO_6 only.

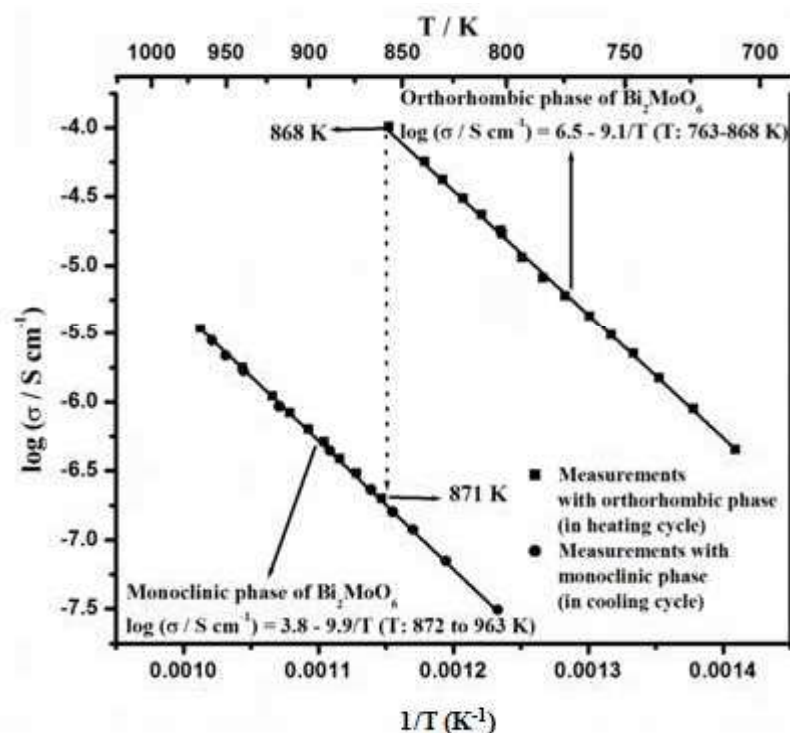


Fig. 3.17 Variation of electrical conductivity of orthorhombic and monoclinic phases of Bi_2MoO_6 as a function of temperature

3.4.9 Oxygen potential measurements

3.4.9.1 Standard molar Gibbs energy of formation of Bi_2MoO_6 (s)

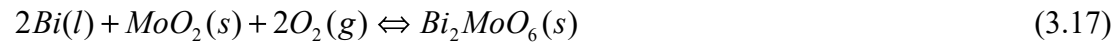
The XRD analysis of the sample pellets retrieved at the end of emf measurements showed the presence of Bi, MoO_2 and Bi_2MoO_6 phases. Monoclinic phase of Bi_2MoO_6 was observed to be present. As mentioned earlier, first temperature of operation in each cell was in the temperature range of 1023 K for cell-I and 936 K for cell-II, where the monoclinic phase of Bi_2MoO_6 is stable. It is known that the transition of Bi_2MoO_6 from the orthorhombic phase to monoclinic phase is irreversible and the electrical conductivity measurements have shown that the transformation occurring at ~ 868 K. The monoclinic form of Bi_2MoO_6 is known to be metastable at room temperature. Hence, the phase that was present during emf measurements was the monoclinic form of Bi_2MoO_6 .

The emf values measured as a function of temperature in the case of sample with composition within the Bi- MoO_2 - Bi_2MoO_6 phase field are given in Table 3.12. The variation of cell emf with temperature is shown in Fig. 3.18 and can be expressed by the following least squares fitted expression:

$$E \pm 0.7 / \text{mV} = 1039.7 - 0.4358 (T/\text{K}) \quad (T: 772\text{-}1023 \text{ K}) \quad (3.16)$$

The error indicated is the expanded uncertainty with 0.95 level of confidence.

The chemical equilibrium at the sample electrode is represented as below:



$$\Delta_f G_m^\circ < \text{Bi}_2\text{MoO}_6 > = \Delta_f G_m^\circ < \text{MoO}_2 > + 2RT \ln p_{\text{O}_2}^s \quad (3.18)$$

where $p_{\text{O}_2}^s$ is the partial pressure of oxygen at the sample electrode.

Table 3.12 Variation of EMF with temperature in the Bi-MoO₂-Bi₂MoO₆ phase field

Sample 1		Sample 2	
Temperature / K	Emf / mV	Temperature / K	Emf / mV
1022.7	595.4	936.3	631.8
921.5	638.2	911.6	642.5
823.9	680.9	886.5	653.6
998.5	605.3	873.7	659.5
899.1	648.3	861.1	664.6
947.0	627.2	1014.3	597.6
849.0	670.0	911.2	641.2
1010.5	599.7	936.9	630.2
985.4	610.2	864.3	662.3
961.0	620.9	962.1	619.3
-	-	987.9	608.3
-	-	772.6	703.3
-	-	799.2	691.7

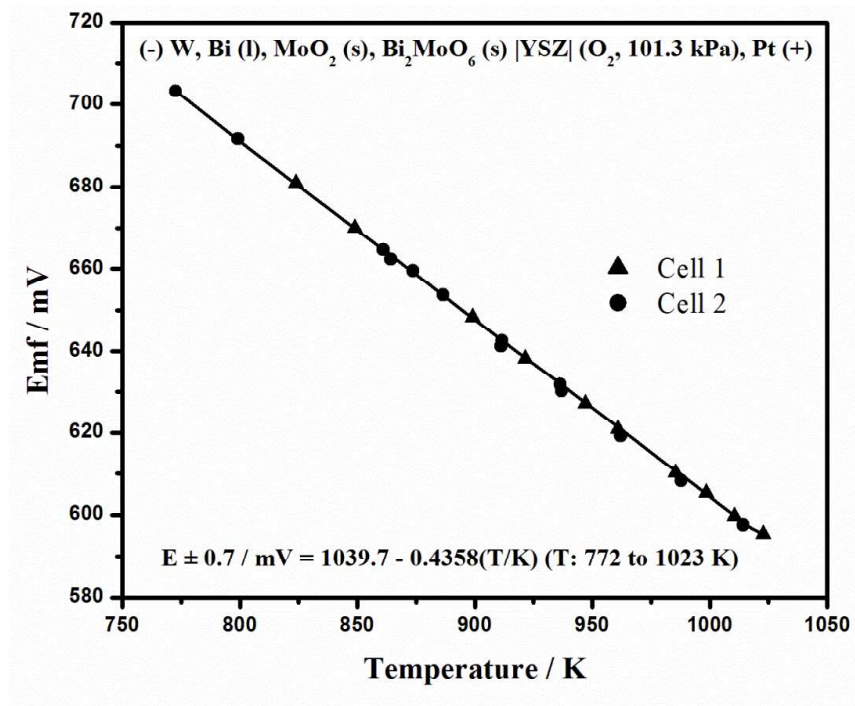


Fig. 3.18 Variation of emf with temperature with Bi- MoO₂-Bi₂MoO₆ as sample

The cell emf is given by

$$E = \frac{RT}{4F} \ln \frac{P_{O_2}^R}{P_{O_2}^S} \quad (3.19)$$

where E is the electromotive force in volts, R is the universal gas constant (8.314 J K⁻¹ mol⁻¹), F is the Faraday constant (96485 C mol⁻¹) and $P_{O_2}^R$ is the partial pressure of oxygen in the reference electrode. Equation (3.19) can be written as

$$4FE = RT \ln P_{O_2}^R - RT \ln P_{O_2}^S \quad (3.20)$$

Since $P_{O_2}^R = 1 \text{ atm}$, $RT \ln p_{O_2}^S = -4FE$

Thus the standard molar Gibbs energy of formation of the monoclinic phase of $\text{Bi}_2\text{MoO}_6(\text{s})$ can be obtained from the measured emf values as given below:

$$\Delta_f G_m^\circ < \text{Bi}_2\text{MoO}_6 > = \Delta_f G_m^\circ < \text{MoO}_2 > - 8FE \quad (3.21)$$

By substituting the emf data given by expression (3.16) and using the following data on molar Gibbs energy of formation of $\text{MoO}_2(\text{s})$ from ref. 23

$$\Delta_f G^\circ < \text{MoO}_2 > \pm 0.6 / \text{kJ mol}^{-1} = -579.8 + 0.1700(T / K) \quad (T : 925 - 1533 \text{ K}) \quad (3.22)$$

The standard molar Gibbs energy of formation of monoclinic phase of $\text{Bi}_2\text{MoO}_6(\text{s})$ was derived and is given below:

$$\Delta_f G^\circ < \text{Bi}_2\text{MoO}_6 > \pm 0.8 / \text{kJ mol}^{-1} = -1382.3 + 0.5064(T / K) \quad (T : 772 - 1023 \text{ K}) \quad (3.23)$$

To determine the uncertainties introduced in the Gibbs energy of formation of $\text{Bi}_2\text{MoO}_6(\text{s})$ due to variation in the total local atmospheric pressure of the site, atmospheric pressure during the experimental period was continuously monitored.

The variation was found to be $\pm 0.008 \text{ atm}$.

The uncertainties introduced due to this variation are calculated as below:

The standard molar Gibbs energy of formation of $\text{Bi}_2\text{MoO}_6(\text{s})$ is deduced from the following equation:

$$\Delta_f G_m^\circ < Bi_2MoO_6 > = \Delta_f G_m^\circ < MoO_2 > + 2RT \ln P_{O_2}^R - 8FE \quad (3.24)$$

When $P_{O_2}^R = 1$ atm, the expression (3.24) could be written as:

$$\Delta_f G_m^\circ < Bi_2MoO_6 > = \Delta_f G_m^\circ < MoO_2 > - 8FE$$

At the maximum temperature of emf measurement ($T = 1023$ K),

$$\Delta_f G_m^\circ < Bi_2MoO_6 > = -864.3 \pm 0.8 \text{ kJ mol}^{-1}.$$

When there is deviation in $P_{O_2}^R$ from 1 atm, i.e. $P_{O_2}^R = 1 \pm 0.008$ atm, the errors introduced at the maximum temperature of 1023 K is calculated as below:

At $T = 1023$ K and $P = 1.008$ atm,

$$2RT \ln 1.008 = 0.136 \text{ kJ mol}^{-1}$$

And when $P = 0.992$ atm,

$$2RT \ln 0.992 = -0.136 \text{ kJ mol}^{-1}$$

Hence, the error due to the variation of reference pressure = $\pm 0.136 \text{ kJ mol}^{-1}$.

Therefore,

$$\Delta_f G_m^\circ < Bi_2MoO_6 > = \Delta_f G_m^\circ < MoO_2 > + 2RT \ln P_{O_2}^R - 8FE = -864.3 \pm 0.136 \text{ kJ mol}^{-1}$$

at 1023 K.

This error is negligible compared to the uncertainty reported for the Gibbs energy of formation of Bi_2MoO_6 (s) ($\pm 0.8 \text{ kJ mol}^{-1}$).

3.4.10 Standard molar enthalpies of formation of bismuth molybdates

The experimental results obtained for the enthalpy of dissolution of TRIS are given in Table 3.13. The molar enthalpy of solution of TRIS obtained in the present work is $(-29.62 \pm 0.44) \text{ kJ mol}^{-1}$ which is in good agreement with the reported value of $(-29.770 \pm 0.032) \text{ kJ mol}^{-1}$ [70]. Thus it ensures the suitability of the experimental set up for calorimetric measurements.

Table 3.13 Enthalpy of solution ($\Delta_{sol}H_m^{\circ}$) of TRIS* in 0.10 ± 0.01 mol / kg HCl (mass of solvent = 99.52 ± 0.01 g) at 298.15 K[@] and 0.1 MPa^a (Molar mass of TRIS = 121.1 g mol⁻¹)

Run	Weight of TRIS (w / g) ^a	Experimental enthalpy change (ΔH / J)	Molar enthalpy of solution ($\Delta_{sol}H_m^{\circ}$ / kJ mol ⁻¹)
1	0.2354	-57.73	-29.70
2	0.2313	-57.07	-29.87
3	0.2295	-55.71	-29.40
4	0.2295	-56.15	-29.63
5	0.2161	-52.62	-29.48
			Average: (-29.62 ± 0.44)^b

*Tris(hydroxymethyl)aminomethane (s), [@]Temperature stability inside the calorimeter prior to start of experiment was within ± 0.001 K. ^a Standard uncertainty, *u*, are $u(P) = 0.8$ kPa and $u(w) = 0.001$, ^b Expanded uncertainty $U(\Delta_{sol}H_m^{\circ})$ is calculated as 2σ of the mean with 0.95 level of confidence. Uncertainty from calibration was also included into the final uncertainty of the dissolution enthalpies.

In the present study, the standard molar enthalpies of formation of bismuth molybdates were determined by measuring their enthalpies of dissolution. A suitable solvent which can dissolve the ternary bismuth molybdates as well as the component oxides, Bi₂O₃ (s) and MoO₃ (s) has to be used for the dissolution experiments. Also the samples should dissolve in the solvent in a reasonable period of time. Several mineral acids and alkalis were tried for the solubility experiments and the bismuth molybdates were found to be insoluble in all of them.

It is known from literature that triethanolamine (TEA) is a versatile ligand and can readily form coordination complexes with almost all metal ions and behave as N and O-donor ligands [71]. TEA can form complexes with Bi³⁺ and Mo⁶⁺ ions as well. The complexes of TEA with Bi find its application in medical fields. For the preparation of medically relevant Bi-TEA complexes, the ratio of Bi to TEA used was reported to be ranging from 1:2.6 to 1:5.2 [72]. Miller described the conditions for the

formation of complexes of TEA with bismuth and reported that TEA forms 1:1 complex with bismuth ions [72]. Based on differential pulse polarography experiments, Hancock et al. [73] determined the formation constant ($\log K$) of this 1:1 complex and it is found to be 9.2. The complexation of molybdenum ions with TEA was studied by Szalontai et al. [74]. Under alkaline pH, the mononuclear molybdate anion exists in the tetrahedral form while upon chelation with triethanolamine, it forms soluble oxomolybdate (VI) complexes which exist in the octahedral or distorted octahedral configuration. It is also reported that water soluble complexes of Mo-TEA could form when the ratio of Mo to TEA is 1:3 [74]. In the present experiments, the ratio of metals to TEA was maintained as 1:80, so as to maintain a large excess of TEA. The final solution obtained after the dissolution of bismuth molybdates as well as the component oxides were clear and there were no perceptible precipitates. Based on the reports in literature, it is clear that both bismuth and molybdenum salts can form water soluble complexes with triethanolamine under alkaline conditions. This fact has been employed in the present study. The solubility of ternary bismuth molybdates along with that of Bi_2O_3 (s) and MoO_3 (s) was checked in a mixture of triethanolamine and NaOH solution. It was observed that all the ternary bismuth molybdates as well as the component oxides were soluble in the solvent and the maximum time taken for the dissolution was found to be ~ 4 min under the chosen experimental conditions.

The experimental results obtained for the measurement of enthalpy of solution of the starting components, Bi_2O_3 (s) and MoO_3 (s) and that for ternary components are given in Tables 3.14 and 3.15, respectively.

Table 3.14 Experimentally determined values of enthalpies of dissolution (ΔH) and molar enthalpies of dissolution ($\Delta_{sol}H_m^o$) of Bi_2O_3 (s) and MoO_3 (s) in a mixture of 100 ml of 3 mol kg^{-1} NaOH and 25 ml of triethanolamine at 298.15 K* and 0.1 MPa^a

Sample	Weight of sample (w / g) ^a	Experimental enthalpy change (ΔH / J)	Molar enthalpy of solution ($\Delta_{sol}H_m^o$ / kJ mol^{-1})
Bi_2O_3 (s) (molar mass = 465.96 g mol^{-1})	0.6923	-62.34	-41.96
	0.4020	-36.97	-42.86
	0.4400	-39.84	-42.18
	0.4388	-41.00	-43.54
	0.2650	-24.52	-43.11
	0.3645	-33.37	-42.66
	0.2002	-18.87	-43.93
	0.3152	-28.30	-41.83
	0.2568	-23.45	-42.56
Average: (-42.74 \pm 0.77)^b			
MoO_3 (s) (molar mass = 143.9382 g mol^{-1})	0.3239	-178.67	-79.39
	0.2459	-136.19	-79.72
	0.2699	-150.62	-80.32
	0.2392	-131.89	-79.36
	0.2450	-136.71	-80.32
Average: (-79.82 \pm 1.19)^b			

*Temperature stability inside the calorimeter prior to start of experiment was within ± 0.001 K. ^a Standard uncertainties, u , are $u(P) = 0.8$ kPa and $u(w) = 0.0001$ g. ^bExpanded uncertainty, $U(\Delta_{sol}H_m^o)$, is calculated as 2σ of the mean with 0.95 level of confidence. Uncertainty from calibration was also included into the final uncertainty of the dissolution enthalpies.

The molar enthalpies of solution, $\Delta_{sol}H_m^o$ of Bi_2O_3 (s), MoO_3 (s), $\text{Bi}_2\text{Mo}_3\text{O}_{12}$ (s), orthorhombic- Bi_2MoO_6 (s), monoclinic- Bi_2MoO_6 (s), $\text{Bi}_6\text{Mo}_2\text{O}_{15}$ (s), and $\text{Bi}_6\text{MoO}_{12}$ (s), obtained are (-42.74 \pm 0.77), (-79.82 \pm 1.19), (-172.72 \pm 2.69), (-31.28 \pm 0.98), (-52.79 \pm 1.24), (-145.40 \pm 2.55) and (-60.15 \pm 1.08) kJ mol^{-1} , respectively. The molar enthalpy of formation of the ternary compounds from the component elements were obtained by considering suitable thermochemical reaction schemes

presented in Tables 3.16 to 3.20. For the calculation of enthalpies of formation from elements, values of enthalpies of formation of binary oxides were taken from references 74 and 75. The calculated enthalpies of formation from elements, $\Delta_f H_{298}^\circ$, are (-2915.8 ± 5.7) , (-1407.2 ± 3.8) , (-1385.7 ± 3.9) , (-3345.0 ± 10.9) and (-2605.2 ± 10.4) kJ mol⁻¹, respectively for Bi₂Mo₃O₁₂ (s), orthorhombic Bi₂MoO₆ (s), monoclinic Bi₂MoO₆ (s), Bi₆Mo₂O₁₅ (s) and Bi₆MoO₁₂ (s).

3.4.11 Heat capacity measurements

3.4.11.1 Molar heat capacity of MoO₃ (s)

The performance of the differential scanning calorimeter was verified by measuring the heat capacity of MoO₃ (s) in the temperature range of 318 to 763 K and shown in Fig. 3.19 and the selected values are given in Table 3.21. The measured data given in Table 3.21 is the mean of ten measurements. The experimental heat capacity is compared with the literature data [77]. It is seen that the measured C_p values are in good agreement with the reported C_p values at temperatures between 428 and 703 K. Deviations from the literature data are observed at temperatures below and above this range. The maximum deviation is found to be 3%.

The combined expanded uncertainty associated with the heat capacity measurements of the samples were calculated by incorporating the relative uncertainties of experimental data and the relative uncertainty attributed to the instrument. The relative uncertainty of the instrument was determined from the measured C_p values of MoO₃(s) (Table 3.21). The relative uncertainty in the measured heat capacity of the samples were calculated as $\Delta x/x$ where Δx is the maximum standard uncertainty observed and x is the smallest measured C_p value.

Table 3.15 Experimentally determined values of enthalpies of dissolution (ΔH) and molar enthalpies of dissolution ($\Delta_{sol}H_m^o$) of $\text{Bi}_2\text{Mo}_3\text{O}_{12}(\text{s})$, orthorhombic $\text{Bi}_2\text{MoO}_6(\text{s})$, monoclinic $\text{Bi}_2\text{MoO}_6(\text{s})$, $\text{Bi}_6\text{Mo}_2\text{O}_{15}(\text{s})$ and $\text{Bi}_6\text{MoO}_{12}(\text{s})$ in a mixture of 100 ml of 3 mol kg^{-1} NaOH and 25 ml of triethanolamine at 298.15 K^{*} and 0.1 MPa^a.

Sample	Weight of sample (w / g) ^a	Experimental enthalpy change ΔH (J)	Molar enthalpy of solution $\Delta_{sol}H_m^o$ (kJ mol ⁻¹)
$\text{Bi}_2\text{Mo}_3\text{O}_{12}(\text{s})$ (molar mass = 897.7728 g mol ⁻¹)	0.4921	-94.11	-171.69
	0.5156	-99.64	-173.49
	0.5338	-103.83	-174.63
	0.5340	-102.63	-172.54
	0.5442	-103.81	-171.26
Average: (-172.72 ± 2.69)^b			
$\text{Bi}_2\text{MoO}_6(\text{s})$ - orthorhombic phase (molar mass = 609.8964 g mol ⁻¹)	0.3043	-15.76	-31.59
	0.2758	-14.71	-32.53
	0.2392	-11.94	-30.44
	0.2204	-10.89	-30.14
	0.2952	-15.35	-31.71
Average: (-31.28 ± 0.98)^b			
$\text{Bi}_2\text{MoO}_6(\text{s})$ - monoclinic phase (molar mass = 609.8964 g mol ⁻¹)	0.4308	-38.62	-54.68
	0.3217	-27.46	-52.06
	0.3745	-31.57	-51.42
	0.3240	-27.57	-51.89
	0.4677	-41.13	-53.63
0.5418	-47.12	-53.04	
Average: (-52.79 ± 1.24)^b			
$\text{Bi}_6\text{Mo}_2\text{O}_{15}(\text{s})$ - (molar mass = 1685.7534 g mol ⁻¹)	0.3892	-32.11	-142.76
	0.3556	-29.68	-144.80
	0.1739	-15.06	-145.98
	0.4455	-38.96	-147.42
	0.2834	-24.55	-146.06
Average: (-145.40 ± 2.55)^b			
$\text{Bi}_6\text{MoO}_{12}(\text{s})$ - (molar mass = 1541.8152 g mol ⁻¹)	0.2653	-10.25	-59.61
	0.3770	-14.79	-60.48
	0.2108	-8.29	-60.66
	0.4186	-16.53	-60.91
	0.4363	-16.72	-59.10
Average: (-60.15 ± 1.08)^b			

^{*}Temperature stability inside the calorimeter prior to start of experiment was within ± 0.001 K. ^aStandard uncertainties, u , are $u(P) = 0.8$ kPa and $u(w) = 0.0001$ g. ^bExpanded uncertainty, $U(\Delta_{sol}H_m^o)$, is calculated as 2σ of the mean with 0.95 level of confidence. Uncertainty from calibration was also included into the final uncertainty of the dissolution enthalpies.

Table 3.16 Thermodynamic reaction schemes for obtaining the enthalpies of formation from oxides and elements for $\text{Bi}_2\text{Mo}_3\text{O}_{12}$ (s) at $T = 298.15 \text{ K}^a$. (s = solid, soln = aqueous solution, g = gas)

No	Reaction	Enthalpies (kJ mol^{-1})	Source of data
1	Bi_2O_3 (s) + 6 NaOH (soln) = $(2 \text{ Bi}^{3+} + 6 \text{ OH}^- + 6 \text{ Na}^+ + 3 \text{ O}^{2-})$ (soln)	$\Delta H_1 = (-42.74 \pm 0.77)^b$	This work
2	MoO_3 (s) + 2 NaOH (soln) = $(2 \text{ Na}^+ + \text{MoO}_4^{2-} + \text{H}_2\text{O})$ (soln)	$\Delta H_2 = (-79.82 \pm 1.19)^b$	This work
3	$\text{Bi}_2\text{Mo}_3\text{O}_{12}$ (s) + 12 NaOH (soln) = $(2 \text{ Bi}^{3+} + 6 \text{ OH}^- + 12 \text{ Na}^+ + 3 \text{ O}^{2-} + 3 \text{ MoO}_4^{2-} + 3 \text{ H}_2\text{O})$ (soln)	$\Delta H_3 = (-172.72 \pm 2.69)^b$	This work
4	2 Bi (s) + $3/2 \text{ O}_2$ (g) = Bi_2O_3 (s)	$\Delta H_4 = \Delta_f H_{298}^\circ$ of Bi_2O_3 (s) = (-570.70 ± 3.35)	[75]
5	Mo (s) + $3/2 \text{ O}_2$ (g) = MoO_3 (s)	$\Delta H_5 = \Delta_f H_{298}^\circ$ of MoO_3 (s) = (-745.2 ± 0.4)	[76]
6	2 Bi (s) + 3 Mo (s) + 6 O_2 (g) = $\text{Bi}_2\text{Mo}_3\text{O}_{12}$ (s)	$\Delta H_6 = \Delta H_1 + 3\Delta H_2 + \Delta H_4 + 3 \Delta H_5 - \Delta H_3 =$ $\Delta_f H_{298}^\circ$ of $\text{Bi}_2\text{Mo}_3\text{O}_{12}$ (s) = $(-2915.8 \pm 5.7)^c$	-

^aTemperature of the calorimeter prior to the actual experiment was stable within $\pm 0.001 \text{ K}$. ^bExpanded uncertainties, U_c (ΔH_i) are calculated as 2σ of the mean and are at the 95 % confidence level. ^cCombined expanded uncertainties, $U_c(\Delta H)$, are calculated as 2σ of the mean and are at the 95 % confidence level.

Table 3.17 Thermodynamic reaction schemes for obtaining the enthalpies of formation from oxides and elements for orthorhombic Bi₂MoO₆(s) at T = 298.15 K^a (s = solid, soln = aqueous solution, g = gas)

No	Reaction	Enthalpies (kJ mol ⁻¹)	Source of data
1	Bi ₂ O ₃ (s) + 6 NaOH (soln) = (2 Bi ³⁺ + 6 OH ⁻ + 6 Na ⁺ + 3 O ²⁻) (soln)	ΔH ₁ = (-42.74 ± 0.77) ^b	This work
2	MoO ₃ (s) + 2 NaOH (soln) = (2 Na ⁺ + MoO ₄ ²⁻ + H ₂ O) (soln)	ΔH ₂ = (-79.82 ± 1.19) ^b	This work
3	Bi ₂ MoO ₆ (s) + 8 NaOH (soln) = (2 Bi ³⁺ + 6 OH ⁻ + 8 Na ⁺ + 3 O ²⁻ + MoO ₄ ²⁻ + H ₂ O) (soln)	ΔH ₃ = (-31.28 ± 0.98) ^b	This work
4	2 Bi (s) + 3/2 O ₂ (g) = Bi ₂ O ₃ (s)	ΔH ₄ = Δ _f H ₂₉₈ ^o of Bi ₂ O ₃ (s) = (-570.70 ± 3.35)	[75]
5	Mo (s) + 3/2 O ₂ (g) = MoO ₃ (s)	ΔH ₅ = Δ _f H ₂₉₈ ^o of MoO ₃ (s) = (-745.2 ± 0.4)	[76]
6	2 Bi (s) + Mo (s) + 3 O ₂ (g) = Bi ₂ MoO ₆ (s)	ΔH ₆ = ΔH ₁ + ΔH ₂ + ΔH ₄ + ΔH ₅ - ΔH ₃ = Δ _f H ₂₉₈ ^o of Bi ₂ MoO ₆ (s) = (-1407.2 ± 3.8) ^c	-

^aTemperature of the calorimeter prior to the actual experiment was stable within ± 0.001 K. ^bExpanded uncertainties, U_c(ΔH), are calculated as 2σ of the mean and are at the 95 % confidence level. ^cCombined expanded uncertainties, U_c(ΔH), are calculated as 2σ of the mean and are at the 95 % confidence level.

Table 3.18 Thermodynamic reaction schemes for obtaining the enthalpies of formation from oxides and elements form monoclinic $\text{Bi}_2\text{MoO}_6(\text{s})$ at $T = 298.15 \text{ K}^{\text{a}}$ (s = solid, soln = aqueous solution, g = gas)

No	Reaction	Enthalpies (kJ mol^{-1})	Source of data
1	$\text{Bi}_2\text{O}_3(\text{s}) + 6 \text{ NaOH}(\text{soln}) = (2 \text{ Bi}^{3+} + 6 \text{ OH}^- + 6 \text{ Na}^+ + 3 \text{ O}^{2-})(\text{soln})$	$\Delta H_1 = (-42.74 \pm 0.77)^{\text{b}}$	This work
2	$\text{MoO}_3(\text{s}) + 2 \text{ NaOH}(\text{soln}) = (2 \text{ Na}^+ + \text{MoO}_4^{2-} + \text{H}_2\text{O})(\text{soln})$	$\Delta H_2 = (-79.82 \pm 1.19)^{\text{b}}$	This work
3	$\text{Bi}_2\text{MoO}_6(\text{s}) + 8 \text{ NaOH}(\text{soln}) = (2 \text{ Bi}^{3+} + 6 \text{ OH}^- + 8 \text{ Na}^+ + 3 \text{ O}^{2-} + \text{MoO}_4^{2-} + \text{H}_2\text{O})(\text{soln})$	$\Delta H_3 = (-52.79 \pm 1.24)^{\text{b}}$	This work
4	$2 \text{ Bi}(\text{s}) + 3/2 \text{ O}_2(\text{g}) = \text{Bi}_2\text{O}_3(\text{s})$	$\Delta H_4 = \Delta_f H_{298}^\circ \text{ of Bi}_2\text{O}_3(\text{s}) = (-570.70 \pm 3.35)$	[75]
5	$\text{Mo}(\text{s}) + 3/2 \text{ O}_2(\text{g}) = \text{MoO}_3(\text{s})$	$\Delta H_5 = \Delta_f H_{298}^\circ \text{ of MoO}_3(\text{s}) = (-745.2 \pm 0.4)$	[76]
6	$2 \text{ Bi}(\text{s}) + \text{Mo}(\text{s}) + 3 \text{ O}_2(\text{g}) = \text{Bi}_2\text{MoO}_6(\text{s})$	$\Delta H_6 = \Delta H_1 + \Delta H_2 + \Delta H_4 + \Delta H_5 - \Delta H_3 =$ $\Delta_f H_{298}^\circ \text{ of Bi}_2\text{MoO}_6(\text{s}) = (-1385.7 \pm 3.9)^{\text{c}}$	-

^aTemperature of the calorimeter prior to the actual experiment was stable within $\pm 0.001 \text{ K}$. ^bExpanded uncertainties, $U_c(\Delta H_i)$ are calculated as 2σ of the mean and are at the 95 % confidence level. ^cCombined expanded uncertainties, $U_c(\Delta H)$, are calculated as 2σ of the mean and are at the 95 % confidence level.

Table 3.19 Thermodynamic reaction schemes for obtaining the enthalpies of formation from oxides and elements for Bi₆Mo₂O₁₅ (s) at T = 298.15 K^a (s = solid, soln = aqueous solution, g = gas)

No	Reaction	Enthalpies (kJ mol ⁻¹)	Source of data
1	Bi ₂ O ₃ (s) + 6 NaOH (soln) = (2 Bi ³⁺ + 6 OH ⁻ + 6 Na ⁺ + 3 O ²⁻) (soln)	$\Delta H_1 = (-42.74 \pm 0.77)^b$	This work
2	MoO ₃ (s) + 2 NaOH (soln) = (2 Na ⁺ + MoO ₄ ²⁻ + H ₂ O) (soln)	$\Delta H_2 = (-79.82 \pm 1.19)^b$	This work
3	Bi ₆ Mo ₂ O ₁₅ (s) + 22 NaOH (soln) = (6 Bi ³⁺ + 18 OH ⁻ + 22 Na ⁺ + 9 O ²⁻ + 2 MoO ₄ ²⁻ + 2 H ₂ O) (soln)	$\Delta H_3 = (-145.40 \pm 2.55)^b$	This work
4	2 Bi (s) + 3/2 O ₂ (g) = Bi ₂ O ₃ (s)	$\Delta H_4 = \Delta_f H_{298}^\circ \text{ of Bi}_2\text{O}_3 \text{ (s)} = (-570.70 \pm 3.35)$	[75]
5	5Mo (s) + 3/2 O ₂ (g) = MoO ₃ (s)	$\Delta H_5 = \Delta_f H_{298}^\circ \text{ of MoO}_3 \text{ (s)} = (-745.2 \pm 0.4)$	[76]
6	6 Bi (s) + 2 Mo (s) + 15/2 O ₂ (g) = Bi ₆ Mo ₂ O ₁₅ (s)	$\Delta H_6 = 3\Delta H_1 + 2\Delta H_2 + 3\Delta H_4 + 2\Delta H_5 - \Delta H_3 =$ $\Delta_f H_{298}^\circ \text{ of Bi}_6\text{Mo}_2\text{O}_{15} \text{ (s)} = (-3345.0 \pm 10.9)^c$	-

^aTemperature of the calorimeter prior to the actual experiment was stable within ± 0.001 K. ^bExpanded uncertainties, U_c (ΔH_i) are calculated as 2σ of the mean and are at the 95 % confidence level. ^cCombined expanded uncertainties, $U_c(\Delta H)$, are calculated as 2σ of the mean and are at the 95 % confidence level.

Table 3.20 Thermodynamic reaction schemes for obtaining the enthalpies of formation from oxides and elements for Bi₆MoO₁₂(s) at T = 298.15 K^a (s = solid, soln = aqueous solution, g = gas)

No	Reaction	Enthalpies (kJ mol ⁻¹)	Source of data
1	Bi ₂ O ₃ (s) + 6 NaOH (soln) = (2 Bi ³⁺ + 6 OH ⁻ + 6 Na ⁺ + 3 O ²⁻) (soln)	ΔH ₁ = (-42.74 ± 0.77) ^b	This work
2	MoO ₃ (s) + 2 NaOH (soln) = (2 Na ⁺ + MoO ₄ ²⁻ + H ₂ O) (soln)	ΔH ₂ = (-79.82 ± 1.19) ^b	This work
3	Bi ₆ MoO ₁₂ (s) + 20 NaOH (soln) = (6 Bi ³⁺ + 18 OH ⁻ + 20 Na ⁺ + 9 O ²⁻ + MoO ₄ ²⁻ + H ₂ O) (soln)	ΔH ₃ = (-60.15 ± 1.08) ^b	This work
4	2 Bi (s) + 3/2 O ₂ (g) = Bi ₂ O ₃ (s)	ΔH ₄ = Δ _f H ₂₉₈ ^o of Bi ₂ O ₃ (s) = (-570.70 ± 3.35)	[75]
5	Mo (s) + 3/2 O ₂ (g) = MoO ₃ (s)	ΔH ₅ = Δ _f H ₂₉₈ ^o of MoO ₃ (s) = (-745.2 ± 0.4)	[76]
6	6 Bi (s) + Mo (s) + 6 O ₂ (g) = Bi ₆ MoO ₁₂ (s)	ΔH ₆ = 3ΔH ₁ + ΔH ₂ + 3ΔH ₄ + ΔH ₅ - ΔH ₃ = Δ _f H ₂₉₈ ^o of Bi ₆ MoO ₁₂ (s) = (-2605.2 ± 10.4) ^c	-

^aTemperature of the calorimeter prior to the actual experiment was stable within ± 0.001 K. ^bExpanded uncertainties, U_c(ΔH), are calculated as 2σ of the mean and are at the 95 % confidence level. ^cCombined expanded uncertainties, U_c(ΔH) are calculated as 2σ of the mean and are at the 95 % confidence level.

Using these relative uncertainties, the combined expanded uncertainty was calculated by multiplying with the highest value of the measured heat capacity and is given in the fitted expressions of heat capacities of bismuth molybdates.

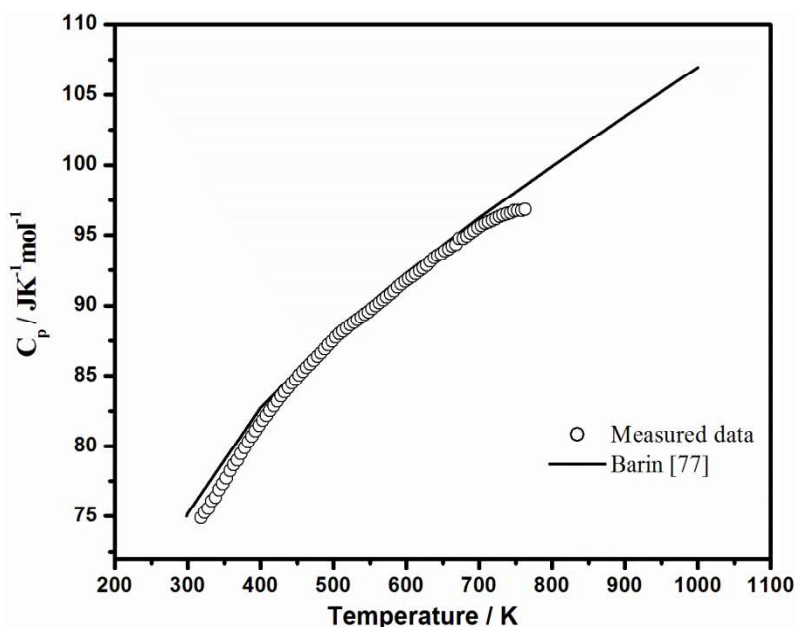


Fig. 3.19 Variation of molar heat capacity of MoO_3 (s) with temperature

Table 3.21 Heat capacity of MoO_3 (s) at $P = 0.1\text{MPa}^a$

T / K^a	$C_p / \text{J K}^{-1} \text{mol}^{-1}$		Observed deviation from the reported values / $\text{J K}^{-1} \text{mol}^{-1}$
	Measured data ^b	Reported values [77] ^c	
318	74.9	76.9	2.0
353	77.7	79.7	2.0
403	81.8	82.9	1.1
453	85.1	85.7	0.6
503	87.7	88.1	0.4
553	89.8	90.4	0.6
603	91.9	92.4	0.5
653	93.9	94.4	0.5
703	95.7	96.4	0.7
753	96.7	98.2	1.5
763	96.8	98.6	1.8

^a Standard uncertainties, u , are $u(T) = 0.4 \text{ K}$ and $u(P) = 0.8 \text{ kPa}$. ^b Maximum relative uncertainty is 0.03 with 0.95 level of confidence. ^c Barin [77]

3.4.11.2 Molar heat capacity of $\text{Bi}_2\text{Mo}_3\text{O}_{12}$ (s)

The XRD patterns of the $\text{Bi}_2\text{Mo}_3\text{O}_{12}$ (s) samples retrieved after heat capacity measurements were identical to their XRD patterns before the measurements indicating that the compound had not undergone any changes during the measurements. Fig. 3.20 represents the experimental heat capacity of $\text{Bi}_2\text{Mo}_3\text{O}_{12}$ (s) as a function of temperature over the range of 328 to 818 K. The data can be fitted to the following least squares expression:

$$C_p \pm 16.4 / \text{J K}^{-1} \text{mol}^{-1} = 416.7 - 7.1 \times 10^{-3} T - 8.8 \times 10^6 T^{-2}; T = 328\text{-}818 \text{ K} \quad (3.25)$$

The error given in the expression is the combined expanded uncertainty with 0.95 level of confidence.

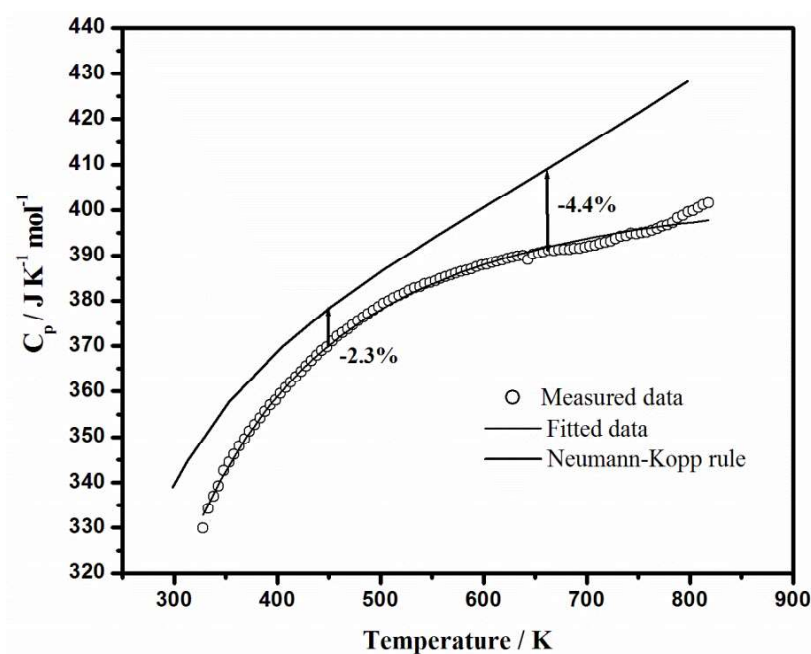


Fig. 3.20 Variation of molar heat capacity of $\text{Bi}_2\text{Mo}_3\text{O}_{12}$ (s) with temperature

The measured heat capacity values of $\text{Bi}_2\text{Mo}_3\text{O}_{12}$ (s) along with the fitted values for the selected temperatures are given in Table 3.22. The heat capacity of $\text{Bi}_2\text{Mo}_3\text{O}_{12}$ (s) was also computed by Neumann-Kopp's rule (NKR) using the heat capacity data for Bi_2O_3 (s) and MoO_3 (s) [78], and is compared with the measured

data in Fig. 3.20. The comparison plot reveals that the experimental heat capacity is lower than the estimated data and the percentage deviation is $\sim 3\%$ at 573 K, which is the mean temperature of the measurement.

Table 3.22 Thermodynamic functions of $\text{Bi}_2\text{Mo}_3\text{O}_{12}$ (s) at $P = 0.1 \text{ MPa}^a$

T / K ^a	$C_p / \text{J K}^{-1} \text{ mol}^{-1}$		$H_T^\circ - H_{298}^\circ$ / J mol^{-1b}	S_T° / $\text{J K}^{-1} \text{ mol}^{-1b}$	$-(G_T^\circ - H_{298}^\circ) / T$ / $\text{J K}^{-1} \text{ mol}^{-1b}$
	Measured data	Fitted values			
298.15	-	315.6	0	358.2 ± 1.4	358.5 ± 1.4
328	329.9	332.6	9687.0 ± 489.5	389.1 ± 1.6	359.9 ± 2.2
353	344.4	343.6	18144.8 ± 899.5	414.0 ± 2.8	362.9 ± 3.8
403	359.5	359.7	35754.6 ± 1719.5	460.6 ± 4.9	372.2 ± 6.5
453	371.0	370.6	54029.6 ± 2539.5	503.3 ± 6.9	384.4 ± 8.9
503	379.4	378.3	72766.3 ± 3359.5	542.6 ± 8.6	398.2 ± 10.9
553	384.5	384.0	91834.6 ± 4179.5	578.7 ± 10.1	413.0 ± 12.6
603	388.1	388.2	111147.8 ± 4999.5	612.1 ± 11.6	428.2 ± 14.2
653	390.6	391.4	130645.6 ± 5819.5	643.2 ± 12.9	443.5 ± 15.6
703	392.1	393.9	150284.8 ± 6639.5	672.2 ± 14.1	458.7 ± 16.9
753	395.0	395.8	170033.8 ± 7459.5	699.3 ± 15.2	473.9 ± 18.1
798	399.5	397.2	187882.0 ± 8197.5	722.3 ± 16.1	487.2 ± 19.1
818	401.6	397.7	195833.3 ± 8525.5	732.1 ± 16.6	493.1 ± 19.6

^aStandard uncertainties, u , are $u(T) = 0.4 \text{ K}$ and $u(P) = 0.8 \text{ kPa}$. The reported uncertainties are the combined expanded uncertainties. The combined expanded uncertainty, U_c , is $U_c(C_p) = 16.4 \text{ J K}^{-1} \text{ mol}^{-1}$.

As no thermochemical data are available for $\text{Bi}_2\text{Mo}_3\text{O}_{12}$ (s), the S_{298}° value of $\text{Bi}_2\text{Mo}_3\text{O}_{12}$ (s) was computed by NKR using the S_{298}° values of Bi_2O_3 (s) and MoO_3 (s) [78]. Since the experimental value of C_p of $\text{Bi}_2\text{Mo}_3\text{O}_{12}$ (s) at 298.15 K is 6.9% lower than that obtained by the NKR estimation, it is assumed that the S_{298}° value of $\text{Bi}_2\text{Mo}_3\text{O}_{12}$ (s) will also be 6.9% lower than the estimated S_{298}° value. Similar assumption has been made in the earlier works [79-81]. Based on this assumption, the

S_{298}° value computed for $\text{Bi}_2\text{Mo}_3\text{O}_{12}$ (s) is $358.2 \text{ J K}^{-1} \text{ mol}^{-1}$. Using this value, other thermodynamic functions of $\text{Bi}_2\text{Mo}_3\text{O}_{12}$ (s) were computed and are given in Table 3.22.

3.4.11.3 Molar heat capacity of monoclinic phase of Bi_2MoO_6 (s)

XRD pattern of the monoclinic phase of Bi_2MoO_6 (s) pellets after the heat capacity measurements were identical to the initial pattern, indicating that no changes had happened to the compound during the calorimetric runs. The temperature dependence of heat capacity of Bi_2MoO_6 (s) obtained by measurement over the temperature range of 318 to 818 K is shown in Fig. 3.21 and can be represented by the least squares fitted expression:

$$C_p \pm 8.8 / \text{J K}^{-1} \text{ mol}^{-1} = 221.4 - 1.5 \times 10^{-3} T - 3.9 \times 10^6 T^{-2} \quad (T : 318 - 818 \text{ K}) \quad (3.26)$$

The error given in the expression is the combined expanded uncertainty with 0.95 level of confidence.

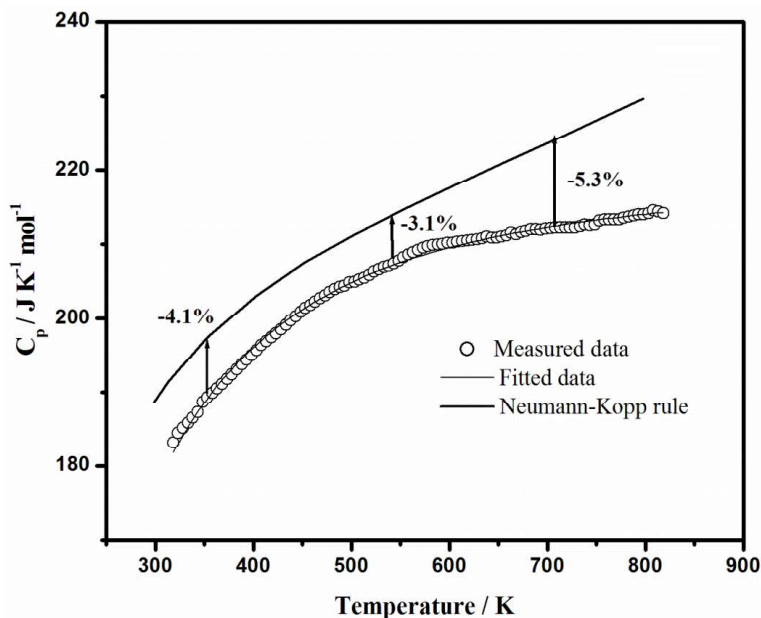


Fig. 3.21 Variation of molar heat capacity of monoclinic- Bi_2MoO_6 with temperature

The measured heat capacity values of Bi_2MoO_6 (s) along with the fitted values for the selected temperatures are given in Table 3.23. Each measured data is the mean of sixteen measurements obtained by measuring the C_p using two sample pellets. The heat capacity of Bi_2MoO_6 (s) was also computed by Neumann-Kopp's rule (NKR) using the heat capacity data for Bi_2O_3 (s) and MoO_3 (s) [78], and is compared with the measured data in Fig. 3.21.

Table 3.23 Thermodynamic functions of monoclinic- Bi_2MoO_6 (s) at $P = 0.1\text{MPa}$ ^a

T / K ^a	$C_p / \text{J K}^{-1} \text{mol}^{-1}$		$H_T^\circ - H_{298}^\circ$ / J mol^{-1b}	S_T° / $\text{J K}^{-1} \text{mol}^{-1b}$	$-(G_T^\circ - H_{298}^\circ) / T$ / $\text{J K}^{-1} \text{mol}^{-1b}$
	Measured data	Fitted values			
298.15	-	177.1	0	214.3 ± 0.5	214.3 ± 0.5
318	183.2	182.4	3569.1 ± 174.7	225.8 ± 0.6	214.7 ± 0.8
328	185.1	184.7	5404.4 ± 262.7	231.5 ± 0.8	215.1 ± 1.2
353	189.3	189.6	10084.5 ± 482.7	245.2 ± 1.5	216.7 ± 2.0
403	195.7	196.8	19755.4 ± 922.7	270.8 ± 2.7	221.9 ± 3.5
453	201.4	201.7	29725.2 ± 1362.7	294.1 ± 3.7	228.6 ± 4.8
503	204.9	205.2	39903.5 ± 1802.7	315.4 ± 4.6	236.2 ± 5.8
553	208.2	207.8	50232.9 ± 2242.7	334.9 ± 5.4	244.2 ± 6.8
603	210.2	209.8	60674.8 ± 2682.7	353.0 ± 6.2	252.5 ± 7.6
653	211.0	211.3	71202.4 ± 3122.7	369.7 ± 6.9	260.9 ± 8.4
703	212.2	212.5	81796.8 ± 3562.7	385.4 ± 7.5	269.2 ± 9.1
753	213.2	213.4	92443.8 ± 4002.7	400.0 ± 8.2	277.4 ± 9.7
818	214.2	214.3	106346.7 ± 4574.7	417.7 ± 8.9	287.8 ± 10.5

^a Standard uncertainties, u , are $u(T) = 0.4 \text{ K}$ and $u(P) = 0.8 \text{ kPa}$. ^bThe reported uncertainties are the combined expanded uncertainties. The combined expanded uncertainty, U_c , is $U_c(C_p) = 8.8 \text{ J K}^{-1} \text{mol}^{-1}$

As seen in the figure, the experimental heat capacity is lower than the estimated data and the percentage deviation is $\sim 3.1\%$ at 568 K, which is the mean temperature of the measurement. As no thermochemical data of Bi_2MoO_6 (s) are available, its S_{298}° value was computed by Neumann-Kopp Rule (NKR) using the S_{298}° values of Bi_2O_3 (s) and MoO_3 (s) [78]. Based on this assumption, the S_{298}° value

computed for Bi_2MoO_6 (s) is $208.8 \text{ J K}^{-1} \text{ mol}^{-1}$. Using this value, the thermodynamic functions of Bi_2MoO_6 (s) were computed and given in Table 3.23.

3.4.11.4 Molar heat capacity of $\text{Bi}_6\text{Mo}_2\text{O}_{15}$ (s)

The XRD pattern of $\text{Bi}_6\text{Mo}_2\text{O}_{15}$ (s) retrieved after DSC measurements was identical to the initial pattern indicating that no changes had happened to the compound during the calorimetric runs. The variation of molar heat capacity of $\text{Bi}_6\text{Mo}_2\text{O}_{15}$ (s) obtained is shown in Fig. 3.22 and the fitted expression is given below:

$$C_p \pm 23.4 / \text{J K}^{-1} \text{ mol}^{-1} = 529.8 - 67.9 \times 10^{-3} T - 6.3 \times 10^6 T^{-2} \quad (T : 318 - 808 \text{ K}) \quad (3.27)$$

The error given in the expression is the combined expanded uncertainty with 0.95 level of confidence.

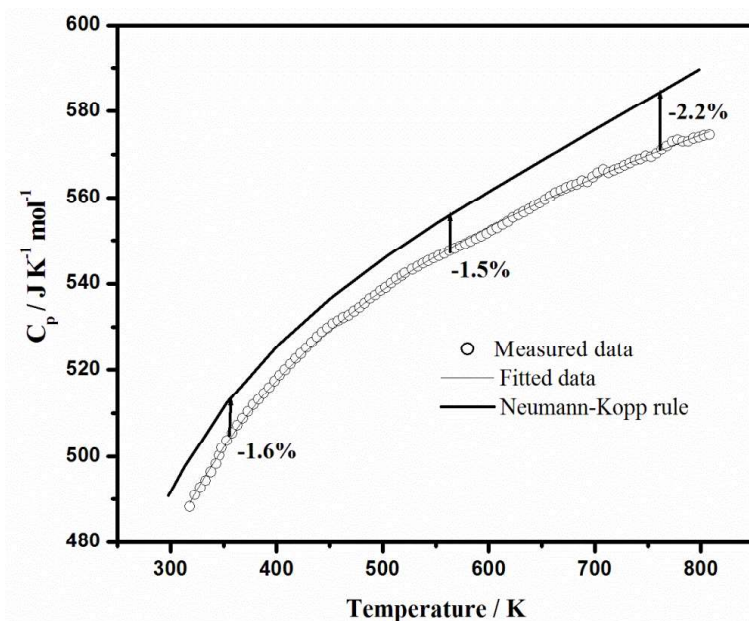


Fig. 3.22 Variation of heat capacity of $\text{Bi}_6\text{Mo}_2\text{O}_{15}$ (s) with temperature

The thermodynamic functions of $\text{Bi}_6\text{Mo}_2\text{O}_{15}$ (s) were calculated based on the measured heat capacity data and presented in Table 3.24. Fig.3.22 also shows the comparison of experimentally obtained heat capacities and those estimated by NKR. It is found that the measured heat capacities are lower than the estimated heat

capacities and the percentage deviation is ~1.5 % at the mean temperature of measurement (563 K).

Table 3.24 Thermodynamic functions of Bi₆Mo₂O₁₅ (s) at P = 0.1MPa^a

T / K ^a	C _p / J K ⁻¹ mol ⁻¹		H _T ^o - H ₂₉₈ ^o / J mol ^{-1b}	S _T ^o / J K ⁻¹ mol ^{-1b}	-(G _T ^o - H ₂₉₈ ^o)/T / J K ⁻¹ mol ^{-1b}
	Measured data	Fitted values			
298.15	-	479.1	0	545.0 ± 1.1	545.0 ± 1.1
318	489.1	489.0	9610.8 ± 464.5	576.2 ± 1.5	545.9 ± 2.1
343	499.5	499.5	21970.9 ± 1049.5	613.6 ± 3.3	549.5 ± 4.5
401	517.9	517.8	51504.5 ± 2406.7	693.1 ± 6.9	564.6 ± 9.2
451	529.4	529.4	77697.6 ± 3576.7	754.6 ± 9.7	582.3 ± 12.5
500	538.7	538.5	103870.4 ± 4723.3	809.7 ± 12.1	602.0 ± 15.3
550	546.4	546.3	130997.5 ± 5893.3	861.4 ± 14.3	623.2 ± 17.9
600	553.1	553.1	158485.8 ± 7063.3	909.2 ± 16.4	645.1 ± 20.2
650	559.1	559.1	186291.3 ± 8233.3	953.8 ± 18.2	667.2 ± 22.2
700	564.5	564.5	214382.3 ± 9403.3	995.4 ± 20.0	689.1 ± 24.1
750	569.6	569.6	242735.8 ± 10573.3	1034.5 ± 21.6	710.9 ± 25.8
800	574.3	574.3	271334.4 ± 11743.3	1071.4 ± 23.1	732.3 ± 27.4
808	575.0	575.1	275932.0 ± 11930.5	1077.1 ± 23.3	735.6 ± 27.6

^aStandard uncertainties, *u*, are $u(T) = 0.4 \text{ K}$ and $u(P) = 0.8 \text{ kPa}$. ^bThe reported uncertainties are the combined expanded uncertainties. The combined expanded uncertainty, U_c , is $U_c(C_p) = 23.4 \text{ J K}^{-1} \text{ mol}^{-1}$

3.4.12 Consistency of the measured thermodynamic data

The consistency between the standard enthalpy of formation of Bi₂MoO₆(s) determined by solution calorimetry experiments, with the standard enthalpy of formation at the mid temperature of emf measurements is determined as follows:

3.4.12.1 Monoclinic Bi₂MoO₆ (s)

The standard molar Gibbs energy of formation of monoclinic Bi₂MoO₆ (s) obtained by emf method is given by the expression (3.23);

$$\Delta_f G^\circ < Bi_2MoO_6 > \pm 0.8 / kJ mol^{-1} = -1382.3 + 0.5064(T / K) \quad (T : 772 - 1023K) \quad (3.23)$$

The mid temperature of this measurement is 898 K. By expressing the standard Gibbs energy of formation as $\Delta G = \Delta H - T\Delta S$, the enthalpy of formation of $Bi_2MoO_6(s)$ at 898 K can be deduced as

$$\Delta_f H_{898}^\circ < Bi_2MoO_6 > = -1382.3 kJ mol^{-1}$$

This can be related to the standard molar enthalpy of formation of $Bi_2MoO_6(s)$ at 298.15 K as below:

$$\Delta_f H_{298K}^\circ < Bi_2MoO_6 > = \Delta_f H_{898K}^\circ < Bi_2MoO_6 > - \left[\int_{298}^{544} \Delta C_p dT - 2\Delta H_{fusion}^{Bi} + \int_{544}^{898} \Delta C_p dT \right] \quad (3.28)$$

where ΔC_p is the difference in the heat capacities of $Bi_2MoO_6(s)$ and its constituent elements Bi (solid / liquid), Mo and O_2 and ΔH_{fusion}^{Bi} is the enthalpy of fusion of Bi at 544 K. The second term of the equation (3.28) can be obtained as:

$$\begin{aligned} \int_{298}^{544} \Delta C_p dT - 2\Delta H_{fusion}^{Bi} + \int_{544}^{898} \Delta C_p dT &= \int_{298}^{544} [C_p^{Bi_2MoO_6} - (2C_p^{Bi(s)} + C_p^{Mo(s)} + 3C_p^{O_2(g)})] dT - \\ 2\Delta H_{fusion}^{Bi} + \int_{544}^{898} [C_p^{Bi_2MoO_6} - (2C_p^{Bi(l)} + C_p^{Mo(s)} + 3C_p^{O_2(g)})] dT & \quad (3.29) \end{aligned}$$

The data of heat capacity for Bi, Mo and O_2 were taken from ref [78] and that of $Bi_2MoO_6(s)$ from our experimental studies as given by equation (3.26) and are given below:

$$C_p < Bi_2MoO_6 > / JK^{-1} mol^{-1} = 221.4 - 1.5 \times 10^{-3} T - 3.9 \times 10^{-6} T^{-2} \quad (T : 318 - 818K) \quad (3.26)$$

$$C_p < Bi > / JK^{-1} mol^{-1} = 28.033 - 24.267 \times 10^{-3} T + 50.208 \times 10^{-6} T^2 \quad (T : 298 - 544K) \quad (3.30)$$

$$C_p \{Bi\} / JK^{-1} mol^{-1} = 23.359 - 9.736 \times 10^{-3} T - 0.280 \times 10^{-6} T^{-2} + 3.238 \times 10^{-6} T \quad (T : 544 - 1835K) \quad (3.31)$$

$$C_p < Mo > / JK^{-1} mol^{-1} = 29.732 + 3.138 \times 10^{-3} T + 1.661 \times 10^{-6} T^{-2} - 0.720 \times 10^{-6} T \quad (T : 298 - 2896K) \quad (3.32)$$

$$C_p(O_2) / JK^{-1}mol^{-1} = 29.154 + 6.477 \times 10^{-3} T - 0.184 \times 10^{-6} T^2 - 1.017 \times 10^{-6} T \quad (T: 298-3200 K) \quad (3.33)$$

By substituting the above values in equation (3.29), we get

$$\int_{298}^{544} \Delta C_p dT - 2\Delta H_{fusion}^{Bi} + \int_{544}^{898} \Delta C_p dT = -5.24 kJ mol^{-1} \text{ and hence,}$$

$$\Delta_f H_{298K}^o < Bi_2MoO_6 > = -1382.3 + 5.24 = -1377.1 kJ mol^{-1}.$$

$\Delta_f H_{298K}^o < Bi_2MoO_6 >$ obtained by solution calorimetry experiment is -1385.7 kJ mol⁻¹ and is found to be in agreement with the deduced value of -1377.1 kJ mol⁻¹.

3.5 References

1. L. Brewer, Molybdenum: Physico-chemical properties of its compounds and alloys, Atomic Energy Review Special issue No.7, International Atomic Energy Agency, Vienna, 1980.
2. R.P. Elliott, Constitution of binary alloys, First supplement, McGraw Hill book company, USA, 1965.
3. T.B. Massalski (Ed.), Binary Alloy Phase Diagrams, 2nd Ed., ASM International, 1990.
4. G.W. Horsley, J.T. Maskreg, J. Inst. Metals, 86 (1957) 401-402.
5. D. Risold, B. Hallstedt, L.J. Gauckler, The bismuth-oxygen system, J. Phase. Equilibria. 16 (1995) 223-234.
6. R. Ganesan, T. Gnanasekaran, R.S. Srinivasa, Electrochemical study on determination of diffusivity, activity and solubility of oxygen in liquid bismuth, J. Chem. Thermodyn. 38 (2006) 739-747.

7. L. Brewer, R.H. Lamoreaux, The Mo-O system, Bull. Alloy Phase Diagr. 1 (1980) 85-89.
8. K. Tonosaki, Bull. Inst. Phys. Chem. Res. Jpn. 19 (1940) 126-132.
9. N.A. Gokcen, Thermodynamic properties of molybdenum dioxide, J. Met. 197 (1953) 1019-1020.
10. M. Gleiser, J. Chapman, Free energy of formation of molybdenum oxide and carbide, J. Phys. Chem. 66 (1962) 1539-1540.
11. R.A. Rapp, The standard free energy of formation of MoO₂, Trans. Metall. Soc. AIME 227 (1963) 371-374.
12. G.B. Barbi, Thermodynamic functions and phase stability limits by electromotive force measurements on solid electrolyte cells, J. Phys. Chem. 68 (1964) 1025-1029.
13. V.N. Drobyshev, T.N. Rezhukhina, L.A. Tarasova, Thermodynamic properties of cobalt-molybdenum alloys, Russ. J. Phys. Chem. 39 (1965) 70-73.
14. C. Vassilev, T. Nikolov, M. Chimbulev, Trans. Inst. Min. Metall. 77 (1968) C36-C38.
15. S. Berglund, P. Kierkegaard, The free energies of formation of WO₂ and MoO₂, Acta Chem. Scand. 23 (1969) 329-330.
16. C.B. Alcock, J.C. Chan, The oxygen permeability of stabilized zirconia electrolytes at high temperatures, Can. Metall. Quart. 11 (1972) 559-567.

17. M. Iwase, M. Yasuda, T. Mori, Free energy of formation of MoO₂ at steelmaking temperature from EMF measurement, *Electrochim. Acta* 24 (1979) 261-266.
18. H. Kleykamp, A. Supawan, Gibbs energies of formation of MoO₂ and Mo₄O₁₁, *J. Less Comm. Met.* 63 (1979) 261L.
19. L. Pejryd, Phase relations and stabilities in the system Ni-MoO₂-O in the temperature range 850-1500 K, *High Temp-High Press.* 16 (1984) 403-408.
20. H.St.C. O'Neill, Mo-MoO₂ (MOM) oxygen buffer and the free energy of formation of MoO₂, *Am. Mineral.* 71 (1986) 1007-1010.
21. K.T. Jacob, G.M. Kale, G.N.K. Iyengar, Phase equilibria and thermodynamic properties in the system Ni-Mo-O, *J. Mater. Sci.* 22 (1987) 4274-4280.
22. J. Bygden, D. Sichen, S. Seetharaman, A thermodynamic study of the molybdenum-oxygen system, *Metall. Mater. Trans. B* 25 (1994) 885-891.
23. K.T. Jacob, V.S. Saji, J. Gopalakrishnan, Y. Waseda, Thermodynamic evidence for phase transition in MoO₂-δ, *J. Chem. Thermodyn.* 39 (2007) 1539-1545.
24. M.R. Antonio, R.G. Teller, D.R. Sandstrom, M. Mehicic, J.F. Brazdil, Structural characterization of bismuth molybdates by X-ray absorption spectroscopy and powder neutron diffraction profile analysis, *J. Phys. Chem.* 92 (1988) 2939-2944.

25. F.D. Hardcastle, I.E. Wachs, Molecular structure of molybdenum oxide in bismuth molybdates by Raman spectroscopy, *J. Phys. Chem.* 95 (1991) 10763-10772.
26. M.T. Le, W.J.M.V. Well, I.V. Driessche, S. Hoste, Spray drying, a versatile synthetic method to control purity in single phases and mixed phases of bismuth molybdates, *Can. J. Chem. Eng.* 83 (2005) 336-343.
27. R.B. Licht, D. Vogt, A.T. Bell, The mechanism and kinetics of propene ammoxidation over α -bismuth molybdates, *J. Catal.* 339 (2016) 228-241.
28. A.P.V. Soares, L.D. Dimitrov, M.C.R.A. Oliveira, L. Hilaire, M.F. Portela, R.K. Grasselli, Synergy effects between β and γ phases of bismuth molybdates in the selective catalytic oxidation of 1-butene, *Appl. Catal. A.* 253 (2003) 191-200.
29. B. Farin, A.H.A.M. Videla, S. Specchia, E.M. Gaigneaux, Bismuth molybdates prepared by solution combustion synthesis for the partial oxidation of propene, *Catal. Today.* 257 (2015) 11-17.
30. L. Sillen, K. Lundberg, *Arkiv Kemi*, 17A (1943) 21.
31. R. Kohlmuller, J. P. Baduad, Etude du systeme $\text{Bi}_2\text{O}_3\text{-MoO}_3$, *Bull. Soc. Chim. Fr.* 10 (1969) 3434-3439.
32. M. Egashira, K. Matsuo, S. Kagawa, T. Seiyama, Phase diagram of the system $\text{Bi}_2\text{O}_3\text{-MoO}_3$, *J. Catal.* 58 (1979) 409-418.

33. C.D. Ling, R.L. Withers, J.G. Thompson, S. Schmid, Structures of $\text{Bi}_{14}\text{WO}_{24}$ and $\text{Bi}_{14}\text{MoO}_{24}$ from neutron powder diffraction data, *Acta. Cryst. B* 55 (1999) 306-312.
34. C. Tomasi, G. Spinolo, G. Chiodelli, A. Magistris, Phase equilibria in the Bi-rich part of the Bi, Mo/O system, *Solid State Ionics*. 99 (1997) 263–268.
35. I.N. Belyaev, N.P. Smolyaninov, The Bi_2O_3 - MoO_3 - PbO ternary system, *Russ. J. Inorg. Chem.* 5 (1962) 579–581.
36. A.C.A.M. Bleijenberg, B. C. Lippens, G. C. A. Schuit, Catalytic oxidation of 1-Butene over bismuth molybdate catalysts: the system Bi_2O_3 - MoO_3 , *J. Catal.* 4 (1965) 581–585.
37. L.M. Vitting, *Vestnik Moskow. Univ., Ser. Khim.* 2 (1966) 60.
38. G. Gattow, Beitrag zur kristallchemie des systems Bi_2O_3 - MoO_3 , *Z. Anorg. Chem.* 298 (1958) 64-71.
39. D.J. Buttrey, D.A. Jefferson, J.M. Thomas, Characterization of a new bismuth molybdate phase – $\text{Bi}_{38}\text{Mo}_7\text{O}_{78}$, *Mat. Res. Bull.* 21 (1986) 739–744.
40. G. Spinolo, C. Tomasi, Fluorite-related phases in the Bi-rich part of the Bi, Mo/O system, *Powder Diffraction*. 12 (1997) 16-19.
41. N. Sharma, R.B. Macquart, M. Christensen, M. Avdeev, Y.S. Chen, C.D. Ling, Structure and crystal chemistry of fluorite-related $\text{Bi}_{38}\text{Mo}_7\text{O}_{78}$ from single crystal X-ray diffraction and ab initio calculations, *J. Solid. State. Chem.* 182 (2009) 1312-1318.

42. E. Vila, J.E. Iglesias, J. Galy, A. Castro, Synthesis and characterization of a novel bismuth-molybdenum oxide and study of its ionic conducting behavior, *Solid State Sci.* 7 (2005) 1369-1376.
43. J. Galy, J.H. Velasco, A.R.L. Canovas, E. Vila, A. Castro, Ab initio structure determination and Rietveld refinement of $\text{Bi}_{10}\text{Mo}_3\text{O}_{24}$ the member $n = 3$ of the $\text{Bi}_{2n+4}\text{Mo}_n\text{O}_{6(n+1)}$ series, *J. Solid. State. Chem.* 182 (2009) 1177-1187.
44. S. Miyazawa, A. Kawana, H. Koizumi, H. Iwasaki, Single crystals in the Bi_2O_3 - MoO_3 binary system: growth and optical properties, *Mat. Res. Bull.* 9 (1974) 41–52.
45. L. Boon, R. Metselaar, Transport properties of $\text{Bi}_6\text{Mo}_2\text{O}_{15}$, *Solid State Ionics.* 16 (1985) 201–210.
46. E. Vila, J.M. Rojo, J.E. Iglesias, A. Castro, Polymorphism and electrical properties in the new oxide $\text{Bi}_6\text{Mo}_2\text{O}_{15}$, *Chem. Mater.* 16 (2004) 1732-1739.
47. E. Vila, A.R.L. Canovas, J. Galy, J.E. Iglesias, A. Castro, $\text{Bi}_{2n+4}\text{Mo}_n\text{O}_{6(n+1)}$ with $n = 3, 4, 5, 6$: A new series of low-temperature stable phases in the $m\text{Bi}_2\text{O}_3$ - MoO_3 system ($1.0 < m < 1.7$): Structural relationships and conductor properties, *J. Solid State Chem.* 180 (2007) 661-669.
48. J. Zemann, Die Kristallstruktur von koechlinit, Bi_2MoO_6 , *Heidelberger Beitr. Mineral. Petrogr.* 5 (1956) 139-145.
49. L.Ya. Erman, E.L. Galperin, B.P. Sobolev, Equilibrium diagram of the Bi_2O_3 - MoO_3 system, *Russ. J. Inorg. Chem.* 16 (1971) 258-261.

50. T. Chen, G.S. Smith, The compounds and the phase diagram of MoO₃-rich Bi₂O₃-MoO₃ system, *J. Solid State Chem.* 13 (1975) 288–297.
51. G. Blasse, Polymorphism of Bi₂MoO₆, *J. Inorg. Nucl. Chem.* 28 (1966) 1124–1125.
52. L.Ya. Erman, E.L. Galperin, Modifications of Bi₂MoO₆, *Russ. J. Inorg. Chem.* 13 (1968) 487.
53. A. Watanabe, H. Kodama, Polymorphic transformations of Bi₂MoO₆, *J. Solid State Chem.* 35 (1980) 240–245.
54. H. Kodama, A. Watanabe, The relative stabilities of Bi₂MoO₆ polymorphs, *J. Solid State Chem.* 56 (1985) 225-229.
55. A.R. Lim, J.H. Chang, S.H. Choh, M.S. Jang, A study of the phase transition in Bi₂MoO₆ single crystals, *J. Korean Phys. Soc.* 25 (1992) 109-112.
56. D.J. Buttrey, T. Vogt, B.D. White, High-temperature incommensurate-to-commensurate phase transition in the Bi₂MoO₆ catalyst, *J. Solid State Chem.* 155 (2000) 206-215.
57. L.Ya. Erman, E.L. Galperin, I.K. Kolchin, G.F. Dobrzhanskii, K.S. Chernyshev, The Bi₂O₃-MoO₃ system, *Russ. J. Inorg. Chem.* 9 (1964) 1174-1176.
58. L.Ya. Erman, E.L. Galperin, New data on the crystal structure of Bi₂O₃.2MoO₃, *Russ. J. Inorg. Chem.* 11 (1966) 122.

59. Ph.A. Batist, A.H.W.M. der Kinderen, Y. Leeuwenburgh, F.A.M.G. Metz, G.C.A. Schuit, Catalytic oxidation of 1-Butene over bismuth molybdate catalysts: dependence of activity on structures of catalysts, *J. Catal.* 12 (1968) 45-60.
60. B. Grzybowska, J. Haber, J. Komorek, Chemistry of Bi-Mo oxide catalysts: phase composition of catalysts and its relation to structure of precursors, *J. Catal.* 25 (1972) 25-32.
61. F. Zambonini, *Gazz. Chim. Ital.* 50 (1920) 128.
62. T. Chen, Crystal growth of BaMoO_4 , $\text{Bi}_2\text{O}_3 \cdot 3\text{MoO}_3$ and $\text{Bi}_2\text{O}_3 \cdot 2\text{MoO}_3$ from molten salt solution by pulling seed method, *J. Cryst. Growth.* 20 (1973) 29-37.
63. R.N. Vannier, G. Mairesse, F. Abraham, G. Nowogrocki, $\text{Bi}_{26}\text{Mo}_{10}\text{O}_8$ solid solution type in the Bi_2O_3 - MoO_3 - V_2O_5 ternary diagram, *J. Solid State Chem.* 122 (1996) 394-406.
64. R.N. Vannier, F. Abraham, G. Nowogrocki, G. Mairesse, New structural and electrical data on Bi-Mo mixed oxides with a structure based on $[\text{Bi}_{12}\text{O}_{14}]_\infty$ columns, *J. Solid State. Chem.* 142 (1999) 294-304.
65. D.J. Buttrey, T. Vogt, G.P.A. Yap, A.L. Rheingold, The structure of $\text{Bi}_{26}\text{Mo}_{10}\text{O}_{69}$, *Mat. Res. Bull.* 32 (1997) 947-963.
66. R. Enjalbert, G. Hasselmann, J. Galy, $[\text{Bi}_{12}\text{O}_{14}\text{E}_{12}]_n$ columns and lone pairs E in $\text{Bi}_{13}\text{Mo}_4\text{VO}_3\text{E}_{13}$: synthesis, crystal structure and chemistry of the Bi_2O_3 - MoO_3 - V_2O_5 system, *J. Solid. State. Chem.* 131 (1997) 236-245.

67. M. Huve, R.N. Vannier, G. Mairesse, EDS and TEM study of the family of compounds with a structure based on $[\text{Bi}_{12}\text{O}_{14}]_{\infty}$ columns in the Bi_2O_3 - MoO_3 binary system, *J. Solid. State. Chem.* 149 (2000) 276-283.
68. D.J. Buttrey, A survey of the Bi_2O_3 - MoO_3 binary system in Turning points in solid state materials and surface science- A book in celebration of the life and work of Sir John Meurig Thomas edited by K.D.M. Harris, P.P. Edwards, Royal Society of Chemistry, Cambridge, UK, 2008, p. 754-777.
69. M. Hartmanova, M.T. Le, I.V. Driessche, S. Hoste, F. Kundracik, Phase composition and charge transport in bismuth molybdates, *Russ.J. Electrochem.* 41 (2005) 455-460.
70. R. Sabbah, A.X. Wu, J.S. Chickos, M.L.P. Leitao, M.V. Roux, L.A. Torres, Reference materials for calorimetry and differential thermal analysis, *Thermochim. Acta.* 331 (1999) 93-204.
71. K. Majid, R. Mushtaq, S. Ahmad, Synthesis, characterization and coordinating behavior of aminoalcohol complexes with transition metals, *E-J.Chem.* 5 (2008) 969-979.
72. W.T. Miller, Some complex sodium bismuth salts of triethanolamine and triisopropanolamine, *J. Am. Chem. Soc.* 62 (1940) 2707-2709.
73. R.D. Hancock, I. Cukrowski, J. Baloyi, J. Mashishi, The affinity of bismuth (III) for nitrogen donor ligands, *J. Chem. Soc. Dalton Trans.* (1993) 2895-2899.

74. G. Szalontai, G. Kiss, L. Bartha, Equilibria of mononuclear oxomolybdenum (VI) complexes of triethanolamine- A multinuclear dynamic magnetic resonance study of structure and exchange mechanisms, *Spectrochim. Acta Part A* 59 (2003) 1995-2007.
75. O. Kubachewski, C.B. Alcock, *Metallurgical thermochemistry*, fifth ed., Pergamon, Oxford, 1979.
76. G.B. Naumov, B.N. Ryzhenko, I.L. Khodakovsky, *Reference book of thermodynamic values (for geologists) (in Russian)*: Atomizdat: Moskva, 1971
77. I. Barin, *Thermochemical data of pure substances*, third ed., VCH, Weinheim (Federal Republic of Germany), 1995.
78. O. Knacke, O. Kubachewski, K. Hesselmann, *Thermochemical properties of inorganic substances*, Vol 2, second ed., Springer, Berlin, 1991.
79. R. Venkatakrisnan, K. Nagarajan, P.R. Vasudeva Rao, Heat capacity measurements on BaThO₃ and BaCeO₃, *J. Nucl. Mater.* 299 (2001) 28–31.
80. R. Ganesan, R. Venkatakrisnan, R. Asuvathraman, K. Nagarajan, T. Gnanasekaran, R.S. Srinivasa, Heat capacities of PbBi₁₂O₁₉(s) and Φ -Pb₅Bi₈O₁₇(s), *Thermochim Acta* 439 (2005) 27-31.
81. S.K. Sahu, M. Sahu, R.S. Srinivasa, T. Gnanasekaran, Determination of heat capacities of PbCrO₄(s), Pb₂CrO₅(s) and Pb₅CrO₈(s), *Monatsh Chem.* 143 (2012) 1207-1214.

Chapter 4

Thermochemical studies on Pb-Mo-O system

4.1. Introduction

Studies carried out towards the determination of phase diagram of ternary Pb-Mo-O system and thermochemical data of ternary compounds in this system are described in the present chapter.

4.2 Literature survey

4.2.1 Pb-Mo system

The binary phase diagram of Pb-Mo system is shown in Fig. 4.1 [1]. No intermetallic compounds are formed between Pb and Mo. The melting point of Pb is 600.5 K. The solubility of Mo in liquid Pb is reported to be $<10^{-4}$ at% at 1143 K [2] and <0.011 at% at 1479 K [3]. Solubility of Pb in Mo is nearly zero.

4.2.2 Pb-O system

The binary phase diagram of Pb-O system is shown in Fig. 4.2 [4]. The stable oxides present in the system are PbO, Pb₃O₄, Pb₁₂O₁₇, Pb₁₂O₁₉ and PbO₂. Among these oxides, both PbO and Pb₃O₄ exhibit polymorphism. PbO exists in the tetragonal form up to 762 K and above this temperature it exists in the orthorhombic form up to its melting point of 1160 K. Pb₃O₄ exists in orthorhombic and tetragonal form and the transition from orthorhombic to tetragonal phase occurs at ~143 K. Ganesan et al. [5] reported the solubility of oxygen in liquid lead and is given by the following equation:

$$\log(S / \text{at\% O}) = -5100/T + 4.32 \quad (T : 815 - 1090 \text{ K}) \quad (4.1)$$

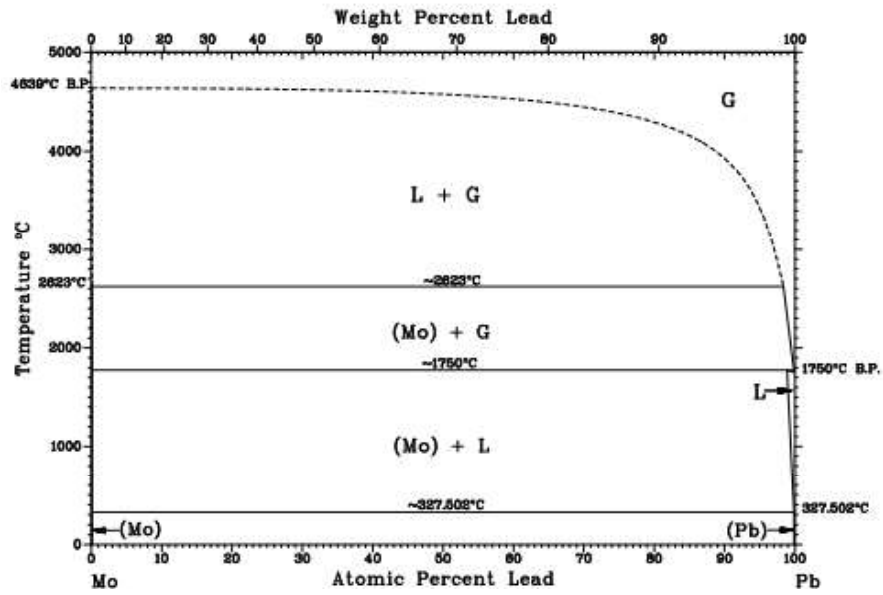


Fig. 4.1 Phase diagram of Pb-Mo system [1]

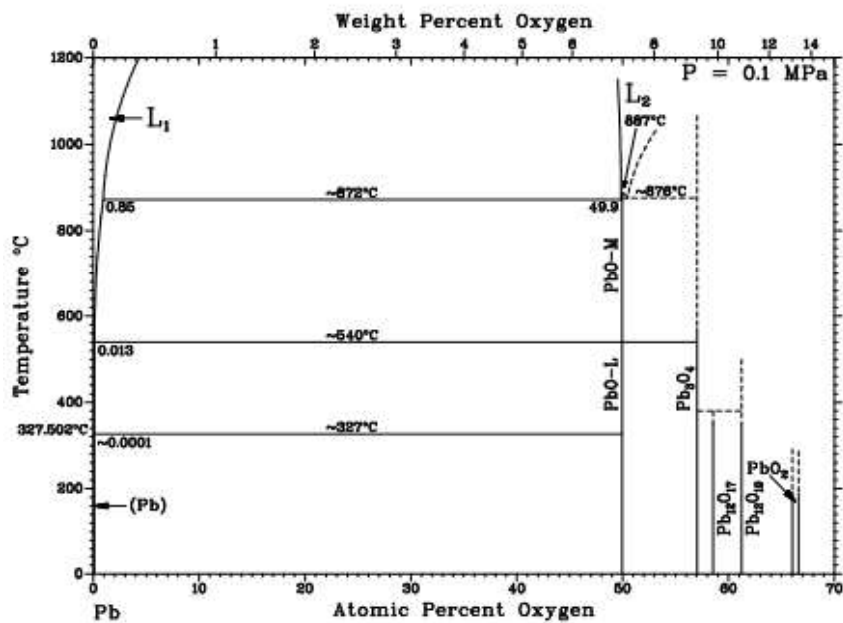


Fig. 4.2 Phase diagram of Pb-O system [4]

4.2.3 PbO-MoO₃ system

Several groups have studied the PbO-MoO₃ pseudo binary system in the past [6-16] and salient aspects of these studies are given in Table 4.1. The first detailed investigation was carried out by Jaeger and Germs [6] using thermal analysis and they investigated the system in the composition range of 0–50 mol% MoO₃. They

identified a new compound of composition Pb_2MoO_5 between PbO and PbMoO_4 . Based on their experiments, the authors reported PbMoO_4 and Pb_2MoO_5 to be congruently melting at 1338 and 1224 K, respectively. They also reported Pb_2MoO_5 to be forming an eutectic with PbO at 1035 K and another eutectic with PbMoO_4 at 1206 K. Later, Belyaev and Smolyaninov [7] studied the system in the entire composition range of PbO-MoO_3 system as part of their investigation on the ternary $\text{Bi}_2\text{O}_3\text{-PbO-MoO}_3$ system. Their results agreed with those reported by Jaeger and Germs [6] between 0 to 50 mol% MoO_3 . They also reported that PbMoO_4 formed an eutectic with MoO_3 at 953 K with the composition of eutectic as 17.5 mol% PbO -82.5 mol% MoO_3 .

Doyle and Forbes [8] employed diffuse reflectance measurements for the identification of compounds formed by solid state reaction between PbO and MoO_3 . They employed samples with different ratios of PbO and MoO_3 which covered from 0 to 100 mol% PbO and equilibrated them in air at elevated temperatures. The difference in the absorption function [the quantity $(A/R)^{1.383}$ where R is the percentage reflectance and $A = 100-R$, is the percentage absorbance] of each sample before and after the equilibration was measured and plotted against the respective composition [9]. The compound formation was indicated by the presence of either a maximum or a minimum in the plot. Based on these studies, they identified the existence of a new compound of composition Pb_5MoO_8 in this binary system in addition to PbMoO_4 and Pb_2MoO_5 . Detailed structural investigation of this newly reported compound was later carried out by Mentzen et al. [10] and Vassilev and Nihtianova [11]. The presence of this eutectic between MoO_3 and PbMoO_4 was further confirmed by the studies of Kunev et al. [12]. However, these authors reported the eutectic temperature and melting point of PbMoO_4 as 943 K and 1336 K, respectively. Bukhalova et al.

[13] studied the solid state reaction between PbO and MoO₃ using DTA and XRD. Their observations are in agreement with those reported by Jaeger and Germs [6] and Belyaev and Smolyaninov [7]. Similar conclusions were drawn by Lee et al. [14] during their studies. However, it is to be pointed out that the presence of Pb₅MoO₈ in this system had not been identified in references [6], [7], and [12]- [14].

Eissa et al. [15] studied the reaction between PbO₂ and MoO₃ by thermogravimetry in air. Based on mass loss characteristics, they identified all the three ternary compounds, namely, PbMoO₄, Pb₂MoO₅ and Pb₅MoO₈ in the PbO-MoO₃ system. They also reported the coexisting phases and the temperatures at which the equilibrium oxygen partial pressure was 0.21 bar. The studies on the crystal growth of Pb₅MoO₈ by Nihtianova et al. [16] have shown it to be incongruently melting and its peritectic temperature to be 1036 K. They also investigated the PbO rich portion of the PbO-MoO₃ system in detail and concluded that Pb₅MoO₈ formed an eutectic with PbO at 1017 K. It is quite likely that Jaeger and Germs [6] and Belyaev and Smolyaninov [7] misinterpreted the peritectic decomposition of Pb₅MoO₈ reported by Nihtianova et al. [16] as eutectic between PbO and Pb₂MoO₅. Similarly, the eutectic between PbO and Pb₅MoO₈ reported by Nihtianova et al. [17] might have been misinterpreted as eutectic between PbO and Pb₂MoO₅ by Bukhalova et al. [13].

Table 4.1 Literature data on PbO-MoO₃ pseudo binary system

S. No	Author	Experimental techniques employed	Salient features
1	Jaeger and Germs, 1921 [6]	Differential thermal analysis of samples in PbO-MoO ₃ system from 0 to 50 mol% MoO ₃ .	<ul style="list-style-type: none"> ➤ Reported the existence of PbMoO₄ and Pb₂MoO₅. Also reported that they congruently melt at 1338 K and 1224 K, respectively. ➤ Eutectic reaction between PbO and Pb₂MoO₅ at 1035 K ➤ Eutectic reaction between Pb₂MoO₅ and PbMoO₄ at 1206 K
2	Belyaev and Smolyaninov, 1962 [7]	Investigation of Bi ₂ O ₃ -MoO ₃ -PbO system. Mixtures of oxides were melted. By observing the crystallization temperature, the liquidus of the system was constructed.	<ul style="list-style-type: none"> ➤ Reported PbMoO₄ and Pb₂MoO₅ to be congruently melting at 1338 K and 1225 K, respectively. ➤ Eutectic reaction between PbO and Pb₂MoO₅ at 1035 K ➤ Eutectic reaction between Pb₂MoO₅ and PbMoO₄ at 1205 K ➤ Eutectic reaction between PbMoO₄ and MoO₃ at 953 K
3	Doyle and Forbes, 1965 [8]	Measurement of diffuse reflectance of samples in the PbO-MoO ₃ system	<ul style="list-style-type: none"> ➤ Reported the presence of three ternary compounds: PbMoO₄, Pb₂MoO₅ and Pb₅MoO₈
4	Kunev et al., 1966 [12]	Thermal and microscopic analysis of samples in the PbMoO ₄ -MoO ₃ system	<ul style="list-style-type: none"> ➤ Congruent melting of PbMoO₄ at 1336 K ➤ Eutectic reaction between PbMoO₄ and MoO₃ at 943 K
5	Bukhalova et al., 1971 [13]	DTA and XRD of different compositions of PbO-MoO ₃ mixtures	<ul style="list-style-type: none"> ➤ Congruent melting of PbMoO₄ at 1343 K ➤ Congruent melting of Pb₂MoO₅ at 1223 K ➤ Eutectic reaction between PbO and Pb₂MoO₅ at 1017 K

			<ul style="list-style-type: none"> ➤ Eutectic reaction between Pb_2MoO_5 and PbMoO_4 at 1183 K ➤ Eutectic reaction between PbMoO_4 and MoO_3 at 933 K ➤ Observations similar to those reported by Kunev et al. [12]
6	Lee et al., 1988 [14]	XRD	
7	Eissa et al., 1996 [15]	Thermogravimetric analysis of different compositions of PbO_2 and MoO_3	<ul style="list-style-type: none"> ➤ PbO_2-Pb-MoO_3 isobaric ternary phase diagram is reported ➤ Congruent melting of PbMoO_4 at 1336 K ➤ Congruent melting of Pb_2MoO_5 at 1224 K ➤ Reported the existence of Pb_5MoO_8
8	Nihtianova et al., 1997 [16]	DTA analysis in the PbO rich portion of the PbO - MoO_3 system	<ul style="list-style-type: none"> ➤ Congruent melting of Pb_2MoO_5 at 1223 K ➤ Peritectic decomposition of Pb_5MoO_8 at 1036 K ➤ Eutectic reaction between PbO and Pb_5MoO_8 at 1017 K
9	Dronskowski and Simon, 1989 [17]	Investigated the structures of various oxomolybdates of Na, In, Pb, La, etc based on XRD studies	<ul style="list-style-type: none"> ➤ Reported the existence of PbMo_5O_8 ➤ Crystal structure of PbMo_5O_8 was reported to be monoclinic
10	Wang and Yeh, 1991 [18]	Single crystal XRD studies on $\text{Pb}_3\text{Mo}_{16}\text{O}_{24}$	<ul style="list-style-type: none"> ➤ Crystal structure of $\text{Pb}_3\text{Mo}_{16}\text{O}_{24}$ was determined to be tetragonal

Dronskowski and Simon [17] carried out structural studies of numerous oxomolybdate species and identified a compound of composition PbMo_5O_8 . The compound was synthesized at 1473 K and based on XRD investigation, its structure was reported to be monoclinic. Later, Wang and Yeh [18] reported a new compound of composition $\text{Pb}_3\text{Mo}_{16}\text{O}_{24}$ and carried out single crystal XRD studies on this compound. The compound was prepared at 1215 K under vacuum using a stoichiometric mixture of Mo, MoO_3 and PbMoO_4 .

Though the pseudo binary phase diagram of PbO-MoO_3 system has been investigated in detail, the data available on the ternary Pb-Mo-O system is scanty. Feja and Reichelt [19] investigated the ternary Pb-Mo-O system. The coexistence of different phase fields in the system was identified by thermodynamic modeling in the system and later confirmed by carrying out long term equilibration experiments. Based on this work, they reported the ternary phase diagram of the system valid in the temperature range of 773 to 1273 K. The phase diagram shows the existence of seven phase fields namely, $\text{Pb-Mo-Pb}_3\text{Mo}_{16}\text{O}_{24}$, $\text{Mo-MoO}_2\text{-Pb}_3\text{Mo}_{16}\text{O}_{24}$, $\text{Pb-MoO}_2\text{-Pb}_3\text{Mo}_{16}\text{O}_{24}$, $\text{Pb-MoO}_2\text{-PbMoO}_4$, $\text{Pb-PbMoO}_4\text{-Pb}_2\text{MoO}_5$, $\text{Pb-Pb}_2\text{MoO}_5\text{-Pb}_5\text{MoO}_8$ and $\text{Pb-Pb}_5\text{MoO}_8\text{-PbO}$.

To summarise, five ternary oxides viz., PbMoO_4 , Pb_2MoO_5 , Pb_5MoO_8 , PbMo_5O_8 and $\text{Pb}_3\text{Mo}_{16}\text{O}_{24}$ have been reported to exist in the Pb-Mo-O ternary system. However, thermochemical data on these ternary compounds are limited.

Thermochemical properties of $\text{PbMoO}_4(\text{s})$ have been investigated by different authors [20-28]. Data on the standard molar enthalpies of formation at 298.15 K and molar heat capacity of $\text{PbMoO}_4(\text{s})$ have been reported by various authors and are listed in Table 4.2. Muldrow and Hepler [20] determined the heat of precipitation of $\text{PbMoO}_4(\text{s})$ by reacting crystalline lead nitrate with aqueous sodium molybdate.

Using the enthalpy of formation of $\text{Pb}(\text{NO}_3)_2$ (s) and Na_2MoO_4 (s) and literature data on the enthalpies of formation of MoO_4^{2-} (aq) and NO_3^- (aq) ions, $\Delta_f H_{298}^\circ$ of PbMoO_4 (s) was deduced. Similar experiments were carried out to determine the heat of precipitation of PbMoO_4 (s) from the heat of reaction of crystalline sodium molybdate with aqueous lead nitrate. Based on these results, the authors reported a value of (-1049.1 ± 3.7) kJ mol^{-1} for $\Delta_f H_{298}^\circ$ of PbMoO_4 (s). Using the data reported by Muldrow and Hepler [20], O'Hare et al. [21] estimated the Gibbs energy of dissociation of PbMoO_4 (s) into Pb^{2+} (aq) and MoO_4^{2-} (aq) ions. They also estimated the same by using the solubility product data. The authors observed a difference of about 16 kJ mol^{-1} between their data and that of the data reported by Muldrow and Hepler [20] and attributed it to the formation of polymolybdate species in the experimental condition (acidic media) employed by Muldrow and Hepler [20] and the associated uncertainties. In order to reconcile these two sources of data, O'Hare et al. [21] suggested a value of $-1025 \text{ kJ mol}^{-1}$ for the $\Delta_f H_{298}^\circ$ of PbMoO_4 (s). Dellien et al. [22] determined $\Delta_f H_{298}^\circ$ of PbMoO_4 (s) by solution calorimetry using a mixture of NaOH and Na_4EDTA solution as the calorimetric solvent and with the data on enthalpies of formation of PbO (s) and MoO_3 (s) from NBS tables [23]. Their reported value for $\Delta_f H_{298}^\circ$ of PbMoO_4 (s) is $(-1052.6 \pm 0.5) \text{ kJ mol}^{-1}$ and this is in good agreement with the value reported by Muldrow and Hepler [20] as well as with the NBS value [23] of $-1051.9 \text{ kJ mol}^{-1}$. Dellien et al. [22] indicated the difficulties associated with measuring the solubility of PbMoO_4 (s) and associated large uncertainties to be responsible for the deviation in the values reported by O'Hare et al. [21]. Later, Bissengaliyeva [24] et al. reported a value of $(-1051.2 \pm 4.3) \text{ kJ mol}^{-1}$

¹for the $\Delta_f H_{298}^\circ$ of PbMoO_4 (s) based on high temperature melt calorimetry experiments using $2\text{PbO} \cdot \text{Bi}_2\text{O}_3$ as the solvent. This value is in good agreement with the earlier reported values.

Weller and Kelley [25] measured the low temperature heat capacity of PbMoO_4 (s) (51 to 298 K) and reported a value of $119.7 \text{ J K}^{-1} \text{ mol}^{-1}$ at 298.15 K. Barin [26] has assessed all the available thermochemical data of PbMoO_4 (s) and estimated its molar heat capacity from 298 to 1200 K. Using vacuum adiabatic calorimetry, Bissengaliyeva et al. [27] measured the heat capacity of PbMoO_4 (s) in the temperature range of 55 to 320 K and reported a value of $(119.41 \pm 0.13) \text{ J K}^{-1} \text{ mol}^{-1}$ at 298.15 K. They also estimated the heat capacity of PbMoO_4 (s) over the temperature range of 0 to 55 K by means of a semi - empirical method. In a later study, Bissengaliyeva et al. [28] measured the heat capacities of PbMoO_4 (s) in the temperature range of 4.3 to 80 K and calculated the thermodynamic functions of PbMoO_4 (s) in the temperature range from 0 to 320 K.

From the experimentally obtained data on heat capacity, enthalpy of formation and entropy of formation, Gibbs energy of formation of PbMoO_4 (s) at 298.15 K has been deduced. A value of $-951.4 \text{ kJ mol}^{-1}$ is reported in NBS table [23] for the $\Delta_f G_{298}^\circ$ of PbMoO_4 (s) while Bissengaliyeva et al. [27] have reported a value of $-949.1 \text{ kJ mol}^{-1}$. Bissengaliyeva et al. [27] also cited a value of $-948.47 \text{ kJ mol}^{-1}$ for the same from the thermodynamic compilation of Naumov et al. [29]. Weller and Kelley [25] reported a value of $-944.3 \text{ kJ mol}^{-1}$ for the same. Barin [26] has estimated the variation of Gibbs energy of formation of PbMoO_4 (s) in the temperature range of 298 to 1200 K. Thermochemical data is available only for Pb_2MoO_5 (g), reported by Kunkel et al. [30] based on high temperature vaporization studies using mass spectrometric

Knudsen-cell method. Thermochemical data on other ternary compounds are not available.

4.3 Experimental details

4.3.1 Materials

The starting reagents used were Pb powder (99.95% purity on metal basis, M/s Alfa Aesar, USA), Mo powder (99.9% purity on metal basis, M/s Alfa Aesar, USA), PbO, MoO₃ and MoO₂ powders. MoO₃ required for this work was prepared by heating ammonium heptamolybdate tetrahydrate (99.96%, purity on metal basis, M/s Sigma-Aldrich, USA) at 723 K in air for 24 h. MoO₂ was prepared by the reduction of MoO₃ at 823 K under flowing hydrogen gas saturated with water vapour. During this reduction process, the temperature was slowly increased to 823 K to avoid the volatilization of MoO₃. Pure orthorhombic phase of PbO (yellow PbO) was used in the entire experimental studies and it was prepared by heating PbCO₃ (obtained by the precipitation of Pb(NO₃)₂ (99.999% purity on metal basis, M/s Alfa Aesar, USA) and (NH₄)₂CO₃ (99.999 % purity, M/s Alfa Aesar, USA) at 853 K as reported in ref. [31]. The XRD patterns of the synthesized compounds, PbO, MoO₃ and MoO₂ were matched with the PCPDF patterns 00-038-1477, 00-032-0671, and 00-05-0508, respectively. No additional peaks were observed in the XRD patterns of the prepared compounds, indicating the phase purity of the prepared compounds.

Table 4.2 Literature data on thermochemical properties of PbMoO₄ (s)

a) Enthalpy of formation		
No	Reference	$\Delta_f H_{298}^\circ / \text{kJ mol}^{-1}$
1	Muldraw and Hepler, 1958 [20]	-1049.1 ± 3.7 [@]
2	Wagman et al., 1969 [23]	-1051.9 ± 0.85 [@]
3	O'Hare et al., 1974 [21]	-1025.08 [*]
4	Dellien et al., 1976 [22]	-1052.6 ± 0.5 ^a

Remarks	
1	<ul style="list-style-type: none"> Determined enthalpy of formation of PbMoO₄ (s) from the heat of reaction of crystalline Pb(NO₃)₂ with dilute solution of Na₂MoO₄ and from the heat of reaction of crystalline Na₂MoO₄ with dilute solution of Pb(NO₃)₂ Compilation of thermochemical data
3	<ul style="list-style-type: none"> Estimated the Gibbs energy of dissociation of PbMoO₄ (s) into Pb²⁺ (aq) and MoO₄²⁻ (aq) ions using the $\Delta_f H_{298}^\circ$ of PbMoO₄ (s) reported by Muldraw and Hepler [20] Another estimation was made for the same using the solubility product data. Observed a difference of about 16 kJ mol⁻¹ between these two data and attributed it to the formation of unaccountable polymolybdate species formed under the experimental conditions employed by Mulrow and Hepler [20] Suggested $\Delta_f H_{298}^\circ$ of PbMoO₄ (s) = -1025.08 kJ mol⁻¹ to have consistency between the data determined by two methods Determined $\Delta_f H_{298}^\circ$ of PbMoO₄ (s) by solution calorimetry using a mixture of NaOH and Na₄EDTA as the calorimetric solvent

5	Bissengaliyeva et al., 2013 [24]	-1051.2 ± 4.3 ^b	<ul style="list-style-type: none"> Determined $\Delta_f H_{298}^\circ$ of PbMoO₄ (s) based on high temperature melt calorimetry experiments using 2PbO·Bi₂O₃ as the solvent
b) Heat capacity			
No	Reference	$C_p^{298} / \text{J K}^{-1} \text{mol}^{-1}$	Remarks
1	Weller and Kelley, 1964 [25]	119.7 ^c	<ul style="list-style-type: none"> Measured the heat capacity of PbMoO₄ (s) in the temperature range of 51 to 298 K Reported S_{298}° of PbMoO₄ (s) as 166.1 ± 2.1 J K⁻¹ mol⁻¹
2	Barin [26]	119.7 ^c	<ul style="list-style-type: none"> Compilation of thermochemical data Reported S_{298}° of PbMoO₄ (s) as 166.1 J K⁻¹ mol⁻¹
3	Wagman et al., 1969 [23]	119.7 ^c	<ul style="list-style-type: none"> Compilation of thermochemical data Reported S_{298}° of PbMoO₄ (s) as 166.6 ± 2.09 J K⁻¹ mol⁻¹
4	Bissengaliyeva et al., 2010 [27]	119.41 ± 0.13 ^b	<ul style="list-style-type: none"> Measured the heat capacity of PbMoO₄ (s) by vacuum adiabatic calorimetry in the temperature range of 55 to 320 K Estimated S_{298}° of PbMoO₄(s) as 168.33 ± 2.06 J K⁻¹ mol⁻¹
	Bissengaliyeva et al., 2011 [28]	119.4 ± 0.13 ^b	<ul style="list-style-type: none"> Measured the heat capacity of PbMoO₄ (s) by vacuum adiabatic calorimetry in the temperature range of 4.3 to 80 K Estimated S_{298}° of PbMoO₄ (s) as 161.5 ± 0.3 J K⁻¹ mol⁻¹

^aType of uncertainty is not mentioned by the author. ^bSuggested data. ^cStandard uncertainty with 0.68 level of confidence, ^bExpanded uncertainty with 0.95 level of confidence. ^cUncertainty not mentioned by the author.

4.3.2 Preparation of ternary compounds

The ternary compounds, namely, PbMoO_4 , Pb_2MoO_5 and Pb_5MoO_8 were prepared by compacting the mixtures of PbO and MoO_3 taken in appropriate molar ratios and heating them in air for prolonged periods. PbMoO_4 and Pb_2MoO_5 were prepared by heating the compacts of the oxide mixtures at 873 K for 48 h while Pb_5MoO_8 was prepared by heating at 1003 K for 192 h in platinum crucibles with one intermediate grinding and repelletising followed by heating at the same temperature. For the preparation of $\text{Pb}_3\text{Mo}_{16}\text{O}_{24}$ compound, starting materials chosen were PbMoO_4 , MoO_3 and Mo powders. The homogeneous mixture of these reactants in the appropriate molar ratio was sealed in alumina crucibles under vacuum and heated at 1215 K for 10 days as reported in ref. [18]. Towards the preparation of PbMo_5O_8 compound, sample pellets were made by using a mixture of stoichiometric amounts of Mo , MoO_2 and Pb powders. The pellets were kept in alumina crucibles and enclosed in evacuated quartz ampoules. The reactant mixture was heated at 1473 K for about 7 days as reported in ref. [17]. The preparation of PbMo_5O_8 compound was also carried out at 773 and 998 K using the same starting components. The resulting products were characterized using X-ray diffractometer (M/s Inel, France) with $\text{Cu K}\alpha$ radiation and graphite monochromator. The details of procedure adopted for the preparation of $\text{Pb}_3\text{Mo}_{16}\text{O}_{24}$ and PbMo_5O_8 and the observations made are given in Table 4.3.

Table 4.3 Preparation of compounds PbMo_5O_8 and $\text{Pb}_3\text{Mo}_{16}\text{O}_{24}$

Composition chosen	Phases taken for equilibration	Temperature and duration of heating	Phases obtained after heating (based on XRD analysis)	Inference
$\text{Pb}_{0.07}\text{Mo}_{0.36}\text{O}_{0.57}$	Mo: MoO_2 : Pb in the ratio of 1: 4: 1	1473 K, 168 h	Pb, Mo, MoO_2	PbMo_5O_8 was not formed
		773 K, 960 h	Pb, Mo, MoO_2	PbMo_5O_8 was not formed
		998 K, 432 h	Pb, Mo, MoO_2	PbMo_5O_8 was not formed
$\text{Pb}_{0.07}\text{Mo}_{0.37}\text{O}_{0.56}$	Mo: MoO_3 : PbMoO_4 in the ratio of 3: 1.3: 1	1215 K, 240 h	Pb, Mo, MoO_2 , $\text{Pb}_3\text{Mo}_{16}\text{O}_{24}$	Partial formation of $\text{Pb}_3\text{Mo}_{16}\text{O}_{24}$
		773 K, 960 h	Pb, Mo, MoO_2	$\text{Pb}_3\text{Mo}_{16}\text{O}_{24}$ is unstable at 773 K
	Mixture of partially formed $\text{Pb}_3\text{Mo}_{16}\text{O}_{24}$ along with unreacted Pb, Mo and MoO_2	998 K, 432 h	Pb, Mo, MoO_2	$\text{Pb}_3\text{Mo}_{16}\text{O}_{24}$ is unstable at 998 K

4.3.3 Phase equilibration studies

4.3.3.1 Equilibrations of samples with compositions on the PbO-MoO₃ pseudo binary line and the line joining PbO and MoO₂

To examine the possible existence of any additional compound in the PbO-MoO₃ pseudo binary system, samples with different molar ratios of PbO and MoO₃ in the form of pellets were equilibrated under vacuum at 773 K and at 998 K for prolonged duration. Similar experiments were carried out with samples having different molar ratios of PbO and MoO₂ for identifying the possible existence of any ternary compound with composition falling between PbO and MoO₂. In both the cases, mixture of oxides were compacted into pellets and taken in alumina crucibles. The crucibles were then hermetically sealed in quartz ampoules under vacuum and subjected to long term equilibration at 773 K as well as at 998 K. The coexisting phases were then identified by XRD after quenching the samples to room temperature. Details of these experiments are given in Table 4.4.

4.3.3.2 Partial reduction of ternary compounds followed by long term equilibrations

With a view to deduce preliminary information on the phase relations in this ternary system, the three ternary compounds namely, PbMoO₄, Pb₂MoO₅ and Pb₅MoO₈ were subjected to partial reduction under flowing hydrogen gas at 773 K followed by equilibration of products formed for prolonged periods at that temperature. For these experiments, samples were taken in alumina crucibles and heated slowly under a flow of hydrogen gas up to 773 K and held at that temperature for about 5 min.

Table 4.4 Equilibrations of samples with mixtures of (a) PbO and MoO₃ and (b) PbO and MoO₂

Sample No	Molar ratio of oxides taken	Temperature and duration of equilibration *	Phases obtained after equilibration
(a) Experiments with PbO and MoO₃			
1	1PbO : 3MoO ₃	773 K, 960 h	PbMoO ₄ , MoO ₃
		998 K, 432 h	PbMoO ₄ , MoO ₃
2	3PbO : 2MoO ₃	773 K, 960 h	PbMoO ₄ , Pb ₂ MoO ₅
		998 K, 432 h	PbMoO ₄ , Pb ₂ MoO ₅
3	3PbO : 1MoO ₃	773 K, 960 h	Pb ₂ MoO ₅ , PbO
		998 K, 432 h	Pb ₂ MoO ₅ , Pb ₅ MoO ₈
4	14PbO : 1MoO ₃	773 K, 960 h	Pb ₂ MoO ₅ , PbO
		998 K, 432 h	Pb ₅ MoO ₈ , PbO
(b) Experiments with PbO and MoO₂			
5	1PbO : 1MoO ₂	773 K, 960 h	Pb, MoO ₂ , PbMoO ₄
		998 K, 432 h	Pb, MoO ₂ , PbMoO ₄
6	1PbO : 3MoO ₂	773 K, 960 h	Pb, MoO ₂ , PbMoO ₄
		998 K, 432 h	Pb, MoO ₂ , PbMoO ₄
7	2PbO : 1MoO ₂	773 K, 960 h	Pb, PbMoO ₄ , Pb ₂ MoO ₅
		998 K, 432 h	Pb, PbMoO ₄ , Pb ₂ MoO ₅
8	5PbO : 1MoO ₂	773 K, 960 h	Pb, Pb ₂ MoO ₅ , PbO
		998 K, 432 h	Pb, Pb ₂ MoO ₅ , Pb ₅ MoO ₈
9	11PbO : 1MoO ₂	773 K, 960 h	Pb, Pb ₂ MoO ₅ , PbO
		998 K, 432 h	Pb, Pb ₅ MoO ₈ , PbO

**Same phases were obtained at the end of 480 h for equilibrations at 773 K and at the end of 216 h for equilibrations at 998 K, indicating attainment of equilibrium.*

The overall composition of the products obtained by this reduction was then determined based on the final mass of each sample assuming the mass loss was solely due to removal of oxygen, i.e. Pb to Mo ratio remained constant during this partial reduction. The products obtained were ground and compacted into pellets. These pellets were kept inside alumina crucibles which in turn were hermetically sealed inside quartz ampoules under vacuum and equilibrated at 773 K for prolonged periods. Similar equilibrations were carried out at 998 K also. The details of the samples (10 to 12) are given in Table 4.5 and the compositions are indicated in Fig. 4.3. After equilibration, samples were quenched to room temperature and the resulting phases were analyzed by XRD.

Table 4.5 Equilibrations of partially reduced ternary compounds

No	Starting compound	Overall composition after partial reduction	Temperature and duration of equilibration	Phases obtained after equilibration (based on XRD analysis) *
10	PbMoO ₄	Pb _{0.20} Mo _{0.20} O _{0.60}	773K, 960h	Pb, PbMoO ₄ , MoO ₂
			998, 432h	Pb, PbMoO ₄ , MoO ₂
11	Pb ₂ MoO ₅	Pb _{0.28} Mo _{0.14} O _{0.58}	773K, 960h	Pb, Pb ₂ MoO ₅ , PbMoO ₄
			998, 432h	Pb, Pb ₂ MoO ₅ , PbMoO ₄
12	Pb ₅ MoO ₈	Pb _{0.40} Mo _{0.08} O _{0.50}	773K, 960h	Pb, Pb ₂ MoO ₅ , PbO
			998, 432h	Pb, Pb ₅ MoO ₈ , Pb ₂ MoO ₅

**Same phases were obtained at the end of 480 h for equilibrations at 773 K and at the end of 216 h for equilibrations at 998 K, indicating attainment of equilibrium.*

4.3.3.3 Additional equilibrations using different starting components

The coexisting phases identified in the preliminary experiments were further confirmed by carrying out additional equilibrations. Samples of different overall compositions with different starting materials, including metals, metal oxides and

ternary compounds were prepared by thoroughly mixing them and compacting them into pellets. Each of these sample pellets was then placed inside an alumina crucible which was hermetically sealed in quartz tubes under vacuum. Each sample in the sealed tube was equilibrated for a prolonged period at a chosen temperature. After equilibration, samples were quenched to room temperature and the equilibrium phases were analyzed by XRD. Details of the samples (13 to 27) and equilibration parameters are given in Table 4.6 and the compositions of the samples are shown in Fig. 4.3. Equilibrations were also performed to examine whether PbMo_5O_8 and $\text{Pb}_3\text{Mo}_{16}\text{O}_{24}$ would coexist with liquid lead at 773 and 998 K. For these equilibrations, samples of compositions lying within the region bound by Pb, Mo and MoO_2 (samples 28 to 33) were prepared.

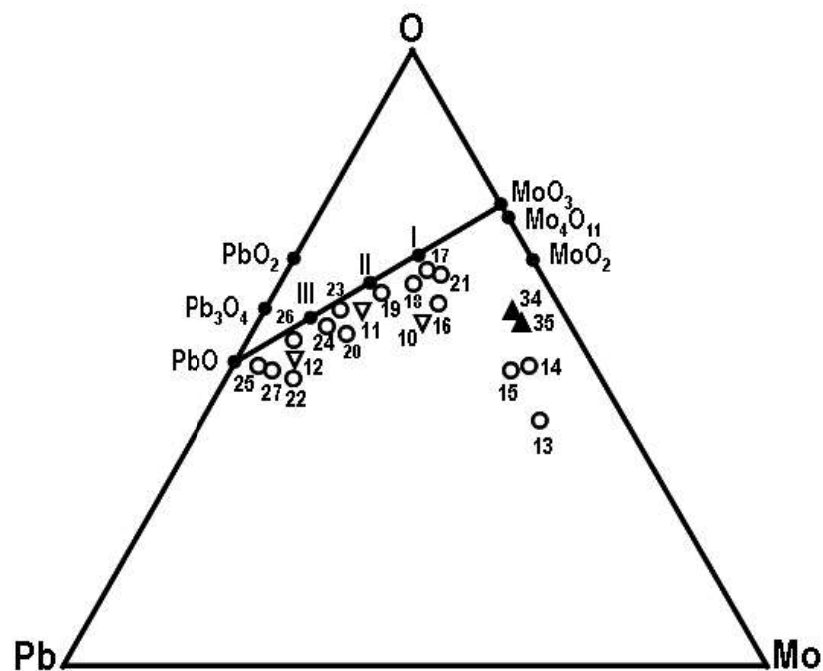


Fig. 4.3 Compositions chosen for equilibrations, I- PbMoO_4 , II- Pb_2MoO_5 , III- Pb_5MoO_8 10-12(▼): Overall compositions of products obtained after partial reduction of ternary compounds (Table 4.5), 13-27(○): Overall compositions of samples chosen for equilibration using different starting components (Table 4.6), 34, 35(▲): Compositions corresponding to ' PbMo_5O_8 ' and ' $\text{Pb}_3\text{Mo}_{16}\text{O}_{24}$ ' compounds.

The starting phases were a mixture of PbO, Mo and MoO₂ of different overall compositions and the equilibrations were carried out at both 773 and 998 K. The details are given in Table 4.7 and the overall compositions of these samples are shown in Fig. 4.4.

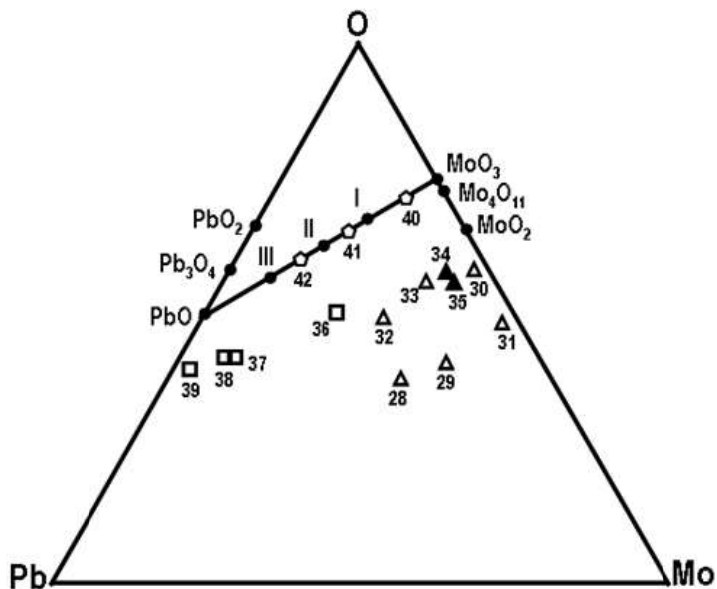


Fig. 4.4 Compositions chosen for equilibrations, I-PbMoO₄, II-Pb₂MoO₅, III-Pb₅MoO₈

28-33(▲): Overall compositions of samples chosen for equilibration in the Pb-Mo-MoO₂ region (Table 4.7), 34, 35(▲): Compositions corresponding to PbMo₅O₈ and Pb₃Mo₁₆O₂₄ compounds, 36-39(■): Overall compositions chosen for equilibration with excess of liquid Pb (Table 4.8), 40-42(○): Overall compositions of samples (coated on alumina strips) used for equilibration in excess of liquid lead (Table 4.9)

4.3.3.4 Equilibrations in liquid lead

Two sets of additional equilibration experiments were carried out for deducing the phases that coexist in liquid lead. In one set of experiments, samples of chosen composition with lead powder as one of the reactants were prepared in the form of porous pellet. Each of the pellets was kept immersed in excess liquid lead contained in an alumina crucible by forcing it down by an alumina strip which was later tied to the crucible using a wire.

Table 4.6 Details of additional equilibrations

No	Composition chosen	Phases taken for equilibration	Temperature and duration of equilibration *	Phases obtained after equilibration (based on XRD analysis)
13	Pb _{0.12} Mo _{0.48} O _{0.40}	PbO, Mo, MoO ₃	773 K, 960 h	Pb, Mo, MoO ₂
			998 K, 432 h	Pb, Mo, MoO ₂
14	Pb _{0.09} Mo _{0.42} O _{0.49}	Pb ₂ MoO ₅ , Mo, MoO ₃	773 K, 960 h	Pb, Mo, MoO ₂
			998 K, 432 h	Pb, Mo, MoO ₂
15	Pb _{0.12} Mo _{0.40} O _{0.48}	Pb ₅ MoO ₈ , Mo, MoO ₃	773 K, 960 h	Pb, Mo, MoO ₂
			998 K, 432 h	Pb, Mo, MoO ₂
16	Pb _{0.17} Mo _{0.24} O _{0.59}	PbO, Mo, MoO ₃	773 K, 960 h	Pb, MoO ₂ , PbMoO ₄
			998 K, 432 h	Pb, MoO ₂ , PbMoO ₄
18	Pb _{0.19} Mo _{0.19} O _{0.62}	Pb ₂ MoO ₅ , Mo, MoO ₃	773 K, 960 h	Pb, MoO ₂ , PbMoO ₄ ,
			998 K, 432 h	Pb, MoO ₂ , PbMoO ₄
19	Pb _{0.16} Mo _{0.21} O _{0.63}	Pb ₂ MoO ₅ , Mo, MoO ₃	773 K, 960 h	Pb, MoO ₂ , PbMoO ₄
			998 K, 432 h	Pb, MoO ₂ , PbMoO ₄
20	Pb _{0.32} Mo _{0.13} O _{0.55}	PbO, Mo, MoO ₃	773 K, 960 h	Pb, PbMoO ₄ , Pb ₂ MoO ₅
			998 K, 432 h	Pb, PbMoO ₄ , Pb ₂ MoO ₅
21	Pb _{0.25} Mo _{0.14} O _{0.61}	PbO, MoO ₂ , MoO ₃	773 K, 960h	Pb, PbMoO ₄ , Pb ₂ MoO ₅
			998 K, 432h	Pb, PbMoO ₄ , Pb ₂ MoO ₅
22	Pb _{0.42} Mo _{0.08} O _{0.50}	PbO, Mo, MoO ₃	998K, 432h	Pb, Pb ₂ MoO ₅ , Pb ₅ MoO ₈
23	Pb _{0.32} Mo _{0.10} O _{0.58}	PbO, PbMoO ₄ , Mo	998K, 432h	Pb, Pb ₂ MoO ₅ , Pb ₅ MoO ₈
24	Pb _{0.34} Mo _{0.09} O _{0.57}	PbO, MoO ₂ , MoO ₃	998K, 432h	Pb, Pb ₂ MoO ₅ , Pb ₅ MoO ₈
25	Pb _{0.47} Mo _{0.03} O _{0.50}	PbO, Mo, MoO ₃	998K, 432h	Pb, Pb ₅ MoO ₈ , PbO
26	Pb _{0.41} Mo _{0.06} O _{0.53}	PbO, MoO ₂ , MoO ₃	998K, 432h	Pb, Pb ₅ MoO ₈ , PbO
27	Pb _{0.46} Mo _{0.04} O _{0.50}	PbO, PbMoO ₄ , Mo	998K, 432h	Pb, Pb ₅ MoO ₈ , PbO

**Same phases were obtained at the end of 480 h for equilibrations at 773 K and at the end of 216 h for equilibrations at 998 K, indicating attainment of equilibrium.*

Table 4.7 Details of equilibration of samples of composition falling within the Pb-Mo-MoO₂ region

Sample No	Composition chosen	Phases taken for equilibration	Temperature and duration of equilibration *	Phases obtained after equilibration (based on XRD analysis)
28	Pb _{0.24} Mo _{0.38} O _{0.38}	PbO, Mo, MoO ₃	773 K, 960 h	Pb, Mo, MoO ₂
			998 K, 432 h	Pb, Mo, MoO ₂
29	Pb _{0.15} Mo _{0.44} O _{0.41}	PbO, Mo, MoO ₃	773 K, 960 h	Pb, Mo, MoO ₂
			998 K, 432 h	Pb, Mo, MoO ₂
30	Pb _{0.02} Mo _{0.40} O _{0.58}	PbO, Mo, MoO ₃	773 K, 960 h	Pb, Mo, MoO ₂
			998 K, 432 h	Pb, Mo, MoO ₂
31	Pb _{0.03} Mo _{0.49} O _{0.48}	PbO, Mo, MoO ₃	773 K, 960 h	Pb, Mo, MoO ₂
			998 K, 432 h	Pb, Mo, MoO ₂
32	Pb _{0.22} Mo _{0.29} O _{0.49}	PbO, Mo, MoO ₃	773 K, 960 h	Pb, Mo, MoO ₂
			998 K, 432 h	Pb, Mo, MoO ₂
33	Pb _{0.11} Mo _{0.33} O _{0.56}	PbO, Mo, MoO ₃	773 K, 960 h	Pb, Mo, MoO ₂
			998 K, 432 h	Pb, Mo, MoO ₂

**Same phases were obtained at the end of 480 h for equilibrations at 773 K and at the end of 216 h for equilibrations at 998 K, indicating attainment of equilibrium.*

This crucible was hermetically sealed in a quartz tube undervacuum and allowed for equilibration for prolonged periods. In the second set of experiments, alumina strips were coated with molten mixture of the starting materials and kept immersed in liquid lead taken in an alumina crucible. The crucible was later sealed under vacuum in a quartz tube and allowed for equilibration at a chosen temperature. Details of these samples (34 to 42) and equilibration parameters are given in Tables 4.8 and 4.9 and the overall compositions of the samples chosen are marked in Fig. 4.4. After equilibrations, sample pellets and alumina strips were retrieved from lead metal and analyzed by XRD.

Table 4.8 Details of samples equilibrated with excess liquid lead and the products obtained

Sample No	Composition chosen for pellets	Phases taken for equilibration	Temperature and duration of equilibration	Phases obtained after equilibration (based on XRD analysis)
34	PbMo ₅ O ₈	Mo, MoO ₂ , Pb (in the molar ratio of 1: 4: 1)	773 K, 960 h	Pb, Mo, MoO ₂
			998 K, 432 h	Pb, Mo, MoO ₂
35	Pb ₃ Mo ₁₆ O ₂₄	Mo, MoO ₃ , PbMoO ₄ (in the molar ratio of 3: 1.3: 1)	773 K, 960 h	Pb, Mo, MoO ₂
			998 K, 432 h	Pb, Mo, MoO ₂
36	Pb _{0.28} Mo _{0.21} O _{0.51}	Pb, Mo, MoO ₃	773 K, 960 h	Pb, MoO ₂ , PbMoO ₄
			998 K, 432 h	Pb, MoO ₂ , PbMoO ₄
37	Pb _{0.49} Mo _{0.09} O _{0.42}	Pb, PbO, MoO ₃	773 K, 960 h	Pb, PbMoO ₄ , Pb ₂ MoO ₅
			998 K, 432 h	Pb, PbMoO ₄ , Pb ₂ MoO ₅
38	Pb _{0.50} Mo _{0.07} O _{0.43}	Pb, PbO, MoO ₃	998K, 432h	Pb, Pb ₂ MoO ₅ , Pb ₅ MoO ₈
			998K, 432h	Pb, Pb ₅ MoO ₈ , PbO
39	Pb _{0.58} Mo _{0.02} O _{0.40}	Pb, PbO, MoO ₃	998K, 432h	Pb, Pb ₅ MoO ₈ , PbO

In all the phase equilibration experiments, except during the experiments which involve the immersion of sample pellets or strips in excess of liquid lead, the sample pellets were retrieved from the quartz ampoules at the end of ca. 50% of period of equilibration, ground well and analyzed by XRD. Samples were then repelletised and equilibration was continued by sealing them in quartz ampoules under vacuum.

Table 4.9 Details of samples coated on alumina strips and equilibrated with excess liquid lead

No	Composition chosen	Phases taken	Temperature and time of equilibration	Phases obtained after equilibration (based on XRD analysis)
40	Pb _{0.07} Mo _{0.21} O _{0.72}	PbO, MoO ₃	773 K, 960 h	Pb, MoO ₂ , PbMoO ₄
			998 K, 432 h	Pb, MoO ₂ , PbMoO ₄
41	Pb _{0.21} Mo _{0.15} O _{0.64}	Pb ₅ MoO ₈ , MoO ₃	773 K, 960 h	Pb, PbMoO ₄ , Pb ₂ MoO ₅
			998 K, 432 h	Pb, PbMoO ₄ , Pb ₂ MoO ₅
42	Pb _{0.31} Mo _{0.09} O _{0.60}	Pb ₅ MoO ₈ , MoO ₃	998K, 432h	Pb, Pb ₂ MoO ₅ , Pb ₅ MoO ₈

4.3.3.5 Equilibrations to determine the temperature range of stability of Pb₅MoO₈

In order to determine the temperature range of existence of Pb₅MoO₈, long term equilibrations were carried out at different temperatures using three different sets of starting components. In one set of experiments, Pb₅MoO₈ was taken as the starting component whereas 1:3 mixtures of Pb₂MoO₅ and PbO were used as the starting components in the second set of experiments. The third set of experiments was performed using a 5:1 mixture of PbO and MoO₃ as the starting components. For these equilibration studies, homogeneous mixture of the starting components were made and compacted into pellets. The pellets were kept in alumina crucibles, which in turn kept enclosed in evacuated small volume quartz ampoules. The samples were subjected to long term equilibration at the chosen temperatures for prolonged

duration. At the end of the reaction, samples were quenched to room temperature and the resulting phases were analyzed by XRD. Details of these equilibrations are given in Table 4.10.

Table 4.10 Details of long term equilibration experiments to deduce the temperature range of stability of Pb_5MoO_8

a) Using Pb_5MoO_8 as the starting component		
Sample No	Temperature and duration of heating	Phases obtained (based on XRD analysis)
1	748 K / 720 h	Pb_2MoO_5 , PbO
2	753 K / 720 h	Pb_2MoO_5 , PbO
3	773 K / 720 h	Pb_2MoO_5 , PbO
4	848 K / 720 h	Pb_2MoO_5 , PbO
5	873 K / 720 h	Pb_2MoO_5 , PbO
6	898 K / 720 h	Pb_2MoO_5 , PbO
7	918 K / 720 h	Pb_5MoO_8
8	923 K / 360 h	Pb_5MoO_8
9	998K / 432h	Pb_5MoO_8
10	1003 K / 360 h	Pb_5MoO_8
b) Using 1:3 mixture of Pb_2MoO_5 and PbO as the starting component		
11	773 K / 720 h	Pb_2MoO_5 , PbO
12	898 K / 720 h	Pb_2MoO_5 , PbO
13	923 K / 360 h	Pb_5MoO_8
c) Using 5:1 mixture of PbO and MoO_3 as the starting component		
14	765 K / 840 h	Pb_2MoO_5 , PbO
15	867 K / 840 h	Pb_2MoO_5 , PbO
16	920 K / 840 h	Pb_5MoO_8
17	948 K / 840 h	Pb_5MoO_8
18	956 K / 840 h	Pb_5MoO_8
19	978 K / 840 h	Pb_5MoO_8
20	981 K / 840 h	Pb_5MoO_8

4.3.4. Emf measurements

Three galvanic cells were constructed for the determination of Gibbs energy of formation of $\text{PbMoO}_4(\text{s})$, $\text{Pb}_2\text{MoO}_5(\text{s})$ and $\text{Pb}_5\text{MoO}_8(\text{s})$ which are represented below:

(-) Kanthal, Ir, Pb (l), $\text{MoO}_2(\text{s})$, $\text{PbMoO}_4(\text{s})$ | YSZ | (O_2 , 101.3 kPa), Pt (+) (I)

(-) Kanthal, Ir, Pb (l), $\text{PbMoO}_4(\text{s})$, $\text{Pb}_2\text{MoO}_5(\text{s})$ | YSZ | (O_2 , 101.3 kPa), Pt (+) (II)

(-) Kanthal, Ir, Pb (l), $\text{Pb}_2\text{MoO}_5(\text{s})$, $\text{Pb}_5\text{MoO}_8(\text{s})$ | YSZ | (O_2 , 101.3 kPa), Pt (+) (III)

The schematics of the experimental assembly of the galvanic cells are shown in Fig. 4.5.

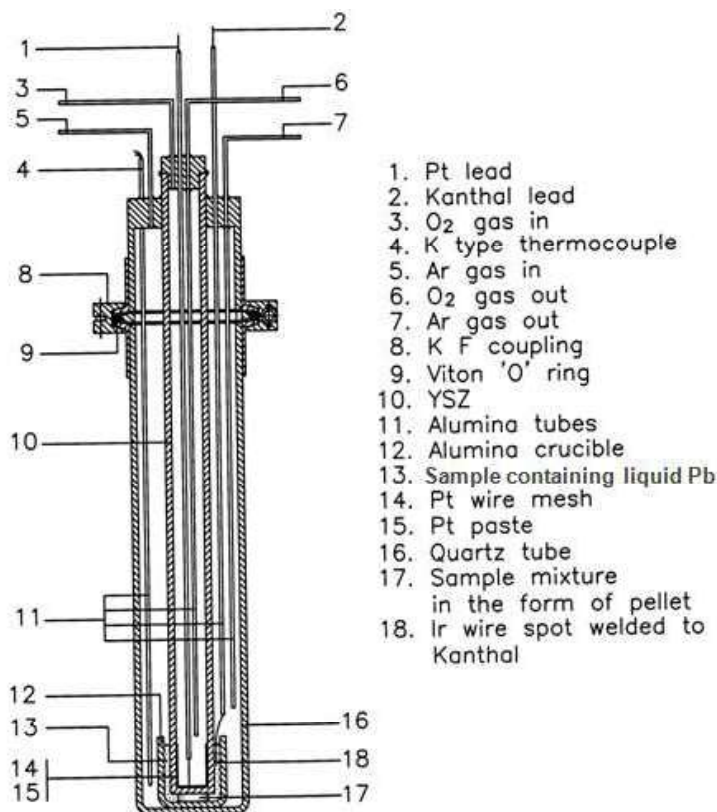


Fig. 4.5 Schematic representation of the emf cell

One end closed yttria stabilized zirconia (YSZ) solid electrolyte tube with a flat bottom (13 mm OD, 9 mm ID and 300 mm long, M/s Nikkato Corporation, Japan) was used for constructing the galvanic cells. The reference electrode for the

cells was prepared by applying platinum paste (M/s Eltecks Corporation, India) over the inner bottom surface of the solid electrolyte tube and heating it in air at 1373 K for 2 h. This resulted in a uniform and porous platinum coating over the electrolyte surface. A platinum wire, which had been spot welded to platinum mesh was cofired with the platinum paste. This served as the electrical lead for the reference electrode. A similar porous platinum electrode was formed at the external bottom surface of the electrolyte tube. The solid electrolyte tube was then fastened to a stainless steel KF coupling by means of a high temperature epoxy seal. A K-type thermocouple was inserted through the stainless steel coupling and kept very close to the electrode-electrolyte assembly for measuring the cell temperature. This thermocouple used in the experiment was calibrated prior to the actual measurements against a standard calibrated thermocouple supplied by National Physical Laboratory, India. Uncertainty in the temperature measurement is found to be ± 1 K. The mating component of the KF coupling was attached to a one end closed quartz tube using the epoxy seal. The entire cell assembly was then kept enclosed in this one end closed quartz tube and sealed using a viton O-ring and KF clamp. The cell assembly had provisions for flowing gases through the sample and reference compartments. The performance of the emf cell was tested by measuring the null emf as a function of temperature by maintaining identical oxygen pressures on both sides of the electrolyte (air-air and oxygen-oxygen). Data obtained for null emf measurement are given in Table 1 in the Appendix. The performance of the cell was also checked at several temperatures by passing oxygen at one electrode and air at the other electrode. Later, the Pt-electrode and the Pt lead present at the external surface of the electrolyte tube were removed, thoroughly cleaned and used for measurements with sample electrodes of cells (I), (II) and (III).

Two sample pellets of different compositions falling within the phase field of Pb-MoO₂-PbMoO₄ were used for measurements with cell (I). Similarly two sets of emf measurements were carried out with cell (II) using two sample electrodes of different compositions and falling within Pb-PbMoO₄-Pb₂MoO₅ phase field. Two different sample pellets with composition falling within Pb-Pb₂MoO₅-Pb₅MoO₈ were used for cell (III). As iridium is compatible with Pb, a short iridium wire (0.5 mm diameter and 35 mm long, M/s Goodfellow Cambridge Limited, England) spot welded to kanthal wire was used as the electrical lead for the sample. Pellets of the sample electrodes were made by compacting the homogeneous mixture of constituent phases. Assembling of the emf cell was carried out inside an argon atmosphere glove box. Appropriate amount of Pb metal was taken in a recrystallized alumina crucible and melted. The sample pellet was then kept immersed in liquid Pb by placing the solid electrolyte tube over it in such a way that the lower end of the iridium wire dipped into liquid Pb. The cell assembly was cooled slowly and taken outside the glove box and placed in the constant temperature zone of a furnace. A 55 mm long hollow cylindrical stainless steel block was also kept in the constant temperature zone of the furnace to further enhance the uniformity of the temperature in the zone. Any a.c pick up in the emf signal was avoided by grounding the stainless steel block. During emf measurements, high purity argon and oxygen gases were passed through the sample and reference compartments, respectively. Cell emf was measured using a high impedance electrometer (input impedance > 10¹⁴Ω, Keithley, Model 617) and the thermocouple output was measured using a multimeter (M/s Agilent Technologies, Malaysia, Model 34970A, data acquisition/switch unit). Data were recorded using a computer interface.

Emf measurements were carried out by performing several random heating and cooling cycles. At each temperature, the readings were recorded when the cell emf was stable within ± 0.05 mV at least for four hours. The reproducibility of the cell emf and attainment of equilibrium in the cell was checked by shorting the electrical leads briefly. The cell emf restored to the pre-test emf value within five minutes. The reproducibility of the cell emf was also confirmed by the emf data obtained during the random heating and cooling cycles. The thermo-emf between the two dissimilar electrical leads, i.e. kanthal and platinum was measured in a separate experiment by forming a junction between the two electrical leads followed by the measurement of the thermo-emf between them as a function of temperature. The cell emf was corrected using this thermo emf data. As the junction between kanthal and iridium was present at the constant temperature zone of the furnace along with the sensor head, the thermo-emf due to this junction need not be considered. At the end of the emf measurements, sample pellets were retrieved and analyzed by XRD to confirm the coexisting phases.

4.3.5 Determination of enthalpies of formation of lead molybdates by solution calorimetry

The enthalpies of dissolution of the ternary compounds were determined by using a homemade version of the isoperibol calorimeter described in Chapter 2. The chemical calibration of the calorimeter was carried out by using tris(hydroxyl methyl) aminomethane (s) (TRIS) (99.8% purity, M/s Merck, UK). The calorimetric solvent used was 0.1 mol kg^{-1} HCl. Calorimetric measurements of samples of ternary lead molybdates as well as the binary oxides PbO (s) and MoO₃ (s) were performed using 125 ml of 2.02 mol kg^{-1} NaOH as the calorimetric solvent. The current and duration of its passage for the insitu electrical calibration were decided by the time taken for

the sample to dissolve completely under the experimental conditions and the weight of the sample taken for each experiment. The maximum time taken for the dissolution of the samples was around 3 min. The temperature change, ΔT , during the experiment with the ternary compounds and starting components was also corrected for the heat exchange between calorimeter and surroundings and was used for the evaluation of the enthalpy change for the reaction. Calorimetric measurements were repeated several times to obtain the reproducible data.

4.3.6. Determination of molar heat capacities of lead molybdates by differential scanning calorimetry

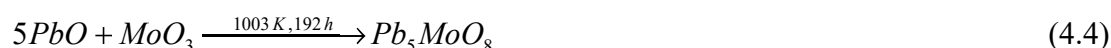
The heat capacity of PbMoO_4 (s) and Pb_2MoO_5 (s) were measured using a heat flux DSC (Mettler Toledo, Model No. HP DSC827e, Switzerland). Temperature calibration was carried out by measuring the melting points of high purity indium and zinc metals. The classical three step procedure was adopted for the measurement of heat capacity. The three steps are: i) blank run, ii) calibration run and iii) sample run. In the blank run, the heat flow rate is determined using empty aluminium pans of equal weight in the sample and reference sides. A disc of sapphire (NIST, USA) is used as the calibration reference. In the calibration run, sapphire is placed in the sample pan while the reference side is unchanged and the heat flow rate is measured as in the case of blank run. During the sample run, sapphire in the sample pan is replaced by the sample and the heat flow rate is measured. In addition to the heat flow calibration by sapphire, performance of the DSC was also verified by measuring the heat capacity of MoO_3 (s). The sample pellets were prepared by compaction of the powders followed by sintering them under vacuum. The sintered pellets were then sealed in 40 mm^3 aluminium pans and used for the measurement. For each sample, the reproducibility was checked by repeating the measurement at least for five to six

times. Measurements were also repeated with two different pellets of the same sample. The DSC measurements were carried out in high purity argon atmosphere at a flow rate of 50 ml min⁻¹ over the temperature range of 300 to 800 K at a heating rate of 10 K min⁻¹. The temperature program used for the measurement consisted of three segments: an isothermal segment at the initial temperature with a dwelling period of 10 min, followed by a dynamic segment at a heating rate of 10 K min⁻¹ and finally an isothermal segment at the final temperature for 10 min. The samples used for measurements were characterized by XRD before and after the calorimetric runs. The heat capacity data at each temperature was obtained by taking the average of calorimetric runs carried out with two sample pellets.

4.4 Results and discussion

4.4.1 Preparation of ternary compounds

The solid state reactions leading to the formation of three ternary compounds existing on the PbO-MoO₃ line can be represented by the following equations:



The XRD patterns of PbMoO₄, Pb₂MoO₅ and Pb₅MoO₈ prepared were matched with PCPDF patterns viz., 00-044-1486, 04-010-3859, 04-011-4216, respectively. The attempts to prepare Pb₃Mo₁₆O₂₄ with Mo, MoO₂ and Pb as starting components at 1215 K resulted only in the partial formation of the compound (XRD pattern of partially formed Pb₃Mo₁₆O₂₄ is matched with PCPDF pattern 00-080-2096) even after prolonged heating (480 h). Upon heating the partially formed compound along with the unreacted starting components at 773 K and 998 K, it decomposed to

give PbMoO_4 , Mo and MoO_3 mixture indicating that the compound is unstable at 773 and 998 K. The preparation of PbMo_5O_8 with a stoichiometric mixture of Pb, Mo and MoO_2 at 1473 K was not successful and has not yielded the compound. XRD analysis of the product obtained after the equilibration has shown the presence of Pb, Mo and MoO_2 . Similar results were obtained in the case of preparation of PbMo_5O_8 at 773 and 998 K (Table 4.3).

4.4.2 Studies involving equilibrations using PbO-MoO_3 and PbO-MoO_2 mixtures

Table 4.4 summarizes the results from equilibration studies carried out to examine the possible existence of additional ternary compounds in the Pb-Mo-O system. The XRD patterns of the equilibrium phases in samples with different molar ratios of PbO and MoO_3 have shown the presence of either a mixture of two ternary compounds or that of a ternary compound and the metal oxide. These results conclusively indicated that only three ternary compounds, namely PbMoO_4 , Pb_2MoO_5 and Pb_5MoO_8 , are present in the PbO-MoO_3 pseudo binary system. The results also show that Pb_5MoO_8 does not appear as equilibrium phase at 773 K (see sample nos. 3 and 4 in Table 4.4).

The long term equilibrations of samples with different molar ratios of PbO and MoO_2 have shown that there are no additional ternary compounds involving PbO and MoO_2 . However, the results revealed the existence of different phase fields, of which Pb is found to be one of the coexisting phases. The phase fields identified to be present at 773 K are (i) Pb- MoO_2 - PbMoO_4 (ii) Pb- PbMoO_4 - Pb_2MoO_5 and (iii) Pb- Pb_2MoO_5 -PbO. At 998 K, the phase fields identified are: (i) Pb- MoO_2 - PbMoO_4 (ii) Pb- PbMoO_4 - Pb_2MoO_5 (iii) Pb- Pb_2MoO_5 - Pb_5MoO_8 and (iv) Pb- Pb_5MoO_8 -PbO. The results of these equilibrations also indicated that Pb_5MoO_8 is not stable at 773 K.

4.4.3 Studies involving partial reduction of ternary compounds followed by long term equilibrations

The equilibrium phases obtained after the long term equilibration of the products from partial reduction of the ternary compounds are given in Table 4.5. It can be seen that upon partial reduction, the overall compositions of the samples, namely, PbMoO_4 , Pb_2MoO_5 , and Pb_5MoO_8 have moved towards lower oxygen content (indicated as sample nos. 10, 11 and 12 in Fig. 4.3). The XRD analysis of these samples after long term equilibration at 773 K and at 998 K has confirmed the existence of the following phase fields at 773 K: (i) $\text{Pb-MoO}_2\text{-PbMoO}_4$ (ii) $\text{Pb-PbMoO}_4\text{-Pb}_2\text{MoO}_5$ and (iii) $\text{Pb-Pb}_2\text{MoO}_5\text{-PbO}$. The coexisting phase fields at 998 K are: (i) $\text{Pb-MoO}_2\text{-PbMoO}_4$ (ii) $\text{Pb-PbMoO}_4\text{-Pb}_2\text{MoO}_5$ and (iii) $\text{Pb-Pb}_2\text{MoO}_5\text{-Pb}_5\text{MoO}_8$. The appearance of same phases at the end of first and second spells of equilibrations confirmed the attainment of equilibrium in all these experiments.

4.4.4 Studies involving long term equilibrations using different starting components and equilibrations in liquid lead

Additional equilibrations using different starting components and equilibrations in liquid Pb further confirmed the coexisting phase fields and the summary of these results are given in Tables 4.6 to 4.9. In the ternary phase diagram of Pb-Mo-O system reported by Feja and Reichelt [19], the existence of additional three phase fields namely, $\text{Pb-Mo-Pb}_3\text{Mo}_{16}\text{O}_{24}$, $\text{Mo-MoO}_2\text{-Pb}_3\text{Mo}_{16}\text{O}_{24}$ and $\text{Pb-MoO}_2\text{-Pb}_3\text{Mo}_{16}\text{O}_{24}$ have been reported. To examine the existence of these phase fields, equilibrations were carried out using PbO, Mo and MoO_3 as the starting materials (Table 4.7). Two samples with different overall compositions falling within each reported phase fields were chosen for equilibration. Equilibrations were performed at both 773 and 998 K and the results obtained after XRD analysis are given in Table 4.7. If the phase fields reported in ref. [19] exist, the long term

equilibration of the samples 28 and 29 would have given Pb, Mo and $\text{Pb}_3\text{Mo}_{16}\text{O}_{24}$ as the equilibrium phases and the equilibration of samples 30 and 31 would have given Mo, MoO_2 and $\text{Pb}_3\text{Mo}_{16}\text{O}_{24}$. In both cases we observed the presence of only Pb, Mo and MoO_2 as equilibrium phases. Similarly, the equilibration of samples 32 and 33 whose overall compositions fall in the proposed field of Pb-Mo- $\text{Pb}_3\text{Mo}_{16}\text{O}_{24}$ has also resulted in a mixture of Pb, Mo and MoO_2 . These results conclusively indicate the non existence of the three phase fields suggested by Feja and Reichelt [19]. Also our experiments showed that $\text{Pb}_3\text{Mo}_{16}\text{O}_{24}$ was only partially formed at 1215 K but this decomposed to Pb, Mo and MoO_2 on prolonged equilibration. It is also to be mentioned that PbMo_5O_8 was not formed at 1473, 998 and 773 K in spite of equilibration of Pb, Mo and MoO_2 for prolonged duration (Table 4.3). Hence we conclude that the two compounds $\text{Pb}_3\text{Mo}_{16}\text{O}_{24}$ and PbMo_5O_8 are unstable at 773 K and 998 K.

4.4.5 Studies involving long term equilibrations to determine the temperature range of stability of Pb_5MoO_8

Long term equilibrations were performed to identify the range of temperature at which Pb_5MoO_8 compound is stable. The results are presented in Table 4.10. It can be seen that when Pb_5MoO_8 was used as the starting component, it had undergone decomposition to give a mixture of PbO and Pb_2MoO_5 phases for equilibrations in the temperature range of 748 to 898 K. However, the equilibration of Pb_5MoO_8 at temperatures between 918 and 1003 K had shown the presence of Pb_5MoO_8 phase only. Thus it is clear that Pb_5MoO_8 decomposes between 898 and 918 K. In the case of equilibration experiments performed using a mixture of 1:3 Pb_2MoO_5 :PbO, the same phases were retained when equilibrations were performed at 773 and 898 K even after heating for a duration of 720 h. However, the equilibration at 923 K has

yielded the single phase of Pb_5MoO_8 . These results also indicate that Pb_5MoO_8 appears as stable phase between 898 and 923 K. Equilibrations were also performed to see the formation of Pb_5MoO_8 from a mixture of PbO and MoO_3 taken in the 5:1 molar ratio. While the equilibrations at 765 and 867 K have retained the two phases even after heating for a duration of 840 h, the equilibrations in the temperature range of 920-981 K resulted in the formation of Pb_5MoO_8 single phase. Based on these equilibration studies using different starting components, it is concluded that Pb_5MoO_8 becomes thermodynamically stable phase only at temperatures above 898 K.

Based on the results obtained from the above series of long term phase equilibration experiments, the existence of the following phase fields are deduced: At 773 K: (1) Pb-Mo-MoO_2 (2) $\text{Pb-MoO}_2\text{-PbMoO}_4$ (3) $\text{Pb-PbMoO}_4\text{-Pb}_2\text{MoO}_5$ (4) $\text{Pb-Pb}_2\text{MoO}_5\text{-PbO}$. At 998 K (1) Pb-Mo-MoO_2 (2) $\text{Pb-MoO}_2\text{-PbMoO}_4$ (3) $\text{Pb-PbMoO}_4\text{-Pb}_2\text{MoO}_5$ (4) $\text{Pb-Pb}_2\text{MoO}_5\text{-Pb}_5\text{MoO}_8$ and (5) $\text{Pb-Pb}_5\text{MoO}_8\text{-PbO}$.

Based on these results, partial phase diagrams of Pb-Mo-O system valid at 773 and 998 K were constructed and are shown in Figs. 4.6 and 4.7. It can be seen that upon increasing the oxygen concentration in liquid Pb coexisting with Mo metal, MoO_2 would precipitate first. With further increase of oxygen concentration, PbMoO_4 appears as stable phase with simultaneous disappearance of Mo metal. Further increase in the oxygen content in liquid Pb would lead to the appearance of Pb_2MoO_5 .

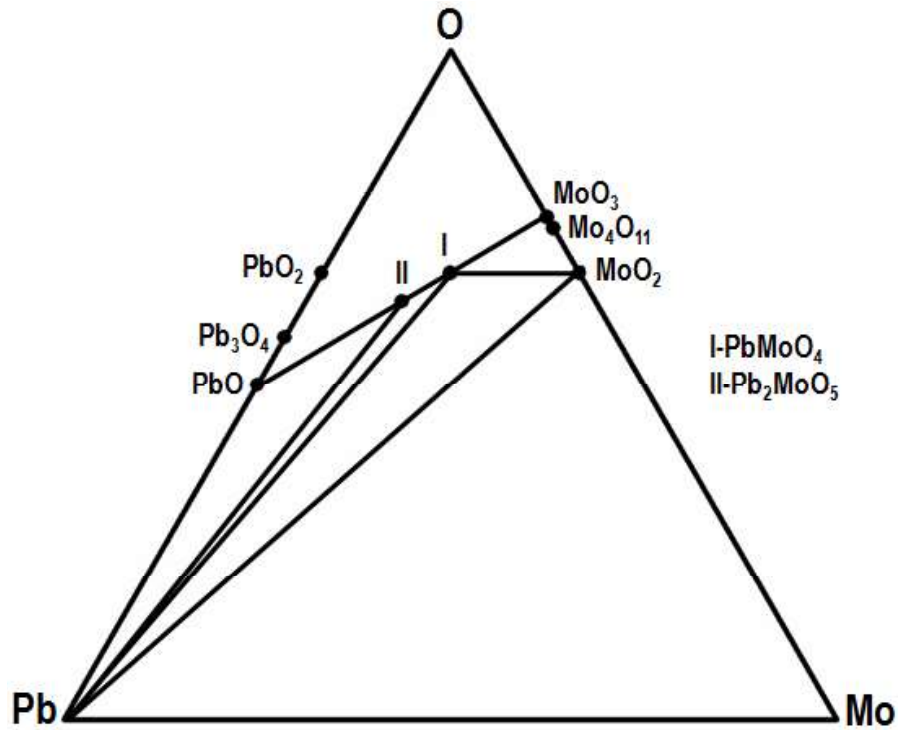


Fig. 4.6 Isothermal section of Pb-Mo-O system at 773 K

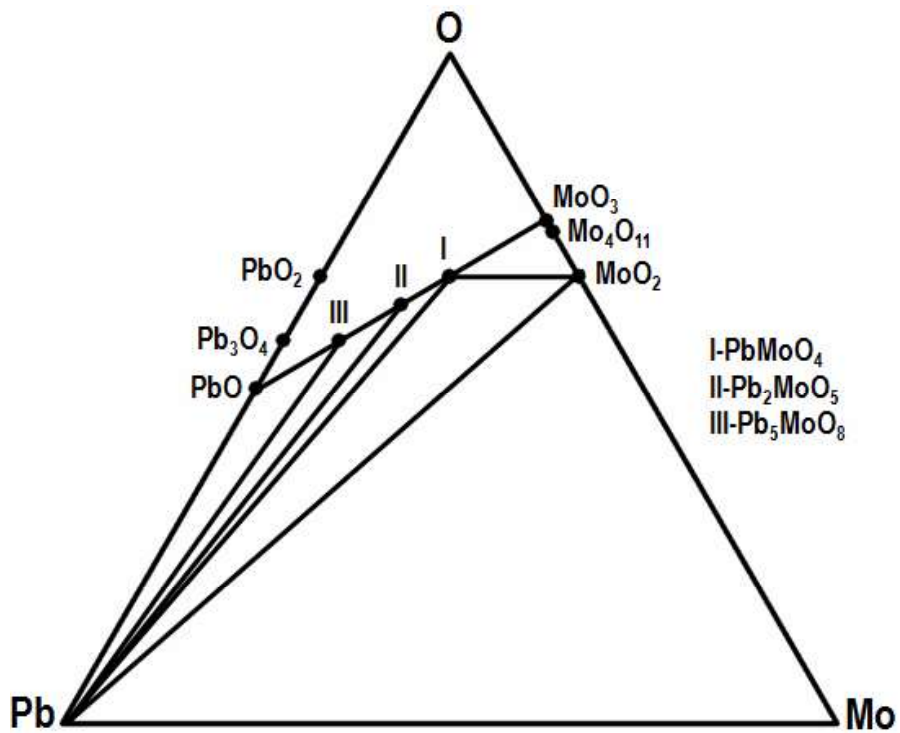


Fig. 4.7 Isothermal section of Pb-Mo-O system at 998 K

4.4.6 Oxygen potential measurements

4.4.6.1 Standard molar Gibbs energy of formation of $PbMoO_4$ (s)

The emf values that were measured in cell (I) as a function of temperature are given in Table 4.11. The variation of cell emf with temperature is shown in Fig. 4.8 and the data was fitted to the following expression:

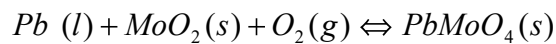
$$E \pm 1.1/mV = 1166.8 - 0.3508(T/K) \quad (T : 772 - 1017 K) \quad (4.5)$$

The uncertainty expressed is the expanded uncertainty with 0.95 level of confidence.

Table 4.11 Variation of emf of cell (I) with temperature

<i>Sample 1</i>		<i>Sample 2</i>	
Temperature / K	Emf / mV	Temperature / K	Emf / mV
867.9	860.6	772.0	897.4
1017.7	810.4	917.8	845.1
821.3	878.4	924.4	842.7
994.5	817.2	970.7	826.5
898.1	851.0	957.1	831.0
800.5	886.6	846.6	868.4
805.7	884.9	785.0	892.4
952.1	832.5	905.0	848.7
986.8	819.9	885.1	854.2
-	-	921.9	842.8
-	-	1012.6	813.2
-	-	972.2	826.8
-	-	947.7	835.1

The chemical equilibrium at the sample electrode is represented as below:



$$\Delta_f G_m^\circ < PbMoO_4 > = \Delta_f G_m^\circ < MoO_2 > + RT \ln p_{O_2}^S \quad (4.6)$$

where $p_{O_2}^S$ is the partial pressure of oxygen at the sample electrode. As discussed in

Chapter 3, the cell emf can be given as:

$$E = \frac{RT}{4F} \ln \frac{p_{O_2}^R}{p_{O_2}^S} \quad (4.7)$$

where E is the electromotive force in volts, R is universal gas constant (8.314 J K⁻¹ mol⁻¹), F is the Faraday constant (96485 C mol⁻¹) and $p_{O_2}^R$ is the partial pressure of oxygen in the reference electrode.

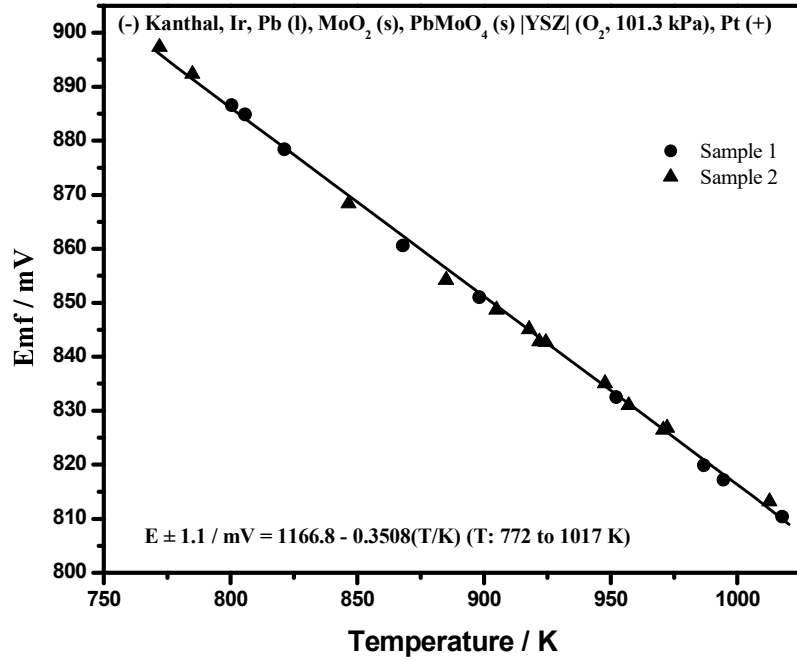


Fig. 4.8 Variation of emf with temperature in cell (I) for Pb-MoO₂-PbMoO₄ phase field

Equation (4.7) can be written as

$$4FE = RT \ln p_{O_2}^R - RT \ln p_{O_2}^S \quad (4.8)$$

Since $p_{O_2}^R = 1$ atm,

$$RT \ln p_{O_2}^S = -4FE \quad (4.9)$$

Thus the standard molar Gibbs energy of formation of PbMoO₄(s) can be obtained from the measured emf values as given below:

$$\Delta_f G_m^\circ < PbMoO_4 > = \Delta_f G_m^\circ < MoO_2 > - 4FE \quad (4.10)$$

By substituting the emf data given by expression (4.5) and by using the literature data for $\Delta_f G_m^\circ < MoO_2 >$ from ref. [33],

$$\Delta_f G_m^\circ < MoO_2 > \pm 0.6 / kJ mol^{-1} = -579.8 + 0.1700 (T / K) \quad (T: 925 - 1533 K) \quad (4.11)$$

the standard molar Gibbs energy of formation of $PbMoO_4$ (s) was derived and is given below:

$$\Delta_f G^\circ < PbMoO_4 > \pm 0.7 / kJ mol^{-1} = -1030.1 + 0.3054(T / K) \quad (T: 772 - 1017 K) \quad (4.12)$$

The error given in the expression is the combined expanded uncertainty with 0.95 level of confidence.

Figure 4.9 compares the Gibbs energy of formation of $PbMoO_4$ (s) obtained from this work with that estimated by Barin [26]. It is seen that the values are in good agreement. The $\Delta_f G_{298}^\circ < PbMoO_4 >$ can be obtained by extrapolation of the data given by equation (4.12) and this value is $-939.0 \text{ kJ mol}^{-1}$. This value is compared with the reported values and given in Table 4.12. The present value is found to be in agreement with those reported by the previous investigators [23, 25-27, 29].

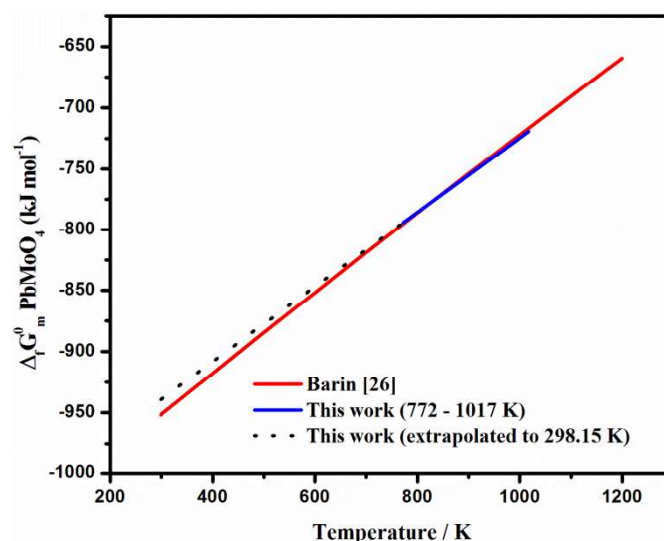


Fig. 4.9 Comparison of $\Delta_f G_m^\circ < PbMoO_4 >$ from the present work and that reported in ref. [26]

Table 4.12 Comparison of $\Delta_f G_{298}^\circ < PbMoO_4 >$ reported in literature and that obtained in the present work

Reference	$\Delta_f G_{298}^\circ < PbMoO_4 >$ / $kJ mol^{-1}$
Wagman et al. [23]	951.4
Weller and Kelley [25]	-944.3
Barin [26]	-951.7
Bissengaliyeva et al. [27]	-949.1
Naumov et al. [29]	948.47
Present work	-939.0

4.4.6.2 Standard molar Gibbs energy of formation of Pb_2MoO_5 (s)

The emf values obtained as a function of temperature from cell (II) are given in Table 4.13 and shown in Fig. 4.10. They can be represented by the following least squares fitted expression:

$$E \pm 1.5 / mV = 1129.5 - 0.4238(T / K) \quad (T : 741 - 1021 K) \quad (4.13)$$

The uncertainty expressed is the expanded uncertainty with 0.95 level of confidence.

Table 4.13 Variation of emf of cell (II) with temperature

<i>Sample 1</i>		<i>Sample 2</i>	
Temperature / K	Emf / mV	Temperature / K	Emf / mV
988.5	709.2	971.7	714.3
1006.8	704.5	1021.4	697.0
741.7	814.1	959.5	723.4
836.3	776.3	1009.6	702.3
920.6	737.7	933.6	731.9
756.6	807.9	911.0	742.1
881.6	756.6	961.6	722.1
898.5	750.0	811.9	786.8
868.3	763.2	862.2	766.3
823.6	781.4	788.7	794.2
-	-	770.5	802.3
-	-	946.8	729.3

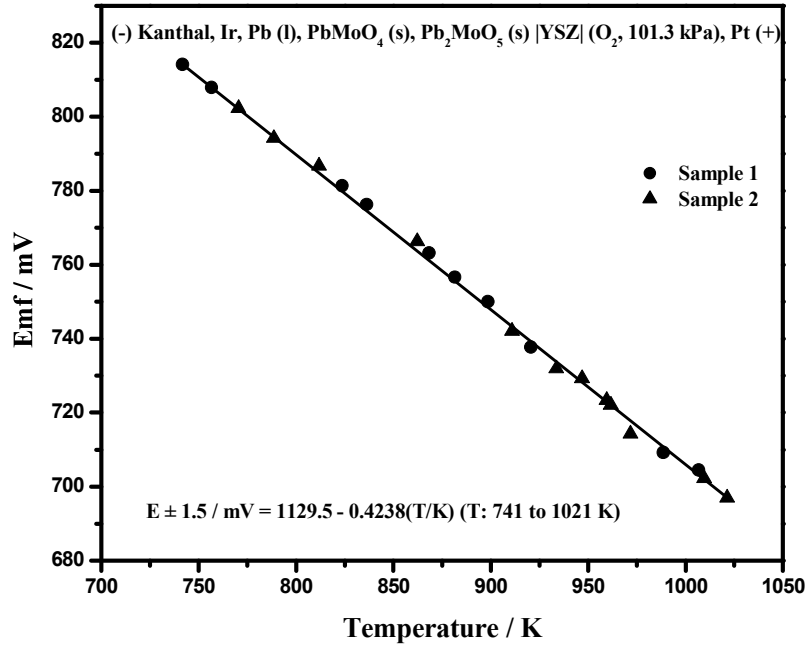
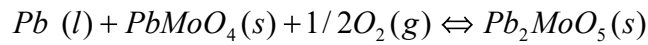


Fig. 4.10 Variation of emf with temperature in cell (II) for Pb-PbMoO₄-Pb₂MoO₅ phase field

For cell (II), the cell reaction can be represented as below:



The standard molar Gibbs energy of formation of Pb₂MoO₅(s) can be related to the measured cell emf values by the following expression:

$$\Delta_f G_m^\circ < Pb_2MoO_5 > = \Delta_f G_m^\circ < PbMoO_4 > - 2FE \quad (4.14)$$

By incorporating the values of emf from equation (4.13) and using the value of

$\Delta_f G_m^\circ < PbMoO_4 >$ from expression (4.12) $\Delta_f G_m^\circ < Pb_2MoO_5 >$ could be obtained as:

$$\Delta_f G^\circ < Pb_2MoO_5 > \pm 0.8 \text{ kJ mol}^{-1} = -1248.1 + 0.3872(T/K) \text{ (T: 741-1021K)} \quad (4.15)$$

The error given in the expression is the combined expanded uncertainty with 0.95 level of confidence.

4.4.6.3 Standard molar Gibbs energy of formation of Pb_5MoO_8 (s)

As Pb_5MoO_8 is found to be stable only above 898 K, emf measurements were carried out in the temperature range of 967 to 905 K. The emf values obtained as a function of temperature from cell (III) are given in Table 4.14 and shown in Fig. 4.11.

Table 4.14 Variation of emf of cell (III) with temperature

<i>Sample 1</i>		<i>Sample 2</i>	
Temperature / K	Emf / mV	Temperature / K	Emf / mV
904.8	695.7	966.6	685.4
905.3	695.6	960.7	686.5
909.6	694.9	958.6	686.6
916.3	693.8	957.5	686.8
921.8	692.8	957.8	686.7
934.6	690.6	956.2	687.3
915.6	693.9	949.9	688.2
925.0	692.3	949.4	688.5
		945.7	689.2
		945.2	689.5
		936.1	690.8
		935.8	690.5
		930.6	691.4

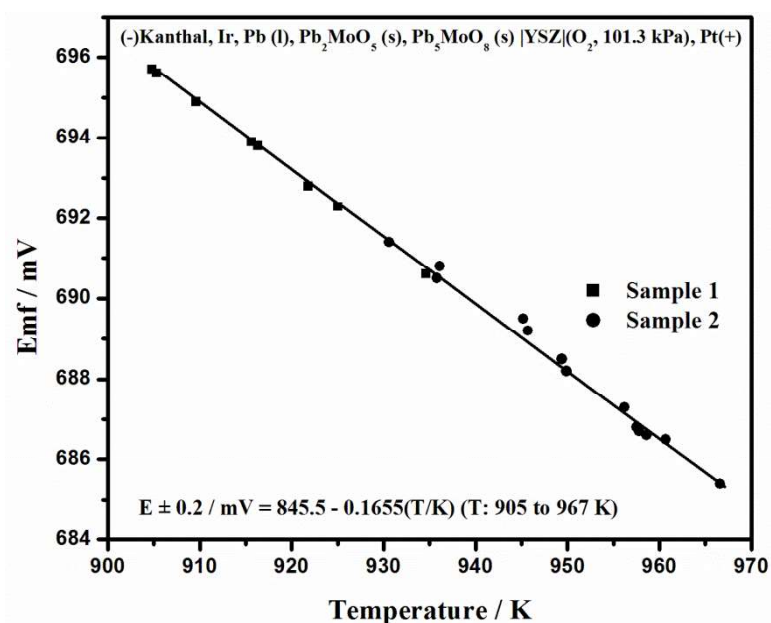


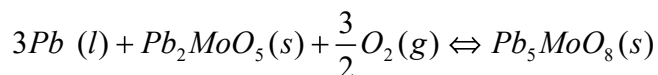
Fig. 4.11 Variation of emf with temperature in cell (III) for Pb-Pb₂MoO₅-Pb₅MoO₈ phase field

They can be represented by the following least squares fitted expression:

$$E \pm 0.2 / mV = 845.5 - 0.1655(T / K) \quad (T : 905 - 967 K) \quad (4.16)$$

The uncertainty expressed is the expanded uncertainty with 0.95 level of confidence.

For cell (III), the cell reaction can be represented as below:



The standard molar Gibbs energy of formation of $Pb_5MoO_8(s)$ can be related to the measured cell emf values by the following expression:

$$\Delta_f G_m^\circ < Pb_5MoO_8 > = \Delta_f G_m^\circ < Pb_2MoO_5 > - 6FE \quad (4.17)$$

By incorporating the values of emf from equation (4.16) and using the value of $\Delta_f G_m^\circ < Pb_2MoO_5 >$ from expression (4.15), the $\Delta_f G_m^\circ < Pb_5MoO_8 >$ could be obtained as

$$\Delta_f G_m^\circ < Pb_5MoO_8 > \pm 0.8 / kJ mol^{-1} = -1737.6 + 0.4831(T / K) \quad (T : 884 - 967 K) \quad (4.18)$$

The error given in the expression is the combined expanded uncertainty with 0.95 level of confidence.

4.4.7 Standard molar enthalpies of formation of $PbMoO_4 (s)$, $Pb_2MoO_5 (s)$ and $Pb_5MoO_8 (s)$

The experimental results obtained for the measurement of enthalpy of solution of $PbMoO_4 (s)$, $Pb_2MoO_5 (s)$ and $Pb_5MoO_8 (s)$ along with the starting components $PbO (s)$ and $MoO_3 (s)$ are given in Table 4.15. The molar enthalpies of solution of $PbMoO_4(s)$, $Pb_2MoO_5 (s)$, $Pb_5MoO_8 (s)$, $PbO (s)$ and $MoO_3 (s)$, $\Delta_{sol} H_m^\circ$ obtained are (21.87 ± 0.82) , (35.04 ± 0.84) , (60.70 ± 1.52) , (15.36 ± 0.27) and (-90.61 ± 1.93) $kJ mol^{-1}$, respectively. The molar enthalpy of formation of the ternary compounds from the component oxides and elements were obtained by considering suitable thermochemical reaction schemes presented in Tables 4.16, 4.17 and 4.18 for

PbMoO₄ (s), Pb₂MoO₅ (s) and Pb₅MoO₈ (s), respectively. For the calculation of enthalpies of formation from elements, values of enthalpies of formation of binary oxides were taken from ref. [29].

Table 4.15 Experimentally determined values of enthalpies of dissolution (ΔH) and molar enthalpies of dissolution ($\Delta_{sol}H_m^o$) of PbMoO₄ (s), Pb₂MoO₅ (s), PbO (s) and MoO₃ (s) in 2.02 ± 0.01 mol / kg NaOH (mass of solvent = 134.08 ± 0.01 g) at 298.15 K^{*} and 0.1 MPa^a

Sample	Weight (w / g) ^a	Experimental enthalpy change (ΔH / J)	Molar enthalpy of solution ($\Delta_{sol}H_m^o$ / kJ mol ⁻¹)
PbMoO ₄ (molar mass = 367.1376 g mol ⁻¹)	0.5065	30.07	21.80
	0.5004	29.88	21.92
	0.5053	29.40	21.36
	0.5005	30.76	22.57
	0.5050	29.60	21.52
	0.4521	27.36	22.22
	0.4893	29.04	21.79
	0.4358	25.90	21.82
Average: (21.87 ± 0.82)^b			
Pb ₂ MoO ₅ (molar mass = 590.335 g mol ⁻¹)	0.5052	29.91	34.95
	0.5079	30.35	35.27
	0.5004	30.58	36.07
	0.5014	31.25	36.79
	0.5053	29.37	34.31
	0.4992	29.17	34.50
	0.5064	29.38	34.25
	0.4916	29.71	35.67
	0.4954	28.17	33.57
Average: (35.04 ± 0.84)^b			
PbO (molar mass = 223.191 g mol ⁻¹)	0.4980	33.62	15.07
	0.4644	31.94	15.35
	0.5645	39.32	15.54
	0.4812	33.32	15.45
	0.4025	27.80	15.41
Average: (15.36 ± 0.27)^b			
MoO ₃ (molar mass = 143.937g mol ⁻¹)	0.4743	-304.45	-92.38
	0.4650	-293.41	-90.82
	0.5060	-317.87	-90.42
	0.4709	-290.60	-88.82
Average: (-90.61 ± 1.93)^b			

*Temperature stability inside the calorimeter prior to start of experiment was within ± 0.001 K. ^aStandard uncertainties, u , are $u(P) = 0.8$ kPa and $u(w) = 0.0001$ g. ^bExpanded uncertainty $U(\Delta_{sol}H_m^o)$, is calculated as 2σ of the mean with 0.95 level of confidence. Uncertainty from calibration was also included into the final uncertainty of the dissolution enthalpies.

Table 4.16 Thermodynamic reaction schemes for obtaining the enthalpies of formation from oxides and elements for PbMoO₄ (s) at T = 298.15 K^a (s = solid, soln = aqueous solution, g = gas) and P = 0.1 MPa^{*}

No.	Reaction	Enthalpy change (ΔH / kJ mol ⁻¹)	Source of data
From oxides	1 PbO (s) + 2 NaOH (soln) = (2 Na ⁺ + PbO ₂ ²⁻ + H ₂ O) (soln)	$\Delta H_1 = 15.36 \pm 0.27^b$	This work
	2 MoO ₃ (s) + 2 NaOH (soln) = (2 Na ⁺ + MoO ₄ ²⁻ + H ₂ O) (soln)	$\Delta H_2 = -90.61 \pm 1.93^b$	This work
	3 PbMoO ₄ (s) + 4 NaOH (soln) = (4 Na ⁺ + PbO ₂ ²⁻ + MoO ₄ ²⁻ + 2 H ₂ O) (soln)	$\Delta H_3 = 21.87 \pm 0.82^b$	This work
	4 PbO (s) + MoO ₃ (s) = PbMoO ₄ (s)	$\Delta H_4 = \Delta H_1 + \Delta H_2 - \Delta H_3 = \Delta_f H_{ox, 298}^\circ$ of PbMoO ₄ (s) = -97.12 ± 2.11^c	-
From elements	5 Pb (s) + 1/2 O ₂ (g) = PbO (s)	$\Delta H_5 = \Delta_f H_{298}^\circ$ of PbO (s) = -217.3 ± 0.3	[29]
	6 Mo (s) + 3/2 O ₂ (g) = MoO ₃ (s)	$\Delta H_6 = \Delta_f H_{298}^\circ$ of MoO ₃ (s) = -745.2 ± 0.4	[29]
	7 Pb (s) + Mo (s) + 2 O ₂ (g) = PbMoO ₄ (s)	$\Delta H_7 = \Delta H_5 + \Delta H_6 + \Delta H_4 = \Delta_f H_{298}^\circ$ of PbMoO ₄ (s) = -1059.6 ± 2.2^c	-

^a Temperature of the calorimeter prior to the actual experiment was stable within ± 0.001 K. ^{*} Standard uncertainty in pressure $u(P) = 0.8$ kPa. ^b Expanded uncertainties, $U(\Delta H)$ are calculated as 2σ of the mean and are at the 95 % confidence level. ^c Combined expanded uncertainties, $U_c(\Delta H)$ are calculated as 2σ of the mean and are at the 95 % confidence level. Uncertainty from calibration was also included into the final uncertainty of the dissolution enthalpies.

Table 4.17 Thermodynamic reaction schemes for obtaining the enthalpies of formation from oxides and elements for $\text{Pb}_2\text{MoO}_5(\text{s})$ at $T = 298.15 \text{ K}^a$ (s = solid, soln = aqueous solution, g = gas) and $P = 0.1 \text{ MPa}^*$

No.	Reaction	Enthalpy change ($\Delta H / \text{kJ mol}^{-1}$)	Source of data
From oxides	8 $\text{PbO}(\text{s}) + 2 \text{NaOH}(\text{soln}) = (2 \text{Na}^+ + \text{PbO}_2^{2-} + \text{H}_2\text{O})(\text{soln})$	$\Delta H_8 = 15.36 \pm 0.27^b$	This work
	9 $\text{MoO}_3(\text{s}) + 2 \text{NaOH}(\text{soln}) = (2 \text{Na}^+ + \text{MoO}_4^{2-} + \text{H}_2\text{O})(\text{soln})$	$\Delta H_9 = -90.61 \pm 1.93^b$	This work
	10 $\text{Pb}_2\text{MoO}_5(\text{s}) + 6 \text{NaOH}(\text{soln}) = (6 \text{Na}^+ + 2 \text{PbO}_2^{2-} + \text{MoO}_4^{2-} + 3 \text{H}_2\text{O})(\text{soln})$	$\Delta H_{10} = 35.04 \pm 0.84^b$	This work
	11 $2\text{PbO}(\text{s}) + \text{MoO}_3(\text{s}) = \text{Pb}_2\text{MoO}(\text{s})$	$\Delta H_{11} = 2\Delta H_8 + \Delta H_9 - \Delta H_{10} = \Delta_f H_{\text{ox},298}^\circ$ of $\text{Pb}_2\text{MoO}_5(\text{s}) = -94.93 \pm 2.17^c$	-
From elements	12 $\text{Pb}(\text{s}) + \frac{1}{2} \text{O}_2(\text{g}) = \text{PbO}(\text{s})$	$\Delta H_{12} = \Delta_f H_{298}^\circ$ of $\text{PbO}(\text{s}) = -217.3 \pm 0.3$	[29]
	13 $\text{Mo}(\text{s}) + \frac{3}{2} \text{O}_2(\text{g}) = \text{MoO}_3(\text{s})$	$\Delta H_{13} = \Delta_f H_{298}^\circ$ of $\text{MoO}_3(\text{s}) = -745.2 \pm 0.4$	[29]
	14 $2\text{Pb}(\text{s}) + \text{Mo}(\text{s}) + \frac{5}{2} \text{O}_2(\text{g}) = \text{Pb}_2\text{MoO}_5(\text{s})$	$\Delta H_{14} = 2\Delta H_{12} + \Delta H_{13} + \Delta H_{11} = \Delta_f H_{298}^\circ$ of $\text{Pb}_2\text{MoO}_5(\text{s}) = -1274.7 \pm 2.3^c$	-

^a Temperature of the calorimeter prior to the actual experiment was stable within $\pm 0.001 \text{ K}$. ^{*} Standard uncertainty in pressure $u(P) = 0.8 \text{ kPa}$. ^b Expanded uncertainties, $U_c(\Delta H)$ are calculated as 2σ of the mean and are at the 95 % confidence level. ^c Combined expanded uncertainties, $U_c(\Delta H)$ are calculated as 2σ of the mean and are at the 95 % confidence level. Uncertainty from calibration was also included into the final uncertainty of the dissolution enthalpies.

Table 4.18 Thermodynamic reaction schemes for obtaining the enthalpies of formation from oxides and elements for $\text{Pb}_5\text{MoO}_8(\text{s})$ at $T = 298.15 \text{ K}$ ^a ($\text{s} = \text{solid}$, $\text{soln} = \text{aqueous solution}$, $\text{g} = \text{gas}$) and $P = 0.1 \text{ MPa}$ ^{*}

No.	Reaction	Enthalpy change ($\Delta H / \text{kJ mol}^{-1}$)	Source of data
From oxides	15 $\text{PbO}(\text{s}) + 2 \text{NaOH}(\text{soln}) = (2 \text{Na}^+ + \text{PbO}_2^{2-} + \text{H}_2\text{O})(\text{soln})$	$\Delta H_{15} = 15.36 \pm 0.27$	This work
	16 $\text{MoO}_3(\text{s}) + 2 \text{NaOH}(\text{soln}) = (2 \text{Na}^+ + \text{MoO}_4^{2-} + \text{H}_2\text{O})(\text{soln})$	$\Delta H_{16} = -90.61 \pm 1.93$	This work
	17 $\text{Pb}_5\text{MoO}_8(\text{s}) + 12 \text{NaOH}(\text{soln}) = (12 \text{Na}^+ + 5 \text{PbO}_2^{2-} + \text{MoO}_4^{2-} + 6 \text{H}_2\text{O})(\text{soln})$	$\Delta H_{17} = 60.70 \pm 1.52$	This work
18 $5 \text{PbO}(\text{s}) + \text{MoO}_3(\text{s}) = \text{Pb}_5\text{MoO}_8(\text{s})$	$\Delta H_{18} = 5\Delta H_{15} + \Delta H_{16} - \Delta H_{17} = \Delta_f H_{\text{ox},298}^\circ$ of $\text{Pb}_5\text{MoO}_8(\text{s}) = -74.51 \pm 2.80$	-	
From elements	19 $\text{Pb} + \frac{1}{2} \text{O}_2 = \text{PbO}$	$\Delta H_{19} = \Delta_f H_{298}^\circ$ of $\text{PbO}(\text{s}) = -217.3 \pm 0.3$	[29]
	20 $\text{Mo} + 3/2 \text{O}_2 = \text{MoO}_3$	$\Delta H_{20} = \Delta_f H_{298}^\circ$ of $\text{MoO}_3(\text{s}) = -745.2 \pm 0.4$	[29]
	21 $5\text{Pb} + \text{Mo} + 4\text{O}_2 = \text{Pb}_5\text{MoO}_8$	$\Delta H_{21} = 5\Delta H_{19} + \Delta H_{20} + \Delta H_{18} = \Delta_f H_{298}^\circ$ of $\text{Pb}_5\text{MoO}_8(\text{s}) = -1906.2 \pm 3.2$	-

^aTemperature of the calorimeter prior to the actual experiment was stable within $\pm 0.001 \text{ K}$. ^{*}Standard uncertainty in pressure $u(P) = 0.8 \text{ kPa}$. ^b Expanded uncertainties, $U(\Delta H)$ are calculated as 2σ of the mean and are at the 95 % confidence level. ^c combined expanded uncertainties, $U_c(\Delta H)$ are calculated as 2σ of the mean and are at the 95 % confidence level. Uncertainty from calibration was also included into the final uncertainty of the dissolution enthalpies.

The calculated enthalpies of formation from the corresponding oxides, $\Delta_f H_{ox,298}^\circ$, for PbMoO_4 (s), Pb_2MoO_5 (s) and Pb_5MoO_8 (s) are (-97.12 ± 2.11) , (-94.93 ± 2.17) and (-74.51 ± 2.80) kJ mol^{-1} respectively, whereas the calculated enthalpies of formation from elements $\Delta_f H_{298}^\circ$, are (-1059.6 ± 2.2) , (-1274.7 ± 2.3) and (-1906.2 ± 3.2) kJ mol^{-1} , respectively. The enthalpy of formation of PbMoO_4 (s) obtained in the present study is found to be in good agreement with values obtained by the previous investigators [20-24] given in Table 4.2.

4.4.8 Heat capacity measurements

The performance of the differential scanning calorimeter was verified by measuring the heat capacity of MoO_3 (s) as described in Chapter 3. The combined expanded uncertainty associated with the heat capacity measurements of the lead molybdates were calculated by incorporating the relative uncertainties of experimental data and the relative uncertainty attributed to the instrument. The relative uncertainty of the instrument was determined from the measured C_p values of MoO_3 (s) (Table 3.21 and Fig. 3.19 in Chapter 3). The relative uncertainty in the measured heat capacity of the samples were calculated as $\Delta x/x$ where Δx is the maximum standard uncertainty observed and x is the smallest measured C_p value.

4.4.8.1 Molar heat capacity of PbMoO_4 (s)

The XRD patterns of PbMoO_4 (s) samples retrieved after heat capacity measurements were identical to their XRD patterns before measurement indicating that the compound has not undergone any changes during the measurements. Figure 4.12 represents the experimental heat capacity of PbMoO_4 (s) as a function of temperature over the range of 313 to 798 K.

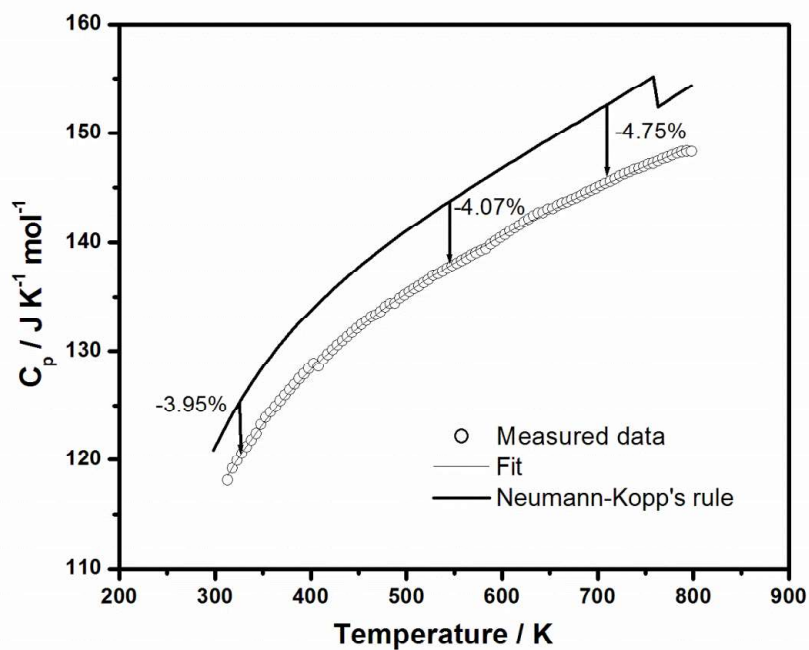


Fig. 4.12 Variation of molar heat capacity of $\text{PbMoO}_4(\text{s})$ with temperature

The data can be fitted to the following least squares expression:

$$C_p \pm 4.1 / JK^{-1} mol^{-1} = 127.31 + 30.47 \times 10^{-3} T - 1.79 \times 10^{-6} T^{-2} \quad (T : 313 - 798 K) \quad (4.19)$$

The error given in the expression is the combined expanded uncertainty with 0.95 level of confidence.

The measured heat capacity values of $\text{PbMoO}_4(\text{s})$ along with the fitted values for the selected temperatures are given in Table 4.19. Each measured data is the mean of twenty one measurements. The heat capacity of $\text{PbMoO}_4(\text{s})$ was also computed by Neumann-Kopp's rule (NKR) using the heat capacity data for $\text{PbO}(\text{s})$ and $\text{MoO}_3(\text{s})$ [34], and is compared with the measured data in Fig 4.12. A small step at 762 K present in the heat capacity data derived using NKR is due to the tetragonal to orthorhombic transition of $\text{PbO}(\text{s})$. The comparison plot reveals that the

experimental heat capacity is lower than the estimated data and the percentage deviation is $\sim 4\%$ at 555 K, which is the mean temperature of the measurement.

The experimental heat capacity of PbMoO_4 (s) is compared with the reported data of Weller and Kelley [25], Barin [26] and Bissengaliyeva et al. [27, 28] in Fig. 4.13. The C_p of PbMoO_4 (s) at 298.15 K obtained in the present study is in good agreement with the values reported by these authors. But deviation is observed at higher temperatures. The S_{298}° of PbMoO_4 (s) has been estimated by many authors [25-28]. Weller and Kelley [25] have given a value of $(166.1 \pm 2.1) \text{ J K}^{-1} \text{ mol}^{-1}$. Barin [26] also has mentioned the same value in his compilation. Bissengaliyeva et al. [27, 28] reported (168.33 ± 2.06) and $(161.5 \pm 0.3) \text{ J K}^{-1} \text{ mol}^{-1}$ for S_{298}° of PbMoO_4 (s) based on their two different studies. Using the S_{298}° value of PbMoO_4 (s) reported by Bissengaliyeva et al. [27], the thermodynamic functions of PbMoO_4 (s) were estimated from the molar heat capacity measured in this work and are given in Table 4.19.

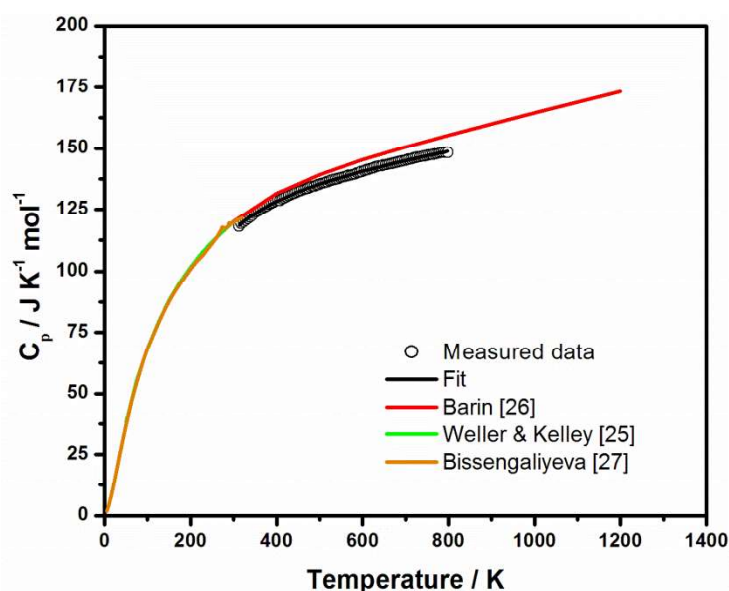


Fig. 4.13 Comparison of measured heat capacity values of PbMoO_4 (s) with the values reported in literature

Table 4.19 Thermodynamic functions of PbMoO₄ (s) at P = 0.1MPa^a

T / K ^a	C _p / J K ⁻¹ mol ⁻¹		H _T ^o - H ₂₉₈ ^o / J mol ^{-1b}	S _T ^o / J K ⁻¹ mol ^{-1b}	-(G _T ^o - H ₂₉₈ ^o)/T / J K ⁻¹ mol ^{-1b}
	Measured data	Fitted values			
298.15	-	116.3	0	161.5 ± 0.3	161.5 ± 0.3
313	118.2	118.6	1744.0 ± 60.9	167.2 ± 0.4	161.6 ± 0.4
353	123.8	123.7	6594.2 ± 224.9	181.8 ± 0.8	163.1 ± 1.0
403	128.7	128.6	12906.5 ± 429.9	198.5 ± 1.3	166.5 ± 1.7
453	132.4	132.4	19433.8 ± 634.9	213.8 ± 1.7	170.9 ± 2.2
503	135.4	135.6	26134.7 ± 839.9	227.8 ± 2.2	175.8 ± 2.7
553	137.9	138.3	32982.9 ± 1044.9	240.8 ± 2.6	181.1 ± 3.2
603	140.6	140.8	39960.5 ± 1249.9	252.8 ± 2.9	186.6 ± 3.6
653	142.9	143.0	47055.5 ± 1454.9	264.2 ± 3.2	192.1 ± 3.9
703	145.0	145.1	54259.0 ± 1659.9	274.8 ± 3.5	197.6 ± 4.2
753	146.9	147.1	61564.5 ± 1864.9	284.8 ± 3.8	203.1 ± 4.5
798	148.1	148.8	68222.7 ± 2049.4	293.4 ± 4.0	207.9 ± 4.8

^aStandard uncertainties, *u*, are *u*(T) = 0.4 K and *u*(P) = 0.8 kPa. The combined expanded uncertainty, *U_c*, is *U_c*(C_p) = 4.1 J K⁻¹ mol⁻¹. ^bThe reported uncertainties are the combined expanded uncertainties.

4.4.8.2 Molar heat capacity of Pb₂MoO₅ (s)

The XRD pattern of the Pb₂MoO₅ (s) pellets after the heat capacity measurements was identical to the initial pattern, indicating that no changes had happened to the compound during the calorimetric runs. The temperature dependence of heat capacity of Pb₂MoO₅ (s) obtained by measurement over the temperature range of 308 to 798 K is shown in Fig. 4.14 and can be represented by the least squares fitted expression:

$$C_p \pm 6.2 / J K^{-1} mol^{-1} = 169.20 + 66.69 \times 10^{-3} T - 1.99 \times 10^6 T^{-2} \quad (T : 308 - 798 K) \quad (4.20)$$

The error given in the expression is the combined expanded uncertainty with 0.95 level of confidence.

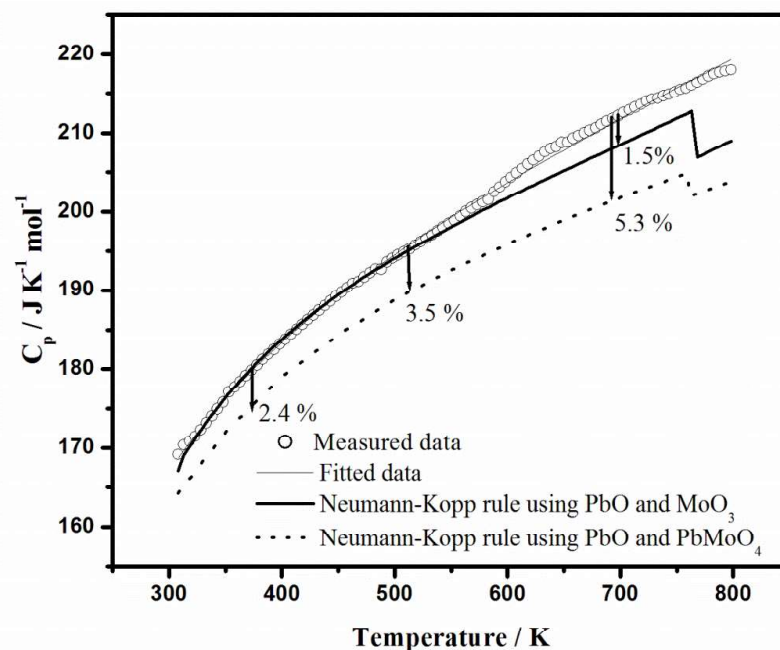


Fig. 4.14 Variation of molar heat capacity of $\text{Pb}_2\text{MoO}_5(\text{s})$ with temperature

The measured heat capacity data of $\text{Pb}_2\text{MoO}_5(\text{s})$ was compared with the data estimated using the C_p values of $\text{PbO}(\text{s})$ and $\text{MoO}_3(\text{s})$ by NKR and it is shown in Fig. 4.14. It can be seen that there is good agreement between the measured and estimated C_p data at low temperatures but there is deviation at temperatures higher than 550 K. The experimental heat capacity is 0.6% higher than the estimated C_p data at 553 K, the mean temperature of measurement. The heat capacity of Pb_2MoO_5 was also estimated using the sum of the C_p data of $\text{PbMoO}_4(\text{s})$ and $\text{PbO}(\text{s})$ and shown in Fig. 4.14. The C_p value estimated from the data of $\text{PbO}(\text{s})$ and $\text{PbMoO}_4(\text{s})$ is lower than the experimental value at all temperatures of measurement. At the mean temperature of measurement (550 K), the deviation is found to be ~3.5%.

As no thermochemical data are available for $\text{Pb}_2\text{MoO}_5(\text{s})$, the S_{298}° value of $\text{Pb}_2\text{MoO}_5(\text{s})$ was computed by NKR using the S_{298}° values of $\text{PbO}(\text{s})$ and $\text{MoO}_3(\text{s})$ [34]. Based on this data, the S_{298}° value computed for $\text{Pb}_2\text{MoO}_5(\text{s})$ is $208.8 \text{ J K}^{-1} \text{ mol}^{-1}$

¹. Using this value, the thermodynamic functions of Pb_2MoO_5 (s) were computed and given in Table 4.20.

Table 4.20 Thermodynamic functions of Pb_2MoO_5 (s) at $P = 0.1\text{MPa}$

T / K^{a}	$C_p / \text{J K}^{-1} \text{mol}^{-1}$		$H_T^\circ - H_{298}^\circ$ $/ \text{J mol}^{-1 \text{b}}$	S_T° $/ \text{J K}^{-1} \text{mol}^{-1 \text{b}}$	$-(G_T^\circ - H_{298}^\circ) / T$ $/ \text{J K}^{-1} \text{mol}^{-1 \text{b}}$
	Measured data	Fitted values			
298.15	-	166.7	0	208.8 ± 0.2	208.8 ± 0.3
308	169.3	168.8	1652.3 ± 61.1	214.3 ± 0.2	208.9 ± 0.3
353	177.1	176.8	9434.5 ± 340.1	237.8 ± 1.0	211.1 ± 1.4
403	183.9	183.8	18455.5 ± 650.1	261.7 ± 1.9	215.9 ± 2.5
453	189.8	189.7	27797.6 ± 960.1	283.6 ± 2.6	222.2 ± 3.3
503	194.6	194.9	37414.8 ± 1270.1	303.7 ± 3.2	229.3 ± 4.1
553	199.0	199.6	47277.7 ± 1580.1	322.4 ± 3.8	236.9 ± 4.8
603	204.4	203.9	57366.7 ± 1890.1	339.8 ± 4.4	244.7 ± 5.4
653	209.0	208.1	67668.1 ± 2200.1	356.3 ± 4.9	252.6 ± 5.9
703	212.7	212.1	78172.1 ± 2510.1	371.8 ± 5.3	260.6 ± 6.4
753	215.6	215.9	88871.7 ± 2820.1	386.5 ± 5.7	268.4 ± 6.9
798	218.2	219.3	98663.9 ± 3099.1	399.1 ± 6.1	275.4 ± 7.2

^a Standard uncertainties, u , are $u(T) = 0.4 \text{ K}$ and $u(P) = 0.8 \text{ kPa}$, The combined expanded uncertainty, U_c , is $U_c(C_p) = 6.2 \text{ J K}^{-1} \text{ mol}^{-1}$, ^b The reported uncertainties are the combined expanded uncertainties

The temperature dependence of the enthalpies of formation of PbMoO_4 (s) from room temperature to the highest temperature of C_p measurement was calculated using the experimental values of enthalpy of formation of PbMoO_4 (s) and C_p data of PbMoO_4 (s) along with the C_p data of elements (represented as $\Delta H_{f,\text{exp}}^\circ$). The temperature dependence of the enthalpies of formation was also calculated using the C_p data of PbMoO_4 (s) estimated by NKR (represented as $\Delta H_{f,\text{NKR}}^\circ$). These are plotted against temperature and shown in Fig. 4.15-a. Similar calculations were carried out for Pb_2MoO_5 (s) also and presented in Fig. 4.15-b. The difference between $\Delta H_{f,\text{exp}}^\circ$ and $\Delta H_{f,\text{NKR}}^\circ$ was then determined and plotted against temperature. These data are shown in Fig. 4.15-c. It is seen that for PbMoO_4 (s), the difference in the enthalpies of formation increases steadily with increase in temperature. In the case of Pb_2MoO_5 (s)

this difference is close to zero up to 700 K and it is 0.5 kJ mol⁻¹ at 800 K. These deviations are evident from the deviations of the estimated C_p data of the compounds from those of the experimental data.

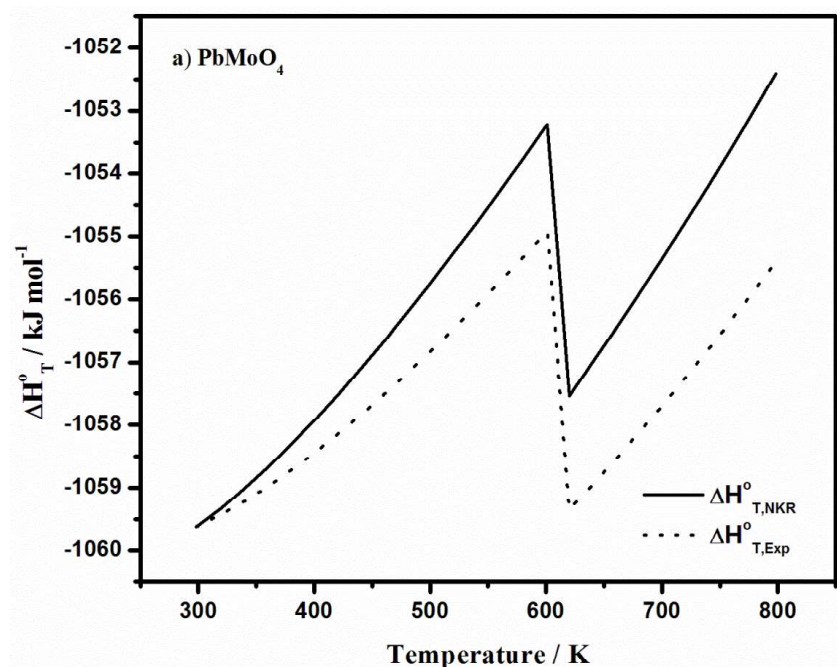


Fig. 4.15-a Temperature dependence of enthalpies of formation of PbMoO₄ (s)

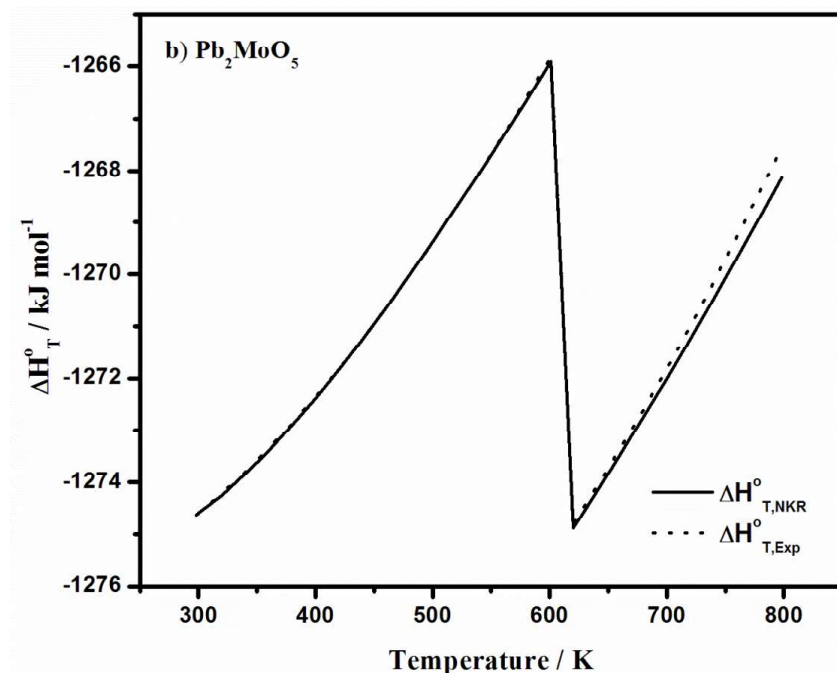


Fig. 4.15-b Temperature dependence of enthalpies of formation of Pb₂MoO₅(s)

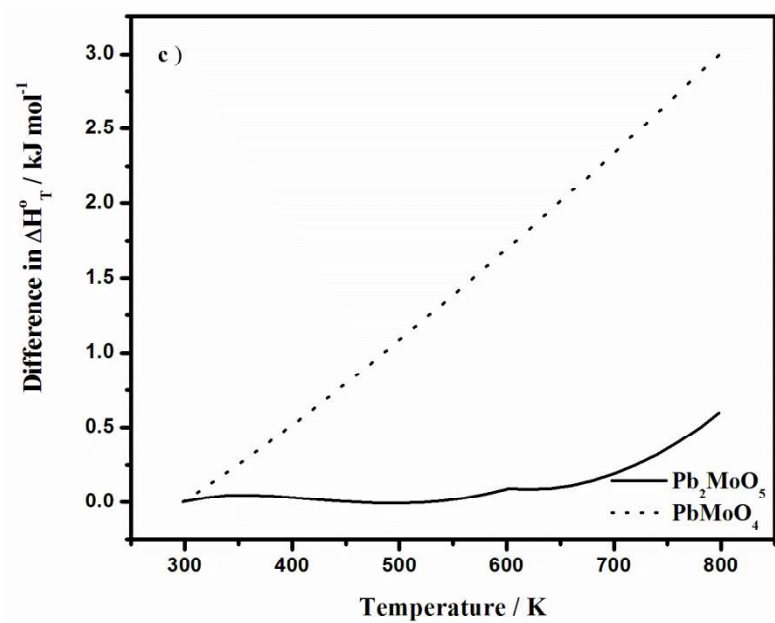


Fig. 4.15-c Difference in the temperature dependence of enthalpies of formation of $\text{PbMoO}_4(\text{s})$ and $\text{Pb}_2\text{MoO}_5(\text{s})$

4.4.8.3 Deviations of C_p from Neumann-Kopp's rule (NKR)

The experimental heat capacities of $\text{PbMoO}_4(\text{s})$ and $\text{Pb}_2\text{MoO}_5(\text{s})$ were compared with the heat capacity values estimated by Neumann-Kopp's rule in Figs 4.12 and 4.14. It can be seen that the measured heat capacity of $\text{PbMoO}_4(\text{s})$ is lower than the estimated values at all temperatures whereas for $\text{Pb}_2\text{MoO}_5(\text{s})$, the experimental and estimated heat capacities are in good agreement at low temperatures and positive deviations are observed at high temperatures. In both cases, the percentage deviation increases with increase in temperature.

The causes for the observed deviation in the measured heat capacities from the estimated heat capacities by NKR have been described in ref 35. NKR is an empirical method to predict the heat capacities of complex compounds from the heat capacities of the constituent elements and binary components and it works well for those cases in which the crystal structures of the compound as well as those of the constituent components match. In the present cases of $\text{PbMoO}_4(\text{s})$ and $\text{Pb}_2\text{MoO}_5(\text{s})$, the crystal

structures are tetragonal and monoclinic, respectively whereas the binary oxides, PbO (s) and MoO₃ (s) crystallize in tetragonal and orthorhombic forms, respectively. Several factors contribute to the molar heat capacity of a solid at constant pressure. Thus C_p can be expressed as

$$C_p = C_{ph} + C_{dil} + C_{others} \quad (4.21)$$

where C_{ph} represents contribution of lattice vibrations (phonons), C_{dil} is the contribution from lattice dilatations and C_{others} comprises of contributions from conduction electrons, excitation of localized electrons, formation of vacancies, etc. The contributions of localized and conduction electrons and excitations for pure ionic crystals of PbMoO₄ (s) and Pb₂MoO₅ (s) are expected to be low. Additionally, the contribution due to the formation of vacancies such as V_O^{••} and V_{Pb}^{''} are also expected to be low [36] in the temperature range of present measurement.

The phonon contribution C_{ph}, can be expressed as the sum of heat capacities described within harmonic crystal approximation C_{har}, and an additional correction to the anharmonicity of vibration modes, C_{anh}. Similarly for the dilatation term C_{dil}, the following expression is often applied.

$$C_{dil} = C_p - C_v = TV\alpha^2/\beta \quad (4.22)$$

where C_v is the molar heat capacity at constant volume, V is the molar volume, α is the isobaric volume expansion and β is the isothermal compressibility. At low temperatures, only the contribution from harmonic phonon vibrations are important while at high temperatures, the dilatation term and anharmonic correction terms become particularly important and the harmonic part approaches the Dulong-Petit law limit of 3NR, where N is the number of atoms per formula unit and R is the universal gas constant. So at high temperatures, the C_p can be expressed as

$$C_p = C_{\text{har}} + C_{\text{anh}} + C_{\text{dil}} = 3NR + C_{\text{anh}} + TV\alpha^2/\beta \quad (4.23)$$

Thus it is clear that at high temperatures the deviation from NKR prediction is essentially determined by C_{anh} and C_{dil} terms. However, it is known from the literature that the contribution of C_{anh} are significant at temperatures 1000 K and above [36]. Thus in the present work, the observed experimental deviation in the temperatures <800 K could be mainly due to C_{dil} . This would depend upon the difference in molar volumes of oxides, their temperature coefficients of expansions, and compressibility factors.

$$\Delta C_{\text{dil}}/T = V_{\text{AB}} (\alpha_{\text{AB}}^2/\beta_{\text{AB}}) - x_{\text{A}} V_{\text{A}} (\alpha_{\text{A}}^2/\beta_{\text{A}}) - x_{\text{B}} V_{\text{B}} (\alpha_{\text{B}}^2/\beta_{\text{B}}) \quad (4.24)$$

where AB represents the ternary oxide formed from the constituent oxides A and B.

Thus according to equation (4.24), if there is an expansion during the formation of a ternary oxide, it would result in an increase in the heat capacity. The reverse is applicable if the compound formation is accompanied by a contraction in molar volume. Table 4.21 gives the unit cell volumes of the ternary oxides calculated from the component binary oxides. It is seen that the formation of PbMoO_4 (s) is accompanied by contraction of molar volume while Pb_2MoO_5 (s) formation results in the expansion of the unit cell. Accordingly, the measured heat capacities of PbMoO_4 (s) showed negative deviation and Pb_2MoO_5 (s) showed positive deviations from the heat capacities estimated by NKR. However, to calculate the dilatational contribution exactly, it is necessary to have data on the α and β parameters of the ternary compounds and the constituent oxides, which are seldom available at elevated temperatures.

Table 4.21 Unit cell volumes of ternary oxides and component oxides

Ternary oxide	Unit cell volume / Å ^{3*}		Expansion/ Contraction in volume	Percent volume change	Source of data*
	Compound	Constituent oxides			
PbMoO ₄	89.36	(PbO + MoO ₃), 90.38	Contraction	-1.12 %	PCPDF
Pb ₂ MoO ₅	135.81	(2PbO + MoO ₃), 130.01	Expansion	4.46 %	PCPDF

*Unit cell volumes were taken from JCPDS files 00-044-1486, 04-010-3859, 00-005-0570 and 00-005-0508 respectively for PbMoO₄, Pb₂MoO₅, PbO and MoO₃.

4.4.9 Consistency of the measured thermodynamic data with the data reported in literature

The consistency between the standard enthalpy of formation of PbMoO₄(s) and Pb₂MoO₅(s) determined by solution calorimetry experiments, with the standard enthalpy of formation at the mid temperature of emf measurements is determined as follows:

4.4.9.1 PbMoO₄ (s)

The standard molar Gibbs energy of formation of PbMoO₄(s) obtained by emf method is given by the expression (4.12) ;

$$\Delta_f G^\circ < PbMoO_4 > \pm 0.7 / kJ mol^{-1} = -1030.1 + 0.3054(T / K) \quad (T: 772-1017K) \quad (4.12)$$

This can be related to the standard molar enthalpy of formation of PbMoO₄(s) at 298.15 K as below:

$$\Delta_f H_{298K}^\circ < PbMoO_4 > = \Delta_f H_{894K}^\circ < PbMoO_4 > - \left[\int_{298}^{601} \Delta C_p dT - \Delta H_{Pb}^{Fusion} + \int_{601}^{894} \Delta C_p dT \right] \quad (4.25)$$

where ΔC_p is the difference in the heat capacities of $\text{PbMoO}_4(\text{s})$ and its constituent elements Pb (solid / liquid), Mo and O_2 and $\Delta H_{\text{fusion}}^{\text{Pb}}$ is the enthalpy of fusion of Pb at 601 K. The second term of the equation (4.25) can be obtained as:

$$\int_{298}^{601} \Delta C_p dT - \Delta H_{\text{fusion}}^{\text{Pb}} + \int_{601}^{894} \Delta C_p dT =$$

$$\int_{298}^{601} [C_p^{\text{PbMoO}_4} - (C_p^{\text{Pb(s)}} + C_p^{\text{Mo(s)}} + 2C_p^{\text{O}_2(\text{g})})] dT - \Delta H_{\text{fusion}}^{\text{Pb}} + \int_{601}^{894} [C_p^{\text{PbMoO}_4} - (C_p^{\text{Pb(l)}} + C_p^{\text{Mo(s)}} + 2C_p^{\text{O}_2(\text{g})})] dT \quad (4.26)$$

The data of heat capacity for Pb, Mo and O_2 were taken from ref. [34] and that of PbMoO_4 (s) from the present experimental studies (equation 4.19) and are given below.

$$C_p \langle \text{PbMoO}_4 \rangle / \text{J K}^{-1} \text{mol}^{-1} = 127.31 + 30.47 \times 10^{-3} T - 1.79 \times 10^6 T^{-2}$$

$$(T: 313-798 \text{ K}) \quad (4.19)$$

$$C_p \langle \text{Pb} \rangle / \text{J K}^{-1} \text{mol}^{-1} = 24.221 + 8.711 \times 10^{-3} T \quad (T: 298-601 \text{ K}) \quad (4.27)$$

$$C_p \{ \text{Pb} \} / \text{J K}^{-1} \text{mol}^{-1} = 36.112 - 9.736 \times 10^{-3} T - 0.280 \times 10^6 T^{-2} + 3.238 \times 10^{-6} T^2$$

$$(T: 601-1200 \text{ K}) \quad (4.28)$$

$$C_p \langle \text{Mo} \rangle / \text{J K}^{-1} \text{mol}^{-1} = 29.732 - 5.699 \times 10^{-3} T - 0.439 \times 10^6 T^{-2} + 4.665 \times 10^{-6} T^2$$

$$(T: 298-2896 \text{ K}) \quad (4.29)$$

$$C_p (\text{O}_2) / \text{J K}^{-1} \text{mol}^{-1} = 29.154 + 6.477 \times 10^{-3} T - 0.184 \times 10^6 T^{-2} - 1.017 \times 10^{-6} T^2$$

$$(T: 298-3200 \text{ K}) \quad (4.30)$$

By substituting the above values in equation (4.26), the following relation is obtained:

$$\int_{298}^{601} \Delta C_p dT - \Delta H_{\text{fusion}}^{\text{Pb}} + \int_{601}^{894} \Delta C_p dT = 6.7 \text{ kJ mol}^{-1} \text{ and hence}$$

$$\Delta_f H_{298\text{K}}^{\circ} \langle \text{PbMoO}_4 \rangle = -1030.1 - 6.7 = -1036.8 \text{ kJ mol}^{-1}.$$

$\Delta_f H_{298K}^{\circ} < PbMoO_4 >$ obtained by solution calorimetry experiment is $-1059.6 \text{ kJ mol}^{-1}$ and is found to be in fair agreement with the deduced value of $-1036.8 \text{ kJ mol}^{-1}$. This deduced value of standard molar enthalpy of formation of $PbMoO_4(s)$ at 298.15 K is compared with the literature data and the good agreement between them is seen.

4.4.9.2 $Pb_2MoO_5 (s)$

The standard Gibbs energy of formation of $Pb_2MoO_5(s)$ obtained by emf measurement is given by equation 4.15.

$$\Delta_f G_m^{\circ} < Pb_2MoO_5 > \pm 0.8 / \text{kJ mol}^{-1} = -1248.1 + 0.3872T \quad (T : 741 - 1021 \text{ K}) \quad (4.15)$$

The mid temperature of the measurement is 881 K . As $\Delta G = \Delta H - T\Delta S$, the enthalpy of formation of $Pb_2MoO_5 (s)$ at the mid temperature, $\Delta_f H_{881K}^{\circ} = -1248.1 \text{ kJ mol}^{-1}$.

$\Delta_f H_{881K}^{\circ} < Pb_2MoO_5 >$ can be related to $\Delta_f H_{298K}^{\circ} < Pb_2MoO_5 >$ by the following expression:

$$\Delta_f H_{298K}^{\circ} < Pb_2MoO_5 > = \Delta_f H_{881K}^{\circ} - \left[\int_{298}^{601} \Delta C_p dT - 2\Delta H_{fusion}^{Pb} + \int_{601}^{881} \Delta C_p dT \right] \quad (4.31)$$

where ΔC_p is the difference in the heat capacities of $Pb_2MoO_5(s)$ and its constituent elements Pb (solid / liquid), Mo and O_2 and ΔH_{fusion}^{Pb} is the enthalpy of fusion of Pb at 601 K . Thus the second term of equation (4.31) can be obtained as

$$\int_{298}^{601} \Delta C_p dT - 2\Delta H_{fusion}^{Pb} + \int_{601}^{881} \Delta C_p dT = \int_{298}^{601} [C_p^{Pb_2MoO_5} - (2C_p^{Pb(s)} + C_p^{Mo(s)} + \frac{5}{2}C_p^{O_2(g)})]dT - 2\Delta H_{fusion}^{Pb} + \int_{601}^{881} [C_p^{Pb_2MoO_5} - (2C_p^{Pb(l)} + C_p^{Mo(s)} + \frac{5}{2}C_p^{O_2(g)})]dT \quad (4.32)$$

The heat capacity of $Pb_2MoO_5(s)$ has been measured in this work and is given by:

$$C_p < Pb_2MoO_5 > / JK^{-1}mol^{-1} = 169.20 + 66.69 \times 10^{-3}T - 1.99 \times 10^{-6}T^{-2} \quad (T : 308 - 798 \text{ K}) \quad (4.20)$$

By using equation (4.20) along with equations (4.27-4.301), we get

$$\int_{298}^{601} \Delta C_p dT - 2\Delta H_{fusion}^{Pb} + \int_{601}^{881} \Delta C_p dT = 11.7 \text{ kJ mol}^{-1}$$

By substituting the above value and $\Delta_f H_{881K}^o < Pb_2MoO_5 > = -1248.1 \text{ kJ mol}^{-1}$ in equation (20), we get $\Delta_f H_{298K}^o < Pb_2MoO_5 > = -1248.1 - 11.7 = -1259.8 \text{ kJ mol}^{-1}$.

$\Delta_f H_{298K}^o < Pb_2MoO_5 >$ obtained by solution calorimetry experiment is $-1274.7 \text{ kJ mol}^{-1}$, which is in good agreement with the data deduced from emf experiments.

4.5 References

1. T.B. Massalski (Ed.), Binary Alloy Phase Diagrams, 2nd Ed., ASM International, 1990.
2. R. Parkman, O.C. Shepard, Rep. ORO-45, U.S. Atomic Energy Commission, (1951) 1-33.
3. T. Alden, D.A. Stevenson, J. Wulff, Trans. AIME, 212 (1958) 15-17.
4. H.A. Wredt, Bull. Alloy Phase Diagrams 9 (1988) 106. (reported in: T.B. Massalski (Ed.), Binary Alloy Phase Diagrams, 2nd Ed., ASM International, 1990)).
5. R. Ganesan, T. Gnanasekaran, R.S. Srinivasa, Diffusivity, activity and solubility of oxygen in liquid lead and lead-bismuth eutectic alloy by electrochemical methods, J. Nucl. Mater. 349 (2006) 133-149.
6. F.M. Jaeger, H.C. Germs, Uber die binarn der sulfates, chromate, molybdate und wolframate des bleies, Z. Anorg. Allg. Chem. 119 (1921) 145-173.

7. I.N. Belyaev, N.P. Smolyaninov, The $\text{Bi}_2\text{O}_3\text{-MoO}_3\text{-PbO}$ ternary system, Russ. J. Inorg. Chem. (Engl. Transl.) 5 (1962) 579-581.
8. W.P. Doyle, F. Forbes, Determination by diffuse reflectance of the stoichiometry of solid products in solid-solid additive reactions, J. Inorg. Nucl. Chem. 27 (1965) 1271-1280.
9. W.P. Doyle, F. Forbes, Quantitative analysis of solid mixtures by diffuse reflectance measurements, Anal. Chim. Acta, 33 (1965) 108-114.
10. B.F. Mentzen, A. Latrach, J. Bouix, Superstructure in pentalead(II) octaoxomolybdate (VI) Pb_5MoO_8 and the $\text{Pb}_5\text{S}_x\text{Mo}_{(1-x)}\text{O}_8$ solid solution, CR Acad Sci. Paris. 297 (1983) 887-889.
11. P. Vassiliev, D. Nihtianova, $\text{Pb}_5\text{O}_4\text{MoO}_4$, Acta Crystallogr, 54 (1998) 1062-1064.
12. D.K. Kunev, L.V. Belyaevskaya, A.N. Zelikman, The $\text{MoO}_3\text{-CaMoO}_4$, $\text{MoO}_3\text{-PbMoO}_4$ and $\text{MoO}_3\text{-ZnMoO}_4$ systems, Russ. J. Inorg. Chem (Engl. Transl.). 11 (1966) 1063-1064.
13. G.A. Bukhalova, V.M. Manakov, V.T. Mal'tsev, $\text{PbO-PbSiO}_3\text{-PbWO}_4$ ternary system, Russ. J. Inorg. Chem.(Engl. Transl.) 16 (1971) 280-281.
14. H.S. Lee, I.H. Oh, J.H. Lee, Y. H. Park, PbMoO_4 , Sae Mulli. 28 (1988) 574-579.
15. M.A. Eissa, M.A.A. Elmasry, S.S. Younis, The $\text{PbO}_2\text{-Pb-MoO}_3$ system in air, Thermochem Acta, 288 (1966) 169-178.

16. D.D. Nihtianova, D.P. Shumov, S.S. Angelova, Y.B. Dimitriev, L.L. Petrov, Investigation of Pb_5MoO_8 crystal growth in PbO-MoO₃ system, *J. Cryst. Growth*, 179 (1997) 161-167.
17. R. Dronskowski, A. Simon, PbMo_5O_8 and $\text{Tl}_{0.8}\text{Sn}_{0.6}\text{Mo}_7\text{O}_{11}$, Novel clusters of molybdenum and thallium, *Angew. Chemie*. 101 (1989) 775.
18. S.L. Wang, J.Y. Yeh, Pb^{2+} cation ordering in $\text{Pb}_3(\text{Mo}_4\text{O}_6)_4$, *Acta Crystallogr. B* 47 (1991) 446-451.
19. S. Feja, W. Reichelt, Thermodynamische modellierung im system Mo-Pb-O, *Z. Anorg. Allg. Chem.* 628 (2002) 2181.
20. C.N. Muldrow, Jr., L.G. Hepler, Heats of precipitation and formation of lead and calcium molybdates, *J. Phys. Chem.* 62 (1958) 982-984.
21. P.A.G. O'Hare, K.J. Jensen, H.R. Hoekstra, Standard enthalpy of formation of lithium molybdate, thermodynamic properties of the aqueous molybdate ion and thermodynamic stabilities of the alkali metal molybdates, *J. Chem. Thermodyn.* 6 (1974) 681-691.
22. I. Dellien, K.G. McCurdy, L.G. Hepler, Enthalpies of formation of lead chromate, lead molybdate and lead tungstate and the entropy of aqueous tungstate ion, *J. Chem. Thermodyn.* 8 (1976) 203-207.
23. D.D. Wagman, W.H. Evans, V.B. Parker, I. Halow, S.M. Bailey, R.H. Schumm, The NBS tables of chemical thermodynamic properties, *Nat. Bur. Stand. (U.S) Tech. Note 270-4*, U.S. Govt. Printing Office, Washington, 1969.

24. M.R. Bissengaliyeva, L.P. Ogorodova, M.F. Vigasina, L.V. Melchakova, Enthalpy of formation of wulfenite (Natural lead molybdate), *Russ. J. Phys. Chem. A.* 87 (2013) 163-165.
25. W.W. Weller, K.K. Kelly, Low temperature heat capacities and entropies at 298.15 K of lead molybdate and lead tungstate, U.S. Bur. Mines Rept. Inv. 6357, (1964).
26. I. Barin, Thermochemical data of pure substances, Third ed., VCH, Weinheim (Federal Republic of Germany), 1995, pp.1293.
27. M.R. Bissengaliyeva, M.A. Bespyatov, D.B. Gogol, Experimental measurement and calculation of mole heat capacity and thermodynamic functions of wulfenite PbMoO_4 , *J. Chem. Eng. Data.* 55, (2010) 2974-2979.
28. M.R. Bissengaliyeva, D.B. Gogol, N.S. Bekturganov, S.T. Taymasova, Heat capacity and thermodynamic functions of the wulfenite PbMoO_4 over the temperature range of (0 to 320) K, *J. Chem. Eng. Data.* 56 (2011) 1941-1945.
29. G.B. Naumov, B.N. Ryzhenko, I.L. Khodakovsky, Reference book of thermodynamic values (for geologists) (in Russian): Atomizdat: Moskva, 1971
30. K. Kunkel, E. Milke, M. Binnewies, Formation of ternary lead molybdenum oxides PbMoO_4 , PbMo_2O_7 , Pb_2MoO_5 and $\text{PbMo}_3\text{O}_{10}$ in the gas phase: A mass spectrometric and quantum chemical investigation, *Int. J Mass Spec.* 374 (2014) 12-19.

31. E.G. King, Low temperature heat capacities and entropies at 298.15 K of lead sesquioxide and red and yellow lead monoxide, *J. Amer. Chem. Soc.* 80 (1958) 2400-2401.
32. R. Sabbah, A.X. Wu, J.S. Chickos, M.L.P. Leitao, M.V. Roux, L.A. Torres, Reference materials for calorimetry and differential thermal analysis, *Thermochim. Acta.* 331 (1999) 93-204.
33. K.T. Jacob, V.S. Saji, J. Gopalakrishnan, Y. Waseda, Thermodynamic evidence for phase transition in $\text{MoO}_2\text{-}\delta$, *J. Chem. Thermodyn.* 39 (2007) 1539-1545.
34. O. Knacke, O. Kubachewski, K. Hesselmann, Thermochemical properties of inorganic substances, Vol 2, second ed., Springer, Berlin, 1991.
35. J. Leitner, P. Vonka, D. Sedmidubsky, P. Svoboda, Application of Neumann-Kopp rule for the estimation of heat capacity of mixed oxides, *Thermochim. Acta* 497 (2010) 7-13.
36. W. V. Loo, Crystal growth and electrical conduction of PbMoO_4 and PbWO_4 , *J. Solid State Chem.* 14 (1975) 359-365.

Chapter 5

Development of piezoelectric material for high temperature applications in liquid metals

5.1 Introduction

The opacity of liquid metal coolants hinders the visual inspection of in-vessel components in liquid metal cooled nuclear systems by conventional methods. High temperature ultrasonic transducers are employed for this purpose. Conventional ultrasonic transducers consist of a piezoelectric element, a protection layer between the medium under investigation and the piezoelectric element, and a damping element attached to the back surface of the piezoelectric element [1]. Selection of a suitable piezoelectric material is very important in the development of ultrasonic transducers. The properties which decide the choice of a particular piezoelectric material are its Curie temperature and piezoelectric coefficient. The chosen piezoelectric material should have high Curie temperature and also should have high piezoelectric coefficient. There are many piezoelectric materials that possess high Curie temperatures. But the piezoelectric response of these materials is generally poor. Lead zirconate titanate (PZT) based ceramics with favourable piezoelectric properties are currently used in ultrasonic transducers. As the Curie temperature of PZT is around 623 K, it can be used only at the low temperature ranges. However, the operating temperature of the advanced nuclear systems is in the range of 823-873 K. Thus different piezoelectric materials with high Curie temperature and favourable piezoelectric properties have been examined and investigated for their piezoelectric applications in the service condition at high temperatures.

5.1.1 Overview of piezoelectric elements suitable for high temperature applications

There are many piezoelectric materials which possess high Curie temperature. However, their piezoelectric properties are generally poor in comparison to PZT based materials. These piezoelectric materials belong to different crystalline structures: perovskites, pyrochlores, tungsten-bronzes, illmenites, layered perovskites and Aurivillius compounds. All these structures consist of an ion of small size and high charge, inside an oxygen octahedron that shares corners to form oxygen-metal-oxygen chains [2]. This favours the appearance of ferroelectricity in these structures. A comparison of the piezoelectric properties of selected piezoelectric materials is given in Table 5.1.

Table 5.1 Properties of selected piezoelectric materials

Compound	Curie temperature / K	d_{33} / pCN ⁻¹
BaTiO ₃	403	190
PbTiO ₃	743	51
Pb(ZrTi)O ₃ (PZT)	403	300
La ₂ Ti ₂ O ₇	1773	16
LiNbO ₃	1423	68
Sr ₂ Nb ₂ O ₇	1573	18
PbNb ₂ O ₆	833	85
Bi ₄ Ti ₃ O ₁₂	948	8-25
Na _{0.5} Bi _{4.5} Ti ₃ O ₁₂	933	18
SrBi ₄ Ti ₄ O ₁₅	803	17
CaBi ₄ Ti ₄ O ₁₅	1063	8
PbBi ₄ Ti ₄ O ₁₅	833	12
Bi ₃ TiNbO ₉	1213	5

The first widely used piezoelectric material was BaTiO₃, which possess a Curie temperature of 403 K. Because of the superior piezoelectric properties and higher operating temperature, PZT has largely replaced barium titanate. PZT has the perovskite structure and it is a solid solution of tetragonal PbTiO₃ and orthorhombic

PbZrO_3 . It exhibits high values of electromechanical coupling coefficients and electrical permittivity. Useful variations in the properties of PZT can be obtained by compositional additives. Although its electrical resistivity remains quite high up to 633 K, its use is limited to below 473 K because of its tendency to age very rapidly and leading to depoling [3]. Lead metaniobate (PbNb_2O_6) is another piezoelectric material which belongs to the tungsten-bronze family. Because of its relatively high d_{33} value, it finds greatest applications. However, limitations are imposed by its high conductivity above 573 K. Other problems associated with this material are its high level of porosity and relatively low mechanical strength [3]. The piezoelectric lithium niobate has the corundum structure and possesses a Curie temperature of 1423 K. Only single crystals of lithium niobate are preferred because of the higher piezoactivity and due to the difficulties encountered in conventional sintering of the polycrystalline form [3]. The benefit of the high Curie temperature of lithium niobate is thus offset by the difficulty of fabrication [4]. Perovskite layer structured ferroelectrics such as $\text{Sr}_2\text{Nb}_2\text{O}_7$ and $\text{La}_2\text{Ti}_2\text{O}_7$ possess the highest known Curie temperatures of 1615 and 1773 K, respectively. They have been proposed for use in high temperature transducers. However, the cost of growing high quality single crystals is expensive due to the high melting points of these compounds [3]. Bismuth titanate based ferroelectric materials are another category. The chemical stability of bismuth titanate at high temperatures combined with its high Curie temperature make it an ideal candidate for high temperature applications [4].

The important feature of ferroelectric materials is the presence of polarised domains which induces strong coupling between electrical and mechanical properties. However, in polycrystalline ferroelectrics, the individual domains are randomly

oriented and cancel each other and hence, the net polarisation is zero. By the process of poling, the bulk material is subjected to a high electric field at a temperature below the Curie point, so that all the domains align themselves in the direction of the applied field and the materials will have a net polarisation [5].

5.1.2 Bismuth titanate – structure and characteristic properties

Bismuth titanate ($\text{Bi}_4\text{Ti}_3\text{O}_{12}$), a layered ferroelectric oxide and belonging to the Aurivillius family, has attracted considerable interest for high temperature piezoelectric applications due to its high Curie temperature (948 K), high dielectric constant, large spontaneous polarization (50 $\mu\text{C}/\text{cm}$) and better piezoelectric properties (d_{33} -8 to 21 pC/N) [6-9]. The layered structure of bismuth titanate is characterized by the perovskite-like $(\text{Bi}_2\text{Ti}_3\text{O}_{10})^{2-}$ layers sandwiched between $(\text{Bi}_2\text{O}_2)^{2+}$ layers along its crystallographic c-axis [10, 11]. An idealized structure of bismuth titanate showing the bismuth oxide layers and pseudo perovskite units is shown in Fig. 5.1.

It is well known that the preparation of bismuth titanate at high temperatures is accompanied by the vaporization of Bi_2O_3 along with the generation of bismuth and oxide ion vacancies ($V_{\text{Bi}}^{\text{m}}, V_{\text{O}}^{\text{••}}$), which largely affect the electrical properties of bismuth titanate [12]. Upon cooling the product in air, majority of the oxide ion vacancies get compensated by absorption of oxygen and the charge neutrality is acquired by the generation of holes. A detailed structural analysis of bismuth titanate showed that some of the bismuth ions in the perovskite layers are overbonded with a valence state higher than 3+ [13] and the generation of holes in bismuth titanate is associated with the oxidation of Bi^{3+} to Bi^{4+} [12, 14]. The measurements on Seebeck coefficient of bismuth titanate by Kim et al. [15] also proved that the conduction to be

of p-type. Takahashi et al. [16] showed the polycrystalline bismuth titanate ceramics exhibited ionic and p-type mixed conduction and the ionic conduction dominated at high temperatures. The dependence of the electrical conductivity of single crystals of bismuth titanate on the oxygen pressure was also studied by Takahashi et al. [16]. They observed anisotropic conductivity along the a- and c axes with the maximum value along the c-axis. p-type conduction was dominant along the c-axis whereas ionic conduction was dominant along the a-axis of the crystal. They also suggested that the defects responsible for the electrical conduction preferentially existed in the perovskite layer. As the conductivity of bismuth titanate is relatively high, it is very difficult to polarize polycrystalline bismuth titanate ceramics prepared by conventional methods, which has been an obstacle for the piezoelectric applications of bismuth titanate [12]. Conductivity of bismuth titanate along the c-axis can be reduced by restricting the growth of the crystal along the c-axis and allowing its growth along the a-b plane. It is also known from literature that a significant reduction in the conductivity of bismuth titanate can be achieved by the substitution at the Ti^{4+} site by ions such as Nb^{5+} , W^{6+} , Ta^{5+} , etc [17-22].

Different methods have been adopted in the past for the synthesis of highly homogeneous bismuth titanate powder. As mentioned above, synthesis by conventional solid state methods leads to the vaporization of Bi_2O_3 and causes coarsening and agglomeration of particles resulting in poor microstructure and structural/mechanical strength of the ceramic [23, 24]. It is also reported that use of high temperatures for preparing bismuth titanate could result in the formation of an additional pyrochlore phase of $Bi_2Ti_2O_7$ by the vaporization of Bi_2O_3 from the parent $Bi_4Ti_3O_{12}$ phase [16]. Different wet chemical methods such as co-precipitation,

hydrothermal synthesis, etc can also be used for the synthesis of bismuth titanate which will allow control over the size and morphology of the particles [25-28]. But the subsequent heat treatment results in loss of Bi_2O_3 by vapourisation and the desired reduction in the electrical conductivity of bismuth titanate could not be achieved by these methods.

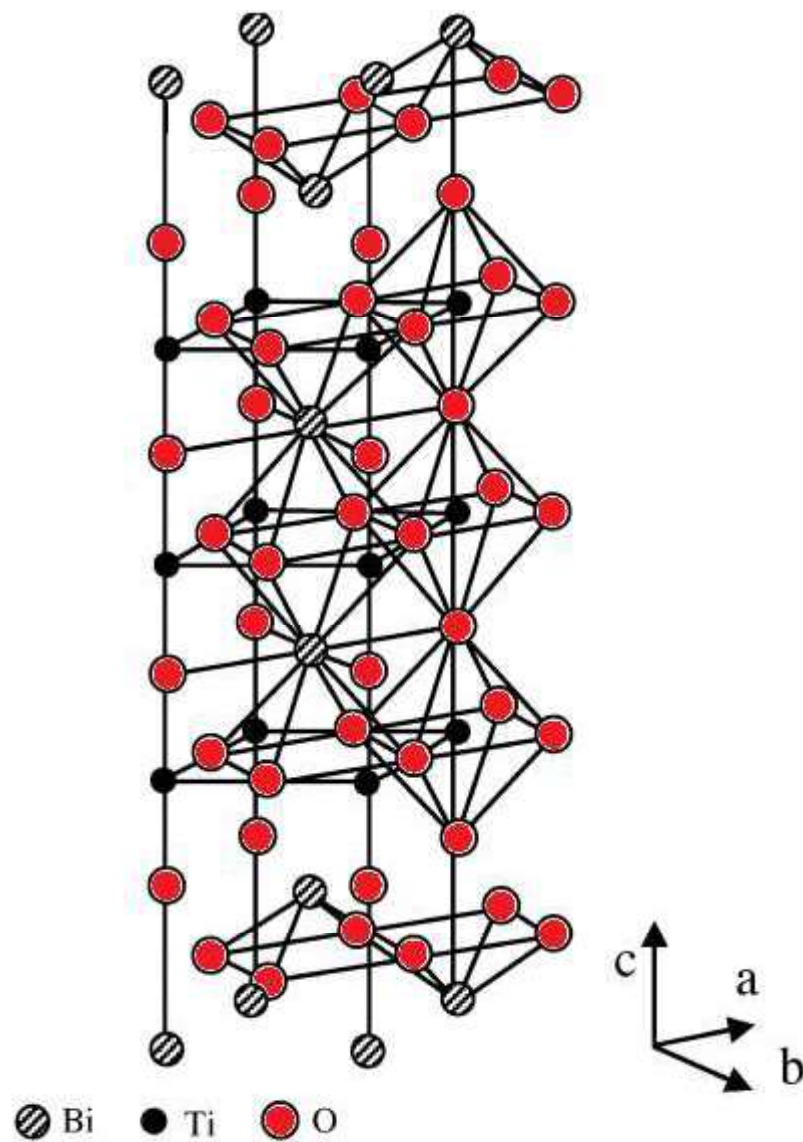


Fig. 5.1 Structure of bismuth titanate

It is known from literature that highly textured and flake like structures can be prepared by molten salt synthesis [29]. Here, the reactant mixture is heated with a low melting salt at a temperature above the melting point of the salt. At the reaction temperature, the medium melts and acts as a solvent to facilitate the interaction of the reactants. The products formed by this method are found to be highly textured and homogeneous. Also, as the reaction is mediated by the liquid, Bi_2O_3 vaporization losses would be low.

Synthesis of bismuth titanate by molten salt method is reported in literature [30-32]. Zaremba [30] and ChenJie [31] employed molten salt method for the synthesis of bismuth titanates with flake like structures using NaCl-KCl medium and observed that both temperature and duration of heating can affect the shape and size of the crystals. Kimura and Yamaguchi [32] investigated the effect of salt species on the morphology and structure of bismuth titanate using chloride and sulphate fluxes. They reported that the shape of the product particles formed depends upon the flux species. As chlorides have a larger interaction with the oxide than the sulphates, it can cause extensive imperfections, and resulting in a larger (001)-stabilizing effect. This large (001)-stabilizing effect of the chloride flux would reduce the growth rate along the (001) plane and resulting in the formation of plate-like product particles.

In the present work, highly textured and sufficiently resistive bismuth titanate ceramics were prepared by molten salt synthesis and further reduction in the electrical conductivity was achieved by doping with Nb^{5+} . The electrical conductivities of the prepared ceramics were compared with those obtained by solid state reaction and co-precipitation.

5.2 Experimental details

5.2.1 Synthesis of bismuth titanate

Bismuth titanate was prepared by three different methods: i) solid state reaction, ii) co-precipitation reaction and iii) reaction in molten salt medium.

5.2.1.1 Solid state reaction

The starting materials used were Bi_2O_3 (99.99% purity on metal basis, M/s Alfa Aesar, USA), TiO_2 (99.99% purity on metal basis, M/s Alfa Aesar, USA). The Bi_2O_3 powder used was calcined at 1023 K in air for about 6 h to remove any carbonate impurities and moisture present in it. The TiO_2 powder was also subjected to heating before use to remove any moisture content in it. For preparing bismuth titanate, stoichiometric amounts of Bi_2O_3 and TiO_2 were mixed well and pelletized. The pellet was placed in alumina crucible and heated in air at 1073 K for 48 h. At the end of 24 h of heating, the pellet was crushed and uniformly mixed. The powder was repelletized and heated again for another 24 h. The resulting product was quenched to room temperature, powdered and characterized by XRD. The powders were pelletized and sintered in air at 1373 K for 2 h.

5.2.1.2 Co-precipitation reaction

Titanium butoxide ($\text{Ti}(\text{C}_4\text{H}_9\text{O})_4$) (98+% purity on metal basis, M/s Alfa Aesar, USA) and $\text{Bi}(\text{NO}_3)_3 \cdot 5\text{H}_2\text{O}$ (prepared by dissolving high purity Bi metal (99.999 % purity) in concentrated HNO_3) were used as the precursors for Ti^{4+} and Bi^{3+} ions, respectively. The trace impurities in the titanium butoxide were identified by ICP-AES and the total amount of the impurities was determined to be ~140 ppm. They were mixed in the stoichiometric ratio and then dispersed in isopropyl alcohol. The

mixture thus obtained was precipitated as oxalate by the drop wise addition of the dispersion in isopropyl alcohol into an excess of 0.3 mol kg^{-1} oxalic acid solution under constant stirring. A small amount of NH_4OH solution was added at the end of the precipitation process. The co-precipitate thus obtained was washed with isopropyl alcohol. The amorphous powder obtained was dried and calcined at 1023 K for 1 h. The calcined powder was thoroughly ground in isopropyl alcohol medium for about 2 h and made into pellets. The compacted pellets were then sintered at 1123 K for 2 h. One of the sintered pellets was crushed, ground well and the ensuing sample was characterized by XRD.

5.2.1.3 Reaction in molten salt medium

A homogeneous mixture of Bi_2O_3 and TiO_2 in the stoichiometric ratio was prepared. 75 wt% of an eutectic mixture of 44 wt% NaCl (99.9% purity on metal basis, M/s Sarabhai Chemicals, India) and 56 wt% KCl (99.98% purity on metal basis, M/s Sarabhai Chemicals, India) was added to it and thoroughly ground in acetone medium. The well ground mixture was taken in an alumina crucible, covered with an alumina lid and sealed using alumina cement to prevent evaporation of the constituents. The sample was heated at 1323 K for 2 h, which is above the eutectic temperature of NaCl-KCl (923 K). The crucible was cooled and the product was repeatedly washed with hot distilled water until all the alkali metal chlorides were removed. The effluent was tested for any residual chlorides using silver nitrate solution. The product was further repeatedly ultra sonicated under water and washed to remove adsorbed or occluded impurities in it. The product thus obtained was dried in an oven, compacted into pellets and sintered in air at 1373 K for 2 h. The sintered samples were later characterized by XRD.

5.2.2 Synthesis of Nb-doped bismuth titanates

Nb-doped bismuth titanates were synthesized both by solid state reaction method and reaction in molten salt medium. The nominal composition employed was $\text{Bi}_4\text{Ti}_{3-x/4}\text{Nb}_{x/5}\text{O}_{12}$ where $x = 0.25, 0.5, 0.75, 1$ and 1.25 and they are designated as BITN-1, BITN-2, BITN-3, BITN-4 and BITN-5, respectively. Preparations were carried out in a similar manner as mentioned in section 5.2.1.1 and 5.2.1.3 using Nb_2O_5 (99.9% purity on metal basis, M/s Alfa Aesar, USA) as the precursor. The details of the various compositions chosen are given in Table. 5.2.

5.2.3 Structural and morphological characterizations

The samples of bismuth titanate prepared were characterized by X-ray diffraction method (XRD) using a powder X-ray Diffractometer (M/s Inel, France) operating with Cu K_α radiation and graphite monochromator. Their surface morphology was investigated by scanning electron microscopy (SEM) imaging using Model XL 30, M/s Philips, Netherlands. The bulk density of the sintered pellets was measured by Archimedes method.

Table 5.2 Composition of Nb doped bismuth titanates ($\text{Bi}_4\text{Ti}_{3-x/4}\text{Nb}_{x/5}\text{O}_{12}$)

Sample	x	Formula
BIT	0	$\text{Bi}_4\text{Ti}_3\text{O}_{12}$
BITN-1	0.25	$\text{Bi}_4\text{Ti}_{2.9375}\text{Nb}_{0.05}\text{O}_{12}$
BITN-2	0.5	$\text{Bi}_4\text{Ti}_{2.875}\text{Nb}_{0.1}\text{O}_{12}$
BITN-3	0.75	$\text{Bi}_4\text{Ti}_{2.8125}\text{Nb}_{0.15}\text{O}_{12}$
BITN-4	1	$\text{Bi}_4\text{Ti}_{2.75}\text{Nb}_{0.2}\text{O}_{12}$
BITN-5	1.25	$\text{Bi}_4\text{Ti}_{2.69}\text{Nb}_{0.25}\text{O}_{12}$

5.2.4 Conductivity measurements

The electrical conductivity of the samples was measured by complex impedance spectroscopy. For these experiments, sintered sample pellets of pristine

and doped bismuth titanates were used. The conductivity cell used for the measurement is described in Chapter 2. The cell had consisted of two silver electrical leads which were brazed to silver pellets of identical dimension (10 mm diameter). The sample pellet of known diameter (<10 mm) and thickness was mounted between the silver pellets by a spring loading arrangement. A K- type thermocouple was kept close to the sample pellet, so that the sample temperature could be accurately measured. Entire assembly was kept inside a quartz chamber, which in turn was kept in a furnace for heating. The electrical conductivity was measured using a frequency response analyzer (Model SI 1255, Solartron, M/s Schlumberger, UK) coupled with an electrochemical interface (Model 1287, Solartron, M/s Schlumberger, UK). The measurements were carried out in air in the temperature range of 700 to 1050 K in the frequency range of 10 Hz to 1 MHz with an applied perturbation potential of 500 mV. The impedance data obtained at each temperature was fitted using the software Zview® [33]. The bulk resistance of the material was obtained by fitting a semicircle to the experimentally obtained Nyquist plot. By incorporating the dimensions of the sample pellet, the conductivity (σ) of the sample at that temperature (T) was determined. The Arrhenius plot for conductivity was obtained by plotting $\log \sigma$ as a function of $1/T$. The activation energy was calculated from the slope of the Arrhenius plot.

5.2.5 Piezoelectric characterization

Poling of the Nb-doped bismuth titanate samples was performed in silicone oil bath at 448 K at an applied field of 30 kV/cm for 4 h using a dc poling unit (M/s Marine, India). Piezoelectric sensitivity (d_{33}) was measured using the direct piezoelectric effect and for this a piezometer system (M/s Piezotest, UK) was used.

Dynamic force was applied through a lead zirconate titanate (PZT) actuator, and a quartz sensor was used as a reference.

5.3 Results and Discussion

5.3.1 Structural and morphological characterization of bismuth titanates

The comparison of XRD patterns of bismuth titanate samples synthesized by solid state method and molten salt method is presented in Fig. 5.2.

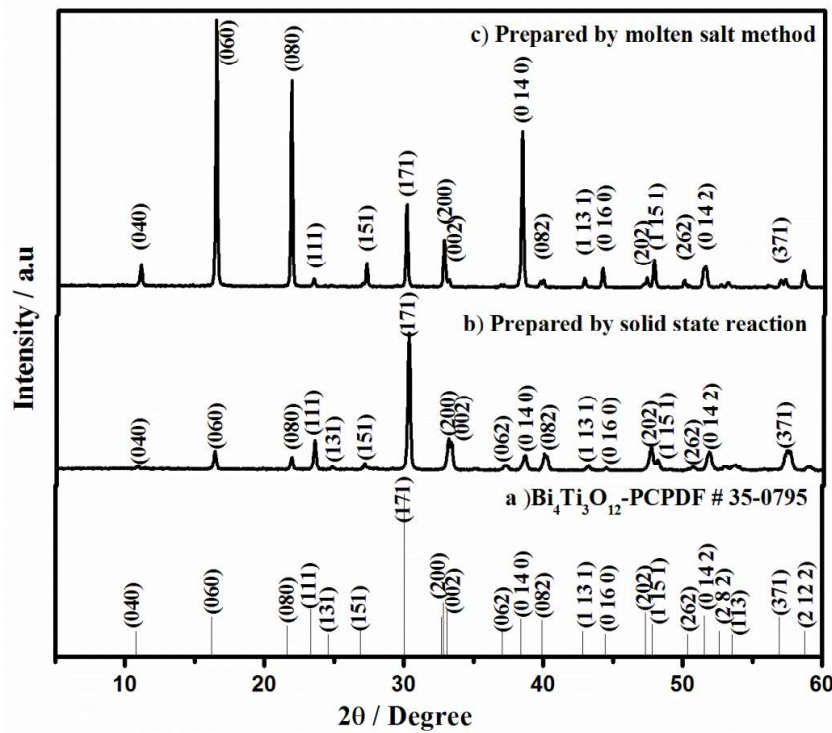


Fig. 5.2 Graphical comparison of XRD patterns of $\text{Bi}_4\text{Ti}_3\text{O}_{12}$ a) PCPDF pattern b) prepared by solid state reaction method c) prepared by reaction in molten salt medium

All the XRD patterns showed the presence of pure orthorhombic phase of $\text{Bi}_4\text{Ti}_3\text{O}_{12}$, which were indexed according to the PCPDF file # 35-0795 as shown in Fig. 5.2a. There were no additional peaks, suggesting that the compounds formed are phase pure. Bismuth titanate prepared by solid state method (Fig. 5.2b) exhibited the highest intensity peak at $2\theta = 30.05^\circ$, which is attributed to the diffraction at the (171)

plane of $\text{Bi}_4\text{Ti}_3\text{O}_{12}$. The intensities of other diffracted peaks are lower, indicating predominant polycrystalline nature of the sample. In the case of bismuth titanate prepared by molten salt method, the XRD pattern (Fig. 5.2c) had shown increased intensity along the (0k0) planes, viz., (060), (080) and (0 14 0), indicating the preferential growth of the crystal along the b axis.

Figure 5.3a shows the XRD patterns obtained for bismuth titanate prepared by oxalate coprecipitation method followed by calcination at 1023 K. The XRD pattern is similar to the one prepared by solid state reaction with the highest intensity peak at 2θ corresponding to 30.05° . However, it is seen from Fig. 5.3b that after sintering at 1123 K, the intensity of the diffraction peaks along the (0k0) planes increased.

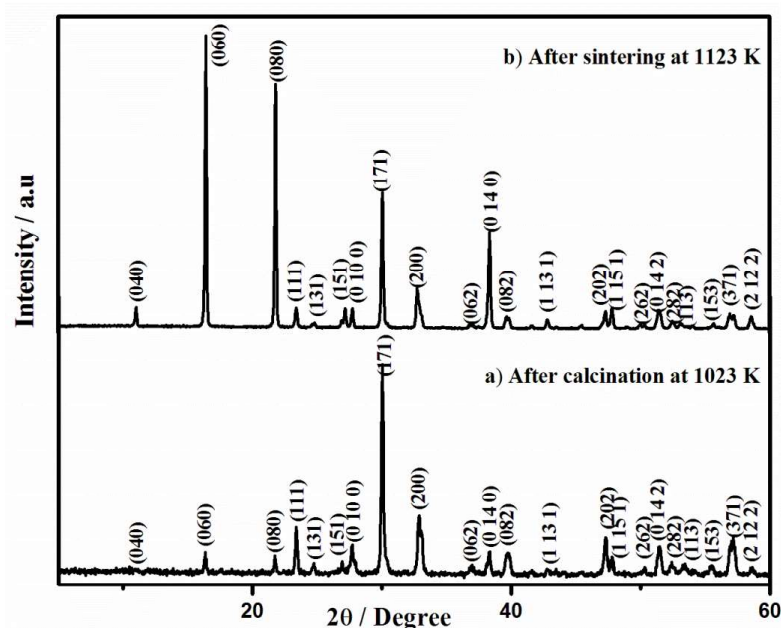


Fig. 5.3 XRD patterns of $\text{Bi}_4\text{Ti}_3\text{O}_{12}$ prepared by oxalate co-precipitation method
a) after calcination at 1023 K b) after sintering at 1123 K

The influence of Nb addition in bismuth titanate was also investigated by XRD. The XRD profiles of bismuth titanate obtained before and after Nb doping by both solid state reaction and by reaction in molten salt medium are shown in Figs.

5.4 and 5.5. The XRD patterns of pristine and Nb-doped bismuth titanates are similar. All diffraction data showed the existence of a single orthorhombic phase, without any detectable secondary phase.

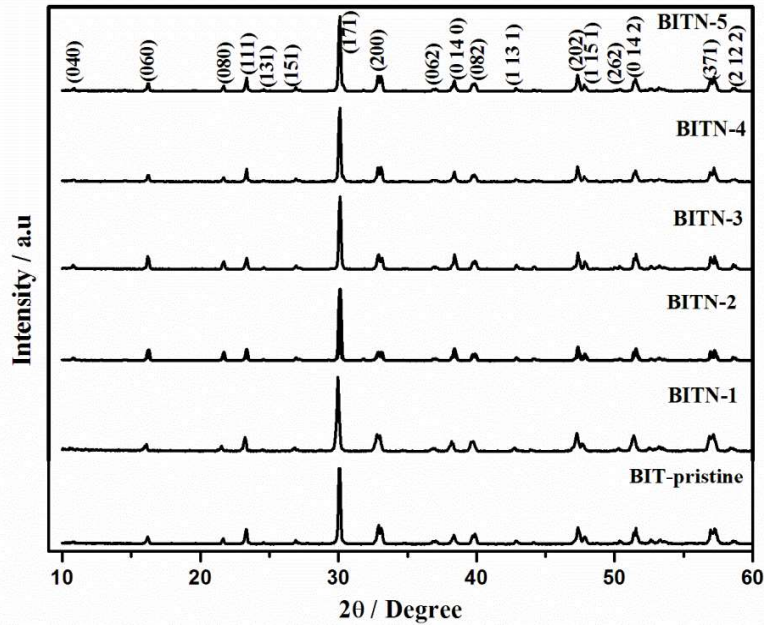


Fig. 5.4 Comparison of XRD patterns of Nb-doped bismuth titanate prepared by solid state reaction

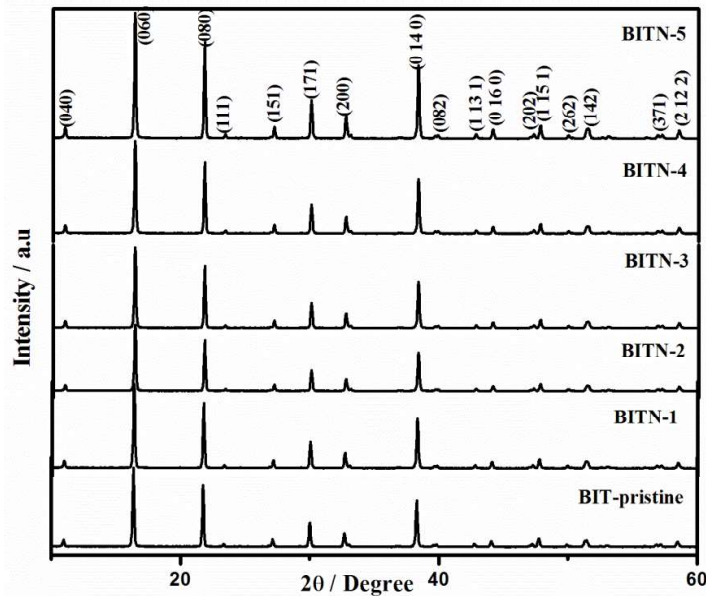


Fig. 5.5 Comparison of XRD patterns of Nb-doped bismuth titanate prepared by the reaction in molten salt medium

The relative densities of the sintered pellets of bismuth titanate synthesized by various routes were determined by Archimedes method and found that all the specimens had attained 95-98% of theoretical density.

The microstructures of pristine bismuth titanate samples prepared by both solid state reaction and reaction in molten salt medium were followed by SEM analysis. The morphological changes that occurred in the bismuth titanate samples upon Nb doping were also studied by SEM imaging of the sintered specimens. Fig. 5.6 represents SEM images of bismuth titanate prepared by solid state reaction and Fig. 5.7 shows those of bismuth titanate prepared by reaction in molten salt medium.

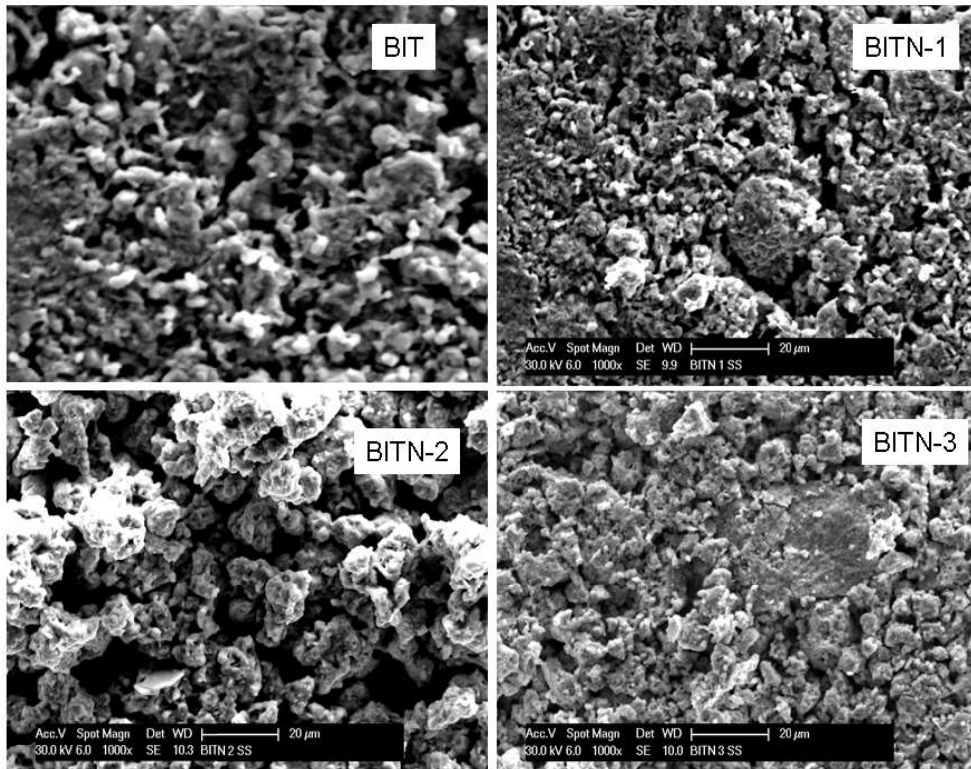


Fig. 5.6 SEM images of pristine and Nb doped BIT prepared by solid state method

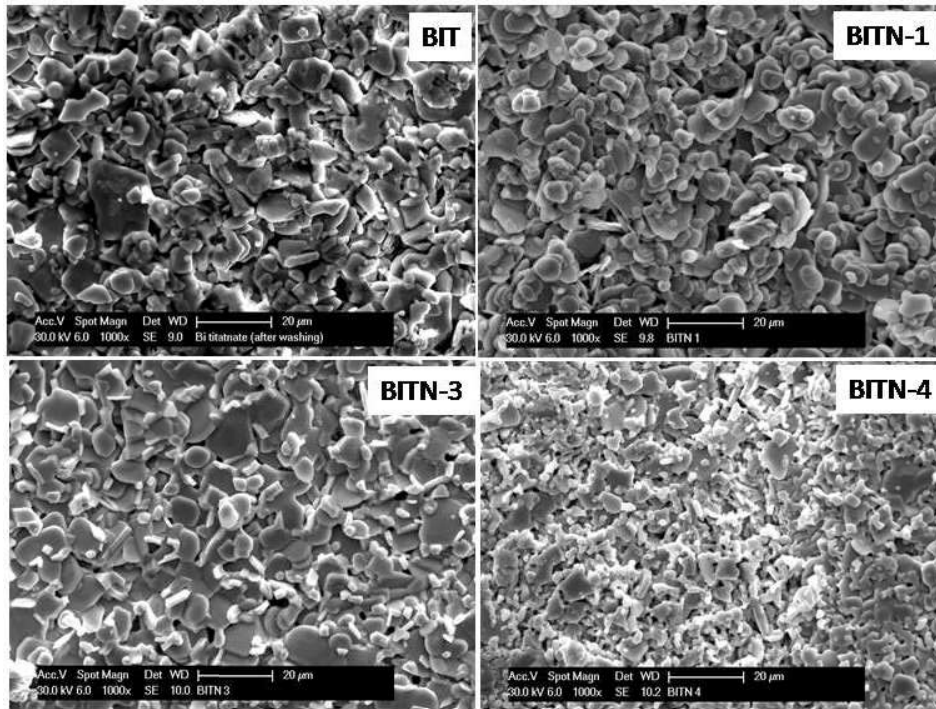


Fig. 5.7 SEM images of pristine and Nb doped BIT prepared by molten salt method

The micrographs of bismuth titanate prepared by solid state reaction shows the presence of small agglomerates of grains. Nb doping has resulted in an increase in the agglomeration of particles. It is seen that the spherical agglomerates are randomly scattered and the average size of the agglomerates ranges from 10-20 μm . The SEM images of the samples prepared by reaction in molten salt medium showed the presence of flake-like microstructures. The flake like structures arises due to the restricted growth of the crystal along the c-axis. Doping with Nb has also modified the appearance of the flakes. Instead of plane flakes as obtained for pristine bismuth titanate, Nb-doped bismuth titanate showed the presence of a globule-like structure within each flake. The incorporation of Nb has led to the evolution of microstructures which is indicated by the increased flowering of the flakes with increase in the Nb content.

5.3.2 Electrical characterization of bismuth titanates

Figure 5.8 shows the variation of electrical conductivity with temperature for pristine bismuth titanates prepared by three different methods.

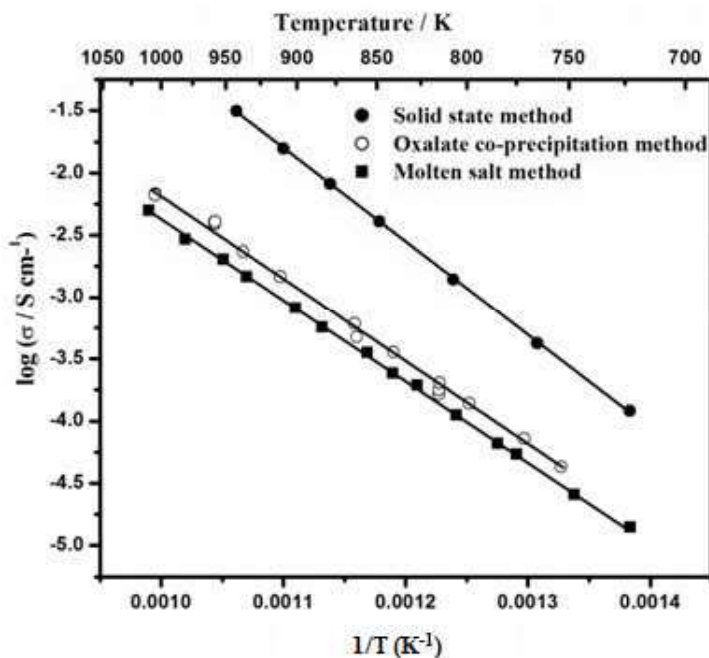


Fig. 5.8 Arrhenius plots of electrical conductivity of bismuth titanates prepared by different methods

It is seen that bismuth titanate prepared by the reaction in molten salt medium has shown the lowest conductivity. The observed reduction in electrical conductivity can be attributed to two factors: 1) as the preparation by molten salt method is mediated by the liquid, evaporation losses of Bi_2O_3 would be low. Thus formation of bismuth and oxide ion vacancies is suppressed during the preparation itself. However, Bi_2O_3 losses can occur during the high temperature sintering of the specimen in air. As the compound has already formed, activity of Bi_2O_3 in the compound would be less as it is in the bound state and consequently evaporation losses would be low and hence, conductivity will be low. 2) It is evident from SEM images that the preparation of bismuth titanate by reaction in molten salt medium had resulted in the formation of

flake like structures which are indicative of the restricted growth of the crystal along the c-axis (i.e. a-b plane oriented). As bismuth titanate shows maximum conductivity along the c-axis, this component of conductivity would get reduced in the case of a-b plane oriented crystal. During the preparation as well as sintering of bismuth titanate by solid state reaction, bismuth and oxide ion vacancies will get generated due to the evaporation of Bi_2O_3 . Even though majority of the oxide ion vacancies get compensated by absorption of oxygen upon cooling, ionic conductivity can be still there in the compound due to the presence of very low concentration of oxide ion vacancies. In addition to this, for compensating the charge for the presence of bismuth ion vacancies holes would be generated which results in p-type conductivity. This is the reason for the high conductivity exhibited by bismuth titanates prepared by solid state reaction. It is also to be noted that electrical conductivity of bismuth titanate prepared by oxalate co-precipitation method is lower than that prepared by solid state method and closer to that prepared by molten salt method. The XRD pattern of the sintered specimen of bismuth titanate obtained by oxalate co-precipitation method had also shown increased intensity of the diffracted peaks along the (0k0) planes suggesting the growth of the crystal along the a-b plane. The conductivity observed is lower and is in accordance with the XRD results. The activation energies observed are 1.50, 1.35 and 1.29 eV, respectively for bismuth titanates prepared by solid state method, oxalate co-precipitation method and molten salt method.

The variation of electrical conductivity obtained after doping with Nb^{5+} for bismuth titanates prepared by solid state method is shown in Fig. 5.9.

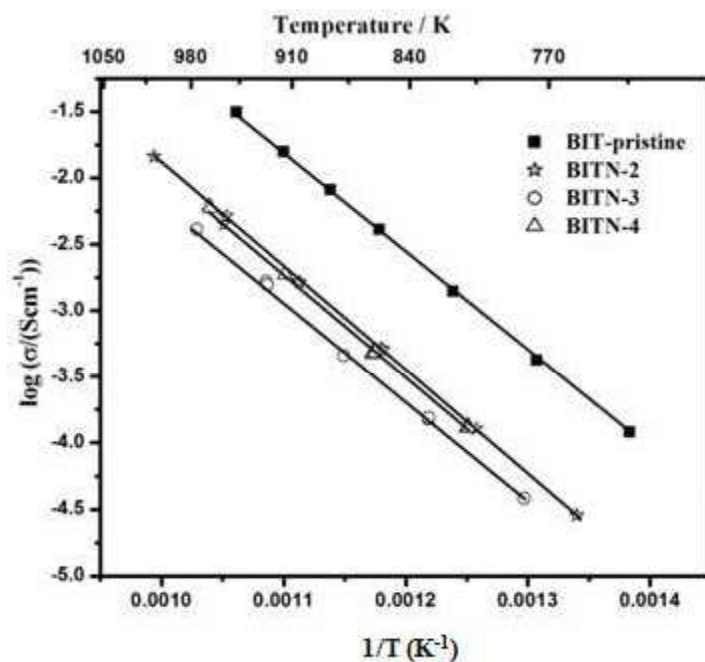


Fig. 5.9 Comparison of electrical conductivities of pristine and Nb-doped bismuth titanates prepared by solid state method

It is observed that the conductivity of Nb-doped bismuth titanates is lower than that of the pristine bismuth titanate. The conductivity was significantly reduced with a very small Nb content. However, the variation of electrical conductivity with increase in Nb content is not much pronounced.

The conductivity measurements on Nb-doped bismuth titanates prepared by molten salt method revealed that the incorporation of Nb has led to the lowering of conductivity by two to three orders of magnitude in comparison with the pristine bismuth titanates synthesized by the same method. The Arrhenius plots of conductivity for all compositions of Nb-doped bismuth titanates are shown in Fig. 5.10. It is found that all compositions showed similar activation energies. However, there is a drastic change in the conductivity values upon doping with Nb⁵⁺.

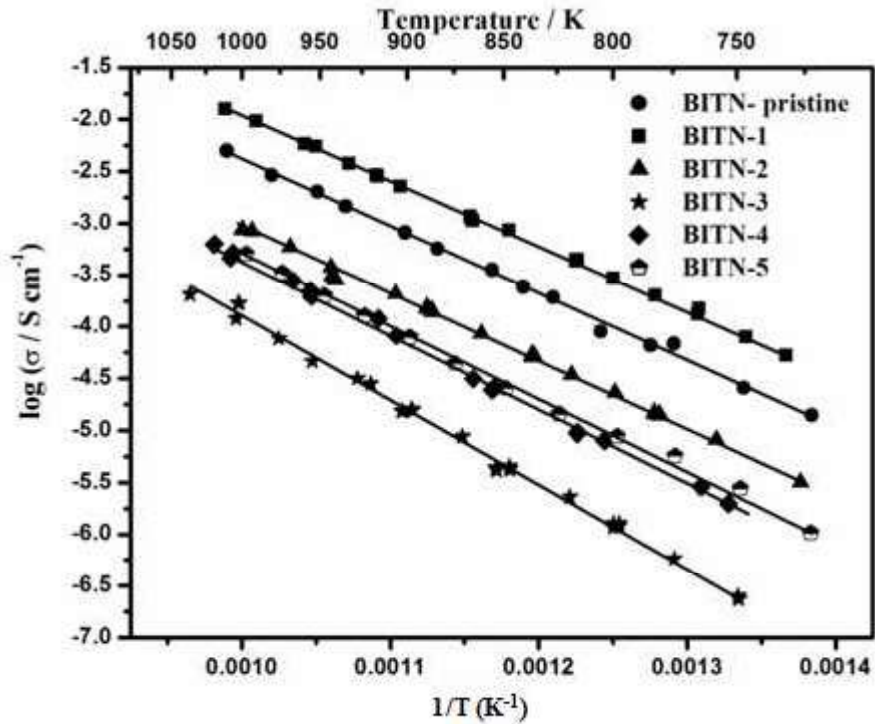


Fig. 5.10 Comparison of electrical conductivities of pristine and Nb-doped bismuth titanates prepared by molten salt method

The conductivity values slightly increased for the lowest Nb concentration and it continued to decrease until it reached the composition with $x = 0.75$ which corresponds to BITN-3. After that, further increase in the Nb concentration has led to an increase in the conductivity. A similar observation in the conductivity of Nb-doped bismuth titanate was reported in the studies of Martin et al. [34].

The lowering of conductivity of bismuth titanate with increasing Nb content can be explained on the basis of the defect structure of bismuth titanate. As discussed earlier, bismuth titanate exhibit both ionic and p-type conduction. The introduction of Nb_2O_5 in bismuth titanate results in the substitution of Nb^{5+} at the Ti^{4+} site with the generation of metal vacancy or by accommodating oxygen ion in the already existing vacant oxygen sites. The filling up of vacant oxygen sites causes a reduction in the ionic conductivity as expressed by equation 5.1.



Once all the oxide ion vacancies are filled up, further substitution of Nb_2O_5 will lead to the generation of electrons. These electrons neutralize the effect of holes, which result in the reduction of conductivity. The conductivity will decrease with Nb_2O_5 doping to a minimum value until the concentration of the electrons equals to the hole concentration. Further introduction of Nb_2O_5 causes an increase in the conductivity. This is evident from the electrical conductivity behavior of Nb-doped bismuth titanates shown in Fig. 5.10. The Nb doped bismuth titanate of composition BITN-3 with $x = 0.75$ has showed the lowest conductivity among the different samples. However, the initial increment in the conductivity for the least concentration of Nb in bismuth titanate could not be explained.

The variation of electrical conductivity as a function of Nb concentration has been plotted and shown in Fig. 5.11. This shows that the behavior of samples is same for all temperatures.

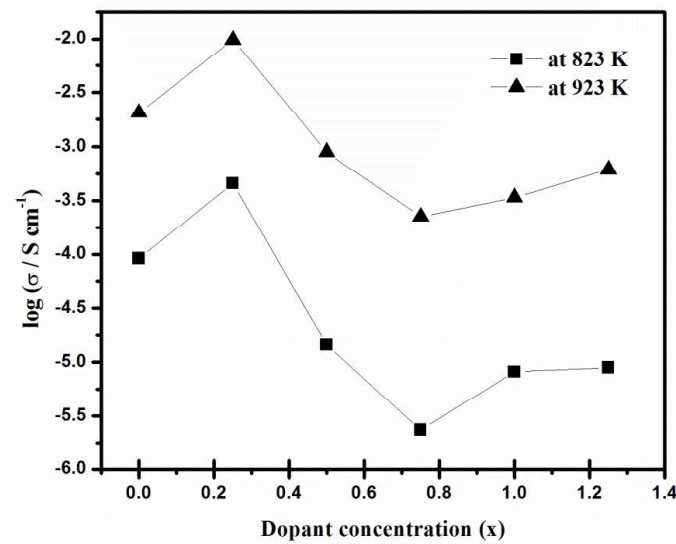


Fig. 5.11 Variation of electrical conductivity as a function of Nb concentration

Based on the experimental studies described so far, it is clear that a reduction in electrical conductivity can be achieved by Nb doping by both solid state method and molten salt method. However, compared to solid state method, highly textured and sufficiently resistive bismuth titanates could be prepared by the reaction in molten salt medium. A pronounced effect in conductivity was observed with Nb doping by this method. The lowest electrical conductivity was obtained for the sample BITN-3 with composition $\text{Bi}_4\text{Ti}_{2.8125}\text{Nb}_{0.15}\text{O}_{12}$. The high electrical resistivity allows for applying high poling fields, which is beneficial to polarize the ceramics and obtain high piezoelectric properties.

5.3.3 Piezoelectric characterization of bismuth titanates

The Nb-doped bismuth titanate sample which exhibited the highest electrical resistance, BITN-3 with composition $\text{Bi}_4\text{Ti}_{2.8125}\text{Nb}_{0.15}\text{O}_{12}$ was poled. The d_{33} value obtained was found to be ~ 16 pC/N.

5.4 References

1. Kazys, R. Sliteris, A. Voleisis, B. Voleisiene, A. Abderrahim, P. Kupschus, Development of ultrasonic transducers for ranging and imaging in heavy liquid metal, Report 0-7803-8692-2/04, IEEE, 2004, 646-649.
2. T. Jardiel, A.C. Cabellero, M. Villegas, Aurivillius ceramics: $\text{Bi}_4\text{Ti}_3\text{O}_{12}$ -based piezoelectrics, J. Ceram. Soc. Jpn. 116 (2008) 511-518.
3. R.C. Turner, P.A. Fuiere, R.E. Newnham, T.R. Shrout, Materials for high temperature acoustic and vibration sensors: A review, App. Acoustics. 41 (1994) 299-324.

4. K.L. Mcaughey, S.E. Burrows, R.S. Edwards, S. Dixon, Investigation into the use of bismuth titanate as a high temperature piezoelectric transducer, 18th World Conference on Non-destructive Testing, 16-20 April 2012, Durban, South Africa.
5. D. Krsmanovic, High temperature ultrasonic gas flow sensor based on lead free piezoelectric material, A dissertation submitted for the degree of Doctor of Philosophy at the University of Cambridge, 2009.
6. L.B. Kong, J. Ma, W. Zhu, O.K. Tan, Preparation of Bi₄Ti₃O₁₂ ceramics via a high-energy ball milling process, Mater. Lett. 51 (2001) 108-114.
7. Q. Yang, Y. Li, Q. Yin, P. Wang, Y.B. Cheng, Bi₄Ti₃O₁₂ nanoparticles prepared by hydrothermal synthesis, J. Eur. Ceram. Soc. 23 (2003) 161-166.
8. P. Pookmanee, P. Uriwilast, S. Phanichpant, Hydrothermal synthesis of fine bismuth titanate powders, Ceram. Int. 30 (2004) 1913-1915.
9. J.S. Patwardhan, M.N. Rahaman, Compositional effects on densification and microstructural evolution of bismuth titanate, J. Mater. Sci. 39 (2004) 133-139.
10. B. Aurivillius, Mixed oxides with layer lattices, Ark. Kemi. 1 (1950) 499-512.
11. C. Jovalekic, S. Stevic, A study of ferroelectric properties of Bi₄Ti₃O₁₂ ceramics prepared from chemically derived powders, Ferroelectrics. 132 (1992) 185-196.

12. C. Long, Q. Chang, H. Fan, Differences in nature of electrical conduction among $\text{Bi}_4\text{Ti}_3\text{O}_{12}$ -based ferroelectric polycrystalline ceramics, *Scientific Reports*, 7 (2017) 1-15.
13. R.L. Withers, J.G. Thompson, A.D. Rae, The crystal chemistry underlying ferroelectricity in $\text{Bi}_4\text{Ti}_3\text{O}_{12}$, $\text{Bi}_3\text{TiNbO}_9$ and Bi_2WO_6 , *J. Solid. State. Chem.* 94 (1991) 404-417.
14. H.S. Shulman, M. Testorf, D. Damjanovic, N. Setter, Microstructure, electrical conductivity, and piezoelectric properties of bismuth titanate, *J. Am. Ceram. Soc.* 79 (1996) 3124-3128.
15. S.K. Kim, M. Miyayama, H. Yanagida, Electrical anisotropy and a plausible explanation for dielectric anomaly of $\text{Bi}_4\text{Ti}_3\text{O}_{12}$ single crystal, *Mater. Res. Bull.* 31 (1996) 121-131.
16. M. Takahashi, Y. Noguchi, M. Miyayama, Electrical conduction mechanism in $\text{Bi}_4\text{Ti}_3\text{O}_{12}$ single crystal, *Jpn. J. Appl. Phys.* 41 (2002) 7053-7056.
17. J.H. Park, J.S. Bae, H.J. Park, Y.S. Kim, B.E. Jun, B.C. Choi, J. H. Jeong, Electric response as a function of applied voltage of Nb-doped $\text{Bi}_4\text{Ti}_3\text{O}_{12}$ thin films, *Thin Solid Films.* 516 (2008) 5304-5308.
18. S.H. Hong, S.T. McKinstry, G.L. Messing, Dielectric and electromechanical properties of textured niobium-doped bismuth titanate ceramics, *J. Am. Ceram. Soc.* 83 (2000) 113-118.

19. J.K. Kim, J. Kim, T.K. Song, S.S. Kim, Effects of niobium doping on microstructures and ferroelectric properties of bismuth titanate ferroelectric thin films, *Thin Solid Films*. 419 (2002) 225-229.
20. T. Sakai, T. Watanabe, M. Osada, M. Kakihana, Y. Noguchui, M. Miyayama, H. Funakubo, Crystal structure and ferroelectric property of tungsten-substituted $\text{Bi}_4\text{Ti}_3\text{O}_{12}$ thin films prepared by metal-organic chemical vapor deposition, *J. Appl. Phys.* 42 (2003) 2850-2852.
21. J.K. Kim, T.K. Song, S.S. Kim, J. Kim, Ferroelectric properties of tungsten-doped bismuth titanate thin film prepared by sol-gel route, *Mater. Letter*. 57 (2002) 964-968.
22. L.N. Zhang, G.R. Li, S.C. Zhao, A.L. Ding, Q.R. Yin, Integrated Ferroelectrics. 79 (2006) 253-263.
23. S.H. Ng, J. Xue, J. Wang, Bismuth titanate from mechanical activation of a chemically coprecipitated precursor, *J. Am. Ceram. Soc.* 85 (2002) 2660-2665.
24. W.F. Su, J.F. Lee, M.Y. Chen, R.M. Ho, Bismuth titanate nanoparticles dispersed polyacrylates, *J. Mater. Res.* 19 (2004) 2343-2348.
25. A.Q. Jiang, H.G. Li, L.D. Zhang, Dielectric study in nanocrystalline $\text{Bi}_4\text{Ti}_3\text{O}_{12}$ prepared by chemical coprecipitation, *J. Appl. Phys.* 83 (1998) 4878-4883.
26. S.H. Hong, J.A. Horn, S.T. McKinstry, G.L. Messing, Dielectric and ferroelectric properties of Ta-doped bismuth titanate, *J. Mater. Sci. Lett.* 19 (2000) 1661-1664.

27. J.A. Horn, S.C. Zhang, U. Selvaraj, G.L. Messing, S.T. McKinstry, Templated grain growth of textured bismuth titanate, *J. Am. Ceram. Soc.* 82 (1999) 921-926.
28. G. Tomandl, A. Stiegelschmitt, R. Bohner, *Proceedings in Science of Ceramic Chemical Processing*, John Wiley & Sons, New York, 1986.
29. T. Kimura, Molten salt synthesis of ceramic powders (in *Advances in ceramics-synthesis and characterization, processing and specific applications*, Edited by C. Sikalidis), InTech, 2011.
30. T. Zaremba, Anisotropic grain growth of bismuth titanate in molten salt fluxes, *X. Kristallogr. Suppl.* 30 (2009) 477-482.
31. G. ChenJie, Z.C. Song, Molten salt synthesis of anisotropic $\text{Bi}_4\text{Ti}_3\text{O}_{12}$ particles, *Adv. Mater. Res.* 284 (2011) 1452-1455.
32. T. Kimura, Y. Yamaguchi, Fused salt synthesis of $\text{Bi}_4\text{Ti}_3\text{O}_{12}$, *Ceram. Int.* 9 (1983) 13-17.
33. Z view®-Impedance software, Scribner Associates, Inc. North Carolina, USA.
34. D. Martin, C. Voisard, D. Damjanovic, N. Setter, Study and control of the conductivity of Nb-doped $\text{Bi}_4\text{Ti}_3\text{O}_{12}$ for high temperature piezoelectric applications, *Bol. Soc. Esp. Ceram. Vidrio.* 38 (1999) 582-586.

Chapter 6

Summary and Conclusions

The results reported in the chapters 3, 4 and 5 can be summarized as follows:

- 1) Partial phase diagram of ternary Bi-Mo-O system valid at 773, 873 and 1023 K has been established by phase equilibration studies. Existence of the following phase fields were identified: (1) Bi-Mo-MoO₂, (2) Bi-MoO₂-Bi₂MoO₆, (3) Bi₂MoO₆-MoO₂-Bi₂Mo₃O₁₂, (4) Bi-Bi₂MoO₆-Bi₆Mo₂O₁₅, (5) Bi-Bi₆Mo₂O₁₅-Bi₁₀Mo₃O₂₄, (6) Bi-Bi₁₀Mo₃O₂₄-Bi₆MoO₁₂, (7) Bi-Bi₆MoO₁₂-Bi₁₄MoO₂₄ and (8) Bi-Bi₁₄MoO₂₄-Bi₂O₃ at 773 K, (1) Bi-Mo-MoO₂, (2) Bi-MoO₂-Bi₂MoO₆, (3) Bi₂MoO₆-MoO₂-Bi₂Mo₂O₉, (4) Bi₂Mo₂O₉-MoO₂-Bi₂Mo₃O₁₂, (5) Bi-Bi₂MoO₆-Bi₈Mo₃O₂₁, (6) Bi-Bi₈Mo₃O₂₁-Bi₁₄Mo₅O₃₆, (7) Bi-Bi₁₄Mo₅O₃₆-Bi₆Mo₂O₁₅, (8) Bi-Bi₆Mo₂O₁₅-Bi₁₀Mo₃O₂₄, (9) Bi-Bi₁₀Mo₃O₂₄-Bi₆MoO₁₂, (10) Bi-Bi₆MoO₁₂-Bi₁₄MoO₂₄ and (11) Bi-Bi₁₄MoO₂₄-Bi₂O₃ at 873 K and (1) Bi-Mo-MoO₂, (2) Bi-MoO₂-Bi₂MoO₆, (3) Bi-Bi₂MoO₆-‘Bi₂₆Mo₁₀O₆₉’, (4) Bi-‘Bi₂₆Mo₁₀O₆₉’-Bi₁₀Mo₃O₂₄, (5) Bi-Bi₁₀Mo₃O₂₄-‘Bi₃₈Mo₇O₇₈’, (6) Bi-‘Bi₃₈Mo₇O₇₈’-Bi₁₄MoO₂₄ and (7) Bi-Bi₁₄MoO₂₄-Bi₂O₃ at 1023 K.

The phase diagrams show that on increasing the dissolved oxygen concentration in liquid bismuth in equilibrium with molybdenum metal, molybdenum oxide (MoO₂) would precipitate first as the coexisting phases. With further increase in oxygen concentration, Bi₂MoO₆ would appear as the first ternary compound stable in liquid bismuth.

Experiments were also carried out to determine the temperatures at which the three ternary compounds, namely, Bi₈Mo₃O₂₁, Bi₁₄Mo₅O₃₆ and Bi₆Mo₂O₁₅ undergo transition into the high temperature solid solution phase ‘Bi₂₆Mo₁₀O₆₉’. The

corresponding transition temperatures are determined to be 917 ± 5 K, 963 ± 5 K and 891 ± 5 K, respectively. Electrical conductivity measurements on $\text{Bi}_2\text{Mo}_2\text{O}_9$ have proved that at temperatures below 817 ± 5 K it undergoes decomposition to $\text{Bi}_2\text{Mo}_3\text{O}_{12}$ and Bi_2MoO_6 phases. Studies carried out on the polymorphic transformations of Bi_2MoO_6 have revealed that the orthorhombic to monoclinic transition of Bi_2MoO_6 is irreversible and occurs between 868 and 871 K.

The standard molar Gibbs energies of formation of monoclinic phase of Bi_2MoO_6 (s) was determined by measuring the oxygen potentials in the relevant ternary phase fields by solid oxide electrolyte based emf cell and is given as below.

$$\Delta_f G^\circ \langle \text{Bi}_2\text{MoO}_6 \rangle / \text{kJmol}^{-1} = -1382.3 + 0.5064 (T / \text{K})$$

$$(T: 772-1023 \text{ K}) \quad (3.23)$$

The standard molar enthalpies of formation of $\text{Bi}_2\text{Mo}_3\text{O}_{12}$ (s), orthorhombic and monoclinic phases of Bi_2MoO_6 (s), $\text{Bi}_6\text{Mo}_2\text{O}_{15}$ (s) and $\text{Bi}_6\text{MoO}_{12}$ (s) were determined by solution calorimetry experiments and the values obtained are (-2915.8 ± 5.7), (-1407.2 ± 3.8), (-1385.7 ± 3.9), (-3345.0 ± 10.9) and (-2605.2 ± 10.2) kJ mol⁻¹, respectively.

Molar heat capacities of $\text{Bi}_2\text{Mo}_3\text{O}_{12}$ (s), monoclinic- Bi_2MoO_6 (s) and $\text{Bi}_6\text{Mo}_2\text{O}_{15}$ (s) were determined by differential scanning calorimetry and are given below:

$$C_p \langle \text{Bi}_2\text{Mo}_3\text{O}_{12} \rangle / \text{J K}^{-1} \text{mol}^{-1} = 416.7 - 7.1 \times 10^{-3} T - 8.8 \times 10^6 T^{-2}$$

$$(T: 328-818 \text{ K}) \quad (3.25)$$

$$C_p \langle \text{Bi}_2\text{MoO}_6 \rangle / \text{J K}^{-1} \text{mol}^{-1} = 221.4 - 1.5 \times 10^{-3} T - 3.9 \times 10^6 T^{-2}$$

$$(T: 318-818 \text{ K}) \quad (3.26)$$

$$C_p \langle \text{Bi}_6\text{Mo}_2\text{O}_{15} \rangle / \text{J K}^{-1} \text{mol}^{-1} = 529.8 - 67.9 \times 10^{-3} T - 6.3 \times 10^6 T^{-2}$$

(T: 318-808 K) (3.27)

From the measured heat capacity data, thermodynamic functions such as enthalpy increments, entropies and Gibbs energy functions were derived.

2) The partial phase diagram of the ternary Pb-Mo-O system has been established at 773 and 998 K by phase equilibration studies. The following phase fields were identified in the system: At 773 K: (1) Pb-Mo-MoO₂ (2) Pb-MoO₂-PbMoO₄ (3) Pb-PbMoO₄-Pb₂MoO₅ (4) Pb-Pb₂MoO₅-PbO. At 998 K (1) Pb-Mo-MoO₂ (2) Pb-MoO₂-PbMoO₄ (3) Pb-PbMoO₄-Pb₂MoO₅ (4) Pb-Pb₂MoO₅-Pb₅MoO₈ and (5) Pb-Pb₅MoO₈-PbO.

The results have shown that in the Pb-Mo-O system, with increase in the oxygen content in liquid lead that is coexisting with Mo metal, molybdenum oxide (MoO₂) would appear first followed by the ternary compounds.

The standard molar Gibbs energies of formation of PbMoO₄ (s), Pb₂MoO₅ (s) and Pb₅MoO₈ (s) were determined by using emf cells. The following results are obtained:

$$\Delta_f G^\circ \langle \text{PbMoO}_4 \rangle \pm 0.7 / \text{kJmol}^{-1} = -1030.1 + 0.3054 (T / \text{K})$$

(T: 772-1017 K) (4.12)

$$\Delta_f G^\circ \langle \text{Pb}_2\text{MoO}_5 \rangle \pm 0.8 / \text{kJmol}^{-1} = -1248.1 + 0.3872 (T / \text{K})$$

(T: 741-1021 K) (4.15)

$$\Delta_f G^\circ \langle \text{Pb}_5\text{MoO}_8 \rangle \pm 0.8 / \text{kJmol}^{-1} = -1737.5 + 0.4830 (T / \text{K})$$

(T: 884-967 K) (4.18)

The standard molar enthalpies of formation of PbMoO_4 (s), Pb_2MoO_5 (s) and Pb_5MoO_8 (s) were determined by solution calorimetry using 2.02 mol kg^{-1} NaOH as the calorimetric solvent and results obtained are (-1059.6 ± 2.2) , (-1274.7 ± 2.3) and $(-1906.2 \pm 3.2) \text{ kJ mol}^{-1}$, respectively.

The molar heat capacities of PbMoO_4 (s) and Pb_2MoO_5 (s) were determined by differential scanning calorimetry and the results obtained are given below:

$$C_p \langle \text{PbMoO}_4 \rangle / \text{J K}^{-1} \text{mol}^{-1} = 127.31 + 30.47 \times 10^{-3} T - 1.79 \times 10^6 T^{-2}$$

(T: 313-798 K) (4.19)

$$C_p \langle \text{Pb}_2\text{MoO}_5 \rangle / \text{J K}^{-1} \text{mol}^{-1} = 169.20 + 66.69 \times 10^{-3} T - 1.99 \times 10^6 T^{-2}$$

(T: 308-798 K) (4.20)

3) Work towards the development of a high temperature piezoelectric material for use in liquid metals was carried out. In this regard, highly textured and piezoelectric bismuth titanate was prepared by reaction in molten salt medium. In order to achieve sufficient resistivity for the material, doping has been carried out by the same method using Nb as the dopant. A pronounced lowering in conductivity was observed with Nb doping. The lowest electrical conductivity was obtained for the sample with composition $\text{Bi}_4\text{Ti}_{2.8125}\text{Nb}_{0.15}\text{O}_{12}$ (BITN-3). The material prepared was subjected to poling and the d_{33} value was measured.

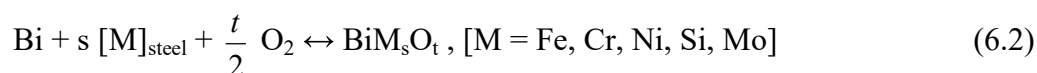
6.1 Prediction of the nature of passive oxide layer

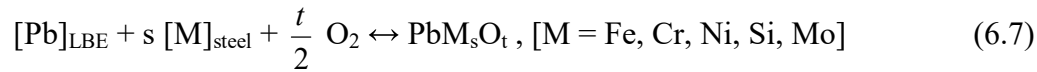
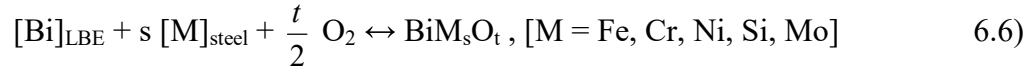
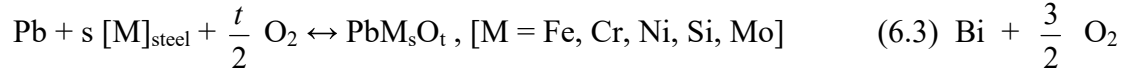
The nature of the protective oxide layer formed at the steel-liquid Bi and steel-liquid Pb interface can be predicted by using the results obtained on Bi-Mo-O and Pb-Mo-O systems along with the data on solubility of oxygen in liquid Bi and liquid Pb. The threshold concentration of oxygen above which a ternary compound appears in

the liquid metal system is determined by the thermodynamic stability of the compound, chemical activity of the the structural steel components and the activity and solubility of oxygen in the coolant. Studies by Sahu et al.. [1-3] carried out a detailed study on Pb-Fe-O and Pb-Cr-O systems and predicted the nature of the passive oxide layer formed on the steel–liquid Pb interface. Meera et al. [4, 5] studied the Bi-Fe-O and Bi-Cr-O systems and used the data to predict the nature of the passive oxide layer formed on the steel–Bi interface. Using the earlier reported data along with the present data, further insights can be obtained on the nature of oxide layer on the steel-liquid metal interface.

In order to understand the nature of the ternary compound formed on Bi-stainless steel system and Pb- stainless steel system, equilibrium oxygen potentials of various equilibria that would exist in these systems were computed. Based on the studies on Bi-Mo-O and Pb-Mo-O systems, it is concluded that at low levels of dissolved oxygen, only MoO₂ would coexist with liquid Bi in equilibrium with Mo metal. Ternary compounds appear only at high oxygen concentrations. Similarly in the case of liquid Pb coexisting with Mo metal only MoO₂ would coexist at low oxygen concentrations.

The following equilibria were considered for computation of oxygen potentials:





In equilibria 6.2, 6.3, 6.6 and 6.7, the s and t can have different values for different elements, viz., Fe, Cr, Ni, Si, Mo, etc. As PbO is more stable than Bi₂O₃ in LBE, the equilibrium considered for computing oxygen potential with different levels of dissolved oxygen concentration in LBE is:



For these computations, data on Gibbs energies of formation of bismuth molybdates and lead molybdates from this work, MoO₂ from reference [6] were used. Data on lead ferrates and chromates were from references 1 to 3 and data on bismuth ferrates and chromates from references 4 and 5 were used. For oxides of Ni, Si and Mo, the data from reference 7, for oxides of iron, data from references 8 and 9, and for chromium sesquioxide, data from 10 were used. Oxygen potentials of the above mentioned equilibria were calculated for 9Cr-1Mo steel. The chemical activity of the alloying elements in steel was obtained by assuming the steel to be an ideal solid solution obeying Raoult's law.

The oxygen potentials of the different equilibria in liquid Bi, liquid Pb and LBE in 9Cr-1Mo steel are shown in Figs. 6.1 to 6.3. Fig. 6.1 shows the oxygen potentials of different chemical equilibria in liquid Bi –9Cr-1Mo steel system. The oxygen potentials in liquid Bi containing different levels of dissolved oxygen concentrations are also shown in the same figure. It can be seen from the figure that at low oxygen concentrations, SiO_2 and Cr_2O_3 layers would be formed on the steel surface depending upon the amount of Si and Cr present in the steel. With increase in the oxygen concentration, iron oxides and molybdenum oxides would be formed at the steel – liquid Bi interface. If the oxygen concentration in the molten bismuth is further increased, Bi_2MoO_6 would appear. Further increase in the oxygen concentration can lead to the formation of $\text{Bi}_2\text{Fe}_4\text{O}_9$ and $\text{Bi}_{22}\text{Cr}_{18}\text{O}_{60}$ ternary compounds.

Fig. 6.2 shows the oxygen potentials in liquid Pb containing different dissolved oxygen concentrations and chemical equilibria computed for 9Cr–1Mo steel. As in the case of liquid Bi - 9Cr-1Mo steel, SiO_2 and Cr_2O_3 layers would be formed at low oxygen levels followed by the formation of molybdenum and iron oxides with increase in the oxygen concentration. If the oxygen concentration in liquid Pb is further increased, PbMoO_4 would appear. Further increase in the oxygen concentration can lead to the formation of $\text{PbFe}_5\text{O}_{8.5}$ and $\text{Pb}_2\text{Fe}_2\text{O}_5$ ternary compounds.

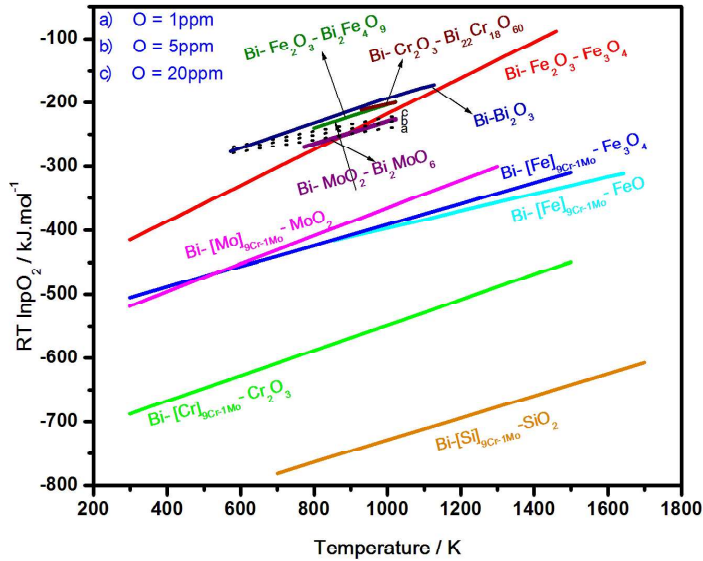


Fig. 6.1 Oxygen potentials in liquid Bi containing different oxygen concentrations and with different chemical equilibria for 9Cr-1Mo steel

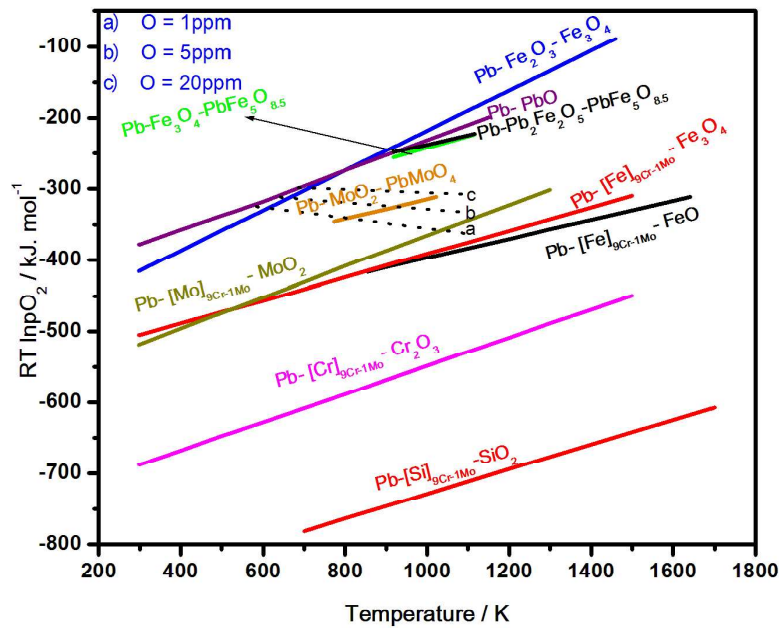


Fig. 6.2 Oxygen potentials in liquid Pb containing different oxygen concentrations and with different chemical equilibria for 9Cr-1Mo steel

Figure 6.3 shows the oxygen potentials of different chemical equilibria in LBE and 9Cr-1Mo steel. As in the previous cases, at lower oxygen concentrations, SiO_2 , Cr_2O_3 and MoO_2 layers could be formed at the LBE - steel interface. With increase in

the oxygen concentration, iron oxides would be formed at the steel–LBE interface. At higher oxygen concentrations, the first ternary compound formed would be PbMoO_4 .

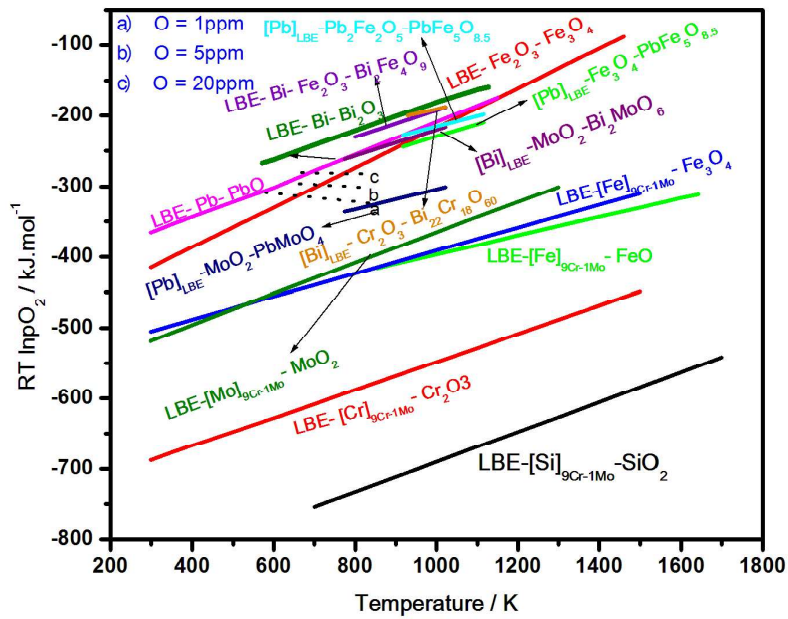


Fig. 6.3 Oxygen potentials in LBE containing different oxygen concentrations and with different chemical equilibria for 9Cr-1Mo steel

6.2 References

1. S.K. Sahu, R. Ganesan, T. Gnanasekaran, Studies on phase diagram of Pb–Cr–O system, *J. Nucl. Mater.* 376 (2008) 366-370.
2. S.K. Sahu, R. Ganesan, T. Gnanasekaran, Standard molar Gibbs free energy of formation of Pb_5CrO_8 (s), Pb_2CrO_5 (s), and PbCrO_4 (s), *J. Chem. Thermodyn.* 42 (2010) 1–7.
3. S.K. Sahu, R. Ganesan, T. Gnanasekaran, Studies on the phase diagram of Pb–Fe–O system and standard molar Gibbs energy of formation of ‘ $\text{PbFe}_5\text{O}_{8.5}$ ’ and $\text{Pb}_2\text{Fe}_2\text{O}_5$, *J. Nucl. Mater.* 426 (2012) 214-222.

4. A.V. Meera, R. Ganesan, T. Gnanasekaran, Partial phase diagram of Bi-Fe-O system and the standard molar Gibbs energy of formation of $\text{Bi}_2\text{Fe}_4\text{O}_9$, *J. Alloys. Comp.* 692 (2017) 841-847.
5. A.V. Meera, J. Basu, R. Ganesan, T. Gnanasekaran, Studies on the phase diagram of Bi-Cr-O system, *J. Nucl. Mater.* 487 (2017) 174-185.
6. K.T. Jacob, V.S. Saji, J. Gopalakrishnan, Y. Waseda, Thermodynamic evidence for phase transition in $\text{MoO}_2\text{-}\delta$, *J. Chem. Thermodyn.* 39 (2007) 1539-1545.
7. O. Kubaschewski, C.B. Alcock, *Metallurgical Thermochemistry*, fifth ed., Pergamon, Oxford, 1979.
8. B. Sundman, An assessment of the Fe-O system, *J. Phase Equilibria*, 12 (1991) 127-140.
9. A.F. Guillermet, P. Gustafson, An assessment of the thermodynamic properties and the (p, T) phase diagram of iron, *High Temp. – High Press.* 16 (1985) 591–610.
10. A. Holzheid, H. St.C. O'Neill, The Cr-Cr₂O₃ oxygen buffer and the free energy of formation of Cr₂O₃ from high-temperature electrochemical measurements, *Geochim. Cosmochim. Acta.* 59 (1995) 475-479.

Chapter 7

Scope for future studies

Based on the discussion in the preceding chapters it is clear that a comprehensive knowledge on the composition and thermochemical data of the passive oxide layer is required for the effective mitigation of corrosion in LBE-steel systems. In this regard, the interaction of structural steel components with Pb and Bi is important. A detailed study on Bi-M-O and Pb-M-O (M: Fe, Cr) systems has been carried out by Sahu et al. [1-6] and Meera et al. [7, 8]. Bi-Mo-O and Pb-Mo-O systems were studied in the present work.

In Bi-Mo-O ternary system, the Gibbs energy of formation of $\text{Bi}_2\text{MoO}_6(\text{s})$ has been determined in the present work. Gibbs energies of formation of other ternary compounds which are coexisting with liquid Bi are needed to be determined. Their enthalpies of formation and heat capacities are also needed to be measured.

Interaction of other alloying components of steels with Pb and Bi in the presence of dissolved oxygen deserves greater importance. Pb (Bi) –Ti-O systems and Pb (Bi) –Si-O systems can be studied in this regard to understand and exploit the corrosion protection phenomena in lead and LBE circuits.

In the present study, predominantly textured bismuth titanate ceramics were prepared by molten salt method using Nb as the dopant. Further studies can be carried out to modify the electrical properties of bismuth titanate using different dopants.

7.1 References

1. S.K. Sahu, R. Ganesan, T. Gnanasekaran, Studies on phase diagram of Pb–Cr–O system, *J. Nucl. Mater.* 376 (2008) 366-370.

2. S.K. Sahu, R. Ganesan, T. Gnanasekaran, Standard molar Gibbs free energy of formation of Pb_5CrO_8 (s), Pb_2CrO_5 (s), and PbCrO_4 (s), *J. Chem. Thermodyn.* 42 (2010) 1–7.
3. S.K. Sahu, R. Ganesan, T.G. Srinivasan, T. Gnanasekaran, The standard molar enthalpies of formation of Pb_2CrO_5 (s) and Pb_5CrO_8 (s) by acid solution calorimetry, *J. Chem. Thermodyn.* 43 (2011) 750-753.
4. S.K. Sahu, R. Ganesan, T. Gnanasekaran, Studies on the phase diagram of Pb–Fe–O system and standard molar Gibbs energy of formation of ‘ $\text{PbFe}_5\text{O}_{8.5}$ ’ and $\text{Pb}_2\text{Fe}_2\text{O}_5$, *J. Nucl. Mater.* 426 (2012) 214-222.
5. S.K. Sahu, M. Sahu, R.S. Srinivasa, T. Gnanasekaran, Determination of heat capacities of PbCrO_4 (s), Pb_2CrO_5 (s), and Pb_5CrO_8 (s), *Monatsh. Chem.* 143 (2012) 1207–1214.
6. S.K. Sahu, R. Ganesan, T. Gnanasekaran, The standard molar enthalpies of formation of $\text{Pb}_2\text{Fe}_2\text{O}_5$ (s) and $\text{PbFe}_5\text{O}_{8.5}$ (s) by acid solution calorimetry, *J. Chem. Thermodyn.* 56 (2013) 57–59.
7. A.V. Meera, R. Ganesan, T. Gnanasekaran, Partial phase diagram of Bi-Fe-O system and the standard molar Gibbs energy of formation of $\text{Bi}_2\text{Fe}_4\text{O}_9$, *J. Alloys. Comp.* 692 (2017) 841-847.
8. A.V. Meera, Joysurya Basu, R. Ganesan, T. Gnanasekaran, Studies on the phase diagram of Bi-Cr-O system, *J. Nucl. Mater.* 487 (2017) 174-185.

Appendix

Table 1. Data of null emf measurements

Variation of emf with temperature for cell with oxygen gas on either side of the electrolyte	
Temperature / K	Emf / mV
1015.6	0.026
967.0	0.046
917.4	0.064
887.3	0.081
868.3	0.098

Variation of emf with temperature for cell with air on either side of the electrolyte	
Temperature / K	Emf / mV
1012.1	0.016
962.9	0.025
919.6	0.048
867.9	0.093
773.8	0.125

Fig.1. Schematic of the experimental set up used for long term equilibrations of $\text{Bi}_8\text{Mo}_3\text{O}_{21}$, $\text{Bi}_{14}\text{Mo}_5\text{O}_{36}$ and $\text{Bi}_6\text{Mo}_2\text{O}_{15}$

